NUMERICAL ANALYSIS OF TEST PILE DATA FROM INSTRUMENTED LARGE DIAMETER BORED PILES FORMED IN KEUPER MARL (MERCIA MUDSTONE)

by

J.R.OMER*, B.Sc. (Hons.), M.Sc.

A thesis presented in fulfilment of the requirement for the degree of Doctor of Philosophy of the University of Glamorgan

June 1998

Collaborating establishments

- South Glamorgan County Council
- Building Research Establishment

Grant support

- Overseas Development Administration
- University of Glamorgan
- Institution of Civil Engineers (Research Enablement fund)

* The candidate was the winner of the inaugural David Douglas prize awarded by the South Wales Institute of Engineers, U.K., May 1994

CERTIFICATE OF RESEARCH

This is to certify that, apart from where specific reference to other publications is made the work in this thesis is the result of the investigation by the candidate.

....
J.R Omer
(Candidate)

26/3/99
....
(Date)

R.B. Robinson
....
Dr R.B. Robinson
(Director of studies)

26th March 1999
....
(Date)

R Delpak
....
Dr R. Delpak
(Supervisor)

26th March 1999
....
(Date)

DECLARATION

This is to certify that neither this thesis, nor any part of it has been presented, in candidature form for any degree at any other academic institution.

....
(Candidate)

ACKNOWLEDGEMENTS

The author is indebted to Drs. R. Delpak and R.B. Robinson (Supervisor and Director of Studies, respectively) for their advice and support. Special thanks are due to Cardiff County Council for permitting full access to their pile load test and site investigation reports and for providing the main research funding. The enthusiasm of Mr John Church (formerly of the Department of Highways and Transportation, South Glamorgan County Council) in encouraging the research is greatly appreciated. Messrs Davies Middleton & Davies (DMD), Cardiff, are thanked for carrying out the pile load tests and for being generous with their expertise and facilities.

Other thanks go to the Building Research Establishment (Geotechnics Division), Garston, Hertfordshire, for their collaborative input and for installing and monitoring the instrumentation used in the test piles. The author is indebted to Messrs England and Fleming at Kvaerner Cementation Piling & Foundations for their helpful advice and for providing pile analysis software gratis.

Finally the author wishes to express gratitude to his wife Hilda and children Winnie and Tonnie for their understanding and patience throughout the duration of this study.

The author was supported by research grants awarded by the Institution of Civil Engineers (Research and Development Enabling Fund), Overseas Development Administration (O.D.A.) and the University of Glamorgan.

SUMMARY

A study of the behaviour of large diameter, bored, cast in-situ piles founded in Keuper marl (Mercia mudstone) is presented. The work is based on instrumented full-scale pile load tests carried out as part of the design of a major Highway communication project in Cardiff, U.K. This research also forms part of an on-going research programme within the Soil/Structure research unit at the University of Glamorgan. The test piles were 0.9m in diameter by 28-32m long and were constructed following the procedure to be used in the actual contract piles. Vibrating wire strain gauges, extensometers and load cells were installed in the test piles at selected locations.

The load test generated extensive data in terms of the strain levels along each pile shaft. All instrument readings were monitored and automatically stored on computer. In addition, a 2m long reinforced concrete column with the same cross-section properties and instrumentation as the test piles was load tested under controlled conditions. The measured stress-strain characteristics of the short column were used to model the deformation parameters of the test piles. Utilising the load test data and the results of a comprehensive site investigation, the initial design of the contract piles has been evaluated. It is established that the design method suggested in the interpretative report of the site investigation, which is partially based on C.I.R.I.A. report No.47, leads to conservative predictions of ultimate shaft resistance. The predicted values are 40-57% of the measured values.

A semi-empirical method is developed which can predict the characteristics of large diameter, bored, cast in-situ piles in Keuper marl, at every stage of loading up to the ultimate state of the pile-soil system. The formulation is supported by load test-data from fully instrumented test piles in Cardiff (South Wales, U.K.) as well as other published pile test data. The analysis is based on separation of shaft resistance and end bearing by formulating the variation in load sharing between the pile shaft and base. The method takes into consideration the influence of non-linear stress-strain behaviour of concrete on pile deformation and the influence on pile settlement of additional compressibility due to any loose soil possibly present at the pile base level.

The proposed method is validated against a large database of full-scale pile loading tests, with a wide range of diameters and lengths, installed in a variety of clays. There are provisions in the model, to accommodate pile conditions with negligible components of either shaft resistance or end bearing. In every case, the predictive capability is judged to be accurate and satisfactory. The improved predictive capability of this method, in pile analysis, is expected to result in a more cost-effective construction. A computer program is written for the complete analysis of a pile using the proposed numerical model. The program can accommodate pile conditions in which the contribution to load resistance of either shaft or end bearing is negligible. The parameters required for input into the numerical model are those that would be available from a standard site investigation, but may also be back-figured from pile test data. These data may then be used to predict the complete load-settlement curve for a pile of different dimensions and material properties under different ground conditions.

NOTATIONS

A_o, A_1, A_2, A_3	Constants in the hyperbolic function for base performance
A_b	Area of a pile base
	Cross-sectional area of reinforced concrete
A_c	Area of concrete at the pile cross-section
A_s	Area of steel at the pile cross-section
C_o, C_1, C_2, C_3	Constants in the cubic function for shaft load versus base movement
D_b	Diameter of pile base
D_s	Diameter of pile shaft
E_b	Deformation modulus for soil beneath the pile base
	Young's modulus of reinforced concrete
$E_c(z)$	Young's modulus of pile concrete at a given depth z
E_s	Young's modulus of steel reinforcement in a pile
G	Gradient of a plot of base load versus base movement using a the linear function for settlement calculation given by Randolph and Wroth(1978)
K(z)	Earth pressure coefficient at depth z (Burland,1973)
K_o	Coefficient of earth pressure at rest
K_{ob}	Value of K_o at the level of the pile base
K_{ot}	Value of K_o at the bottom of the upper portion of the pile not involved in load transfer
L	Length of pile
L_o	Upper length of a pile carrying little or no load in shaft resistance
L_m	Distance from the bottom of the upper portion of the pile not involved in load transfer to the point of maximum or minimum shaft resistance
L_s	Length of a pile transferring load to soil by shaft resistance
N	Blow count in a Standard Penetration Test (S.P.T.)
N_c, N_q, N_γ	Bearing capacity factors
P	Applied axial force or load
P_b	Load applied at pile base
P_h	Load applied at pile head
P_s	Load carried by pile in shaft resistance
P_{ub}	Ultimate pile base resistance
P_{us}	Ultimate pile shaft resistance
P(z)	Axial force in pile at depth z
R_s	Residual shaft resistance divided by ultimate shaft resistance for a pile
S	Imaginary shift, to the left, of the origin of the base load versus base movement curve due to the effects of a pile base resting on debris
a, b, c, d	General constants, to be determined from the boundary conditions of a function
a_o, a_1	Numerical constants in the expression for the variation of Young's modulus of concrete versus strain
c'_s	Effective cohesion of a softened soil
c_u	Undrained cohesion of soil
c'	Drained cohesion of soil
e_o	Elastic shortening of the upper length of a pile not involved in load transfer
e_p	Total elastic shortening of a pile
e_s	Elastic shortening of the length of a pile transferring load to soil by shaft resistance

f_b	Maximum base pressure for a pile
f_s	Maximum unit shaft resistance at a pile shaft
k	Ratio of $K_o \tan\delta$ at the top of the lower pile portion involved in load transfer to that at the pile base level
m	Base movement at ultimate base load expressed as a proportion of the pile base diameter
n	Value of $\frac{P_b}{P_{ub}}$ at which the parabolic function and the linear function of P_b versus Δ_b merge
$\bar{q}$	Mean effective overburden pressure along a pile shaft
q_b	Ultimate base pressure
q_{ub}	Ultimate bearing pressure at a pile base
r	Base movement at ultimate shaft load divided by pile shaft diameter Radius, Radial co-ordinate
s_τ	Equivalent spring stiffness for a given soil stratum, in the notation of Cole and Stroud(1976)
u	Radial displacement
z	Depth, below a given level (also depth in general) Co-ordinate along the main axis of a cylinder
$\tau(z)$	Shaft resistance at depth z
τ_{max}	Maximum shaft resistance that can occur anywhere on a pile shaft (Reese et al.,1969)
$\tau_{us}(z)$	Ultimate shaft resistance at depth z
τ_t	Shaft resistance at the top of the pile shaft length transferring load to soil by friction
τ_b	Shaft resistance at the level of the pile toe
Δ_b	Movement of a pile base
Δ_h	Pile head settlement under applied load
Δ_{ub}	Base movement at ultimate base load
Δ_{us}	Base movement at ultimate shaft load
$\Delta(z)$	Pile displacement at a given depth, z
Δ_k	Value of Δ_b when $P_b=nP_{ub}$ using the linear foundation settlement formula
Δ_ϕ	Value of Δ_b when $P_b=\phi P_{ub}$ using the linear foundation settlement formula
θ	Circumferential angle
ν	Poisson's ratio of soil
ν_b	Poisson's ratio of reinforced concrete
ν_c	Poisson's ratio of concrete
ν_s	Poisson's ratio of steel
η	Settlement reduction factor (related to depth of foundation below ground) as used in the foundation settlement formula
ϕ	Value of $\frac{P_b}{P_{ub}}$ at which the linear function and the hyperbolic cosine function of P_b versus Δ_b merge
ϕ'	Drained angle of friction of soil
ϕ_s'	Effective angle of internal friction of a softened soil (Foley and Davis,1971)
ϕ_r'	Residual effective angle of internal friction of soil
ϕ_d	Remoulded drained angle of friction of soil
ε_z	Strain in the longitudinal direction of a cylinder

ε_r	Strain in the radial direction of a cylinder
ε_θ	Strain in the circumferential direction of a cylinder
$\varepsilon(z)$	Strain in a pile at depth z
σ_b	Stress in the reinforced concrete zone of a composite column
σ_c	Stress in concrete
σ_r	Direct stress in the radial direction of a cylinder
σ_s	Stress in steel
σ_θ	Direct stress in the circumferential direction of a cylinder
σ_z	Direct stress in the longitudinal direction of a cylinder
σ_h'	Horizontal effective stress in soil
$\sigma_v'(z)$	Effective vertical stress at depth z
σ_{vt}'	Effective vertical stress in soil at the top of the pile lower pile portion transferring load to soil by skin resistance
σ_{vb}'	Effective vertical stress in soil at the level of the pile base
$\delta(z)$	Effective angle of friction of soil at depth z
δ_t	Effective angle of friction of soil at the top of the pile shaft length transferring load to soil by shaft resistance
δ_b	Effective angle of friction of soil at the level of the pile base
ω	Factor which when multiplied by L_s gives the position of the point of maximum or minimum shaft resistance below the top of the lower pile portion transferring load to soil by shaft resistance
λ	Compound parameter
Ω	Compound parameter
α	Adhesion factor (Tomlinson,1971)
β	Average ultimate shaft resistance divided by average effective overburden pressure along a pile shaft (Burland,1973)
ψ	Ratio of Shaft load to applied pile head load

ABBREVIATIONS

Ax..	Axial
A.C.I.	American Concrete Institute
A.P.I.	American Petroleum Institute
A.S.C.E.	American Society of Civil Engineers
A.S.T.M.	American Society of Testing and Materials
BH	Bore hole
B.R.E.	Building Research Establishment
B.S.	British Standards
B.S.I.	British Standards Institution
C.G.J.	Canadian Geotechnical Journal
C.I.R.I.A.	Construction Industry Research Information Association
Conf.	Conference
C.P.T..	Cone Penetration Test
C.R.P.	Continuous Rate of Penetration
Dia.	Diameter, Diametral
Geot.	Geotechnical
H.Y.S.	High Yield Steel
I.C.E.	Institution of Civil Engineers
I.nt.	International
Jnl.	Journal
L.C.	Load Cycle
LL	Liquid Limit
LI	Liquidity Index
L.V.D.T.	Linear Vertical Displacement Transducer
M.L.	Maintained Load
nc	normally consolidated
oc	over-consolidated
OCR	Over-consolidation Ratio
P.D.R.	Peripheral Distributor Road
PL	Plastic Limit
PI	Plasticity Index
Proc.	Proceedings
S.G.C.C.	South Glamorgan County Council
S.M. & F.D.	Soil Mechanics and Foundations Division
S.M. & F.E.	Soil Mechanics and Foundation Engineering
S.P.T.	Standard Penetration Test
Symp.	Symposium
T.C.R.	Total Core Recovery
U.C.S.	Unconfined Compression Strength
U.o.G.	University of Glamorgan

LIST OF TABLES

LIST OF FIGURES

LIST OF PLATES

CHAPTER 1

INTRODUCTION AND OBJECTIVES

CHAPTER 1: INTRODUCTION AND OBJECTIVES

1.1 PREVIOUS RESEARCH WORK AT THE UNIVERSITY OF GLAMORGAN

This study is part of an on-going research programme on pile foundations at the University of Glamorgan (formerly The Polytechnic of Wales). Since its inception in the mid-1970's, the research work has produced a number of publications and theses. The following is a brief account of the work already undertaken by various research workers and successfully presented for Ph.D awards.

Perren(1978) carried out an investigation into the design, construction and performance of bored piles installed in glacial tills. Amongst his findings were that a satisfactory pile could successfully be formed in a granular material (e.g glacial tills) through the use of a temporary casing down to the underlying strata. This technique effectively sealed off the pile base, thereby preventing any further ingress of water from the till. Thus a "dry condition" was achieved, making it possible to form concrete piles.

Kay(1980) studied the behaviour of a tubular steel pile founded in a layered soil profile by using model laboratory test piles. He eliminated end-bearing by passing the pile base into a frictionless cylinder. He also used sand placed in layers around the pile, to model the overlying granular material. It was shown that there was a linear increase in shaft resistance at a shallow depth, becoming constant at greater depths.

Lake(1986) adopted a dynamic approach to pile installation. A pneumatic drop hammer system, incorporating a static axial core load cell and a dynamic load cell, was installed into the model test pile. Thus he was able to measure transient forces along the pile as well as the static load distribution. He found out that:

(a) The pile top impact force was dependent on the ram impact velocity only,

(b) Depending on the nature of the bearing surface, the transient force at the pile tip could equal, be greater or less than the impact force

(c) It was possible to predict the static bearing capacity using the dynamic equations of motion through a theoretical method, which he outlined. A good agreement was achieved between the experimental and theoretical results.

Wersching(1987) carried forward Kay's work by improving the accuracy with which the pile axial forces, shear and normal stresses at the pile-soil interface could be measured. He used various contact stress transducers at the sand/clay interface to monitor the development of effective vertical and radial shear stresses acting at the interface level. He also developed instrumentation to monitor soil vertical movements and density variations. His findings were that:

a) The local unit shaft resistance and radial effective stress remain practically constant along a pile shaft in sand and increase at a diminishing rate with pile embedded length,

b) At the maximum embedded pile length and ultimate load, the local coefficient of earth pressure acting on pile shaft at failure may greatly exceed the passive earth pressure coefficient near the pile top. Also it tends to a lower limit of 0.5 near the pile base,

c) The development of shaft resistance is directly related to the displacements within the sand and on the sand/clay interface, and

d) Vertical stresses within the sand around the pile shaft are reduced by the development of arching. The radial effective stress is the major principal stress at a location adjacent to the pile shaft.

Robinson(1989) examined the behaviour of single 60mm and 114mm segmented tubular steel model piles driven into loose sand and loose sand overlying clay. This was carried out under laboratory conditions using a 3.0m diameter by 3.0m deep concrete tank. He monitored the static and dynamic axial force distributions in the smaller pile. He also measured the variation in local shaft resistance, axial load and radial effective stresses along the 114mm pile. Vertical and radial displacements were monitored within the sand layer; and for the two layers, radial shear and vertical effective stresses were measured at a selected level. The following were established:

a) The radial soil displacements during pile installation are directly related to the pile diameter. Within the sand layer, the peak radial displacement may be predicted by the use of an empirical compaction factor to adjust and correct a theoretically obtained representation of soil movements

b) Adjacent to the pile shaft, the radial effective stress is the major principal stress

c) The development of shaft resistance is directly related to the displacements within the surrounding sand and on the sand/clay interface

d) The underlying clay layer affects the development of shaft resistance to different limits above and below the sand/clay interface

e) For shallow pile penetrations into the clay layer, the draw-down of sand and sand plug driven ahead of the pile significantly reduces the pore water pressure generated at the soil/pile interface

f) The development and radial distribution of pore water pressure within the clay may be accurately predicted by a logarithmic function.

Jones(1991) carried out a series of analyses of both shallow and deep foundations using soil-structure interaction techniques. This work involved theoretical modelling of raft and piled foundations using beam-column idealisations. No experimental testing was carried out but a number of theories were proposed to study the interaction of uniformly loaded piles. Consistent matrices were also presented to idealise the uniform distribution of soil stiffness along both axially and laterally loaded pile elements.

1.2 CURRENT RESEARCH WORK

1.2.1 Introduction

The previous research work outlined above have addressed different objectives and involved extensive laboratory testing of model piles and soils. In each case useful information regarding particular aspects of pile behaviour in different soil conditions was uniquely achieved. The present research work has utilised an opportunity to analyse data from full scale instrumented test piles load tested in an environment of real and intense civil engineering activity. The load tests were undertaken as part of the design of the Butetown Road Link in Cardiff, U.K. The Butetown Road Link is the penultimate section of the Cardiff Peripheral Distributor Road (P.D.R.).

1.2.2 Peripheral Distributor Road, Cardiff

The P.D.R, approved in principle by South Glamorgan County Council (SGCC) in 1973, has the objective of improving access from the M4 in the west and east to the Cardiff area and the Vale of Glamorgan. The construction of the road was programmed in a number of stages:

(a) The Eastmoors Viaduct, opened in 1984

(b) The Grangetown Viaduct, opened in 1988

(c) The Cogan Viaduct opened, in 1988.

The 2.7 km long Butetown Road Link, which forms the penultimate section of the P.D.R, was completed and opened in 1995. The final phase of the P.D.R will be the Eastern Bay Link. The Butetown Link, although the shortest section scheme of the P.D.R, has been the most challenging and expensive costing £135m. With the route passing through deep Keuper marl cuttings, over river courses filled with refuse and through the Cardiff docklands, each P.D.R scheme has presented major challenges and problems to be overcome.

The P.D.R consists of several long span structures constructed to provide crossings over rivers, railways, existing roads and weak ground. Among the available alternatives, large diameter, bored, cast in-situ bored piles provided the most appropriate solution. These piles were installed in the Keuper marl (Mercia mudstone) of the Triassic period, which occurs extensively in Vale of Glamorgan. It is a sedimentary deposit consisting of red-brown silty mudstones, sometimes with bands of sandstone and siltstone. Within the

Cardiff region, these strata are notorious for having variable engineering properties both in lateral extent and with depth.

The design of the Butetown Road Link commenced in the mid-1980's. During the design of the above structures, engineers from Cardiff County Council-C.C.C. (formerly South Glamorgan County Council) utilised the technique of "voided toe" piles to verify the design parameters for bored piles in Keuper marl. The data generated from this technique, although valuable, proved to be of limited use as far as the assessment of soil/pile interaction is concerned within such highly variable strata. To gain a fuller understanding of this subject C.C.C. considered placing instrumentation within the test piles for the Butetown Road Link project.

The School of the Built Environment (formerly the Department of Civil Engineering and Building), University of Glamorgan, was invited to participate in the selection of instruments and monitoring systems suitable for the pile testing programme. In addition, the school had developed and maintained strong links with the Building Research Establishment (B.R.E.), Hertfordshire, particularly on pile load testing. As a consequence the BRE (Structures and Geotechnics Group) installed and monitored all the instruments used in the pile load tests.

A 2,000 tonne pile load-testing rig was developed by C.C.C. in conjunction with Davies Middleton and Davies (DMD) Cardiff Ltd. This equipment was used in the load testing of six full-scale instrumented piles within the project area. The piles were 0.9m in diameter with lengths varying from 26-32m. The instrumentation comprised vibrating wire strain gauges, rod extensometers, load-cells and displacement transducers. One of the test piles was constructed with a "voided toe" in order to measure shaft resistance only. The load tests generated significant data in terms of strain levels at different cross-sections along the pile shafts.

1.2.3 Objectives of the current research

The purpose of this research was to utilise the extensive information and data produced from the site investigation and the six instrumented pile loading tests for the Butetown Road Link to achieve five prime objectives, namely to:

1. Verify, or otherwise, the design of the working piles for the Butetown Road Link
2. Develop an information base which will aid future pile designs in Keuper marl
3. Move forward from the traditional concept of "voided toe" pile testing by using the data to separate end-bearing from shaft resistance
4. Develop and validate a theoretical model which can predict the behaviour of large diameter, bored, cast in-situ piles in Keuper marl in terms of (a) the development of shaft resistance and end bearing (b) the load transfer and pile shortening (c) the load-settlement variation up to the point of pile failure
5. Test the theoretical model for its suitability and application for other soil/pile types and loading conditions.

CHAPTER 2

LITERATURE REVIEW

CHAPTER 2:LITERATURE REVIEW

2.1 INTRODUCTION

This chapter examines the fundamental principles and key factors defining the performance of large diameter, bored, cast-in situ piles formed in Keuper marl. The research is concerned with straight-shafted vertically loaded piles. An extensive search of the available information indicates that little knowledge is available regarding pile behaviour in Keuper marl. Much of the existing information, gleaned from literature, is based on piles formed in London clay, chalk and glacial tills. A number of case studies are discussed whereby a variety of theoretical models and numerical techniques are applied to establish the load capacity of piles formed in Keuper marl and weathered mudstones.

2.2 ENGINEERING PROPERTIES OF KEUPER MARL

2.2.1 Nature of Keuper marl

The process of designing piled foundations to transmit large amounts of load to any soil requires adequate knowledge of the engineering properties of the soil. Keuper marl (Mercia mudstone) is an ancient sedimentary deposit of the Triassic age. The term "Keuper" originated in Germany but has been informally used in Great Britain since 1835 to refer to the lower arenaceous and upper argillaceous Triassic. In the South-western part of Britain, "Keuper" deposits are the red mudstone sequences that make up the lower division of the Mercia mudstone Group. Keuper marl accumulated in a series of red-brown silty mudstones, which are often interspersed with sandstone bands containing frequent siltstones (or skerry). However, these siltstones and sandstones (which are usually grey-green in colour) may not be present in some Keuper marl deposits. White to pink gypsum may also occur, either dispersed throughout, or as discrete nodules and bands.

Mudstones of limited weathering contain a large proportion of silt-sized particles whereas the more weathered mudstones have predominantly clay-sized fractions. Minor quantities of unweathered material are sometimes present even in the fully weathered marl. The unweathered fragments (or "litherolicts") are recognisable by their structure and fabric which are features of the parent rock, Brewer(1964). According to evidence presented by Dumbleton(1967), the clay sized particles originally exist as aggregates during the early stages of weathering. The aggregates constitute much of the silt-sized materials which are predominant in the hitherto less weathered marl.

Besides employing the methods of site investigation recommended in BS 5930(1981), it is usual practice to further identify Keuper marl using the weathering zone classification system proposed by Davis and Chandler(1973) as shown in Table 2.1.

2.2.2 Typical index and strength properties of Keuper marl

The plasticity and shear strength properties of the various zones of Keuper marl present in the Midlands area have been reported by Davis and Chandler and are given in Table 2.2, along with various properties established from the site investigation associated with this research. It is seen that zones I-III strata exhibit similar plasticity and grading properties whereas zone IV marls are considerably more plastic in nature.

Weathering zone		Descriptions
Fully weathered	IVb	• Matrix only. • Can be confused with solifluction or drift deposits, but contains no pebbles. • Plastic slightly silty clay. • May be fissured.
Partially weathered	IVa	• Matrix with occasional clay-stone pellets less than 3mm diameter but more usually coarse sand size. • Little or no trace of original (zone I) structure, though clay may be fissured. • Lower permeability than underlying layers.
	III	• Matrix with frequent litherolicts, up to 25mm in diameter. • Litherolicts become less angular as weathering progresses. • Water content of matrix greater than that of lithorelicts.
	II	• Angular blocks of unweathered marl with virtually no matrix. • Spheroidal weathering. Matrix starting to encroach along joints. • First indications of chemical weathering.
Unweathered	I	• Mudstone (often fissured). • Water content varies due to depositional variations.

Table 2.1: Weathering zones of Keuper marl, after Davis and Chandler(1973)

The bulk density, effective angle of friction and cohesion decrease with prolonged weathering. However, zones III and IV marls may exhibit nearly equal values of effective cohesion. It has been noted that fine graded material in zones I and II may sometimes be non-plastic.

	Davis and Chandler(1973)			Present work			
Weathering zones	I and II	III	IV	I	II	III	IV
Bulk density (Mg/m^3)	2.480-2.245	2.32-2.08	2.16-1.84				
Liquid Limit (%)	25-35*	25-40	35-60				
Plastic Limit (%)	17-25*	17-25	17-33				
Plasticity Index	10-15*	10-18	17-35				
c_u (kN/m^2)				558#	502#	80.5[$] 340#	65.8[$] 211#
c' (kN/m^2)†	>27.5	≤17.2	≤17.2				27.2
ϕ'†	>40°	40°-32°	32°-25°				33°
ϕ_r'	32°-23°	29°-22°	24°-18°				
S.P.T. "N" values	>60‡ (zone I) >40‡ (zone II)	20-50‡	<30‡	-	275 157‡ 150♣	123 86‡ 80-140♣	81 57‡ 40-100♣
Modulus of volume change m_v (m^2/MN)	0.004-0.032 (zone I) 0.01-0.1 (zone II)	0.04-0.4	0.06-0.4				
Deformation modulus E (MN/m^2)	26-250 (zone I) 9-70 (zone II)	2-48	2-13		30	13-70	38

*Legend * May be non-plastic, † Unfissured marl, ‡ Corrected for overburden pressure by Gibbs and Holtz(1957) method, #Point load test results, $ Triaxial undrained test results (for $\phi_u=0$), ♣Values by Kilbourn et.al(1988) for Keuper marl in Cardiff. Underlined results are based on limited number of tests, typically less than 10.*

Table 2.2: Engineering properties of Keuper marl- A comparison between Davis and Chandler's (1973) data and the results obtained from the present work (P.D.R. project area in Cardiff)

The standard penetration "N" values and the deformation modulus values for various weathering zones of Keuper marl in Cardiff are significantly greater than those reported by Davis and Chandler(1973). The effective cohesion and effective angle of friction of

Zone IV Keuper marl in Cardiff are also greater than those given by Davis and Chandler(1973).

2.3 PILE LOAD TEST METHODS

2.3.1 Introduction

Fundamental design parameters such as bearing capacity and expected settlement of a piled foundation under working load are best assessed by load testing. Once a piled foundation has been constructed, neither can it be readily inspected in order to ascertain compliance with design requirements nor can variations in the bearing strata be detected. Therefore, it is essential to carry out load testing, in addition to comprehensive site investigation. Pile load testing is usually an expensive undertaking and a careful cost comparison should be made between risk reduction and assurance of satisfactory behaviour provided by pile testing. The most common type of test is a compression test but piles may also be tested to assess resistance to uplift, lateral loads and torsion.

Pre-contract piles are usually installed and tested to prove the suitability of the proposed piling system and to verify the design parameters inferred from the site investigation. Contract piles may be subjected to integrity testing to check the construction technique, workmanship and performance as foundation elements. The scale of the pile test programme and the extent of instrumentation depend on the availability of piling experience in the prevailing ground conditions and the capital cost of the works. The objectives of pile load testing for foundation design and construction are:

1) To provide assurance that failure of the pile does not occur before the design load is reached.

2) To determine the ultimate bearing capacity for comparison with the theoretically predicted value, or to back-analyse soil data for use in the design of other piles.
3) To determine the foundation settlement at working load. This data may then be used to predict the settlement of other single piles and of pile groups.
4) To assess the structural soundness of a typical pile.

2.3.2 Methods of conducting pile load tests

2.3.2.1 Introduction

There are three methods for carrying out compression load tests on piles, namely:

a) Maintained load (M.L.) tests.
b) Constant-rate-of- penetration (C.R.P.) tests.
c) Method of equilibrium (M.E.) tests.

2.3.2.2. Maintained load test

Where load-settlement relationship for a test pile is required, it is usual to use the maintained load (M.L.) test procedure. In this method, load is applied in stages, the load at each stage being maintained at a constant level until the resulting settlement of the pile head virtually ceases, before applying the next increment. The loading increments to be applied and the time periods over which these loads are to be held constant are carefully specified prior to the start of the test. A limit is also placed on the rate of pile head settlement to be achieved before the next load increment is applied. It is also a frequent requirement to hold the load constant for 24 hours at the calculated design load of the pile. The maintained load test procedure is sometimes modified, by removing the load so that the pile is allowed to undergo some recovery, before proceeding to the next increment.

The ICE *Specification for Piling* states a limit of 0.25mm/h, provided that the settlement is decreasing. Fleming et.al(1992) points out that in granular soils or soft rocks, the cessation of movement is not as difficult to establish as in clay soils This is because consolidation settlement occurs over an extended period. Since settlement is a function of the pile/soil system, relatively short intervals between load increments may be acceptable, especially at load levels not approaching failure and a limiting settlement criterion is maintained.

The ultimate or failure load condition can be interpreted in several different ways. Based on ultimate failure in shear of the supporting soil, pile failure is regarded as the condition whereby the pile plunges down into the ground without any further increase in applied load. However, the pile may be deemed to have failed when its settlement reaches a stage where unacceptable distortion and cracking is caused to the superstructure. In order to determine the pile load capacity from the results of M.L. tests, Whitaker(1970) suggested that it is helpful to define a certain physical event by which the failure state of the pile may be recognised. Among the commonly used definitions of ultimate load are:

1) The load that produces a settlement equal to 10% of the pile diameter (Terzhaghi, 1942).
2) The load at which the rate of settlement continues to increase without additional loading, unless this rate is so low as to indicate that the settlement is due to consolidation of the soil (British Standards BS8004,1986) .

The M.L. test method enables the prediction of the expected settlement under the working load of the pile. Such a settlement obviously relates more closely to a maintained load rather than to a constant rate of soil strain. However, some difficulties are usually encountered in interpreting M.L. test results, depending on the ground conditions, namely

a) If, at a particular stage, the loading is terminated before settlement has ceased, the actual settlement corresponding to that particular load increment is not obtained.

b) If the periods over which applied loads are held vary from one stage to another, the resulting load-settlement curve is often irregular.

c) For piles formed in cohesive soils, it is usually difficult to identify the failure point based on the definition that failure occurs when the settlement continues undiminished without further load increments.

2.3.2.3. Constant rate of penetration test

The C.R.P. test method was developed by Whitaker(1957) for testing model piles and was subsequently used in full-scale pile load tests (Whitaker,1963 and Whitaker and Cooke,1961). The main purpose of this test is to determine the ultimate bearing capacity of the pile. In the C.R.P. test method, the pile is made to penetrate the soil at a constant speed from its original position by applying the necessary load at the head and continuously measuring the penetration produced. Whitaker(1976) states that a penetration rate of 0.75mm/min is suitable for friction piles formed in clay where the penetration at failure is likely not to exceed 25mm.

If the C.R.P. test is carried out at the same speed as an undrained shear test of a sample of the soil, there is a reasonable basis on which the two tests can be compared. It is therefore argued that the conditions under which the supporting soil is stressed approach a constant rate of strain. Hence the ultimate bearing capacity of the pile is reached when the soil is made to fail in shear. The C.R.P. test can be performed rapidly and is therefore suitable as for use in field pile testing. The main disadvantage of the C.R.P. test is that force-penetration curve obtained does not represent an equilibrium load-settlement relationship for the pile, hence it is difficult to determine the expected settlement under the working load of the pile.

2.3.2.4 Method of equilibrium

The method of equilibrium (M.E.) was proposed by Mohan et.al.(1967). It is a slight modification of the maintained load test procedure in order to reduce the time required for the pile to attain an equilibrium settlement rate. At each stage, a slightly greater load than the prescribed load is applied to the test pile and the jack pressure is allowed to relax until the load decreases to the desired value (rather than being maintained). Using this technique, the rate of settlement decreases much more rapidly than in the M.L. test procedure. Equilibrium is reached in a matter of minutes as compared to hours in the maintained load test and the total time required for the test is reduced by up to 65%. This method is mainly intended to determine the ultimate load capacity of a pile but may also be used to provide settlement data.

Mohan et.al.(1967) observed that the ultimate capacity and load-settlement behaviour of a pile determined using M.E. and M.L. test methods were generally in good agreement. The M.E. test procedure is particularly useful in testing preliminary piles to relatively high load levels whereby difficulty is experienced in maintaining or decreasing the applied load.

2.4 EVALUATION OF PILE LOAD CAPACITY IN COHESIVE SOILS

2.4.1 General

The load resistance of a pile is shared, in varying proportions, between its shaft and base. A pile penetrating a relatively soft layer of soil to found on a stiffer stratum derives most of its load capacity from base resistance. Where a particularly stiff soil stratum is not present, most of the applied load on a pile is carried in shaft resistance. In cohesive soil, the shaft resistance is generally paramount, whereas in granular soil (or for an under-reamed pile base in clay), the load capacity is more evenly divided between the shaft and base. Fleming et.al(1992) gives typical ratios of end-bearing pressure to shaft resistance for piles formed in sand as 50-100 as compared to 10-20 for piles formed in clay. This statistics underscores the importance of shaft resistance for piles formed in clay which is relatively more significant than for piles formed in sand.

Most pile design problems involve consideration of bearing capacity under downward loading. In special circumstances, lateral loading, uplift loading and torsion are also taken into account. There is limited data on the shaft resistance of piles subjected to uplift loading. Data presented by Sowa(1970) and Downs and Chieurzzi(1966) indicated considerable variations in shaft resistance between withdrawal and compression loading. The data revealed a tendency for the shaft resistance for upward loading to be lower than those for compression loading. Based on these data it was suggested that the shaft resistance values for upward loading were approximately 0.67 times those for compression loading. However, Ireland(1957) examined load test data from piles driven into fine sand and found that there was no difference between the average shaft resistance for upward loading and downward loading.

Conventional design methods for piles formed in weathered mudstone make use of the principles of bearing capacity for piles formed in cohesive soils. Dauncey and Woodland(1984) have explained that it is appropriate to apply the bearing capacity formulae for cohesive soils in the design of bored piles formed in Keuper marl. The results of loading tests on driven piles formed in the Keuper marls of the Severn estuary (Leach and Mellard,1980) support Dauncey and Woodland's(1984) approach to pile design in Keuper marl. There are three basic methods for the calculation of pile load capacity in clay, the first two of which make use of the principles of soil mechanics, whereas the third is based on empiricism and site experience:

(a) Total Stress method.

(b) Effective Stress method.

(c) Empirical correlation.

The above procedures are examined in more detail in the following sections.

2.4.2 Total stress method - Design for end resistance

2.4.2.1 Piles formed in soft to hard clays

The design of piles formed in clay has been based on a conventional total stress method of estimating the ultimate load carrying capacity both in shaft and end resistance. Burland(1973) has pointed out that the use of undrained strength in estimating base resistance may be justified for the following reasons:

1) Failure usually occurs through the soil at a distance beneath the base where disturbance during pile installation normally does not affect the clay involved in the shearing process.

2) In the long term, the soil beneath the base will normally experience an increase in effective stress and consequently an increase in strength. Thus the undrained bearing capacity represents a safe lower limit.

The method makes use of the undrained strength of the clay c_u below the foundation base and along the pile shaft. The ultimate bearing capacity of the pile base P_{ub} is given by,

$$P_{ub}=A_b.N_c.c_u \qquad (2.1a)$$

where A_b is the area of pile base and N_c is a bearing capacity factor, which is usually taken as 9 (Skempton,1951). For D/B<4 (where D= depth and B= Base diameter), BS8004:1986 recommends N_c=6. Fleming *et.al.*(1992) suggested that a linear interpolation should be made between a value of N_c=6 for the case of a pile tip just reaching a stiff bearing stratum, and N_c=9 where the pile tip penetrates the stratum by 3 diameters or more. Robinson(1989) analysed the behaviour of driven piles formed in sand overlying clay and established that N_c=7.5 for the case of a pile tip just reaching the sand/clay interface. This value was back-analysed for 60mm and 114mm diameter model tubular steel piles driven into clay overlain by sand. There was an increase in the value of N_c with increasing embedded length into the clay. The N_c value closely approached the conventional value of 9 when the pile tip had been embedded approximately 700mm into the clay.

2.4.2.2 Piles formed in weathered rock

Partially weathered and unweathered Keuper marl may be regarded as weak rock, for which the general end-bearing capacity formulae for piles founded on rock are appropriate. Bored piles formed by drilling to some depth into weak or weathered rock act in both shaft resistance and end bearing. The development of skin resistance along the embedded length is more complex than in the case of friction piles installed in soft or stiff soil. The factors which influence the skin resistance of rock socket piles have been described by Wyllie(1991). These include (a) the length to diameter ratio of the socket, (b) the strength and stiffness of the rock (c) the roughness of the socket face and extent of disturbance at the base (d) settlement of the pile in relation to the elastic limit of the socket strength.

The ultimate end bearing resistance of bored, cast in-place piles formed in weak rocks is influenced by the drilling techniques employed. Any soft sludge accumulating at the bottom of the drill hole can significantly affect the results hence not revealing the true character of the rock. The ultimate base resistance of bored, cast in-situ piles formed in rock is determined based on the unconfined compression strength and angle of shearing resistance of the rock. Tomlinson(1994) gives the following formula for ultimate base resistance, for driven as well as bored piles.

$$q_{ub} = 2N_{\phi} q_{UCS} \tag{2.1b}$$

Where q_{UCS} is the unconfined compression strength of the intact rock and N_{ϕ} is a bearing capacity factor given by $N_{\phi} = \tan^2\left(45^{\circ} + \frac{\phi}{2}\right)$. For piles formed in marl, Wyllie(1991) reported values of angle of shearing resistance ϕ=20°-27°, which may be used as guidelines since these values can vary widely from one site to another.

Kulhawy and Goodman(1980) have suggested that the ultimate end-bearing capacity for piles bearing on jointed rock may be represented by a wedge failure condition beneath the pile base. Hence the ultimate base pressure q_{ub} is given by

$$q_{ub} = cN_c + \frac{\gamma B N_{\gamma}}{2} + \gamma D N_q \tag{2.1c}$$

Where

c= cohesion

B= width of pile base

D= depth of base below rock surface

γ= effective unit weight of rock mass

N_c, N_γ and N_q = bearing capacity factors evaluated for a wedge failure condition, as functions of ϕ, based on curves presented by Pells and Turner(1980). For a circular pile cross-section, a factor of 1.2 is applied to the term cN_c and 0.7 to the term $\frac{\gamma B N_\gamma}{2}$. The latter quantity is usually small in comparison to the former and may be neglected.

Kulhawy and Goodman(1980) point out that *c* and ϕ values are difficult and expensive to obtain from laboratory tests on large samples of jointed rock. To help overcome this difficulty, Kulhawy and Goodman(1987) have suggested the following approximate relationships between c and ϕ values and Rock Quality Designation (RQD) values (where RQD is the sum of lengths of intact pieces of core greater than 100mm in length divided by length of core advance, expressed as a percentage of the latter).

RQD	c	ϕ
0%-70%	$0.1q_{UCS}$	30°
70%-100%	$0.1q_{UCS}$	30°-60°

2.4.3 Total stress method- Design for shaft resistance

2.4.3.1 Introduction

Traditionally, the calculation of shaft resistance for bored piles formed in cohesive soils has been based on the undrained shear strength parameters of soil. Currently, both the total and effective stress methods are widely used, either singly or in combination. The choice of a particular method is dictated by the available database of successful application in a given locality. There are two methods available for the prediction of the ultimate shaft resistance of a pile in clay based on the total stress approach:

a) α method originally devised by Tomlinson(1957) and

b) λ method suggested by Vijayvergiya and Focht(1972)

An average value of shaft resistance can be evaluated for the entire pile length, however a better prediction is to sum the shaft resistance contributions from each stratum penetrated, using the best estimates of the properties of that stratum.

2.4.3.2 The α method

Historically, the α method has been the most widely used procedure for calculating the shaft resistance of both driven and bored piles formed in cohesive soils. The average shaft resistance c_a along the pile shaft is taken to be related to the mean undrained shear strength $\bar{c}_u$ along the pile shaft and is given by,

$$c_a = \alpha \bar{c}_u \qquad (2.2a)$$

Where α is an empirical factor, which is now commonly known as the adhesion coefficient (Tomlinson,1957). The general form of this equation, for layered soil conditions, was given by Tomlinson (1971) and includes both the adhesion and friction components, thus

$$c_a = \alpha \bar{c}_u + \bar{q} K \tan\delta \qquad (2.2b)$$

Where,

$\bar{q}$ = average effective vertical stress along the pile shaft

K= coefficient of lateral earth pressure

δ= effective angle of internal friction of the soil, or the friction angle of the pile-soil interface, as appropriate

(a) Limiting values of c_a : It is interesting to speculate as to how the value of c_a should vary with depth, given the form Eqn.2.2(b) takes. Early studies by Vesic(1964) and Kerisel(1964) indicated that, for cohesionless soil, there is a certain depth (known as the critical depth), below which the unit shaft and base resistances are quasi-constant. This concept was later supported by load tests on full-scale piles reported by Vesic(1970,1977) and Meyerhof(1976). See section 2.4.6 on "Critical Depth".

(b) Values of the adhesion factor, α : Poulos(1980) stated that the value of α depends on a number of factors, such as (i) the shear strength of the clay (ii) the method of pile installation (iii) the effective overburden stress and (iv) the pile type. Early studies by Skempton(1959) showed that the adhesion factor α ranges from 0.3 to 0.6 for piles formed in London clay, for a variety of load tests. For a normal pile shaft condition (where concrete is placed rapidly after drilling), a value of 0.45 was established for London clay. A lower value of 0.3 was taken for short piles where a large proportion of the shaft passed through heavily fissured clay. The American Petroleum Institute (API,1984) also recommends the use of α values which vary with c_u values. In addition, it stipulates a maximum shaft resistance value, based on the state of consolidation of the clay.

For driven piles formed in clay, McClelland(1974) has presented a collection of several plots of adhesion factor, α versus undrained cohesion, c_u as reported by various authors. These curves show that the adhesion factor decreases with increasing strength of clay, both for bored as well as driven piles. In all cases, there is a wide scatter in the observed variation of adhesion factor with undrained strength. Some of the α values corresponding to particular c_u values indicated by the curves are:

	c_u=50 kN/m^2	c_u=150 kN/m^2
Peck(1958)	0.90	0.45
Woodward and Boitano(1961)	0.86	0.32
Kerisel(1961)	0.72	0.35
Tomlinson(1970)	0.72	0.24

Randolph and Murphy(1985) have deduced α values from load tests on driven piles based on the average in-situ strength ratio. Based on a linear regression analysis of these data it was established that

$$\alpha=\frac{0.5}{\left(\frac{c_u}{\bar{q}}\right)^{0.5}}\text{, when }\frac{c_u}{\bar{q}}\leq 1\text{ and} \tag{2.2c}$$

$$\alpha=\frac{0.5}{\left(\frac{c_u}{\bar{q}}\right)^{0.25}}\text{, for }\frac{c_u}{\bar{q}}>1, \tag{2.2d}$$

Where $\bar{q}$ is the average effective overburden stress.

These observations seem to agree well with the findings of Sladen(1992) who gives the following relationship for the evaluation of α ,

$$\alpha = C_1\left(\frac{\bar{q}}{c_u}\right)^{0.45}, \tag{2.2e}$$

in which C_1 is an empirical constant, and $\bar{q}$ and c_u are as previously defined. For bored piles, C_1 lies in the range 0.4-0.5 whereas for driven piles C_1>0.5. Information becomes more scant for α values for bored piles in comparison to driven piles. Weltman and Healy(1978) have analysed a number of pile tests and produced plots of adhesion factor α versus undrained strength for bored and driven piles formed in glacial till. These curves show that α varies from approximately 0.9 to 0.375 as the undrained cohesion increases from 80 kN/m^2 to 200 kN/m^2. For similar pile-soil conditions, the test data indicated that α values for bored were approximately 80% of those for driven piles.

Kulhawy and Phoon(1993) proposed the following correlation for α based on 127 case studies of bored piles load tested to failure in clay at 46 sites.

$$\alpha = 0.5\left(\frac{p_a}{c_u}\right)^{0.5} \tag{2.2f}$$

where p_a is atmospheric pressure (approximated for simplicity to 100kN/m^2 rather than 101.4kN/m^2). Based on the load test data, this relationship was judged to be in close agreement with other relationships for driven piles.

(c) Values of α for piles under uplift loading: The shaft resistance of straight-shafted piles under static uplift loading is usually estimated using the same procedures as in piles under downward loading. The shaft resistance of piles under uplift loading is influenced by both the rate of loading and the extent of remoulding of the soil immediately around the pile shaft. Tomlinson(1994) suggested that, in the short term, the uplift resistance of a bored pile in clay is likely to be equal to its shaft resistance in downward loading. St John et.al.(1983) showed that the first pull on a previously unloaded pile in clay would give an uplift resistance equal to the ultimate shaft resistance under compression loading. However, under cyclic loading or creep caused by sustained loading, the uplift shaft resistance could decrease from the peak to the residual value, especially for long piles.

As noted by Poulos(1980), test data for piles loaded in uplift are still rather limited to definitively support the use of the same values of adhesion factors as for downward loading. However, test pile data reported by Sowa(1970) indicated no significant difference in α values for piles subjected to upward or downward loading.

(d) Determination of c_u for shaft resistance prediction: The undrained strength may be determined using the standard shear strength testing methods for soils and rocks or by empirical correlation with in-situ measurements. For bored piles formed in stiff over-consolidated clay, design procedures have been largely developed on c_u determinations on undrained triaxial tests performed on 38mm diameter specimens. Of late, it has become common practice to test 100mm diameter samples rather than 38mm samples. Patel(1992) has analysed a series of pile loading tests in London clay for which shear strength measurements were carried out using 100mm diameter triaxial samples, rather than the standard 38mm samples. The results indicate that with the use of 100mm diameter samples, a better correlation between the observed shaft resistance and undrained strength is obtained. In addition, it was found that an adhesion factor of 0.6, rather than the conventional value of 0.45, is appropriate when shear strength measurement is based on 100mm diameter triaxial test samples.

For over-consolidated clays, various relationships have been suggested for calculating c_u directly based on the overburden pressure. Azzouz and Lutz(1986) have suggested the relationship $c_u = \sigma'_v s(OCR)^m$ in which

σ'_v =	effective overburden pressure
OCR=	over-consolidation ratio (defined as the ratio of the past effective pressure to the present overburden pressure)
s, m=	empirical constants

(e) Rock-socket piles: Rowe and Armitage(1987) and Horvath and Kenney(1979) have suggested the following relationship between the ultimate shaft resistance f_S and the unconfined compression strength q_{UCS} of the rock,

$$f_s = \chi(q_{UCS})^{0.5} \text{ in MN/m}^2 \tag{2.2g}$$

where χ is a coefficient. Based on full-scale loading tests using variable pile diameters and rock strengths, Rowe and Armitage(1987) found that χ values lie in the range 0.45-0.6, the units being $[MN/m^2]^{0.5}$.However, different results were obtained by Horvath and Kenney(1979), who inferred values of χ as 0.2-0.25. Carrubba(1997) has suggested an analytical model, based on two-constant hyperbolic load transfer functions which may be used to evaluate the limiting skin resistance at the pile-rock interface. Such functions were initially adopted in pile analysis by Kondner(1963) and later used by Chin(1970), Hirayama(1990) and Fleming(1992), The results of numerical simulation showed that friction along the socketed length generally developed earlier than base resistance. Carrubba(1997) presented test results from five large diameter drilled piles socketed into different types of rock (including marl). The results revealed χ values lying in the range 0.13-0.25, which are close to Horvath and Kenney's(1979) lower limit.

Seidel and Haberfield(1995) have developed a computer program by the name ROCKET which encompasses the various analytical methods to provide a rational basis for the prediction of rock socket behaviour in geomaterials varying from hard soils to strong rock. Limited parametric studies are presented in this reference to demonstrate that the predictions of the program are in general agreement with international databases on pile socket load testing. The program predicts a transition from hard soils to rocks using the method postulated by Kulhawy and Phoon(1993) and takes into account the effects of (a) rock socket roughness (b) pile diameter (c) rock mass modulus (d) Intact strength parameters.

2.4.3.3 The λ method

The λ method has not found as much popularity as the α method. In this method, the ultimate skin resistance f_s is given by Vijayvergiya and Focht(1972) as

$$f_s = \lambda(\bar{q} + 2c_u) \tag{2.2h}$$

where $\bar{q}$ is the average effective vertical stress along the pile shaft and λ is a coefficient (typically 0.10-0.50), the value of which increases with pile penetration. This coefficient is applicable for the entire pile shaft. This relationship was developed on the basis of regression curve fitting for a large number of load tests on long pile installed for offshore oil production structures in the Gulf of Mexico. The format in which the correlation is expressed is such the method includes both adhesion and friction components of shaft resistance.

According to studies by Kraft(1981), the λ method over-predicts the shaft capacity for piles longer than 15m, in both normally and over-consolidated clays. Values of λ in the range 0.2-0.4 are applicable for such pile lengths.

There are two limitations in the λ method, namely: (a) It uses a single value of λ for the pile, rather than different values for various soil strata and (b) It is not consistent with the widely accepted concept that shaft resistance tends to reach a limiting value, so that $\bar{q}$ does not infinitely increase pile capacity.

2.4.4 Limitations of the total stress method

The total stress approach has proved very useful in pile design, but its empirical nature implies that it is far less reliable when extrapolated to circumstances for which there is no precedent. There is still a lot of uncertainty as to the exact condition of a pile shaft after construction and during sustained loading. Burland(1973) suggests that the use of undrained strength in calculating shaft resistance has little justification because:

1) "Only a relatively thin zone of clay around the pile shaft is involved in the shearing process (Cooke and Price,1973). Thus drainage to and from this narrow zone takes place rapidly during loading or has already occurred in the delay between pile construction and loading.
2) Pile installation, whether driven or cast in-situ, inevitably must disturb and remould the ground adjacent to the pile shaft. Therefore excess pore pressures (either positive or negative) will be set up in the soil around the pile.
3) Quite apart from the disturbance caused by pile installation, there is no simple relationship between the undrained strength and drained shear strength of the clay".

Indrasurya et.al.(1988) measured ultimate shaft resistance of model piles formed in clay using a special apparatus whereby the boundary stresses of the clay could be independently controlled in the vertical and horizontal directions. The undrained cohesion of the clay was measured both by the laboratory miniature vane shear test and the unconfined compression test. The results showed that there was no correlation between the deduced angle of pile-soil friction and the undrained cohesion values. This observation supports Burland's(1973) conclusion that there is no simple relationship between the undrained and drained strength of a clay.

Chandler(1968) has suggested that when the rate of pile loading is sufficiently slow to ensure drained conditions in the clay, the shaft resistance is controlled by the lateral effective stresses in the ground. Drained conditions are expected to exist in maintained load tests and particularly in long term in-service foundation conditions.

2.4.5 Effective Stress approach

Vesic(1967) and Chandler(1966,1968) have suggested that for piles formed in stiff, over-consolidated clay, the drained load capacity, rather than undrained, may be the critical value. They recommended the use of effective-stress approach in such conditions. Chandler(1968) proposed that the drained strength ,τ of the clay around a pile shaft may be expressed as

$$\tau = c' + \sigma_{h'} \tan\phi' \qquad (2.3)$$

where c'= effective cohesion

σ_h'= horizontal effective stress acting on the pile, and

ϕ'= effective angle of friction of the clay.

Poulos(1980) suggests that for a pile installed in sand, the vertical stress near the shaft may be less than the overburden, whereas for a pile in clay, the vertical stress near the shaft is reasonably close to the overburden. Assuming that the effective horizontal stress is proportional to the effective overburden pressure, the ultimate shaft resistance per unit area f_S, may be expressed from Eqn 2.3 as

$$f_s = c' + K\,\overline{\sigma_v'} \tan\phi' \qquad (2.4)$$

where K= coefficient of effective earth pressure, and

$\overline{\sigma'_v}$ = mean value of effective overburden stress along pile shaft.

As a consequence of remoulding during pile installation, the soil has no effective cohesion and c' may be neglected. Therefore the average ultimate shaft resistance along the pile shaft $\overline{\tau_s}$ will be given by

$$\overline{\tau_s} = \beta . \overline{\sigma'_v} \tag{2.5}$$

where,

$$\overline{\beta} = \overline{K_o} \tan\phi' \tag{2.6}$$

Thus β is similar to the empirical adhesion factor α in the total stress method except that it relates ultimate shaft resistance to fundamental effective stress parameters. Burland(1973) suggests that for bored piles, provided the pile is formed promptly after excavation of the shaft, there is little change in the in-situ effective stress state of the soil hence the use of K_o is appropriate. In heavily over-consolidated clay, where the value of K_o is large, it appears reasonable to make some allowances for stress relaxation by reducing the value of K_o. Alpan(1967) presented a formula relating K_o for an over-consolidated clay $K_{o,oc}$ to that for a normally consolidated clay $K_{o,nc}$ of the form $K_{o,oc} = K_{o,nc} OCR^n$ in which n is an empirical constant. Other empirical relationships for estimating these parameters are given by Mayne(1984) and Semple and Rigden(1984), based on a number of clay soils studied, typically:

$$K_{o,oc} = \left(A + \frac{c_u}{\sigma'_{vo}} \right) \tag{2.7}$$

where the constant A lies in the range 0.7-1.0, depending on the laboratory test used to obtain the ratio of undrained strength to effective current overburden pressure $\left(\frac{c_u}{\sigma'_{vo}} \right)$.

The effective friction angle appropriate for a particular situation is thought to depend on a number of factors. Burland and Twine(1988) suggested that a residual angle of friction is appropriate, at least for bored piles formed in heavily over-consolidated clay. This is based on the argument that the friction angle mobilised on the vertical failure surface at ultimate shear stress depends on the complete state of stress.

Indrasurya et.al.(1988) have measured the load transfer along the shaft of a model pile inserted in a specimen of clay soil. They used special apparatus whereby the boundary stresses of the clay specimen could be independently controlled in the vertical and horizontal directions. The top and lateral surfaces of the clay specimen were free to deform freely. They established that the angle of pile-clay friction is independent of the vertical consolidation pressure in the clay, the over-consolidation ratio (both in the vertical and horizontal directions) and the length of the pile-soil contact.

Flaate and Selnes(1977) have back-computed a number of reported pile load tests to plot ultimate shaft resistance against the mean undrained strength using the β method of Burland(1973). In a similar study, Esrig and Kirby(1979) have used separately the α method and the λ method on observed pile test results to plot similar graphs. On comparing their findings with those of Flaate and Selnes(1977), it was found that although the extent of scatter in the β method was substantial, it was not as great as that encountered when using the α and the λ methods.

As stated by Milititsky(1983), despite the apparent attraction of a fundamental analysis, the difficulties of predicting lateral soil stresses, and accounting for installation effects is an impediment to the universal use of the effective stress and total stress methods. The lateral soil stresses are generally empirically rather than theoretically determined.

2.4.6 Critical depth considerations

Vesic(1967) explained a mechanism for the occurrence of critical depth by suggesting that vertical arching takes place which causes the average vertical effective stress immediately adjacent to the pile shaft to reach a constant value. According to Bhushan(1982), at some critical length to diameter ratio value, c_a increases at an ever-decreasing rate. Zeitlen and Paikowsky(1982) have suggested that the limiting value of c_a is automatically explained by the decrease in the value of ϕ' with effective normal confining pressure.

More recently, there has been mixed opinions regarding the concept of critical depth. Fellenius(1995) has concluded that critical depth is a fallacy which arises from neglect of residual loads in full-scale and model test piles. The same view has been expressed by Randolph(1993) and Kulhawy(1984). In driven piles, residual loads are probably caused by such factors as (a) wave action during driving, (b) soil quakes along the pile shaft, and (c) re-consolidation of the soil subsequent to the disturbance caused by pile installation. In bored, cast in-place piles, residual loads can arise from (i) concrete shrinkage and (ii) pile self-weight.

Fellenius's(1995) analyzed the results of instrumented full-scale and model piles by measuring the initial distribution of shaft resistance due to residual loads. With the residual load effects excluded from the analysis, Fellenius(1995) showed that a critical depth existed at 10-20 pile diameters. Lings(1997) suggested that it is the *average* shear stress along a pile shaft that reaches a quasi-constant value with depth and not the *local* shear stress. The author's view is that the variation of average unit shaft resistance with depth is significantly influenced by the estimated values of earth pressure coefficient. If critical depth is defined in relation to a limiting unit shaft resistance, then the interpretation of data from a pile load test relies on the accuracy of the assessed values of earth pressure coefficient.

2.4.7 Empirical correlation methods

There are a number of empirical relationships available for predicting the bearing capacity of piles in shaft resistance and end resistance. For shaft resistance of piles formed in cohesive soils, Table 2.3(a) lists the most commonly used formulae for the estimation of undrained strength, c_u. In Table 2.3(b), empirical formulae are given for the evaluation of shaft resistance directly from of S.P.T. and C.P.T. results. The formulae for calculating ultimate base resistance are given in Table 2.3(b).

Reference	Empirical formula	Remarks
Kilbourn et.al(1988)	c_u=6N (kN/m^2)	Large diameter, bored, cast in-place piles formed in Keuper marl- Case studies of P.D.R., Cardiff, South Wales, U.K.
Foley and Davis (1971)	c_u=18.5+5.74N (kN/m^2)	Bored, cast in-situ piles formed in Keuper marl- Case study at Leicester, U.K.
Reese et.al(1976)	c_u=7N (kN/m^2)	Piles formed in stiff clays
Stroud(1989)	c_u=4N to 6N (kN/m^2)	Piles formed in silt and piles formed in hard clays

Table 2.3(a): Empirical formulae for undrained strength, c_u for the design of bored, cast in-place piles formed in cohesive soils based on in-situ tests

Reference	Empirical formula	Remarks
Present work@	f_s=3.2N	Large diameter, bored, cast in-situ piles formed in Keuper marl, P.D.R.-Cardiff.
Yamashita et al(1987)*	f_s=5N (kN/m^2)	Cast in place piles formed in cohesive soils. f_s(max.)=150kN/m^2
Shioi and Fukui(1982)*	f_s=10N (kN/m^2)	Cast in place piles formed in cohesive soils
Decourt(1982)*	f_s=10+3.3N (kN/m^2)	Piles cast under bentonite in cohesive soils; 50>N>3; f_s(max.)=170kN/m^2
Shioi and Fukui(1982)*	f_s=5N (kN/m^2)	Piles formed in cohesive soils.
Meyerhof(1976)	f_s=N (kN/m^2)	Low-displacement piles (any soil type)
Fleming & Thorburn(1983)	f_s=0.1q_c *(q_c=cone resistance)*	Driven and bored piles formed in cohesive soils
Price & Wardle (1982)	f_s=0.49q_s *(q_s=cone sleeve friction)*	Small diameter (168mm) bored pile in stiff clay
Thorburn & McVicar(1979)	f_s=0.025q_c	Driven and bored piles formed in cohesive soils

Legend: *@ Back-analysed from pile load tests for P.D.R. (Cardiff), *In Poulos(1989)*

Table 2.3(b): Empirical formulae for shaft resistance of bored and cast in place piles formed in cohesive soils based on in-situ tests

The suggested values in Tables 2.3(a)- (c) vary widely, hence the empirical formulae given should be checked against actual results from field or laboratory soil tests, if available for the particular soil stratum being investigated. Fleming et.al.(1992) have noted that, for non-sensitive clays, the relationship between "N" and c_u proposed by Stroud(1989) is frequently adopted in the U.K.

Reference	Formula	Remarks
Present work[@]	f_b=110-150N	Large diameter, bored, cast in-situ piles formed in Keuper marl, P.D.R.-Cardiff.
Shioi and Fukui(1982)*	f_b=150N (kN/m^2)	Bored piles formed in clay
Yamashita et al(1987)*	f_b=90(1+0.16z) in kN/m^2 where z= depth of pile tip in metres	Cast in place piles formed in cohesive soils
Meyerhof(1976)	$f_b = 12 N_{Pt} \frac{L_b}{B}$ (kN/m^2) N_{Pt}= N value near pile toe (corrected for 100kN/m^2 overburden pressure) L_b= length of penetration of into bearing stratum B= pile width (diameter)	Bored piles (any soil type) Maximum base pressure: f_b=<120N
Hobbs & Healy (1979)	f_b=240N (kN/m^2) ; N<30; f_b=200N for N>40	Piles formed in Chalk

Table 2.3(c): Empirical formulae for end resistance of bored and cast in place piles formed in cohesive soils based on in-situ tests

2.4.8 Summary

The available methods of pile load capacity calculation based on classical soil mechanics theories and empiricism have been discussed. Several empirical formulae have been suggested for calculating pile load capacity based on in-situ soil properties. This suggests that emprical coefficients determined for a given site may not be applicable to another site. Most classical methods of predicting pile load capacity are faced with difficulties in evaluating the various soil properties required. The major cause of this problem is the effect of pile installation. Disturbance to soil during pile installation can cause complex conditions to develop both within the soil mass and at the pile-soil interface thereby affecting shaft and end bearing resistance.

A large collection by Meyerhof(1992) of data from instrumented test piles installed in clay reveals that none of the above described approaches can realistically be said to represent a fundamental design method. Design options are usually reduced by the inadequacy of information regarding the soil properties at a site. Consequently it becomes necessary to either carry out a pile load test programme or resort to a conservative design, with uneconomically high safety factors. In view of these uncertainties, the necessity of further research into pile-soil interaction cannot be over-emphasised.

2.5 CASE STUDIES OF PILE TESTING IN KEUPER MARL

2.5.1 Introduction

A search of the existing publications revealed that the extent of published information regarding the behaviour of large diameter, bored piles installed in Keuper marl (Keuper marl) is limited. It is understood that load testing of piles as a part of site investigation is often an expensive undertaking. Nevertheless, there are situations where pile load tests may be necessary, depending on the

(a) Significance and scale of the foundation problem

(b) Information available regarding the ground conditions

(c) Complexity of the soil condition and of the loading on the foundation

(d) Financial resources available for foundation design.

A brief review of the some published case histories on the observed behaviour of piles formed in weathered mudstones is discussed in the following sections. Particular attention has been paid to instrumented piles and to situations where conventional construction and testing techniques have been used.

2.5.2 Large diameter, bored, cast in-situ piles formed in Cardiff (P.D.R.)

2.5.2.1 Previous piling experience in Cardiff

Large diameter piles were used for the foundations of the Penarth Bridge in 1967. This created an awareness of the nature and variability of Keuper marl and how these factors affect pile behaviour. In the same year, 1.07m diameter bored piles were required for the foundation work for the 26-storey Pearl Assurance building which was to be built at the Greyfriars site in Cardiff. Plate bearing tests were used to provide the design information for the piles. However, more detailed soil investigation was recommended in order to reveal extensive profiles of the marl and the variations in positions and strengths of the strata. The results of this investigation led to substantial amendments of the original pile design.

During the design and construction of the previously completed sections of the P.D.R., several pile load test programmes were carried out in order to provide certain design parameters and to assess the performance of the working piles. Most of the foundations of the various bridges and other structures constructed utilised large diameter, bored, cast-in-situ piles. Among the available options, these pile types were found to provide the most appropriate solution. Load testing was carried out on actual working piles and experimental piles installed at selected locations along the proposed routes.

2.5.2.2 Test piles at Clarence Road bridge, Cardiff P.D.R.

In 1973, trial tests were carried out using 790mm diameter by 26m long bored, cast in-situ piles for the Clarence Road Bridge project. One test pile was provided with a voided toe, whilst the other was constructed so as to allow the mobilisation of end resistance to occur. Bentonite was used while boring into the marl. The ground stratification profile comprises layers of fill, sand/cobbles and soft silty clay to 9m depth. Below these is a layer of ballast and large cobbles up to 18m depth, at which the Keuper marl surface is located.

Fig 2.1(a) shows the load-settlement plots for the voided toe test (test 1) and the test on the normally constructed pile (test 2). The curve for the voided toe test represents load carried in shaft resistance only. At each settlement value, the difference between the ordinates in test 1 and test 2 may be taken to represent the load carried in end bearing resistance. The deduced plot of base load versus settlement is given in Fig 2.1(b). This calculation may be justified because the voided toe pile and the normal pile were (i) identical in diameter and length, (ii) installed in similar ground conditions and (iii) constructed with the same equipment and care. However, despite the similarity of construction, it is appreciated that some differences in load capacity between the two test piles might still exist.

By using the method given by Mazurkiewicz(1972), the ultimate shaft load was determined by extrapolation of this curve (i.e test 1). Hence by reference to the same curve, Kilbourn et.al.(1988) deduced that at 25mm settlement, some 80% of the ultimate shaft load was mobilised. In addition, by the 25mm settlement stage, the rate of increase of load of the normal pile would be increasing almost directly in response to the stiffness of its base. This implies that, beyond a settlement value of 25mm, the rate of increase of shaft resistance would be low. Hence, at 25mm settlement, the vertical intercept of the tangent from the load-settlement graph (for the normally constructed pile) would give a measure of the mobilised shaft load at this stage. By comparison to the plot of the voided toe test, the shaft load inferred from the tangent at 25mm settlement is taken to be approximately 80% of the ultimate shaft load. This method of determining ultimate shaft load by drawing a tangent line at a given settlement is similar to the procedure initially suggested by Van Weele(1957). In this procedure, the base load versus settlement graph was adopted as a line drawn through the origin and parallel to the tangent on the load-settlement curve at the point of ultimate shaft load mobilisation. Brierley et.al.(1979) and Leonards and Lovėll(1979) have also used similar methods to separate bearing capacity into shaft resistance and end bearing.

2.5.2.3 Test piles at Grangetown Link and Cogan Spur, Cardiff P.D.R.

In 1985, the Grangetown Road link contract required the load testing of three large diameter bored, cast in-situ piles. The details of the test piles are:

	Type	Diameter (m)	Length (m)
Test 1	Normal	0.9	34
Test 2	Voided toe	1.35	34
Test 3	Voided toe	0.9	27

The voided toe piles were installed at a site adjacent to that of the normal pile. The piles were successfully loaded to three times the working load. The load-settlement curves obtained in tests 1 and 2 showed that at the maximum applied load (equivalent to three times the working load), the gradients of the graphs were still high. Hence, unless brittle failure was imminent, the both piles were still below ultimate load capacity. There were large variations in the soil conditions between these sites and hence the ultimate load capacity of the voided toe pile could not be compared with the ultimate shaft resistance of the normally constructed pile.

At Cogan Spur (test 4) where a 0.9m diameter by 30m long pile was tested, the soil conditions were found to be comparable to the stratification profile encountered at Grangetown Link (test 3). It was intended to compare the performances of these piles in order to test the validity of the method of evaluating ultimate shaft resistance previously developed from the pile test results at Clarence Road bridge. Fig 2.1(c) shows a comparison between the load-settlement plots for the two test piles. By comparing the mobilised shaft load with the total load at 25mm settlement, the results were found to support the previously suggested pattern.

2.5.2.4 Test piles at East moors Link, Cardiff P.D.R.

Three piles, each 1.05m in diameter, were successfully load tested to failure at selected sites within the proposed project area. The test piles were embedded to different lengths in the Keuper marl. Above the Keuper marl surface, the pile portions passing through superficial soil strata were sleeved. No strain gauges or load cells were installed in the test piles. Therefore, in order to separate shaft resistance and end bearing, the method previously developed from pile tests at Clarence Road Bridge, Grangetown Road Link and Cogan spur was applied. This method was used to calculate the ultimate shaft and base resistance values shown in Table 2.3(c).

Pile No.	Length (m)	Permanent casing to (m)	Load capacity (MN)	Ultimate shaft load (MN)	Ultimate base load (MN)
2	23.0	12.0	14.0	9.0	5.0
3	21.0	11.0	9.0	4.8	4.2
4	21.0	9.6	15.5	10.8	4.7

Table 2.3(d): Pile load test results-East moors Link (P.D.R.), Kilbourn et.al(1988)

It was proposed to use the pile data collected to develop a design method for the working piles based on SPT "N" values obtained from the site investigation. Figure 2.2 shows the predicted variation of ultimate shaft capacity with embedded length in the marl, based on SPT "N" values. The observed results are plotted on the same graph for comparison. Kilbourn et.al.(1988) deduced that the use of SPT "N" values in estimating ultimate shaft load was reasonably accurate. There was close agreement between the predicted and the measured values of ultimate shaft load for c_u=6N and α=0.375.

2.5.3 Piles formed in Keuper marl at Leicester

Foley and Davis(1971) have reported a case study of pile load testing for a large shopping centre and Civic Theatre in Leicester. The site had layers of Keuper marl commencing from 3.3m to 5m below ground level and extending to a depth of 16m. Below this depth, there was a marked increase in strength up to the proposed installation depth of the working piles. The standing water level was at 9.5m depth below ground level.

Two 0.6m diameter by 18m long, bored, cast-in-situ piles were tested in order to examine the design parameters. One of the piles had a soft toe to separate end bearing from shaft resistance while the other was normally constructed. Laboratory tests were carried out on undisturbed samples of material from depths 4m, 6.5m and 10m. The tests were,

(i) Undrained triaxial tests,

(ii) Drained shear box tests, and

(iii) Capillary tension measurements for in-situ values of the coefficient of earth pressure at-rest, K_o.

Tests for the determination of the effective stress parameters, c'_S and ϕ_s' were carried out on remoulded and softened samples from depths 4m and 10m. As shown in Table 2.4, c' was substantially reduced but remoulding had very little effect on ϕ_s'.

Depth (m)	Consolidated undrained triaxial	Shear box tests	Unconfined comp. strength	S.P.T. result
4m	$c'=17.6kN/m^2$ $\phi'=35°$ $c'_s=3.5kN/m^2$ $\phi_s'=34°$	-	$c_u=107$ kN/m^2	-
6.5m	$c'=17.6kN/m^2$ $\phi'=36°$	$c'=27.4\ kN/m^2$ $\phi'=38°$ $c'_r=0$ $\phi_r'=27°$	$c_u=85.4$ kN/m^2	N=32 ($c_u=195\ kN/m^2$)
10m	$c'=24.6kN/m^2$ $\phi'=40°$ $c'_s=3.5kN/m^2$ $\phi_s'=38°$	-	$c_u=89.3$ kN/m^2	N=30 ($c_u=195\ kN/m^2$)
12.5m	-	-	-	N=20 ($c_u=136.7$ kN/m^2)
14m	-	-	-	N=36 ($c_u=219.7$ kN/m^2)
15.5m	-	-	-	N=47 ($c_u=293\ kN/m^2$)
18m	-	-	-	N=35 ($c_u=220\ kN/m^2$)

Table 2.4 In-situ and laboratory soil test results for test piles at Leicester, Foley and Davis(1971)

The shaft resistance values of the two test piles were calculated using the following three methods,

(i) Total stress method based on c_u derived from unconfined compression tests

(ii) Total stress method with c_u derived from empirical relationships with SPT "N" values, and

(iii) Effective stress method.

The results from these methods were compared with the results of the load test given in Table 2.5.

Design method	Shaft resistance result@ (tonnes)	
	Voided toe pile	Normal pile
Total stress method (c_u from UCS test) α=0.45	142	165
Total stress method (c_u from SPT) α=0.45	320	370
Effective stress method c'_s=0 ϕ_s'=36° K_o=1.5	590	710
Load test result	300	450

@ Shaft resistance values averaged over 13.72m (voided toe pile) and 15.24m (normal pile)

Table 2.5 Comparison of the results of three approaches to the calculation of shaft resistance for test piles at Leicester, Foley and Davis(1971)

It was shown that the total stress method based on unconfined compression tests underestimated the pile shaft capacity by more than 50%. The S.P.T based total stress method is convincing. The effective stress method was found to provide an upper bound solution to the ultimate shaft resistance capacity.

2.5.4 Piles formed in Keuper marl for the Birmingham International Arena

Dauncey and Woodland(1984) have reported a case study of pile testing in Keuper marl for the Birmingham International arena. The main foundations comprised bored, cast in-situ piles installed in predominantly zone III marl. The ground strata was described according to the weathering zone as follows:

Depth	Zone
1.4-4.0m	IVa
4.0-18.0m	III
Below 18.0m	II

The Keuper marl was described as a firm, becoming stiff and then very stiff red-brown and grey-brown silty clay or clayey sandy silt. Less weathered material, described as very weak or weak mudstone was encountered in some deep boreholes, below 13-19m depths. Standard Penetration Tests (S.P.T.) and Cone Penetration Tests (C.P.T.) were carried out in the mudstone at regular intervals. The S.P.T. results from the borehole closest to the test pile site showed an approximately linear increase in undrained shear strength from an average of 75 kN/m^2 at 3m depth to 725kN/m^2 at 20m depth. The relationship $c_u = 6N$ was adopted in converting S.P.T. "N" values to equivalent undrained strength.

To confirm the design of the working piles, preliminary trial compression pile and tension pile testing was carried out to loads approaching ultimate capacities. The details of the test piles are:

	Diameter	Length	Casing to
Compression pile	0.75 m	13.6 m	5.0 m
Tension pile	0.75 m (cased length) 0.6 m (embedded section)	18.8 m	3.5 m

The ultimate capacities of the trial piles were not achieved in either test and the method of Mazurkiewicz(1972) was used to extrapolate the maximum loads. The estimated ultimate capacity of the compression pile was 5400kN whilst that of the tension pile was 3780kN. Hence, the ultimate base capacity of the compression pile is estimated to be 1920kN. Assuming a bearing capacity factor N_c=9, the c_u value at the base of the compression pile was obtained as 482 kN/m^2. This value was therefore consistent with the S.P.T. results at that depth.

Mazurkiewicz's method assumes that the load-deflection curve is approximately parabolic in shape. An alternative method of projecting ultimate load was suggested by Chin(1972), which assumes a hyperbolic load-deflection relationship. This gave ultimate load values about 15% higher than those obtained by Mazurkiewicz's method. However, as Fellenius(1980) pointed out, the Chin's method tends to over-predict pile load capacity. The ultimate shaft resistance values were obtained as 3220kN and 3580kN, for the compression pile and the tension pile respectively. Therefore the average ultimate shaft resistances were calculated to be 105kN/m^2 for both piles. Hence the adhesion factor, α and the effective stress parameter, β (where β=K$\tan\delta$) were deduced as:

	α	β
Compression pile	0.44	1.06
Tension pile	0.31	0.82

As will be discussed in chapter 5, the average α and β values for the Butetown Road link test piles TP1-TP6 are back-analyzed as 1.42 and 0.53 respectively. Based on the assumption that the ultimate shaft resistance is fully developed at a pile head movement of 20mm (at which the applied load is 4400kN), the stiffness of the material beneath the

base E_b was back-analysed using the relationship $E_b = \frac{q_b D_b \left(1-\nu^2\right) If}{D_b}$, where:

q_b= base stress

D_b=base diameter

ν= Poisson's ratio of soil beneath the base

I= influence factor (taken as $\frac{\pi}{4}$)

f= depth correction factor (taken as 0.5)

Δ_b= base settlement.

It was assumed that at 20mm deflection, approximately half of the ultimate base capacity was developed. The E_b value was back analysed to be 40MN/m^2.

2.5.5 Piles formed in weathered mudstone at County Antrim, Northern Ireland

Piled foundations were required at Kilroot, County Antrim where a power station for Northern Ireland Electricity Service was being built. Preliminary pile testing was carried out to confirm the load capacity of bored piles at the site. The case record has been reported by Leach et al.(1976). It was intended to compare the performance of the test piles against predictions based on conventional design methods using laboratory and in-situ soil tests. Three concrete test piles A,B and C, detailed below ,were installed and load tested.

	Pile type	Diameter	Embedded Length	Test type
A	Voided toe	0.74 m	6.37 m	C.R.P.
B	Voided toe	0.74 m	8.98 m	M.L.
C	Normal	0.74 m	7.60 m	C.R.P.

The ground strata comprised glacial deposits of stiff clay with gravel up to 0.3-7.0m depth below which Keuper marl was encountered. The water table was located at a depth of about 2.0m. Table 2.6 gives a comparison between the measured ultimate shaft resistance for test piles A and B and the predicted value using effective stress methods.

	Pile A	Pile B
Material around shaft	Mainly zone II marl	Zones III and IV marl
Embedded length into marl (m)	6.37m	8.98m
Ultimate shaft resistance (effective stress method using c' and ϕ' values) (kN/m^2)	152	162
Measured shaft resistance (kN/m^2)	210	119
Values of ultimate shaft resistance (Davis and Chandler,1973)	250-280	150-180

Table 2.6: Comparison of ultimate shaft resistance values for two piles A and B at County Antrim, Leach et al(1976)

The bearing capacity for test pile C was predicted using the following five different methods as shown in Table 2.7. It was found that all the above methods underestimated the ultimate capacity of test pile C. The use of laboratory determined c_u values gave only 40% of the measured capacity of the pile. This indicates that laboratory undrained tests on undisturbed samples result in an underestimation of the in-situ strength of Keuper marl. The methods based on c_u values determined from pressuremeter tests gave 85% of the load capacity of the pile. The results also indicated that the use of β=0.8 in Burland(1973) lead to a conservative design. The following design methods resulted in the closest estimate of pile capacity (accurate to within 10%).

(i) The basic effective stress approach of Davis and Chandler(1973) with α=0.45 and using pressuremeter c_u values, and

(ii) Chandler's(1968) method using pressuremeter K_o and c_u values and taking N_c=9.

	Design constants and soil properties		Calculated ultimate load capacities (kN)			
Design method	Shaft	Base	Shaft (kN)	Base (kN)	Total Q_u (kN)	$\frac{Q_{u(predicted)}}{Q_{u(actual)}}$
Skempton (1959)	α=0.3, c_u laboratory	N_c=9, c_u laboratory	770	620	1390	0.23
	α=0.3, c_u pressuremeter	N_c=9, c_u pressuremeter	2650	2440	5090	0.84
Menard (1965)	Pressuremeter	Pressuremeter	1590	2720	4310	0.71
Chandler (1968)	ϕ' recompacted K_o pressuremeter	N_c=9, c_u laboratory	3080	620	3700	0.61
		N_c=9, c_u pressuremeter	3080	2440	5520	0.92
Burland (1973)	$\bar{\beta}$=0.8	N_c=9, c_u laboratory	2150	620	2770	0.46
		N_c=9, c_u pressuremeter	2150	2440	4590	0.76
Davis & Chandler (1973)	α=0.45,c_u laboratory	Effective stress parameters for undisturbed zone III marl	1150	1580	2730	0.45
	α=0.45, c_u pressuremeter		3980	1580	5560	0.92
	Average of quoted typical values		3060	1580	4640	0.77

Table 2.7: Different design methods for pile C (Leach et al,1976)

2.5.6 Piles formed in Keuper marl at Redcar, Teesside

Bored, driven, cast-in-situ piles were constructed to provide a foundation for a large blast furnace structure for British Steel Corporation at Redcar, Teesside. The piles were 0.6m in diameter by 15m long and were designed as end bearing. The piles were provided with enlarged bases founded on relatively unweathered Keuper marl bedrock. The substrata consisted of slag fill and beach sand up to 14.5m depth overlying a 1.2-10m thick layer of clay. Keuper marl was present underneath the clay. The piles were embedded to between 1m and 2m into the marl.

Jorden and Dobie(1977) have reported a case study of preliminary load tests on four piles carried out at the site. The first one was designed to measure base resistance, whereas the second was to measure shaft resistance and the remaining two were intended to measure combined base and shaft resistance. The load-deflection curves obtained were used to correlate and to check the results of plate loading tests on 865mm and 584mm diameter discs which were proposed to predict the strength parameters. The plate loading tests gave in-situ modulus values of the marl between $50MN/m^2$ (highly weathered) and $3000MN/m^2$ (unweathered).

From the results of the end-bearing pile, the deformation modulus of the material beneath the base was back-analysed as $1230MN/m^2$. This turned out to be much higher than that obtained from the plate loading tests. This high value of soil modulus was attributed to the possible soil density increase beneath the base during pile installation.

2.5.7 Continuous flight augur pile in Bristol

Fleming(1992) has presented a test on a continuous flight auger pile founded in weathered Keuper marl in the Bristol area. The ground stratification profile and average S.P.T. "N" values were recorded as:

Depth	Description	Mean "N" value
Up to 7.2 m	Fill and soft peaty clays	-
7.2-10.0 m	Soft clayey silt	6
10.0-14.2 m	Sand and gravel	45
Below 14.2 m	Keuper marl	120
17.0 m	Pile toe level	

The pile, which was 600mm in diameter by 17m long, was loaded in increments up to 2.5MN for which the recorded settlement was 43.06mm. The ultimate failure load was not reached. Parallel with the observed pile results, Fleming(1992) has proposed an analytical method for the prediction of pile settlement under load. This method used hyperbolic functions to characterise both shaft and base load mobilisation. These components of load resistance are then combined to give a load-settlement compound function. This function also accounts for pile elastic shortening. For a rigid pile, Fleming(1992) gives the relationship between pile head load P and settlement Δ_n as:

$$P = \frac{U_s \Delta_n}{M_s D_s + \Delta_n} + \frac{D_b E_b U_b \Delta_n}{0.6 U_b + D_b E_b \Delta_n} \tag{2.7}$$

Where U_s= ultimate shaft load, U_b= ultimate base load, D_s= pile shaft diameter, D_b= pile base diameter, E_b= secant modulus of soil beneath pile base (taken at 25% of ultimate load) and M_s= shaft flexibility factor (dimensionless).

For a given load P, the settlement Δ_n was calculated by rearranging the equation, thus

$$(eP - ae - b)\Delta_n^2 + (dP + ecP - ad - bc)\Delta_n + cdP = 0 \tag{2.8}$$

Where a= U_s, b= $D_bE_bU_b$, c= M_sD_s, d= $0.6U_b$, e= D_bE_b.

For convenience, let $f = eP - ae - b$, $g = dP + ecP - ad - bc$ and $h = cdP$. Therefore Δ_n is given by the positive solution of the equation

$$\Delta_n = \frac{-g \pm \sqrt{(g^2 - 4fh)}}{2f} \tag{2.9}$$

For a flexible pile, the additional settlement due to elastic shortening Δ_E is evaluated from one of two functions, depending on whether or not the applied load exceeds the ultimate shaft load. For all values of P such that $P<U_s$, Δ_E was evaluated from:

$$\Delta_E = \frac{4}{\pi}\frac{P(L_o + K_E L_F)}{D_s^2 E_c} \tag{2.10a}$$

whilst for $P>U_s$, the relationship derived was:

$$\Delta_E = \frac{4}{\pi}\frac{1}{D_s^2 E_c}\left[P\left(L_o + L_F\right) - L_F U_s\left(1 - K_E\right)\right] \tag{2.10b}$$

where

L_o= upper length of pile not involved in load transfer

L_F= lower length of pile transferring load to soil by shaft resistance

K_E= coefficient, which when multiplied by L_F gives the depth, below the pile head level, of the centroid of load transfer.

E_c= Young's modulus of concrete.

For all cases, the pile head settlement Δ_h was obtained by adding Δ_n to Δ_E. The ultimate shaft load and ultimate base load were back-figured from the load-settlement data using the "inverse slope" method proposed by Chin(1972).

Values of M_s were found to vary with soil conditions, but could be estimated from empirical correlation with S.P.T. "N" values. The M_s value for a particular test pile may also be back analysed from the load-settlement data using the Chin's(1972) method. For marl and shale, the following M_s values were found to be appropriate for given "N" values:

S.P.T. "N"	Flexibility factor M_s
20	2.0×10^{-3}
50	1.5×10^{-3}
100	1.2×10^{-3}
150	1.0×10^{-3}

Values of E_b were also determined from relationships with "N" values. For a continuous flight auger pile in marl or shale, the E_b value (in kN/m^2) was taken as 1000-1500 times the S.P.T. "N" value.

The value of K_E was reported to depend on the generation of load along the shaft and that the following typical values are appropriate for different conditions:

Condition	**K_E**
Uniform shaft resistance along L_F	0.4
Clay strength increasing with depth	0.45
Sands/Gravels	0.4-0.65

From the geometrical and material properties of the test pile, the following values of various parameters apply: D_s=0.6m, D_b=0.6m, L_o=10m, L_F=7m, E_c =45kN/mm^2; while from the site conditions; U_s=800kN, U_b=3250kN, M_s=0.0007, E_b=0.09161kN/mm^2, K_E=0.5. These values were utilised in the above equations to predict the load-settlement behaviour of the test pile and to separate end bearing and shaft resistance.

Fig.2.3(a) shows a plot of the observed data and the predicted curves of total load, shaft load and base load versus settlement. For the range of loading applied, there is a remarkably close agreement between the predicted and actual settlement values at given applied loads. The result shows that the use of hyperbolic load-transfer functions to represent the shaft and base resistance development produces an accurate prediction of the load-settlement characteristics of the pile.

The hyperbolic transfer function has a major limitation in that it does not represent the settlement characteristics of a pile at load levels approaching failure. The function defines ultimate load by an asymptotic value thereby wrongly suggesting that infinite settlement is required to mobilise the full load capacity of the pile.

2.5.8 Piles formed in pre-consolidated Keuper marls of Southwest Germany

Schmidt and Rumpelt(1993) have presented some experience gained in the design and observed performance of large diameter, bored, cast in-situ concrete piles installed in calcareous mudstone. Loading tests were carried out in order to evaluate and adjust the soil parameters used in the design of the working piles for a large office development in Sttutgart City, Germany. The predominant ground strata in Sttutgart and the surrounding region of Southwest Germany is the Triassic Gypsum Keuper. It consists of a large sequence of mudstones and marlstones. The soils and rocks encountered had a wide range of soil/rock qualities, depending on the state of weathering and dissolution of constituent Gypsum and dolomite.

The Keuper marl at the pile test site was found to be generally completely weathered into a very stiff silty clay having consistency index I_c of approximately 1.02 (Definition: I_c=1-LI) at a mean moisture content of 18.6%. In some places, the Gypsum Keuper could be classified as a hard clay or very weak rock. Based on previous pile test results which showed ultimate shaft resistance values ranging from 150-300 kN/m^2, it was recommended to adopt a design value of 120 kN/m^2 for shaft resistance and ignore any end bearing resistance. Two pile were load tested in order to check these design assumptions:

	Diameter	Embedded length	Design load, Q_d
Pile 1	900 m	9.3 m	3.16 MN
Pile 2	900 m	15.3 m	5.19 MN

The test piles were bored and concreted without casing. Rod extensometers were installed at selected levels to measure the pile deformation and hence load transfer. The load test was conducted according to the ISSMFE recommendations (Smoltczyk, 1985). The failure load, defined as the load at a settlement equivalent to 10% pile diameter, was not reached in both test piles. The maximum applied loads shown below were taken to be the ultimate loads. The ultimate shaft resistance values were estimated based on the German Standard DIN 4014(1990), and taking c_u=150kN/m^2. This Standard stipulates a presumed bearing value of q_{bu}=1150kN/m^2. The total pile capacities were therefore estimated as shown.

	Max. applied load	Ultimate shaft resistance	Total capacity
Pile 1	3.3 MN	1.31 MN	2.05 MN
Pile 2	5.8 MN	2.15 MN	2.89 MN

Therefore, the observed pile capacities were found to be significantly greater than the design values from DIN 4014(1990). Schmidt and Rumpelt(1993) suggested that the design code postulates very low shaft resistance values as functions of undrained strength.

The load transfer data deduced from the extensometers indicated that the shaft resistance increased with depth along each pile shaft, up to a maximum value at 7-8 metres depth (equivalent to 52-75% of embedded pile lengths). There was a decrease in shaft resistance in the lower third of a given test pile. In the longer pile, location of the maximum shaft resistance shifted downward with increasing applied load.

Large diameter triaxial shear tests on soil specimens sampled from adjacent test boreholes indicated effective stress parameters c'= 30 kN/m^2 and $\tan\phi'$=0.5. Based on these data, Schmidt and Rumpelt(1993) deduced the average ultimate shaft resistance as q_{sum}=87 kN/m^2. In comparison to the measured mean values of q_{sm}= 94 and 97 kN/m^2 in pile 1 and pile 2 respectively, it was considered that the effective stress method produced reasonable design parameters.

2.6 CASE STUDIES OF PILES FORMED IN WEAK MUDSTONE ROCK

2.6.1 Introduction

Piles installed in intact rock are largely designed as end-bearing piles and any shaft resistance capacity is neglected, although significant load transfer may occur in the soil strata above the rock. For piles formed in strong rock, the maximum design load of the pile is often determined by the allowable stresses of the pile material itself. However, for pile formed in weak rock, the maximum bearing pressure of the rock is the determining factor.

In weathered rock, accurate estimation of the shaft resistance of driven piles is difficult owing to the disruption of the rock structure caused by driving and the wide variability in strength exhibited by soft rocks. Chalk and marl in the weathered state are examples of weak rocks with highly variable strength parameters. Several factors influence the shear transfer along a pile shaft in rock, such as (a) frictional characteristics of the interface, (b) strength properties of the rock and (c) roughness of the socket.

Codes of practice for foundation design stipulate allowable bearing pressures according to different types of rocks. For a given type of rock, the allowable bearing pressure depends on the quality and joint spacing of the rock. For individual rock types, there are substantial variations in strength and permissible bearing pressures. Therefore, it is helpful to express the allowable bearing pressure in terms of the uniaxial compressive strength, which may be derived from the following laboratory and/or field strength tests on the rock:

a) Unconfined compressive strength tests.

b) Cube crushing tests.

c) Point-load strength index tests.

d) Cross-jacking tests in the pile socket.

e) Standard penetration test.

f) Pressuremeter tests.

In the following sections, some case studies of pile load tests are presented which utilise the above rock testing methods to evaluate pile load capacity. The predicted values are compared and contrasted with observed failure loads of the test piles.

2.6.2 Rock socket piles formed in mudstone and siltstone at Coventry

Cole and Stroud(1976) have reported a case study of rock socket pile foundations for an office block development at Coventry Point, Market Way, Coventry. Two office blocks of fifteen and sixteen storeys were being constructed on a highly developed pedestrian mall layout in the city centre. The ground strata at the site comprised 5.0m of fill with firm silty sandy clay overlying multiple beds of siltstone, sandstone and weathered mudstone.

For economic reasons, it was decided to use rock socket piles although there was only limited design information at the time. Therefore it was decided to carry out trial pile testing in order to obtain adequate design parameters. It was considered that driven piles would cause an unacceptably high noise nuisance during installation and also lead to disturbance and possible damage to existing properties. Cast in-situ, bored, piles designed as rock sockets were selected as being more suitable and economical with lower noise levels. A major disadvantage was that the design of piles of this type, especially in weak rock, was relatively untried in the UK at the time.

The proposed design method for the working piles was based on values of rock strength derived from "N" values obtained from rotary core test data. For shaft resistance along the socket, the adhesion factor α was taken as 0.3;while for base performance, N_c was taken as 9.0 with a safety factor of 3.0.

The test pile was 1.06m in diameter with a design load of 4.5 MN. The pile was tested under maintained load conditions using jacks mounted on a test frame for which reaction was provided by six pre-stressed ground anchors. The pile was jacked progressively to the following loads,

(i) the design load,

(ii) 1.25 times design load, and

(iii) 1.5 times the design load.

The load-settlement plot obtained indicated that even at a load in excess of 1.5 times the design load, the pile was far from failure and probably still had a factor of safety greater than two. It was considered that the design of the foundation was unusual in that the load-settlement behaviour was uncertain.

The mobilisation of shaft resistance at design load was analysed by classifying strata around the shaft into different zones according to strength. Equivalent "spring stiffness" values for the zones were derived from the observed load-settlement curve, allowing for estimated elastic shortening. The shear stiffness s_τ is defined as $s_\tau = \frac{\tau}{\rho}$ whilst the compressive stiffness is $s_q = \frac{q}{\rho}$ where q is the base stress, τ is the shear stress mobilised on the shaft and ρ is the settlement of the rock socket pile. Based on load tests on rock-socket test piles, Thorburn(1966) and Davis(1974) established that $\frac{s_\tau}{s_q}$ values were in the range 0.05-0.07 at loads fully mobilising the allowable concrete stress. Hence a mean value was taken as $\frac{s_\tau}{s_q}=0.06$. Table 2.8 gives the stiffness analysis of the rock socket test pile.

Depth below top of socket (m)	Socket grade & "N" value	Stiffness (s_τ)	Load for ρ=9mm
Up to 1.5m	F N=90	s_qx(90/300)x0.06 =s_qx0.015	0.82s_q
1.5-3.0m	D N=200	s_qx(200/300)x0.06 =s_qx0.033	1.78s_q
3.0-3.75m	E N=130	s_qx(130/300)x0.06 =s_qx0.021	0.56s_q
Base	C N=300	s_q	7.95s_q

<u>Notes</u>
Shaft load=0.82s_q+1.78s_q+0.56s_q=3.16s_q
Base load =7.95s_q
Total load =11.11s_q=4500 kN (design load)
Therefore s_q=405kN/m^2/mm; and base stress q=3650kN/m^2

Table 2.8 Rock socket analysis using stiffness, Cole and Stroud(1976)

From the above results, it is estimated that about 70% of the applied load were transferred to the base of the socket.

2.6.3 Piles formed in cretaceous mudstone in Port Elizabeth, South Africa

Wilson(1977) has reported a case study in which load tests on bored piles founded in mudstone were carried out at the site of a new bridge in Port Elizabeth, South Africa. The site consisted of sand overlying Cretaceous mudstone, which occurred at a depth of 3m below ground level. The mudstone, which was dark grey in colour and even in texture, was found to be heavily over-consolidated in nature.

It was proposed to predict and to check the ultimate pile base load using values of undrained strength of the mudstone determined through different methods. Four methods were used in evaluating the undrained strength of the mudstone, namely,

1. Unconfined compressive strength test,
2. In-situ cross-jacking test at base of pile hole,
3. Cube strength test, and
4. Point-load strength test.

In the cross-jacking test, a loading head 100mm in diameter was forced into the mudstone using a calibrated hydraulic jack. The failure load was taken as the lesser of the ultimate resistance or the load required to produce a penetration of 20mm. Point-load strength tests were performed on cylindrical core samples, both diametrically and axially.

The test pile was end bearing only with a 0.67m diameter toe. The load test result indicated that a settlement of 47mm (i.e 7%of base diameter) was required to reach failure in end bearing. A value for undrained strength at the base was deduced from the ultimate base load by assuming N_c value of 9. The values of c_u deduced from the pile test, laboratory tests and the in-situ tests are given in Table 2.9. It was established that crushing tests on mudstone cubes and cross-jacking tests in the pile socket provided reasonable correlation with the in-situ strength of the mudstone. It was again demonstrated that the unconfined compressive strength test underestimates the in-situ strength of the mudstone.

TEST	AVERAGE RESULT	EQUIVALENT c_u (kN/m^2)	REMARKS
Cross-jacking test	4990 kN/m^2	832	It is assumed that the test pad acts as a surface footing with a bearing capacity of $6c_u$.
Cube crushing test	2096 kN/m^2	786	Taking UCS=3/4 of cube strength, hence $c_u = \frac{1}{2}UCS$
Point-load (54mm core) index I_s	I_s= 104	1248	Taking UCS=$24I_s$ from Bieniawski(1975). Hence $c_u = \frac{1}{2}UCS$
Unconfined compressive strength (UCS)	1091 kN/m^2	545	$c_u = \frac{1}{2}UCS$
Pile load test result (maximum end resistance)	6878 kN/m^2	764	Taking N_c=9

Table 2.9 Values of c_u from different tests compared with the pile load test result correlation, Wilson(1977)

2.6.4 Rock-socket piles formed in mudstone at Melbourne, Australia

Johston and Haberfield(1993) have proposed an analytical model for evaluating skin resistance of piles formed in soft rock. The analytical model was developed into a computer program, which calculates the distribution, magnitudes and continuity of the stresses and deformations for a range of socket geometry and pile-rock interface roughness (asperity). The analytical model requires three groups of parameters for input into the program to analyse a rock-socket pile:

Interface roughness	Mean asperity angle, i_m Standard deviation of asperity angles, i_{sd} Mean asperity height, h_m Standard deviation of asperity height, h_{sd}
Rock-socket geometry	Socket length, L Socket diameter, D Initial normal stress on shaft, σ_{no}
Rock properties* (based on drained conditions)	Uniaxial compressive strength, q_u Cohesion, c Peak angle of friction, ϕ_p Residual angle of friction, ϕ_r Mass modulus, E Poisson's ratio, v Uniaxial tensile strength, σ_t

Table 2.10: Variables considered in the analytical model for rock-socket piles (Johnston and Haberfield, 1993)

Many singularities were found to eventuate with the point contact and localised crushing which occur with truly random asperity shapes. It was found that the simplified method involving the use of triangular asperity avoided these singularities. The initial normal stress on shaft, σ_{no}, was estimated from the head of concrete placed in the socket, by assuming that the horizontal stress is approximately equal to the vertical stress. The analytical model accounts for the effect of softening due to socket dilation, which occurs during pile loading. Dilation leads to the formation of radial cracks around the circumference of the shaft.

Williams(1980) has reported a case study of load testing of 1.2m diameter piles resisting load in shaft resistance only. The test piles were socketed into moderately weathered Melbourne mudstone. These load test data and other test data published elsewhere have been analysed using the model presented by Johnston and Haberfield(1993). Remarkably close agreement was observed between the measured and predicted socket shear stress versus settlement variation. In practical terms, it was found that difficulties are experienced in determining the socket roughness parameters. Hence it was considered advantageous to categorise the mudstone sockets into three groups: (a) smooth sockets, (b) medium sockets, and (c) rough sockets. On the basis of a study of these roughness categories for rock sockets in Melbourne mudstone, Johnston and Haberfield(1993) suggested the use of the roughness parameters given in Table 2.11.

	Range of values for sockets in Melbourne mudstone		
Parameter	smooth	medium	rough
i_m (degrees)	10-12	12-17	17-30
i_{sd} (degrees)	2-4	4-6	6-8
h_m (mm)	1-4	4-20	20-80
h_{sd}/h_m	0.35		
D (m)	0.5-2.0		
q_u (MN/m^2)	0.5-10.0		
σ_{no} (kN/m^2)	50-500		
E (MN/m^2)	50-3000		

Table 2.11: Socket properties in Melbourne mudstone (Johnston and Haberfield, 1993)

In order to produce design charts, the following values of E/q_u and q_u/σ_{no} were chosen as representing the general range of mudstone encountered.

E/q_u	100	200	300		
q_u/σ_{no}	5	25	50	100	200

Using these values, the numerical model was run 200 times with various selections of i_m, i_{sd}, h_m, and D within the ranges given in Table 2.11. For different roughness categories (i.e smooth, medium or rough) at particular values of q_u/σ_{no}, and E/q_u a mean value of the adhesion factor, α, of the 200 results was calculated by back-analysis. The results revealed that there was a trend for the adhesion factor to increase with increasing roughness and increasing E/q_u ratio, but to decrease with an increasing q_u/σ_{no} ratio. The predictions using the simplified design charts were found to agree well even with field correlation of the test conducted in rocks of high uniaxial compressive strength. The calculated variation of adhesion factor with uniaxial strength was found to be in good agreement with the correlation suggested by Horvath(1978).

2.6.5 Large diameter rock socket at Rosignamo, Tuscany (Italy)

Carrubba(1997) has reported loading tests on several 1.2m diameter piles with lengths varying from 13.5-37.0m. The load tests were carried out to provide data for the design of the Poggio-Iberna Viaduct. Depending on the particular site, the pile sockets were formed in marl, diabase, limestone or sandstone. Several continuous borings with undisturbed sampling were performed to characterise the mechanical properties of the rocks. The rock quality designation (RQD) of rock formations was evaluated during sampling. Table 2.12 shows the socket lengths and the geotechnical rock properties at each test pile location.

	Socket length (m)	Total length (m)	Rock type	UCS (MN/m^2)	RQD* (%)	E_R (MN/m^2)
Pile 1	7.5	18.5	Intact marl	0.9	100%	200
Pile 2	2.5	19.0	Highly fractured diabasic breccia	15.0	10%	200*
Pile 3	11.0	37.0	Gypsum	6.0	60%	2000
Pile 4	2.0	20.0	Very hard diabase	40.0	50%	10000
Pile 5	2.5	13.5	Intact limestone	2.5	100%	5000*

UCS =Unconfined compressive strength
RQD=Rock quality designation (defined as the sum of lengths of intact pieces of core greater than 100mm divided by the length of core advance)*
E_R = Longitudinal modulus (denotes values determined from 300mm plate bearing tests; unmarked values are based on UCS tests)*

Table 2.12: Rock socket properties at Rosignamo, Tuscany, Italy (Carrubba,1997)

Loading tests were carried out following a slow-maintained load procedure. During each load increment, pile head settlements were measured at 10 minutes intervals until the settlement rate stabilised to 0.05mm/min. The observed load-settlement behaviour was different under the same load level, depending on the (a) socket length (b) rock strength and (c) upper pile length passing through soil. The shapes of the load-settlement curves showed that shaft resistance appeared to be mobilised first.

Carrubba(1997) carried out numerical analyses in order to evaluate the limiting shaft resistance at the pile-rock interface. This was by using the computer code developed by Castelli et.al.(1992) which is based on a two-constant hyperbolic transfer function approach and pile equilibrium solution by finite element analysis. Three distinct hyperbolic functions were used to represent (a) the overall load transfer in the soil, (b) the overall load transfer along the pile-rock interface and (c) the base resistance development. The estimated hyperbolic function constants for shaft resistance in soil were maintained constant but the function constants for shaft and base resistance mobilisation in the rock were first estimated and then modified in an iterative process until the experimental load-settlement curve was reproduced. Once this was achieved, the limiting shaft resistance τ_{lim} could be directly obtained from the final hyperbolic function for shear transfer in the rock socket.

A comparison is made in Table 2.13 between the back-analysed limiting shaft resistance τ_{lim} and the mobilised shaft resistance τ_{mob} measured in the pile tests. The ratio $\lambda = \frac{\tau_{lim}}{(q_u)^{\frac{1}{2}}}$

has also been calculated and shown (where q_u is the unconfined compressive strength of the rock).

	Rock type	τ_{lmob} (MN/m²)	τ_{lim} (MN/m²)	$\frac{\tau_{mob}}{\tau_{lim}}$ (%)	λ $(MN/m^2)^{\frac{1}{2}}$
Pile 1	Intact marl	0.14	0.14	100	0.15
Pile 2	Highly fractured diabasic breccia	0.49	0.49	100	0.13
Pile 3	Gypsum	0.12	0.47	25	0.19
Pile 4	Very hard diabase	0.89	1.20	74	0.19
Pile 5	Intact limestone	0.40	0.40	100	0.25

Table 2.13: Measured and back-analysed shaft resistance values for test piles at Rosignamo, Tuscany, Italy (Carrubba,1997)

The back-computed λ values of 0.13-0.25 $(MN/m^2)^{0.5}$ were found to be close to the lower limit of 0.2 $(MN/m^2)^{0.5}$ suggested by Horvath and Kenney(1979). These values were found to be in contrast to 0.45-0.60 $(MN/m^2)^{0.5}$ as given by Rowe and Armitage(1987).

2.7 EFFECTS OF TIME AND MAINTAINED LOAD ON PILE SETTLEMENT

2.7.1 Consolidation and creep settlements

For piles formed in sand or unsaturated soils the final settlement comprises mainly the immediate settlement due to load application. The contribution of consolidation settlement in such conditions is of less significance, but additional settlement due to creep may also occur. For piles formed in clay the immediate settlement occurs under undrained conditions, followed by a time-dependent consolidation settlement. Terzaghi's theory of one-dimensional consolidation is fundamentally based on the dissipation of excess pore water pressure. Consolidation takes place when water diffuses through the soil matrix and may also involve the redistribution and spreading of stresses between soil particles within the bearing strata. As a consequence, the soil particles undergo deformation and, if the clay is saturated, the excess pore water pressure is dissipated with time.

Consolidation is known to involve considerable structural changes within the soil and may continue beyond the simple dissipation of excess pore water pressure. The structural changes are responsible for "creep", which is a time dependent effect. Creep settlements occur regardless of the state of soil pore water and is particularly significant at high stress levels. For piles formed in saturated soils, the settlement-time variation may not show any distinction between settlements caused as a result of consolidation and those that are due to creep. Creep continues infinitely but its effects diminish with time, tending towards some ultimate state.

With respect to large diameter piles, load tests reported by Whitaker and Cooke(1966) show that immediate settlement is predominant. The tests reveal that at loads well below the ultimate, there is only a relatively small amount of time-dependent settlement. However, at higher loads, significant time-dependent settlements were observed. These settlements were mainly due to shear creep effects.

2.7.2 Assessment of time-dependent settlement of piles

Theoretical solutions for foundation settlement are often used to calculate the final settlement of piles. The analyses carried out by Poulos(1980) show that, in contrast to surface foundations, the consideration of the rate of settlement for a pile is of relatively minor importance. These analyses were used to calculate immediate settlement as a percentage of the final settlement for incompressible piles having various length to diameter ratios L/d and installed in soils with varying effective Poisson's ratio, ν'_s . The results show that for ν'_s = 0.2 and L/d=25, 89% of the final settlement occurred immediately. For compressible piles having negligible end resistance, the proportion of immediate settlement still remained the most significant portion of final settlement but appeared to decrease with increasing pile compressibility. For end-bearing piles, it was found that the final settlement was almost wholly made up of the immediate settlement.

Cambefort and Chadeisson(1961) have made experimental observations that settlement appears to increase linearly with the logarithm of time. Based on this behaviour, Poulos and Booker(1976) have shown that the slope, C_r of the settlement versus the logarithm of time is given by

$$C_r = \frac{PI_\rho B}{d} \quad . \tag{2.11}$$

Where

P= applied load

d= pile diameter

I_ρ= displacement-influence factor evaluated from elastic theory of pile settlement (Poulos,1980)

B= constant parameter in the logarithmic creep function J(t) of the soil:

$$J(t) = A + B\log_{10}(1 + \alpha t) \tag{2.12}$$

where $A = \frac{1}{E'_s}$ in which E'_s is the drained Young's modulus of the soil. The constants A, B and α are experimentally determined soil parameters. The quantity J(t) is the inverse of the Young's modulus of the soil, which varies with time. Hyperbolic type functions have been found to generally represent pile settlement variation with time, at constant load. Tan et.al.(1991) has proposed a hyperbolic function of the form $\Delta_b = \frac{t}{k_1 + k_2 t}$ in which

Δ_b= settlement of pile base

t= time elapsed

k_1 , k_2 = constants to be determined from a straight line plot of $\frac{t}{\Delta_b}$ versus t

(k$_1$ and k$_2$ are the vertical axis intercept and gradient respectively).

In order that the plot of $\frac{t}{\Delta_b}$ versus time, t, does not deviate from a straight line, Carrier(1993) points out that it is necessary to take settlement and time data for a sufficient length of time.

England(1993) has suggested that pile behaviour under load and in time can be modelled using hyperbolic functions and developed a computer program by the name TIMESET for the analysis of time-dependent pile settlements. The method requires the determination of

1) The asymptotic settlement values W_s and W_b corresponding to the ultimate shaft and base resistances respectively. These are based on individual hyperbolic functions representing shaft and base performances.

2) The half-final strain time T_{50} defined as the time lapsed until 50% of the settlement due to shaft resistance or end bearing has occurred. The half-final strain times for shaft and base are denoted T_s and T_b respectively.

England(1993) used the following double hyperbolic function to predict the settlement Δ_t at any time t

$$\Delta_t = \frac{W_s t}{T_s + t} + \frac{W_b t}{T_b + t} \tag{2.13}$$

Owing to minimal volumetric change, the shaft component of the above function is expected to take place significantly faster than that of the base. Thus the two functions can easily be separated if a sufficient length of time is allowed while monitoring load and displacement readings in a static pile test. There are often variations in the relative displacement recorded under constant load, especially for the shaft. This is common in maintained load tests since pile settlement depends on the applied load, the time of holding the load and also the previous load and its duration. For base behaviour, it is observed that subsequent to the mobilisation of the full shaft resistance, the half-strain time T_b does not vary significantly and only the assymptotic value W_b changes from one load increment to another.

2.7.3 Effect of time on the ultimate capacity of piles

The installation of bored, cast in-situ piles inevitably causes soil softening due to (a) stress relief, (b) migration of moisture towards the pile shaft and (c) presence of extra moisture from concrete as it cures. Subsequent to the installation of the pile, the clay consolidates with time and therefore, in the long term, the load capacity of the pile increases.

For driven piles, pore pressure is generated during driving. This dissipates with time hence resulting in consolidation of the soil around the shaft hence increasing its load capacity.

For this reason, the load capacity of a driven pile may also be expected to increase with time. However, according to evidence presented by Bond and Jardine(1991) and Coop and Wroth(1989), the stress changes around a pile shaft driven into stiff clay may produce negative pore pressures. The dissipation of these pore pressures will therefore lead to a decrease in the strength of the clay. Tomlinson(1994) suggested that possible water entry through radial cracks and the gap between the upper part of the pile shaft and the surrounding soil can cause soil softening with time. Hence this will result in a reduction in the pile load capacity.

Observations made by Bjerrum(1973) indicate that a driven pile in soft clay experiences an increase in both the effective shaft resistance and cohesion over a period of time. This phenomenon has also been reported by Orrje and Broms(1967) who established that most of the strength gain takes place within 1-3 months after pile installation. According to load test data presented by Flaate and Selnes(1977), most of the load capacity regain of piles formed in soft clay occurs within 1-3 months after construction. Tavenas and Audy(1972) also reported a that the load capacity for piles formed in sand increases with time, with the principal regain occurring within one month. Load test data reported by Cooke et.al.(1979) for jacked tubular steel piles installed in London clay showed that the shaft resistance increased by 60% between 2 and 3 years after construction.

Wardle et.al.(1992) investigated the effect of elapsed time and maintained load on the ultimate bearing capacity of differently constructed piles founded in stiff London clay.

The site at Cannons Park in North London has 6-7m of brown London clay overlying blue London clay of considerable depth. The details of the test piles are given below.

Pile type	Diameter and material	Embedded length
Jacked pile No.1	6.4 mm mild steel tubing	6.5 m
Jacked pile No.2	6.4 mm mild steel tubing	6.5 m
Bored cast in-situ pile	170 mm diameter reinforced concrete	6.5 m
Driven pile	6.4 mm mild steel tubing	6.5 m

The jacked piles were instrumented with electrical resistance strain gauges and load cells. The bored, cast in-situ pile was installed and instrumented with vibrating wire load cells various levels and at the base. In all test piles, the initial pore pressure in the ground was monitored using piezometers inserted at selected depths and radial distances from the piles. C.R.P. tests were carried out to failure on each test pile at intervals over a period of about 3 years. In each test, the load variation in the piles and the pore pressure in the adjacent soil were monitored. No pore pressure changes were observed in the surrounding soil during the C.R.P. tests. Therefore any changes were small, or confined to an area very close to the pile shaft. The results by Wardle et.al.(1992) showed that the load capacity of all four test piles increased with time as summarised below.

Pile	Time elapsed	Shaft resistance increase
Jacked pile No. 1	Two months	28% then a further 14% three years later
Jacked pile No.2	Two months	28% then a further 20% three years later
Bored, cast in-situ	Three years	47% of the value at two months
Driven pile	One month	14%

Table 2.14: Observed increases in shaft resistance with time (Wardle et.al.1992)

Wardle et.al.(1992) reported that the increase in load capacity of the jacked and driven piles could be attributed to an increase in the shaft resistance rather than base resistance. Since no significant pore pressure changes were observed, it was considered that the increase of pile load capacity with time could be as a result of the gradual "healing" of the failure surfaces in the soil, rather than a general strength increase due to consolidation. The test results also demonstrated that maintained loads applied to the piles over long periods resulted in no additional increase in load capacity.

2.7.4 Creep settlement of piles formed in Keuper marl from pile load tests

Al-Shaikh-Ali and Davis(1975) have studied the creep-time behaviour of Keuper marl using a model pile load tested at a site near the M5/M6 Lymm interchange in Cheshire. The site had a 1m thick cover of boulder clay and weathered mudstones overlying a series of bands of partially weathered to unweathered Keuper marl mudstones. The water table was located at a depth of 2.5m below ground level. From a previous site investigation for the motorway bridge near the site, typical S.P.T "N" values at 3m depth were 135 and 432 blows corresponding to penetrations of 300mm and 225mm respectively.

A model concrete test pile 108mm in diameter by 2m long, embedded over 1.5m length, was installed into the ground by in-situ construction. The pile shaft was lined with greased polystyrene sheeting in order to eliminate shaft resistance. Load testing was carried out in 7 load cycles by jacking against suitable kentledge. The applied load and settlement were recorded throughout the test. Multi-stage consolidated undrained triaxial tests performed on samples from the pile borehole gave c' values of 14-35 kN/m^2 and ϕ' values of 36-39°.

Failure of the pile occurred in the final load cycle at a stress of 5915 kN/m^2. Using Terzaghi's(1948) bearing capacity formula for a circular footing, a back analysis was performed to evaluate ϕ'. It was found that the best-fit value of ϕ' was 42.5° and this was close to the triaxial test result of 36-39°. It was also expected that the in-situ value of ϕ' would be slightly higher than the laboratory determined value due to sampling disturbances.

At the peak load in each cycle, graphs of settlement (linear scale) against time (log scale) were plotted. At stress levels between 30-80% of ultimate bearing pressure, creep was a significant proportion of total pile settlement. In this range of stress, the variation of creep with the logarithm of time was found to be linear. At higher stress levels, the relationship was non-linear. Moore and Jones(1974) found that creep in well cemented Bunter sandstone may amount to about 20% of total settlement at high stress levels. Al-Shaikh-Ali(1971) carried out plate loading tests on zone II Keuper marl. At an applied pressure of 2800 kN/m^2, which represents the anticipated working bearing stress level in a pile system, the projected creep settlement for one year amounted to about 40-50% of the total settlement. Therefore creep can be of considerable significance in the long-term performance of a piled foundation formed in weak rock. The effects of creep on pile settlement are even greater for applied pile head loads approaching the pile capacity.

2.8 SUMMARY

Several case studies of pile load tests in Keuper marl were carried out. The most important aspects of these studies include the prediction of pile load capacity using different analytical and conventional methods. The findings generally indicate that,

a) The use of unconfined compression tests in estimating the undrained strength of the mudstone results in an underestimate of its in-situ strength by as much as 40%. Pressuremeter tests carried out in the laboratory and cube crushing tests seem to provide more reliable and consistent results.

b) Standard penetration tests provide a reasonable method of determining the in-situ strength of the marl for evaluation of bearing capacity. Cross-jacking tests in pile sockets also predict the in-situ strength reasonably accurately.

c) Effective stress methods provide reasonable predictions of the pile shaft resistance, especially when shear strength values are determined on remoulded samples

d) For given soil conditions, the contribution of creep settlements to the total long term settlement increases with the applied load as a proportion of the load capacity.

e) There is evidence that the installation of a bored pile influences the load capacity from the viewpoint of both shaft resistance and end bearing. This is demonstrated by the fact that different load tests on identical piles installed in similar soil conditions reveal varying load capacities. Drilling a pile hole, by whatever means, will result in a relief of lateral pressure on the walls of the hole. Therefore a particular design method should be judged by how realistic it accounts for the all-important factor of pile installation effects. Even with the use of bentonite during drilling to prevent water inflow into the hole, softening of the clay around the pile shaft still occurs. Based on loading tests in London clay, Fearenside and Cooke(1978) established that the use of bentonite during pile construction has no apparent effect on the ultimate shaft ultimate resistance of the pile.

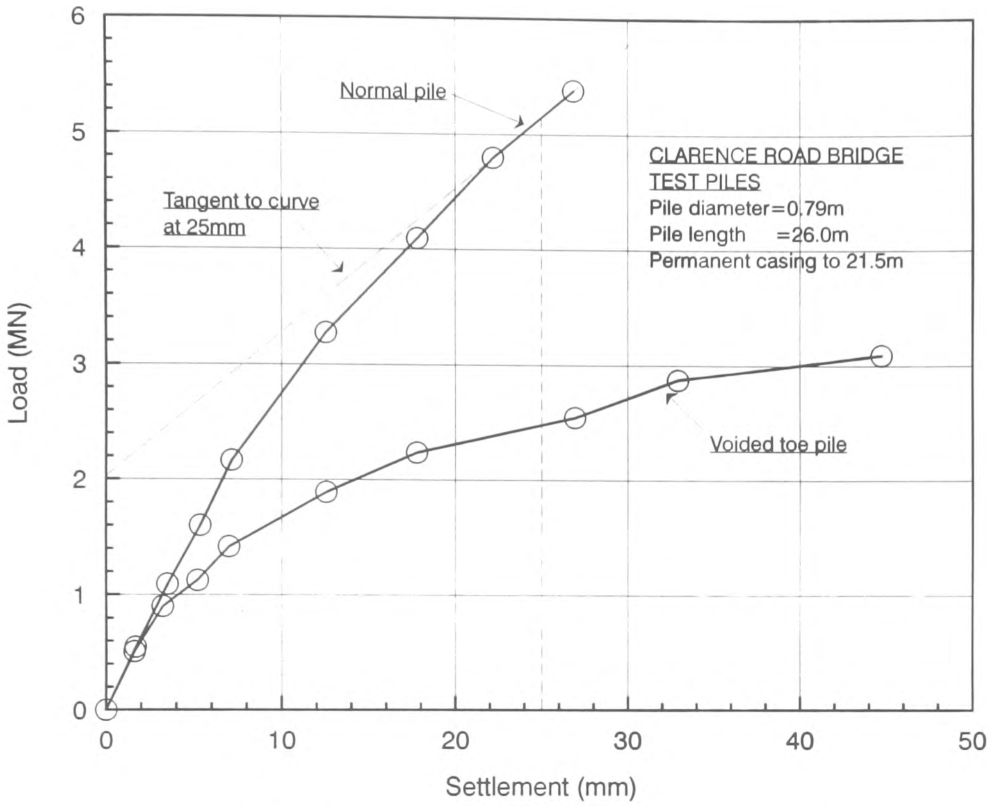

Fig. 2.1(a): Load-Displacement curves for a normal and a voided toe pile at Clarence Road bridge (Kilbourn et.al.,1988)

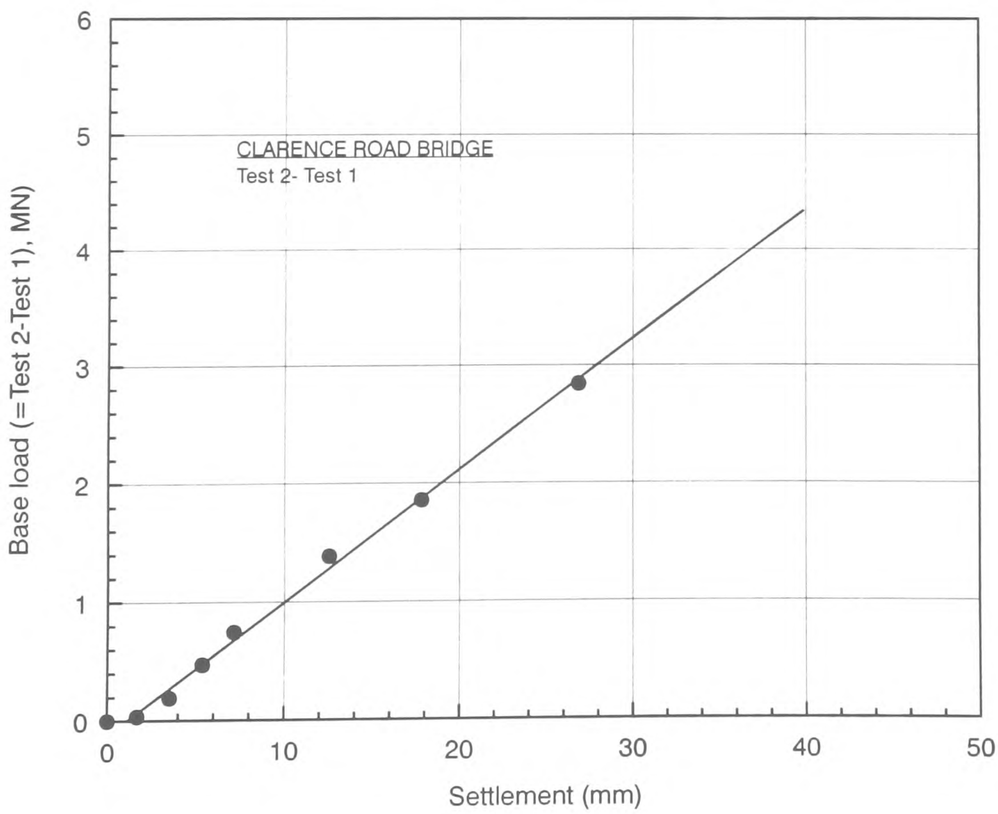

Fig. 2.1(b): Base load versus pile head displacement curve obtained from the load difference between normal and voided toe piles -Clarence Road bridge (Kilbourn et.al.,1988)

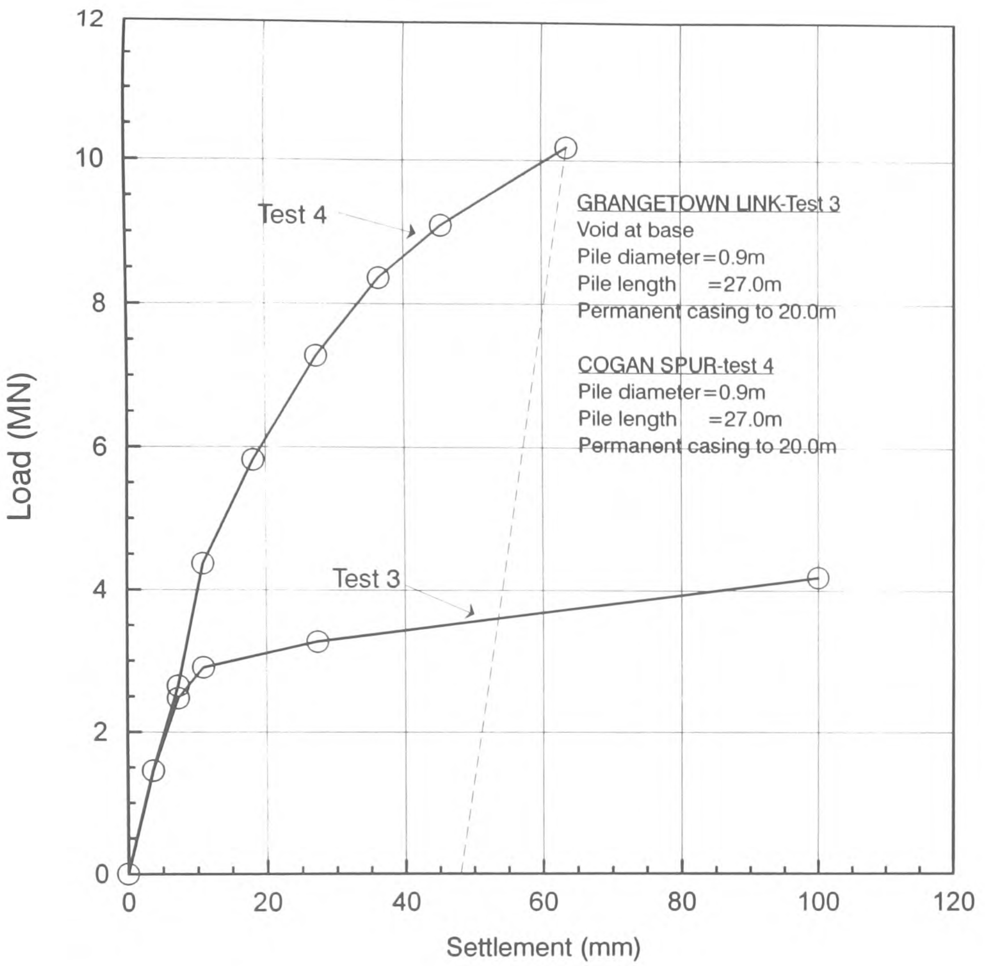

Fig 2.1(c): Load-displacement curves for a voided toe and a normal pile (Kilbourne et al,1988)

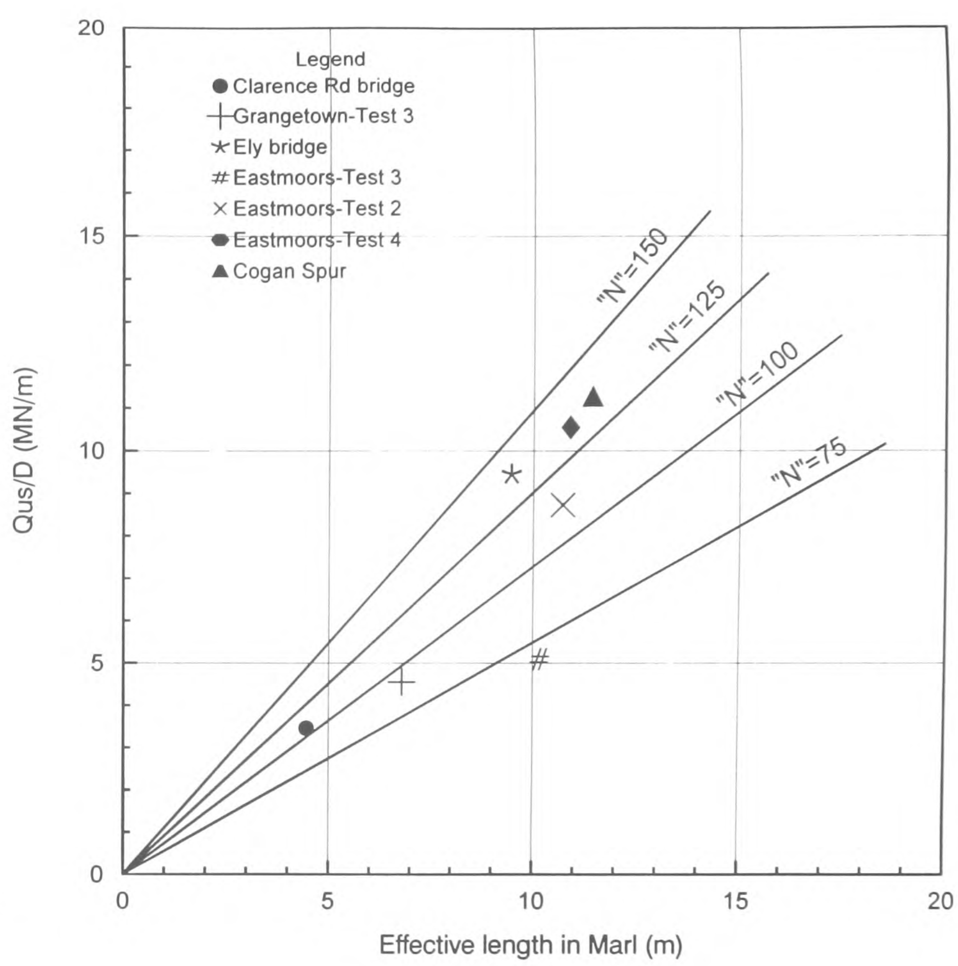

Fig 2.2 : Variation of ultimate shaft load with effective pile length in marl (Kilbourne et.al(1988)

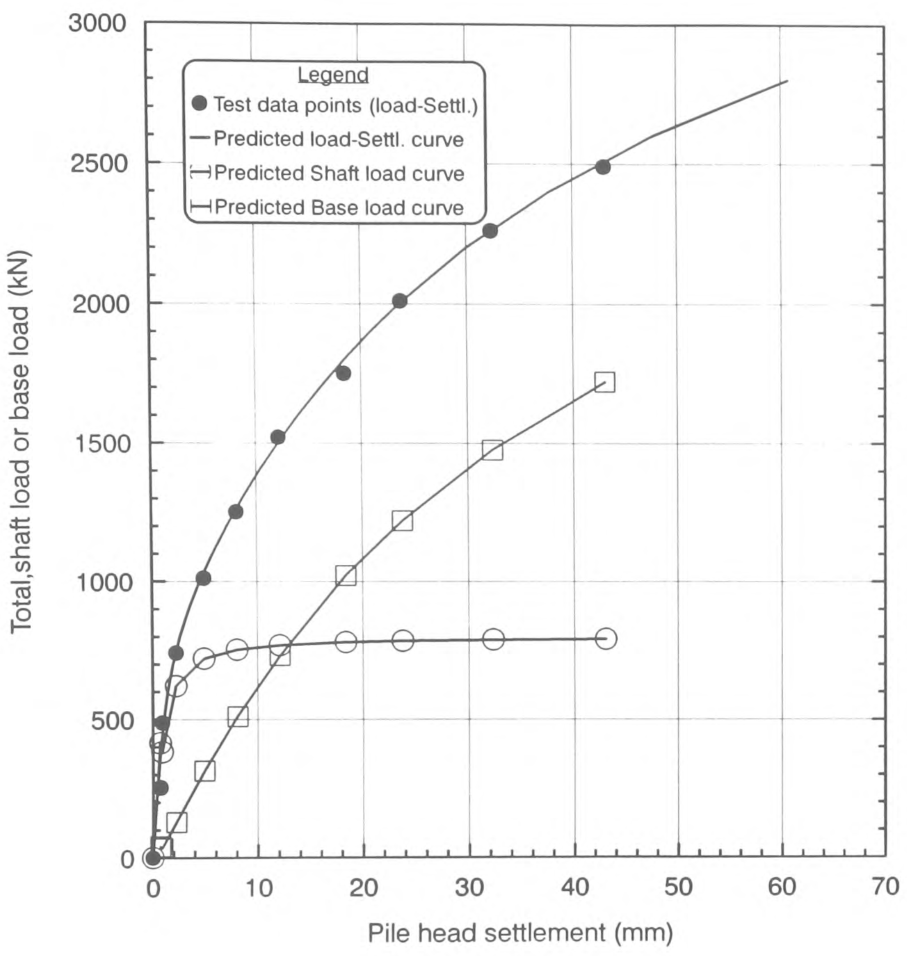

Fig 2.3(a): Comparison between observed and predicted load-settlement patterns and plots of predicted shaft and base load Vs head settlement-CFA pile in Bristol area (Fleming,1992)

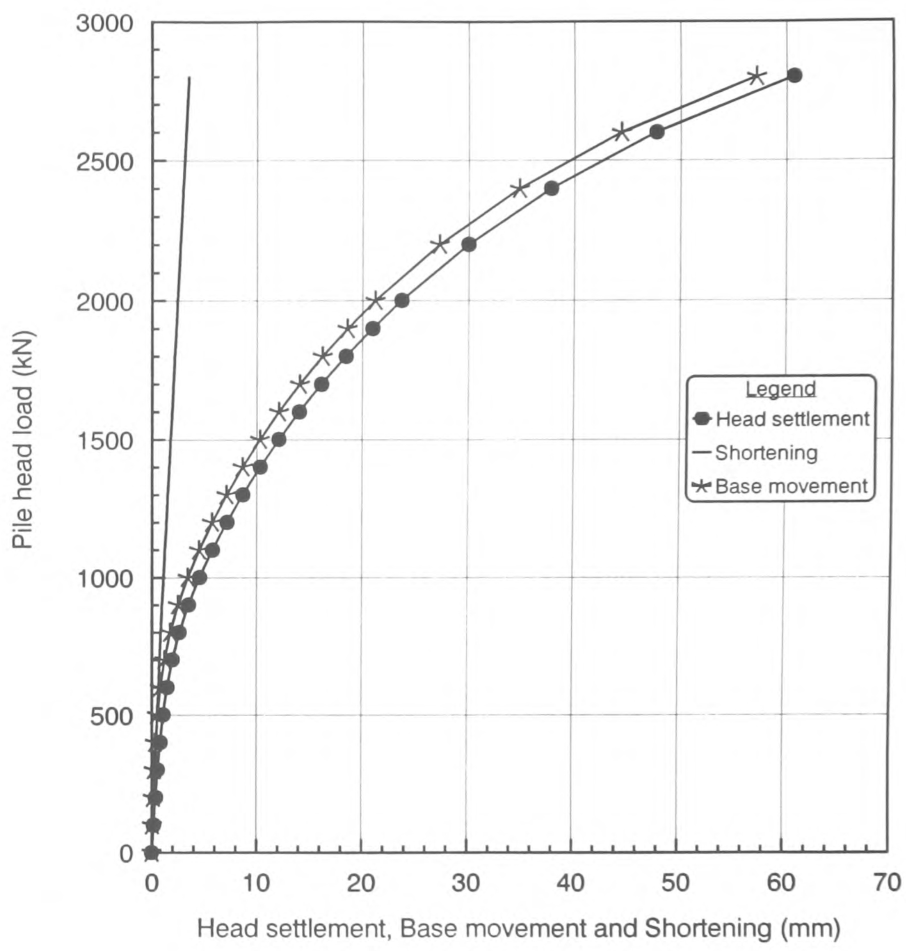

Fig 2.3(b): Predicted variations of pile head settlement,base movement and shortening with applied load for a CFA pile in Bristol area (Fleming,1992)

CHAPTER 3

GROUND INVESTIGATION AND TEST PILE INSTALLATION

CHAPTER 3: GROUND INVESTIGATION AND TEST PILE INSTALLATION

3.1 INTRODUCTION

The economical design of substructure elements requires an extensive investigation of the underground conditions at the site of the proposed development. The elements of the investigation programme usually depend on the project. For the construction of piled foundations, the ground investigation is aimed at providing adequate information to allow the geotechnical engineer to make a recommendation on the allowable load capacity of the foundation, as well as the expected settlement at working load. A load test programme may then be carried out in order to determine the ultimate bearing capacity and load-settlement behaviour, as a check on the values calculated from the soil data.

This chapter describes the programme of ground investigation, the installation and load testing of six full-scale instrumented test piles carried out as part of the Butetown Link of the South Cardiff peripheral distributor road. The main contractor responsible for the construction of the working piles carried out the installation and load testing of the test piles. The ground investigation activity was intended to provide the necessary geotechnical information for various proposed works, including the design of deep foundations in Mercia mudstone. The investigations were carried out to the instructions of the Engineer to the County of South Glamorgan.

3.2 GROUND INVESTIGATION

3.2.1 Geological description of the project area

Relevant geological survey maps indicate that the ground comprises estuarine mud and clay, which rest on glacial sand and gravel. Beneath these superficial deposits, the Triassic red marls (Mercia mudstone) are present. Little structural information is available on these bedrock materials, due to the general lack of exposure, however no major faults or other geological discontinuities are indicated. The general ground stratification profile with increasing depth is described as follows:

(i) Made ground,

(ii) Soft silty and organic clays,

(iii) Sand and gravel, and

(iv) Keuper marl.

The layer of "made ground" is 2-3m deep and consists of artificially deposited superficial materials. This layer contains a high proportion of granular material and is likely to be associated with previous developments and services in the Butetown area. Beneath the made ground layer, or directly beneath the surface in the estuarine area, lies a 10.0m thick stratum of very soft to soft occasionally firm silty clay with some pockets of silt and organic materials. Due to the presence of the river channels, the thickness of the clay decreased locally within the estuarine area. Within the Taff River channel, the clay layer does not exist. Beneath the alluvium exists a layer of variable thickness, of 3-12m, consisting of a medium dense to dense sand and gravel which contains cobbles and some boulders. The Keuper marl is present beneath the superficial material layers along the entire route. This material geologically falls under the Upper Triassic period which, in

Great Britain, is nearly always represented by continental red beds. Ever since Sedgwick imported the term “Keuper” in 1835 from Germany, the word has been used informally to refer to the lower arenaceous and upper muddy Triassic. In the South-Western part of Britain, deposits of “Keuper” are understood to be the red mudstone sequence that forms the lower division of the Mercia Mudstone Group. The upper division of this group is known as the Blue Anchor Formation (the Tea Green Marls of earlier classifications).

The marl was found to comprise very silty mudstone and siltstone with bands of fine grey/green sandstone or siltstone. The upper layers of the marl comprised highly weathered to fully weathered materials constituting weak to very weak zones III and IV marl. These generally occurred at penetrations of around 10m. There was a general increase in strength with increasing depth to zone II and zone III marl. However, the strata contained irregular beds of zone III and IV material throughout. In places, the marl was particularly weathered with zone II marl being encountered at penetrations of 25m. Other locations along the route had deep and variable weathering profiles with zone II material occurring after penetrations of only 6-7m. The marl generally had variable composition, containing regular and irregular bands of both weak and strong materials.

3.2.2 The ground investigation process

3.2.2.1 Introduction

The process of designing piled foundations to transmit and resist large forces requires a thorough understanding of the soil properties of the load bearing strata and any such strata which will influence the performance of the structure. The intention of the ground investigation was to provide the engineering parameters of the Keuper marl and the superficial deposits, for use in the detailed design of large diameter bored pile foundations. The investigations were specifically designed to assess the following:

(i) The nature of the superficial deposits

(ii) The depth to the Keuper marl surface

(iii)The variation of the weathering profile of the Keuper marl

(iv) Groundwater details

(v) Geotechnical properties of the superficial deposits and of the Keuper marl.

3.2.2.2 Test boreholes and drilling through superficial deposits

A detailed site investigation for the Butetown link project was carried out along the route of the proposed road by Messrs Norwest Holst Soil Engineering(1990). A total of 146 boreholes, initially 200mm in diameter, reducing to 120mm, with depths of up to 58m were drilled along the proposed route. For various reasons, several of the designated borehole positions were relocated and others completed using rotary probing equipment.

Each hole was commenced by standard shell and auger equipment utilising both 200mm and 150mm diameter casings. Care was taken throughout in order to ensure that the casing was not advanced ahead of the materials to be sampled or tested. This traditional drilling technique was effective and provided a means of boring through the relatively weak material overlying the Keuper marl. In addition it enabled rotary drilling methods to be carried out down the same hole. The cable Percussion drilling rig was equipped with tools to enable the recovery of undisturbed samples of cohesive strata and carrying out standard penetration tests. Undisturbed samples of 102mm diameter were obtained where suitable cohesive materials were encountered. These were sealed with wax to prevent moisture loss before being transported to the laboratory for testing. Disturbed samples of the materials encountered were obtained and these were placed in sealed jars or large polythene containers for transport to the laboratory.

Penetration tests were carried out using split spoon or solid cone samplers provided with the cable percussion drilling equipment. In order to obtain an indication of the in-situ properties, the Standard Penetration Test (BS 1377 test 19) was carried out within the granular materials and the Keuper marl bedrock, in the boreholes being advanced, using both percussion and rotary drilling. The results of these tests were included on the borehole logs in the form of "N" values or as blow counts for a specified penetration. High blow counts were observed in the upper soil layers when the penetrometer struck larger obstructions within the materials.

3.2.2.3 Drilling through the Keuper marl

Some 102 of the shell and auger boreholes were temporarily cased on completion in order to allow extension into the underlying bedrock by rotary core drilling techniques. These holes were up to 70m in depth below ground level. Once the surface of the Keuper marl was established, coring was generally carried out using a double tube swivel core barrel fitted with either tungsten or diamond tipped bits suitable for providing 76mm diameter cores. Drilling was also carried out using foam or water as the flushing medium in order to provide a gentle cutting action and to increase the stability of the borehole walls.

Good core recovery was generally achieved using the drilling method described. However, some core losses were experienced. This was attributed to the variability of the Keuper marl, which contained bands of both weak clayey material and competent rock. In areas of core loss, data on the in-situ strength was provided where practical by the standard penetration test.

For the main river Taff crossing where a notably weak zone was identified within the Keuper marl strata, larger diameter core drilling, of 112mm and 92mm, was undertaken. Mud was used as the flushing medium and coring was supplemented by the use of a specialist triple barrel for selected use in the weak areas. Where possible, representative samples of the bedrock materials were taken from the core boxes and sealed in cling film and wax to allow further testing in the laboratory.

Calliper tests were undertaken in the boreholes notably through the layers of weak materials located below a marker band of siltstone. This test was to investigate the possible presence of voids in this area.

3.2.2.4 The "marker band" at the river Taff estuary section

A consistent feature was observed in all boreholes drilled at the Taff estuary section of the test area. This was a strong grey green sandy siltstone, with a general thickness of 0.4m. It was directly overlain by up to 4m of moderately strong occasionally strong red brown sandy siltstone. This prominent stratum, which was generally logged as zone II marl, was referred to as "the marker band". It was noted that, above the marker band, the transition from weathering zones IV and III into the moderately strong siltstone was generally very abrupt. A persistent feature observed in many of the boreholes was a brecciated zone, up to 0.5m thick, below the marker band. This zone composed an irregular assemblage of up to coarse gravel sized siltstone fragments, frequently cemented with calcite. This zone was referred to as "the weak zone". At depths below this zone, the rock quality increased, with Keuper marl zones II and II being encountered. It was expected that piles placed in the vicinity of the "weak zone" would experience additional settlement.

3.2.2.5 Groundwater observations

A complete record of the groundwater conditions encountered during drilling is given on the borehole logs. In order to provide detailed information on the groundwater conditions, water records were taken over tidal cycles with the borehole casing sealed at various levels. A number of standpipe piezometers were also installed. The permeability of the upper clay gravel and underlying marl was assessed from both falling and rising head permeability tests within the borehole casing. Falling head tests were also undertaken in several standpipe piezometers after a period of 3-4 weeks in which the piezometers were allowed to stabilise. Packer permeability tests were carried out within the marl notably in the boreholes formed in the river Taff in order to assess the hydro-geological conditions and to investigate further a permeable/porous "weak" zone identified during drilling.

The ground water records made were those encountered at the time of the investigation and might not be representative of the actual state which may prevail at other times or in large excavations. Seasonal and tidal variations of the ground water level were also expected to occur, hence the water levels measured during drilling would not necessarily be constant.

3.2.2.6 Logging of Keuper marl cores

Engineering geologists were maintained on site in order to allow assessment of conditions as the works proceeded, to ensure that the cores were logged and sampled as soon as possible after drilling, and at moisture contents as near as possible to natural moisture contents. Once the rotary cored holes had been drilled, the core-liner was split and, as a first step of the logging process, a photographic record of the cores was taken prior to logging and sampling, with a master copy of the photographs having been presented to the Engineer. On completion of the engineering classification of the cores, a video record of the Keuper marl was produced. This was deemed necessary due to the susceptibility of the Keuper marl matrix to degradation during storage. It enabled an accurate record to be kept of the freshly drilled cores. All this information was made available to the design engineers and the contractors tendering for the works. The video process recorded brief descriptions by an engineering geologist where the Keuper marl cores were physically impacted with a hammer or broken by hand by the geologist.

The Keuper marl strata encountered in each borehole were classified in accordance with the methods stipulated in BS 5930 (1980). In addition, the weathering zone classification system proposed by Davis and Chandler(1973), as indicated in the CIRIA reports numbers 13 and 47, was adopted. The site investigation report used this classification system extensively, with parameters being given for each weathering zone or sub-zone. It was noted that there was considerable variation with depth relating to the degree of weathering, there being a complete intermixing of the zones which did not follow the envisaged pattern of a decrease in weathering with increasing depth.

After logging and sampling, the cores were transported to the contractor's laboratory for storage or for further examination as appropriate, before being returned to the South Glamorgan County Council for long-term storage and for reference purposes.

3.2.3 In-situ and laboratory soil tests

A programme of laboratory testing was agreed between the site investigation contractor and the supervising engineer. The standard penetration test was carried out within the granular materials by percussion and rotary boring in order to assess the in-situ properties of the soils. The following laboratory tests were undertaken on the superficial soil strata, in accordance with British Standards B.S.1377(1975): (1) Moisture content (2) Atterberg Limits (3) Particle size distribution (4) Organic tests (5) Chemical tests (6) Consolidation (7) Triaxial tests: Undrained, Consolidated drained and Consolidated undrained triaxial tests (8) Permeability tests in conjunction with oedometer tests, to determine the horizontal stress coefficients.

Due to the fractured nature of much of the Keuper marl strata, it was not possible to obtain undisturbed material of the weathered marl in sufficient quantities to enable enough tests to be carried out to provide representative average results. Type U100 samplers only provided class 3 samples and thin walled samples were found to be impractical owing to the danger of damage. Therefore, the strength of the more fractured materials was determined on site by the use of the point load test. These tests were carried out according to the procedure given in the Geological Society Engineering Group working party report dated 1970. The size correction for point load testing was based on the values determined for T500.

Further rock testing was carried out to supplement the field point load strength tests. Laboratory point load tests were undertaken as per the procedure used in the field tests. A small number of unconfined compressive strength tests were carried out in accordance with the methods specified in the Geological Society Engineering Group working party report dated 1970. Difficulty was experienced in preparing samples of the upper marl, due to the incipient fractures, which resulted in sample disintegration. Therefore, much of the testing was carried out on the more competent solid layers.

3.3 ANALYSIS OF BOREHOLE DATA

3.3.1 Introduction

The standard engineering description of rock strata is based on (a) colour, (b) fracture, (c) weathering state, (d) particle size, (e) rock name, and (f) strength. The CIRIA report No. 47 gives the strength data and other engineering properties of Keuper marl according to weathering zone classification only. In the present work, the information from the test boreholes is analysed with the aid of a computer spreadsheet to study the relationships between the measured strength data and the physical properties of the soil strata. This enables an investigation to be made of the influence of one or more physical properties of Keuper marl on its strength, based on a database of all borehole records available. Where a large amount of test data is available, it is a simple matter to carry out a statistical analysis on the data to predict the strength of Keuper marl based solely on core description.

3.3.2 Database of borehole records

The classification and properties of the Keuper marl have been established by analysing the strata descriptions, in-situ and laboratory test information given from 85 boreholes and are listed in the Appendix (Table A.1). The test sampling depths and the results of any in-situ and laboratory tests are given alongside the strata description. This information has been transferred from the site investigation factual report into a computer data file. It covers borehole numbers 49 to 128A, which had depths ranging from 30 to 50m. Borehole numbers 1 to 48 were shallower and provided information on the superficial deposits only. No laboratory or in-situ results were available from borehole numbers 129 to the last borehole (No. 136).

The description of the various Keuper marl strata encountered in each borehole was carried out according to the guidelines given in BS 5930 (1980). In addition, each stratum was classified in terms of the weathering zone. Much of the strength information on the Keuper marl was assessed from the standard penetration (S.P.T.) tests and field/laboratory point load tests.

3.3.3 Standard Penetration Test (S.P.T.) data

In the S.P.T. test, the type of drive rod end has been denoted by "split" to mean a split sampler type; and by "cone" to signify that the split sampler was replaced by a standard cone shoe. Where the required total penetration of 450mm could not be achieved, the number of blows corresponding to the final penetration reached has been recorded in the form $\frac{"N"}{p}$ where N is the blow count and **p** is the maximum penetration reached.

In order to standardise the S.P.T. "N" values from different boreholes, the overburden pressure and length of drill rod need to be taken into consideration. Liao and Whitman(1986) have catalogued six methods for correcting measured "N" values for overburden pressure. In the U.K, the most commonly used correction method is that of Gibbs and Holtz(1957), although it is limited to the degree of overburden pressure. This method has been adopted in correcting the observed "N" values.

3.3.4 Point load test results

The point load strength test is generally used as a simple procedure for field classification of rock materials but can be closely correlated with the results of uniaxial compression. The "Point-Load index" I_s, was first calculated from I_s=P/D^2 (where P is the failure load and D is the distance between the platen contact points). This index was then corrected to a reference diameter of 50m using the charts given by Turk and Dearman(1986). The corrected point load index values were arranged in ascending order and the median value determined by systematically deleting highest and lowest values until only two values remained. The average of these two values was taken as the median point load index. The median point load index was then converted to the equivalent uniaxial strength by multiplying by a factor of 24. Hence the undrained cohesion was obtained as half of the uniaxial strength.

The test method is not dealt with in a British Standard, however a detailed experimental procedure and further literature is given in Broch and Franklin(1972). The tests were carried out in accordance with the methods indicated by Norman Brooke, in the international Journal of Rock Mechanics, Mining Science and Geomechanics Abstracts relating to size correction for point load testing, with the values determined for T500. The core specimens, which were in the form of cylindrical cores or irregular lumps, were broken by the application of a concentrated load using a pair of conical platens.

In the "axial" test, the load was applied at the ends of the specimen, whereas in the "diametral" test, the specimen was inserted in the test machine such that the platens make contact along a core diameter. The diametral test was used for core specimens with length/diameter ratio greater than 1.4, while the axial test was applied to core with length/diameter ratio of 1.05-1.15. Long pieces of core were tested diametrically to produce suitable lengths for subsequent axial testing.

3.3.5 Soil description using digital codes

In order to investigate the relationship between the physical properties of Keuper marl and its measured strength values, a spreadsheet database was established to analyse the data from all the 136 borehole logs. The method involves identifying the full description of each stratum by a sequence of 21 digits comprising 7 groups of 3-digit numbers. The seven groups of numbers represent respectively the following properties: (a) colour, (b) weathering state, (c) grain size, (d) fracture state, (e) rock name, (e) strength and, (f) weathering zone. For example, the code number 100|220|310|420|500|605|720 identifies the stratum as (i) *Red brown, (ii) highly weathered, (iii) clayey, (iv) highly fractured, (v) silty MUDSTONE, (vi) very weak to weak, (vii) Keuper marl zone III-IVa.*

Tables 3.1-3.3 give 3-digit identification codes used to describe given physical properties of a soil stratum. The first digit denotes the physical property being considered. The next two digits represent descriptions under the physical property in consideration.

Colour (100-199)	
Description	**Code**
Red brown	100
Red brown and locally grey green	120
Grey	130
Grey green	140
Dark grey	150
Light grey	160
Dark grey green	170
Red brown and grey	180

Fracture state (200-299)	
Description	**Code**
Fragmented	200
Fragmented to fine gravel sized	205
Fragmented to fine to medium/ coarse gravel sized	210
Completely fractured to coarse gravel and cobble sized	215
Highly fractured	220
Highly fractured to fragmented	225
Highly to moderately fractured	230
Moderately fractured	235
Moderately fractured to fragmented	240
Moderately to slightly fractured	245
Slightly fractured	250
Intact to slightly fractured	255
Intact	260
Intact to moderately fractured	265

Table 3.1: Strata description codes for Colour and Fracture state

Weathering state (300-399)	
Description	**Code**
Completely weathered	300
Highly to completely weathered	305
Highly weathered	310
Moderately to highly weathered	315
Moderately weathered	320
Moderately to slightly weathered	325
Slightly to highly weathered	330
Slightly weathered	335
Fresh to slightly weathered	340
Fresh	345

Grain size (400-499)	
Description	**Code**
Silty	400
Sandy	410
Clayey	420

Rock name (500-599)	
Description	**Code**
MUDSTONE	500
SILTSTONE	510
CLAY	520

Zone (700-799)	
Description	**Code**
IVa-III	700
IVa	705
II-IVa	710
III-IVa/II	715
III-IVa	720
III	725
III-II	730
II-III	735
II	740
II-I	745
I-II	750
I	755

Table 3.2: Strata description codes for Weathering state, Grain size, Rock name and weathering Zone

Strength (600-699)	
Description	**Code**
Very weak	600
Very weak to weak	605
Weak	610
Weak to moderately weak	615
Moderately weak	620
Moderately weak and moderately strong	625
Moderately strong	630
Moderately strong to strong	635
Strong	640
Weak with moderately strong lithorelicts	645
Very strong	650
Stiff	655
Extremely strong	660
Firm	665

Table 3.3: Strata description codes for strength

3.3.6 Statistical analysis of test data using digital codes

The above coding system enables the test results on rock cores from various levels to be related to the engineering description of the stratum present at that level. The method enables rapid statistical analyses to be made, which instantly provide information such as the average strength value and frequency of a given stratum, as deduced from as many borehole logs as are available. In addition, the soil test results from a stratum of given description can be analysed taking into account the influence of overburden pressure.

It is possible to assess the influence on strength of weathering, or in combination with one or more additional physical properties. This method was used to study the strength data from the most frequently encountered strata. The classification of point load strength values available from the test summary sheets was carried out on the basis of these strata descriptions and is shown in Fig. 3.1. It is seen that there is a high degree of scatter in the results and no discernible correlation can be said to exist between the engineering description of a stratum and its point load strength.

In Fig. 3.2, the point load data have been classified according to only the strength descriptions of the strata. These descriptions range from *very weak* to *extremely strong*. The test data still highly scattered, with some strata classified as weak apparently having higher strengths than strong strata, and vice versa. Similar scatter of point load data is also observed in Fig.3.3, in which the data have been matched according to weathering zones classification. An analysis of "N" was also carried out based on weathering zone classification only and this is given in Fig. 3.4. The scatter is not as great as with point load values and it is seen that "N" decreases with increasing weathering.

Any number of borehole logs can be analysed using this method. Present experience shows that the statistical analysis of relevant soil parameters are served more effectively by a detailed selection and targeted site investigation procedure, than choosing an all embracing (large volume) type of study, for which the cross-correlation of data becomes unjustifiable.

3.4 FULL SCALE FIELD TEST PILES

3.4.1 Introduction

A number of case histories of pile load tests in Keuper marl are presented in the literature review. In these case studies, pile load capacity predictions are obtained from soil mechanics considerations and compared against the results of load tests. The load tests are generally carried out with only minimum instrumentation to assess the load-settlement behaviour of the test piles. For the Butetown Road link contract, a further initiative was taken in which six test piles were fully instrumented and load tested in an effort to significantly increase the awareness and understanding of soil-pile interaction in the Keuper marl.

The test piles were 0.9m in diameter, with lengths varying between 28 and 31m. Permanent steel casings were installed along the upper portions of the piles passing through superficial deposits. Therefore the embedded pile lengths in the Keuper marl were approximately 12m. The instrumentation comprised vibrating wire strain gauges and extensometers embedded at predetermined locations within the pile concrete. Load cells were also installed at the bases of the test piles. The test piles were installed and tested near the proposed sites of the actual working piles for the foundations of the major structures forming part of the Butetown road link.

3.4.2 General construction of the test piles

The first pile, TP1, because of the contract programme, was undertaken without instrumentation. This test pile was formed in a similar manner to that used during previous piling contracts in the area. It is typically termed a "voided toe" test pile, where as the name suggests, the pile was initially provided with a voided base and load tested to establish the skin resistance. Before subsequent load tests, the pile base was grouted with cement and, after curing, a traditional load test was performed on the simulated full test pile. The results were then used to try and isolate the contribution made by skin resistance and end bearing to the total load capacity of the test pile.

The second pile, TP2, was instrumented except that the base load cell proved too difficult to place. This was due to not only insufficient tolerance in its diameter to that of the steel pile liner but also some possible effects of displacing the drilling fluid. Load testing of this pile was conducted in 4 cycles but not taken to failure. Test piles TP3 and TP5 were successfully installed with full instrumentation and load tested in 5 and 6 load cycles respectively. The failure points were clearly shown and the load-settlement curves depicted clear maximum loads.

Test pile TP4, although formed with full instrumentation, was found to have interference between the liner and the pile shaft. Vibrations caused by earth-moving plant which suddenly erupted close to the site resulted in uncertainty as to whether the pile shaft was formed as intended. Thus a very careful interpretation of the results was required. The test pile was tested in 5 load cycles to failure.

The last test pile, TP6, was successfully instrumented and load tested in a series of 4 compressive load cycles and then subjected to withdrawal loading. A full failure criterion was not reached in either test.

3.4.3 Forming the borehole for a typical test pile

Figures 3.5 to 3.10 illustrate the layout and instrument locations in each of the completed test piles, including descriptions of the ground strata encountered. A full description of the instrumentation needed is given in section 3.5. The following procedure was adopted while forming the pile shaft:

A hole was drilled through the superficial deposits to a predetermined depth (generally about 20m) just below the Keuper marl surface. This was achieved by first driving a 1.3m diameter by 10mm thick mild steel tube to the required depth of the hole. The function of this temporary casing was to prevent the superficial deposits overlying the Keuper marl from collapsing and entering the hole. In addition, this ensured that there was no soil-pile contact along the upper pile portion passing through the superficial soils. Therefore, this enabled the monitoring of load transfer within the pile length embedded in the Keuper marl, which was the material of interest.

Having excavated to the bottom of the steel sleeve, an inner mild steel casing 900mm in internal diameter by 10mm thick was centrally lowered to the bottom of the hole. The casing was then vibrated into the marl and seated at a distance of approximately 1-2m below the top surface of the marl. For the actual working piles, this inner casing was permanently installed so as to prevent "wash out" if substantial hydrostatic pressure was anticipated.

Drilling under bentonite in the marl, within the inner casing, was carried continued to the required length of the pile. The size of the completed borehole was logged using a mechanical calliper along the entire length of the shaft. According to investigations carried out by Barker and Reese(1970) and Fearenside and Cooke(1978) bentonite has no detrimental effects on pile load bearing capacity. Rather, it is the pile/soil properties and the installation technique, which determine the performance of a pile. Bentonite has the property of remaining in suspension in water to form a stiff gel when allowed to become static. However, stirring or pumping agitates the slurry and causes it to have a mobile fluid consistency. When used to support granular soil, the bentonite slurry penetrates the borehole walls and gels there to form a strong and stable "filter-cake". In a clay soil, there is no penetration of the slurry, but the hydrostatic pressure of the fluid prevents collapse at places weakened due to fissures.

3.4.4 "Cleanliness" at the pile base level

The bottom of a borehole for a working pile should not contain any accumulated gravel, which can have a significant effect on the performance of the pile at working loads. The effect of the loose soil present beneath a pile base is to result in relatively high pile movements during the initial stages of base resistance development. However, ultimate end-bearing resistance remains unaffected, because the loose soil will have been fully compressed as the base pressure increases.

The formation of the test piles was expected to continue even under wet borehole conditions since some inflow of groundwater was anticipated. In some cases water could be evacuated, depending on the permeability of the marl strata below the temporary casing and the effectiveness of the seal formed by the casings. In any event care was taken to balance any water pressure by the use of bentonite slurry.

The procedure for cleaning a pile toe involves the use of a bucket with a "slotted" bottom. This is done immediately before placing the reinforcement cage. The bottom of each borehole was tested for cleanliness by measuring the depth with a heavy drop weight attached to the end of the tape. The bore was plumbed and the depth recorded as soon as it had been bottomed out. This process was carried out before installing the reinforcement cage.

After the reinforcement cage was installed, the depth was measured again. Based on experience, up to 500mm thickness of debris was expected to have collected at the bottom of the hole. If the shackle pin slowly sank into the debris, then it was probably slurry, which could simply be lifted out during concrete placement. If the shackle did not sink into the debris, then it was more likely to be a gravel-sized mix, which could stay in place during concrete placing. In this case a suction pump was used to remove the material or alternatively, the material was stirred up into suspension using an air-line, before pouring concrete.

3.4.5 Pile reinforcement and concrete placement

Whilst drilling of the pile shaft was in progress, the steel reinforcement cage for the pile was assembled near the site of the borehole. The reinforcement comprised 18 no. 32mm diameter H.Y.S bars arranged at equal spacing and running the full length of the pile. A concrete cover of 75mm was provided between the reinforcement and the inside surface of the steel casing. The reinforcement were bound together at the periphery by T12 steel bars arranged at equal spacing and welded to the main bars.

The various instruments were installed on the reinforcement cage before the latter was lowered into the hole. A base load cell was installed at the bottom of the hole, (Plate 3.1) and a concrete plug 500mm deep placed over it. In order to protect the instrumentation and to minimise the loosening of material from the sides of the bore, which might cause the cage to fall to the bottom of the hole, the full length of the reinforcement cage was carefully lowered into the hole. (Plate 3.2). Grade 50 normal-weight concrete was specified for the actual contract piles. In order to maintain the same material properties for test piling, the same concrete mix type was used in the test piles. Concrete was placed using a "tremie" pipe, 250mm in diameter, in order to avoid segregation and contamination. A hopper was provided at the top of the first tremie pipe section. At each stage, the required pipe length was achieved by screwing additional segments. Because of the small diameter of the tremie pipes and their long lengths (up to 31m), the concrete mix had to be designed to give a minimum workability of 150mm slump. For each pile hole, concrete placement was commenced not later than 12hrs after drilling.

Sample concrete test cubes and cylinders were prepared and tested at the University of Glamorgan's civil engineering laboratories. The tests were carried out in order to determine the compressive strength and the static modulus of elasticity of the concrete. The test piles were cured, under natural conditions for a minimum of 14 days, before commencement of load tests.

3.4.6 Problems encountered during construction of test piles

The installation of large diameter, bored, cast-in place piles is subject to a wide range of difficulties. The construction problems arising with bored piles have been described by Pandey(1967). Even during placement of workable concrete in a dry open hole, large unfilled voids or pockets of clay and silt may still be created due to a number of causes.

In the U.K, the current practice is to use the guidelines given in the Institution of Civil Engineers Specification for Piling(1988) in order to overcome as many of these difficulties as possible. Additional information and guidance on the installation procedures for bored piles is also given by Thorburn & Thorburn(1977).

3.5 MONITORING OF PILE RESPONSE UNDER LOAD

3.5.1 Instrumentation and test schedule

The following instruments were installed at selected positions in each test pile:

i) Vibrating wire strain gauges,

ii) Rod extensometers,

iii) Pile head displacement transducers, and

iv) Base load cell.

All instruments were electronically connected to a computerised data logger and monitor situated in a small cabin close to the site. The instruments were supplied, installed and monitored by the Geotechnics division of the Building Research Establishment (B.R.E.), Garston, Hertfordshire. Figures 3.5-3.10 illustrate the locations of these instruments as deployed in test piles TP2-to TP6.

The general specifications for each of the instruments the total number required for a given test pile are shown in Table 3.4. These instruments are discussed in more detail in the next section. Table 3.5 lists the various instruments deployed at specific locations with respect to each test pile.

INSTRUMENTATION REQUIRED FOR ONE TEST PILE			
INSTRUMENT	TYPE	QUANTITY	RANGE
Load cell (inclusive of cable from load cell to monitoring unit	Employing a strain gauge sensing unit	1	7500 kN
Embedment strain gauge (inclusive of cable from load cell to monitoring unit)	Vibrating wire strain gauge	12 for TP2 15 for TP3 to TP6	±1500 microstrain
Extensometer (Complete with protective tubes and connecting cable to monitoring unit	Employing LVDT or similar	3 for each pile and in addition 3 short length gauges in TP6	±25 mm

Table 3.4: Instrumentation required for each test pile

Pile	Length	Instrument level No.							
No.	(m)	1	2	3	4	5	6	7	Base
TP2	28.81	VW	VW E1	VW E1	VW E1	*	*	*	-
TP3	30.00	VW	VW	VW E1	VW E1	VW E1	*	*	LC
TP4	24.35	VW	VW	VW E1	VW E1	VW E1	*	*	LC
TP5	30.00	VW	VW	VW E1	VW E1	VW E1	*	*	LC
TP6	31.55	VW	VW	VW	E1 E2	VW E1 E2	E2	VW E1	LC

<u>Legend</u>

VW *Vibrating wire strain gauge*
E1 *Extensometer running from pile head level to this level*
E2 *Short length extensometer (1m gauge length)*
LC *Load cell*
\- *No instrument installed at this level*
* *Instrument level does not exist in this pile*

Table 3.5: Types of instruments installed in the test piles

3.5.2 Vibrating wire strain gauges

A vibrating wire strain gauge is an electrical device consisting of a wire stretched between two points. The strain gauge is mechanically clamped to a structural element such as a steel bar, and can be embedded in concrete when placed inside a protective tube. When vibrated by a small electromagnet, the wire produces a frequency proportional to the tension in it. Any load change in the structural member causes a change in tension, that in turn causes a change in the frequency when the wire is vibrated. To determine the frequency of vibration, the time it takes for the signal generated by the vibrating wire to go through 100 cycles (peak to peak) is measured. Minor seepage of water into the cable containing the strain gauge does not affect the frequency of the signal being generated by the vibrating wire. Nevertheless precautions should be taken to prevent the enclosing tubes from being completely filled with water.

The vibrating wire strain gauges used for these test piles had 150mm gauge lengths and could measure up to 1500 micro strain range. At selected levels, three strain gauges were installed in a 120° pseudo-rosette arrangement. The strain gauges, which were enclosed within protective tubes, were suspended from the reinforcement cage and embedded within the pile concrete (Plate 3.3).

3.5.3 Extensometers

Extensometers were deployed for the measurement of pile shortening at various depths. This was intended to supplement the information provided by the vibrating wire strain gauges and the load cells. The extensometers used in the test piles comprised a Linear

Variable Displacement Transformer (LVDT) which formed the movement sensing transducer. The transducer was fitted at the bottom of the reference rod, which was suspended from the pile head. All extensometers installed in the test piles were accurate to 0.001mm and were embedded in the concrete. For each test pile, three number rod extensometers were longitudinally installed so as to run from the pile head level to certain selected depths along the shaft (Plate 3.4).

It was noted that cracks that develop in the concrete as it is stressed could significantly affect the strain levels measured. Therefore if two cracks are located outside the gauge length covered by a typical vibrating wire strain gauge, the strain gauge will monitor low levels of strain. Conversely, a crack developing in the middle of a strain gauge will cause it to monitor large strain levels. Hence great care is needed in interpreting the strain readings for concrete under tensile loads. For test pile TP6, which was tested in three cycles of upward, additional short length extensometers (1m long) were installed at certain levels within the shaft. This enabled the monitoring of strain over a relatively larger section of pile to include the effects of cracks. It was anticipated that the 1m gauge-lengths would not be significantly influenced by the crack locations within the tensile zone of the composite pile structure.

3.5.4 Pile head movement monitoring

Before concrete was placed in the pile hole, great care was taken in order to ensure that all instruments were correctly identified and connected to the computer logging facility located at the data monitoring cabin. The gap between the inner and outer steel casings

(Plate 3.5) of the test pile was covered in order to prevent any soil or other objects from falling into the hole.

A reference frame was supported on two foundations placed sufficiently far from the test pile and reaction assembly, typically 3 to 5 pile diameters, so as not to be affected by ground movements caused by pile loading (Plate 3.6). Electrical displacement transducers were fixed to the frame and bearing on the top of the pile head. The transducers were accurate to 0.01mm, hence complying with the minimum requirement of 0.1mm according to BS 8004(1986).

3.5.5 Pile base load cells

The load cells were manufactured, calibrated and supplied by BRE. A typical one incorporates vibrating wire sensing elements inside a sealed loading unit. By calibrating the change in frequency of the wire against changes in load applied to the tube, it was possible to use the instrument as a load-measuring unit. Each load cell comprised six vibrating wire-sensing units encased in a cylindrical concrete block, which was provided with an inflatable rubber gasket around its perimeter. When the load cell had been placed in position, using the Kelly bar of the drilling rig, the rubber gasket was inflated in order to prevent fresh concrete from flowing along the sides.

3.6 PILE LOAD TESTS

3.6.1 Load test arrangement

A 2000 tonne load test rig (Plate 3.7) specially developed by the main piling contractor Davis Middleton and Davis Ltd (Cardiff) was used to load test the piles. The frame comprised two main beams situated on opposite sides and stiffened with smaller secondary members in the transverse direction. The ends of the main beams were anchored to four tension piles formed at the corners of the frame. Load was applied to the pile head via a system of four 500 tonne hydraulic jacks symmetrically placed on the pile head so as to apply axial load to the pile (Plate 3.8).

3.6.2 Load test procedure

Each pile was tested under maintained load (ML) conditions. The number of load cycles varied from one test pile to another. In each load cycle, the pile was loaded in increments (or unloaded in decrements) between 500kN and 1500kN. Each load increment or decrement was maintained until the rate of change in pile head settlement with time had fallen to less than 0.25mm/hr, in compliance with BS 8004 (1986). Tables 3.6 and 3.7 give the proposed loading schedule for a typical test pile (TP3).

At each load increment or decrement, and at intervals of 10 minutes, the magnitude of the applied load and the steady state readings on the instruments were automatically logged and stored by computer, which also continuously recorded time. The data logger was housed in a cabin located adjacent to the test pile site (Plate 3.9).

LOAD CYCLE 1				LOAD CYCLE 2			
Increments (kN)		Decrements (kN)		Increments (kN)		Decrements (kN)	
Load	Time held	Load	Time held	Load	Time held	Load	Time held
500	Minimum	5000		500		8000	until
1000	1 hr or	4000	until	1000	Minimum	7000	cessation in
1500	cessation in	3000	cessation in	2000	1 hr or	6000	settlement
2000	settlement	2000	settlement	4000	cessation in	4000	< 0.25mm
3000	< 0.25mm	1500	< 0.25mm	5000	settlement	2000	per hour
4000	per hour	1000	per hour	6000	< 0.25mm	1000	
5000		500		7000	per hour	0	
6000	4-6 hrs	0		8000			
				9000	4-6 hrs		

Table 3.6: Maintained load test schedule for TP3 (load cycles 1 and 2)

LOAD CYCLE 3				LOAD CYCLE 4			
Increments (kN)		Decrements (kN)		Increments (kN)		Decrements (kN)	
Load	Time held	Load	Time held	Load	Time held	Load	Time held
500		10000		1000		15000	
1000	Minimum	8000	until	2000		14000	until
2000	1 hr or	6000	cessation in	4000		12000	cessation in
4000	cessation in	4000	settlement	6000		10000	settlement
6000	settlement	2000	< 0.25mm	8000		8000	< 0.25mm
8000	< 0.25mm	1000	per hour	10000	30 minutes	6000	per hour
9000	per hour	0		11000		4000	
10000				11500		2000	
11000				12000		0	
11500				12500			
12000	12 hrs			13000			
↓	↓			13500			
or minimum load giving 25mm net settl.				14000			
				14500			
				15000			
				↓	↓		
				or load to failure			

Table 3.7: Maintained load test schedule for TP3 (load cycles 3 and 4)

3.6.3 Pile calibration using a short reinforced concrete column

To substantiate and validate the data generated from the pile test programme, a 2.0m long reinforced concrete column with the same diameter, reinforcement and concrete mix type as the test piles was tested. These dimensions gave a satisfactory height to diameter ratio of 2:1. Figure 3.11 illustrates the construction of the short column. The column was formed within a 10mm thick mild steel tube throughout its length and was instrumented with strain gauges to monitor longitudinal, radial and circumferential strains. All the gauges installed in the column were identical to the ones used in the test piles, except that the extensometers were 1220 mm long. The radial, circumferential and axial strain gauges were installed at the mid-height of the column while the extensometers covered the middle 1220mm length of the column, as shown in Fig. 3.11. The instruments were installed as described in Table 3.8.

INSTRUMENT TYPE	DIRECTION OF DEPLOYMENT	MARK	GAUGE LENGTH (mm)	DISTANCE FROM COLUMN AXIS (mm)
Vibrating wire gauge	Axial	VW1 VW2 VW3	150 150 150	343 343 343
Vibrating wire gauge	Radial	VW4 VW5	150 150	253 253
Vibrating wire gauge	Circumferential	VW6 VW7	150 150	343 343
Extensometer	Axial	E1 E2 E3	1220 1220 1220	343 343 343

Table 3.8: Instruments installed in the short column

The co-operation with BRE has taken the work outside of the normal range of university civil engineering research. The short column was load tested using a 1000 tonne Avery compression machine at the BRE laboratories in Garston, Hertfordshire. The base of the test column was laid on a rigid platform beneath the testing frame and the axis of the column aligned with that of the loading frame. This ensured that the load was applied axially. Three compressive load cycles were applied as listed in Table 3.9. Each load increment/decrement was held until steady state readings were achieved (minimum 10 minutes).

LOAD CYCLE 1 (kN)	LOAD CYCLE 2 (kN)	LOAD CYCLE 3 (kN)
0	0	0
50	500	500
500	1000	1000
1000	1500	1500
1500	2000	2000
2000	2500	2500
2500	3000	3000
3000	4000	4000
3500	5000	5000*
4000	6000	6000
4500	7000	7000
5000	7500	8000
		9000
		9500
		10000@
4000	7000	9000
3000	6000	8000
2000	4000	6000
1000	2000	4000
0	1500	2000
	1000	1500
	0	1000
		500
		0

<u>*Legend*</u>

** Denotes load held for 60 minutes*

@ Denotes load held for 30 minutes

Table 3.9: Loading schedule for short column

The results of the load test on the steel encased column were intended to assess the deformation properties of the sleeved portions of the test piles. Several weeks after the test, the steel casing was removed from the column and a similar load test was repeated. This test was intended to assess the effect of the steel casing on the stiffness of the column.

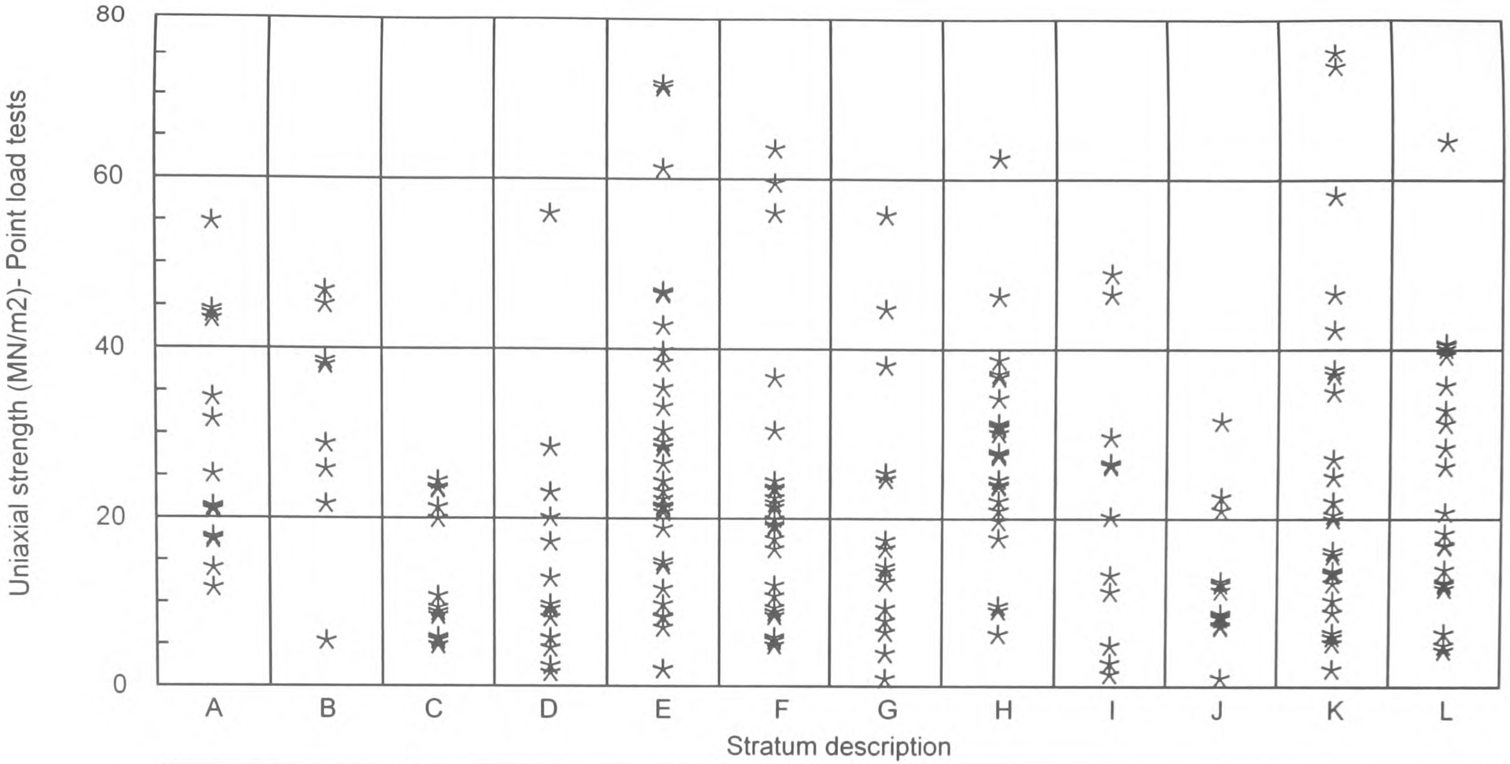

Legend

A Red brown and locally grey green,intact to slightly fractured,fresh to slightly weathered silty MUDSTONE, moderately strong (Zone I-II)
B Red brown and locally grey green slightly fractured slightly weathered silty MUDSTONE moderately weak and moderately strong with occassional strong bands (Zone II)
C Red brown moderately fractured, moderately to slightly weathered,silty MUDSTONE,moderately weak (Zone II-III)
D Red brown slightly weathered,silty MUDSTONE,moderately strong (Zone II)
E Red brown and locally grey green,slightly fractured,fresh to slightly weathered,silty MUDSTONE,moderately strong and strong (Zone I-II).
F Red brown and locally grey green intact to slightly fractured,fresh to slightly weathered,silty MUDSTONE,moderately weak to moderately strong. (Zone I-II)
G Red brown,slightly fractured,slightly weathered,silty MUDSTONE,moderately strong and strong Core length up to 0.4m (Zone I-II).
H Red brown and grey green,slightly fractured,slightly weathered,silty MUDSTONE,moderately strong to strong (Zone II with bands of strong zone II-I)
I Red brown and grey green,slightly fractured to slightly weathered,silty MUDSTONE,moderately strong,with vertical fractures (Zone I-II).
J Red brown,slightly weathered,slightly fractured,silty MUDSTONE,moderately strong to strong (Zone II-I).
K Red brown and locally grey green, moderately to slightly fractured,slightly weathered,silty MUDSTONE,moderately strong, occasionally strong. (Zone II-I).
L Red brown,slightly weathered,moderately to slightly fractured,silty MUDSTONE, moderately strong. (Zone II)

Fig.3.1: Point load test results from Keuper marl strata of various descriptions

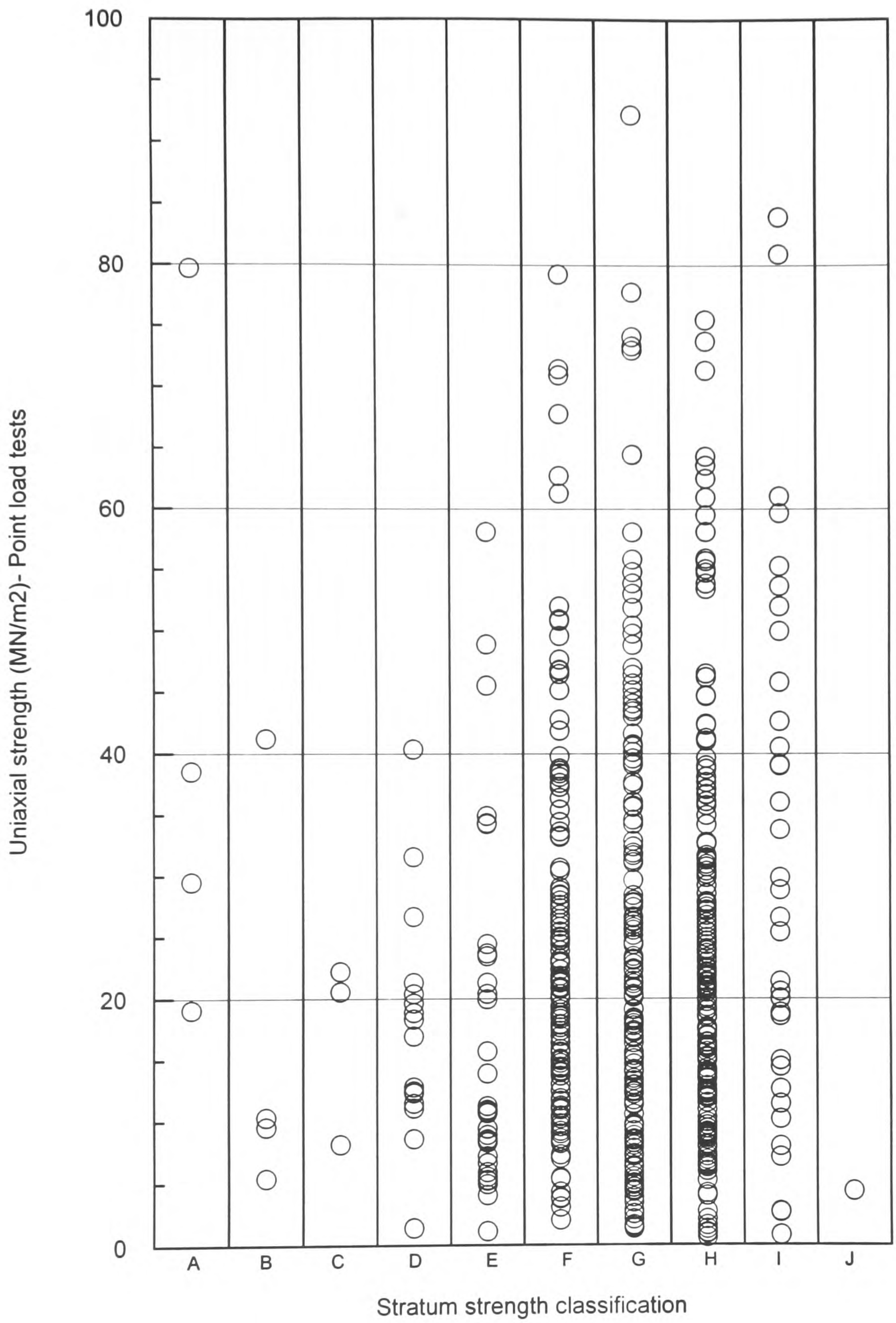

Legend
A=Very weak
B=Very weak to weak
C=Weak
D=Weak to moderately weak
E=Moderately weak
F=Moderately weak and moderately strong
G=Moderately strong
H=Moderately strong to strong
I=Strong
J=Weak with moderately strong lithorelicts

Fig.3.2: Point load test results from Keuper marl strata of various classifications

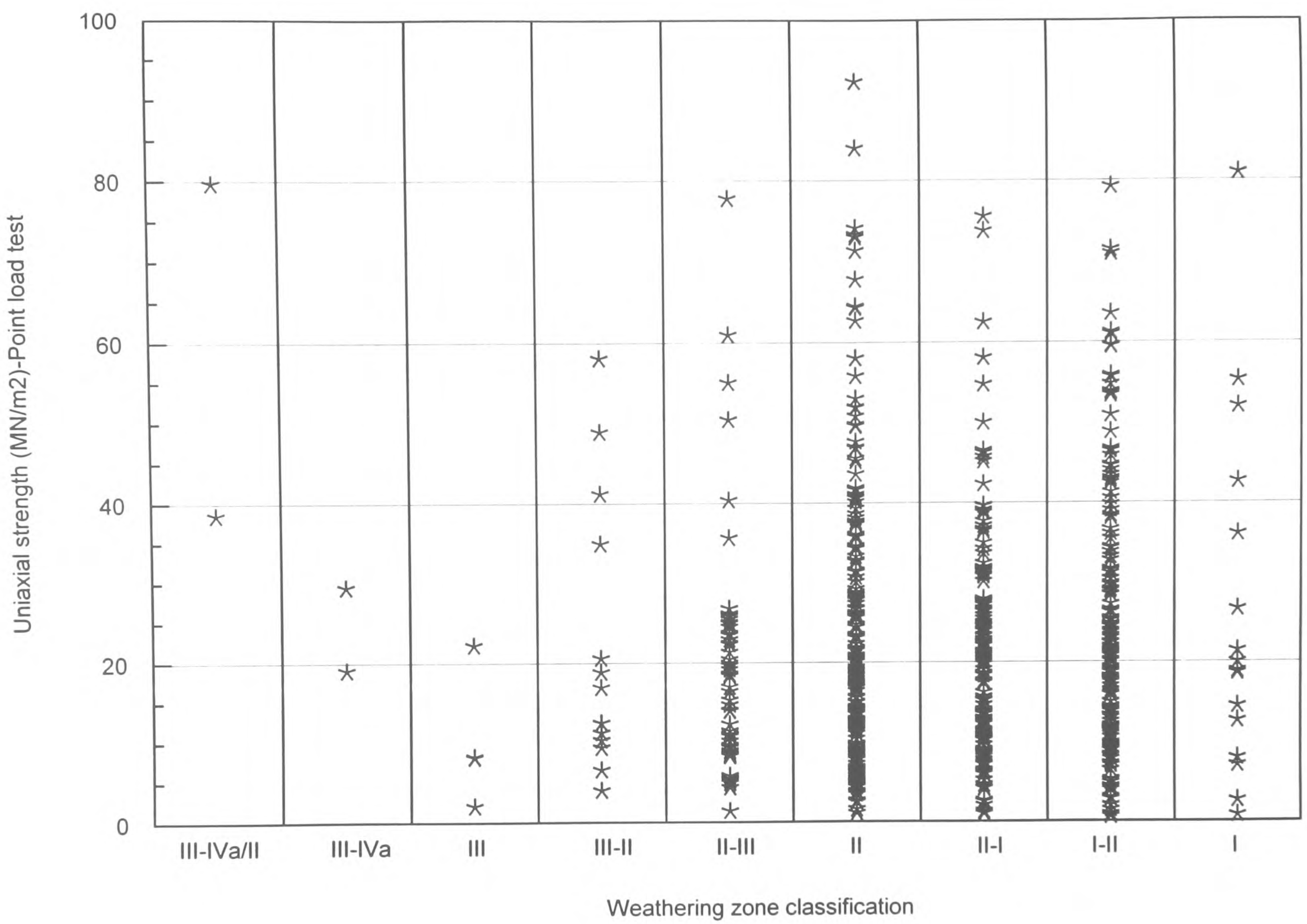

Fig.3.3: Point load test results from various weathering zones of Keuper marl

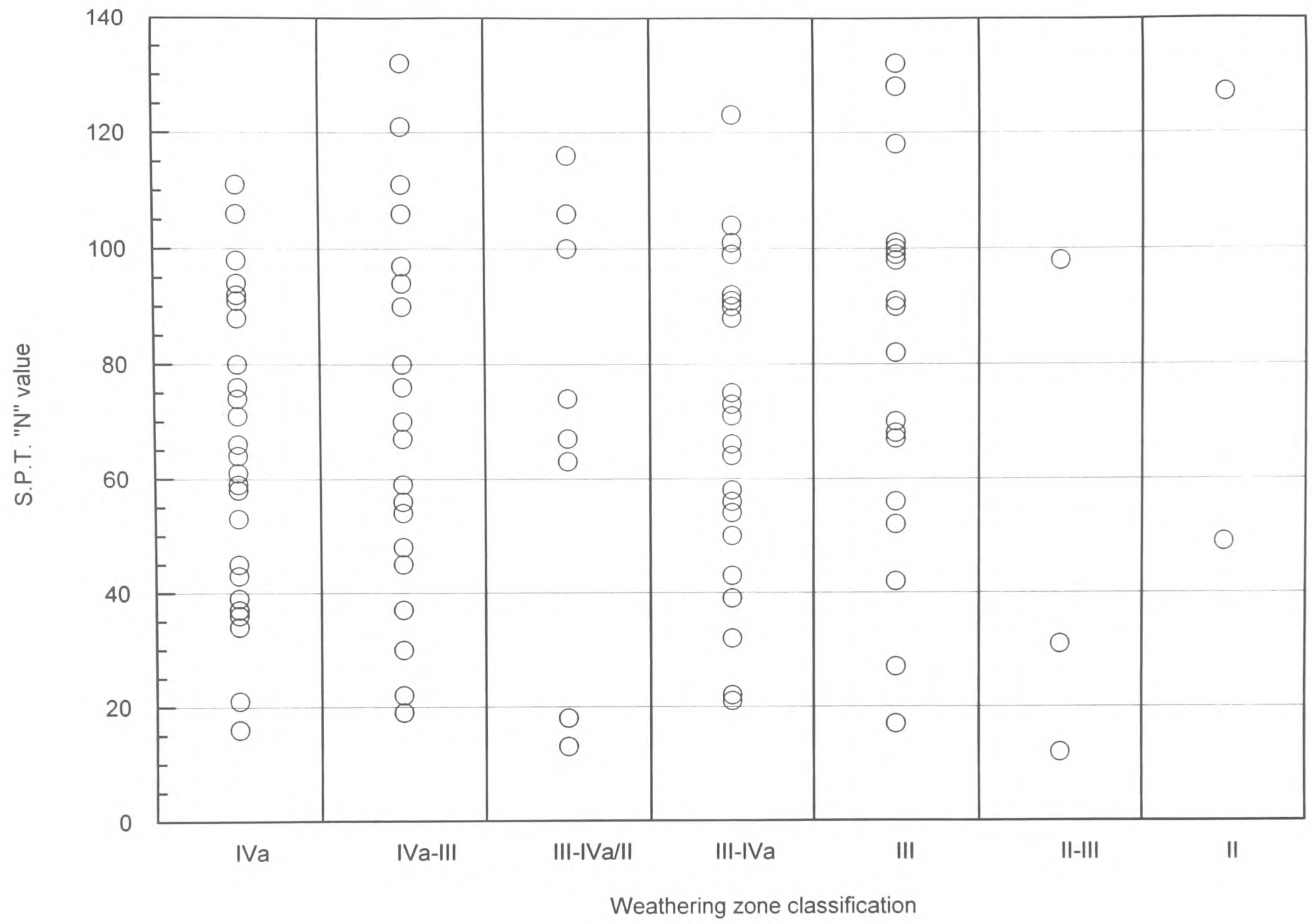

Fig.3.4: S.P.T. "N" values for various weathering zones of Keuper marl

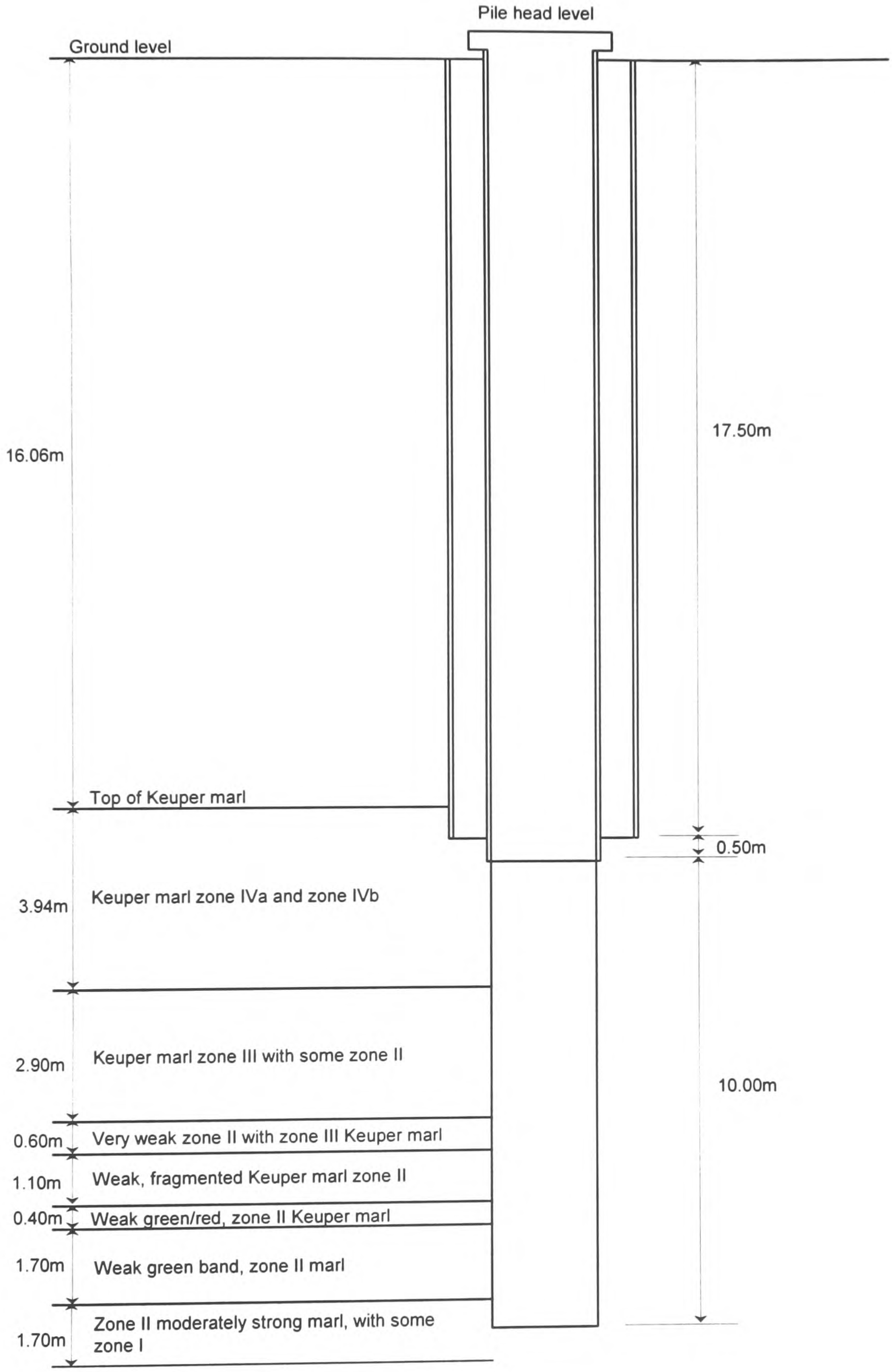

Fig 3.5:TP1-Layout

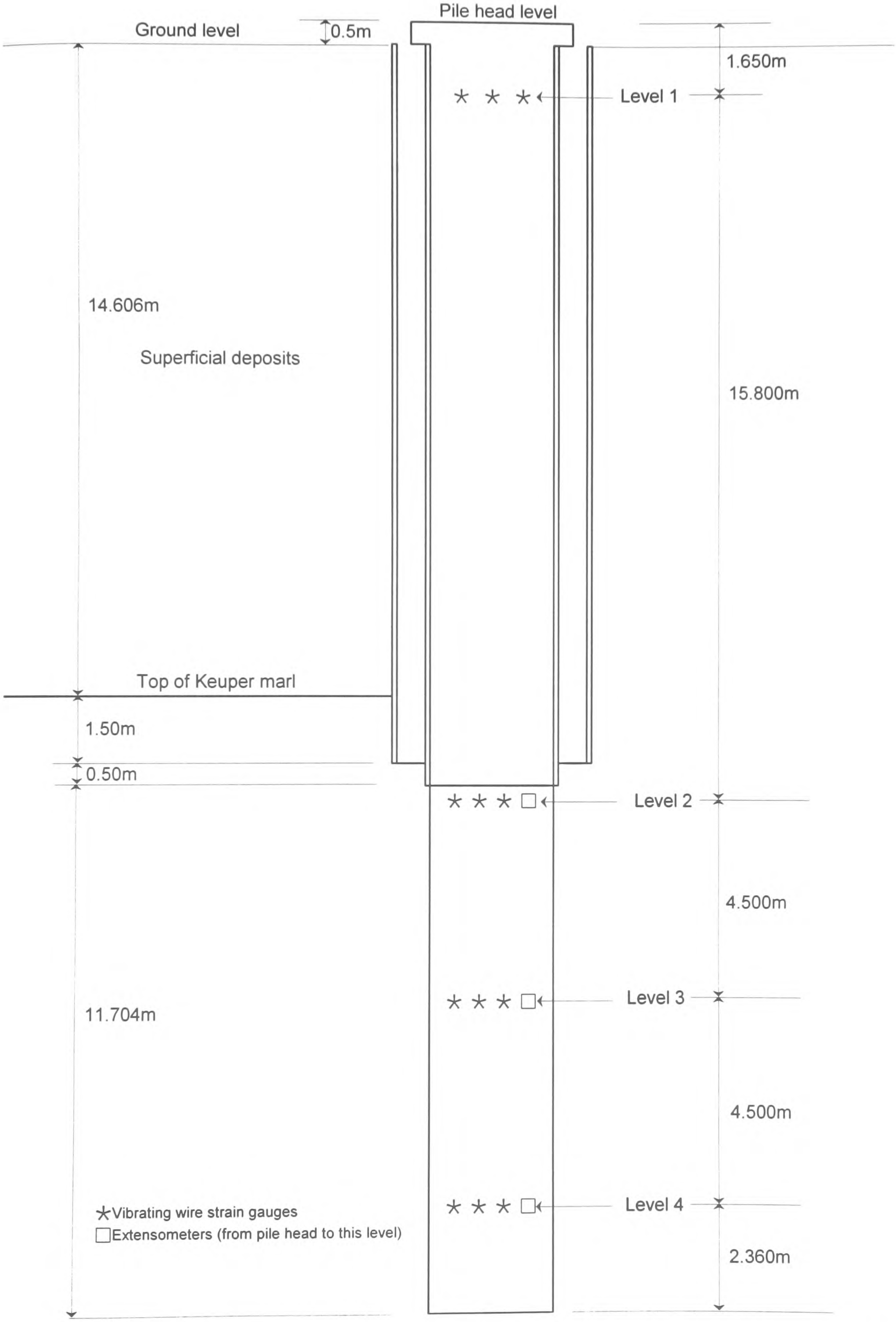

Fig 3.6:TP2-Layout and instrumentation

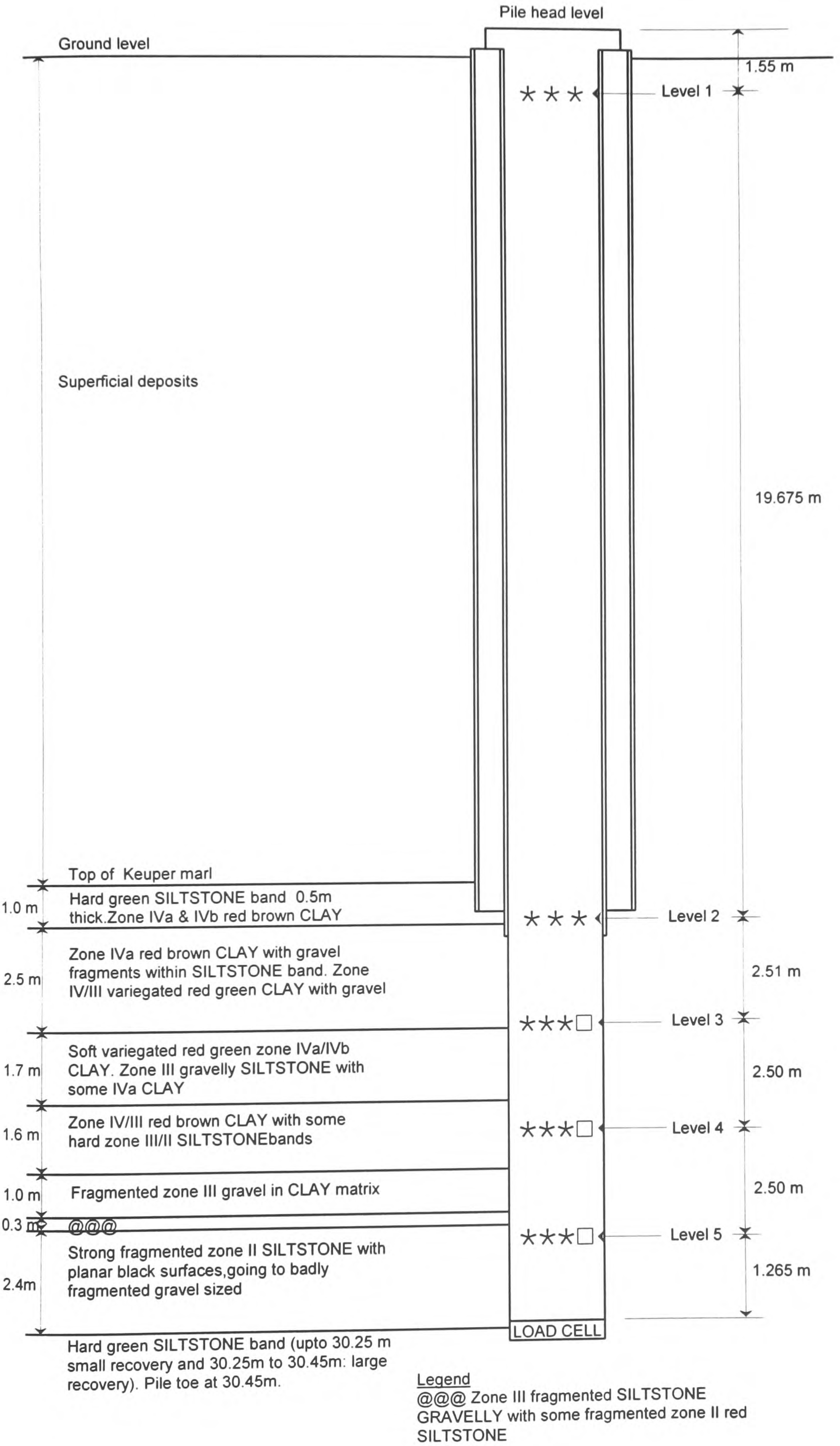

Fig 3.7:TP3-Layout and instrumentation

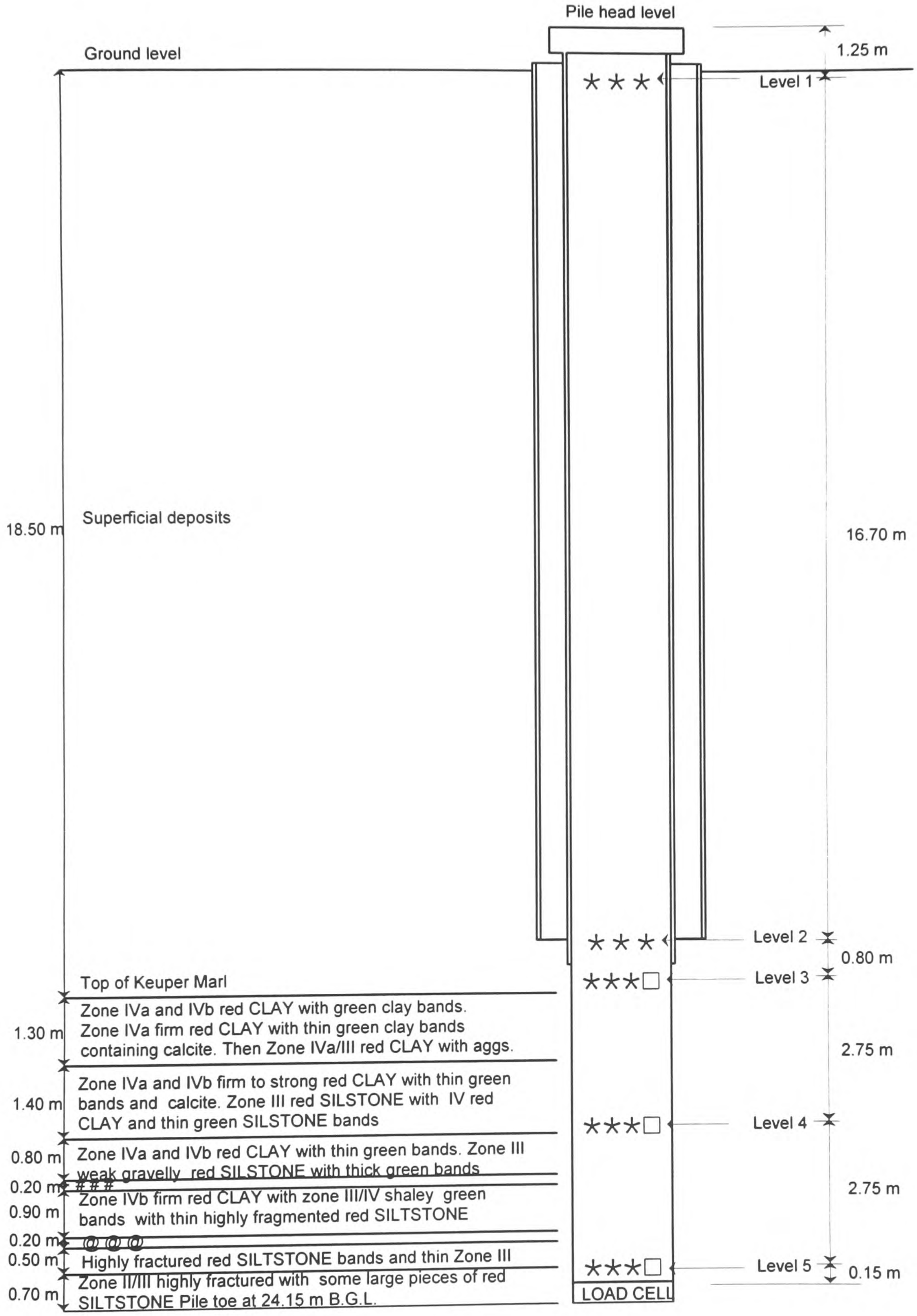

Legend

\# # # Zone IV/III red CLAY with aggregates and thin green bands

@ @ @ Zone III/IV red SILSTONE with some CLAY.

Fig 3.8:TP4-Layout and instrumentation

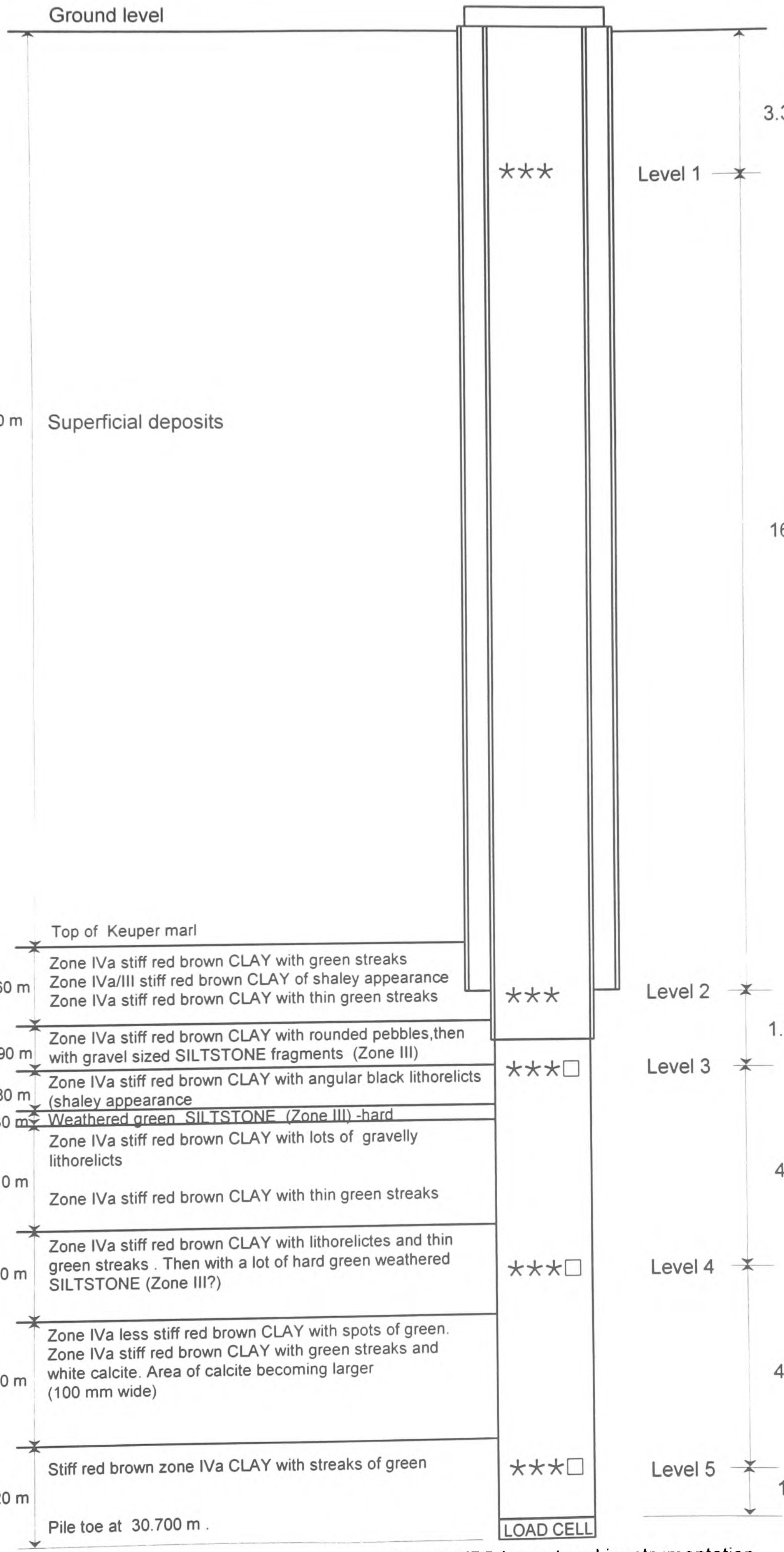

Fig 3.9: TP5-Layout and innstrumentation

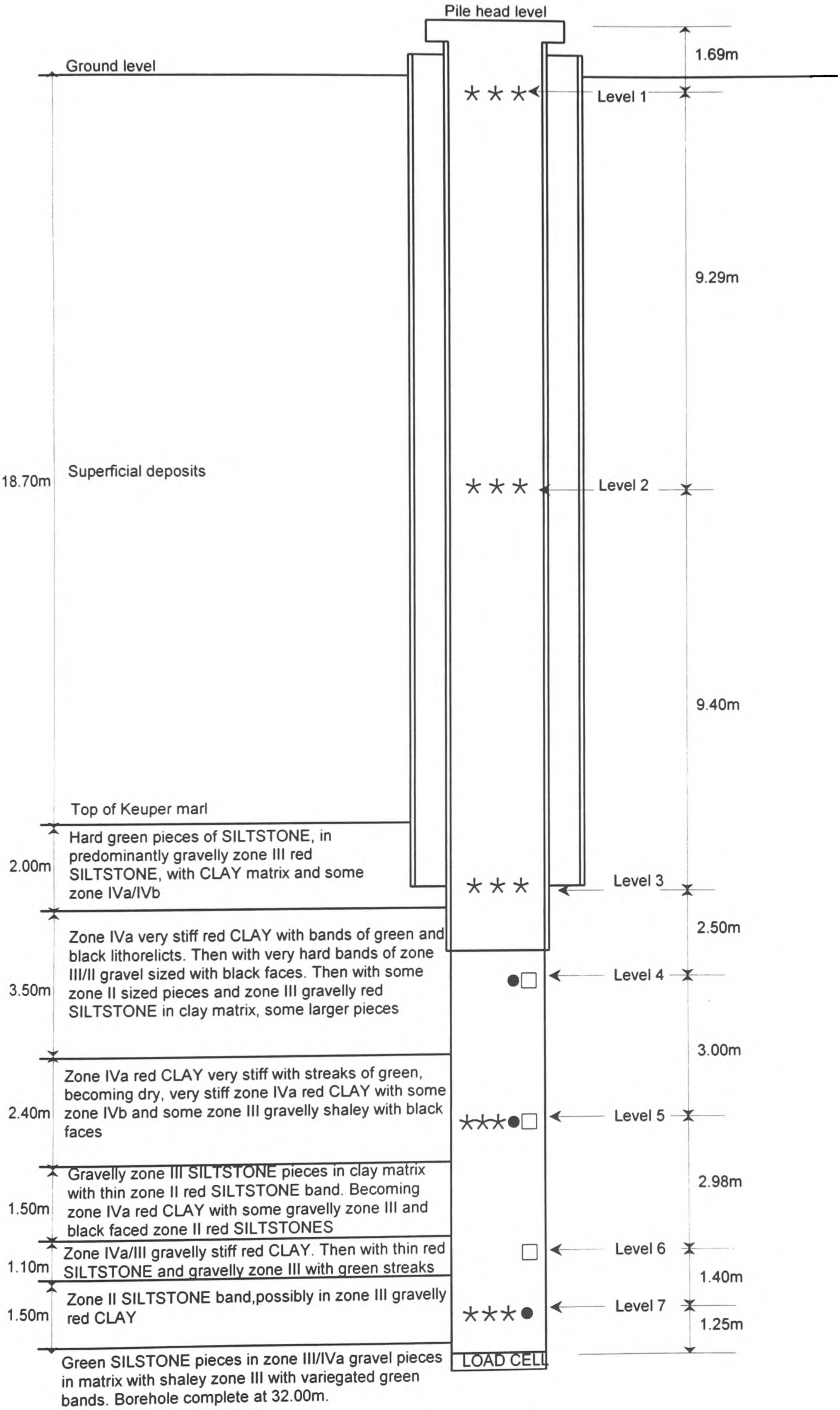

Fig3.10:TP6-Layout and instrumentation

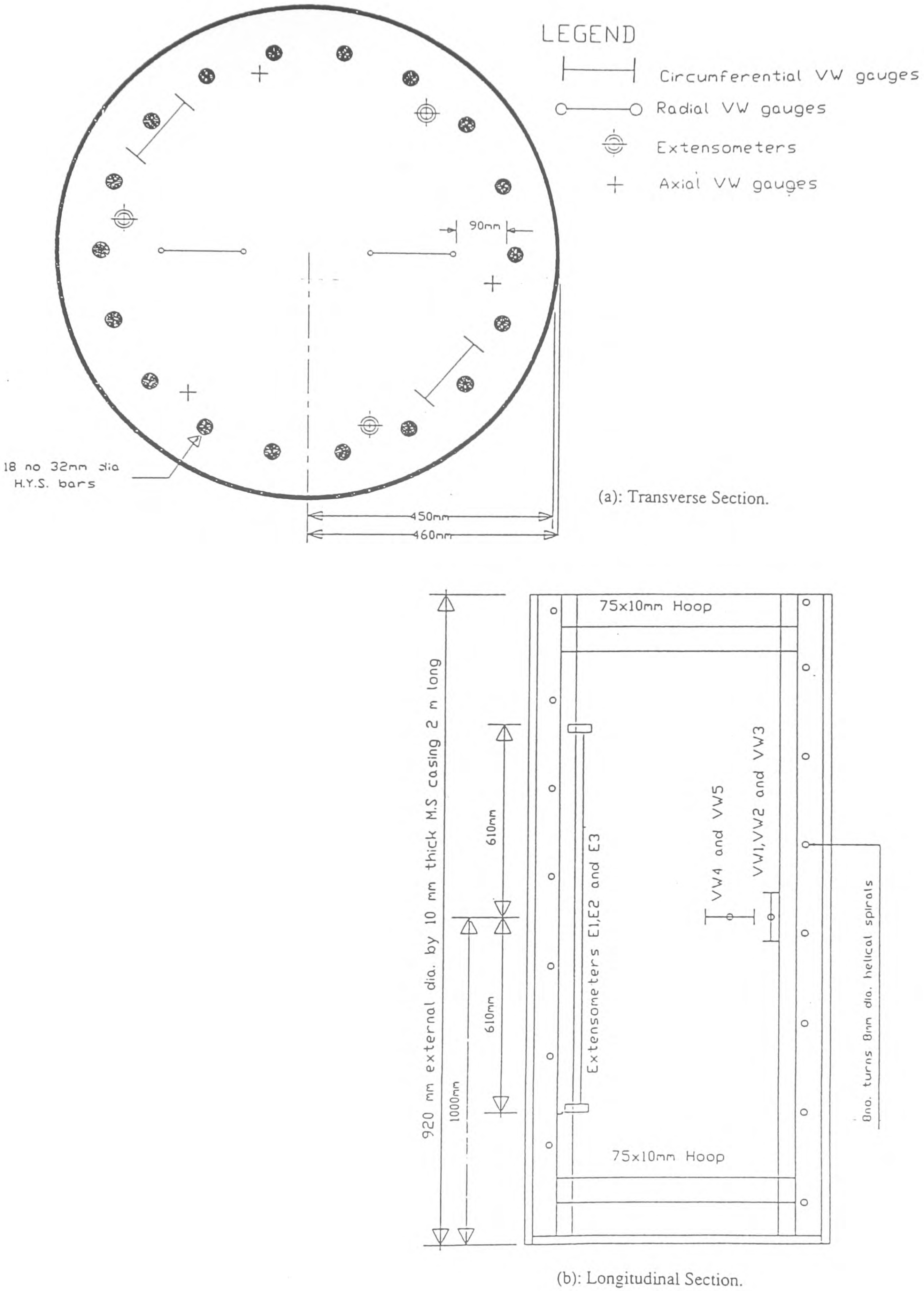

Figure 3.11: Short column construction and instrumentation

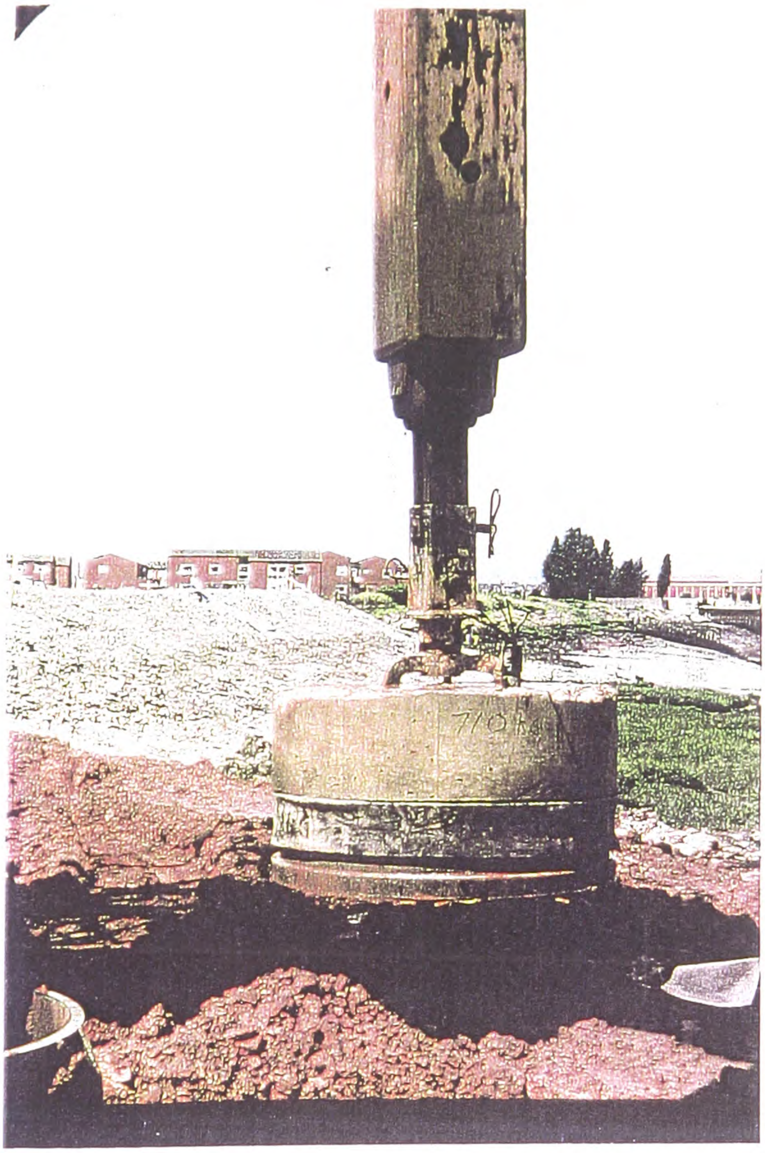

Plate 3.1 A load cell being installed in a test pile hole

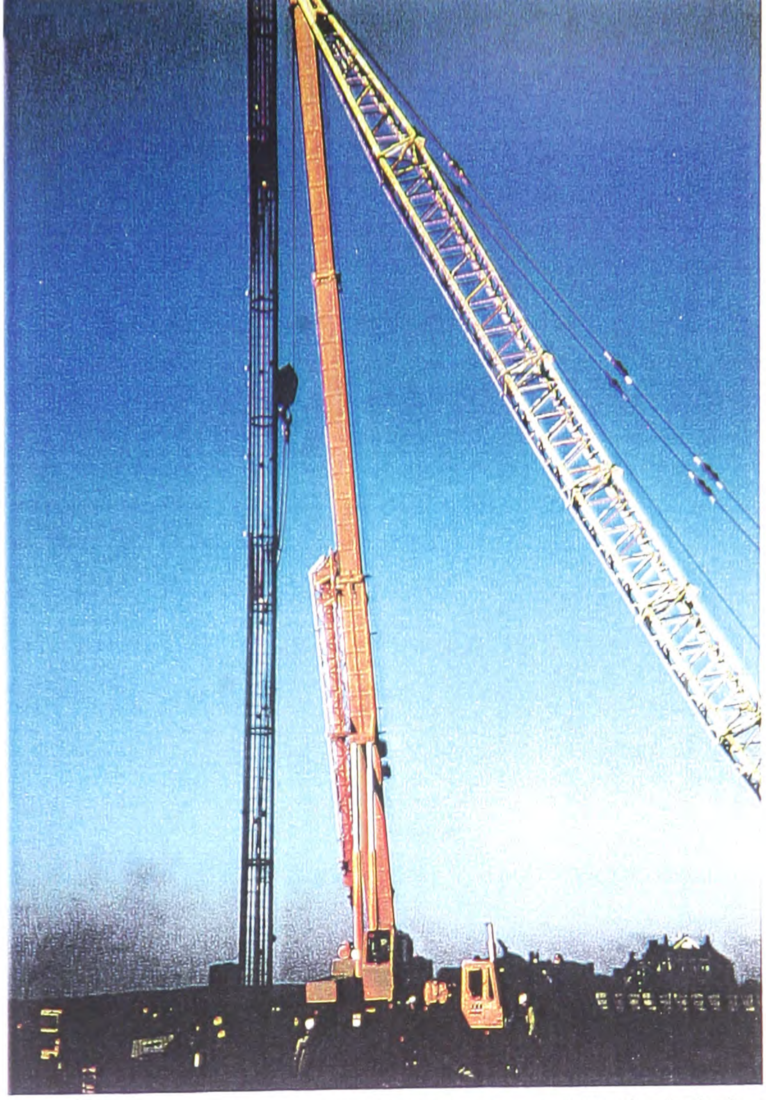

Plate 3.2 Lowering the full length of the reinforcement cage into the hole in order to avoid damage to the instrumentation and electrical connections

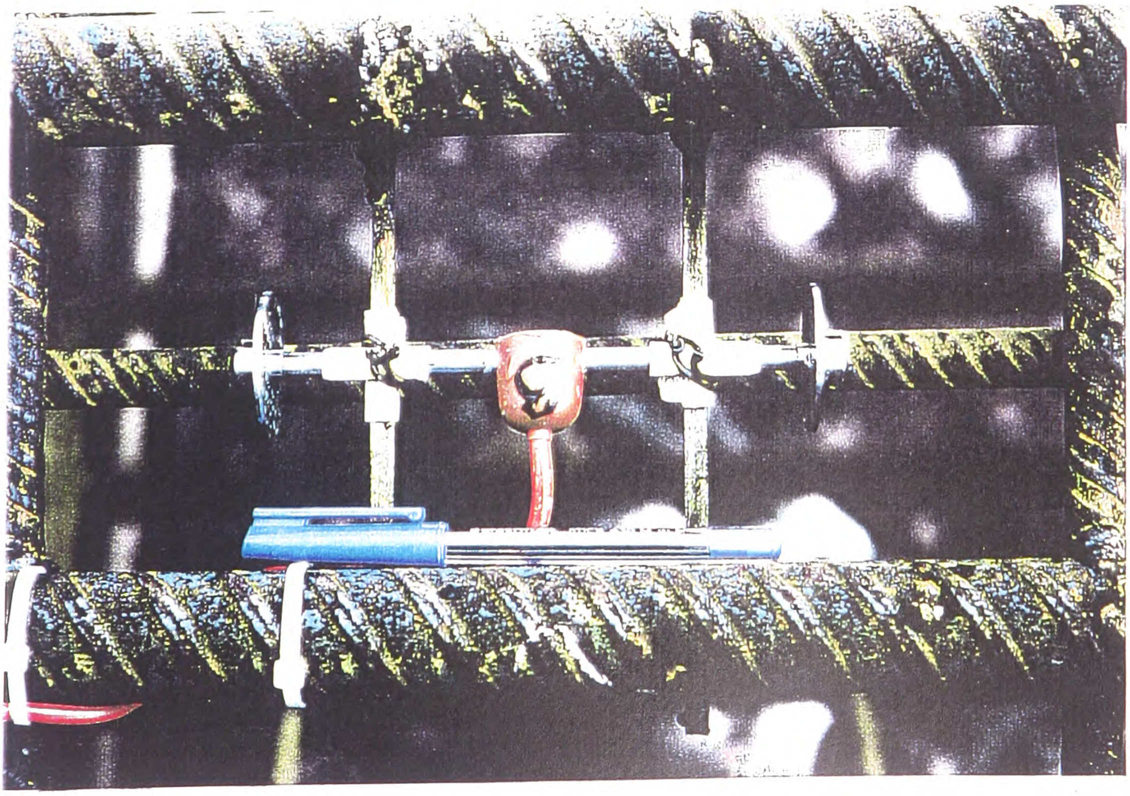

Plate 3.3 Detail of attaching a vibrating wire strain gauge to the pile reinforcement

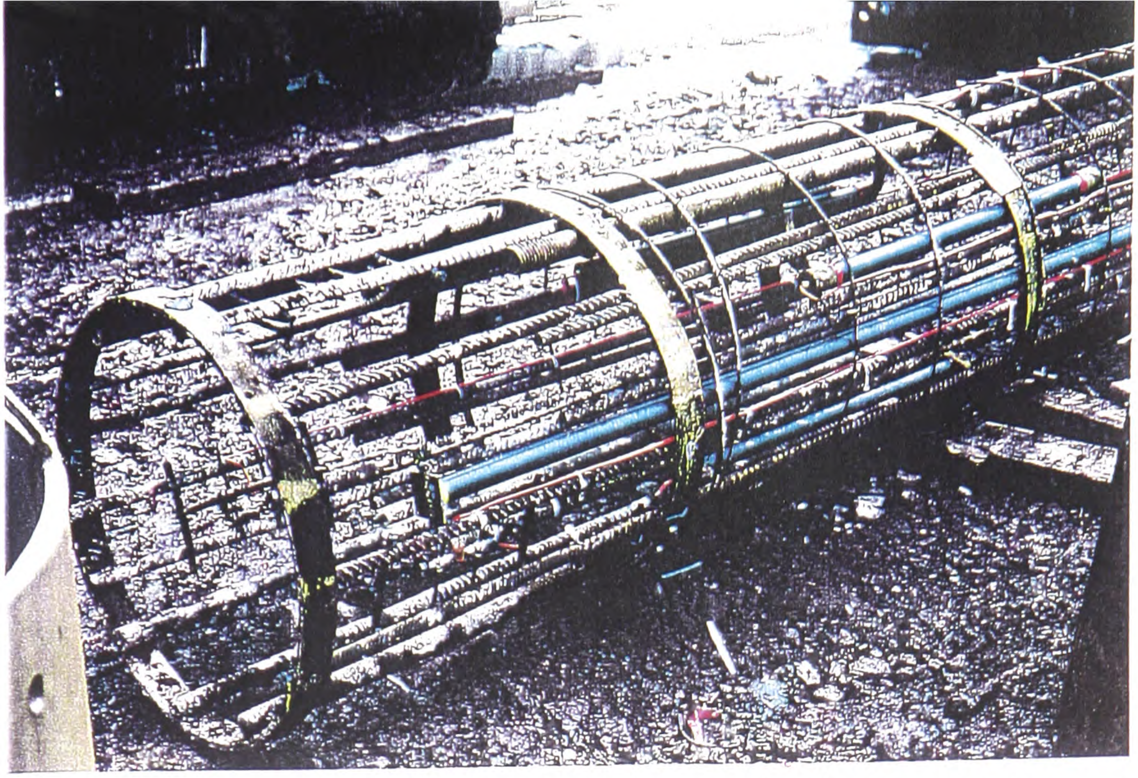

Plate 3.4 Assembling the pile reinforcement and installing the extensometers

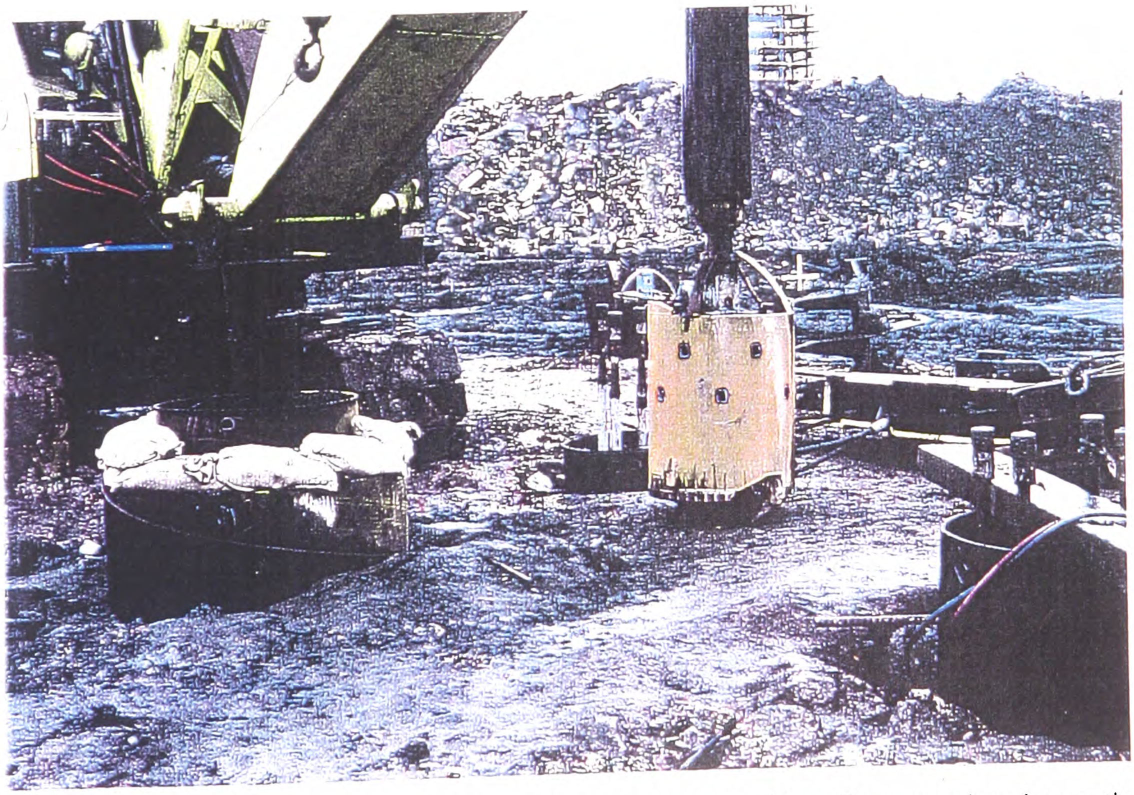

Plate 3.5 (a) Left: Inner and outer casings of the test pile in position. Bags are placed over the gap between the casings in order to prevent debris or other objects falling into the hole. (b) Right: Anchor piles and a bucket augur

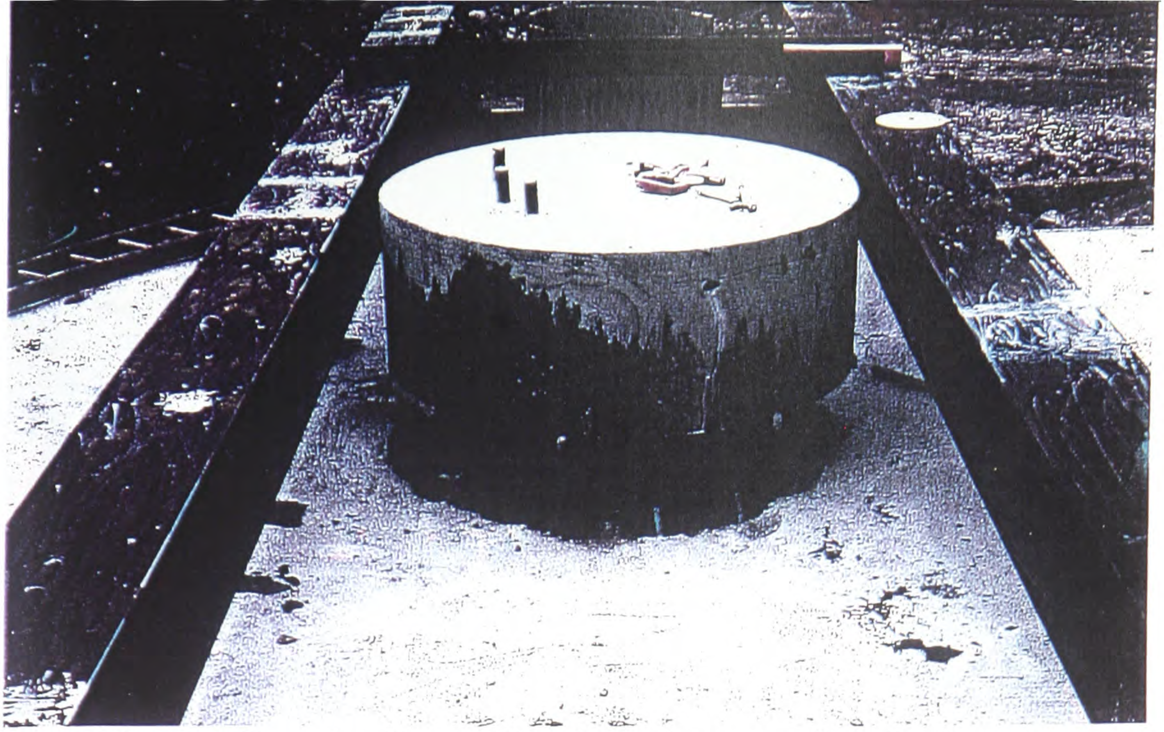

Plate 3.6 Completed test pile with one of the reference beams on which the pile head movement measuring gauges are mounted

Plate 3.7 A 2000 ton test loading rig developed by DMD Piling Ltd (Cardiff) utilising 4 anchor piles

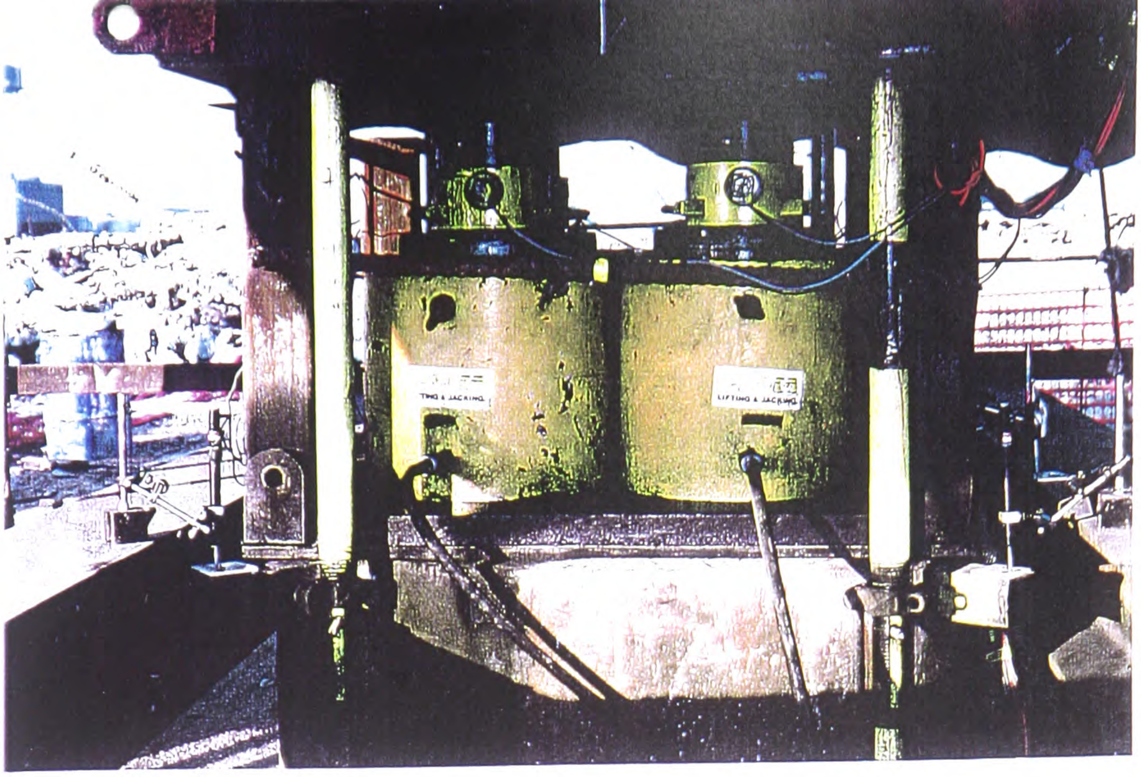

Plate 3.8 Four loading jacks mounted on the pile top

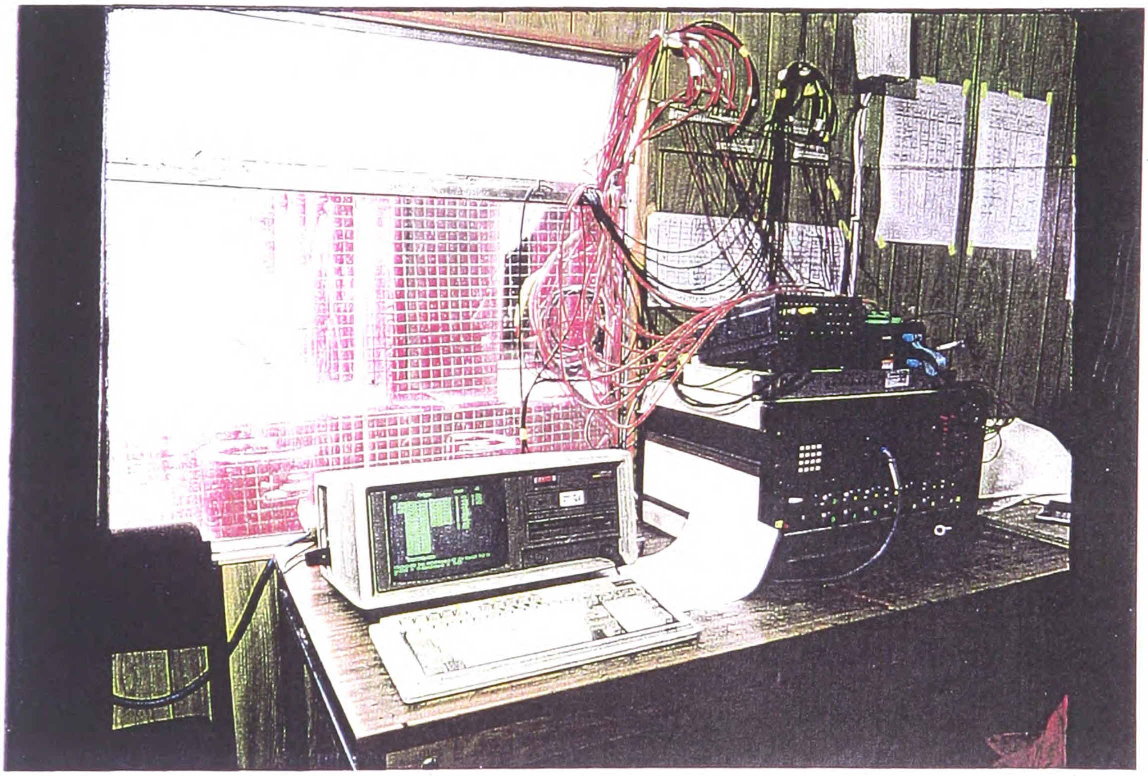

Plate 3.9 Data monitoring cabin located adjacent to a test pile site

CHAPTER 4

ANALYSIS OF PILE LOAD TEST DATA

CHAPTER 4: ANALYSIS OF PILE LOAD TEST DATA

4.1 INTRODUCTION

This chapter presents an analysis and interpretation of the pile load test data in order to establish the load transfer and resistance mechanisms of large diameter, bored, cast in-situ piles formed in Keuper marl. In addition, the pile test data are presented in the traditional form of time, load, and displacement graphs. It was anticipated that the stiffness of a typical test pile would vary both longitudinally and laterally at a given cross-section. These variations are due to (a) the composite nature of the piles (b) the non-linear stress-strain response of concrete, and (c) stiffness variations of plain concrete with distance from the axis of a test specimen. Therefore, it was considered necessary to establish realistic elastic properties of the cross section of each test pile by examining various numerical methods.

Using the established elastic properties of each pile, the variation of shaft resistance and end bearing resistance of each test pile was determined. Due to the nature of the pile tests, no attempt has been made to include the influence of time dependent settlements, although the time/displacement criteria of 0.25mm/min for the maintained load test was complied with, in accordance with the specifications for pile load tests.

4.2 TEST PILE RESULTS

4.2.1 Introduction

A large volume of data was produced from the various pile instruments during load testing in several cycles of load increments and decrements. The data was stored on computer files and was processed by running a purpose designed computer program by the Building Research Establishment (B.R.E.), Geotechnics Division. A listing was made of all instrument readings, corresponding to a given applied pile head load, at every 10 minutes time increment during sustained loading. The listing was carried out for the entire period over which a given load was maintained. In some cases, the load was held for up to 20 hours.

The whole test data was retrieved into a spreadsheet in order to facilitate further analysis. In order to analyse the immediate settlement of each test pile, the readings of strain gauges, extensometers, base load cells and pile head movement gauges were tabulated at various load increments/decrements. Creep behaviour was investigated by including displacement-time variations. The load test data from all test piles are presented in the Appendix. The data for pile TP1 is given in Table A.2. Tables A.3(i)-A.3(xii) show the test data for TP2. The data for test piles TP3-TP6 are given in Tables A.4(i) up to Table A.8(iv). These include the results of the pull-out test on TP6.

4.2.2 Pile head load-Displacement-Time graphs

Plots of Applied load versus time, Pile head displacement versus time and Pile head load versus pile head settlement for test piles TP2-TP6 are given in Figs 4.1-4.5. Table 4.1 summarises the gross and net settlement at working load for each pile. The underlined values are the observed load capacities of the various test piles. These values are based on a definition of pile failure as a clear maximum load reached or the load required to produce a net settlement of 10% of the pile base diameter. Net settlement is defined as the gross pile head settlement less the pile shortening. The working load of a given pile is taken as one third of the load capacity.

	Test duration (hours)	Max. test load (MN)	Gross settlement at working load (mm)	Net settlement at max. load (mm)
TP2	78.5	13.5	8.5	21.5
TP3	169	18.0	6.2	97.0
TP4	95.8	12.0	7.1	61.5
TP5	123.5	11.2	4.7	227.0
TP6	109.6	12.5	7.0	15.0

Table 4.1: Gross and net settlement at working load for piles TP2-TP6

It is seen that whereas the settlement values at maximum loads are so much at variance, the range of settlement at working loads is confined to 4.7-8.5mm. These values are approximately 0.5-1% of pile diameter, which represent the settlement expected to mobilise full shaft resistance. From Figs. 4.1-4.5, the following values of creep at working loads are computed based on an average over the maintained load time periods indicated.

	Creep at working load (mm/hr)	Period over which creep is averaged
TP2	0.23	3.5 hrs
TP3	0.07	16 hrs
TP4	0.10	13 hrs
TP5	0.15	4 hrs
TP6	0.08	4 hrs

These values are less than the limiting settlement rate of 0.25mm/hr, which is the stipulated maximum settlement rate for steady state conditions. In comparison, the creep in pile TP5 at a load corresponding to the ultimate capacity of 11.2MN is 49.7mm/hr. This value represents an average over 19 minutes. Therefore, the increase in deflection as a result of sustained loading with time is insignificant for load values well beyond the working load. During cyclic loading, it is observed that the pile head settlement increases with applied load and on unloading to zero, the unrecoverable displacement remains approximately constant until the next load increment is added. On increasing the load to the next prescribed value, the settlement increases and the cycle is repeated. Due to unrecoverable deformations, there are discontinuities between successive load cycles, in the load-settlement plots for all test piles.

4.2.3 Load-Settlement curves

The plots in Figs 4.1-4.5 also include the load-settlement curves obtained from the test piles. Each curve typifies the variations expected for bored, cast in-situ piles. The difference in the initial gradients of the graphs and in the paths of progress towards failure conditions can be attributed to the variation in the ground conditions and differences in the pile installation process. In addition, the load-settlement curve for a given pile depends on its length and on the deformation properties of the pile cross-section.

Comparisons of pile performance can be made from Figs. 4.1-4.5. In the loading range 0-1000kN, the rates of increase of pile head settlement with applied load for piles TP2 and TP6, which have projected load capacities of 22MN and 19MN respectively, are 0.22 and 0.23mm/MN respectively. In the same load range, the rate of settlement of pile TP5, which has a load capacity of 11.2MN, is 0.09mm/MN. Pile TP3, with a capacity of 18MN indicates a settlement rate of 0.16mm/MN. Excluding pile TP4 in which there was some interference between the permanent casing and the shaft, a common pattern is observed. For these pile lengths and diameters, it can be concluded that the initial slope of the graph of pile head settlement versus applied load is approximately equal to one percent of the ultimate load capacity. Table 4.2 gives a comparative illustration of the differences observed in the load-settlement behaviour of the test piles.

	Applied pile head load								
Pile	2MN	4MN	6MN	8MN	10MN	12MN	14MN	16MN	18MN
TP1	2.90	14.22	-	68.20	-	-	-	-	-
TP2	0.93	3.48	6.07	10.31	18.49	27.94	-	-	-
TP3	0.89	3.33	6.16	10.53	17.40	24.84	36.95	60.79	116.41
TP4	2.38	8.75	20.16	37.53	63.39	155.60	-	-	-
TP5	0.94	4.78	10.86	27.11	62.02	-	-	-	-
TP6	1.17	3.60	6.92	10.92	18.26	24.70	-	-	-

- *Denotes pile head settlement values corresponding to these loads not available*

Table 4.2: Pile head settlement values (mm) corresponding to selected applied loads (TP1-TP6)

The load-settlement response of piles TP2, TP3 and TP6 illustrate a high degree of similarity up to an applied load of 12MN. Pile TP3 was loaded to a maximum of 116.41mm. The piles were of similar length and the soil strata at these sites generally comprised Keuper zone IV/III and III/II. Considering values of applied load in the range 6MN to 12MN, the maximum deviation in pile head deflection in these piles is only about 14%. Figure 4.6(a) shows the load-settlement plot for pile TP1. Since this pile was formed with a voided toe, its load-settlement response cannot be directly compared with those of the other test piles. In addition, it should be noted that TP5 was installed in particularly weak ground where the soil was predominantly Keuper marl zone IVa and IVb. The fact that this pile had the lowest load capacity is also consistent with the ground conditions. The large settlement values observed in pile TP4 strongly indicate the uncertainty with which this pile was installed. It is probable that this pile was significantly weakened by the collapse of the steel casing following strong vibrations of heavy plant and machinery adjacent to the test pile location.

4.2.4 Observed ultimate load capacities

For the test piles being considered, the maintained load test cycles adopted poses some difficulty in expressing the true value of ultimate load capacity. Adopting a pile failure definition as the clear maximum load reached, or the load at which the pile head settlement is equivalent to 10% pile diameter, the following are the ultimate loads for piles TP3-TP5.

Test pile	Ultimate load (MN)
TP3	17.0
TP4	11.5
TP5	11.2

The load-settlement graph for the end-bearing M.L. test in TP1 is shown in Fig 4.6(b) while Fig 4.6(c) illustrates the result of the C.R.P. test. The displacements plotted in the C.R.P. curve are based continued instrument readings above the last recorded readings following the completion of the M.L. test. The ultimate end resistance is clearly evident in the C.R.P. curve and the value is approximately 11.7 MN.

4.3 LOAD-STRAIN CALIBRATION OF THE TEST PILES

4.3.1 Introduction

The technique of load transfer measurement in test piles using strain gauges has been in use for a couple of decades and offers a reasonably cost effective means of obtaining the profile of axial force along a pile shaft when the pile is subjected to loading. The method is also useful in checking the results of analytical formulae for pile settlement The strain gauges located at different depths along the pile axis give the variation of strain with depth as a result of the applied pile head load. This enables the axial load distribution to be determined, for an elastic pile where the elastic properties of the material are known.

4.3.2 Performance of strain gauges

Table 4.3 illustrates the typical strain gauge readings at the first level for applied loads in the range 0-6000 kN, for all the test piles. The mean strain at a given level was obtained by averaging the values of the strains at the pseudo-rosette locations θ, (θ+120°) and (θ+240°). This minimised any effects of load eccentricity on stress distribution. The justification for averaging the strain values was confirmed through a separate but simple mathematical formula as given in section 4.4.3.2. Since all the test piles had identical cross-sections in terms of concrete and steel areas, any differences in the average strains at level No.1 must be due to variations in the concrete strength, which is also a function of the time elapsed since pile installation.

4.3.3 Stress-strain calibration methods

In order to calculate axial forces in the test piles from strain gauge readings, it is necessary to accurately assess the stiffness of each pile. This may be based on a laboratory determined static modulus value for concrete or on the calibration constant for a given strain gauge provided by the manufacturer. Nevertheless, it was considered necessary to study the behaviour of these gauges as installed within the composite pile section. This is because of the non-homogeneity of the pile concrete surrounding the gauges and possible eccentric transmission of load along the pile, which alters the stress distribution from one cross-section to another.

Three approaches to stress-strain calibration were proposed:

a) A linear load-strain relationship based on the observed behaviour of the strain gauges installed within the cased part of each pile,
b) A non-linear load-strain relationship based on the apparent variation of Young's modulus of concrete with strain and
c) A method of back-analysis of the variation of Young's modulus and Poisson's ratio across a given pile cross section, based on load testing of a short instrumented, reinforced concrete column under controlled conditions.

The first method derives a relationship between axial load and strain at a cross-section of known axial load. Based on the assumption that the concrete has constant properties at all other cross sections, the relationship is then used to predict axial force load for the other levels where strain values are available. This method is referred to as the "Linear method" (after O'Riordan,1982) but is modified to account for the composite nature of the pile cross-section. The second method involves curve fitting of the apparent concrete modulus variation with strain using power regression methods. Different regression coefficients are obtained for different load cycles hence this method accounts for the influence of stress history on the Young's modulus of concrete. The load corresponding to a particular measured strain is then calculated using the appropriate value of Young's modulus of concrete calculated from the idealised function.

Load (kN)	Test pile	Strain values (x10^{-6})			
		VW1	VW2	VW3	Mean
1000	TP2	10	17	1	13.5*
	TP3	15	7	7	9.6
	TP4	34	20	0	27.0*
	TP5	6	4	7	5.7
	TP6	27	7	14	16.1
2000	TP2	33	58	10	45.5*
	TP3	50	24	32	35.4
	TP4	73	48	27	60.5*
	TP5	45	25	25	31.7
	TP6	57	40	44	47.2
3000	TP2	62	87	38	74.5*
	TP3	86	60	71	72.3
	TP4	113	76	50	94.5*
	TP5	81	58	57	65.6
	TP6	88	75	76	80.0
4000	TP2	91	118	66	104.5*
	TP3	123	96	109	109.4
	TP4				
	TP5	118	93	89	99.8
	TP6				
5000	TP2	119	148	96	133.5*
	TP3	163	134	150	148.9
	TP4				
	TP5	154	129	122	135.4
	TP6				
6000	TP2	149	181	124	165.0*
	TP3	201	170	188	186.6
	TP4				
	TP5	193	168	157	172.7
	TP6				

* *Mean values for Strain gauges VW1 and VW2 only*

Table 4.3: Strain gauge readings at level No. 1 for all piles (load cycle 1)

The third method enables the assessment of the stiffening effect of steel on concrete, depending on the relative proximity of the steel casing and of the reinforcing bars. The short column tested has cross-sectional dimensions and materials identical to the test piles.

Strains are measured at known locations, along the three cylindrical co-ordinates and the elastic properties of the column are back-figured using a proposed mathematical model.

4.3.4 The linear (Gauge Stiffness) calibration method

This method has been used by O'Riordan(1982) and Fort et al(1989) for a pile with a constant area of steel to represent the load-strain relationship for the entire pile. In the present analysis, an adjustment is made to take into account the composite nature of the pile section. The cross-sectional area of steel changes from the sleeved portion to the embedded portion of the pile. Figs 4.7(a)-(e) are plots of pile head load against strain at instrument level No.1 for test piles TP2-TP6 respectively. For each pile, the strain gauges at level No.1 lie within the sleeved section where the axial force is assumed to be equal to the applied load at the pile head. The graphs show that most of the strain gauges functioned satisfactorily, although there were slight variations in the hysteresis resulting from the effects of cyclic loading. The degradation of concrete stiffness in pile TP3 from one load cycle to another is more rapid than in the other test piles. This probably implies a poor concrete quality at the corresponding instrument level in this pile.

For each load cycle, a linear load-strain relationship for the pile was obtained from these graphs. The mean gradient and the intercept on the vertical axis were calculated by linear regression. Considering force equilibrium, the applied pile head load P can be expressed in terms of the longitudinal stresses, σ_s and σ_c, in the steel and concrete as

$$P = \sigma_s A_s + \sigma_c A_c \qquad (4.1)$$

Where A_s and A_c are the cross-sectional areas of steel and concrete respectively. Assuming that there is no slip between the concrete and the steel at all cross-sections, the axial force P can be expressed in terms of the strain ε as

$$P=\varepsilon(E_sA_s+E_cA_c) \tag{4.2}$$

For the load range for which the graph is linear, the relationship linking P and ε can be written as

$$P=\frac{\Delta P}{\Delta\varepsilon}\varepsilon+P_o \tag{4.3}$$

Where $\frac{\Delta P}{\Delta\varepsilon}$ represents the average stiffness of the strain gauges and P_o is the apparent load at zero strain. Comparing Eqn. (4.3) with Eqn. (4.2), the axial force can be written as

$$P=\varepsilon(E_sA_s+E_cA_c)+P_o \tag{4.4}$$

Hence the gauge stiffness $\frac{\Delta P}{\Delta\varepsilon}$ is given by the expression

$$\frac{\Delta P}{\Delta\varepsilon}=E_sA_s+E_cA_c \tag{4.5}$$

Hence the modulus of the pile concrete E_c is expressed as by

$$E_c=\frac{1}{A_c}\left(\frac{\Delta P}{\Delta\varepsilon}-E_sA_s\right) \tag{4.6}$$

By back substitution of E_c into equation (4.4) the axial force at any section along the pile where the strain is known can be calculated from the expression

$$P=(A_c+\frac{E_sA_s}{E_c})(\varepsilon E_c+\sigma_o) \tag{4.7}$$

Where σ_o is given by

$$\sigma_o = \frac{P_o}{A_c + \frac{E_s A_s}{E_c}} \tag{4.8}$$

For each test pile, the E_c and σ_o values were calculated for each load cycle and the results are presented in Table 4.4. The laboratory determined compressive strength and static modulus values are included at the bottom of the Table. The mean values of E_c for all load cycles are 44.00, 29.20, 35.99 and 34.47 kN/mm^2 for TP2, TP3, TP4 and TP5 respectively. In comparison with the static modulus values, the mean E_c value for TP2 is 16% higher while the mean E_c values for TP4 and TP5 are approximately 14% less. Test pile TP3 shows that the average E_c value is less than the static modulus value by 38%, which leaves some doubt regarding the quality of concrete in this pile. From the experience gained here, it would therefore be inappropriate to adopt the laboratory E_c determined values to evaluate pile axial forces.

4.3.5 Non-linear load-strain relationship by power regression

The elastic modulus of concrete E_c may be back-analysed from the strain ε at the first instrument level where the axial force P is known, hence

$$E_c = \frac{P - E_s A_s \varepsilon}{\varepsilon A_c} \tag{4.9}$$

Curve fitting was carried out on plots of E_c versus ε to express E_c in the form

$$E_c = a_o \varepsilon^{-a_1} \tag{4.9a}$$

in which the constants a_o and a_1 were evaluated by power regression. The force P at a given level was then calculated by making P the subject in Eqn. (4.9) and substituting for E_c from Eqn (4.9a), hence

$$P = a_o \varepsilon^{(1-a_1)} A_c + E_s A_s \varepsilon \tag{4.9b}$$

		E_c, σ_o	TP2*	TP3	TP4*	TP5	TP6
1	Load	E_c	41.05	28.59	33.46	31.85	36.36
		σ_o	0.539	1.175	0.251	1.266	0.596
	Unload	E_c	46.54	32.48	38.04	34.81	39.52
		σ_o	-0.160	0.230	-0.381	0.631	0.274
2	Load	E_c	40.75	28.73	32.85	32.80	36.00
		σ_o	0.423	0.840	0.224	0.990	0.510
	Unload	E_c	45.43	32.18	34.67	34.75	37.75
		σ_o	-0.648	-0.519	-0.340	0.067	0.138
3	Load	E_c	42.53	26.90	33.33	31.58	34.94
		σ_o	0.099	0.504	0.059	0.690	0.509
	Unload	E_c	44.98	31.63	35.65	35.04	36.85
		σ_o	-0.464	-1.570	-0.517	-0.487	-0.368
4	Load	E_c	43.29	24.94	35.36	34.70	34.15
		σ_o	0.369	0.204	-0.097	0.551	0.120
	Unload	E_c	46.09	30.11	39.83	38.45	37.13
		σ_o	-0.291	-3.240	-1.401	-0.419	-0.948
5	Load	E_c	-	25.55	36.93	33.65	-
		σ_o	-	-0.921	-0.556	0.322	-
	Unload	E_c	-	30.88	38.85	37.74	-
		σ_o	-	-4.327	-1.206	-0.670	-
6	Load	E_c	-	-	-	32.96	-
		σ_o	-	-	-	0.446	-
	Unload	E_c	-	-	-	35.84	-
		σ_o	-	-	-	-0.268	-
Mean cylinder strength (kN/mm^2)			47.0	47.3	42.1	51.0	-
Mean static modulus (kN/mm^2)			38.0	40.0	41.1	39.0	-

Notes

*1) * Average readings of 2 strain gauges used because malfunction in the third strain gauge*

2) Both E_c and σ_o values are in kN/mm^2 but σ_o values are to be multiplied by 10^{-3}.

Table 4.4:Gauge stiffness calibration parameters for TP2-TP6

The back-figured variations of E_c with strain for all test piles are illustrated in Figs. 4.8(a)-(e), which also shows the best-fit curves calculated by power regression. For strain values less than $100x10^{-6}$, the apparent E_c value is very sensitive to the strain magnitude. This behaviour is reasonably well represented by the best-fit curve, which is also consistent with the fact that E_c approaches a constant value with high strain levels. The derived E_c versus strain relationships for pile TP5 are presented in Table 4.5.

Cycle	Power regression curve fitting
1	$E_c = 0.36616\varepsilon^{-0.53737}$
2	$E_c = 0.72129\varepsilon^{-0.46515}$
3	$E_c = 8.21102\varepsilon^{-0.176823}$
4	$E_c = 16.35066\varepsilon^{-0.101965}$
5	* As for load cycle 4
6	* As for load cycle 4

Table 4.5 Typical Power regression functions for E_c against ε variation (TP5)

Table 4.6 gives the calibrated values of E_c for various strain values for pile TP5. Virgin concrete generally exhibits considerably high E_c values due to structural changes. During a particular load cycle, the E_c value corresponding to a given strain value depends on the previous loading history.

Load	E_c values (kN/mm^2) for given values of ε (x10^{-6})							
cycle	50	100	150	200	250	300	350	400
1	65.2	51.8	47.4	45.2	43.8	42.9	42.3	41.8
2	57.7	45.4	41.3	39.2	38.0	37.1	36.6	36.1
3	47.0	41.5	38.3	36.5	35.3	33.8	34.2	36.8
4	43.9	41.7	40.2	39.0	38.2	37.4	36.7	36.8
5	As for load cycle 4							
6	As for load cycle 4							

Table 4.6: Typical E_c values obtained by power regression for TP5

4.4 ELASTIC CONSTANTS FROM A SHORT CONCRETE COLUMN

4.4.1 Introduction

According to evidence presented by Klink(1985a) and Klink(1985b), both the Young's modulus and the Poisson's ratio of concrete vary with radius on a cross-section of a cylindrical specimen. Both of these quantities could be 1.5 times greater at the centre than at the periphery of a concrete column. In the case of the test piles being calibrated, the problem is further complicated by the presence of steel casing in the upper part of the pile.

In the present study, the elastic properties of the test piles are investigated by separating the displacement patterns for steel, reinforced concrete and plain concrete. The displacements in these constituent materials are measured at selected radial distances from the centre of the short column, so that the variations in the values of elastic constants with position of measurement are taken into consideration. This provides an analytical capability that represents the composite nature of the column cross-section better than the technique of modular ratio and transformed area of concrete.

4.4.2 Simulation of pile material properties

It was envisaged to model the test pile properties using a 0.9m in diameter by 2m long reinforced concrete column constructed with the same concrete mix type and reinforcement as the test piles. The height of 2m was selected so as to have a suitable height to diameter ratio to minimise slenderness effects. At the same time, this length was adequate to allow the measurement of strains at the column mid height sufficiently away from the ends where stress concentrations would inevitably occur. The column was also provided with the same type and size of steel casing as in the test piles, except that the casing covered the full length of the column.

The instruments used in the column were vibrating wire gauges and extensometers of the kinds used in the test piles. However, in the short column, strains were measured not only in the longitudinal direction but also in the circumferential and radial directions. In order to take into account the behaviour reported by Klink(1985a) and Klink(1985b), the radial and circumferential strains were measured at selected known radial distances from the axis of the column. The behaviour of the sleeved part of the test piles passing through the superficial deposits was modelled using test No.1 of the short column in which the steel casing was present. In test No.2 of the short column, the casing was removed, and this was intended to simulate the deformation patterns in the unlined sections of the test piles.

4.4.3 Numerical modelling of the short column

4.4.3.1 Theoretical representation of pile cross-section

Let the column cross-section be represented by a number of (say N), concentric hollow cylinders with different material properties. This is shown in Fig. 4.8(f). Let the dimensions and properties of the n^{th} cylinder be:

r_{n-1} = internal radius; r_n = external radius; E_n = Young's modulus; ν_n = Poisson's ratio; A_n = Cross-sectional area. For the innermost cylinder, n=1, and for the outermost, n=N.

It is assumed that the deformation of the column comprises the deformations of the individual constituent cylinders. The following three loading stages are considered:

1) A unit applied longitudinal load,
2) Artificially introduced lateral pressures on the contact surfaces of the cylinders to correct the incompatible radial displacements arising from load case (1) above, and
3) Superposition of above load cases to produce the final state of stress and deformation

The following assumptions are made:

(a) Each cylinder is free to displace radially in isolation.

(b) There is no eccentricity in the applied load.

(c) Shear stresses on boundary surfaces may be neglected.

(d) The material of each cylinder obeys Hooke's law, and

(e) There is a small but essential cavity of radius r_o at the centre of the column (the cavity can be mathematically set to zero).

4.4.3.2 Analysis of stresses and strains

In load case (1), elasticity relationships from elementary mechanics (Timoshenko and Gere,1972) are used to derive the axial, radial and circumferential stresses, $\sigma'_{nz}, \sigma'_{nr}, \sigma'_{n\theta}$ in the n^{th} cylinder due to unit applied axial load. Taking tensile stresses as positive, the stresses for load case (i) can be expressed in matrix form as:

$$\begin{Bmatrix} \sigma'_{nz} \\ - \\ \sigma'_{nr} \\ \sigma'_{n\theta} \end{Bmatrix} = \begin{Bmatrix} \dfrac{-1}{A_n + \dfrac{1}{E_n}\left(\sum_{i=1}^{n-1} A_i E_i + \sum_{i=n+1}^{N} A_i E_i\right)} \\ 0 \\ 0 \end{Bmatrix} \tag{4.10}$$

Therefore the resulting axial, radial and circumferential strains $\varepsilon'_{nz}, \varepsilon'_{nr}, \varepsilon'_{n\theta}$ in the n^{th} cylinder due to load case (i) are:

$$\begin{Bmatrix} \varepsilon'_{nz} \\ \varepsilon'_{nr} \\ \varepsilon'_{n\theta} \end{Bmatrix} = \frac{1}{E_n} \begin{bmatrix} 1 & -\nu_n & -\nu_n \\ -\nu_n & 1 & -\nu_n \\ -\nu_n & -\nu_n & 1 \end{bmatrix} \begin{Bmatrix} \sigma'_{nz} \\ \sigma'_{nr} \\ \sigma'_{n\theta} \end{Bmatrix}$$

$$= \frac{1}{E_n} \begin{bmatrix} \underline{1} & \underline{-\nu_n} & \underline{-\nu_n} \\ -\nu_n & 1 & -\nu_n \\ -\nu_n & -\nu_n & 1 \end{bmatrix} \begin{Bmatrix} \dfrac{-1}{A_n + \dfrac{1}{E_n}\left(\sum_{i=1}^{n-1} A_i E_i + \sum_{i=n+1}^{N} A_i E_i\right)} \\ 0 \\ 0 \end{Bmatrix} \tag{4.11}$$

In load case (ii), let contact pressures p_{n-1} and p_n be imposed on the inner and outer surfaces of the n^{th} cylinder. For radial force equilibrium, the contact pressure on the outer surface of the $(n-1)^{th}$ cylinder must equal p_{n-1}. Similarly the pressure on the inner surface of the $(n+1)^{th}$ next cylinder must equal p_n There is no pressure on the inner surface of the first cylinder as well as on the outer surface of the last cylinder.

The stresses induced at any radial co-ordinate r (measured from the centre of the column) within the n^{th} cylinder, may be derived from established formulae from the theory of "thick cylinders" (Popov,1976). Hence the axial, radial and circumferential stresses $\sigma''_{nz}, \sigma''_{nr}, \sigma''_{n\theta}$ in the n^{th} cylinder for load case (ii), which now vary with radial distance, are given by:

$$\begin{Bmatrix} 1\sigma''_{nz} \\ -\sigma''_{nr} \\ -\sigma''_{n\theta} \end{Bmatrix} = \begin{Bmatrix} 0 \\ -p_{n-1}\left(\dfrac{r_{n-1}^2}{r_n^2 - r_{n-1}^2}\right)\left(1-\dfrac{r_n^2}{r^2}\right) + p_n\left(\dfrac{r_n^2}{r_n^2 - r_{n-1}^2}\right)\left(1-\dfrac{r_{n-1}^2}{r^2}\right) \\ -p_{n-1}\left(\dfrac{r_{n-1}^2}{r_n^2 - r_{n-1}^2}\right)\left(1-\dfrac{r_n^2}{r^2}\right) + p_n\left(\dfrac{r_n^2}{r_n^2 - r_{n-1}^2}\right)\left(1+\dfrac{r_{n-1}^2}{r^2}\right) \end{Bmatrix} \tag{4.12}$$

The ensuing strains $\varepsilon''_{nz}, \varepsilon''_{nr}, \varepsilon''_{n\theta}$ are again given in terms of the stresses and elastic constants as,

$$\begin{Bmatrix} \varepsilon''_{nz} \\ \varepsilon''_{nr} \\ \varepsilon''_{n\theta} \end{Bmatrix} = \frac{1}{E_n} \begin{bmatrix} 1 & -\nu_n & -\nu_n \\ -\nu_n & 1 & -\nu_n \\ -\nu_n & -\nu_n & 1 \end{bmatrix} \begin{Bmatrix} \sigma''_{nz} \\ \sigma''_{nr} \\ \sigma''_{n\theta} \end{Bmatrix}$$

$$=\frac{1}{E_n}\begin{bmatrix} 1 & -\nu_n & -\nu_n \\ -\nu_n & 1 & -\nu_n \\ -\nu_n & -\nu_n & 1 \end{bmatrix}\begin{Bmatrix} 0 \\ -p_{n-1}\left(\frac{r_{n-1}^2}{r_n^2-r_{n-1}^2}\right)\left(1-\frac{r_n^2}{r^2}\right)+p_n\left(\frac{r_n^2}{r_n^2-r_{n-1}^2}\right)\left(1-\frac{r_{n-1}^2}{r^2}\right) \\ -p_{n-1}\left(\frac{r_{n-1}^2}{r_n^2-r_{n-1}^2}\right)\left(1-\frac{r_n^2}{r^2}\right)+p_n\left(\frac{r_n^2}{r_n^2-r_{n-1}^2}\right)\left(1+\frac{r_{n-1}^2}{r^2}\right) \end{Bmatrix} \quad (4.13)$$

The stresses and strains in load cases (i) and (ii) can be superimposed, since the problem is assumed to be linearly elastic. Hence the final stresses $\sigma_{nz}, \sigma_{nr}, \sigma_{n\theta}$ in the n^{th} cylinder are given by:

$$\begin{Bmatrix} \sigma_{nz} \\ - \\ \sigma_{nr} \\ \sigma_{n\theta} \end{Bmatrix}=\begin{Bmatrix} \sigma'_{nz} \\ - \\ \sigma'_{nr} \\ \sigma'_{n\theta} \end{Bmatrix}+\begin{Bmatrix} \sigma''_{nz} \\ - \\ \sigma''_{nr} \\ \sigma''_{n\theta} \end{Bmatrix}=\begin{Bmatrix} \dfrac{-1}{A_n+\dfrac{1}{E_n}\left(\sum_{i=1}^{n-1}A_iE_i+\sum_{i=n+1}^{N}A_iE_i\right)} \\ -p_{n-1}\left(\frac{r_{n-1}^2}{r_n^2-r_{n-1}^2}\right)\left(1-\frac{r_n^2}{r^2}\right)+p_n\left(\frac{r_n^2}{r_n^2-r_{n-1}^2}\right)\left(1-\frac{r_{n-1}^2}{r^2}\right) \\ -p_{n-1}\left(\frac{r_{n-1}^2}{r_n^2-r_{n-1}^2}\right)\left(1-\frac{r_n^2}{r^2}\right)+p_n\left(\frac{r_n^2}{r_n^2-r_{n-1}^2}\right)\left(1+\frac{r_{n-1}^2}{r^2}\right) \end{Bmatrix} \quad (4.14)$$

Similarly, the final strains $\varepsilon_{nz}, \varepsilon_{nr}, \varepsilon_{n\theta}$ in the n^{th} cylinder are given by:

$$\begin{Bmatrix} \varepsilon_{nz} \\ \varepsilon_{nr} \\ \varepsilon_{n\theta} \end{Bmatrix}=\begin{Bmatrix} \varepsilon'_{nz} \\ \varepsilon'_{nr} \\ \varepsilon'_{n\theta} \end{Bmatrix}+\begin{Bmatrix} \varepsilon''_{nz} \\ \varepsilon''_{nr} \\ \varepsilon''_{n\theta} \end{Bmatrix} \quad (4.15)$$

4.4.3.3 Boundary conditions

The final state of stress and strain may be applied to satisfy the boundary conditions for force equilibrium and displacement compatibility. Once these conditions are satisfied, the cylinders are "assembled" to form the final state of stress and deformation of the column.

1) At the outside surface of the outermost cylinder (i.e the Nth cylinder), the pressure is atmospheric. Hence the net radial stress there is zero, thus

$$\left(\sigma_{Nr}\right)_{r=\frac{D}{2}} = 0 \qquad (4.16a)$$

Where D= column diameter.

2) The radial stresses at the interfaces of the cylinders must be in equilibrium. Consider the nth and the (n+1)th cylinders. Let the radial stress at the outside face of the nth cylinder be $\left(\sigma_{nr}\right)_{outside}$ while that at the inside face of the (n+1)th cylinder be $\left(\sigma_{(n+1)r}\right)_{inside}$. For equilibrium, we have

$$\left(\sigma_{(n+1)r}\right)_{inside} = \left(\sigma_{nr}\right)_{outside} \qquad (4.16b)$$

3) For compatibility of radial displacements at boundaries, the radial displacement of the outer surface of the nth cylinder must equal the radial displacement of the inner surface of the (n+1)th cylinder. Hence

$$\left(u_{nr}\right)_{outside} = \left(u_{(n+1)r}\right)_{inside} \qquad (4.16c)$$

4) Assuming that there is a small cavity at the centre of the column (the radius r_o of which can be mathematically set to zero), the radial stress at the inner surface of the first cylinder is zero, hence

$$\left(\sigma_{1r}\right)_{r=r_o} = 0 \tag{4.16d}$$

4.4.3.4 Determination of stresses and displacements

Equation 4.16(c) may be re-written to express the boundary radial displacements in terms of circumferential strains. The circumferential strain at the outer surface of the n[th] cylinder is given by

$$\left(\varepsilon_{n\theta}\right)_{outside} = \frac{\left(u_{nr}\right)_{outside}}{r_{outside}} \tag{4.17}$$

The circumferential strain at the inner surface of the (n+1)[th] can be expressed in a similar way. Therefore, the necessary and sufficient condition for displacement compatibility at boundaries is for the corresponding hoop strains to match. In addition, equating hoop strains rather than radial displacements eliminates the need for an integration process. For N number of cylinders, there are (N-1) boundaries. Thus, there will be (N-1) equations of compatibility containing an equal number of unknown radial pressures. These pressures can then be solved if the material properties are known.

4.4.3.5 Application of the analysis to predict the behaviour of the short column

In order to accurately model the behaviour of the short column and to account for the variation of elastic properties with radial distance, a three-cylinder configuration was proposed. The encased column is divided into concentric cylinders of three materials: (a) a plain concrete core, (b) a reinforced concrete zone, and (c) the pure steel casing. This is shown in Fig. 4.8(g). For stress and strain predictions for the column tested without steel casing, there are only two constituent cylinders. Parallel with the load test, the foregoing method has been used to calculate the deformations of the column.

The Young's modulus of steel and concrete were determined from laboratory tests on samples as 205 kN/mm^2 and 38 kN/mm^2 respectively. The Poisson's ratio value for steel and plain concrete were taken as 0.3 (BS5950:1990) and 0.2 respectively (BS8110:1985). The Young's modulus value for the reinforced concrete zone is initially estimated using an "equivalent area" approach, which gives a value of 43 kN/mm^2. Trial values of Poisson's ratio for reinforced concrete are then taken in the range 0.15-0.4.

Graphs of applied load versus the average strains from test No.1 are given in Fig.4.8(h). To avoid clutter, only the results of the first load cycle are shown, since the graphs for load cycles 2 and 3 also show approximately identical gradients. The plots for test No.2 are given in Fig. 4.8(j), for the first load cycle. The average gradients of these graphs represent strain per unit (1 kN) applied load and are called "normalised strains". The normalised strain values from all the gauges are presented in Table 4.7. The normalised strain values shown have been calculated by linear regression on at least 15 test data points.

	Test 1-column with 10mm steel casing				Test 2-column without steel casing			
	Extenso	Axial	Radial	Circum	Extenso	Axial	Radial	Circum
Cycle 1								
Load	33.64	29.90	7.95	8.96	35.45	30.35	8.60	8.20
Unload	33.17	27.58	7.95	8.53	34.79	30.45	8.36	8.35
Cycle 2								
Load	29.63	28.21	7.95	7.26	35.45	30.66	8.58	8.24
Unload	27.38	27.87	7.95	7.26	35.12	30.56	8.49	8.31
Cycle 3								
Load	29.85	27.81	7.78	7.31	35.85	30.42	8.63	8.37
Unload	28.88	26.63	7.78	7.74	35.47	30.89	8.40	8.44
Mean	30.43	28.00	7.89	7.39	35.36	30.56	8.51	8.32
Predicted	31.41		7.74	7.35	38.44		8.38	8.80

Table 4.7: Measured and predicted normalised strains (x 10^{-9}) per kN applied load

A back analysis method was devised to determine the elastic constants from actual measured strains. Tables 4.8-4.10 illustrate the influence of E and ν values on the predicted axial, radial and circumferential strains. In all cases, the following values have been kept constant:

$$E_s=205{,}000\ \text{N/mm}^2,\ \nu_s=0.3 \text{ and } \nu_c=0.2.$$

Various incremental values of the elastic constants E_c, E_b and ν_b were input into a purpose written computer program so that stresses and strains could be generated at required increments. It was also imperative to generate the strain values at radial co-ordinates corresponding to the locations of the embedded strain gauges.

Having carried out a sequence of formulations in order to determine the elastic constants, there are still uncertainties as to the true value of concrete modulus under loading. Therefore a range of values of elastic constants was generated with a view to judging the predicted strains. This study was carried out by the use of a purpose written computer program to compute stresses and strains, in three mutually perpendicular directions, at required locations. The measured strains were "targeted" in order to enable the choice of a range of correct E and ν values.

From this parametric study, the appropriate set of elastic constants to give the most accurate prediction of strain values, in all three directions, are listed in Table 4.11. The experimentally observed strains and the predicted strains in the short column are shown in the last two rows of Table 4.7. It is seen that the predicted strains are accurate to within 5% of the measured values and are remarkably consistent throughout.

Elastic constants for reinforced concrete		Predicted strains ($x10^{-9}$) at Instrument locations		
E_b (N/mm^2)	ν_b	Circum	Radial	Axial
38000	0.20	7.04	7.04	33.88
	0.22	7.37	7.55	33.80
	0.24	7.71	8.06	33.72
	0.26	8.04	8.56	33.65
	0.28	8.38	9.07	33.57
	0.30	8.71	9.58	33.49
40000	0.20	6.84	6.83	32.91
	0.22	7.17	7.33	32.84
	0.24	7.50	7.83	32.77
	0.26	7.82	8.32	32.69
	0.28	8.15	8.82	32.62
	0.30	8.48	9.32	32.54
42000	0.20	6.64	6.63	31.99
	0.22	6.96	7.12	31.92
	0.24	7.29	7.60	31.85
	0.26	7.61	8.09	31.78
	0.28	7.94	8.57	31.71
	0.30	8.26	9.06	31.64
44000	0.20	6.45	6.45	31.12
	0.22	6.77	6.92	31.05
	0.24	7.09	7.40	30.99
	0.26	7.41	7.87	30.92
	0.28	7.73	8.35	30.86
	0.30	8.05	8.82	30.79

Table 4.8: Predicted normalised strains for E_c=36000N/mm^2 per kN applied load

Elastic constants for reinforced concrete		Predicted strains (x10^{-9}) at Instrument locations		
E_b (N/mm^2)	ν_b	Circum	Radial	Axial
40000	0.20	6.74	6.74	32.48
	0.22	7.06	7.23	32.41
	0.24	7.38	7.72	32.33
	0.26	7.71	8.20	32.26
	0.28	8.03	8.69	32.18
	0.30	8.35	9.18	32.11
42000	0.20	6.55	6.54	31.58
	0.22	6.87	7.02	31.51
	0.24	7.19	7.50	31.44
	0.26	7.50	7.97	31.37
	0.28	7.82	8.45	31.30
	0.30	8.14	8.93	31.23
44000	0.20	6.37	6.36	30.74
	0.22	6.68	6.83	30.67
	0.24	6.99	7.30	30.60
	0.26	7.30	7.76	30.54
	0.28	7.62	8.23	30.47
	0.30	7.93	8.70	30.40
46000	0.20	6.20	6.19	29.93
	0.22	6.51	6.65	29.87
	0.24	6.82	7.11	29.80
	0.26	7.12	7.56	29.74
	0.28	7.43	8.02	29.67
	0.30	7.74	8.48	29.61
48000	0.20	6.04	6.02	29.17
	0.22	6.34	6.47	29.11
	0.24	6.65	6.92	29.05
	0.26	6.95	7.37	28.99
	0.28	7.26	7.82	28.93
	0.30	7.56	8.27	28.87

Table 4 9: Predicted normalised strains for E_c=38000N/mm^2 per kN applied load

Elastic constants for reinforced concrete		Predicted strains (x10^{-9}) at Instrument locations		
E_b (N/mm^2)	ν_b	Circum	Radial	Axial
42500	0.20	6.42	6.42	30.98
	0.22	6.73	6.89	30.91
	0.24	7.04	7.35	30.84
	0.26	7.34	7.82	30.78
	0.28	7.65	8.28	30.71
	0.30	7.96	8.75	30.64
45000	0.20	6.16	6.15	29.77
	0.22	6.46	6.61	29.72
	0.24	6.77	7.08	29.68
	0.26	7.07	7.54	29.63
	0.28	7.38	8.01	29.59
	0.30	7.69	8.46	29.54
47500	0.20	6.00	5.99	29.02
	0.22	6.30	6.43	28.96
	0.24	6.60	6.88	28.90
	0.26	6.90	7.32	28.83
	0.28	7.20	7.77	28.77
	0.30	7.50	8.21	28.71
50000	0.20	5.81	5.80	28.13
	0.22	6.10	6.23	28.07
	0.24	6.40	6.66	28.01
	0.26	6.69	7.10	27.95
	0.28	6.99	7.54	27.89
	0.30	7.28	7.97	27.83
52500	0.20	5.64	5.62	27.29
	0.22	5.93	6.04	27.23
	0.24	6.22	6.47	27.18
	0.26	6.50	6.89	27.12
	0.28	6.79	7.32	27.07
	0.30	7.08	7.74	27.01

Table 4.10: Predicted strains for E_c=40000N/mm^2 per kN applied axial load

Material	Young's modulus (kN/mm^2)	Poisson's ratio
Steel casing	205	0.30
Reinforced concrete zone (253mm-450mm radius)	42	0.25
Plain concrete core (0-253 mm radius)	38	0.20

Table 4.11: Appropriate elastic constants for constituent materials of the short column

4.5 EVALUATION OF LOAD TRANSFER FROM PILE TO SOIL

4.5.1 Introduction

The axial load distribution along a pile shaft gives a direct measurement of the pattern of load transfer to soil through the action of shaft resistance and end bearing. A careful interpretation of the axial force profile is necessary where there is potential for anomalies caused as a result of residual forces in the pile. The axial force variation along a given pile shaft is based on the strain gauge results incorporating the calibration methods previously described, namely:

1) The linear gauge stiffness method
2) The non-linear power regression method
3) The back-analysed elastic constants from a short composite column.

In addition to the use of the vibrating wire strain gauge readings, the shortening between various levels have also been calculated form the readings of the extensometers, and this also enables an assessment of axial forces. In this method, the elastic constants are taken from the polynomial function fit, since small values of compression are expected, which can be affected by the use of inaccurate elastic parameters for concrete.

4.5.2 Use of extensometer readings in estimating axial forces

Figures 4.9(a)-4.9(e) present the plots of extensometer readings versus applied load for test piles TP2-TP6. The overall pattern of increase in compression with applied load, even within the friction transferring length of the pile, is approximately linear. Connection of the graphs for successive load cycles produces discontinuities, but this does not substantially affect the calculated shortening, which is based on the algebraic difference between the readings of adjacent extensometers.

In Figures 4.9(f)-(k), the deduced shortening values between the various instrument levels have been plotted against the applied load. In order to use the calculated values of shortening to estimate axial forces, it is important to distinguish between the correct values and the cases of apparent malfunction of the extensometers. In addition, because of the non-linear behaviour of concrete at low strain values, it important to use the correct Young's modulus in order to achieve accurate results. Starting from a level of known axial force P_i, the force P_j at the next extensometer position is calculated from

$$\frac{\frac{1}{2}\left(P_i + P_j\right)L_{ij}}{E_{ij}A_{ij}} = e_{ij} \tag{4.18}$$

where L_{ij} = length of section from level i to j

E_{ij} = Young's modulus of concrete, appropriate for length i-j, depending on the mean value of strain in this section

A_{ij} = Equivalent concrete area for length i-j

e_{ij} = shortening of length i-j, deduced from extensometer readings.

4.5.3 Behaviour of pile TP6 in a pull-out test

Figure 4.9(*l*) is a plot of applied pull-out force versus pile head movement observed in pile TP6. In load cycle No. 1, for applied forces of 0-1MN, the pile head moves upwards at an approximate rate of 1.61mm/MN. The rate of movement of the pile head sharply increases to 6.28mm/MN for loads of 1.5-2.0MN. There is an unrecoverable pile head uplift of 2.46mm on unloading to zero. In load cycle No.2, the applied force versus pile head movement curve follows approximately the same path as that of unloading in the previous load cycle, until the applied load equals the maximum load in the previous load cycle. After this load level, the uplift rate increases steeply to about 12.2 mm/MN. This rate is more or less maintained throughout the load increment loci in cycles 3 and 4, although there is a slight recovery in load cycle 3. The broken line in Fig. 4.9(*l*) represents the variation of shaft resistance with pile head movement. At the maximum load of 8.5MN in load cycle 4, the shaft resistance is still increasing and therefore the failure point has not been reached.

A plot of base load versus applied pull-out force is shown in Fig 4.9(m). It is seen that the base load is constant at 326kN for applied loads of up to 250kN. The base load then decreases approximately linearly with applied load. Although the results available are insufficient to indicate the extent of linearity, if the straight line is projected until it cuts the horizontal axis, the upward force required to produce zero base resistance is estimated as 2.3MN. At this point, the shaft resistance equals the applied force less the self-weight of the pile.

Figure 4.9(n) illustrates the variation of strain at different levels with applied load. When the load reaches 2MN, there are rapid increases in strain at levels 1,2 and 4, which is due to concrete cracking. The cracking at 2.5MN load coincides with the dramatic change in the gradient of the applied force versus pile head movement. Very little tensile load reaches level 5 and hence the strain readings at this level remain approximately constant throughout the test. The level 3 gauges have not registered any cracking effects until the applied load reaches 3.5MN. The load-displacement behaviour and the strain gauge response are also supported by the data from the extensometers. Figure 4.9(p) shows that the all three extensometers record large movements when the applied load reaches 2MN. The concrete is fully cracked at applied loads in excess of 6MN when the extensometer readings become constant with applied load. The initial state of the pile prior to commencement of the pull-out test can be assessed by calculating the residual loads left in the pile at the end of the compression test. Since the strains left in the pile on zero load are small, it is necessary to obtain appropriate calibration curves for the calculation of axial forces, depending on the stress history of the concrete at a given level.

Figure 4.9(q) shows the variation of the apparent concrete modulus with strain as back-analysed from level 1 gauges in the compression test. The path of load increment in the first load cycle is marked 1+ whereas the load decrement curve is marked 1- (and so on). Table 4.12 shows the selected calibration curves for calculating axial forces at a given level, for a given load cycle.

	Level 1*		Level 2*		Level 3*		Level 4		Level 5	
	ε_{max}, ε_{min}	Curve	ε_{max}, ε_{min}	Curve	ε_{max}, ε_{min}	Curve	ε_{max}, ε_{min}	Curve	ε_{max} ε_{min}	Curve
1. LD	97.7	1+	85.0	1+	79.0	1+	59.0	1+	11.7	1+
UNLD	0.3	1-	-1.7	1-	0.3	1-	10.0	1-	0.7	1-
2. LD	166.0	2+	145.7	2+	138.3	2+	105.3	2+	17.3	1+
UNLD	1.0	2-	-2.0	2-	1.0	2-	15.7	2-	-2.3	1-
3. LD	286.0	3+	252.3	3+	254.0	3+	181.0	2+	28.3	1+
UNLD	8.3	3-	-0.3	3-	16.0	3-	23.7	2-	-5.3	1-
4. LD	420.3	4+	367.7	4+	377.7	4+	276.3	3+	69.0	1+
UNLD	26.0	4-	9.3	4-	36.7	4-	36.7	3-	3.7	1-
	Concrete area, A_c= 621.696x10^3 mm^2 Steel area, A_s= 43.065x10^3 mm^2						A_c= 621.696x10^3 mm^2 A_s= 14.476x10^3 mm^2			

* *These levels are located within the sleeved part of the pile*

Table 4.12: Selection of calibration curves for pile TP6

Curves 2+ and 2- are not utilized in the 4th load cycle, for which the axial force profile is required at zero loading. The functions given in Table 4.13 were derived, by regression methods, for the rest of the calibration curves.

	$E_c = a_0 \varepsilon^{a_1}$			$E_c = a_0 + a_1 \ln\varepsilon$		
	Curve numbers			Curve numbers		
	1+	1-	3+	3-	4+	4-
a_0	301.360	226.330	156.330	7.971	21.202	-25.216
a_1	0.431	-0.394	-0.271	4.952	2.442	10.301
r^*	-0.994	-0.964	-0.956	0.965	0.723	0.969

* *Correlation coefficient values*

Table 4.13: Calibration curves for load cycles 1,3 and 4: Pile TP6

Utilising the above stress-strain relationships of concrete, the shaft resistance distribution profile at zero load is shown in Fig. 4.9(r). The total shaft resistance of 311kN is almost balanced by the measured base resistance of 276kN. Therefore the initial positive shaft resistance before the start of the pull-out test is at most 3.7% of the projected peak shaft resistance in upward loading (taken as the maximum value reached of 8.5MN). In comparison, the peak shaft resistance in the compression test is estimated to be 12.0MN, using Chin's(1972) method.

4.5.4 Graphs of axial force versus depth for test piles loaded in compression

The variations of axial force for pile TP2 during load cycles 1-4 are presented in Fig. 4.10(a)- Fig. 4.10(d). Because the base load cell was omitted, the force at the toe has been estimated based on the difference between the total shaft resistance from level 1 to level 4 and the applied pile head load. However, this assumption produces much higher base resistance in comparison to other test piles. The continuous lines refer to the path of incremental loading, whereas the broken lines indicate axial force distributions during load decrements. Figures 4.11-4.14 present the axial force variations in piles TP3, TP4, TP5 and TP6. The force at a given level increases with an increase in the applied load. At a given applied load, the axial force decrease with depth along the pile.

The fashion of axial force variation along a given pile indicates the nature of load transfer to soil. In all cases, the axial force distribution at a given applied load, during load increment, is consistent with that on load decrement. The average unit shaft resistance at the mid-point between instrument levels was derived from the gradients of these graphs. Fig. 4.13(f) shows that, in pile TP5, which was pushed up to 227mm (equivalent to 25% diameter) a negative shaft resistance of 87kN was developed in load cycle 6, owing to pile recovery. With the exception of TP2, the average strain at the gauge level located just below the sleeved section of each pile is marginally less than that at the gauge level nearest to the pile head. At maximum applied loads in piles TP3, TP4, TP5 and TP6 the strain decrements from the pile head level to the bottom of the outer casing were 5%, 13%, 6% and 10% respectively. However, at the maximum applied load in pile TP2, there was a 19% increase in strain from the pile head level to the bottom of the outer casing. These strain differentials resulted in apparent load losses within the sleeved section of a given pile. It is thought that these losses were due to:

1) Friction at the knuckles installed at various points to ensure constant clearance between the inner and outer casings,
2) Possible variations in the pile cross-sectional area from one level to another,
3) Heterogeneity of concrete which makes the calibrated stress-strain relationship not a perfect representative of the behaviour of the entire pile.

In order to check the vertical equilibrium of a given pile, the shaft resistance was calculated from the load shedding curves and compared with the difference between the applied pile head load and the base load cell reading. Taking into account the load losses in the sleeved parts of the test piles, it was found that the maximum out-of-balance force was 13%. However, this margin reduced to 5% with the inclusion of the pile self weight.

Figures 4.12(a)-(e) shows extremely large decreases in axial force, in TP4, from instrument level 2 to level 3. Below strain gauge level 3, the slopes of the graphs are approximately constant, indicating a uniform shaft resistance. It is thought that the apparently large shaft resistance in mid-level 2-3 can be attributed to the interference with the steel liner during the installation of this pile. Therefore, the sudden collapse of the steel liner might have resulted in concrete being placed in the space between the liner and the pile surface, along part of mid-level 2-3.

4.5.5 Comparison between linear and non-linear calibration methods for axial force prediction

The axial forces at various strain gauge levels in each pile were calculated using both the linear and the non-linear concrete stress-strain approaches. Figure 4.15 shows the calculated variation of axial force with depth for test pile TP5, wherein the results of the two methods have been plotted on the same diagram. All the test piles show a similar behaviour, hence the graphs for these piles have not been included. The plots for TP5 show the locus of incremental loading only, from 2MN up to the failure point of approximately 11.2MN. This covers load cycles 1-4 only, since the maximum load of 11.2MN was realised in load cycle 4. Load cycles 5 and 6 were carried out for the purpose of studying the end bearing resistance development, since this required much larger pile deflections.

From Fig. 4.15, it is evident that both the linear and the non-linear calibration methods produce consistent and reliable predictions of the axial force variation along the pile shaft. There are small differences in the results obtained from these methods, which may be due to the imperfect linearity of the load-strain calibration graphs and to errors in representing the variation of concrete modulus with strain.

4.5.6 Comparison between the linear and non-linear calibration methods for pile shortening prediction

The elastic shortening of each test pile was calculated from the load transfer graphs and the pile stiffness results evaluated using both the linear and the non-linear methods. The calculated shortening values were then compared with the measured values, as deduced from the readings of the extensometers covering the entire pile length. For test pile TP5, this comparison is illustrated in Fig. 4.16. All the other test piles produced a similar pattern of behaviour, and hence have not been reproduced here. As expected, the non-linear method gives a more accurate prediction of pile shortening in the initial loading stages. Therefore, the deformation of the pile is sensitive to the variation of the apparent concrete stiffness along the pile.

The linear approach apparently provides a better accuracy in estimating axial load distribution and pile deformation at large load values. Virgin concrete generally shows initially high values of tangent modulus. As the strain is increased, the tangent modulus decreases rapidly and becomes approximately constant, provided the maximum compressive stress is not approached. Since there are strain variations along a typical pile, the total shortening at a given load is sensitive to the average stiffness of the pile.

4.6 MOBILISATION OF SHAFT AND BASE RESISTANCES

4.6.1 Introduction

A typical pile must be made to settle, to some extent, in order to mobilise either shaft resistance or end bearing resistance. The peak shaft resistance of a pile is produced at some small value of relative pile-soil slip. Slip is caused by the accumulated differences in shaft strain from axial load and the soil strain caused by the load transferred to it through shaft resistance. It has been argued by Bowles(1996) that as the applied load is increased, slip progresses downward along the pile. As the slip reaches maximum shaft resistance in the upper regions of the pile, load is transferred to lower regions, which reach maximum shaft resistance, and finally the pile base begins to support load. This mechanism is also a function of the length to diameter ratio for the pile.

Nevertheless, it is thought that the mechanism of load transfer in bored, cast in-situ piles formed in clay or weathered Keuper marl does not necessarily follow the trend suggested by Bowles(1996). The major objective of the instrumentation placed in the test piles was to establish the load transfer mechanism of large diameter, bored piles formed in Keuper marl. The pile test data are analysed to determine how pile settlement influences both shaft and base resistance development. In addition, the data is used to examine the forecasted pile settlement based on the recommendations contained in the soil investigation report. The differences between the rate of development of shaft resistance and end bearing for large diameter bored piles have already been discussed in the literature review.

4.6.2 Shaft resistance at strain gauge mid levels versus settlement

4.6.2.1 Pile TP2

The average shaft resistance between successive strain gauge levels was estimated from the slope of the plots of axial force versus depth. Figures 4.17(a) and (b) are plots of shaft resistance in mid-levels 2-3 and 3-4 respectively versus pile head settlement, for pile TP2. The results indicate that the shaft resistance in mid-level 2-3, in load cycle 1, increases with settlement at a slower rate than in load cycle 2. This is unlikely to be the true behaviour of the pile, since the pile shaft stiffness is expected to be greatest in the virgin load cycle. It is thought that the apparent shaft stiffness increase in load cycle 2 is due to the effects of installation of the pile. Another possibility is error resulting from using an average of only two strain readings to calculate axial forces. The third strain gauge located at the first instrument level did not function consistently. Figure 4.17(b) shows that the shaft resistance mobilised in mid-level 3-4 is much less than that in mid-level 2-3. It can be seen that as the maximum test load of 13.5MN approached, the slope of the shaft resistance versus settlement graph for mid-level 3-4 approaches zero while that of mid-level 2-3 is still high. Therefore, maximum shaft resistance is first developed in mid-level 3-4.

4.6.2.2 Pile TP3

Figures 4.18(a)-(d) present the variation of shaft resistance, at various mid-levels, with pile head settlement for pile TP3. The shaft resistance at all mid-levels are higher than in any other test pile, with the exception of TP4 which was known to have interference between the outer and inner casings. The mobilisation of shaft resistance at a given level, with respect to pile shaft settlement, again reflects variations in the properties of the Keuper marl. It was noted that the strains at levels 3 and 4 were approximately equal throughout all test cycles, hence producing equal forces at these levels. In Fig. 4.18(b), shaft resistance has been calculated over length 2-4. The strain readings indicate apparently very large shaft resistance between level 5 and the pile tip. It is thought that the actual pile diameter at level 5 might have been smaller than intended.

4.6.2.3 Pile TP4

Figure 4.19(a) represents the variation of shaft resistance in mid-level 2-3 with pile head settlement for TP4. There is an anomaly in the sense that shaft resistance is mobilised very rapidly up to $732kN/m^2$ at the peak load in cycle 3. Thereafter no significant increase in shaft resistance occurs during load cycle 4, despite an increase in pile head settlement from 25mm to 90mm. There is a sudden increase in shaft is resistance from $432kN/m^2$ to $1125kN/m^2$ when the pile head settlement increases from 90.4mm to 93.6mm. These anomalies reflect the uncertain condition of the pile shaft, following a suspected collapse of the casing. Figure 4.19(b) shows that a peak shaft resistance of $430kN/m^2$ occurred in mid-level 3-4 at a pile head settlement of 90mm, in load cycle 4. In load cycle 5, there is a decrease in shaft resistance to $320kN/m^2$. The shaft resistance variation with pile head settlement, for mid-level 4-5, is shown in Fig. 4.19(c). At the maximum applied load, the gradient of the graph is high and hence a substantial shaft resistance capacity still exists. Figure 4.19(d) presents the shaft resistance mobilisation in the region between level 5 and the pile tip. Similar to the results of pile TP3, the measured strains produce apparently very large shaft resistance of up to $2200kN/m^2$ in this region.

4.6.2.4 Pile TP5

Figures 4.20(a)-(d) present the shaft resistance variation with pile head settlement for mid-levels 2-3, 3-4, 4-5 and 5-pile toe, respectively. In Fig. 4.20(a), it can be seen that a peak shaft resistance of $330kN/m^2$ is attained in mid-level 2-3 at a settlement of 44.8mm. The shaft resistance remains approximately constant as settlement increases in the subsequent load cycles. At 238mm settlement corresponding to the maximum applied load in cycle 6, the shaft resistance has only decreases to $317kN/m^2$. From Fig. 4.20(b), the peak shaft resistance in mid-level 3-4 is $243kN/m^2$ and occurs at a settlement of 72mm. Hence peak shaft resistance in mid-level 3-4 is less than that in mid-level 2-3 and also requires more settlement to mobilise. As the pile head settlement increases to 178mm, in load cycle 6, the shaft resistance in mid-level 3-4 decreases to only $62kN/m^2$.

From Fig. 4.20(c), it is seen that a peak shaft resistance of $284kN/m^2$ is reached in mid-level 4-5 at a settlement of 44.8mm. Thereafter the shaft resistance decreases with increasing settlement but to a much lesser extent in comparison to mid-level 3-4. At the end of load cycle 6, there is a negative shaft resistance of $-172kN/m^2$ in mid-level 4-5. This may be a function of the pile recovery or of short-term development of residual load in the pile system, after a large pile head movement. Figure 4.20(d) illustrates that shaft resistance develops slower in the region between level 5 and the pile toe as compared to the upper portions of the pile. While peak shaft resistance has been developed in mid-levels 2-3, 3-4 and 4-5, the shaft resistance between level 5 and the pile toe is still increasing in load cycle 6.

4.6.2.5 Pile TP6

The shaft resistance versus settlement plots for the various mid-levels in pile TP6 are shown in Fig. 4.20(e)-(g). Maximum shaft resistance is not achieved anywhere along the pile. In mid-level 7-pile tip, the maximum positive shaft resistance of $240kN/m^2$ is approximately equal to the negative shaft resistance of $230kN/m^2$ on unload. This is consistent with the fact that having subjected the Keuper marl to shearing stresses approaching its peak resistance, in one direction, it should exhibit approximately the same shear strength in the reverse direction. This provides evidence that, prior to the load test, insignificant residual forces existed in the pile.

4.6.3 Comparison of shaft resistance with data from C.I.R.I.A. Report No. 47

The measured peak shaft resistance at various mid-levels in test piles TP3, TP4 and TP5, which were loaded to failure, are presented in Table 4.14. A description, of the Keuper marl strata at these mid-levels, based on weathering zone classification, is also included. The observed peak shaft resistance values are compared with values given in the C.I.R.I.A. Report No. 47, which are based on weathering zone classification. It is seen that the observed shaft resistance values are generally three times greater than the values given in C.I.R.I.A. Report No. 47. Therefore the Keuper marl at the Cardiff test pile sites has a higher strength than that that in the Midlands area on which the C.I.R.I.A. Report No. 47 data are based.

4.6.4 Shaft resistance variation with depth along the test piles

Figures 4.21(a)-(e) present the variation of shaft resistance with depth along each pile shaft, for given load increments up to the last load cycle. The graphs generally show that shaft resistance decreases with depth and reaches a minimum value at a point near the middle of the pile shaft.

	Strata zones	Measured peak shaft resistance (kN/m^2)	C.I.R.I.A. mean shaft resistance values (kN/m^2)
TP3			
2-4	IV & III	350	150
4-5	III	600	240
TP4			
2-3	IVa & IVb	*	75
3-4	IV & III	430	150
4-5	III & IV	*	150
TP5			
2-3	IVa	330	100
3-4	IVa	243	100
4-5	IVa	284	100
5-tip	IVa	450#	100

** Denotes not available; # Maximum value reached in test*

Table 4.14: Shaft resistance compared with C.I.R.I.A. Report No. 47 data

Figure 4.21(a) shows that in TP2, the ratio of shaft resistance in the upper regions of the pile to that in the region near the pile toe decreases to approximately unity as the load is increased from 1MN to 13.5MN. Further, as the load is increased, the middle part of the pile develops shaft resistance at the lowest rate in comparison to other regions. Figure 4.21(b) shows that, at each loading stage, the shaft resistance between depths 24-28m increases only marginally with depth. In contrast, there is a rapid increase in shaft resistance from depth 28m to the pile tot level. The trend observed in TP2 in which there is a minimum shaft resistance near the middle of the pile is also shown in TP4 (Fig. 4.21(c)). In pile TP5, Fig. 4.21(d) reveals that there is also a minimum shaft resistance at a location close to the middle of the pile. The peak shaft resistance in this pile was mobilised at an applied load of 9.5MN. It can be seen from Fig. 4.21(d) that after the mobilisation of peak shaft load, the shaft resistance distribution along the pile becomes approximately constant. In pile TP6, the variation of shaft resistance with depth shows a high sensitivity to the applied load level. Figure 4.21(e) reveals that for applied loads of up to 3.5MN, shaft resistance increases at an increasing rate with depth. At 5MN, the shaft resistance increases approximately linearly with depth. For greater loads, shaft resistance increases with depth at a decreasing rate and depicts a maximum point.

4.6.5 Mobilisation of end bearing resistance

In addition to the available data from the load cells, the load transmitted to the base of each test pile was estimated from the axial force distribution graphs. This was based on the assumption that the shaft resistance distribution between the last instrument level and the pile toe level was equal to that in the mid-level immediately above. In comparison to the base load cell reading, it was found that the estimated base loads from strain gauges were greater.

For low loads and pile head displacement values, it was anticipated that the strain gauges installed close to the pile toe level would record low strain values. Since the Young's modulus of concrete at low strains is subject to wide variations, greater error was expected in the computed axial force at the last instrument level, in comparison to other levels where larger strains were recorded. For this reason, it is thought that the base loads obtained directly from the load cells are more reliable. Figures 4.22(a)-(d) present plots of applied load, shaft load and base load versus net settlement (base movement) for the test piles. The base resistance versus base movement graph for pile TP2 (Fig. 4.22(a)) is thought not to represent the actual behaviour of the pile since the assumptions outlined above had to be made. These assumptions were necessary because no base load cell was installed in this pile. Apart from TP2, for base movements up to 50mm, very little base resistance was developed in the piles. Also, in this loading range, the base resistance appears to increase with base movement at an increasing rate. The excessive base movement initially occurring, with little development of load resistance, indicates that loose soil debris might have been present in the pile holes as concrete was placed.

Figure 4.22(d), which presents the results for pile TP5, reveals the base behaviour most comprehensively. For base movements exceeding 50mm, the base resistance increases with base movement at a decreasing rate. Figure 4.22(d) also shows that, at 228mm movement (equivalent to 25% of pile diameter), the point of ultimate base resistance is approached. In contrast, the peak shaft resistance occurs at a base movement of about 36mm (equivalent to 4% of pile diameter). At this point only about 18% of the ultimate base resistance are developed. Pile TP5 developed a clear maximum load capacity of 11.2MN at a base movement of 100mm (about 11% of the pile diameter). At this point, the shaft resistance had decreased to 7.7MN whereas the base resistance was 2.9MN. Therefore, the ultimate pile load capacity is not the sum of the peak shaft resistance plus the ultimate base resistance but rather, it comprises portions of these components of load resistance.

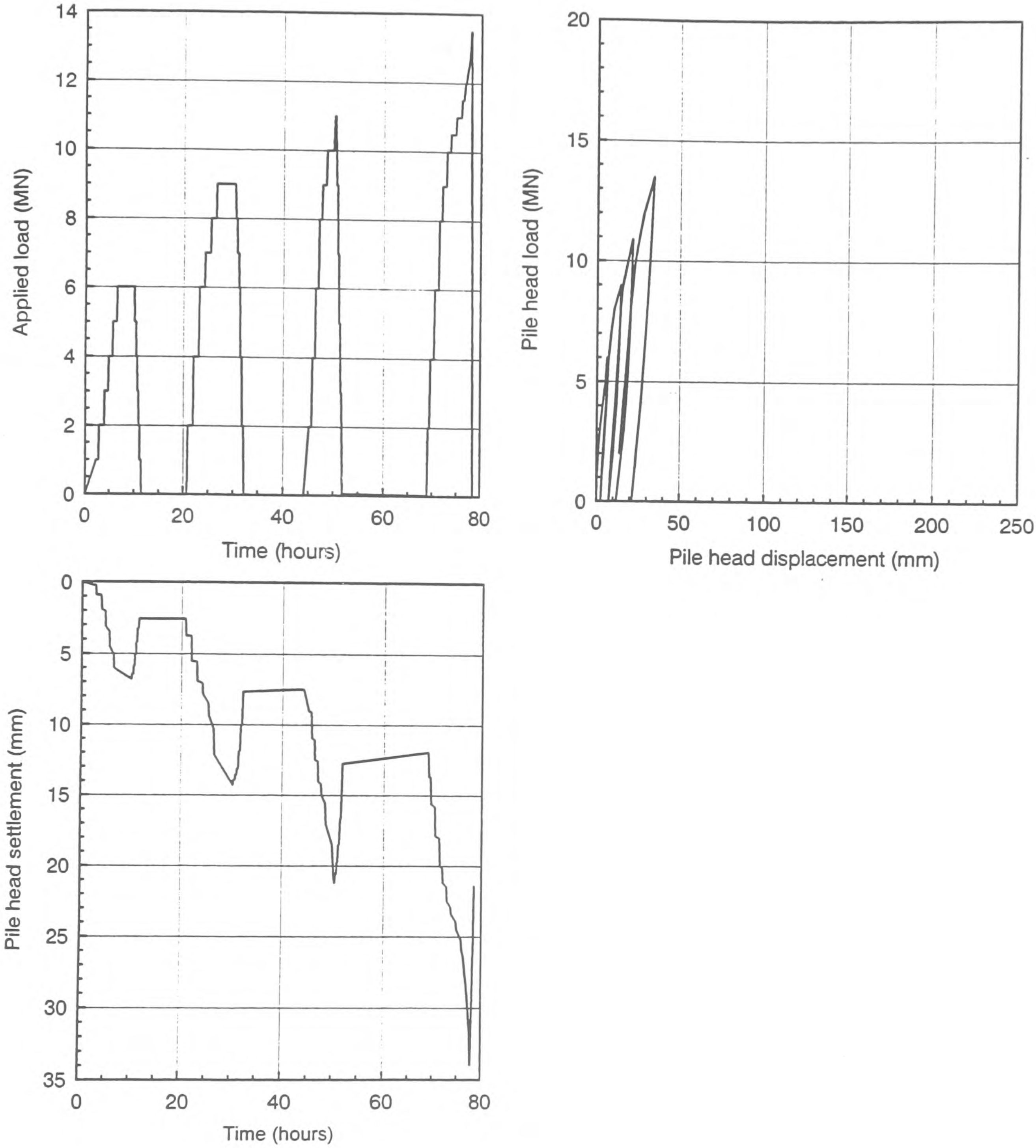

Fig 4.1: Load-Displacement-Time behaviour of TP2

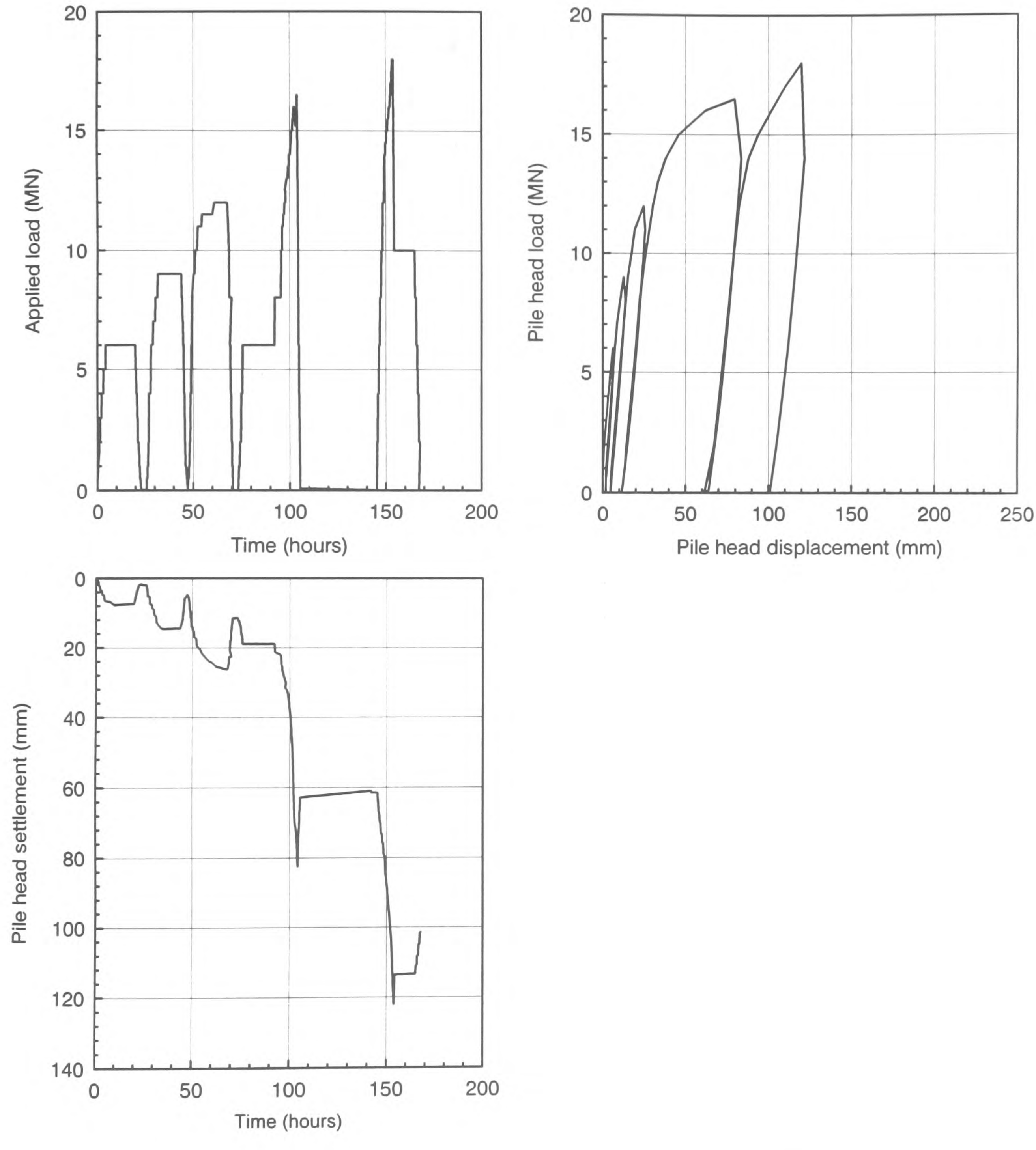

Fig 4.2: Load-Displacement-Time behaviour of TP3

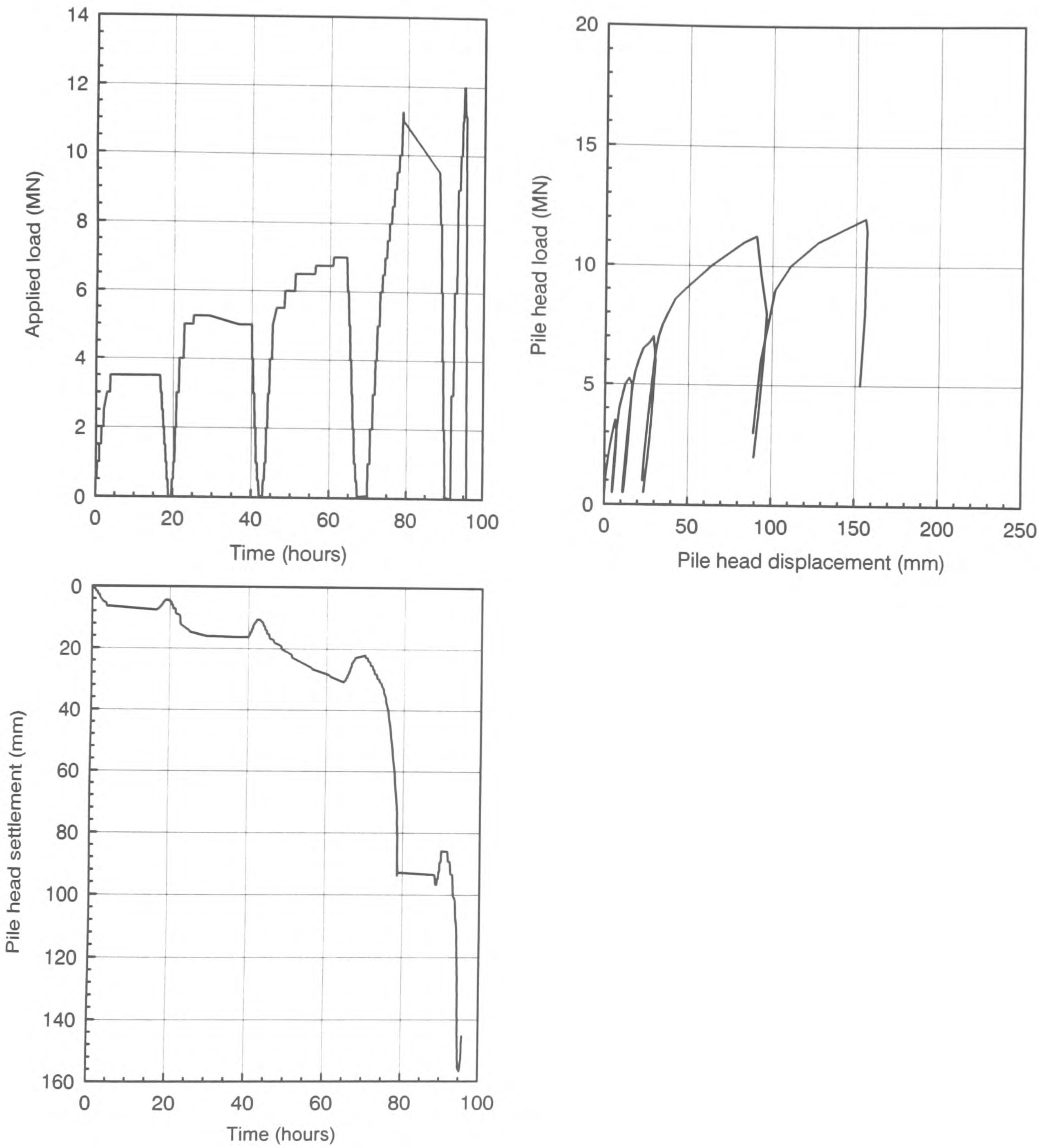

Fig 4.3: Load-Displacement-Time behaviour of TP4

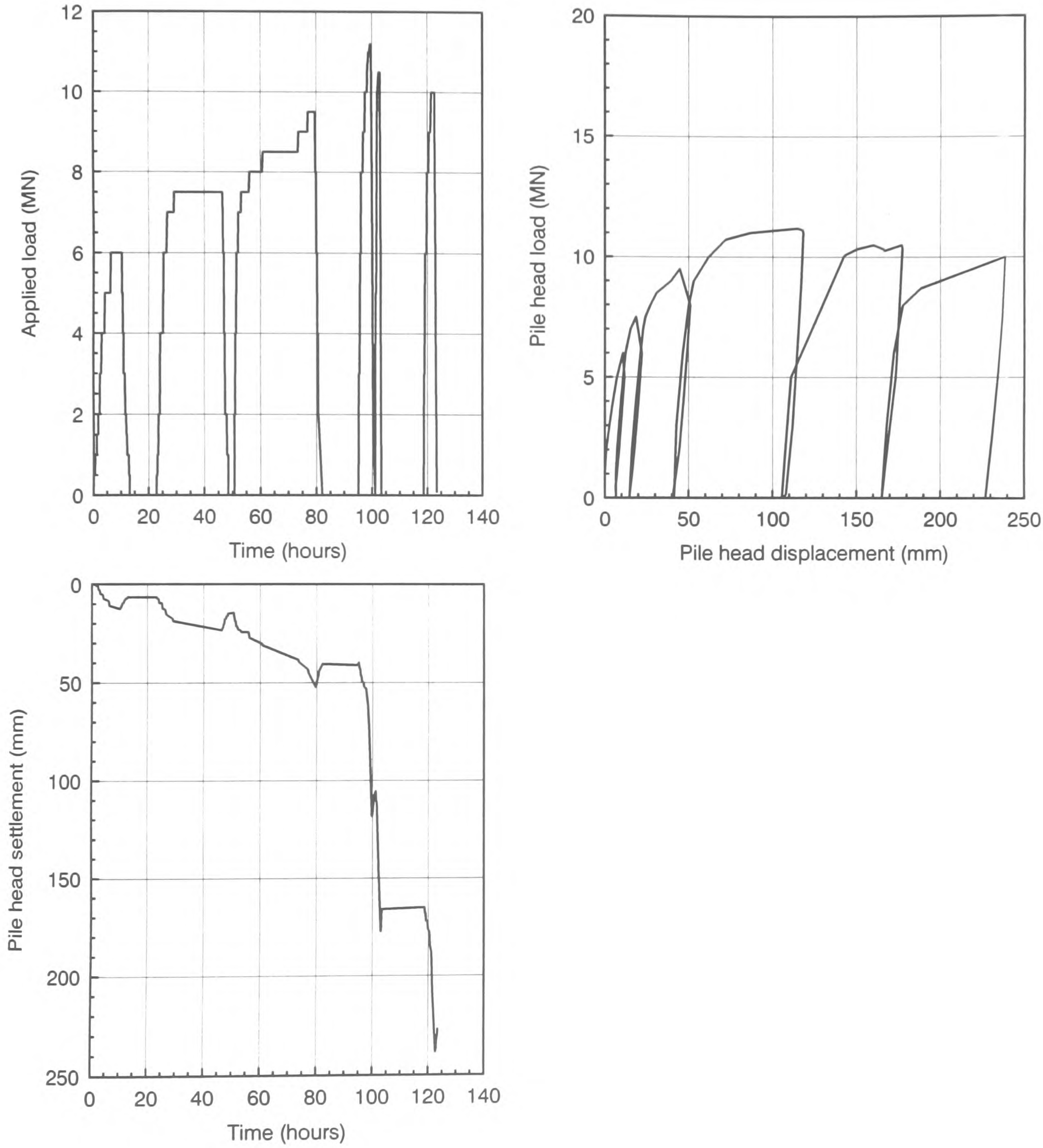

Fig 4.4: Load-Displacement-Time behaviour of TP5

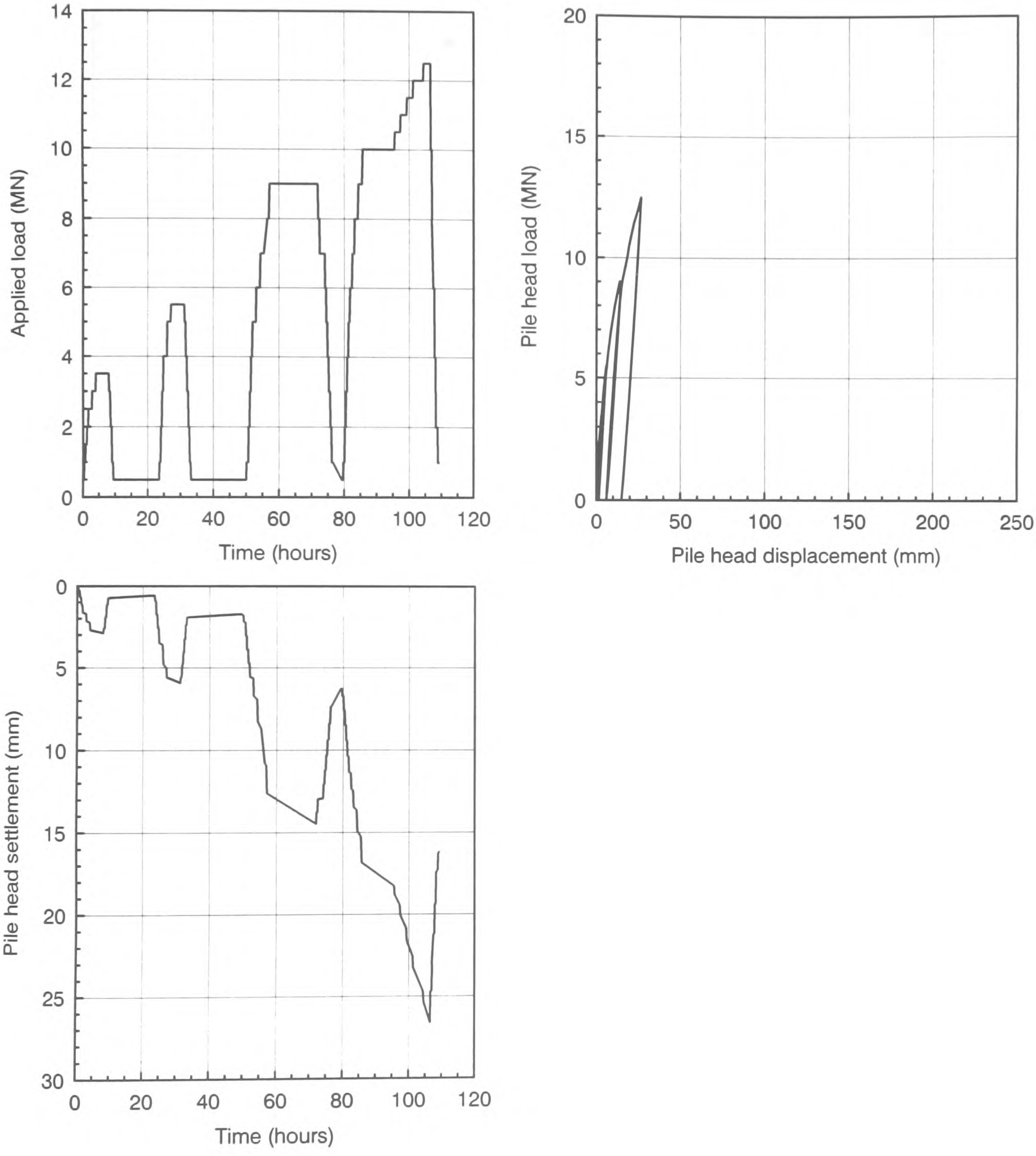

Fig 4.5: Load-Displacement-Time behaviour of TP6

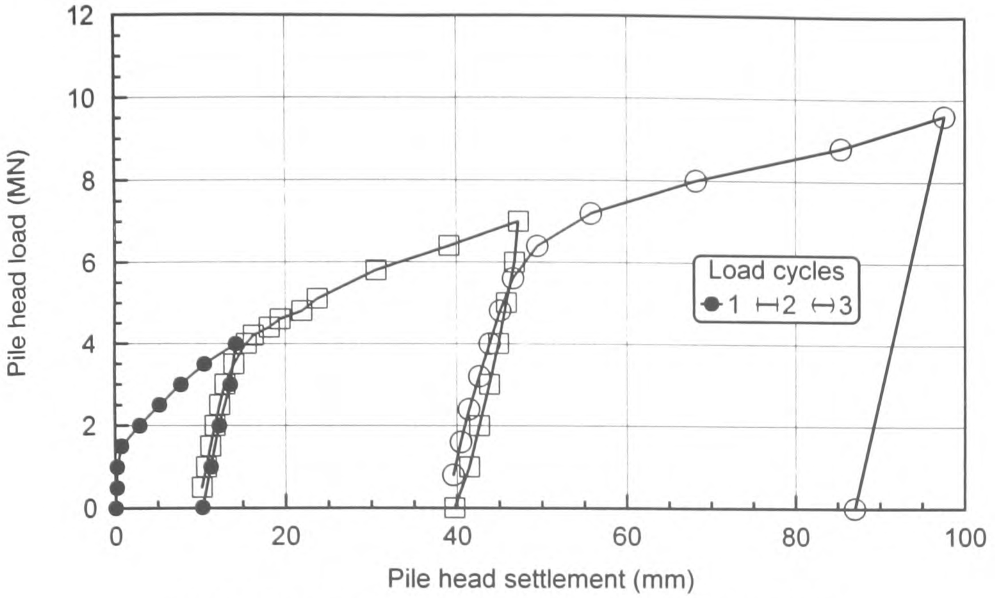

Fig 4.6(a):Load-Settlement graph for TP1(voided toe test)

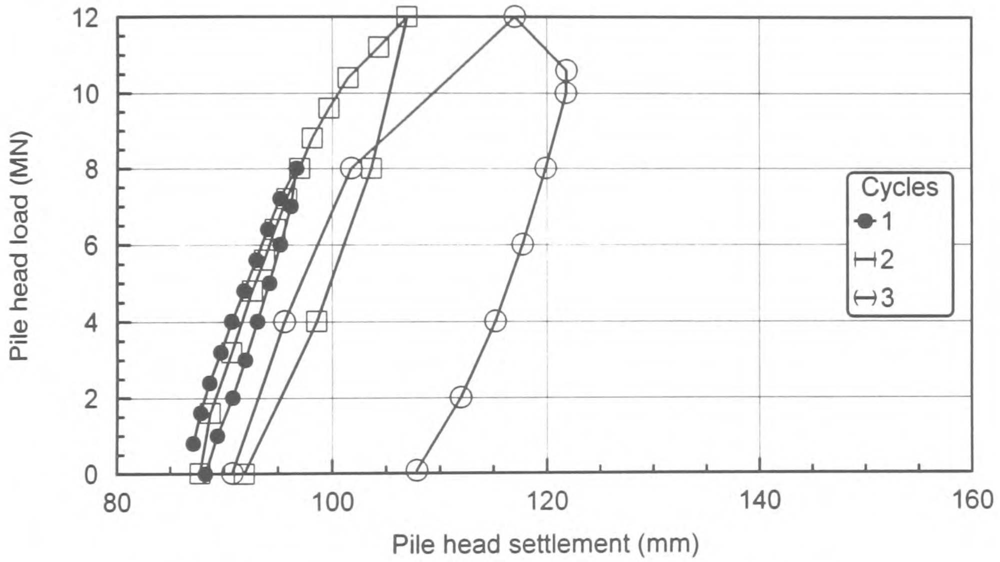

Fig 4.6(b):Load-Settlement graph for TP1(End Bearing M.L. test)

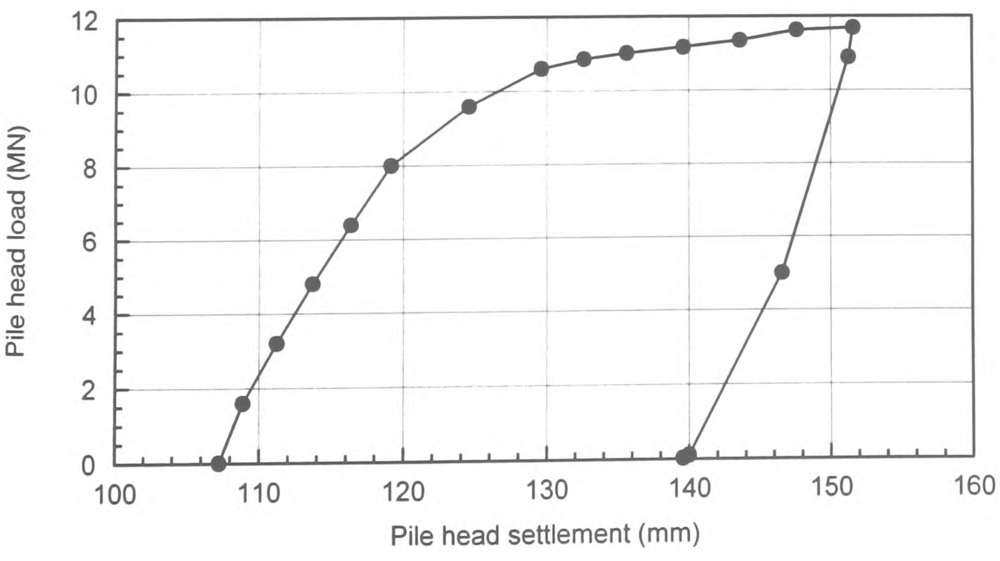

Fig 4.6(c):Load-Settlement graph for TP1(End Bearing C.R.P. test)

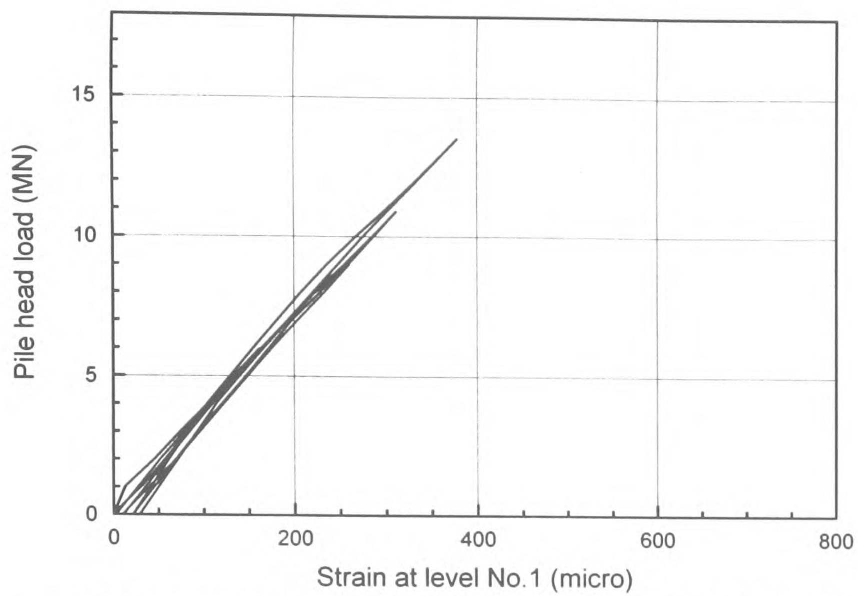

Fig 4.7(a):Applied load Vs pile strain at instrument level No.1 (TP2)

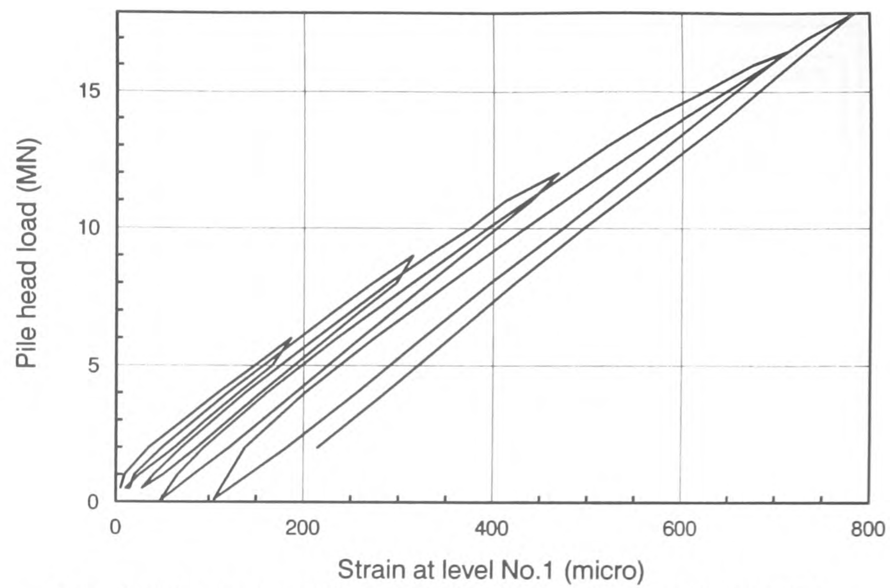

Fig 4.7(b):Applied load Vs pile strain at instrument level No.1 (TP3)

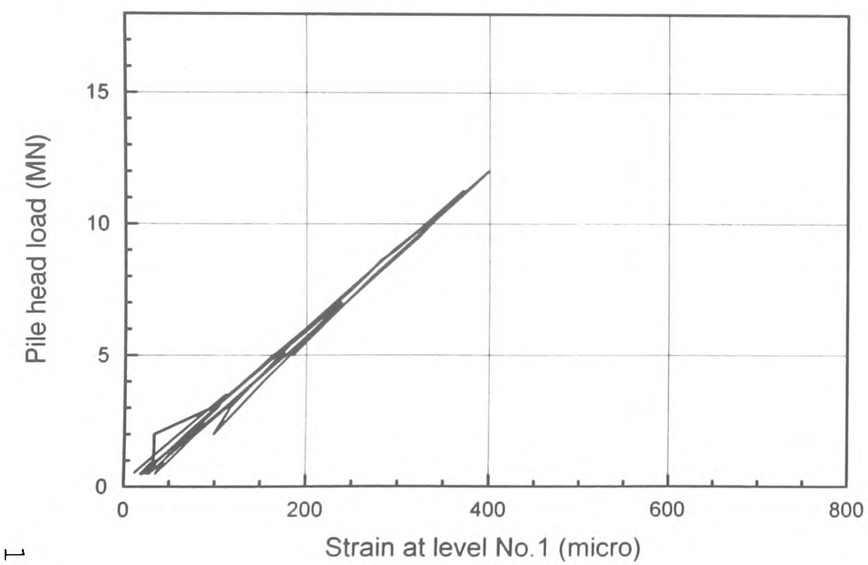

Fig 4.7(c):Applied load Vs pile strain at instrument level No.1 (TP4)

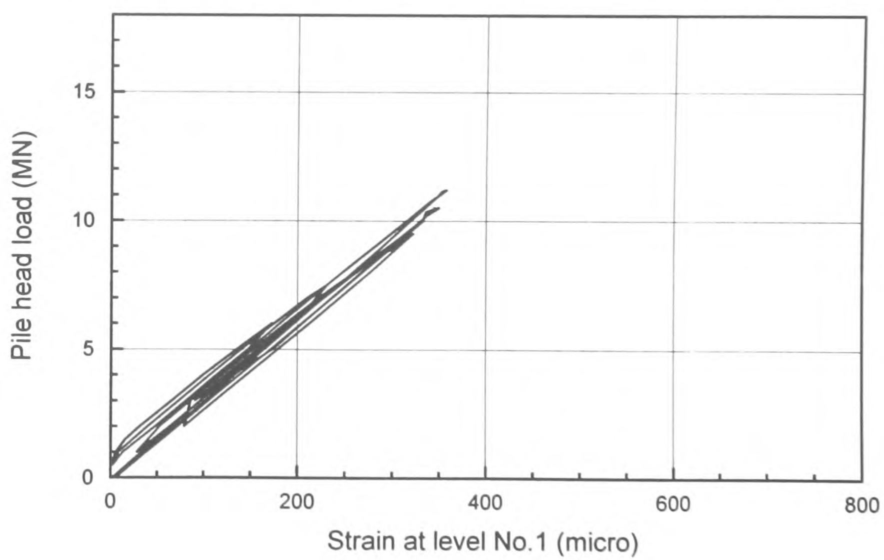

Fig 4.7(d):Applied load Vs pile strain at instrument level No.1 (TP5)

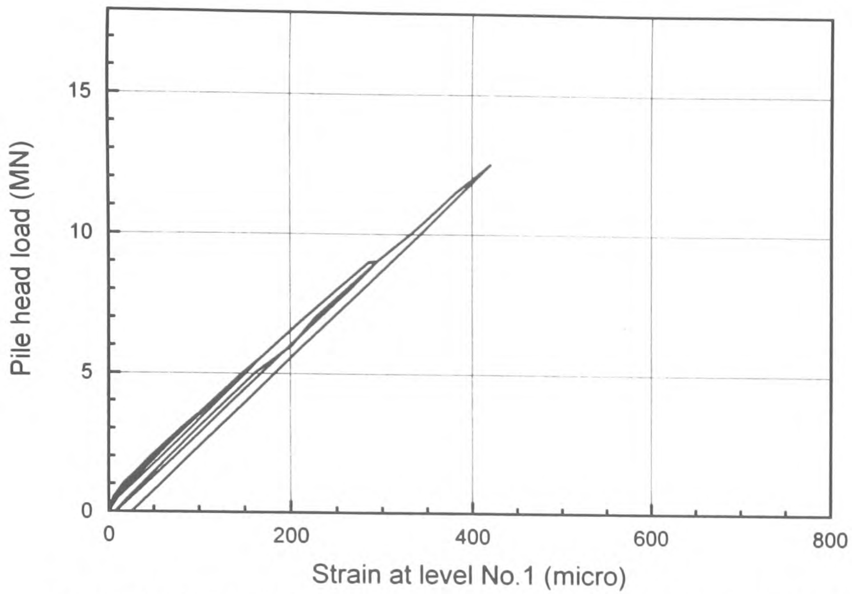

Fig 4.7(e):Applied load Vs pile strain at instrument level No.1 (TP6)

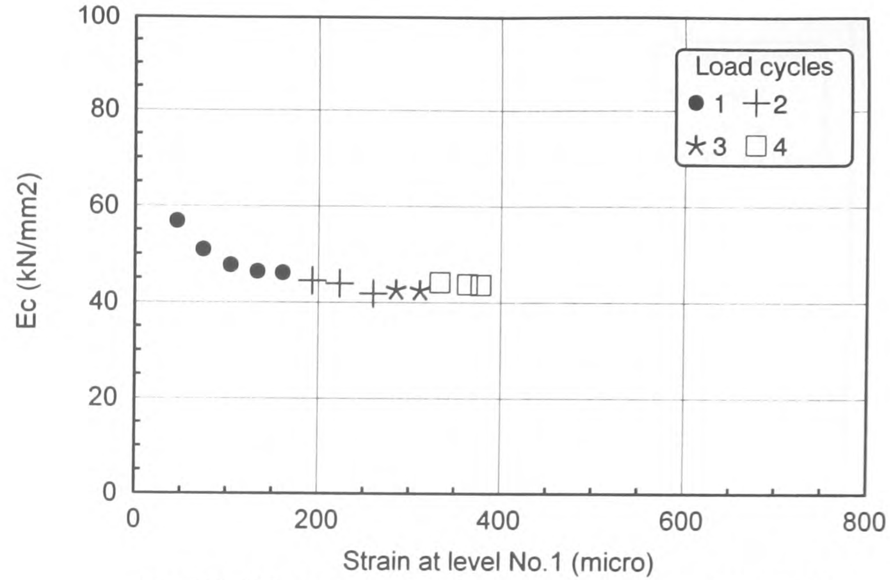

Fig 4.8(a):Young's modulus of concrete versus strain (TP2)

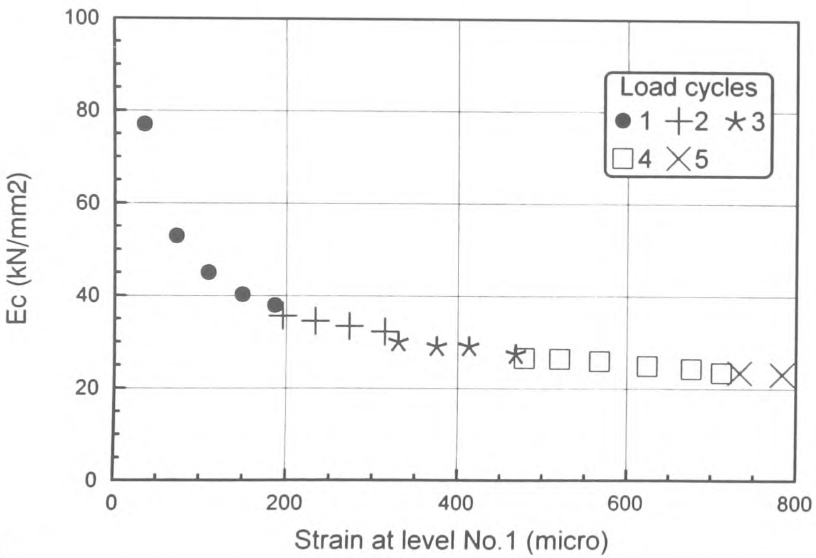

Fig 4.8(b):Young's modulus of concrete versus strain (TP3)

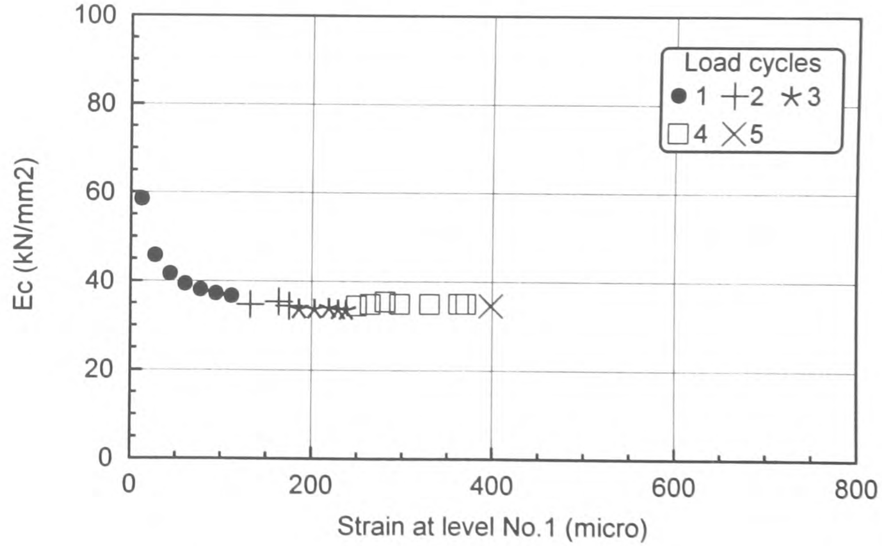

Fig 4.8(c):Young's modulus of concrete versus strain (TP4)

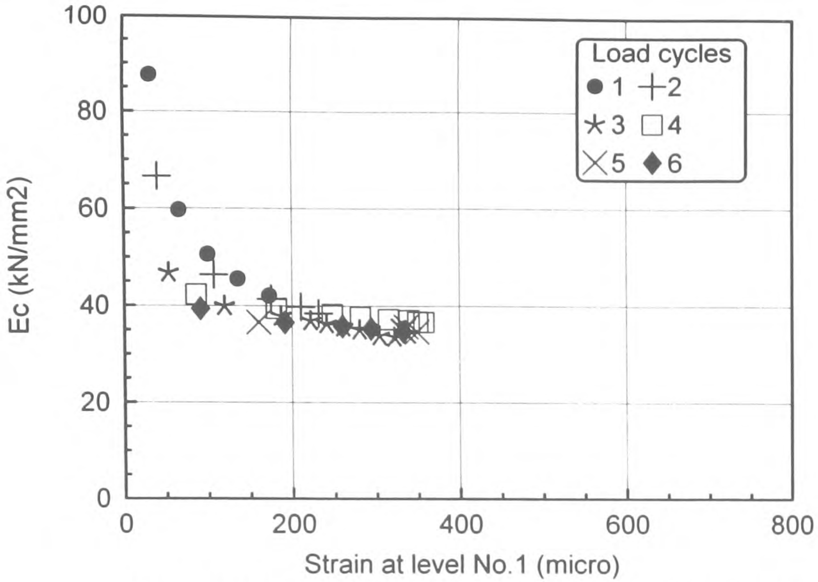

Fig 4.8(d):Young's modulus of concrete versus strain (TP5)

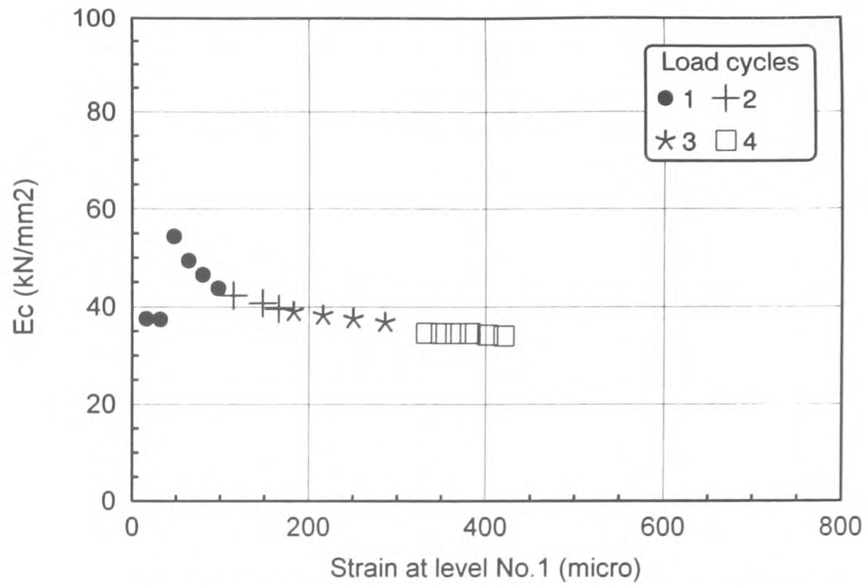

Fig 4.8(e):Young's modulus of concrete versus strain (TP6)

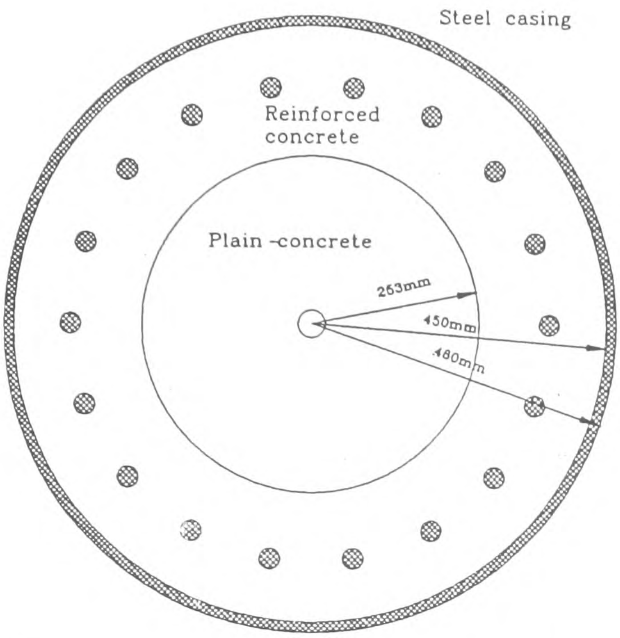

Fig. 4.8(f): Representation of column cross-section by three distinct annuli (steel, plain concrete and reinforced concrete

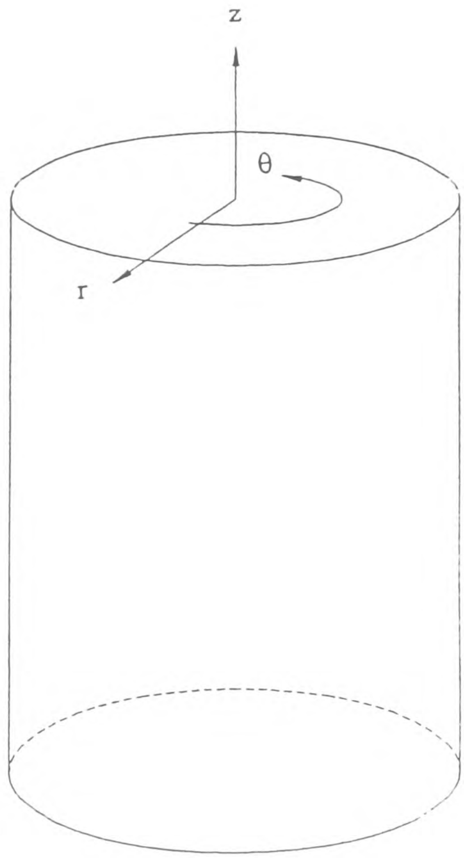

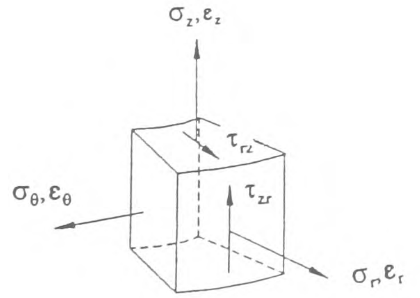

Fig. 4.8(g): Cylindrical co-ordinate system for stresses and strains

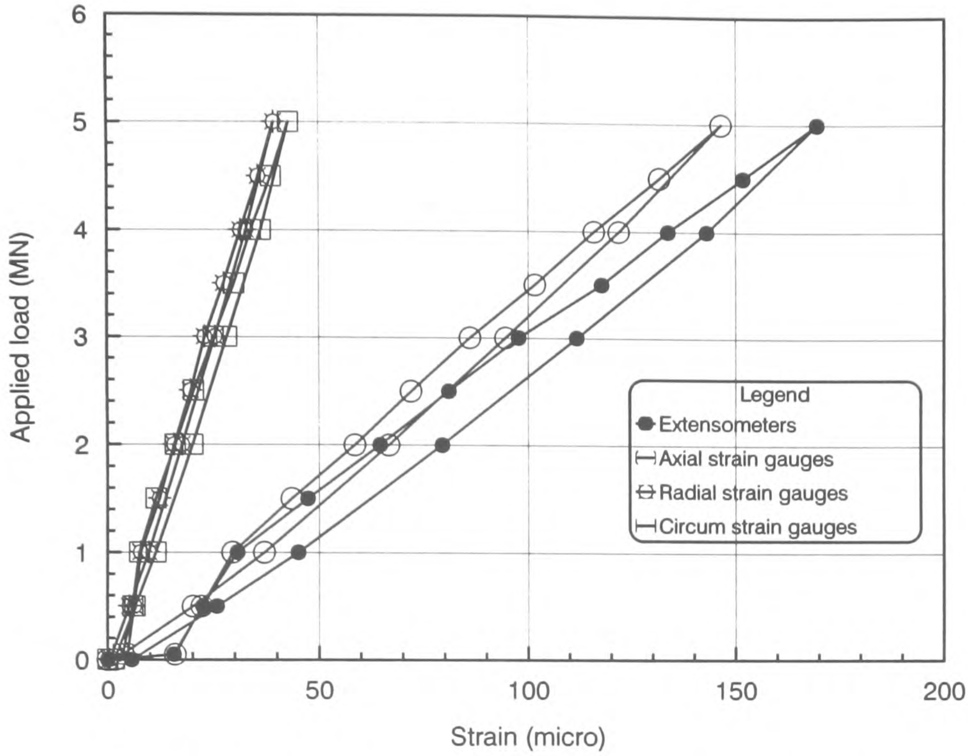

Fig 4.8(h): Applied load versus instrument readings in short column test No.1 (steel casing present)-Load cycle 1

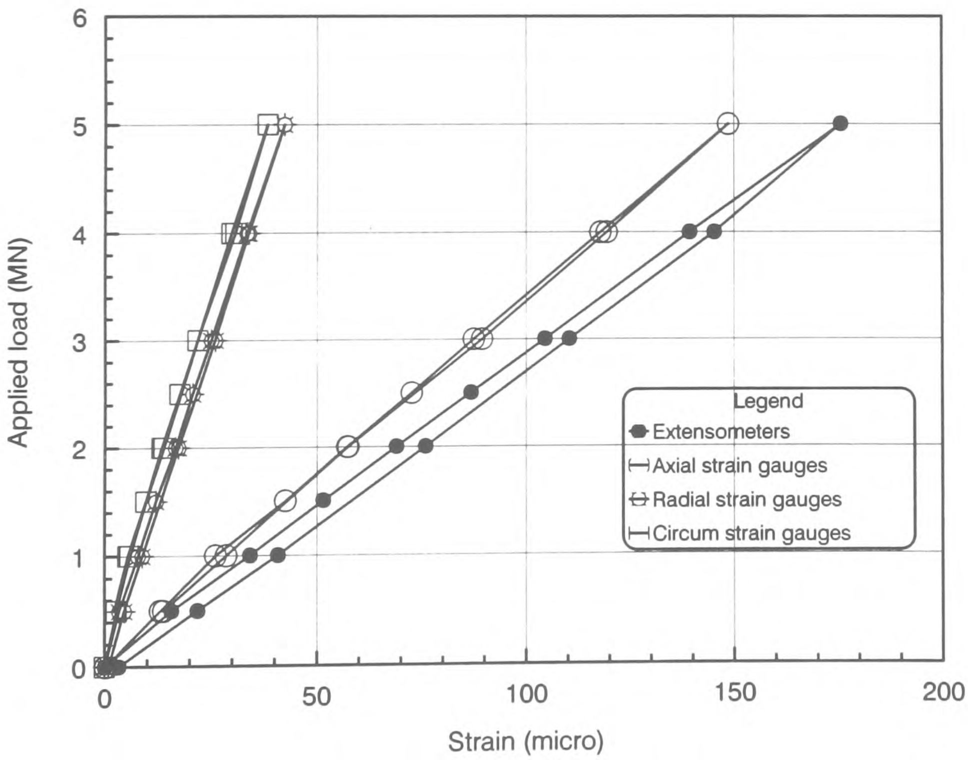

Fig 4.8(j): Applied load versus instrument readings in short column test No.2 (without steel casing)-Load cycle 1

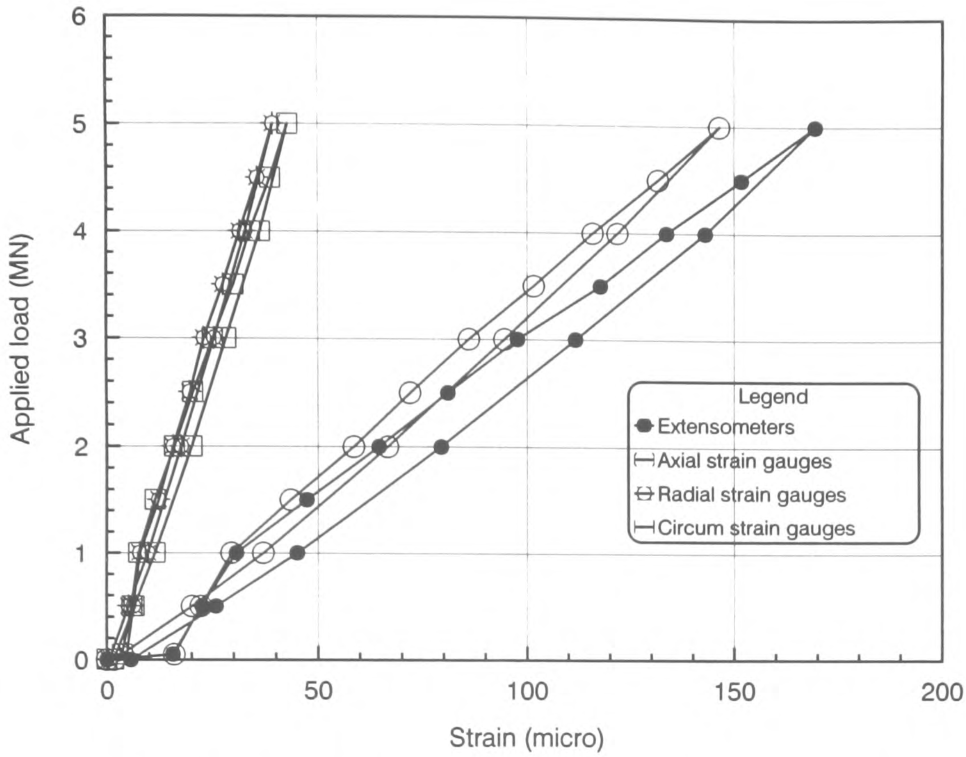

Fig 4.8(k): Applied load versus instrument readings in short column test No.1 (steel casing present)-Load cycle 1

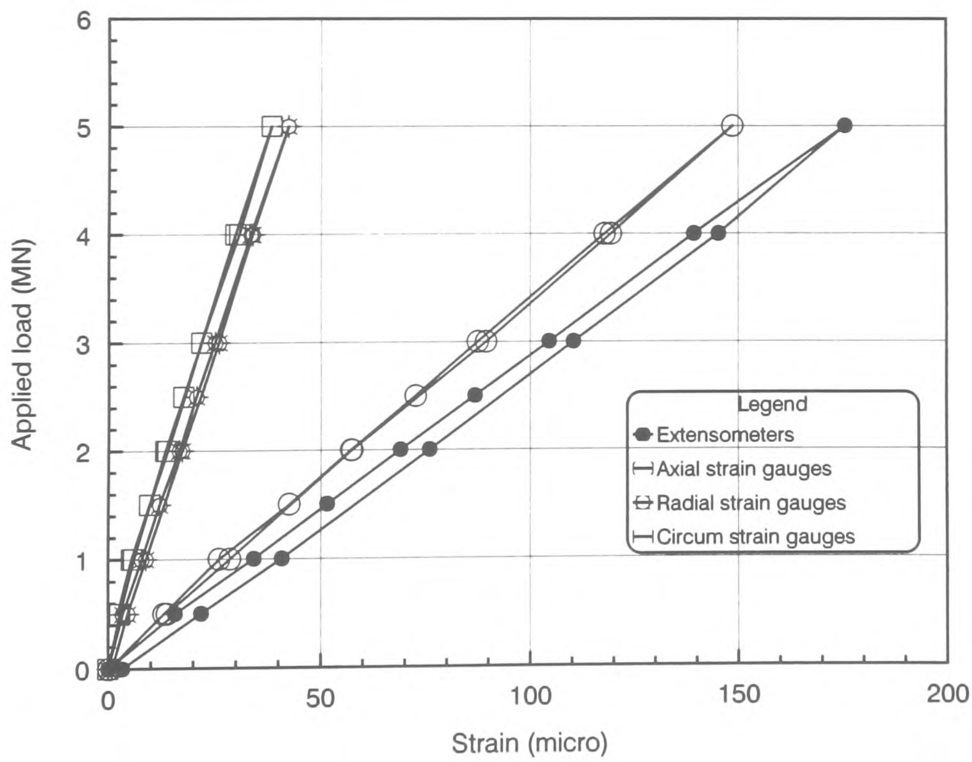

Fig 4.8(l): Applied load versus instrument readings in short column test No.2 (without steel casing)-Load cycle 1

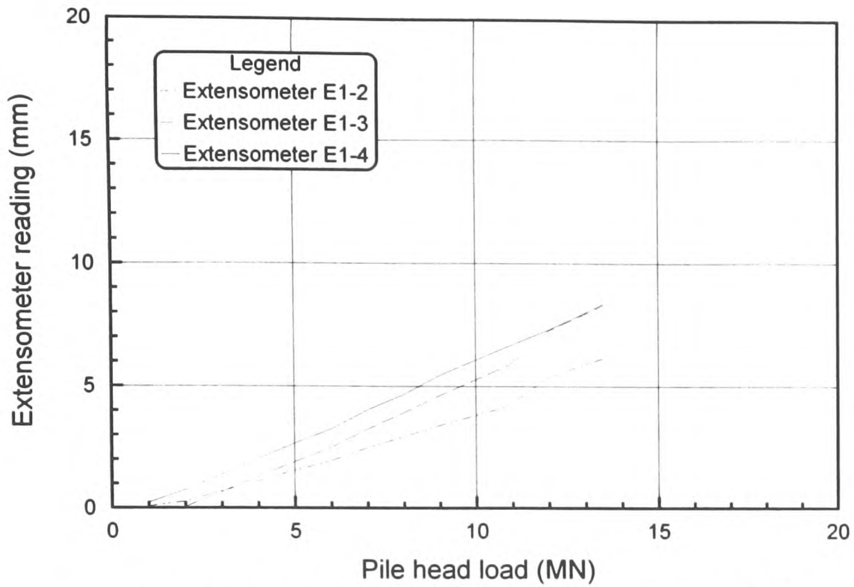

Fig 4.9(a):Extensometer reading versus applied load-TP2

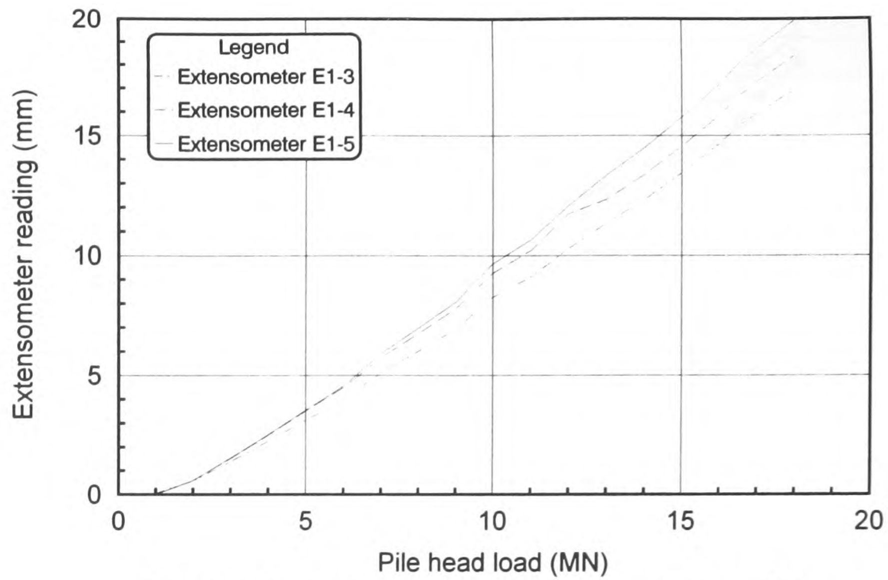

Fig 4.9(b):Extensometer reading versus applied load-TP3

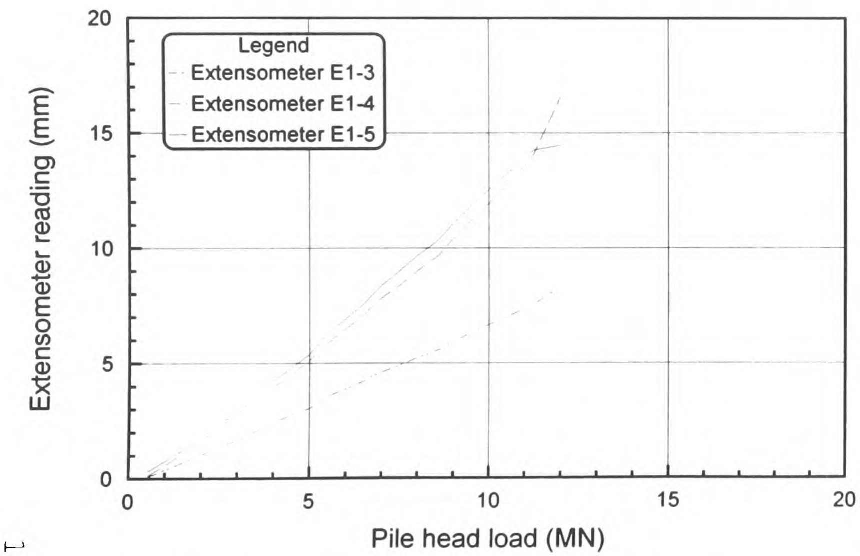

Fig 4.9(c):Extensometer reading versus applied load-TP4

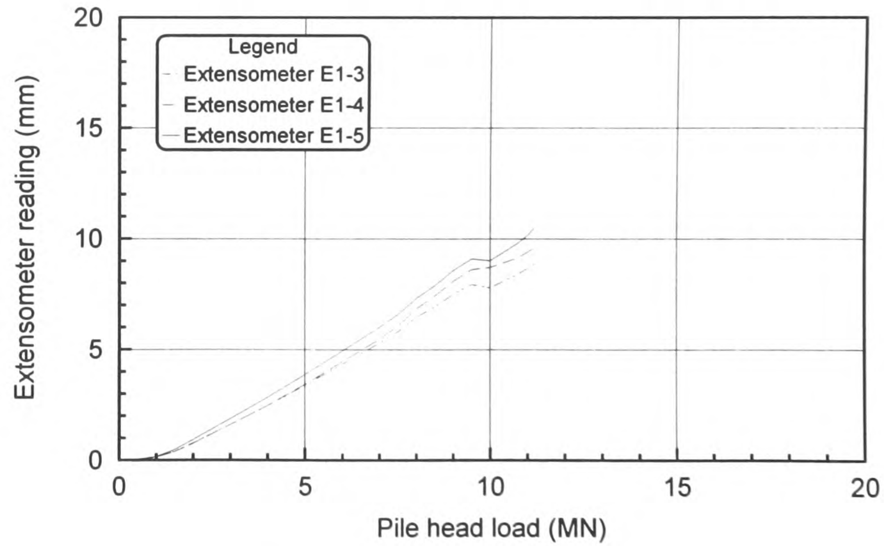

Fig 4.9(d):Extensometer reading versus applied load-TP5

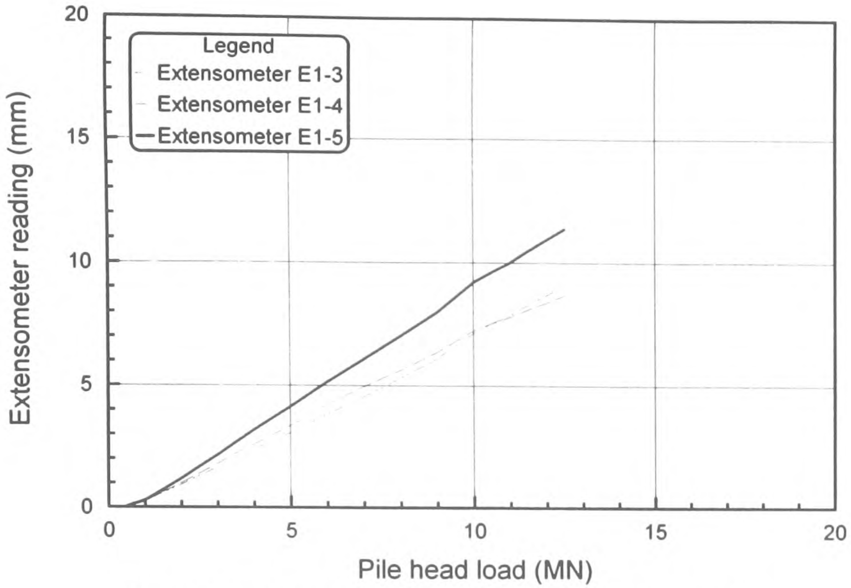

Fig 4.9(e)Extensometer reading Vs applied load-TP6

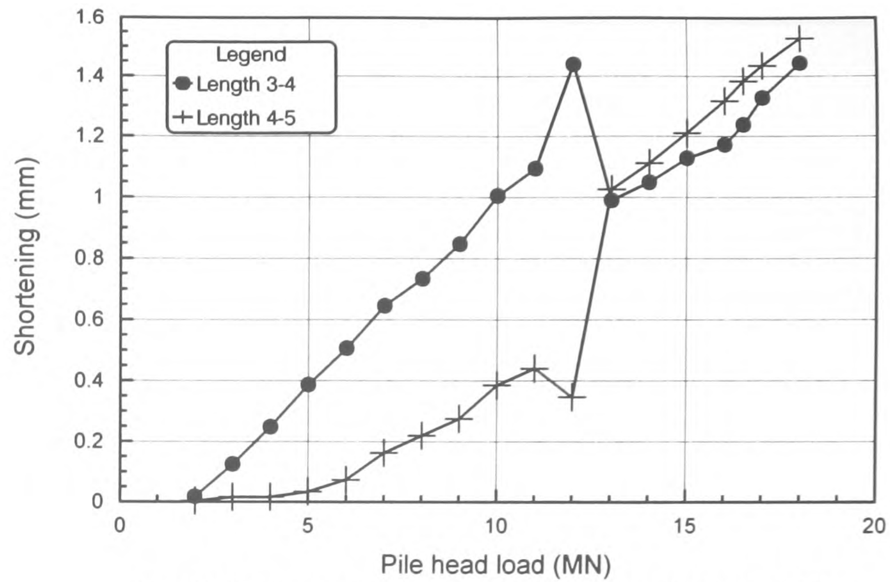

Fig 4.9(f):Shortening between instrument levels Vs load-TP3

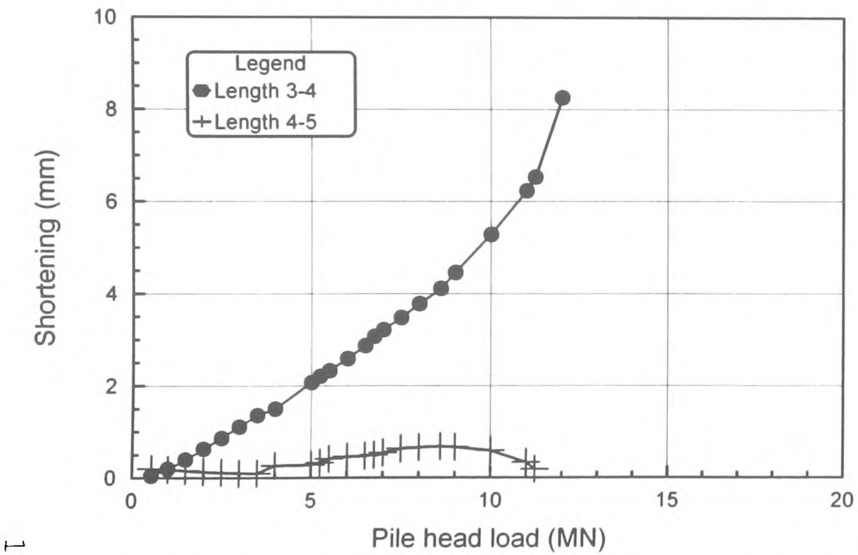

Fig 4.9(g):Shortening between instrument levels Vs load-TP4

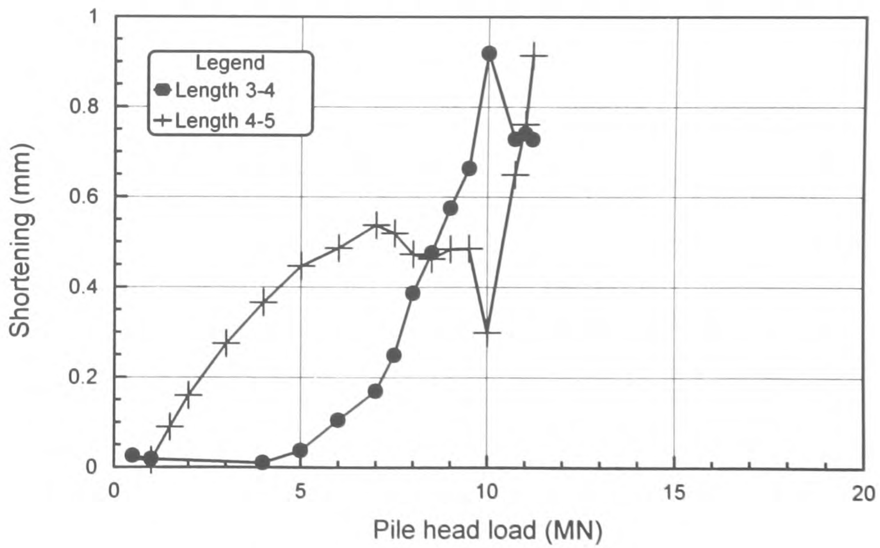

Fig 4.9(h):Shortening between instrument levels Vs load-TP5

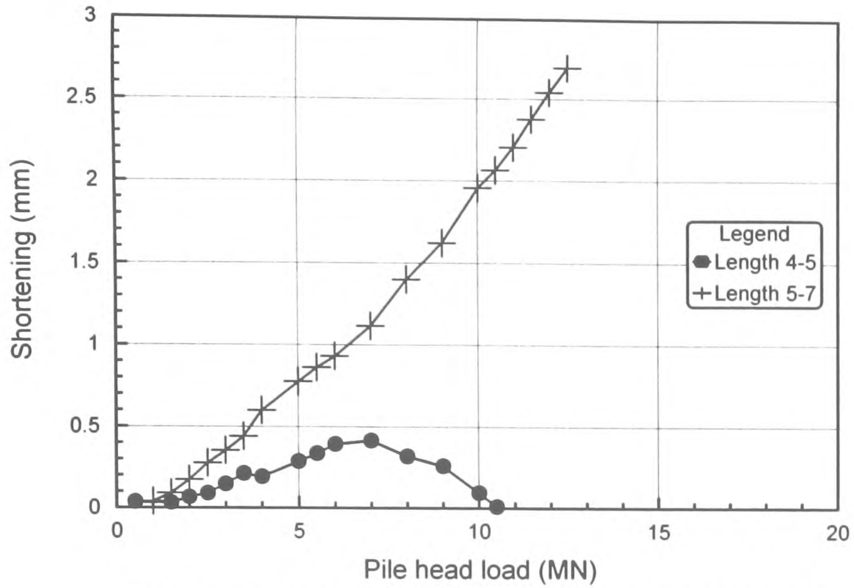

Fig 4.9(j):Shortening between instrument levels Vs load-TP6

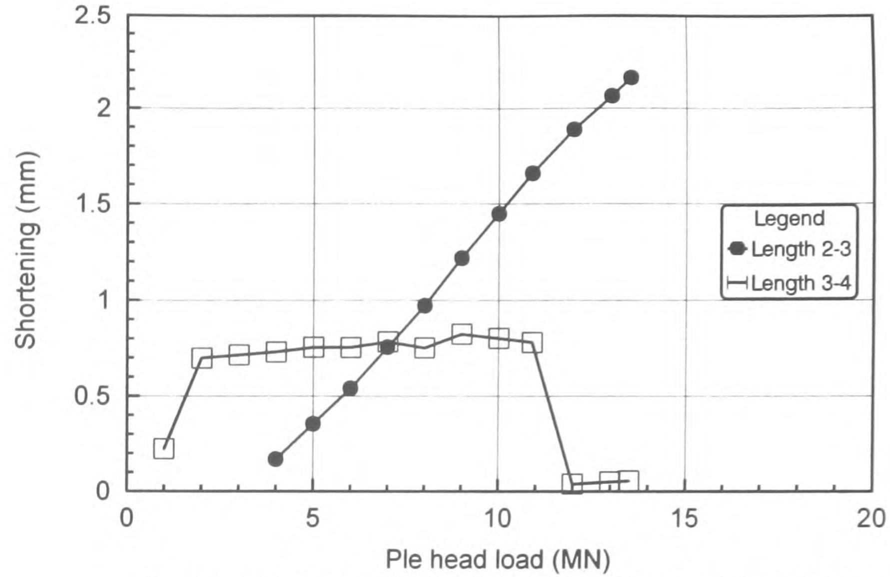

Fig 4.9(k):Shortening between instrument levels Vs load-TP2

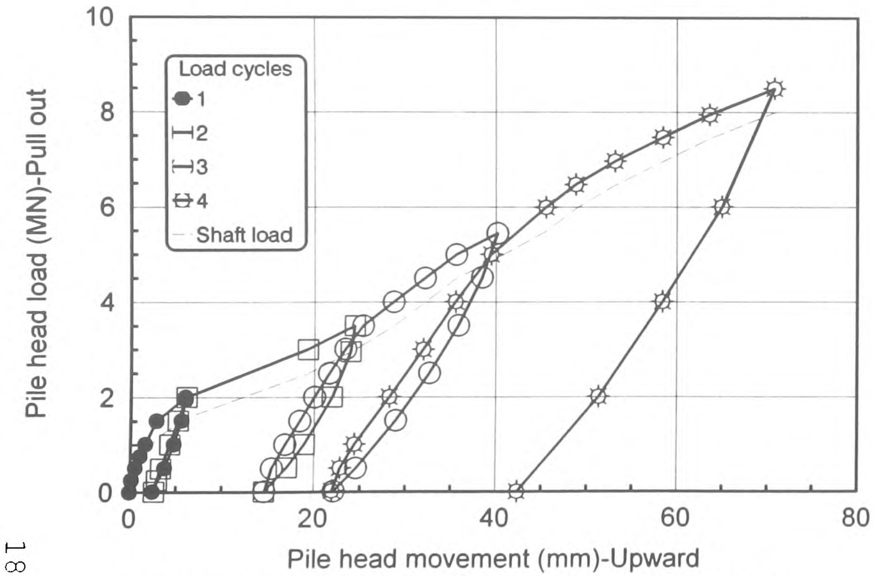

Fig 4.9(l):Pull-out force versus pile head movement-TP6

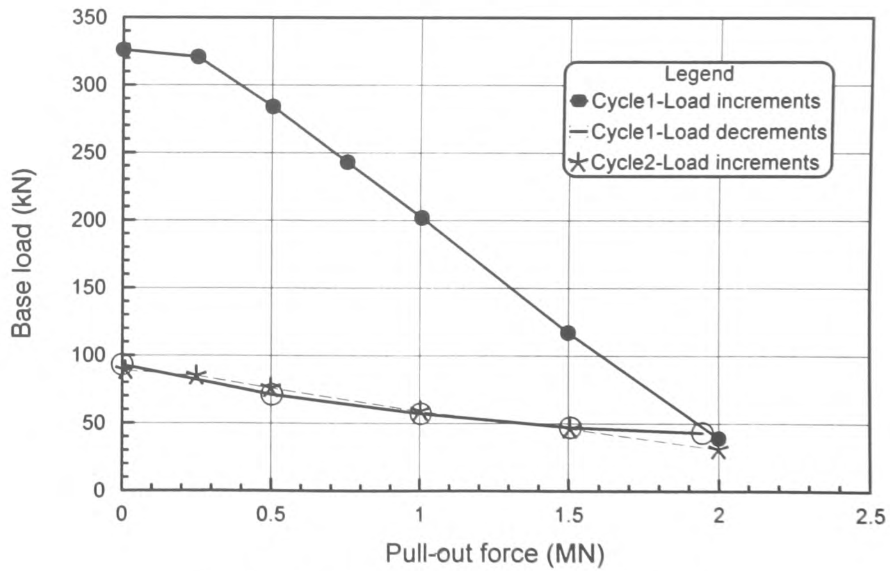

Fig 4.9(m):Base load Vs pull-out force - TP6

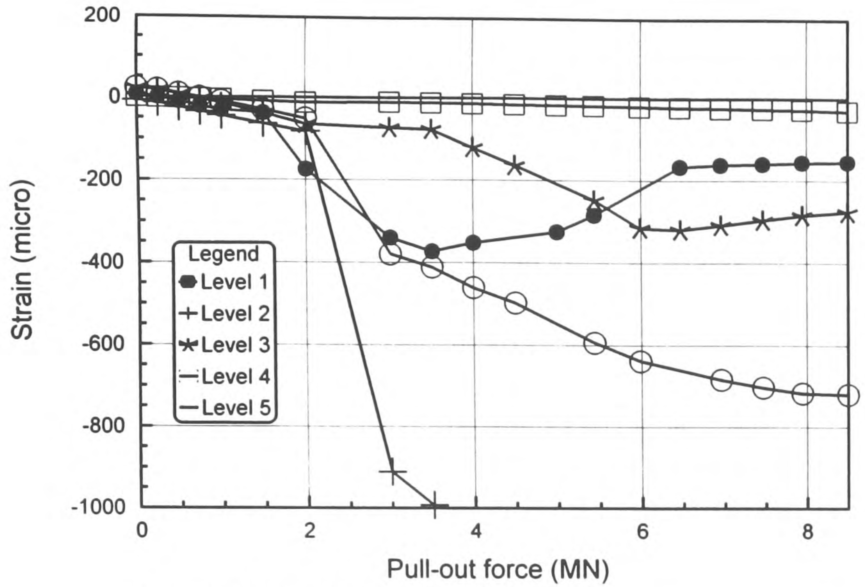

Fig 4.9(n):Strain Vs pull-out force-TP6

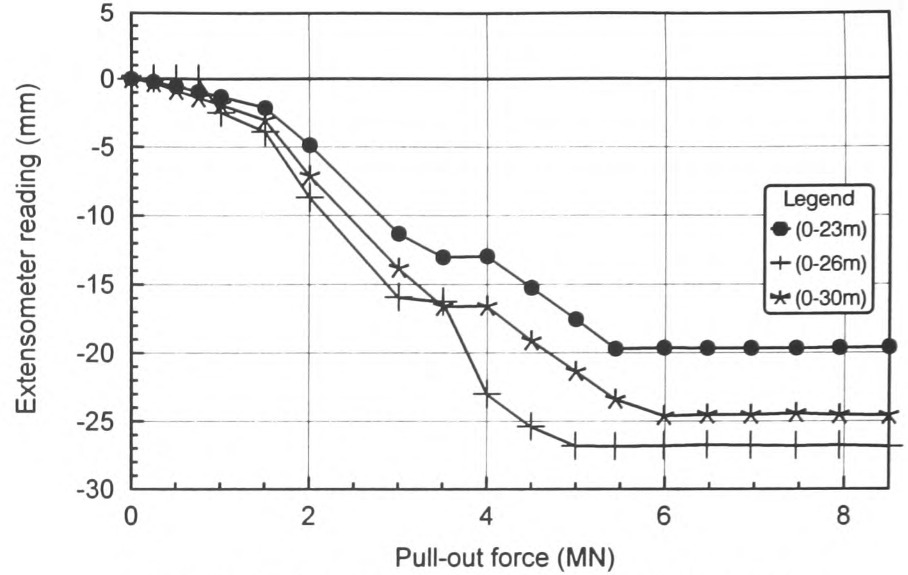

Fig 4.9(p):Extensometer readings Vs pull-out force -TP6

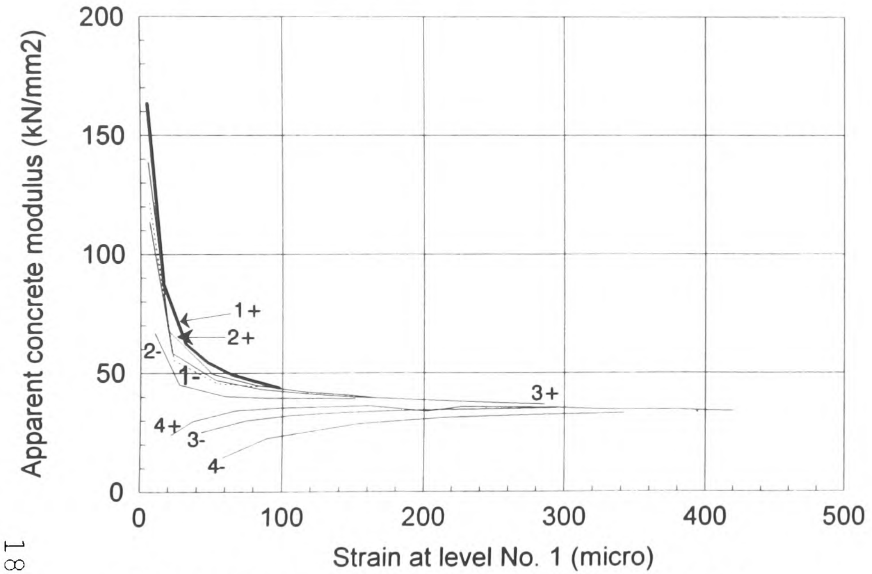

Fig 4.9(q):Apparent concrete modulus Vs strain-TP6

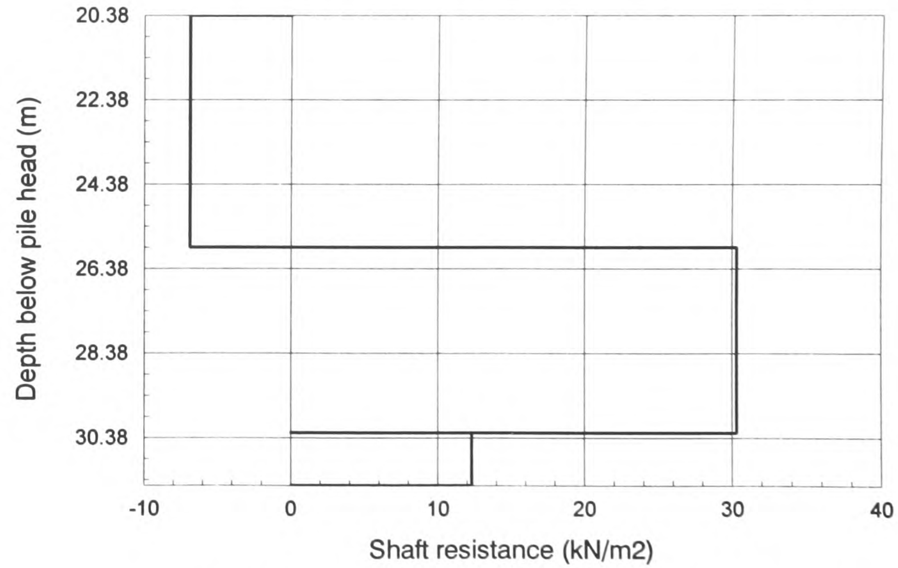

Fig 4.9(r):Shaft resistance Vs Depth at zero load following completion of compression test-TP6

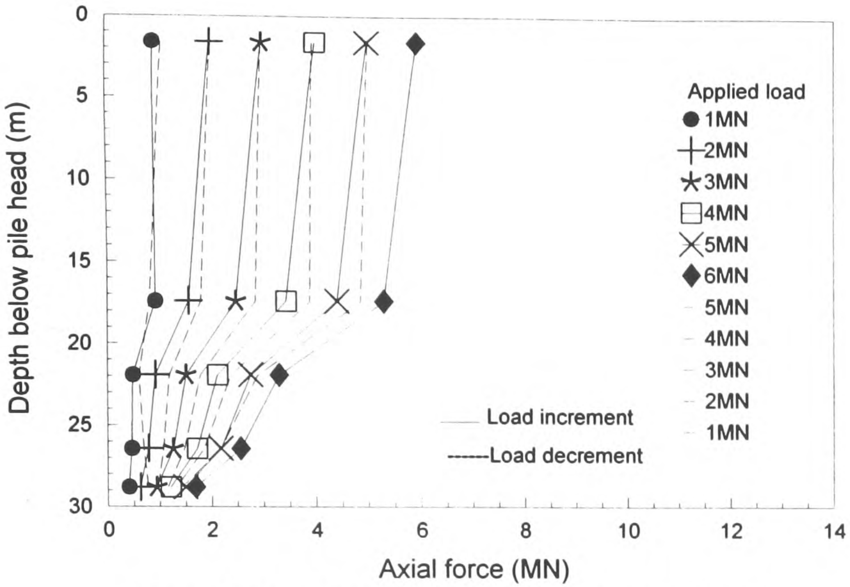

Fig 4.10(a):Axial force versus depth-TP2 (load cycle 1)

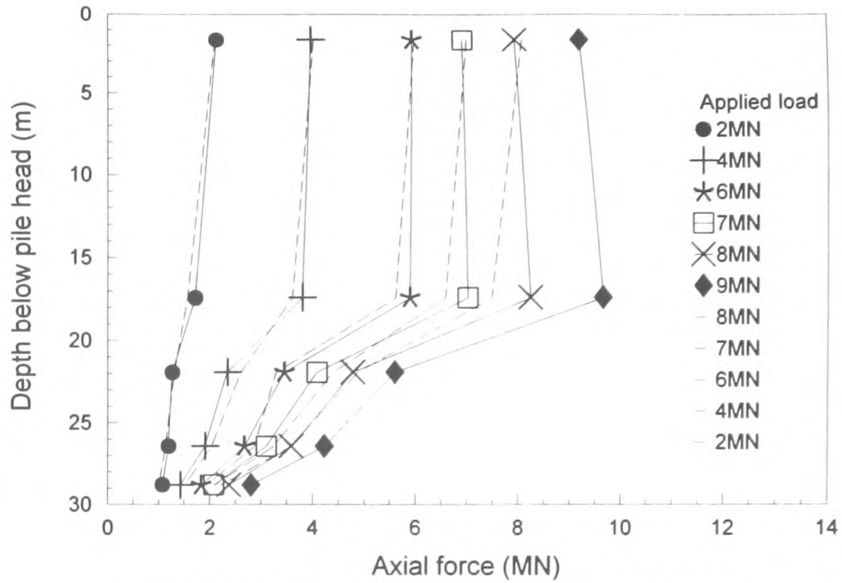

Fig 4.10(b):Axial force versus depth-TP2 (load cycle 2)

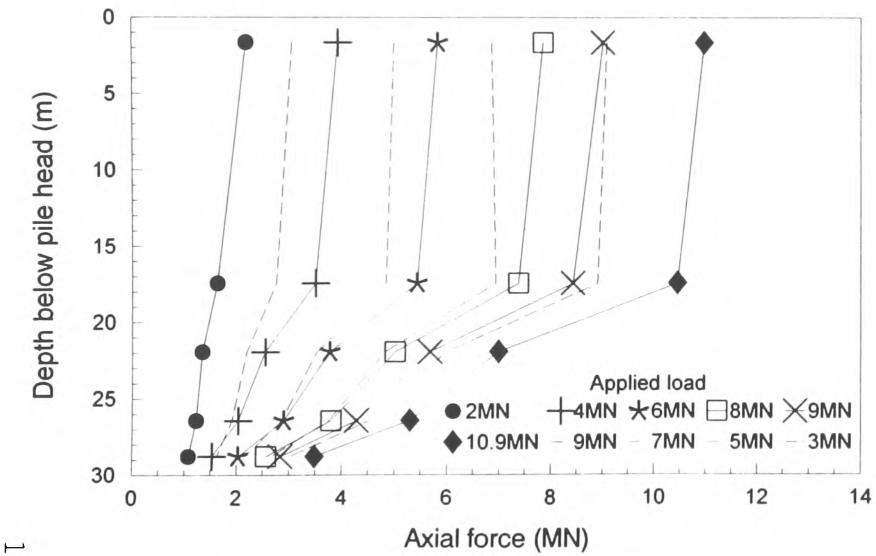

Fig 4.10(c):Axial force versus depth-TP2 (load cycle 3)

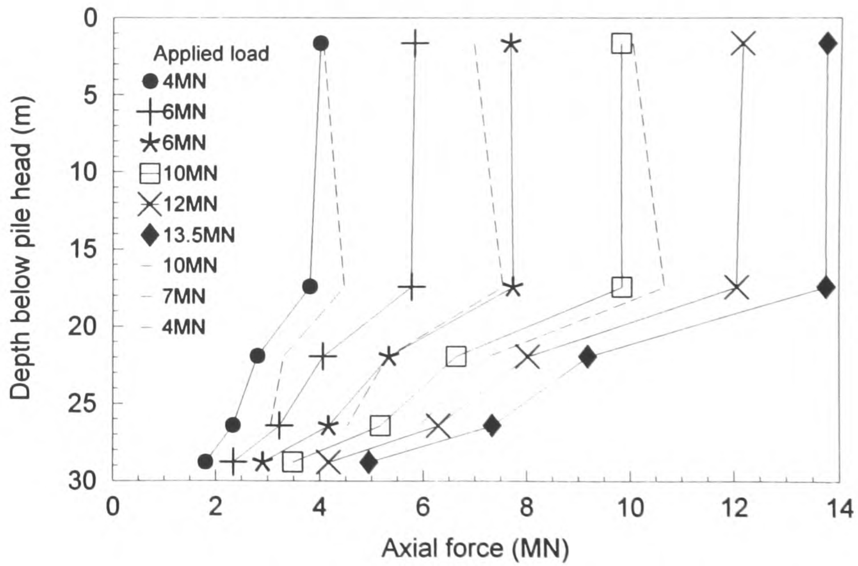

Fig 4.10(d):Axial force versus depth-TP2 (load cycle 4)

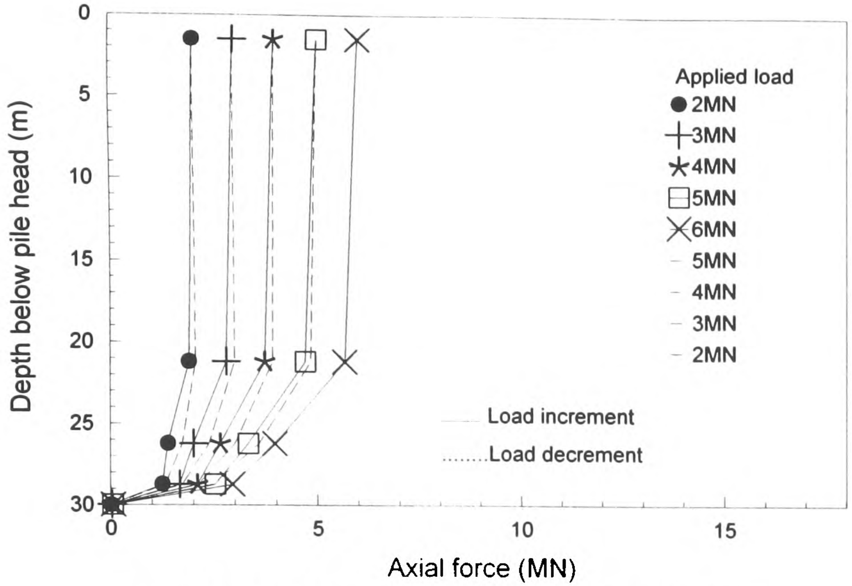

Fig 4.11(a):Axial force versus depth-TP3 (load cycle 1)

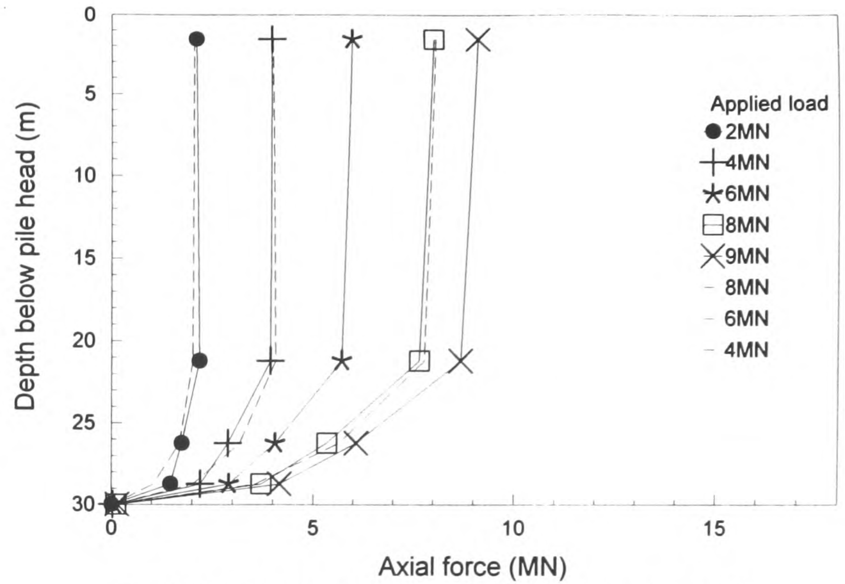

Fig 4.11(b):Axial force versus depth-TP3 (load cycle 2)

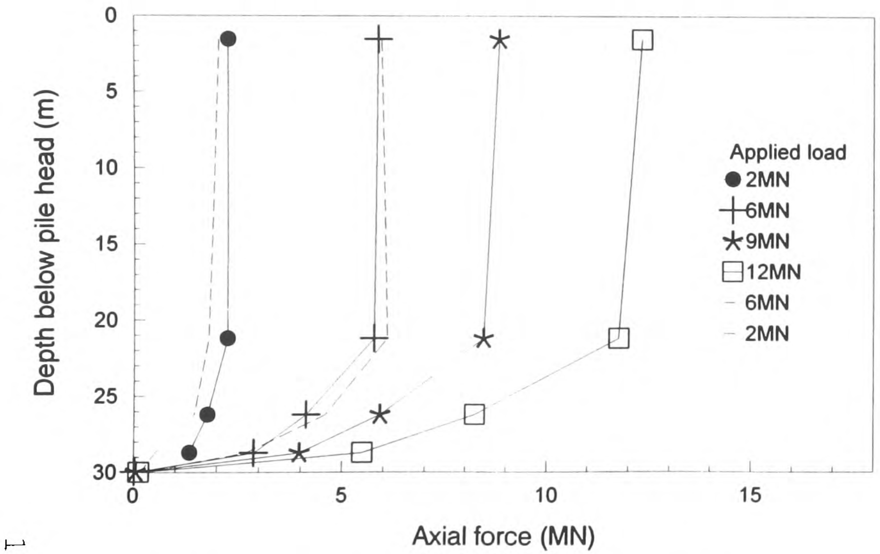

Fig 4.11(c):Axial force versus depth-TP3 (load cycle 3)

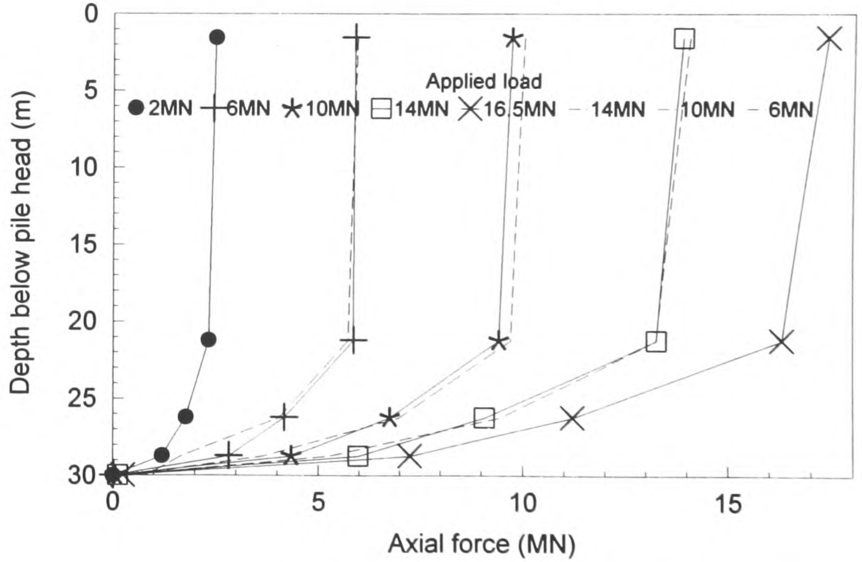

Fig 4.11(d):Axial force versus depth-TP3 (load cycle 4)

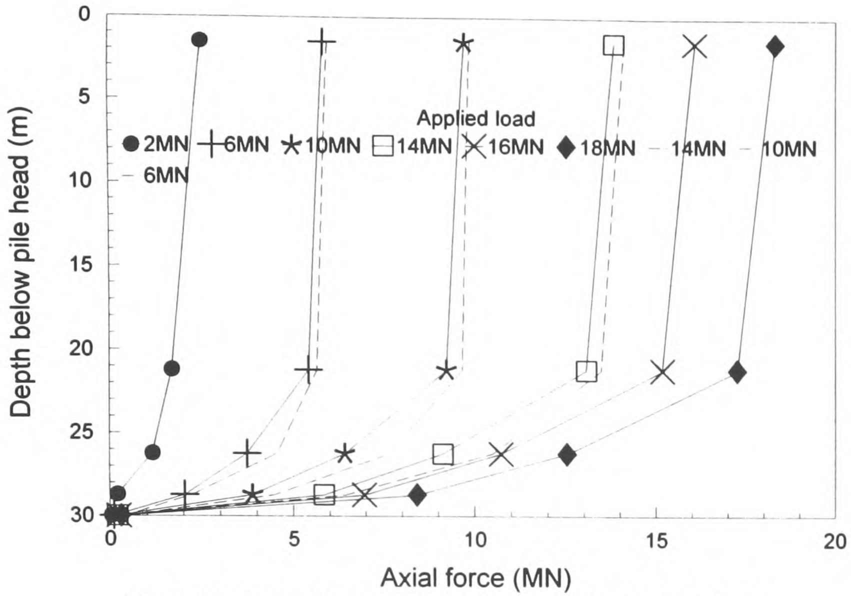

Fig 4.11(e):Axial force versus depth-TP3 (load cycle 5)

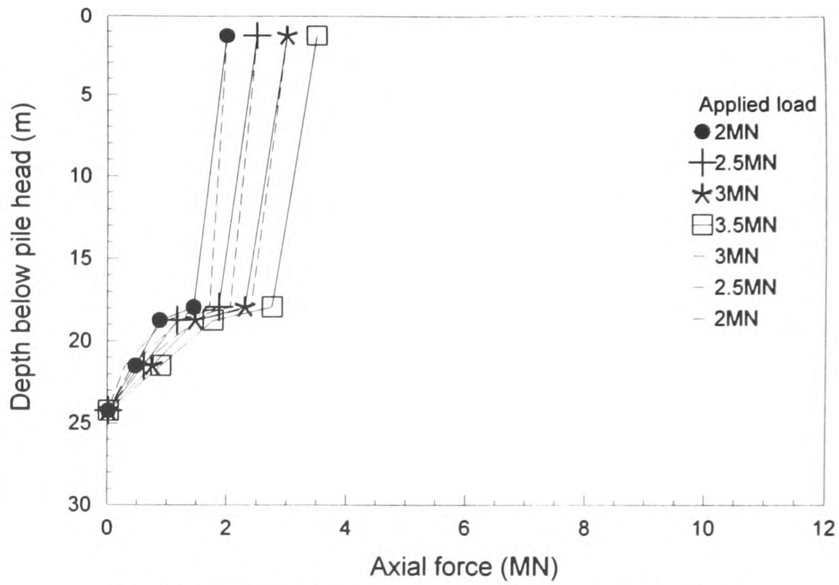

Fig 4.12(a):Axial force versus depth-TP4 (load cycle 1)

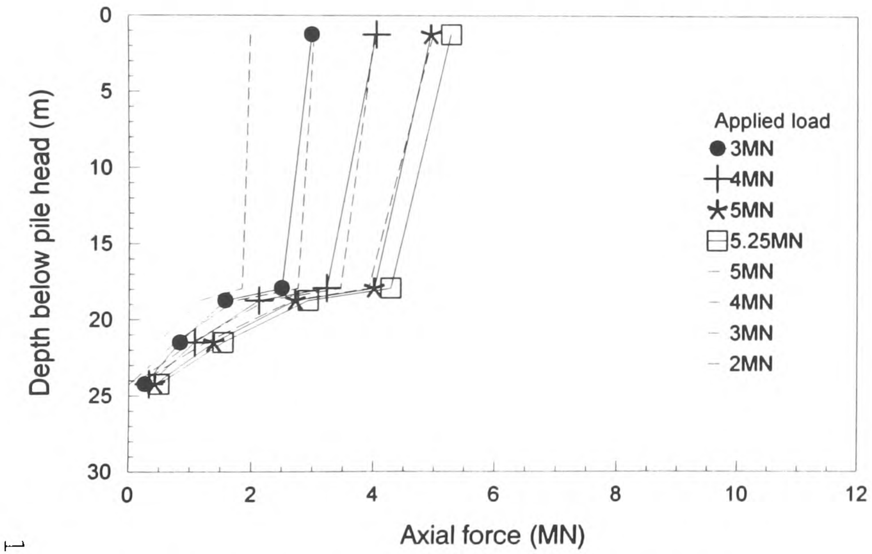

Fig 4.12(b):Axial force versus depth-TP4 (load cycle 2)

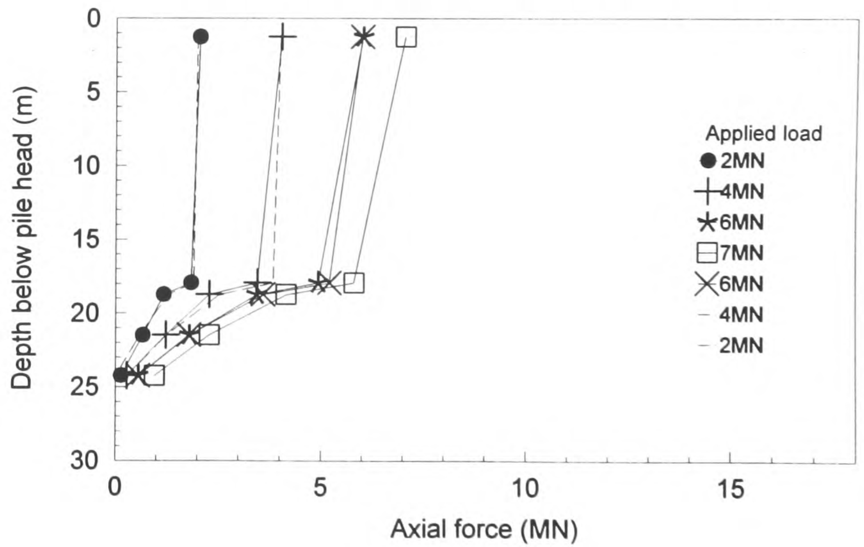

Fig 4.12(c):Axial force versus depth-TP4 (load cycle 3)

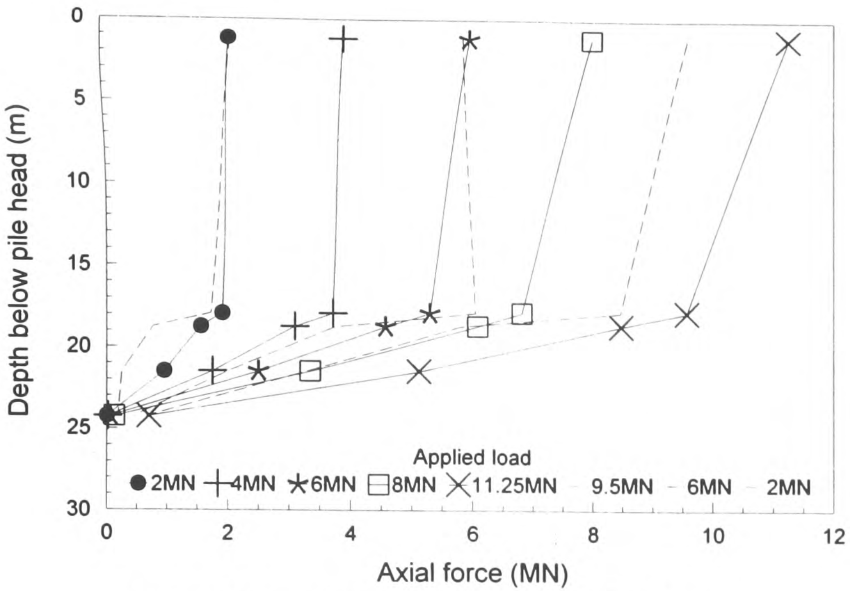

Fig 4.12(d):Axial force versus depth-TP4 (load cycle 4)

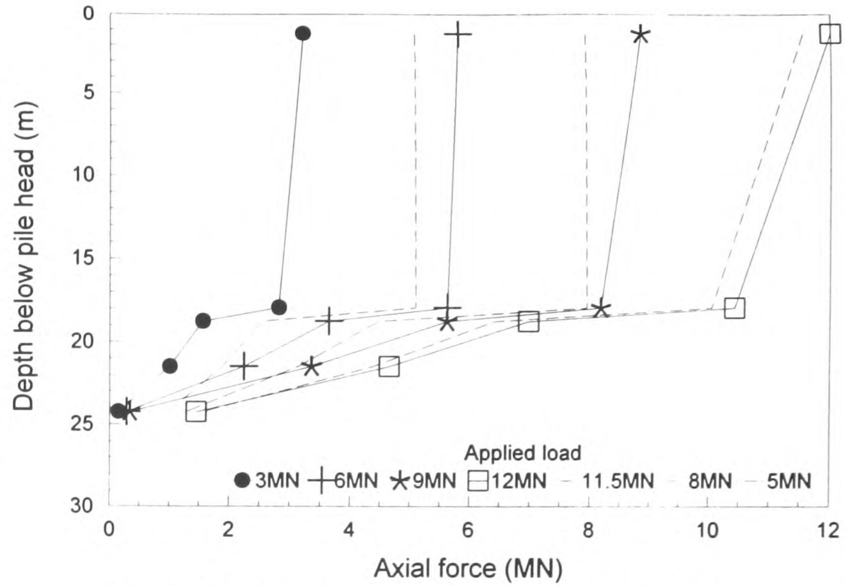

Fig 4.12(e):Axial force versus depth-TP4 (load cycle 5)

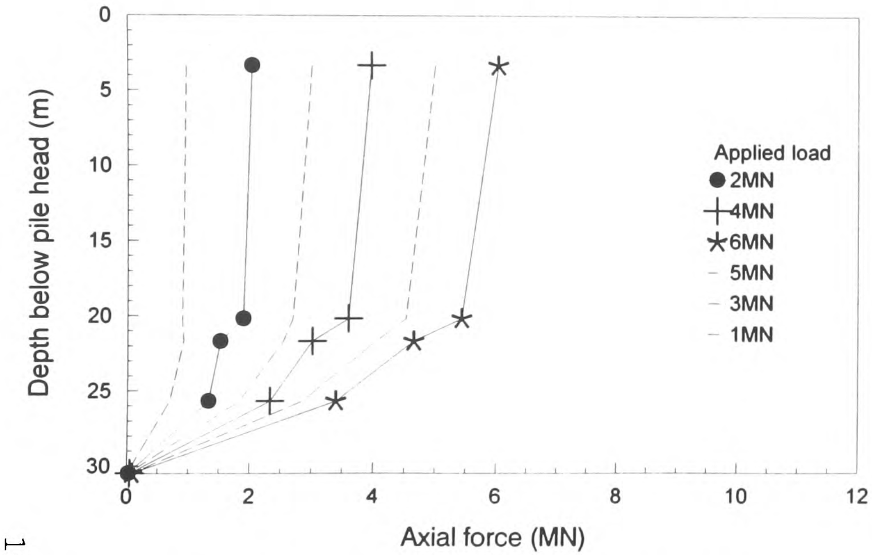

Fig 4.13(a):Axial force versus depth-TP5 (load cycle 1)

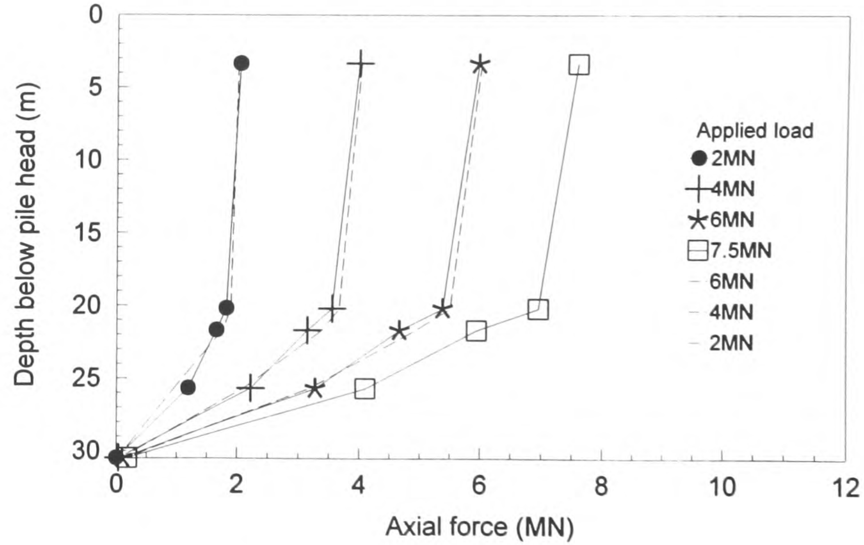

Fig 4.13(b):Axial force versus depth-TP5 (load cycle 2)

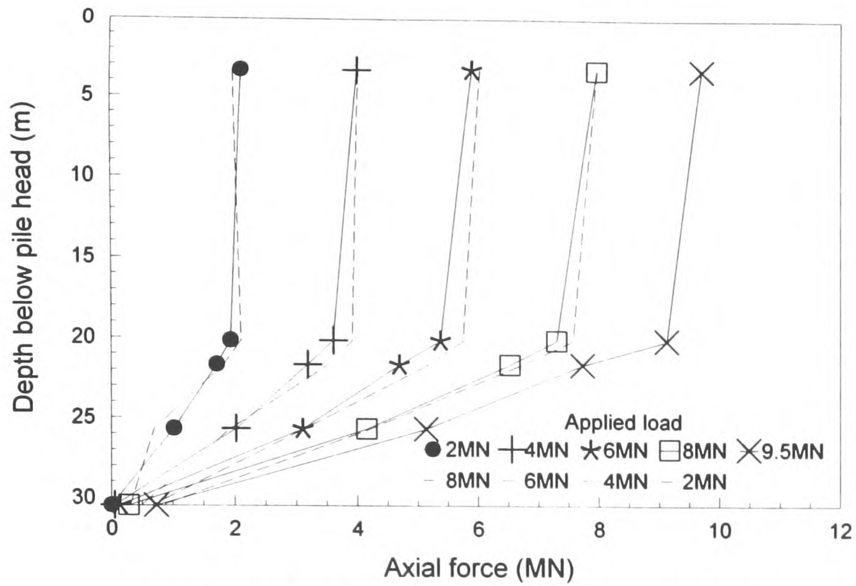

Fig 4.13(c):Axial force versus depth-TP5 (load cycle 3)

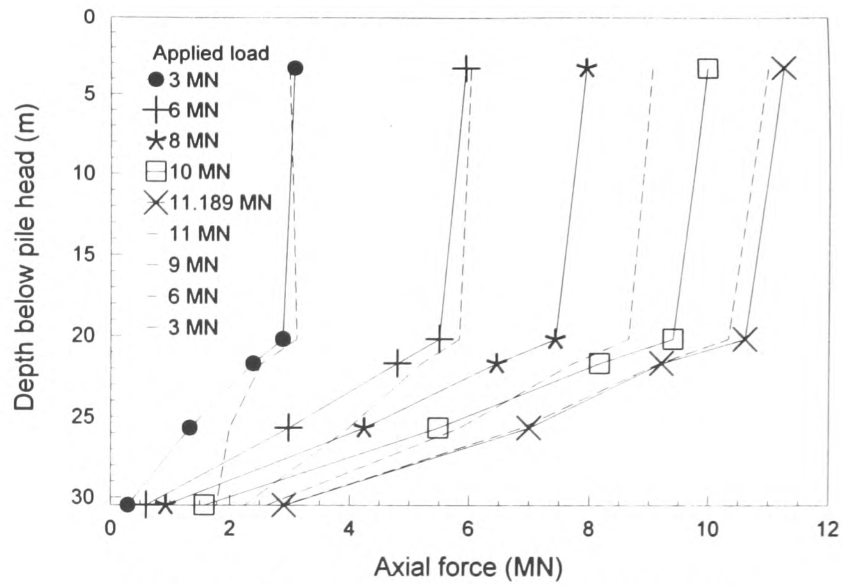

Fig 4.13(d):Axial force versus depth-TP5 (load cycle 4)

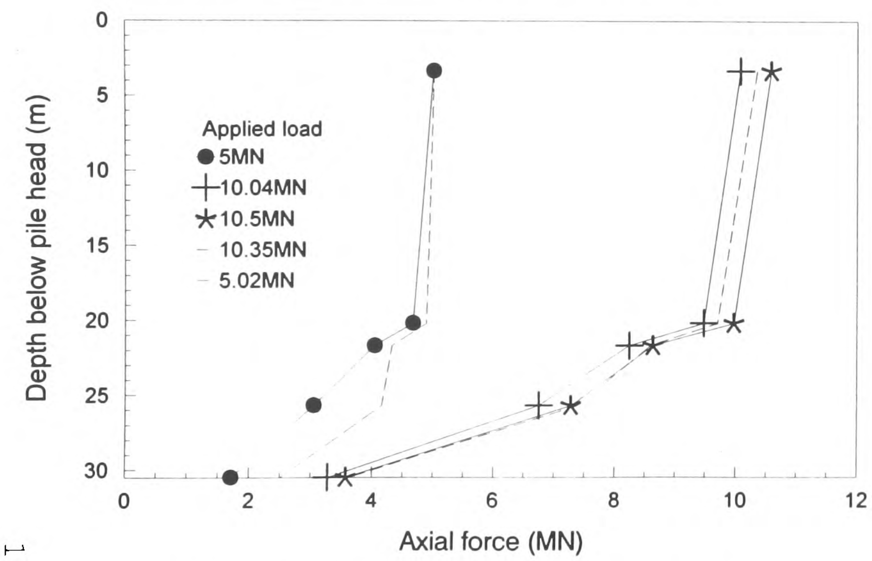

Fig 4.13(e):Axial force versus depth-TP5 (load cycle 5)

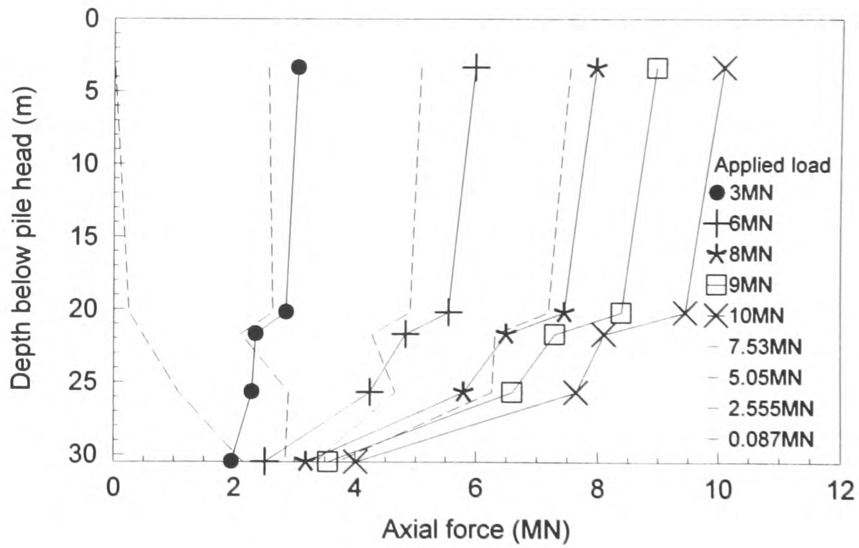

Fig 4.13(f):Axial force versus depth-TP5 (load cycle 6)

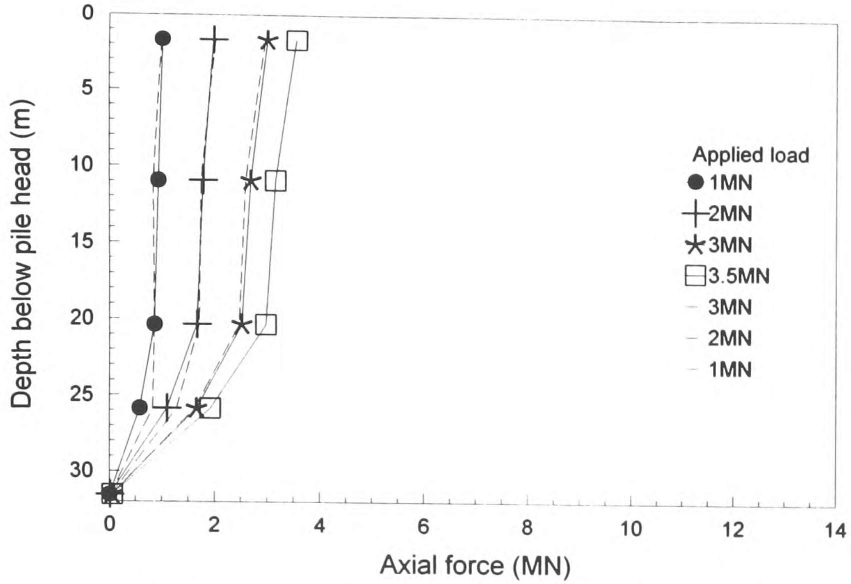

Fig 4.14(a):Axial force versus depth-TP6 (load cycle 1)

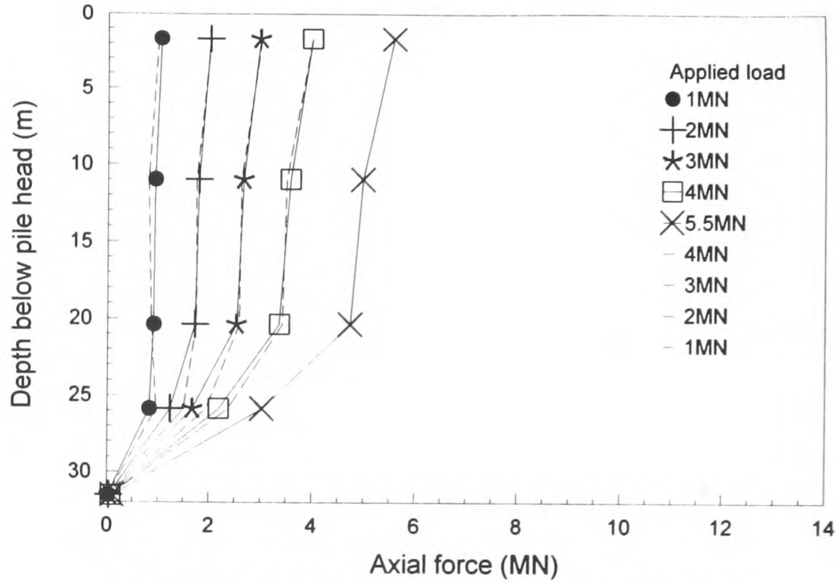

Fig 4.14(b):Axial force versus depth-TP6 (load cycle 2)

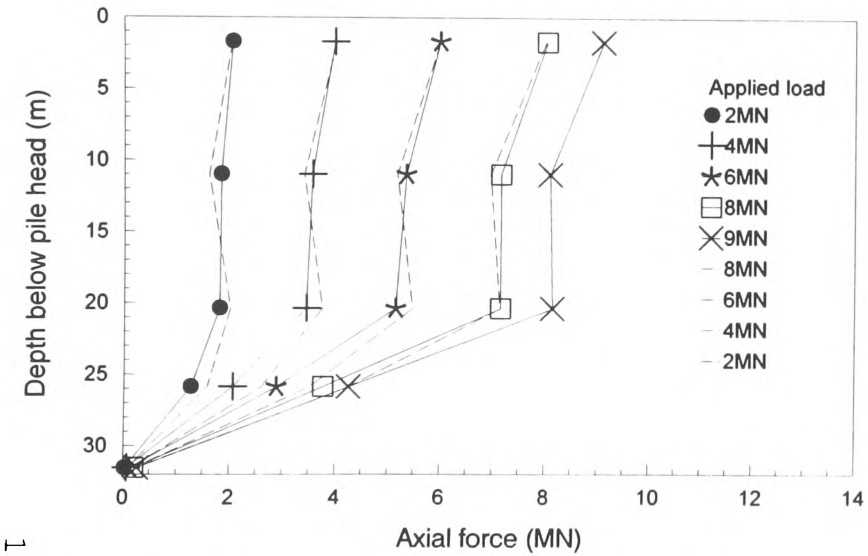

Fig 4.14(c):Axial force versus depth-TP6 (load cycle 3)

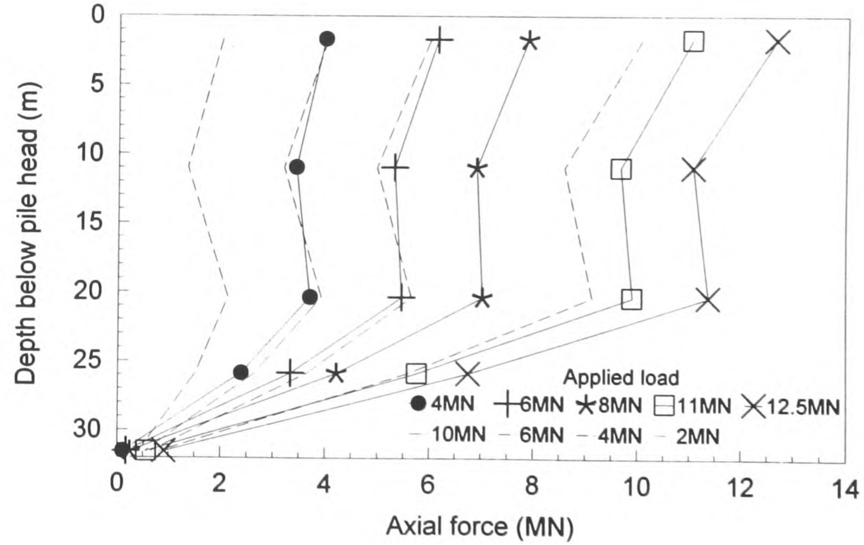

Fig 4.14(d):Axial force versus depth-TP6 (load cycle 4)

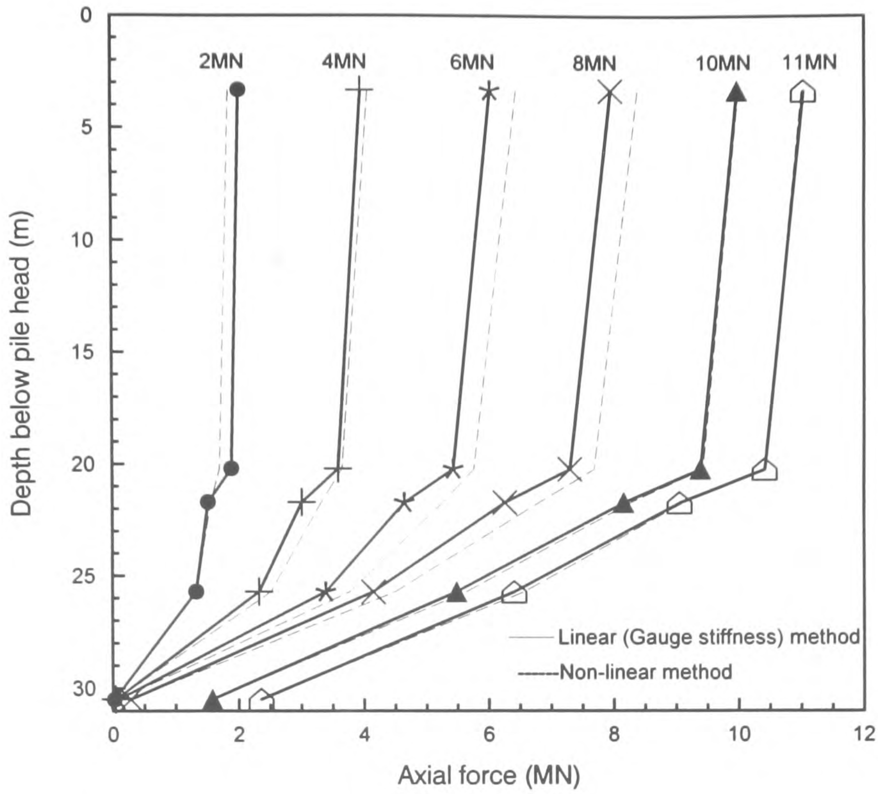

Fig 4.15: Axial force Vs depth-A comparison between the results of linear and non-linear calibration methods -TP5

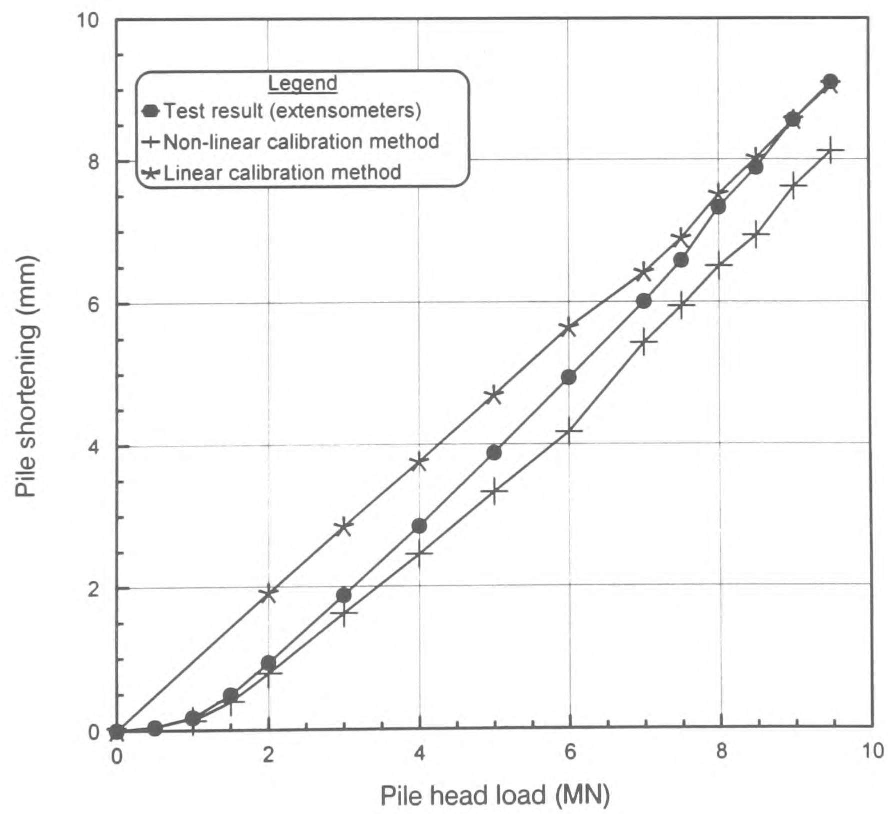

Fig 4.16: Pile shortening Vs applied load-TP5: A comparison between the results of linear and non-linear calibration methods -TP5

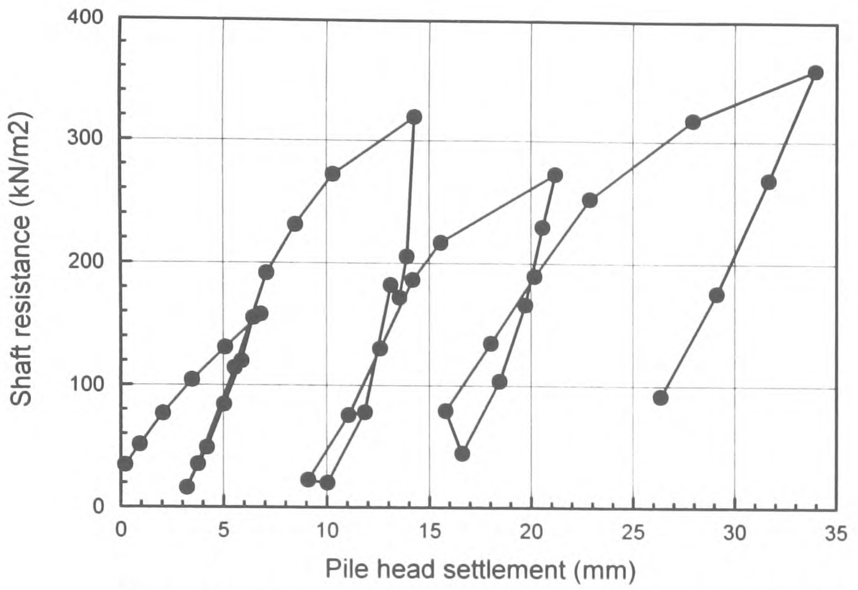

Fig 4.17(a):Shaft resistance (mid level 2-3) Vs settlement-TP2

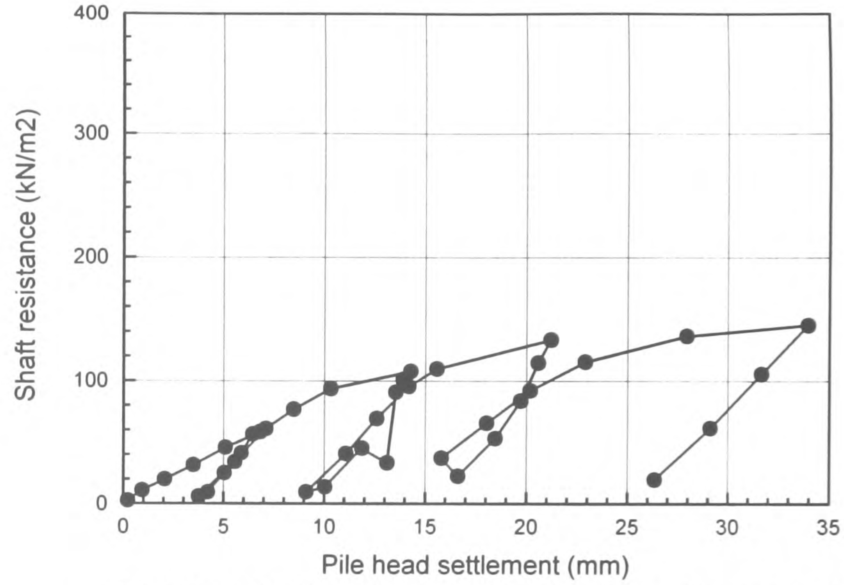

Fig 4.17(b):Shaft resistance (mid level 3-4) Vs settlement-TP2

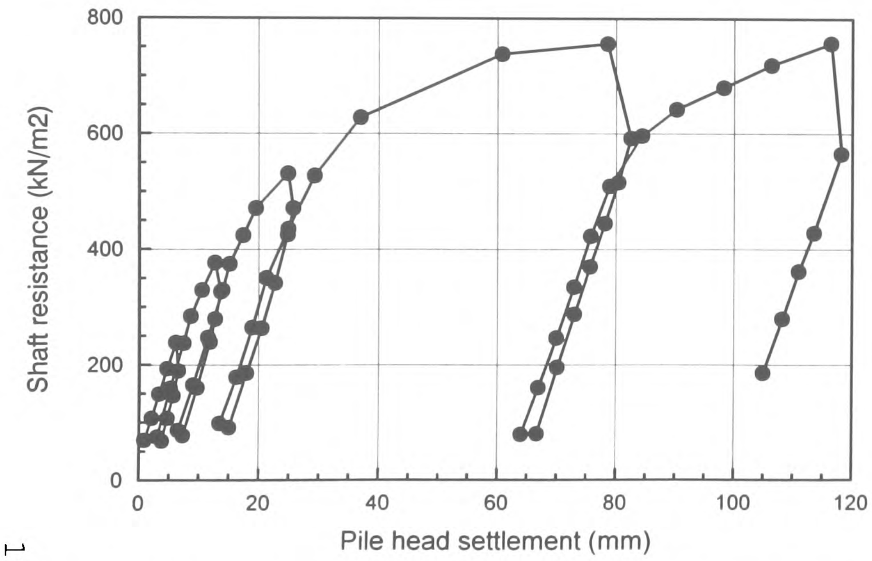

Fig 4.18(a):Shaft resistance (mid level 2-3) Vs settlement-TP3

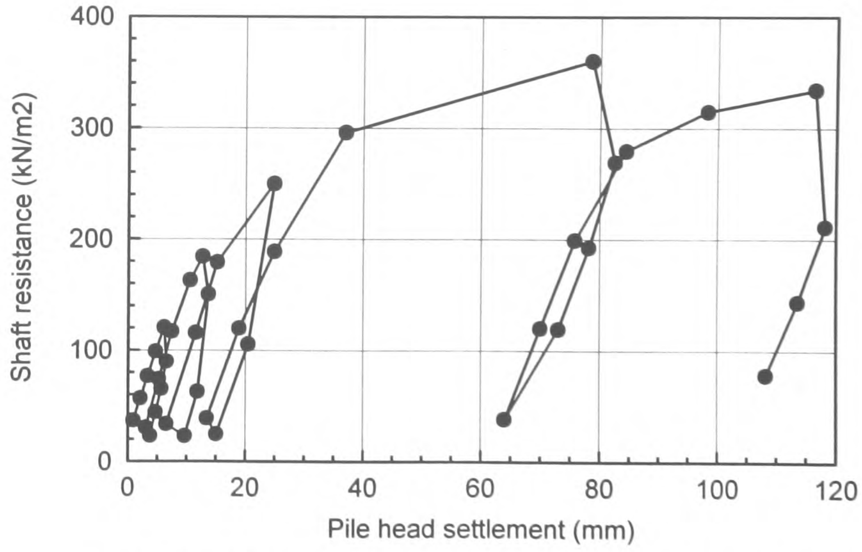

Fig 4.18(b):Shaft resistance (mid level 2-4) Vs settlement-TP3
(Strains in levels 3 and 4 are inconsistent)

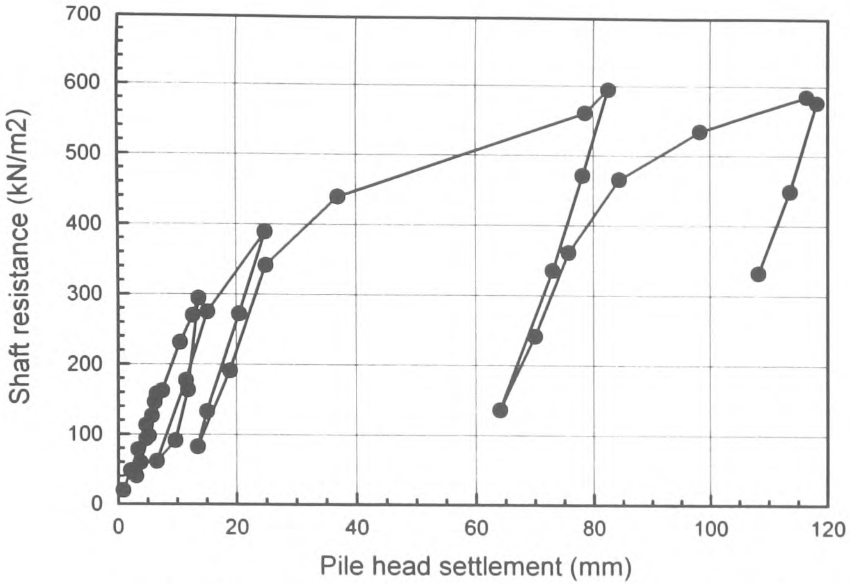

Fig 4.18(c):Shaft resistance (mid level 4-5) Vs settlement-TP3

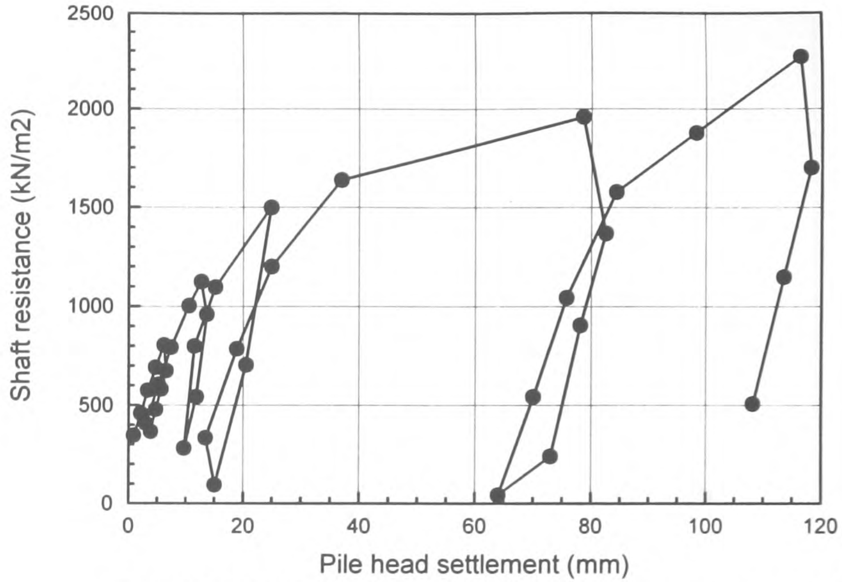

Fig 4.18(d):Shaft resistance (mid level 5-tip) Vs settlement-TP3

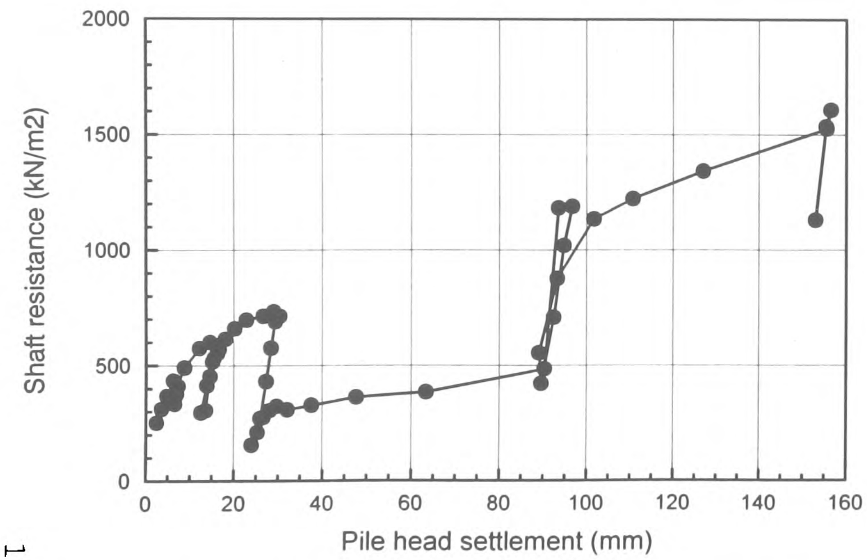

Fig 4.19(a):Shaft resistance (mid level 2-3) Vs settlement-TP4

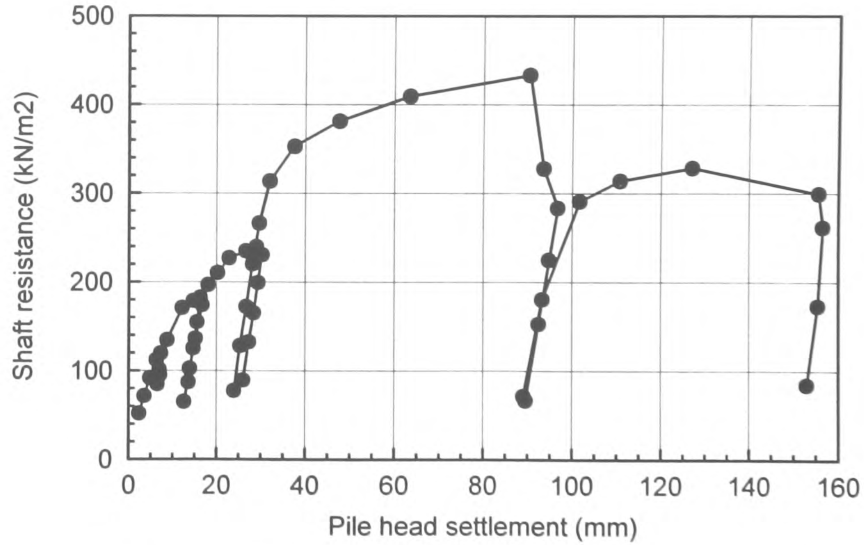

Fig 4.19(b): Shaft resistance (mid level 3-4) Vs settlement-TP4

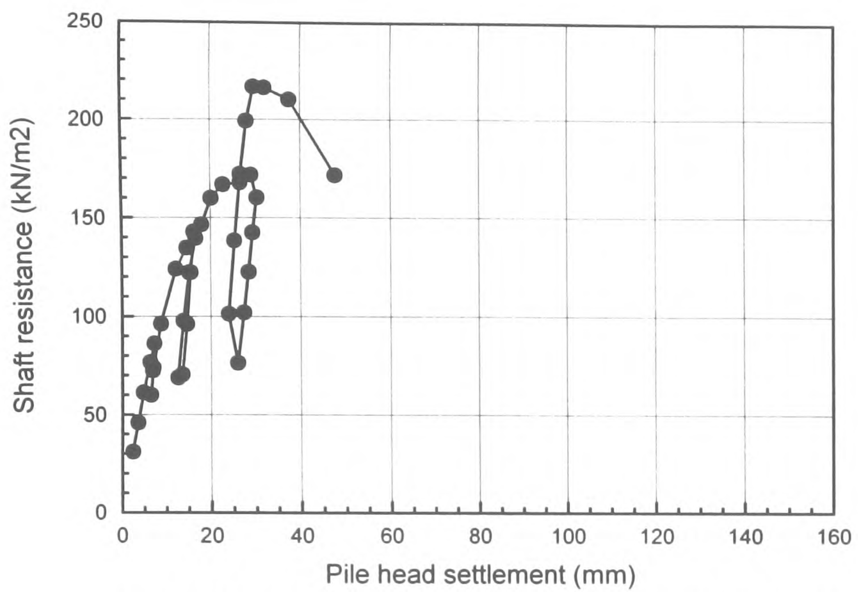

Fig 4.19(c):Shaft resistance (mid level 4-5) Vs settlement-TP4

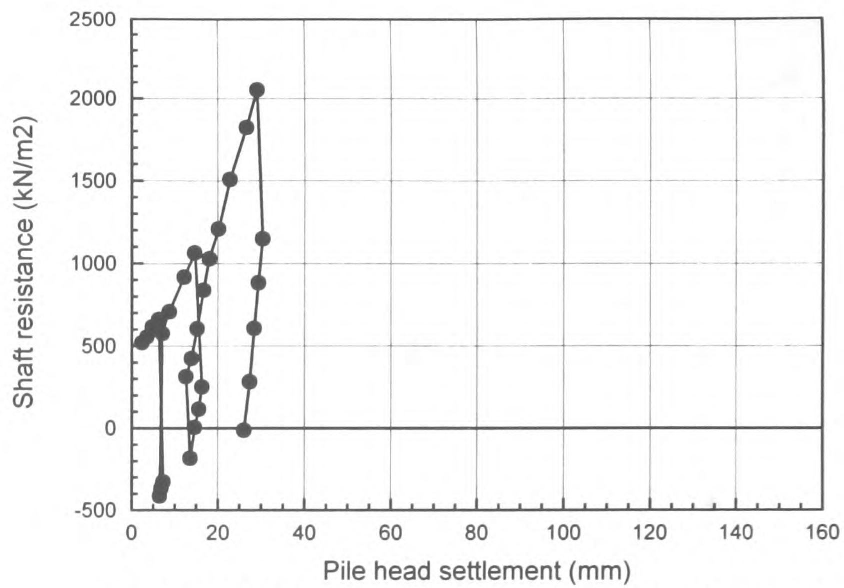

Fig 4.19(d):Shaft resistance (mid level 5-tip) Vs settlement-TP4

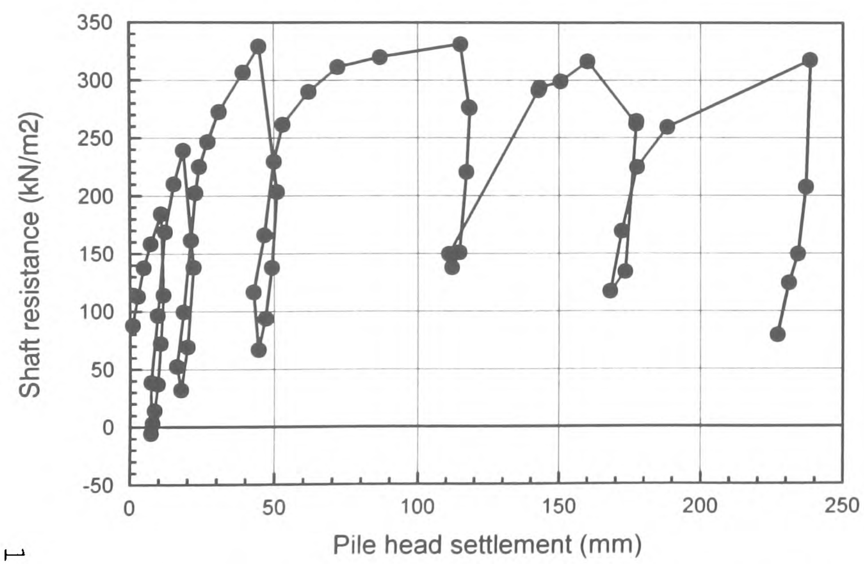

Fig 4.20(a):Shaft resistance (mid level 2-3) Vs settlement-TP5

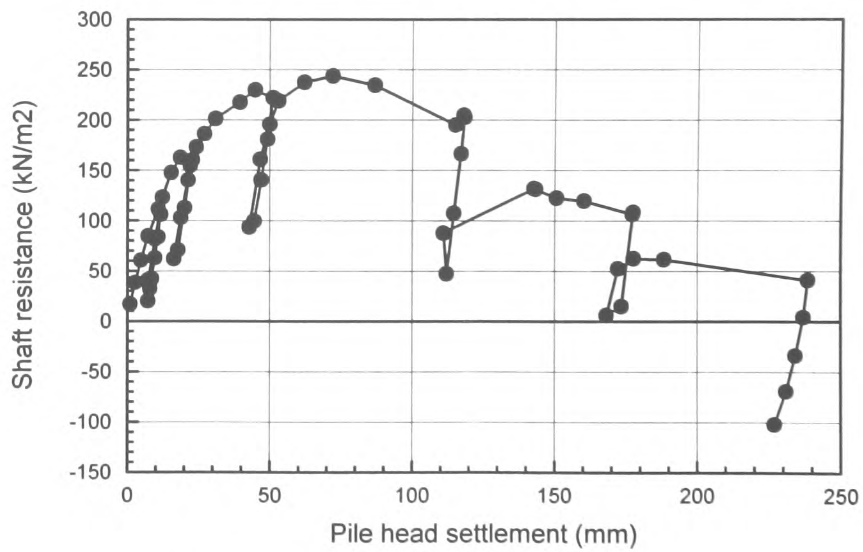

Fig 4.20(b): Shaft resistance (mid level 3-4) Vs settlement-TP5

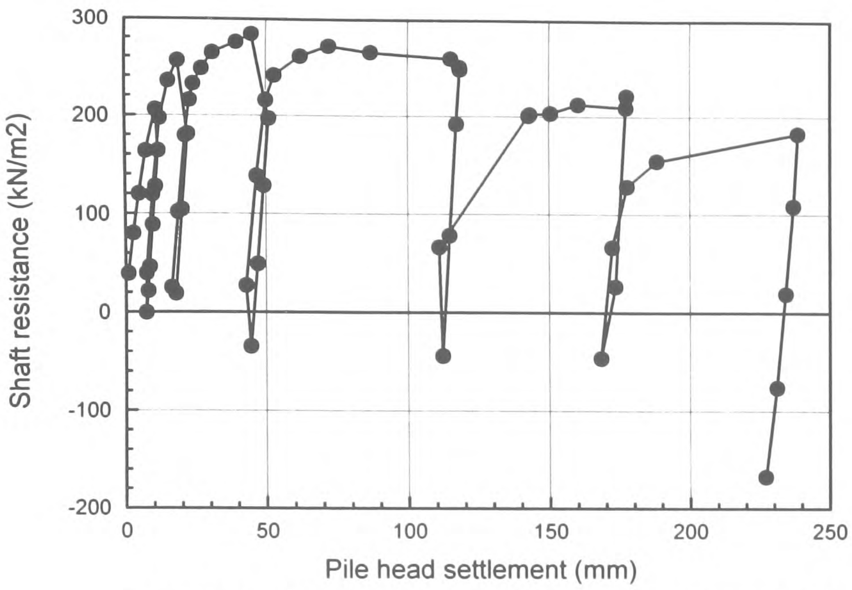

Fig 4.20(c):Shaft resistance (mid level 4-5) Vs settlement-TP5

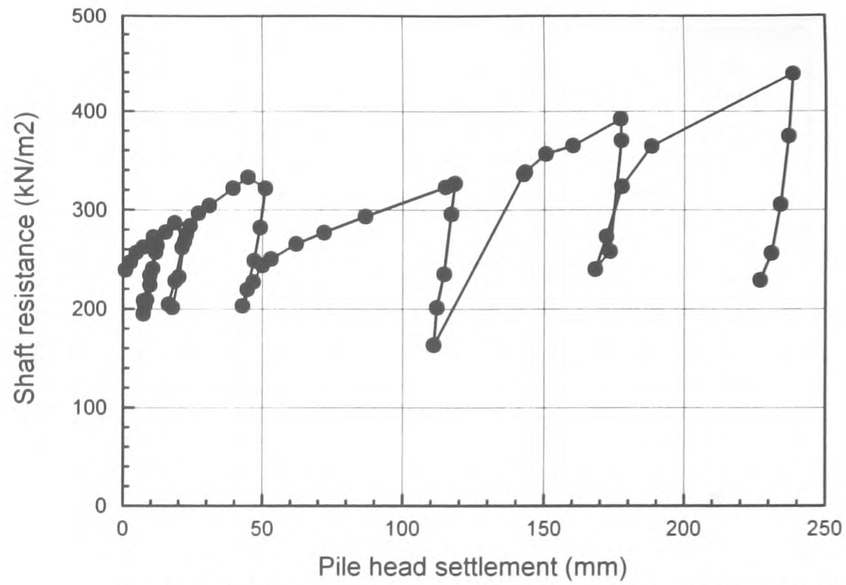

Fig 4.20(d):Shaft resistance (mid level 5-tip) Vs settlement-TP5

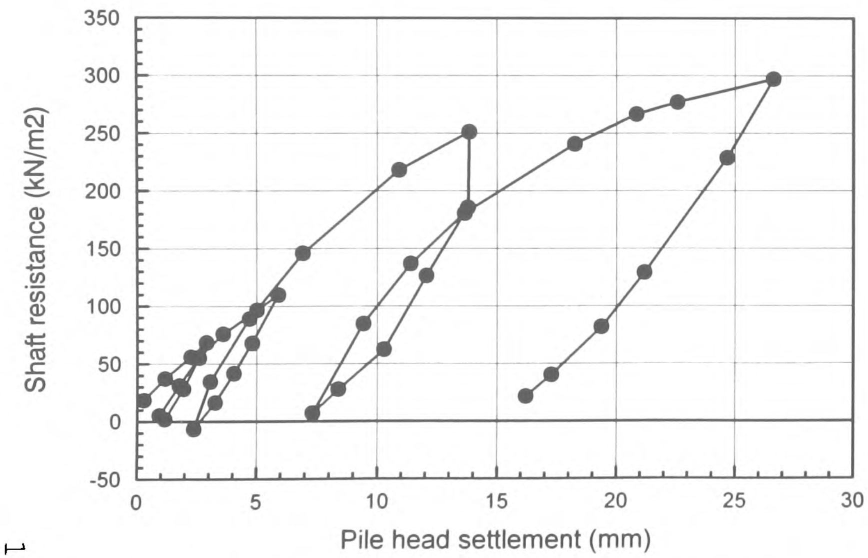

Fig 4.20(e):Shaft resistance (mid level 3-5) Vs settlement-TP6

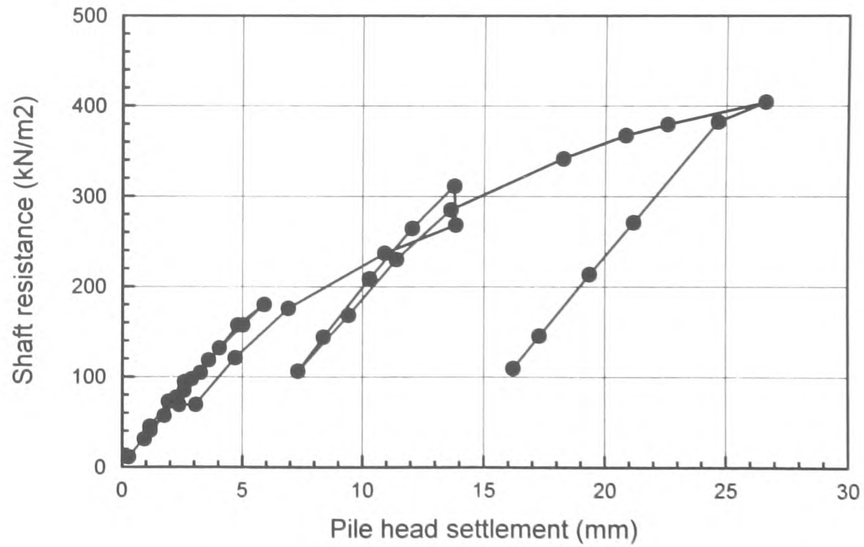

Fig 4.20(f): Shaft resistance (mid level 5-7) Vs settlement-TP6

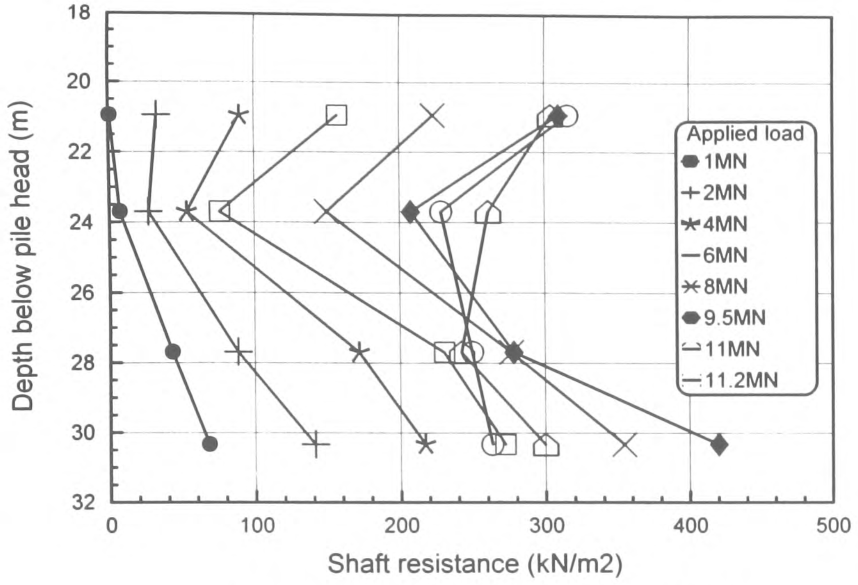

Fig 4.21(d):Shaft resistance Vs depth -TP5

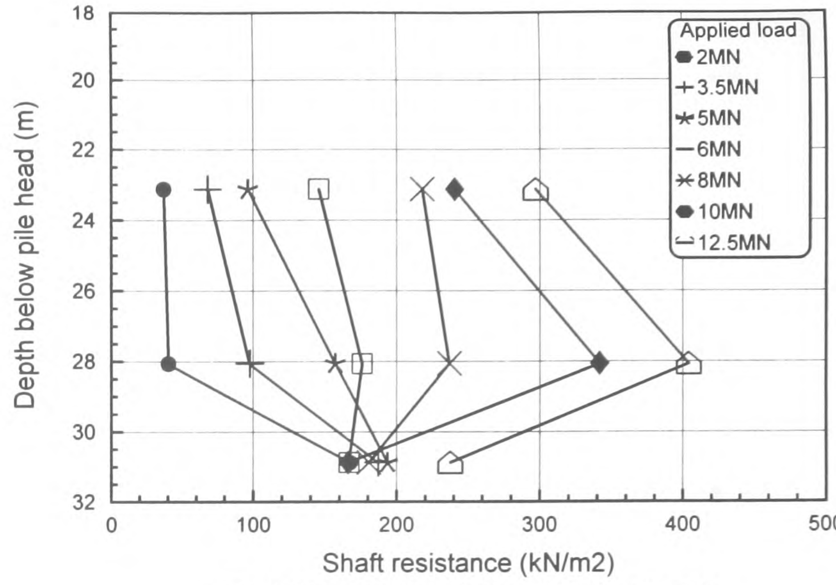

Fig 4.21(e):Shaft resistance Vs depth-TP6

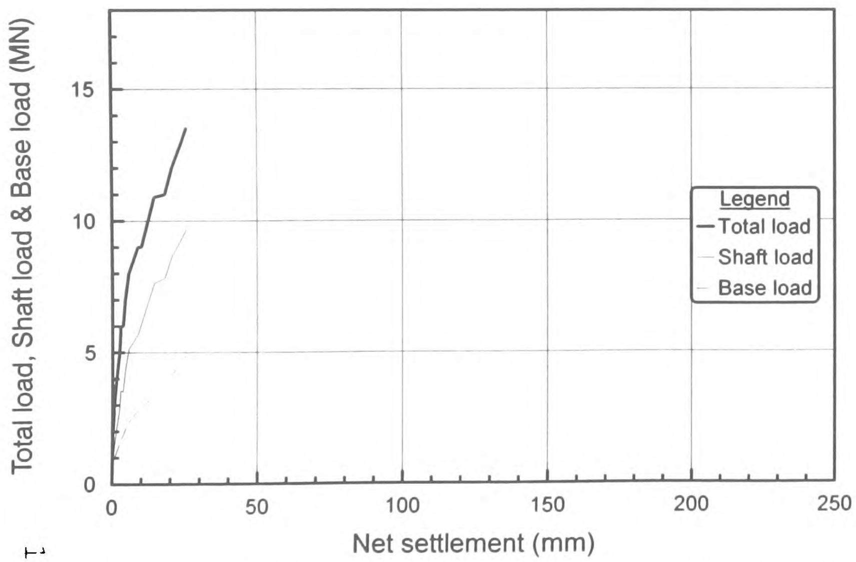

Fig 4.22(a):Total load,Shaft load & Base load Vs net settlement-TP2

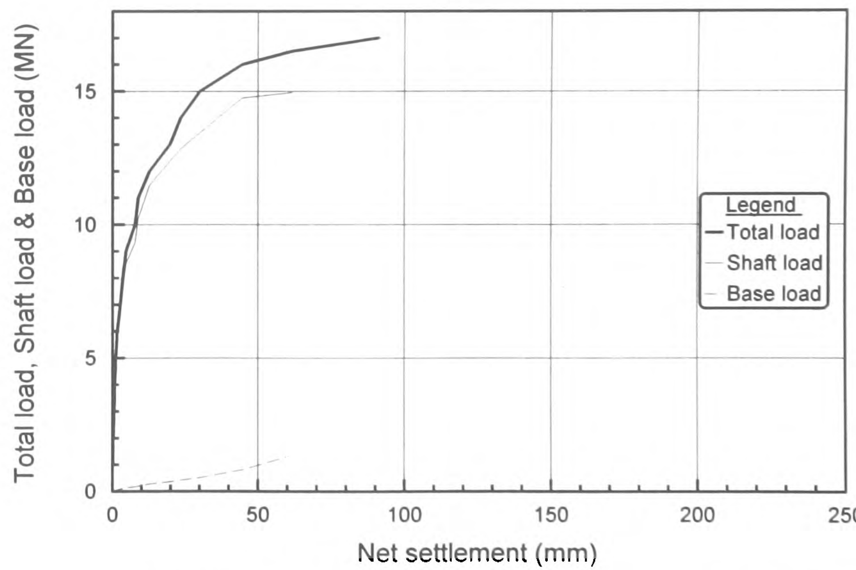

Fig 4.22(b):Total load,Shaft load & Base load Vs net settlement-TP3

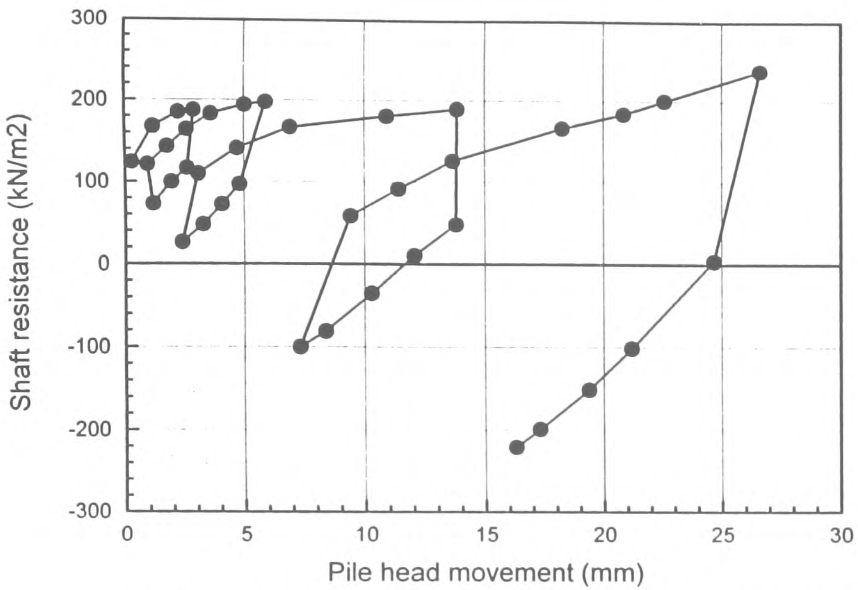

Fig 4.20(g):Shaft resistance (mid-level 7-tip) Vs settlement -TP6

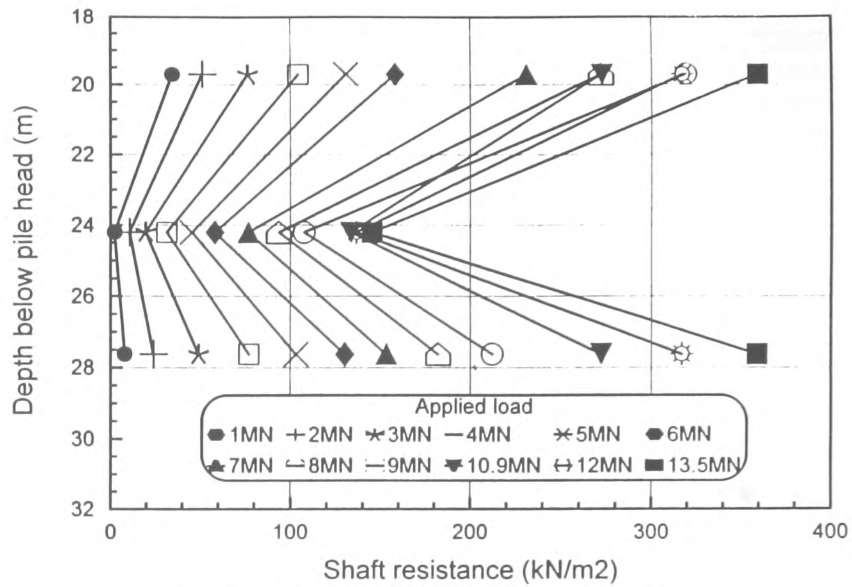

Fig 4.21(a):Shaft resistance versus depth-TP2

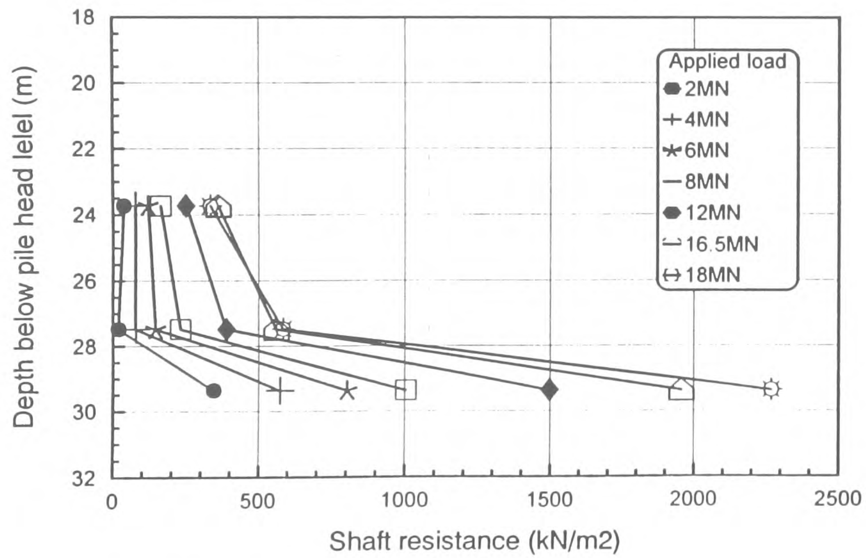

Fig 4.21(b):Shaft resistance versus depth- TP3

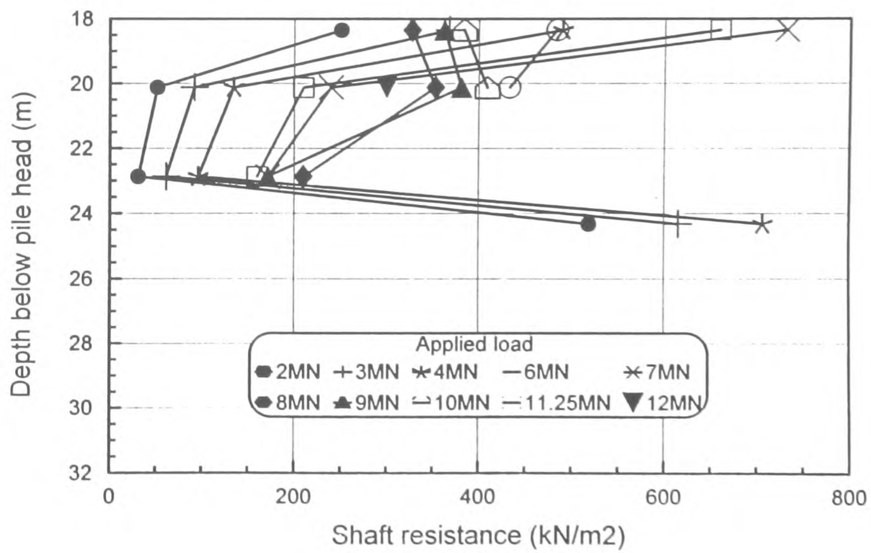

Fig 4.21(c):Shaft resistance versus depth-TP4

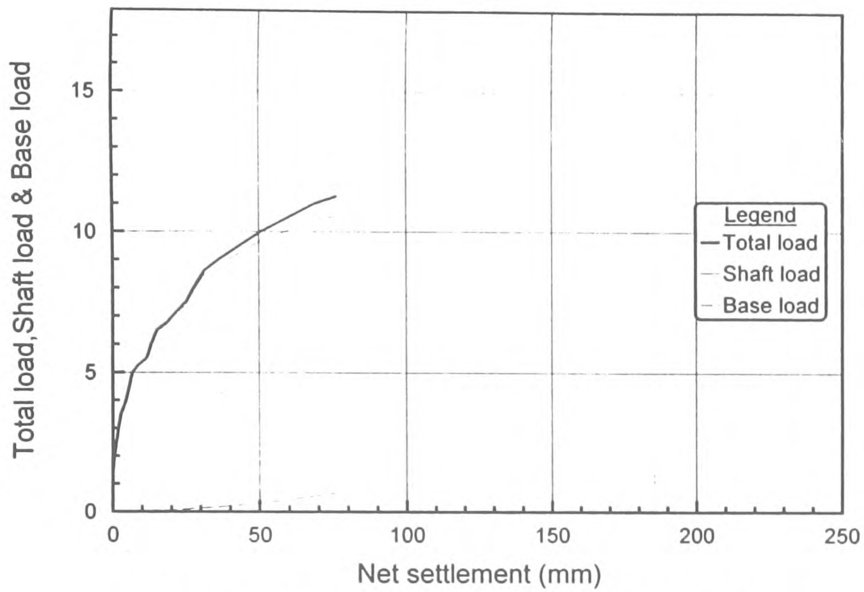

Fig 4.22(c):Total load,Shaft load & Base load Vs net settlement-TP4

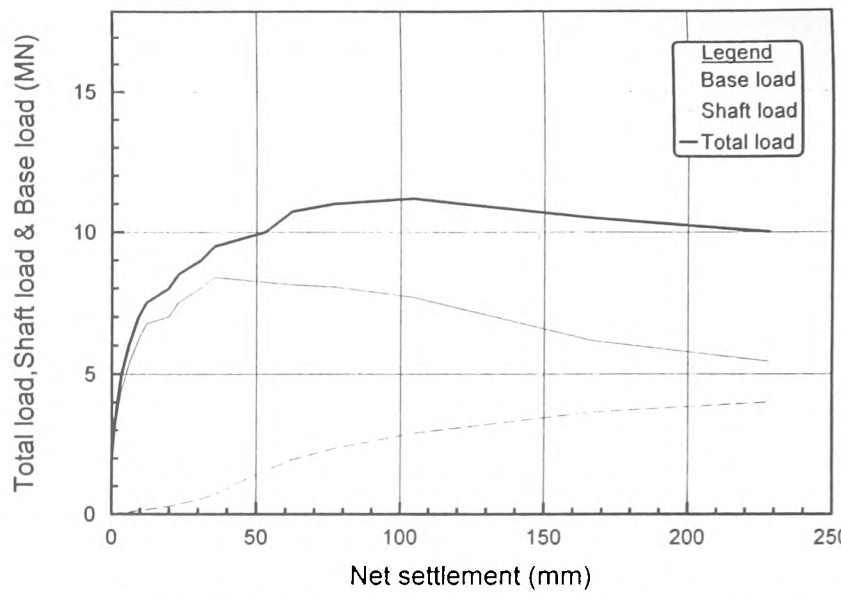

Fig 4.22(d):Total load,Shaft load & Base load Vs net settlement-TP5

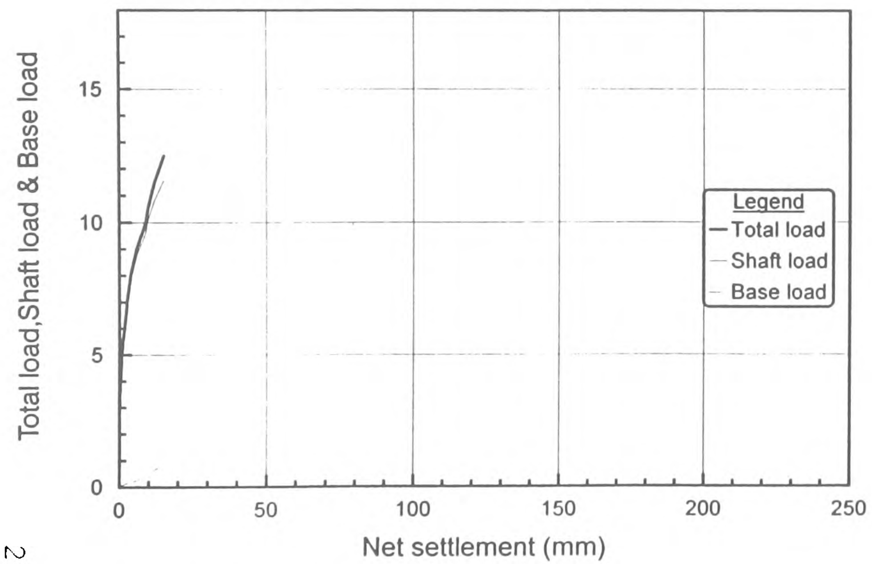

Fig 4.22(e):Total load,Shaft load & Base load Vs net settlement-TP6

CHAPTER 5

EVALUATION OF PILE DESIGN FOR THE BUTETOWN ROAD LINK, P.D.R-CARDIFF

CHAPTER 5: EVALUATION OF PILE DESIGN FOR THE BUTETOWN ROAD LINK

5.1 INTRODUCTION

Several construction projects requiring the use of pile foundations have been undertaken in the Cardiff dock-land area. The most recent occasion is the construction of a number of bridges to link several sections of the new Peripheral Distributor Road. Based on the experience gained, it was considered that driven piles terminated in the Keuper marl would not provide a suitable solution for the Butetown Road link. In addition, the choice of an appropriate pile type depended on other works forming part of the project. The carrying capacity of the selected pile type and size was expected to vary quite significantly due to the variability of the Keuper marl. The load capacity of the piles was also expected to depend on the method of installation.

Large diameter, bored, cast-in place piles were found to offer the most appropriate solution. The following design methods were proposed for the 900mm diameter bored piles:

1) Design method suggested in the interpretative report of the site investigation (this is based on the C.I.R.I.A. Report No. 47 together with previous site experience),
2) Effective stress method (Burland,1973) for shaft resistance prediction, with the drained shear strength values given by Davis and Chandler(1973) ,
3) Total stress design method with undrained cohesion values obtained by empirical correlation with field S.P.T. results, and
4) Total stress design method with undrained cohesion values obtained by empirical

correlation with point load strength data.

5.2 SITE INVESTIGATION RECOMMENDATIONS

5.2.1 Factors of safety

In line with the current piling practice, it was suggested that for these large diameter piles, a factor of safety of 1.5 should be allowed for the shaft resistance and 3 for the base resistance. After incorporating shaft resistance and base resistance, the required pile length was chosen as that which gave an overall factor of safety of at least 2.5. This separation of factors of safety for shaft resistance and end bearing is desirable because of the different degrees to which these components are mobilised at a given pile settlement The safety factors were suggested by Skempton(1966). BS8004 recommends a safety factor of between 2 and 3 subject to various qualifications. However, the regulations given in Eurocode 7 appear to produce an equivalent safety factor of 2 on pile capacity calculated using average shear strengths for the shaft resistance and lower bound strengths for base resistance. In the design of large diameter bored piles, the working load is generally expected to be determined by settlement considerations rather than by ultimate load capacity. This is substantiated by evidence presented by many researchers, notably Whitaker and Cooke(1966) and Burland et al.(1966).

5.2.2 Negative shaft resistance

Because of the instability of the layer of made ground and of the underlying soft clay layers underlying, it was expected that these materials would produce relatively large settlements due to the construction of embankments adjacent to the pile site. Therefore it was considered that the superficial deposits and the upper marl layers would develop negative shaft resistance on the pile shafts. The precise value of negative shaft resistance would vary locally, but it was suggested that an overall negative shaft resistance value of 20kN/m^2 should be allowed for all layers up to the top of the Keuper marl surface. Also as a result of the earthworks, the settlement caused to the superficial layers implied that the full weights of the pile caps had to be carried directly by the piles.

5.2.3 Shaft resistance of the gravel layer above Keuper marl

Generally the unit weight of the gravel layer above the marl was found to be relatively consistent throughout the site. A mean S.P.T. "N" value of 30 was recorded and this was satisfactorily representative of the material. Adopting this value in approximate calculations and assuming that a permanent casing is installed, the average maximum shaft resistance within this layer was estimated to be 40 kN/m^2.

5.2.4 Shaft resistance and base resistance of the Keuper marl

The ground investigation revealed that the Keuper marl was a highly variable material comprising of irregular bands which show a range of strength variations from a firm to stiff clay through to a strong rock. Because of its nature of being intermediate between a rock and clay/silt it is generally not easily analysed, particularly with regard to laboratory strength properties.

Much of the literature available refers to Keuper marl in the Midlands area and the profile of weathering in Cardiff is not the same. The weathered zone associated with a varied depositional environment is much greater in the Cardiff marls. In addition, the Cardiff marls show a general but not consistent decrease in weathering zone with depth and the "N" values also show some variance in comparison with the Midlands.

In using undrained cohesion values, previous experience was relied upon which seemed to indicate that to achieve reasonable results, lower adhesion factors than conventional values for clay, are appropriate. It was also noted that the method of boring and the final state of the pile shaft would have major effect on shaft resistance. For an exposed pile shaft left standing overnight before concrete placement, a much lower adhesion factor of around 0.1 could be required.

5.2.5 Pile settlement

The settlement of a single pile was expected to be a function of the precise length of the pile and the properties of the Keuper marl strata at the exact location of the pile shaft. According to the predictions made by the Soils engineer, it was expected that the maximum shaft resistance would be mobilised when the base movement reached 2-5% of the pile diameter. However, in order to fully mobilise base resistance, a much greater settlement of around 5-10% was expected to be required. This assumption was based on a clean pile toe free from any debris. The magnitude of settlement required for the maximum base resistance to be mobilised could be slightly lower for the more competent zone II and I marl.

Previous studies of load- settlement and load transfer curves for piles (Coyle and Reese,1966) indicated that the pile-soil slip required to develop the maximum shaft resistance is of the order of 5-10 mm. It was suggested that the pile-soil slip is relatively less dependent on shaft diameter, but rather more influenced by the cohesion and friction angle values for the soil. However, whereas the effect of cohesion and friction angle values is a major factor, the contribution of shaft diameter to settlement at a given load cannot be neglected, particularly for large, bored piles.

5.3 DESIGN BASED ON THE SITE INVESTIGATION RECOMMENDATIONS

5.3.1. Shaft resistance

Table 5.1 gives the "N" suggested in the site investigation recommendations, for the various weathering zones of Keuper marl, based on the C.I.R.I.A report No.47. The suggested maximum shaft resistance values are also given.

Weathering zone	S.P.T "N" value	Maximum shaft resistance, q_{us} (kN/m^2)
IVb	<40	50
IVa	40-80	100
IVa with bands of III	80-150	150
III with bands of IVa	**	200
III	150-250	240
III with bands of II	250-350	270
II	>350	350

<u>Notes</u>

1) *Factor for "N" values k=5 to 6 (as suggested for the Midlands area).*
2) *Maximum shaft resistance* $q_{us}=kN\alpha$
3) *Adhesion factors of 0.4 and 0.3 are appropriate for zone IV and zone III marl respectively while a lower value of 0.2 was taken for zone II marl.*

Table 5.1: Maximum shaft resistance from site investigation recommendations

The above maximum shaft resistance values were applied in order to predict the load capacities of the test piles, based on the weathering zone descriptions of the strata encountered during formation of the pile holes. The results are presented in Tables 5.2-

5.7.

Depth (m)	Marl zones	Δl (m)	Site investigation recommendation	
			q_{us} (kN/mm^2) Table 5.1	ΔQ_{us} (kN)
16.56-20.00m	IVa with IVb	3.44	75	729
20.00-22.90m	III with II	2.90	270	2214
22.90-23.50m	II with III	0.60	350	594
23.50-24.60m	II	1.10	350	1089
24.60-25.00m	II	0.40	350	396
25.00-26.70m	II	1.70	350	1682
26.70-27.10m	II	0.40	350	396
		10.54m		**7100**

Table 5.2:Calculation of maximum shaft load for TP1 from "N" values (Design method recommended in the site investigation)

Depth (m)	Marl zones#	Δl (m)	Site investigation recommendation	
			q_{us} (kN/mm^2) Table 5.1	ΔQ_{us} (kN)
16.11-18.00	Gravel	1.89	40@	213
18.00-20.50	II with III	2.50	350	2474
20.50-20.70	III-II	0.20	240	136
20.70-22.00	IVa-III	1.30	150	551
22.00-22.60	III-II	0.60	240	407
22.60-25.00	III-IVa	2.40	200	1357
25.00-25.30	II	0.30	350	297
25.30-26.20	III-II	0.90	240	611
26.20-26.90	II	0.70	350	693
26.90-27.20	III	0.30	270	229
27.20-27.45	II	0.25	350	247
27.45-27.90	III	0.45	270	343
27.90-28.31	II-III	0.41	270	313
		12.20m		**7874**

Borehole No.52 results adopted since TP2 strata log not available
@ *Value recommended for the gravel layer (see section 5.2.3)*

Table 5.3:Calculation of maximum shaft load for TP2 from "N" values (Design method recommended in the site investigation)

Depth (m)	Marl zones	Δl (m)	Site investigation recommendation: q_{us} (kN/mm^2) Table 5.1	Site investigation recommendation: ΔQ_{us} (kN)
20.65-23.15m	IVa with III	2.50	150	1060
23.15-24.00m	IVa	0.85	100	240
24.00-24.85m	III with IVa	0.85	200	481
24.85-26.45m	IV-III and	1.60	210	950
26.45-27.45m	III-II	1.00	240	678
27.45-27.75m	III	0.30	270	229
27.75-30.15m	III with II	2.40	350	2375
30.15-30.45m	II	0.30	350	297
		9.80 m		**6310**

Table 5.4:Calculation of maximum shaft load for TP3 from "N" values (Design method recommended in the site investigation)

Depth (m)	Marl zones	Δl (m)	Site investigation recommendation: q_{us} (kN/mm^2) Table 5.1	Site investigation recommendation: ΔQ_{us} (kN)
17.02-18.15m	IVb	1.13	50	160
18.15-18.58m	IVa with IVb	0.433	75	92
18.58-19.02m	IVa	0.433	100	122
19.02-19.45m	IVa-III	0.433	150	184
19.45-20.15m	IVa with IVb	0.70	75	148
20.15-20.85m	III with IVa	0.70	200	396
20.85-21.25m	IVa with IVb	0.40	75	85
21.25-21.65m	III	0.40	240	271
21.65-21.85m	IV-III	0.20	150	85
21.85-22.75m	IVb&III-IV	0.90	125	318
22.75-22.95m	III-IV	0.20	200	113
22.95-23.45m	III	0.50	240	339
23.45-24.15m	II-III	0.70	270	534
		7.13 m		**2847**

Table 5.5:Calculation of maximum shaft load for TP4 from "N" values (Design method recommended in the site investigation)

Depth (m)	Marl zones	Δl (m)	Site investigation recommendation	
			q_{us} (kN/mm^2) Table 5.1	ΔQ_{us} (kN)
19.70-20.10m	IVa	0.40	100	113
20.10-21.00m	IVa with III	0.90	150	382
21.00-21.80m	IVa	0.80	100	226
21.80-22.10m	III	0.30	240	204
22.10-24.20m	IVa	2.10	100	594
24.20-26.00m	IVa with III	1.80	150	763
26.00-28.50m	IVa	2.50	100	707
28.50-30.20m	IVa	1.70	100	481
		10.50m		**3470**

Table 5.6:Calculation of maximum shaft load for TP5 from "N" values (Design method recommended in the site investigation)

Depth (m)	Marl zones	Δl (m)	Site investigation recommendation q_{us} (kN/mm^2) Table 5.1	ΔQ_{us} (kN)
19.70-20.70m	III with IVa-Vb	1.00	200	566
20.70-21.58m	IVa	0.875	100	247
21.58-22.45m	IVa with III-II	0.875	150	371
22.45-23.33m	IVa with II-III	0.875	150	371
23.33-24.20m	III	0.875	240	594
24.20-25.40m	IVa	1.20	100	339
25.40-26.60m	IVa with IVb-III	1.20	150	509
26.60-27.15m	III with II	0.55	270	420
27.15-27.70m	IVa with III-II	0.55	150	233
27.70-28.45m	IVa with III	0.75	150	318
28.45-29.20m	IVa with III	0.75	150	318
29.20-30.70m	II with III	1.50	350	1484
30.70-30.85m	III with IVa	0.15	200	85
		11.15m		**5855**

Table 5.7:Calculation of maximum shaft load for TP6 from "N" values (Design method recommended in the site investigation)

5.3.2 End bearing resistance

The design method recommended in the site investigation utilises the effective stress parameters given in the C.I.R.I.A. report No. 47 for the calculation of end bearing of piles in Keuper marl. Table 5.8 presents the effective cohesion and the effective angles of friction taken for the various grades of Keuper marl.

Zone	Effective cohesion c' (kN/m^2)	Effective angle of friction ϕ'
IVa	15	30
IVa-III	15	32
III	15	35
III-II	18	37
II	27	40

Table 5.8: Effective stress parameters for different Keuper marl zones (Design method recommended in the site investigation)

The report notes that in order to use the above properties, the material at the base should be at least two pile diameters thick, otherwise the end bearing of the pile should be designed based on the weakest strata present within three pile diameters beneath the base. The ultimate base pressure q_{ub} is then calculated from the following relationship

$$q_{ub} = c'N_c + \sigma'_{vb}N_q + 0.5\gamma DN_\gamma$$

Where N_c, N_q and N_γ are bearing capacity factors

σ'_{vb} = Vertical effective stress at the pile base level

γ = Unit weight of the soil above the pile base level

D = Diameter of pile.

The terms containing the N_c and N_γ may be ignored since they account for only less than 5% of the ultimate base pressure. N_q is calculated from the Prandtl and Reissner(1923) solution, hence:

$$N_q = tan^2\left(45^0 + \frac{\phi'}{2}\right)e^{\pi tan\phi'}$$

Table 5.9 illustrates the calculation of ultimate base resistance values for test piles TP1-TP6. Based on the site investigation data, an average unit weight of the soil strata above the pile base level has been taken as γ = 20kN/m^3, and the water table assumed to be located at the ground surface.

5.3.3 Comparison between predicted and observed load capacities

A comparison between the predicted ultimate bearing values and the results of the pile tests is given in Table 5.10. Where a test pile was not loaded to failure, the "inverse slope" method of extrapolation by Chin(1972) has been used to project the ultimate load. Fellenius(1980) has drawn attention to the fact that Chin's method appears to over-predict. With the exception of TP5, the ultimate base load could not be extrapolated using this method because of low values of base movement achieved.

Pile	Depth to pile toe (m)	Material beneath base	ϕ' (deg)	N_q	q_{ub} (kN/m^2)	Q_b (kN)
TP1	27.10	Zone II	40	64.19	17395	11066
TP2	28.31	Zone II-III	37	42.92	12510	7730
TP3	30.45	Zone II	40	64.19	17395	11066
TP4	24.15	Zone II-III	37	42.92	10365	6594
TP5	30.20	Zone IVa	30	18.40	5557	3535
TP6	31.05	Zone III	35	33.30	10340	6578

Table 5.9:Calculation of ultimate base loads for TP1-TP6 based on the design method recommended in the site investigation

For piles with disturbed bases, such as these ones, the Chin's straight line starts to emerge at base movement values higher than 100mm. Penetrations above this value were achieved in TP5 only.

5.3.4 Comments

It can be seen from Table 5.10 that, using the method recommended in the site investigation report, the calculated shaft resistance values are 40-57% of the measured values. This is true for all test piles, except TP4, where there was interference between the permanent casing and the shaft. Lord(1989) suggested that the S.P.T. approach is not appropriate for assessing the shaft resistance of bored or driven piles bearing on rock. For design purposes, Lord(1989) recommends the use of the maximum shaft resistance derived on the basis of weathering zone classification, as given by Davis & Chandler(1973) and Leach et.al.(1976).

The use of decreasing values of the adhesion factor with increasing Keuper marl shear strength seems satisfactory. Previous research results indicate that the adhesion factor depends on, among others, the cohesive strength of the soil. Early studies by Tomlinson(1957) showed a general trend of decreasing adhesion factors from unity in very soft clays to values as low as 0.2 for clays of very stiff consistency. In the last three decades, several researchers have proposed various formulae relating adhesion factors to shear strength, for various types of clay.

		TP1	TP2	TP3	TP4	TP5	TP6
Shaft (MN)	Predicted	7.100	7.874	6.310	2.847	3.470	5.855
	Measured	**15.90**@	**13.80**@	**15.00**	**8.90**	**8.770**	**12.00**@
	$\frac{Q_{us(predicted)}}{Q_{us(measured)}}$	0.446	0.570	0.421	0.320	0.400	0.488
Base (MN)	Predicted	11.066	-	11.066	6.594	3.535	6.578
	Measured	**12.0**# **11.7**	-	-	-	**5.847**@	-
	$\frac{Q_{ub(predicted)}}{Q_{ub(measured)}}$	0.946	-	-	-	0.605	-
Total (MN)	Predicted	18.166	-	17.376	9.441	7.005	12.433
	Measured	-	**22.0**@	**17.0**	**11.5**	**11.2**	**18.9**@
	$\frac{Q_{u(predicted)}}{Q_{u(measured)}}$	-	-	1.002	0.821	0.625	0.658

Legend
@ *Denotes values extrapolated by the Chin's(1972) method*
\# *Denotes result obtained from an M.L. test*
\- *Denotes result of a C.R.P. test*

Table 5.10: Comparison between the observed load capacities and the predictions from site investigation recommendations

As far as base resistance is concerned, the design method recommended in the site investigation seems to produce reasonable results. Based on the information from TP1, which was designed to provide a direct measurement of base resistance, it is seen from

Table 5.10 that the predicted result is accurate to within about 5%. Both the M.L. and the C.R.P. test results confirm this, coupled with the comparatively higher reliability in the experimental data from this test pile since no interaction between shaft and base behaviour was allowed. The base resistance prediction for TP5 gives a value 60% lower than the value extrapolated using Chin's method.

5.4 EFFECTIVE STRESS DESIGN METHOD

5.4.1 Burland's(1973) formula

This method has already been reviewed in chapter 2 and its use is now explained with regard to the category of bored piles in stiff clay in which the test piles TP1-TP6 fit best. Burland(1973) proposed a relationship between the average maximum shaft resistance $\overline{\tau_s}$ and average effective overburden pressure $\bar{p}$ as $\overline{\tau_s} = \bar{\beta}.\bar{p}$. He showed that, for soft clays, the value of β changes only marginally for a wide range of clays.

For soft clay, assuming that shear failure takes place in the remoulded soil close to the shaft (Tomlinson,1971), the appropriate angle of friction to use is the remoulded drained angle ϕ_r. For a normally consolidated clay, the coefficient of earth pressure at rest is given by $K_o = 1 - \sin\phi_r$, where ϕ_r is the remolded angle of friction. Hence β is given by $\beta = (1 - \sin\phi_r)\tan\phi_r$. Poulos and Davis(1980) suggest that for over-consolidated soils, $K_o = (1 - \sin\phi_r)(OCR)^{1/2}$, in which OCR is the over-consolidation ratio.

5.4.2 Values of earth pressure coefficient, K

An effective stress approach to the evaluation of shaft resistance of stiff clays is subject to a range of uncertainties since it is difficult to evaluate the earth pressure coefficient, K, For heavily over-consolidated clay, the value of K_o ,in the undisturbed state, varies with depth and can have values as high as 3 near the surface decreasing to less than unity at great depth. Because of this variation of K, the calculation of shaft resistance is carried out on a level by level basis.

Wide variations in friction angle values of marl have been reported by Wyllie(1991), who pointed that despite this variation, values of 20-27° may be taken for less weathered and unweathered marl zones approximating to intact rock The following values of remoulded friction angles as given by Davis & Chandler(1973) have been utilised.

Zone	Remoulded angle of friction ϕ_r' (deg)
IVb	18
IVa	20
IVa-III	23
III	25
III-II	28
II	32

Tables 5.11-5.16 give the calculation of maximum shaft loads for TP1-TP6 using the above method. The profile of variation of K_o with depth as reported by Skempton(1961) and Bishop et.al(1965) for stiff over-consolidated clay have been adopted. In each case, the mean of the two values has been utilised in calculating maximum shaft resistance.

Depth (m)	Zones	Δl (m)	ϕ_r' (deg.)	K_o value			$\overline{p}'$ (kN/m^2)	ΔQ_u (kN)
				Skempton (1961)	Bishop et al(1965)	Mean		
16.56				2.010	2.456			
	IVa with IVb	3.44	19			2.156	183	1320
20.00				1.867	2.292			
	III with II	2.9	28			2.014	215	1884
22.90				1.746	2.153			
	II with III	0.6	28			1.936	232	405
23.50				1.721	2.124			
	II	1.1	32			1.898	241	887
24.60				1.675	2.071			
	II	0.4	32			1.864	248	327
25.00				1.658	2.052			
	II	1.7	32			1.817	259	1411
26.70				1.588	1.971			
	II	0.4	32			1.770	269	337
27.10				1.571	1.951			
							Total=	6570kN

Table 5.11:Calculation of maximum shaft load for TP1 using effective stress method (with C.I.R.I.A ϕ_r' values)

Depth (m)	Zones#	Δl (m)	ϕ_r' (deg.)	K_o value			$\overline{p}'$ (kN/m^2)	ΔQ_u (kN)
				Skempton (1961)	Bishop et al(1965)	Mean		
16.11				2.029	2.478			
	Gravel	1.89				2.211		213@
18.00				1.950	2.387			
	II with III	2.50	28			2.113	193	1529
20.50				1.846	2.268			
	III-II	0.20	28			2.052	206	127
20.70				1.838	2.258			
	IVa-III	1.30	23			2.019	214	672
22.00				1.783	2.196			
	III-II	0.60	28			1.976	223	398
22.60				1.758	2.167			
	III-IVa	2.40	23			1.909	238	1309
25.00				1.658	2.052			
	II	0.30	32			1.849	252	246
25.30				1.646	2.038			
	III-II	0.90	28			1.822	258	635
26.20				1.608	1.995			
	II	0.70	32			1.786	266	586
26.90				1.579	1.961			
	III	0.30	25			1.763	271	189
27.20				1.567	1.947			
	II	0.25	32			1.751	273	211
27.45				1.556	1.935			
	III	0.45	25			1.735	277	285
27.90				1.538	1.913			
	II-III	0.41	28			1.716	281	297
28.31				1.521	1.894			
							Total=	6697kN

Borehole No.52 results assumed since TP2 strata log not available
@ *Value recommended for the gravel layer (see section 5.2.3)*

Table 5.12:Calculation of maximum shaft load for TP2 using effective stress method (with C.I.R.I.A ϕ_r' values)

Depth (m)	Zones	Δl (m)	ϕ_r' (deg.)	K_0 value			$\overline{p'}$ (kN/m^2)	ΔQ_u (kN)
				Skempton (1961)	Bishop et al(1965)	Mean		
20.65				1.840	2.261			
	IVa with III	2.5	23			1.994	219	1310
23.15				1.735	2.141			
	IVa	0.85	20			1.919	236	396
24.00				1.700	2.100			
	III with IVa	0.85	23			1.881	244	469
24.85				1.665	2.059			
	IV-III & III-II	1.6	25			1.826	257	988
26.45				1.598	1.983			
	III	1	25			1.768	270	628
27.45				1.556	1.935			
	III with II	0.3	28			1.739	276	216
27.75				1.544	1.920			
	II	2.4	32			1.678	290	2060
30.15				1.444	1.805			
	II	0.3	32			1.618	303	260
30.45				1.431	1.791			
							Total=	6327kN

Table 5.13:Calculation of maximum shaft load for TP3 using effective stress method (with C.I.R.I.A ϕ_r' values)

Depth (m)	Zones	Δl (m)	ϕ_r' (deg.)	K_o value			$\overline{p'}$ (kN/m^2)	ΔQ_u (kN)
				Skempton (1961)	Bishop et al(1965)	Mean		
17.02				1.991	2.434			
	IVb	1.13	18			2.187	176	399
18.15				1.944	2.380			
	IVa with IVb	0.433	19			2.152	184	167
18.58				1.926	2.360			
	IVa	0.433	20			2.133	188	179
19.02				1.908	2.339			
	IVa-III	0.433	23			2.113	192	211
19.45				1.890	2.318			
	IVa with IVb	0.7	19			2.088	198	282
20.15				1.860	2.284			
	III with IVa	0.7	23			2.057	205	354
20.85				1.831	2.251			
	IVa with IVb	0.4	19			2.032	211	167
21.25				1.815	2.232			
	III	0.4	25			2.014	215	228
21.65				1.798	2.213			
	IV-III	0.2	23			2.001	218	104
21.85				1.790	2.203			
	IVb with III-IV	0.9	21			1.976	223	430
22.75				1.752	2.160			
	III-IV	0.2	23			1.952	229	107
22.95				1.744	2.150			
	III	0.5	25			1.936	232	296
23.45				1.723	2.126			
	II-III	0.7	28			1.909	238	478
24.15				1.694	2.093			
							Total =	3402kN

Table 5.14:Calculation of maximum shaft load for TP4 using effective stress method (with C.I.R.I.A ϕ_r' values)

5.4.3 Comparison between predicted and observed shaft resistance values

Table 5.17 gives a comparison between the predicted maximum shaft loads using the effective stress method and the observed pile test results. It can be seen from Tables 5.10 and 5.17 that there is a striking similarity between the predictions obtained using the effective stress method and those evaluated from the S.P.T. design method recommended in the site investigation.

Depth (m)	Zones	Δl (m)	ϕ_r' (deg.)	K_0 value			$\bar{p}'$ (kN/m^2)	ΔQ_u (kN)
				Skempton (1961)	Bishop et al(1965)	Mean		
19.70				1.879	2.306			
	IVa	0.4	20			2.084	199	171
20.10				1.863	2.287			
	IVa with III	0.9	23			2.055	206	456
21.00				1.825	2.244			
	IVa	0.8	20			2.016	214	355
21.80				1.792	2.205			
	III	0.3	25			1.992	220	173
22.10				1.779	2.191			
	IVa	2.1	20			1.938	232	970
24.20				1.692	2.090			
	IVa with III	1.8	23			1.851	251	1004
26.00				1.617	2.004			
	IVa	2.5	20			1.754	273	1230
28.50				1.513	1.884			
	IVa	1.7	20			1.660	294	853
30.20				1.442	1.803			
							Total=	5211kN

Table 5.15:Calculation of maximum shaft load for TP5 using effective stress method (with C.I.R.I.A ϕ_r' values)

Excluding pile TP4 the predicted ultimate loads are 41%-59% of the observed values. Therefore, it both methods appear to be reasonable and appropriate for pile design. The fact that the observed shaft resistance values are higher than predicted may be attributed to the choice of empirical factors and soil parameters. Table 5.17 also gives the $\bar{\beta}$ values back-analysed from the observed maximum shaft resistance values for each test pile. The overal mean value of is $\bar{\beta}$ 1.42. Three assumptions have been made when calculating the mean effective overburden stresses.

Depth (m)	Zones	Δl (m)	ϕ_r' (deg.)	K_o value			$\overline{p}'$ (kN/m^2)	ΔQ_u (kN)
				Skempton (1961)	Bishop et al(1965)	Mean		
19.70				1.879	2.306			
	III with IVa-IVb	1	22			2.070	202	478
20.70				1.838	2.258			
	IVa	0.875	20			2.028	211	386
21.58				1.801	2.216			
	IVa with III-II	0.875	24			1.989	220	482
22.45				1.765	2.174			
	IVa with II-III	0.875	24			1.950	229	492
23.33				1.728	2.132			
	III	0.875	25			1.911	238	524
24.20				1.692	2.090			
	IVa	1.2	20			1.864	248	571
25.40				1.642	2.033			
	IVa with IVb-III	1.2	22			1.810	260	645
26.60				1.592	1.975			
	III with II	0.55	28			1.771	269	394
27.15				1.569	1.949			
	IVa with III-II	0.55	24			1.747	274	332
27.70				1.546	1.923			
	IVa with III	0.75	23			1.717	281	434
28.45				1.515	1.887			
	IVa with III	0.75	23			1.684	288	437
29.20				1.483	1.851			
	II with III	1.5	28			1.633	300	1103
30.70				1.421	1.779			
	III with IVa	0.15	23			1.597	308	88
30.85				1.415	1.772			
							Total =	6366kN

Table 5.16:Calculation of maximum shaft load for TP6 using effective stress method (with C.I.R.I.A ϕ_r' values)

Based on the boreholes data, the bulk density of the Keuper marl has been taken as $26.5kN/m^3$ (and considered unsaturated) and that of the superficial deposits as $20kN/m^3$. Hence the unit weight of water has been subtracted from the unit weight of the superficial soil layers only.

Test pile	Effective stress method result (MN)	Pile test result (MN)	$\frac{Q_{u(predicted)}}{Q_{u(measured)}}$	$\bar{\beta} = \frac{\bar{\tau}_s}{\bar{p}}$ (Back-analysis)
TP1	6.57	15.90	0.41	1.70
TP2	6.70	13.80	0.48	1.22
TP3	6.33	15.00	0.42	1.90
TP4	3.40	8.90	0.38*	1.84
TP5	5.21	8.77	0.59	0.75
TP6	6.37	12.00	0.53	1.08

* *Not reliable since the casing displaced during concreting*

Table 5.17: Comparison between the predicted maximum shaft loads using effective stress method with the test pile results

5.5 TOTAL STRESS DESIGN BASED ON S.P.T. "N" VALUES

5.5.1 Field S.P.T. results

Table 5.16(a) and 5.16(b) present the S.P.T. "N" values measured in various boreholes during the site investigation for the proposed Butetown road link. All other boreholes not listed had S.P.T. data relating to superficial soil strata only. The weathering zone descriptions of the strata penetrated are also given. Where the required total penetration of 450mm was not achieved, the blow count corresponding to the settlement reached has been linearly extrapolated in order to estimate the number of blows required to produce a penetration of 300mm, beyond the initial seating penetration of 150mm.

5.5.2 Kilbourne et.al.(1988) design formula

Based on pile load tests previously carried out in Cardiff, Kilbourne et al.(1988) proposed an empirical formula for calculating the shaft resistance of large diameter, bored, cast in-situ piles formed in Keuper marl. They suggested the use of a factor of 6 to convert field S.P.T. "N" values to equivalent undrained strength.

BH No.	Depth (m)	Split or Cone	"N" for various Keuper marl zones*				
			IVa	IVa & III	III	III & II	II
BH102	16.50	c		16			
	18.00	s		56			
	19.50	s		73			
	22.50	c					200
	37.00	s				402	
	40.00	s					500
BH103	16.50	c		21			
	18.00	c		43			
	19.50	c		71			
	21.00				176		
BH104	18.50	c		56			
	20.00			123			
BH105	16.80	c	45				
	18.30	c	92				
	19.80	c	94				
	21.30	c	111				
	22.80	c					
BH106A	18.50	s		99			
	19.55	s			100		
	20.55	s			42		
	21.55	s				182	
	22.55	s				106	
	23.55	s				200	
	25.50	s				200	
BH107	17.70	s			70		
	18.50	s			68		
	19.50	s				160	
BH108	18.00			99			
	19.00	s					
	20.00	s		202			
	21.00	s	106				
	22.00	s			118		
	23.00	s					
	24.00	s	92				
	25.00				90		
	26.00	s			174		
	27.00	s			128		
	28.00	s					200
	28.70	s					200
	35.00	c					

Table 5.18: Observed S.P.T. "N" values (Borehole Nos 102-108)

With this correlation, Kilbourne et al(1988) established that an adhesion factor of α=0.375 was generally appropriate for the Keuper marl strata in Cardiff. This design method has been applied to piles TP1-TP6 as presented in Tables 5.20-5.25. For the purpose of back-analysing adhesion factors from measured shaft resistance values, a summation $\sum N.\Delta l$ is included in the last columns of these Tables.

BH No.	Depth (m)	Split or Cone	"N" for various Keuper marl zones*				
			IVa	IVa & III	III	III & II	II
BH109	17.55	s		39			
	18.55	s	43				
	19.55	s			132		
	20.55	s			56		
	21.55	s		52			
	22.55	s		17			
	23.55	s		178			
	24.55	s		37			
	25.55	s		173			
	25.55	s		76			
	26.55	s		48			
	27.55	s		45			
	28.55	s		67			
	29.55	s					
	30.55	s			182		
	31.55	s	64				
	32.55	s				74	
	33.55	s			82		
	34.55	s			139		
	35.55	s				396	
	36.55	s				200	
BH110	19.50	s				136	
	21.50	s		19			
	22.50	s		152			
	23.50	s		22			
	24.75	s		148			
BH117	13.30						
	13.80			174			
	15.00					200	
BH118	13.20	c			162		
	15.20	c				154	
	16.20	c			182		
	17.20	c			186		
		Average	80.875	81	122.76	200.83	275

Table 5.19: Observed S.P.T. "N" values (Borehole Nos. 109-118) and overall average values for various weathering zones

Depth (m)	Marl zones	S.P.T. "N"	Δl (m)	ΔQ_u (kN)	N.Δl (m)
16.56-20.00	IVa with IVb	81	3.44	1773	279
20.00-22.90	III with II	201	2.90	3708	583
22.90-23.50	II with III	201	0.60	767	121
23.50-24.60	II	275	1.10	1924	303
24.60-25.00	II	275	0.40	700	110
25.00-26.70	II	275	1.70	2974	468
26.70-27.10	II	275	0.40	700	110
			Totals	**12546**	**1972**

Table 5.20: Kilbourne et.al(1988) design method-TP1

Depth (m)	Marl zones	S.P.T. "N"	Δl (m)	ΔQ_u (kN)	N.Δl (m)
16.11-18.00	Gravel		1.89	213	
18.00-20.50	II with III	201	2.50	3197	503
20.50-20.70	III-II	201	0.20	256	40
20.70-22.00	IVa-III	81	1.30	670	105
22.00-22.60	III-II	201	0.60	767	121
22.60-25.00	III-IVa	81	2.40	1237	194
25.00-25.30	II	275	0.30	525	83
25.30-26.20	III-II	201	0.90	1151	181
26.20-26.90	II	275	0.70	1225	193
26.90-27.20	III	123	0.30	235	37
27.20-27.45	II	275	0.25	437	69
27.45-27.90	III	123	0.45	352	55
27.90-28.31	II-III	201	0.41	524	82
			Totals	**10788**	**1662**

Table 5.21: Kilbourne et.al(1988) design method-TP2

Depth (m)	Marl zones	S.P.T. "N"	Δl (m)	ΔQ_u (kN)	N.Δl (m)
20.65-23.15	IVa with III	81	2.50	1288	203
23.15-24.00	IVa	81	0.85	438	69
24.00-24.85	III with IVa	81	0.85	438	69
24.85-26.45	IV-III & III-II	141	1.60	1435	226
26.45-27.45	III	123	1.00	782	123
27.45-27.75	III with II	201	0.30	384	60
27.75-30.15	II	275	2.40	4199	660
30.15-30.45	II	275	0.30	525	83
			Totals	**9489**	**1492**

Table 5.22: Kilbourne et.al(1988) design method-TP3

Depth (m)	Marl zones	S.P.T. "N"	Δl (m)	ΔQ_u (kN)	N.Δl (m)
17.02-18.15	IVb	81	1.13	582	92
18.15-18.58	IVa with IVb	81	0.43	223	35
18.58-19.02	IVa	81	0.43	223	35
19.02-19.45	IVa-III	81	0.43	223	35
19.45-20.15	IVa with IVb	81	0.70	361	57
20.15-20.85	III with IVa	81	0.70	361	57
20.85-21.25	IVa with IVb	81	0.40	206	32
21.25-21.65	III	123	0.40	313	49
21.65-21.85	IV-III	81	0.20	103	16
21.85-22.75	IVb with III-IV	81	0.90	464	73
22.75-22.95	III-IV	81	0.20	103	16
22.95-23.45	III	123	0.50	391	62
23.45-24.15	II-III	201	0.70	895	141
			Totals	**4448**	**699**

Table 5.23: Kilbourne et.al(1988) design method-TP4

Depth (m)	Marl zones	S.P.T. "N"	Δl (m)	ΔQ_u (kN)	N.Δl (m)
19.70-20.10	IVa	81	0.40	206	32
20.10-21.00	IVa with III	81	0.90	464	73
21.00-21.80	IVa	81	0.80	412	65
21.80-22.10	III	123	0.30	235	37
22.10-24.20	IVa	81	2.10	1082	170
24.20-26.00	IVa with III	81	1.80	928	146
26.00-28.50	IVa	81	2.50	1288	203
28.50-30.20	IVa	81	1.70	876	138
			Totals	**5491**	**863**

Table 5.24: Kilbourne et.al(1988) design method-TP5

Depth (m)	Marl zones	S.P.T. "N"	Δl (m)	ΔQ_u (kN)	N.Δl (m)
19.70-20.70	III with IVa-Ivb	81	1.00	515	81
20.70-21.58	Iva	81	0.88	451	71
21.58-22.45	IVa with III-II	141	0.88	785	123
22.45-23.33	IVa with II-III	141	0.88	785	123
23.33-24.20	III	123	0.88	685	108
24.20-25.40	Iva	81	1.20	618	97
25.40-26.60	IVa with IVb-III	81	1.20	618	97
26.60-27.15	III with II	201	0.55	703	111
27.15-27.70	IVa with III-II	141	0.55	493	78
27.70-28.45	IVa with III	81	0.75	386	61
28.45-29.20	IVa with III	81	0.75	386	61
29.20-30.70	II with III	201	1.50	1918	302
30.70-30.85	III with Iva	81	0.15	77	12
			Totals	**8422**	**1324**

Table 5.25: Kilbourne et.al(1988) design method-TP6

Depth (m)	Marl zones	S.P.T. "N"	Δl (m)	ΔQ_u (kN)	N.Δl (m)
17.02-18.15	IVb	81	1.13	582	92
18.15-18.58	IVa with IVb	81	0.43	223	35
18.58-19.02	IVa	81	0.43	223	35
19.02-19.45	IVa-III	81	0.43	223	35
19.45-20.15	IVa with IVb	81	0.70	361	57
20.15-20.85	III with IVa	81	0.70	361	57
20.85-21.25	IVa with IVb	81	0.40	206	32
21.25-21.65	III	123	0.40	313	49
21.65-21.85	IV-III	81	0.20	103	16
21.85-22.75	IVb with III-IV	81	0.90	464	73
22.75-22.95	III-IV	81	0.20	103	16
22.95-23.45	III	123	0.50	391	62
23.45-24.15	II-III	201	0.70	895	141
			Totals	**4448**	**699**

Table 5.23: Kilbourne et.al(1988) design method-TP4

Depth (m)	Marl zones	S.P.T. "N"	Δl (m)	ΔQ_u (kN)	N.Δl (m)
19.70-20.10	IVa	81	0.40	206	32
20.10-21.00	IVa with III	81	0.90	464	73
21.00-21.80	IVa	81	0.80	412	65
21.80-22.10	III	123	0.30	235	37
22.10-24.20	IVa	81	2.10	1082	170
24.20-26.00	IVa with III	81	1.80	928	146
26.00-28.50	IVa	81	2.50	1288	203
28.50-30.20	IVa	81	1.70	876	138
			Totals	**5491**	**863**

Table 5.24: Kilbourne et.al(1988) design method-TP5

Depth (m)	Marl zones	S.P.T. "N"	Δl (m)	ΔQ_u (kN)	N.Δl (m)
19.70-20.70	III with IVa-Ivb	81	1.00	515	81
20.70-21.58	Iva	81	0.88	451	71
21.58-22.45	IVa with III-II	141	0.88	785	123
22.45-23.33	IVa with II-III	141	0.88	785	123
23.33-24.20	III	123	0.88	685	108
24.20-25.40	Iva	81	1.20	618	97
25.40-26.60	IVa with IVb-III	81	1.20	618	97
26.60-27.15	III with II	201	0.55	703	111
27.15-27.70	IVa with III-II	141	0.55	493	78
27.70-28.45	IVa with III	81	0.75	386	61
28.45-29.20	IVa with III	81	0.75	386	61
29.20-30.70	II with III	201	1.50	1918	302
30.70-30.85	III with Iva	81	0.15	77	12
			Totals	**8422**	**1324**

Table 5.25: Kilbourne et.al(1988) design method-TP6

5.5.3 Comparison between predicted and observed shaft resistance

Table 5.26 presents a comparison between the predicted and measured maximum shaft resistance values. Values of adhesion factor back-analysed from measured shaft resistance are also shown.

Test pile	Kilbourne et.al(1988) (MN)	Measured (MN)	$\frac{Q_{u(predicted)}}{Q_{u(measured)}}$	α (Back-analysis)
TP1	12.55	15.90	0.79	0.475
TP2	10.79	13.80	0.78	0.482
TP3	9.49	15.00	0.63	0.593
TP4	4.45	8.90	0.50	0.750*
TP5	5.49	8.77	0.62	0.599
TP6	8.42	12.00	0.70	0.534

* *Not reliable since the casing displaced during concreting*

Table 5.26: Comparison between predicted and measured shaft resistance values using Kilbourne et. al(1988) method

5.5.4 Comments

From Table 5.20, it can be seen that the method proposed by Kilbourne et.al(1988) also gives consistent predictions for varying soil conditions. This method gives more accurate results than the method suggested in the site investigation interpretative report and the effective stress method. However, it appears that the adhesion factor of α=0.375 suggested by Kilbourne et.al(1988) is inappropriate for the sites of test piles TP1-TP6. Table 5.20 gives back-analysed adhesion factors, α, based on the observed shaft resistance values, for use with the formula proposed by Kilbourne et.al(1988). There is not a significant variation between the back-analysed adhesion factors and an average value of α=0.53 may therefore be considered appropriate.

5.6 TOTAL STRESS DESIGN BASED ON POINT LOAD TEST RESULTS

5.6.1 Analysis of Point Load test data

The point load strength test is generally used as a simple procedure for field classification of rock materials. From the tabulated values of P and D the first step is to calculate the Point-Load strength index I_s from the ratio $I_s = \frac{P}{D^2}$. This is then corrected to a reference specimen diameter of 50 mm by obtaining the index $I_s(50)$ from a correction chart (Turk and Dearman,1986). The $I_s(50)$ values are then arranged in ascending order and the median value is found by systematically deleting highest and lowest values until only two remain. The average of these is the required median value.

5.6.2 Estimation of maximum shaft resistance

Point-Load strength is closely correlated with the results of uniaxial compression. An approximate conversion factor of 24 can be used in order to obtain uniaxial compression strength values from $I_s(50)$ values. The median values of uniaxial strengths of various Keuper marl zones as determined during the site investigation are as follows:

Weathering zone	Comp. Strength (kN/m^2)
IVa	211
IVa-III	274
III	340
III-II	375
II	502
II-I	480
I	558

Using these values in conjunction with the strata descriptions for the test piles sites TP1-TP6 the results shown in Table 5.27 are obtained, for a typical range of values of adhesion factor, α.

		Predicted shaft resistance, $Q_{u(predicted)}$ (MN)					
Pile	$Q_{u(measured)}$ (MN)	α=0.3	α=0.4	α=0.5	α=0.6	α=1.0	α=1.45
TP1	15.90	3.26	4.35	5.15	6.52	10.87	10.00
TP2	13.80	3.29	4.31	5.34	6.36	10.46	15.10
TP3	15.00	2.91	3.87	4.84	5.81	9.68	14.10
TP4	8.90	1.36	2.10	2.63	3.15	5.26	7.60
TP5	8.77	2.06	2.74	3.43	4.11	5.84	8.50
TP6	12.00	2.71	3.62	4.52	5.42	9.04	13.10

Table 5.27: Design based on point load test data-Comparison predicted and observed shaft resistance

5.6.3 Comments

From Table 5.27, it is indicated that the use of point load design method seriously underestimates shaft resistance. For an adhesion factor α=0.5, the calculated maximum shaft resistance values are only 30-40% of the measured values. For α=1.0, the predicted values are still less than the observed ones. A value of α=1.45 is necessary to reduce the discrepancy between the observed and predicted values to an acceptable margin. There is a wide scatter in the point load strength values for a Keuper marl stratum of given weathering zone classification. Therefore, the median point load strength values used to assess the shaft resistance values are subject to variations. These values are also likely to be affected by differences in the population of the point load strength data available for various weathering zone categories.

CHAPTER 6

MODELING PILE BEHAVIOUR

CHAPTER 6: MODELLING PILE BEHAVIOUR

6.1 OVERVIEW OF EXISTING METHODS OF PILE ANALYSIS

6.1.1 Introduction

A number of methods currently exist for the prediction of pile deflection under applied load. These range widely from simple methods to sophisticated methods utilising finite element analysis. Some of the methods present graphical illustrations of the relationship between pile head settlement and various parameters such as pile dimensions, pile stiffness and soil properties. These methods attempt to provide an understanding of the mechanism of load transfer from pile to soil. The methods have varying degrees of success, as judged from back-analysis using pile load test results. The various methods currently available are briefly reviewed below.

6.1.2 Load transfer analysis by linear spring representation

The earliest method is the simple load transfer analysis (Coyle and Reese,1966 and Vesic,1969). This method, to which reference is often made as the t-z analysis, involves representing the relationship between the skin resistance and the relative vertical displacement between the soil and the pile, using linear soil spring modelling. A linear soil spring model is also used to develop curves (q-z curves) relating the pile tip bearing stress to the pile tip vertical displacement. This method is now generally discredited as it does not provide for the influence of the interaction between soil layers on pile settlement.

6.1.3 Boundary Element Method (or Integral Equation Analysis)

This method was invented by Poulos and Davis(1968) and has been extended and modified by Butterfield and Banerjee,(1970&1971). It is an extension of the t-z analysis, to include a consideration of the interaction between various soil elements in which a pile is embedded (by non-linear soil spring modelling). This is achieved using the solution presented by Mindlin(1936) for a point load acting in an elastic half-space. However, both the load transfer and the Boundary element analyses are somewhat limited in the sense that it is difficult to accurately account for a particular site in terms of the non-homogeneity and non-linearity of the soil response under load.

6.1.4 Approximate analysis based on elasticity

Various methods under this category have been developed by Randolph and Wroth(1978), Lee(1993) and Poulos(1980). These are based on considering the pile-soil system as perfectly linearly elastic materials. Some extension to the methods is made to account for non-homogeneity of soil in the lateral and vertical directions.

6.1.5 Functional representation of pile characteristics

These methods (for example Hirayama,1990 and Fleming,1992) utilise mathematical functions to represent various relationships which describe pile load-settlement response. Separate functions may be used to represent individual components of load resistance. The various parameters of the functions are empirically assessed from soil and pile properties. These methods are simple and readily applicable for piles in different soil conditions.

6.1.6 Finite element analysis -FEA

Finite element analysis for piles have been adopted by Frank(1974&1975), Baguelin(1975), Ottaviani(1975), Dasgupta(1985), Chow(1989) and Phoon et.al.,1990). This method has undergone extensive development in recent times and has also gained considerable popularity due to its flexibility and accuracy. The following are examples of the different approaches in which the equations are formulated:

1) **Finite layer analysis** (Small and Booker,1984&1986; Lee and Small,1991). In this method, the soil is treated as consisting of a series of horizontal isotropic or cross-anisotropic elastic layers of infinite lateral extent.
2) **Infinite layer analysis** (Guo et.al.,1987) in which the soil displacement functions are represented by a product of piece-wise polynomial and series expansion functions.
3) **Discrete Fourier Series approach** (Lai and Booker,1989). In this method, the soil displacement fields are represented as discrete Fourier series and solved by finite element methods.
4) **Use of composite filamented beam elements in structural analysis** to model the pile stiffness and non-linear soil springs to model pile displacements by means of hyperbolic functions (San-Shyan Lin, 1997).

With the use of FEA, some of the shortcomings of the Boundary element method have been adequately covered since the former enables the consideration of the variations in soil properties which could extend with depth as well as laterally across the site.

6.2 PERFORMANCE OF LARGE DIAMETER, BORED PILES

6.2.1 The need for a simple numerical model

Poulos(1989) and Fleming(1992) have drawn attention to the fact that, although complex analytical methods are capable of modelling pile-soil systems with significant flexibility, the sophisticated input data required are not available from standard site investigations. Therefore there is need for a simple but accurate numerical model where the required parameters can be readily correlated with conventional soil strength parameters. In addition, the analysis should be easily adaptable and understood by foundation engineers/designers.

In this chapter, a new method is developed which is capable of predicting the load-settlement variation of a pile up to and including the ultimate state of the pile-soil system. The emphasis is on the ease of use by ordinary practising engineers, rather than elaborate theoretical and mathematical sophistication. The analysis is based on mathematical representation of: (a)the development of shaft resistance and end bearing, (b) the variation in load sharing between the pile shaft and base (c) the influence of non-linear concrete stress-strain behaviour on pile compression (d) the influence on pile settlement of additional compressibility due to any loose soil possibly present at the pile base level.

6.2.2 Pile load-settlement prediction

In any pile design activity, settlement control receives considerable attention. Pile settlement is influenced by a number of factors such as installation techniques, group-action and soil conditions. The problem to the designer is not only the consideration of pile integrity and performance as a unit but also the function of the pile as the interface between the superstructure and the surrounding soil.

The elastic theory is of significant help in the development of the numerical model presented. The method is simple and offers a practical solution to the problem of load-settlement prediction and is successful in utilising the parameters readily available from standard site investigations. The model can also be applied to pile-soil systems with variable characteristics.

6.2.3 Load resistance mobilisation

Much of the existing literature on large diameter, bored piles relates to the recorded bahaviour in London clay in which designers often utilise the early investigations carried out by Cooke and Whitaker(1961) and Whitaker and Cooke(1966). These studies show that the shaft and base resistance are developed to different extents for a given pile settlement. Studies such as those carried out by Randolph and Wroth(1982), indicate that shaft resistance at a given applied load also depends on the pile diameter.

Many researchers have attempted to define the settlement at peak shaft load in terms of either the shear strain around the shaft or the penetration of the pile tip. Some of these definitions are summarised in Table 6.1, which also include definitions of the base movement Δ_{ub} at ultimate base resistance, P_{ub}.

Reference	Definition for Δ_{us}	Definition for Δ_{ub}	Soil type
Cooke & Whitaker(1961) and Poulos(1980)	0.5-1% of shaft diameter	10-15% of the base diameter	London clay
Burland et al.(1966)	Occurrence of P_{us} is defined in terms of shear strains around pile shaft and this strain is 0.1 (not dependent on pile diameter)	Not identified	Clay
Whitaker & Cooke(1966), Coyle & Reese(1966), AISI(1975) and Bowles (1996)	Occurrence of Δ_{us} is defined in terms of the relative pile soil slip required, which is 5-10cm and is independent of pile diameter and embedded length, but may depend on the strength properties of the soil	10% and 30% of base diameter for driven and bored piles respectively	Cohesive soils
Fleming et.al.(1992)	Typically 0.5-2% of the pile diameter	5-10% of the pile base diameter (larger for low-displacement piles in granular soil	For a range of soils
Tomlinson(1994)	For piles with diameters greater than 600mm, Δ_{us}=10mm (i.e 1.6% diameter, maximum). Further, at peak shaft load, only 22% of the ultimate base load is developed.	For bored piles in stiff clay with diameters greater than 600mm, Δ_{ub}=150mm (i.e 20% diameter, maximum)	Stiff clay (definition is for bored piles)
Barnes(1995) and BS8004(1986)	1-2% of pile shaft diameter	10-20% pile base diameter	Clay
Present work	1.5-4% pile shaft diameter (for pile diameters greater than 600mm) and 5-15% for small diameter piles, depending on soil stiffness.	15-30% pile base diameter	Keuper marl zones I-IV in South Wales (Based on dedicated load tests and Kilbourn et al,1988).

Table 6.1:Existing definitions for pile base settlements necessary to develop the full shaft resistance and end bearing

6.3 MODELLING OF SHAFT RESISTANCE MOBILISATION

6.3.1 Extension of Reese et.al(1969) method

For large bored piles in clay, Reese et.al.(1969) suggested the following relationship between the local unit shaft resistance at a given level along a pile shaft and the displacement at that level. The symbols used in the equation may differ from the original publication, to maintain the nomenclature adopted by the author.

$$\tau(z) = \tau_{\max}\left[2\sqrt{\frac{\Delta(z)}{s_o}} - \frac{\Delta(z)}{s_o}\right] \qquad (6.1a)$$

Where

$\tau(z)$ =Shaft resistance at depth z (originally in tons/ft^2)

τ_{max} =Maximum shaft resistance that can occur at any depth (tons/ft^2)

$\Delta(z)$ =Pile movement at depth z (originally in inches)

s_o = 2 D_s ε, where

D_s = diameter of pile shaft (in inches)

ε = Average failure strain (in percent) of the soil near the pile toe, obtained from unconfined compression tests.

Equation (6.1a) can be extended to predict the variation between the total load supported by the pile shaft and the settlement of the pile base. Consider the integral of Eqn.(6.1a), with respect to depth, z, between the limits z=0 to z=L_s (where L_s is the shaft length). Two variables are identified, which are both functions z, namely $\tau(z)$ and $\Delta(z)$.

Hence,

$$\int_0^{L_s} \tau(z).dz = \tau_{\max} \int_0^{L_s} \left[\frac{2}{\sqrt{s_o}} \Delta(z)^{\frac{1}{2}} - \frac{\Delta(z)}{s_o} \right].dz \tag{6.1b}$$

On expanding the right hand side, we have

$$\int_0^{L_s} \tau(z).dz = \frac{2\tau_{\max}}{\sqrt{s_o}} \int_0^{L_s} \Delta(z)^{\frac{1}{2}}.dz - \frac{\tau_{\max}}{s_o} \int_0^{L_s} \Delta(z).dz \tag{6.1c}$$

The total shaft load P_s is related to the left-hand side of this equation by

$$P_s = \pi D_s \int_0^{L_s} \tau(z) dz \tag{6.1d}$$

Consider the variations of $\Delta(z)^{\frac{1}{2}}$ and $\Delta(z)$ as functions of z, defined over the domain z=0 to z= L_s. The mean values $\left[\Delta^{\frac{1}{2}}\right]_{mean}$ and $[\Delta]_{mean}$ respectively of these functions are defined by

$$\left[\Delta^{\frac{1}{2}}\right]_{mean} = \frac{1}{L_s} \int_0^{L_s} \Delta(z)^{\frac{1}{2}}.dz \tag{6.1e}$$

(i.e the mean square root displacement for all points along L_s) ,

$$[\Delta]_{mean} = \frac{1}{L_s} \int_0^{L_s} \Delta(z).dz \tag{6.1f}$$

(i.e the mean displacement for all points along L_s).

Substituting for $\int_0^{L_s} \tau(z) dz$, $\int_0^{L_s} \Delta(z)^{\frac{1}{2}}.dz$ and $\int_0^{L_s} \Delta(z).dz$ from Eqns.(6.1d)-(6.1f) into Eqn.(6.1c) gives

$$P_s = \frac{2\pi D_s \tau_{\max} L_s}{\sqrt{s_o}} \left[\Delta^{\frac{1}{2}}\right]_{mean} - \frac{\pi D_s \tau_{\max} L_s}{s_o} [\Delta]_{mean} \tag{6.1g}$$

From physical considerations, the mean displacement for all points along a pile shaft is made up of two components:

1) the base penetration, Δ_b, and

2) the weighted FAPR displacements $\left[\Delta_{es}\right]_{mean}$ for all points along L_s, hence

$$\left[\Delta\right]_{mean} = \Delta_b + \left[\Delta_{es}\right]_{mean} \tag{6.1h}$$

From 5 fully instrumented test piles, it has been assessed that $80{:}1 \le \frac{\left[\Delta_{es}\right]_{mean}}{\Delta_b} \le 10{:}1$, for applied pile head loads down from P_{ult} to $0.3P_{ult}$. Hence $\left[\Delta_{es}\right]_{mean}$ is insignificant in comparison to Δ_b for most of the loading range. Thus it is sufficiently accurate to take

$$\left[\Delta\right]_{mean} = \Delta_b \tag{6.1i}$$

Therefore, in Eqn.(6.1g), $\left[\Delta\right]_{mean} = \Delta_b$, and within the first order of approximations, $\left[\Delta^{\frac{1}{2}}\right]_{mean} = \sqrt{\Delta_b}$. Since τ_{max} and s_o are unknown at this stage, the groups of constants in Eqn.(6.1g) may be replaced by single coefficients, a_o and a_1 which are evaluated from the following boundary conditions. Hence we have,

$$P_s = a_o\sqrt{\Delta_b} - a_1\Delta_b . \tag{6.2}$$

6.3.2 Boundary conditions

1. The function in Eqn.(6.2) obviously satisfies the fact that no shaft load is developed without pile displacement

2. At the peak shaft load, the plot of P_s versus Δ_b must either depict a clear maximum point or reach a plateau, Fig.6.1, hence $\frac{dP_s}{d\Delta_b} = 0$ when $\Delta_b = \Delta_{us}$, where Δ_{us} is the base movement at peak shaft load, P_{us}. Based on a number of case studies, it is sufficient

to assume that the residual shaft load is reached at a settlement equivalent to the base penetration Δ_{ub} necessary to cause failure in end bearing. The residual shaft load is given by $R_s P_{us}$, where R_s is an empirical factor. By differentiating Eqn.(6.2) with respect to Δ_b and invoking this condition, the following relationship is obtained:

$$\frac{a_o}{2\sqrt{\Delta_{us}}} - a_1 = 0. \tag{6.3a}$$

3. When $\Delta_b = \Delta_{us}$, and $P_s = P_{us}$, substituting this into Eqn(6.2) gives

$$a_o\sqrt{\Delta_{us}} - a_1\Delta_{us} = P_{us}. \tag{6.3b}$$

Solving Eqns(6.3a) and (6.3b) simultaneously gives

$$P_s = P_{us}\left(\frac{2\sqrt{\Delta_b}}{\sqrt{\Delta_{us}}} - \frac{\Delta_b}{\Delta_{us}}\right). \tag{6.4a}$$

There is evidence that the settlement of a pile shaft is directly proportional to the pile shaft diameter, D_s. Therefore it is possible to express Δ_{us} as $\Delta_{us} = rD_s$, in which **r** is a constant parameter in the form of a pile shaft flexibility factor. The value of **r** decreases with increasing soil stiffness. The following additional factors are also thought to have an influence on the shaft flexibility: (a) the method of pile installation (b) the pile type (c) the pile length, and (d) the time elapsed since pile installation.

6.3.3 Variation in mobilised shaft resistance

After the mobilisation of full shaft resistance, the shaft resistance either remains constant (the path **XZ**, Fig.6.1) or decreases in value, with increasing base movement (the path **XY**, Fig.6.1). This is a typical variation of shear stress versus shear strain for soils, where peak and residual shear strengths may be experienced. To provide for this situation, it is observed that a cubic power series function can be used to represent the pattern along **XY**, although a number of other functions were attempted. This functional representation is supported by the results of the instrumented test piles in formed in Keuper marl. It is assumed that the shaft resistance decreases to a residual value at a base penetration corresponding to the point of ultimate base resistance (point **Y**, Fig.6.1). The base movement Δ_{ub} at ultimate base load is taken as $\Delta_b = mD_b$, where D_b is the base diameter and ***m*** is a constant parameter as defined in Table 6.1. The relationship is expressed as

$$P_b = C_o + C_1\Delta_b + C_2\Delta_b^2 + C_3\Delta_b^3 \tag{6.4b}$$

where C_o, C_1, C_2, and C_3 are constants to be evaluated from the following boundary conditions:

(1) When $\Delta_b = \Delta_{us}$, $P_s = P_{us}$, (2) and $\frac{dP_s}{d\Delta_b} = 0$, (3) When $\Delta_b = mD_b$, $P_s = R_s\ P_{us}$ and (4) $\frac{dP_s}{d\Delta_b} = 0$, where **m** is the percentage of pile base diameter which defines the base movement at ultimate base load, see Figs.6.1 and 6.2. The coefficient R_s (Fig.6.1) gives the value of the residual shaft resistance when multiplied by the maximum shaft resistance P_{us}. These boundary conditions lead to the following set of equations, from which the unknown coefficients are solved:

$$\begin{bmatrix} 1 & \Delta_{us} & \Delta_{us}^2 & \Delta_{us}^3 \\ 0 & 1 & 2\Delta_{us} & 3\Delta_{us}^2 \\ 1 & mD_b & m^2D_b^2 & m^3D_b^3 \\ 0 & 1 & 2mD_b & 3mD_b^2 \end{bmatrix} \begin{Bmatrix} C_o \\ C_1 \\ C_2 \\ C_3 \end{Bmatrix} = \begin{bmatrix} P_{us} \\ 0 \\ R_sP_{us} \\ 0 \end{bmatrix} \tag{6.4c}$$

On solving these equations, the coefficients are obtained as follows:

$$C_3 = \frac{P_{us}(1-R_s)}{\left[\left\{3m^2D_b^2(mD_b-\Delta_{us})-(m^3D_b^3-\Delta_{us}^3)\right\}-\frac{3}{2}(mD_b+\Delta_{us})(mD_b-\Delta_{us})^2\right]} \tag{6.4d}$$

$$C_2 = -\frac{3}{2}(mD_b+\Delta_{us})C_3 \tag{6.4e}$$

$$C_1 = -2\Delta_{us}C_2 - 3\Delta_{us}^2C_3 \tag{6.4f}$$

$$C_o = P_{us} - \Delta_{us}C_1 - \Delta_{us}^2C_2 - \Delta_{us}^3C_3 \tag{6.4g}$$

6.4 MODELLING OF BASE RESISTANCE MOBILISATION

6.4.1 A normally constructed pile base

Randolph and Wroth(1978) have discussed the "rigid punch" elasticity solution given by Timoshenko and Goodier(1970) in calculating the settlement of pile foundations. For a circular cross-section, the settlement of the base is expressed as

$$\Delta_b = \frac{\pi}{4}\frac{q_b}{E_b}D_b(1-\upsilon^2)\eta \tag{6.5a}$$

where

D_b=base diameter

E_b=Young's modulus of soil beneath the base

υ=Poisson's ratio of soil beneath the base

q_b=base pressure

η=settlement reduction factor (this is related to the foundation depth).

The coefficient η distinguishes the pile base behaviour from the characteristics of a punch, located at the surface of an elastic half-space, for which the original solution was intended. Through calculations for a loaded area embedded in a soil mass, a value of η=0.5 has been calculated for depth/diameter ratio greater than 6. This conclusion is supported by the evidence presented by Banerjee(1970). For a loaded area that is located at the bottom of an open hole, Burland(1969) showed that η=0.85 is the limiting value. For London clay, Marsland(1971) has pointed out that this value is appropriate, depending on the Poisson's ratio of the soil. For the analysis of a pile base, Burland and Cooke(1974) have suggested the use of η=0.5.

For a pile of uniform cross-section (D_b=D_s where D_s is the pile shaft diameter) hence Δ_b can be written as

$$\Delta_b = \frac{P_b\left(1-\upsilon^2\right)}{D_b E_b}\eta = \frac{P_b\left(1-\upsilon^2\right)}{D_s E_b}\eta . \qquad (6.5b)$$

6.4.2 A pile base resting on debris

Figure 6.2 shows a possible plot of base load versus base movement where significant softening of the soil beneath the toe has occurred. This is a typical consequence of a bored pile that has been installed without an effective clean up of soil fragments deposited at the bottom of the hole. It is suggested that the effect of an unclean base may be represented by a shift in the origin, by a distance **S** (from point **E** to point **F**). The path along **FA** represents a progressive increase in the stiffening of the debris beneath the base, as the base pressure increases. Based on a small number of test pile case studies, a parabolic function is found to fit the trend reasonably well. The initial stiffness of the base material before pile installation is assumed to be restored at point **A**. Hence the linear settlement function in Eqn.(6.5b) applies for the path **AB**.

In Fig.6.2 the coefficients **n** and ϕ represent the proportions of P_{ub} which define the three loading ranges considered. The displacements Δ_k and Δ_ϕ are the base movements corresponding to base load values nP_{ub} and ϕP_{ub}, respectively, for a normally constructed pile base. The base movement Δ_{ub} at ultimate base load is defined in terms of a percentage of the base diameter as $\Delta_{ub} = mD_b$. The empirical constants: **n**, ϕ and **m** are determined based on the experience gained from instrumented test piles, whereas P_{ub} is evaluated from well known bearing capacity formulae. The parameters for bearing capacity calculations are based on the site investigation report or other relevant information. From Eqn(6.5b), the displacements Δ_k and Δ_ϕ are expressed as:

$$\Delta_k = \frac{nP_{ub}\left(1-\upsilon^2\right)\eta}{E_b D_b} \tag{6.5c}$$

$$\Delta_\phi = \frac{\phi P_{ub}\left(1-\upsilon^2\right)\eta}{E_b D_b} \tag{6.5d}$$

The suggested parabolic function $P_b = A_o + A_1\Delta_b + A_2\Delta_b^2$ (where A_o, A_1 and A_2 are constants) may be used to evaluate the shift, **S**, for the variation along **FA** if the following boundary conditions are assumed:

1. the parabola has a zero gradient at the new origin **F**
2. the parabolic and linear portions join at the same gradient, G, which is available from Eqn(6.5b) as $G = \dfrac{E_b D_b}{\left(1-\upsilon^2\right)\eta}$

The above conditions yield A_o=A_1=0 and $A_2 = \dfrac{G}{2\left(\Delta_k + S\right)}$. Utilising the condition that P_b=P_{ub} when Δ_b=(Δ_k+S) leads to S=Δ_k , and the parabolic function is now fully defined hence:

$$P_b = \frac{1}{nP_{ub}}\left[\frac{E_b D_b}{2(1-\upsilon^2)\eta}\right]^2 \Delta_b^2. \tag{6.6a}$$

The general equation of the linear portion is

$$P_b = G(\Delta_b - S). \tag{6.6b}$$

For a normal pile base, S is taken as zero whilst for a pile base resting on debris, substituting for S gives

$$P_b = \frac{E_b D_b}{(1-\upsilon^2)\eta}\left[\Delta_b - \frac{nP_{ub}(1-\upsilon^2)\eta}{E_b D_b}\right]. \tag{6.6c}$$

6.4.3 Non-linear base load versus base movement variation

It is considered that, beyond point B (Fig.6.2), the settlements are so large that the linear function is no longer valid. Observed data from test piles at Butetown road link, Cardiff, suggest that the settlement response along the path BC may be represented analytically. A large number of functions have been examined, in attempting to describe the trend **BC**, with varying degrees of success. Of these, the most appropriate is the hyperbolic cosine function expressed in the form:

$$P_b = A_o - A_1 \cosh(A_2\Delta_b - A_3) \tag{6.7}$$

where A_o, A_1 and A_2 and A_3 are constants, to be determined from the following boundary conditions:

(1) When $\Delta_b=(\Delta_\phi+S)$, $P_b=\phi P_{ub}$ (2) When $\Delta_b=(\Delta_\phi+S)$, $\frac{dP_b}{d\Delta_b}=G$

(3) When $\Delta_b=mD_b$, $P_b=P_{ub}$ (4) When $\Delta_b=mD_b$, $\frac{dP_b}{d\Delta_b}=0$.

The boundary conditions (1), (2), (3) and (4) above lead to the following:

$$A_o - A_1 \cosh\left[A_2\left(\Delta_\phi + S\right) - A_3\right] = \phi P_{ub} \tag{6.8a}$$

$$-A_1 A_2 \sinh\left[A_2\left(\Delta_\phi + S\right) - A_3\right] = G \tag{6.8b}$$

$$A_o - A_1 \cosh\left[A_2 m D_b - A_3\right] = P_{ub} \tag{6.8c}$$

$$-A_1 A_2 \sinh\left[A_2 m D_b - A_3\right] = 0 \tag{6.8d}$$

From Eqn.(6.8d), a relationship between A_2 and A_3 emerges, since $A_1 A_2 \neq 0$. Hence the non-trivial solution is $A_3 = A_2 m D_b$. Using this relationship to substitute for A_3 in Eqn.(6.8c) yields $A_o - A_1 = P_{ub}$. Two simultaneous equations containing A_1 and A_2 are obtained, by substituting for A_3 and A_o in Eqn(6.8b) and in Eqn(6.8a). On eliminating A_1, the following expression is obtained, which may be solved by iteration, to evaluate A_2:

$$A_2 = \frac{G\left\{\cosh\left[A_2\left(mD_b - \left(\Delta_\phi + S\right)\right)\right] - 1\right\}}{P_{ub}(1-\phi)\sinh\left[A_2\left(mD_b - \left(\Delta_\phi + S\right)\right)\right]} \tag{6.9a}$$

Hence, by back-substitution, A_1, A_o and A_3 are obtained as follows:

$$A_1 = \frac{G}{A_2 \sinh\left[A_2\left(mD_b - \left(\Delta_\phi + S\right)\right)\right]} \tag{6.9b}$$

$$A_o = A_1 + P_{ub} \tag{6.9c}$$

$$A_3 = A_2 m D_b \tag{6.9d}$$

6.4.4 Minimum value of the coefficient *m*

It is important to recognise the possible mathematical limits of the constants used in the hyperbolic cosine function for base load versus base movement variation. In order to fully define the function, convergence of the iteration process in Eqn. 6.9(a) must be realised, for all practical values of the parameters involved. For given site conditions, the most important parameters controlling the pile base response are the deformation modulus E_b and the ultimate bearing capacity q_{ub}. The gradient of the base load versus base movement curve increases with the ratio $\frac{E_b}{q_{ub}}$. In addition, the higher the ratio $\frac{E_b}{q_{ub}}$ the lower the base displacement at which ultimate base resistance occurs.

The nature of the selected function is such that convergence of the iteration involved in Eqn.6.9(a) is always obtained for all $\frac{E_b}{q_{ub}}$ ratios so that the coefficients A_o, A_1, A_2 and A_3 can always be determined whatever the stiffness and bearing capacity values are at a given site. However, for this to be guaranteed, a situation must be investigated whereby the $\frac{E_b}{q_{ub}}$ ratio at a given site is so small that the slope of line **AB** (Fig.6.2b) reaches its minimum value. This condition is mathematically represented by equating the slope of **AB** to that of a line drawn through **AC** (Fig. 6.2b). In these circumstances, a value of *m* smaller than 30% of base diameter is appropriate. Hence the minimum value of *m* is obtained by equating these slopes, thus

$$m > \frac{P_{ub}\left(1-\upsilon^2\right)\eta + E_b D_b S}{E_b D_b^2} \tag{6.9e}$$

6.5 LOAD TRANSFER/PILE DEFORMATION RELATIONSHIP

6.5.1 Modelling the non-linear stress-strain behaviour of concrete

Consider a typical bored, cast in-situ reinforced concrete pile shown in Fig.(6.3a) and Fig.(6.3b). The dimensions of the pile are:

L_o= friction free length (section of pile passing through material of low friction)

L_s= length of pile shaft transmitting load to soil

L= total length of pile

D_s= diameter of pile shaft

D_b= diameter of pile base.

Particularly at the early stages of loading, proper attention must be given to the non-linear stress-strain variation of concrete. Deformation modulus concrete is usually difficult to evaluate, as it is affected by a number of factors such as creep and loading rates. For normal loading rates applied in pile testing, the Young's modulus of concrete is found to decrease with increasing strain, up to a certain strain level after which it tends to remain approximately constant.

It is reasonable to express the Young's modulus versus strain variation by a simple polynomial function, which can easily be incorporated in the derivation of pile shortening. Figures 6.4(a)-(d) show the apparent Young's modulus-strain variation in test piles TP2, TP3, TP4 and TP6, back-analysed from the strain gauge readings at levels of known axial force. Best fitting polynomial functions are also shown for comparison. In Fig. 6.5, different functions are derived for each load cycle. The general form of the function used is

$$E_c = a_o + \frac{a_1}{\varepsilon} \tag{6.10}$$

where,

E_c= Secant modulus of deformation of concrete (strain dependent)

ε= Strain in concrete ($\varepsilon \neq 0$)

a_o, a_1= numerical constants.

6.5.2 Variation of shaft resistance with depth

Burland(1973) has advocated an effective stress approach to the evaluation of the shaft resistance of pile formed in clay. The shaft resistance τ_{us} (z) at depth z (Fig. 6.3) below the bottom of the sleeved part of the pile is given by

$$\tau_{us}(z) = K(z)\sigma_v'(z)\tan\delta(z) \tag{6.11}$$

where

K(z)=earth pressure coefficient at depth z

σ_v'(z)=effective overburden pressure at depth z

δ(z)=effective angle of friction between the soil and the pile, at depth z.

Two possible patterns of shaft resistance variation are identified. Fig 6.3(a) shows a typical profile for a pile formed sand, such as those reported by Vesic(1969). Fig 6.4(b) describes the shaft resistance versus depth variation for a pile formed in cohesive soil, for example the pile test results reported by Cooke et.al.(1979).

6.5.3 Functional modelling of shaft resistance profiles

It is assumed that the shaft resistance at a given level is consistent with in-situ effective stresses. However, for a given load applied at the pile head, different locations of the pile shaft mobilise different proportions of the maximum shaft resistance available. Hence there will be a re-distribution of shaft resistance along the pile, which is likely to depend on the applied load. It is assumed that the ratio of the final shear stress τ_t at the level of the Keuper marl top (i.e at level z=0), to that at the pile base τ_b (i.e at level $z=L_s$) is given by

$$\frac{\tau_t}{\tau_b} = \frac{K_t \tan(\delta_t)\sigma_v{'}_t}{K_b \tan(\delta_b)\sigma_v{'}_b} \tag{6.12}$$

where K_t and K_b are the coefficients of earth pressure corresponding to the top and bottom of the pile portion involved in load transfer to soil respectively. Similarly, σ_{vt}' and σ_{vb}' are the effective overburden pressures at the level of the top and bottom of the pile portion involved in load transfer to soil respectively. At these levels, the effective angles of internal friction of the soil, or the pile-soil interface friction angle as appropriate, are denoted δ_t and δ_b respectively.

For a bored pile, the earth pressure coefficients K_t and K_b are likely to be less than the coefficient of earth pressure at rest, K_o, due to ground disturbance caused as a result of boring. Hence setting both K_t and K_b to be equal to K_o represents a safe lower limit. For heavily over-consolidated clays, Burland(1973) observed that the value of K_o varies with depth from around 3 near the surface, decreasing to less than unity at great depth. Keuper marl, due to its heavily over-consolidated nature, may be expected to exhibit similar variations of K_o. Therefore, if the shear strength of the clay increases with depth, it is reasonable to expect values of k to lie in the range $1<k<3$ for long piles (typically 60m). For short piles, k is likely to be close to unity.

It is also assumed that the extent of the punching effect on the pile shaft is narrow, so that it is sufficiently accurate to take τ_b at the full shaft length. If it is assumed that the nature of the function representing the variation of shaft resistance variation with depth is independent of the applied load, then Eqn.(6.12) may be written as

$$\frac{\tau_t}{\tau_b} = k\frac{\sigma_v{'}_t}{\sigma_v{'}_b} \tag{6.13}$$

Where $k = \dfrac{K_{ot}\tan(\delta_t)}{K_{ob}\tan(\delta_b)}$ and remains constant with increasing applied pile head load.

The axial force P(z) at any depth z (Figs.6.3a and 6.3b) may be expressed as a function of the shaft resistance $\tau(z)$ at that level as

$$\frac{\partial P_{(z)}}{\partial z} = -\pi D_s \tau(z) \tag{6.14}$$

According to Vesic(1969) and Schmidt and Rumpelt(1993), the shaft resistance variations shown in Figs.6.3(a) and 6.3(b) can be represented by a parabolic function. There is a stationary point at a certain depth, $z=L_m$, below the bottom of the upper pile portion not involved in load transfer to soil. Thus the shaft resistance variation with depth is expressed as

$$\tau(z) = az^2 + bz + c \tag{6.15}$$

Where a, b and c are constants. Integrating Eqn.(6.14) gives

$$P(z) = -\pi D_s\left(\frac{a}{3}z^3 + \frac{b}{2}z^2 + cz + d\right) \tag{6.16}$$

where d is the constant of integration. These constants are determined from the following boundary conditions.

6.5.4 Boundary conditions and solution of equations

a) At level z=L_m the slope of the plot of τ against z is zero (Fig .6.3), thus from Eqn.(6.15), we have $\frac{\partial \tau_{(z)}}{\partial z} = 2az + b = 0$. Hence $b = -2aL_m$.

b) At level z=0, P(z)= P_h, hence from Eqn.(6.16), $d = -\frac{P_h}{\pi D_s}$.

c) At the pile toe level (z=L_s), P(z)=P_b where P_b is the load transferred to the pile base. Hence from Eqn.(6.16), we have

$$\frac{-P_b}{\pi D_s} = a\left(\frac{L_s^3}{3} - L_m L_s^2\right) + cL_s - \frac{P_h}{\pi D_s} \tag{6.17}$$

d) Using Eqn.(6.13) in conjunction with Eqn.(6.15) and assuming a constant unit weight of soil, a relationship involving *a* and *c* can be obtained as

$$\frac{c}{aL_s^2 + bL_s + c} = \frac{kL_o}{L} \tag{6.18}$$

Substituting for b gives

$$\frac{(P_h - P_b)}{\pi D_s} = a\left(\frac{L_s^3}{3} - L_m L_s^2\right) + cL_s \tag{6.19}$$

Equations (6.17) and (6.19) are then solved simultaneously for a and c, hence

$$a = \frac{(P_h - P_b)}{\pi D_s\left\{\frac{L_s^3}{3} - L_m L_s^2 + \frac{kL_o L_s^2}{kL_o - L}\left[2L_m - L_s\right]\right\}}$$

Substituting a from the relationship $b = -2aL_m$ gives

$$b = \frac{-2L_m(P_h - P_b)}{\pi D_s\left\{\frac{L_s^3}{3} - L_m L_s^2 + \frac{kL_o L_s^2}{kL_o - L}\left[2L_m - L_s\right]\right\}}$$

From Eqn.(6.18), the expression for c can be written as

$$c = \frac{-kL_o L_s}{kL_o - L}\left(aL_s + b\right)$$

For convenience, substitute $L_m = \omega L_s$ in which ω is a constant, and let

$$\Omega = \frac{kL_o L_s}{\left(kL_o - L\right)} \tag{6.20}$$

$$\lambda = \pi D_s \left\{ \frac{L_s^3}{3} - \omega L_s^3 + \Omega L_s^2 (2\omega - 1) \right\} \tag{6.21}$$

It will be seen that for $\tau_t < \tau_b$, setting $0.5 < \omega < 1.0$ results in the shaft resistance distribution profile given in Fig. 6.3(b) whilst taking $0 < \omega < 0.5$ gives the profile in Fig. 6.3(c). The former profile was observed, for piles formed in sand, by Vesic(1969), Hirayama(1990) and Altaee et.al.,1993) whereas the latter profile was reported by Cooke et.al.(1979) and O'Riordan(1982), for piles installed in clay. If $\omega < 0$ then there is no stationary point on the shaft resistance versus depth variation. In the present work, the test piles, installed in Keuper marl, exhibit the shaft resistance distribution profile described by $0 < \omega < 0.5$. It is noted that as ω decreases, the rate of decrease of axial force in the pile with depth increases. The effect of an increase in the value of *k* is to decrease the rate of axial force decrease with depth along the pile.

6.5.5 Load sharing between the shaft and base

The proportion of the load carried in shaft resistance P_s may be considered to be related to the applied pile head load P_h by a factor ψ, so that

$$P_s = \psi P_h \tag{6.22}$$

For large diameter, bored piles, ψ actually varies with P_h, and will be calculated by back analysis. Thus the constants *a*, *b* and *c* now become,

$$a=\frac{\psi P_h}{\lambda} \tag{6.23a}$$

$$b=\frac{-2\omega L_s \psi P_h}{\lambda} \tag{6.23b}$$

$$c=-\frac{\Omega\psi P_h}{\lambda}L_s(1-2\omega) \tag{6.23c}$$

The shear stress distribution function $\tau(z)$ is now fully defined and, from Eqn.(6.15), this function may be written as

$$\tau(z)=\frac{\psi P_h}{\lambda}\left[z^2-2\omega L_s z-\Omega L_s(1-2\omega)\right]. \tag{6.24}$$

From Eqn.(6.16), P(z) then becomes

$$P(z)=-\pi D_s P_h\left\{\frac{\psi}{\lambda}\left[\frac{z^3}{3}-\omega L_s z^2-\Omega L_s z(1-2\omega)\right]-\frac{1}{\pi D_s}\right\} \tag{6.25}$$

6.5.6 Axial force profile and pile shortening

The elastic shortening of the pile at a given value of applied load may be obtained by considering the equilibrium of the pile cross-section at any depth, z. Hence $P(z)=\varepsilon(z).\left[E_c(z)A_c+E_sA_s\right]$, where A_c and A_s are the concrete and steel areas respectively. From Eqn.(6.10), the expression for strain at a given level is

$$\varepsilon(z)=\frac{P(z)-A_c a_1}{A_c a_o+E_s A_s} \tag{6.26}$$

Substituting for P(z) from Eqn.(6.25) gives:

$$\varepsilon(z)=\frac{1}{A_c a_o+E_s A_s}\left(-\pi D_s P_h\left\{\frac{\psi}{\lambda}\left[\frac{z^3}{3}-\omega L_s z^2-\Omega L_s z(1-2\omega)\right]-\frac{1}{\pi D_s}\right\}-A_c a_1\right) \tag{6.27}$$

The shortening e_o of the upper portion of the pile not transferring load to soil is given by

$$e_o = \int_0^{L_o} \varepsilon(z)dz \tag{6.28}$$

Substituting for ε(z) from Eqn.(6.26) and recognising that axial force is constant over the sleeved section,

$$e_o = \frac{\left(P_h - A_c a_1\right)L_o}{A_c a_o + E_s A_s} \tag{6.29}$$

The shortening e_s of the lower portion of the pile involved in load transfer is given by

$$e_s = \int_0^{L_s} \varepsilon(z)dz\,. \tag{6.30}$$

Substituting for ε(z) from Eqn.(6.26) and integrating between the limits, we have

$$e_s = \frac{1}{A_c a_o + E_s A_s}\left(-\pi D_s P_h \left\{\frac{\psi}{\lambda}\left[\frac{L_s^4}{12} - \frac{\omega L_s^4}{3} - \frac{\Omega(1-2\omega)L_s^3}{2}\right] - \frac{L_s}{\pi D_s}\right\} - A_c a_1 L_s\right) \tag{6.31}$$

6.5.7 Pile head load versus pile head settlement relationship

The load-settlement relationship for the pile can be obtained by considering the variation of displacements with depth from z=0 to $z=L_s$. The settlement Δ(z) at any depth, z, below the bottom of the upper pile portion not involved in load transfer is related to the strain in the pile ε(z) at that level by the expression

$$\frac{\partial \Delta(z)}{\partial z} = -\varepsilon(z) \tag{6.32}$$

Hence

$$\Delta(z) = -\int \varepsilon(z).dz \tag{6.33}$$

Substituting for $\varepsilon(z)$ from Eqn.(6.27) and integrating leads to,

$$\Delta(z)=\frac{-1}{A_c a_o+E_s A_s}\left(-\pi D_s P_h\left\{\frac{\psi}{\lambda}\left[\frac{z^4}{12}-\frac{\omega L_s z^3}{3}-\frac{\Omega L_s(1-2\omega)z^2}{2}\right]-\right.\right.$$

$$\left.\left.\frac{1}{\pi D_s}z\right\}-A_c a_1 z\right)+c_1 \qquad (6.34)$$

where c_1 is the constant of integration. This constant can be evaluated using the boundary condition that, when z=0, the displacement $\Delta(z)$ is given by $\Delta(z)=e_s+\Delta_b$ in which Δ_b is the base movement, thus

$$c_1=e_s+\Delta_b \qquad (6.35)$$

The settlement of the pile head Δ_h is given by

$$\Delta_h=e_o+e_s+\Delta_b \qquad (6.36)$$

The expressions for e_o and e_s are available from Eqns.(6.29) and (6.31). The solutions for Δ_h are obtained by substituting $P_b=(1-\psi)P_h$ in Eqns.(6.6a), (6.6c) and (6.7) and making Δ_b the subject. Hence

1) For a pile base resting on debris, in the interval: $0\le\Delta_b\le(\Delta_k+S)$

$$\Delta_h=e_o+e_s+\frac{2(1-\upsilon^2)\eta}{E_b D_b}\sqrt{(1-\psi)P_h nP_{ub}} \qquad (6.37)$$

2) For a pile base resting on debris, in the interval: $(\Delta_k+S)\le\Delta_b\le(\Delta_\phi+S)$

$$\Delta_h=e_o+e_s+\frac{(1-\upsilon^2)\eta}{E_b D_b}\left[(1-\psi)P_h+nP_{ub}\right] \qquad (6.38)$$

3) For a normally constructed pile base, in the interval: $0\le\Delta_b\le\Delta_\phi$

$$\Delta_h = e_o + e_s + \frac{(1-\psi)P_h(1-\upsilon^2)\eta}{E_b D_b} \tag{6.39}$$

4) In the interval: $(\Delta_\phi + S) \le \Delta_h \le mD_h$

$$\Delta_h = e_o + e_s + \frac{1}{A_2}\left\{\cosh^{-1}\left[\frac{A_o - (1-\psi)P_h}{A_1}\right] + A_3\right\} \tag{6.40}$$

The coefficients A_o, A_1, A_2 and A_3 are determined from Eqns.(6.9a)-(6.9d).

6.5.8 Summary of the analysis procedure

Since the parameter ψ varies with P_h, the settlement at a given load can only be determined numerically. A computer program has been written for this purpose. The procedure for predicting the load-settlement curve for a pile with known geometry, material properties, and the soil properties is as follows:

1) Take various incremental values of Δ_b from zero up to mD_b
2) Calculate P_b from Eqns.(6.6a), (6.6c) or (6.7), as appropriate
3) Calculate P_s from Eqns.(6.4a) or (6.4b), as appropriate
4) Obtain P_h by summing P_b and P_s
5) Calculate ψ from $\psi = \frac{P_s}{P_h}$
6) Calculate e_O from Eqn.(6.29)
7) Calculate e_S from Eqn(6.31)
8) Obtain the total shortening e_p as $e_p = e_o + e_s$
9) Obtain the total pile head settlement as $\Delta_h = e_p + \Delta_b$
10) Plot the graph of P_h versus Δ_h

11) Read Δ_h value for a given P_h value.

12) If required to know the amounts of shaft load, base load or shortening at a given Δ_h or P_h value, read off directly from relevant graphs.

A FORTRAN coded computer program, by the name OMSET, has been developed in-house for the complete analysis of a pile using the model.

6.6 DESIGN CHARTS UTILISING THE NUMERICAL MODEL

6.6.1 Introduction

Having accepted that the numerical model closely represents pile load-settlement response, the analytical procedure described is clear and is successful in relating the shaft and base response functions to conventional soil parameters. Since the method makes extensive use of observed pile behaviour, the solutions obtained show the familiar characteristics of pile load -settlement relationships.

6.6.2 Design for shaft resistance

Since the settlement at peak shaft resistance directly relates to a failure strain, the parameter ***r*** represents the flexibility of the pile shaft. A range of values r=0.05-0.01 are appropriate for soils ranging from soft to very stiff, respectively. Although these numbers are quoted in percent, the corresponding absolute real number values are equivalent to Fleming's(1992) values of shaft flexibility factor, M_s. The M_s values suggested by Fleming(1992) for a range of soils from soft to very stiff are M_s=0.005-0.0005.

Figure 6.6(a) gives the predicted normalised plots of shaft resistance against base movement, for a range of soil varying from soft to very stiff. These relationships have been calculated from the equations presented. The variations are fully dimensionless and can be used to identify the shaft resistance component of load bearing for a pile with given diameter.

6.6.3 Design for base resistance

The analysis of base load mobilisation is carried out in a similar series of steps using normalised graphs of base load against base movement. The important parameters required are the deformation modulus values E_b and the ultimate bearing capacity q_{ub}. The deformation modulus is one of the most interesting parameters of the numerical method. This parameter is not only manifested in the soil properties at a pile site but is also influenced by the effects of pile installation. In a stiff clay soil type such as Keuper marl, the over-consolidation ratio has a significant effect on the deformation modulus.

Most site investigations presently carried out are focused more on soil strength rather than deformation behaviour. Nevertheless, there are a number of formulae available for calculating deformation modulus values based on correlation with other soil properties. Some of these formulae have been tabulated in the literature review (Chapter 2). Other than published formulae, there may also be opportunities whereby data from pile load tests are available from which the deformation modulus could be back-analysed. In general, this alternative leads to a better estimate, since it incorporates the construction dependent factors.

In Fig. 6.6(b) normalised plots of base load against base movement shown. These values follow from the numerical model, when incremental values of the ratio $\frac{E_b}{q_{ub}}$ are taken and used to compute the base behaviour function for a pile of general dimensions. Selected $\frac{E_b}{q_{ub}}$ values lying in the range 5-100 are examined which increase with increasing soil stiffness.

6.6.4 Summary

The proposed model can be readily utilised for the purpose of designing single piles provided the required soil properties are available. The computer program, which has been developed to facilitate rapid calculations, may be used to assess whether or not the pile satisfies the design requirements. Where a pile load test has been carried out in advance of the main pile construction programme, the model may also be used to back-analyse the required design parameters. However, it good quality test data are required to enable an accurate prediction during back-analysis. In maintained load tests, it may be necessary to project the measured pile head displacements to infinite time before plotting the input data.

Where the capability to maintain applied loads at constant values is significantly affected, some corrections to the measured curve may be necessary. This is necessary to identify and distinguish between creep-related settlements and transient displacements.

Sufficient data points are needed to ensure that a reasonable part of the load-settlement curve is available for back-analysis purposes.

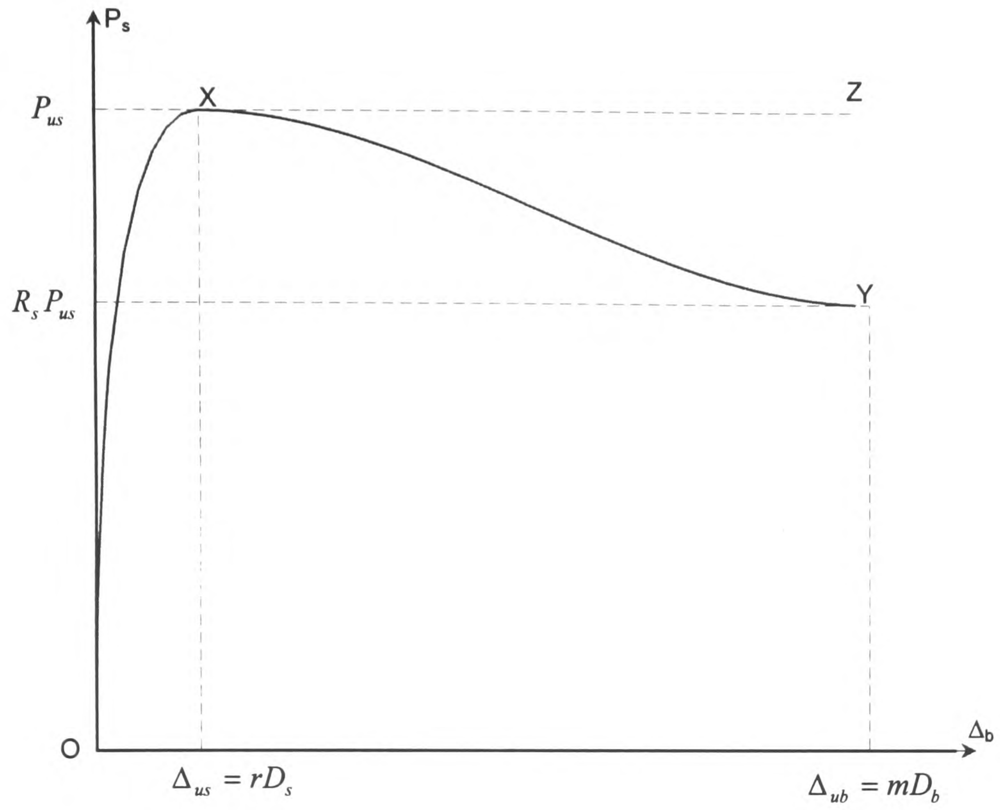

Fig. 6.1: Typical plot of shaft load, P_s versus base movement Δ_b

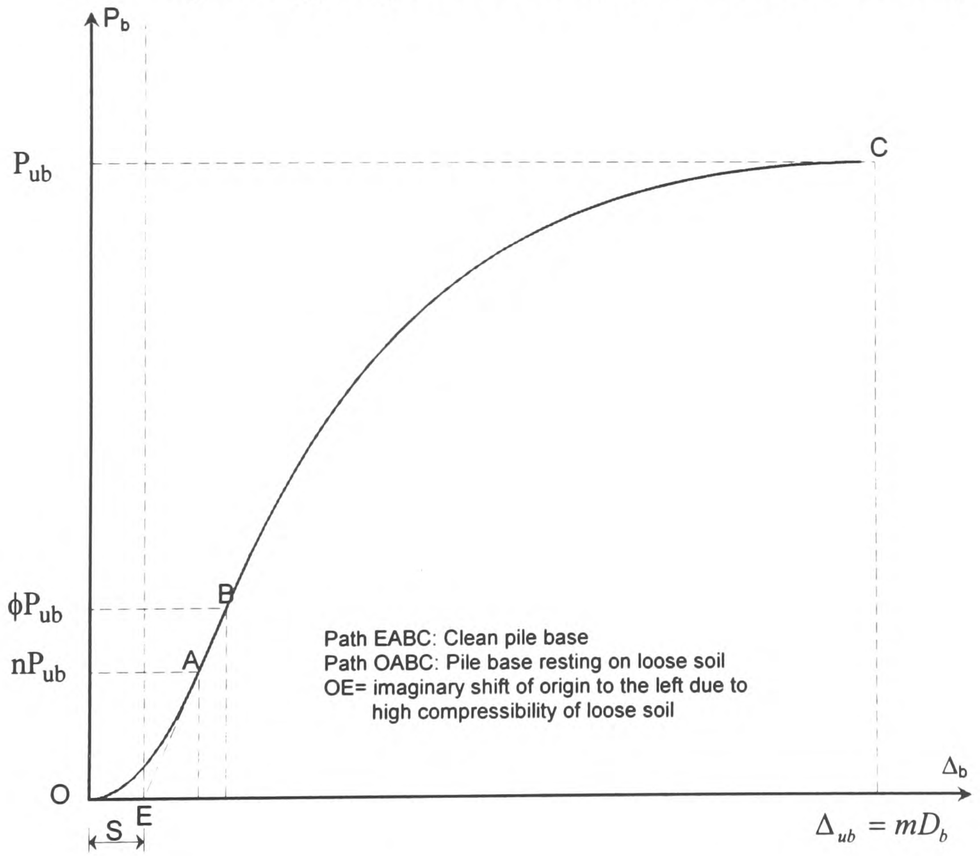

Fig.6.2: Typical plot of base load, P_b versus base movement Δ_b (pile base resting on debris and normal pile base compared)

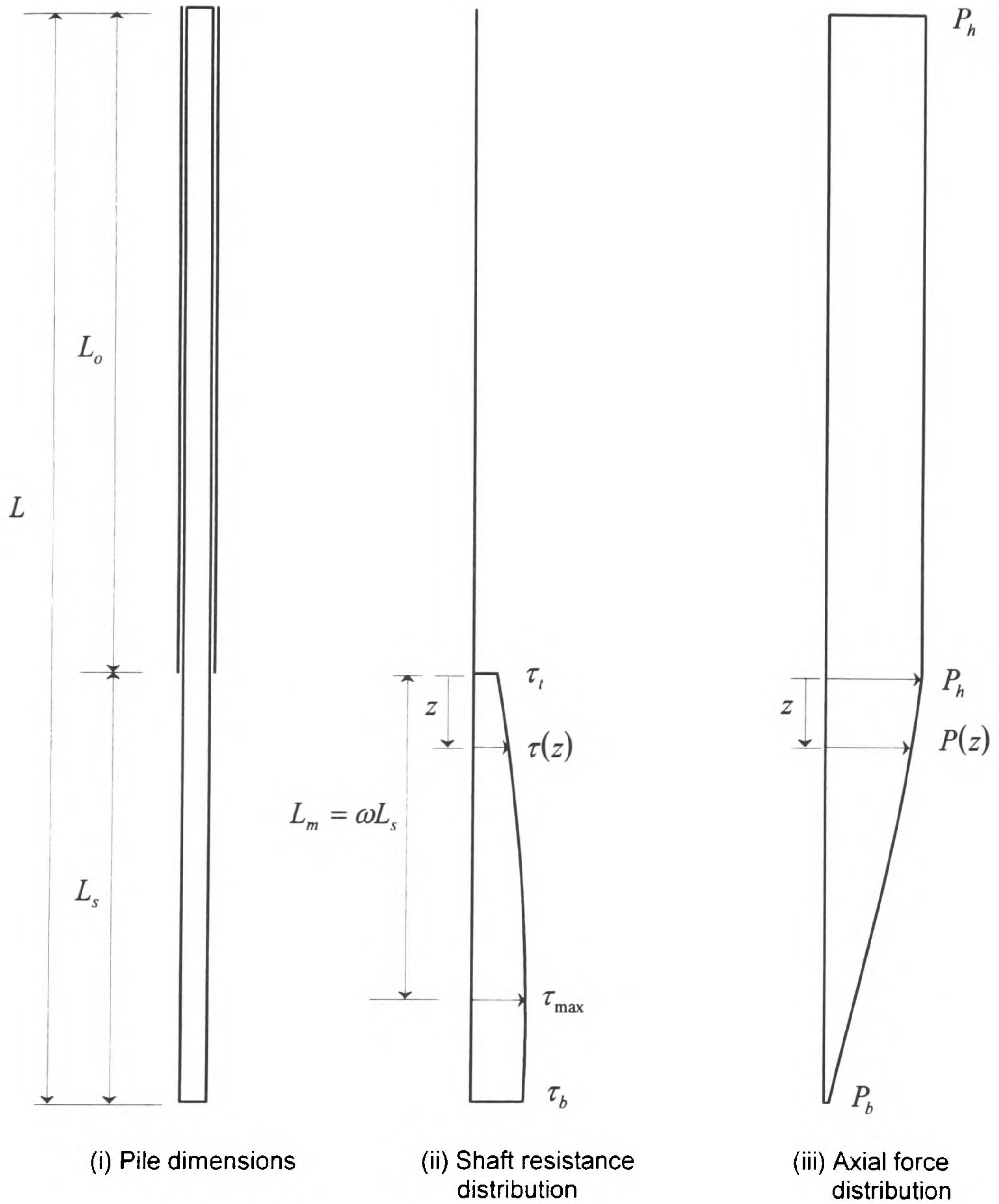

Fig. 6.3(a) Shaft resistance and axial force variation with depth, for k= 0.75 and ω=0.8

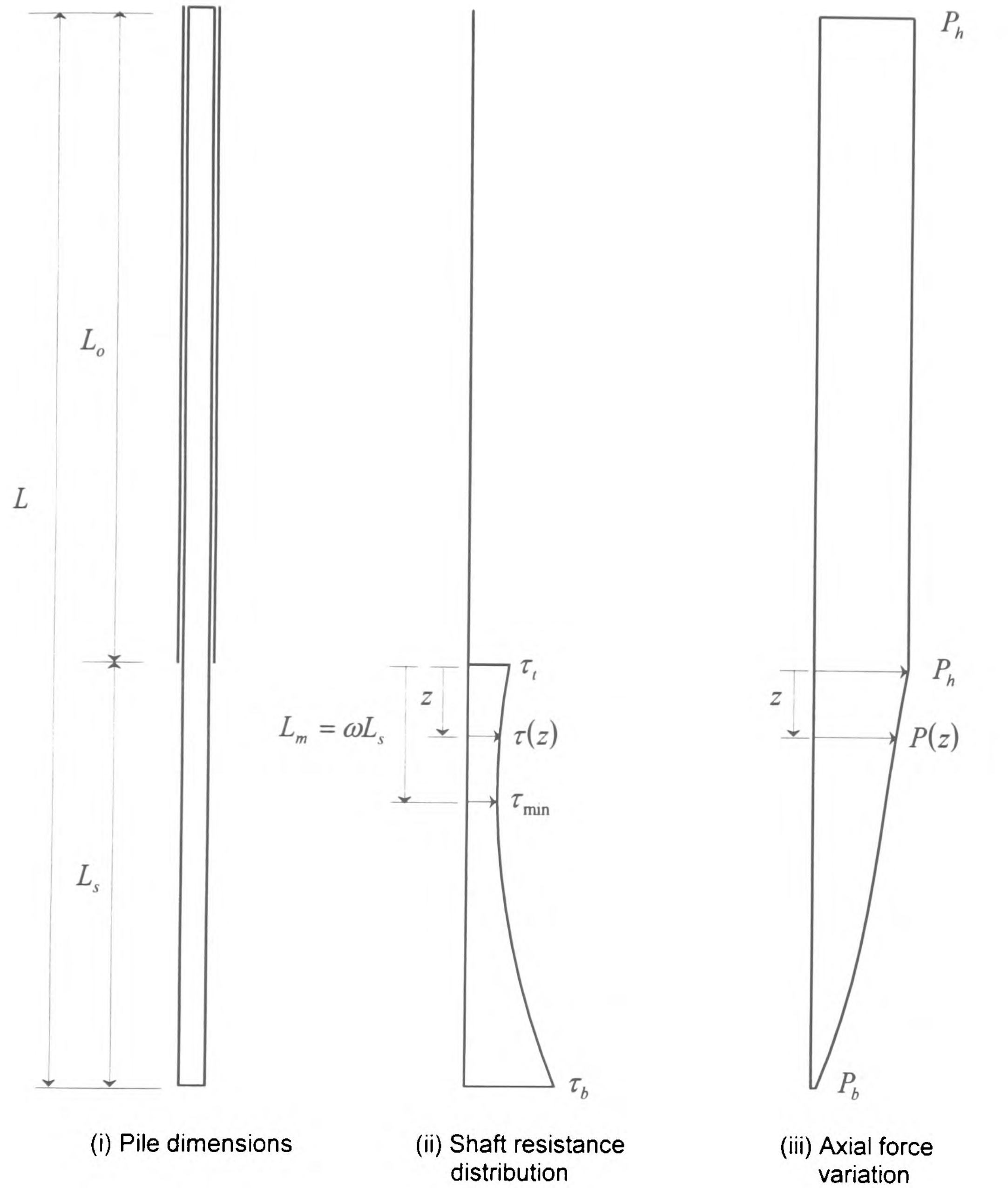

Fig. 6.3(b):Shaft resistance and axial force variation with depth, for k= 0.75 and ω=0.3

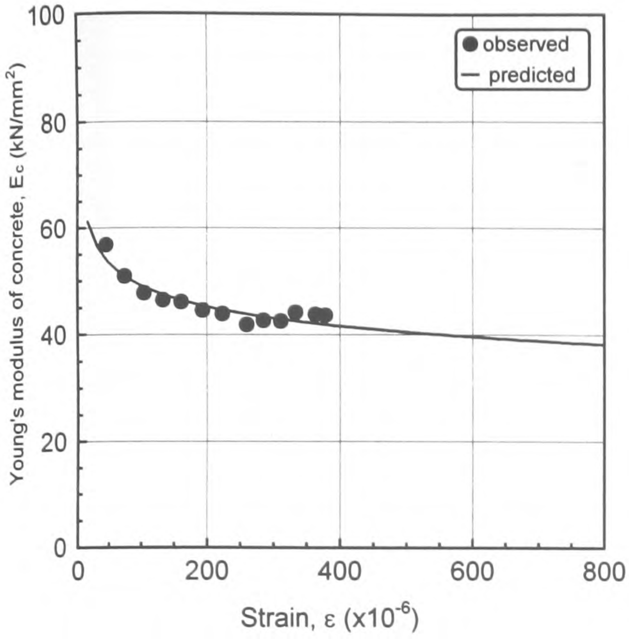

(a) Pile TP2

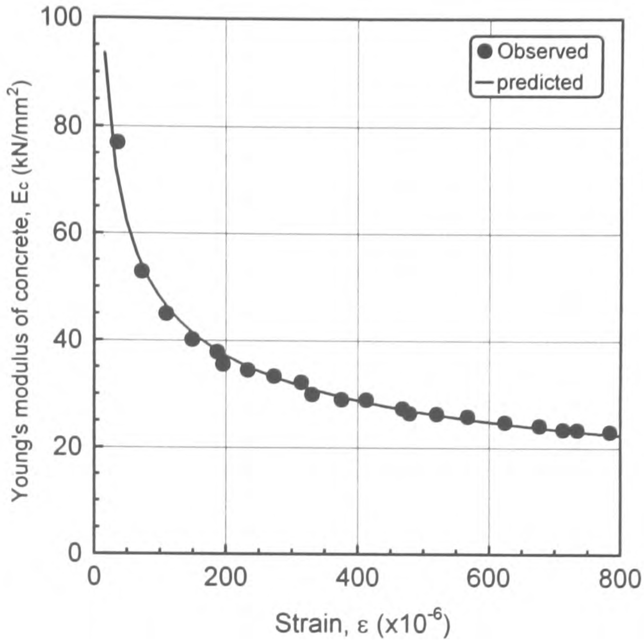

(b) Pile TP3

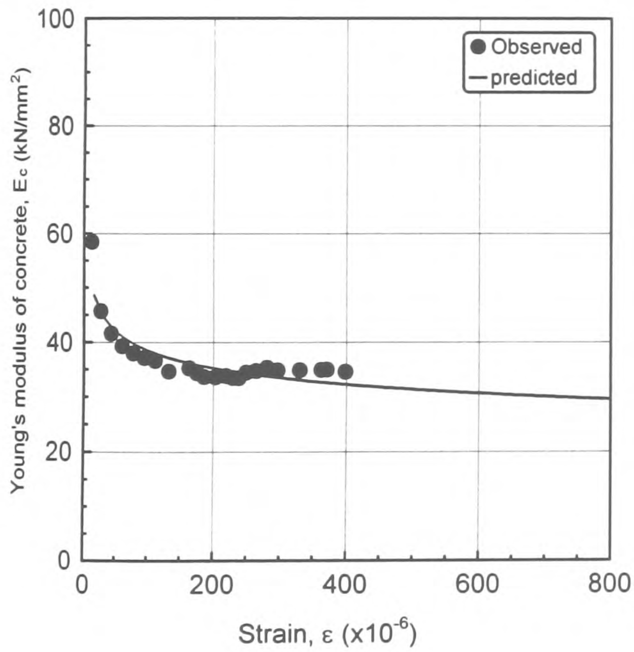

(c) Pile TP4

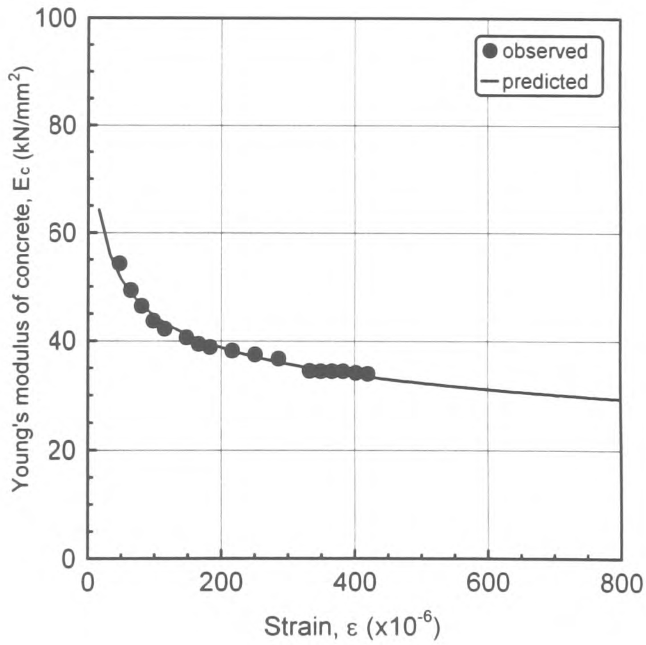

(d) Pile TP6

Figure 6.4: Comparison between the actual and modelled variations of Young's modulus of concrete versus strain (Piles TP2-TP6)

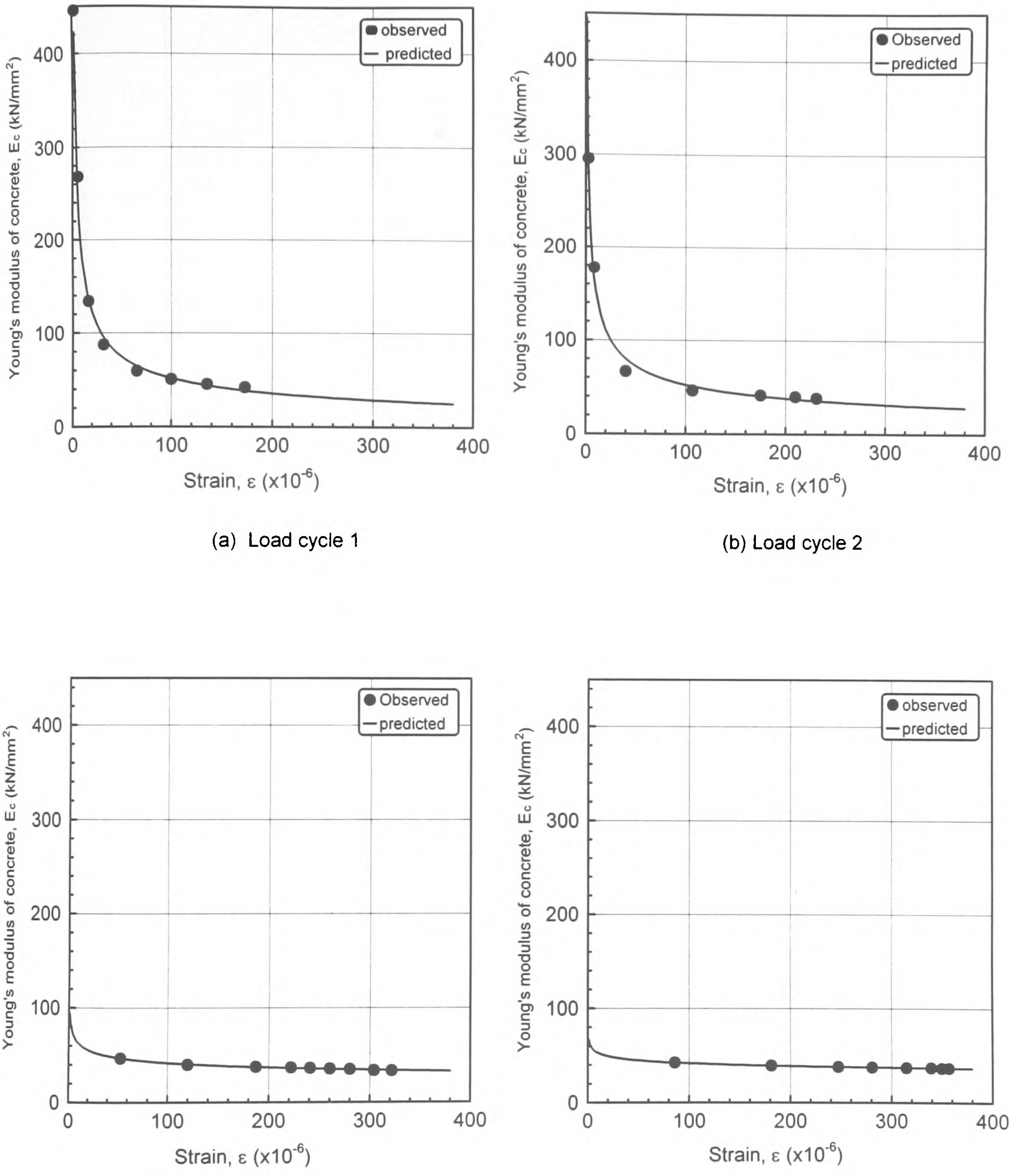

(a) Load cycle 1

(b) Load cycle 2

(c) Load cycle 3

(d) Load cycle 4

Fig. 6.5: Comparison between actual and modeled variation of Young's modulus of concrete versus strain for each load cycle in pile TP5

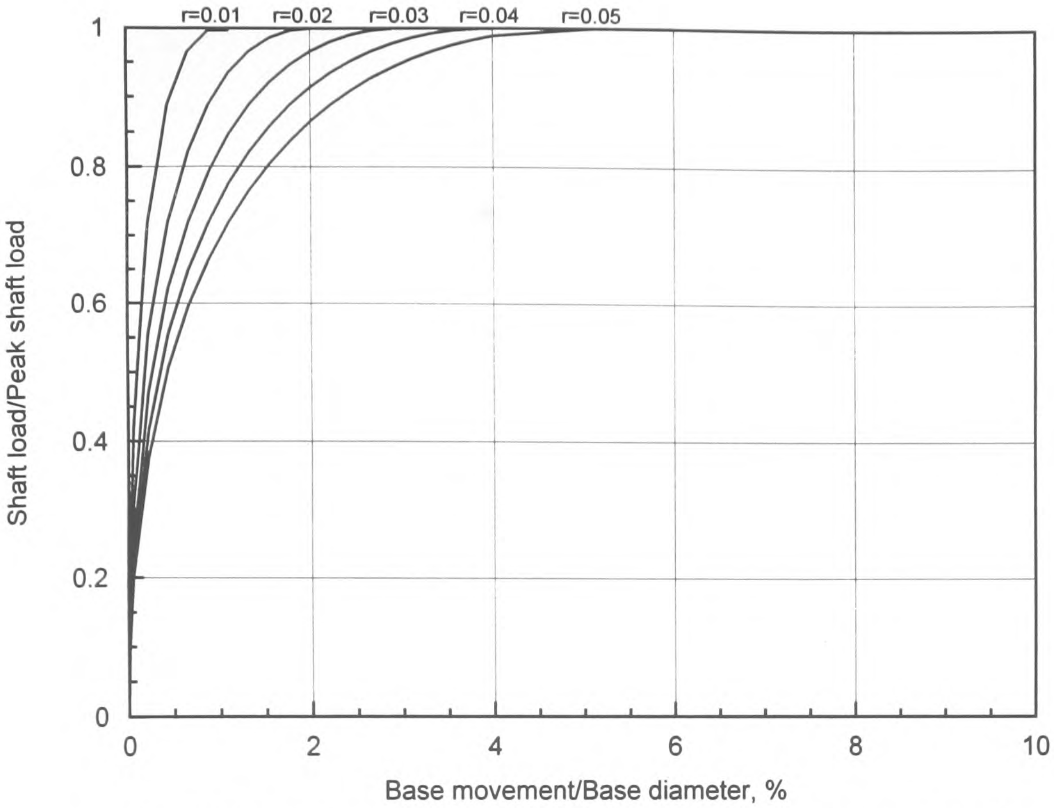

Fig. 6.6(a): Normalised plot of shaft resistance versus settlement relationship for a range of soils from soft to very stiff (r=0.05-0.01)

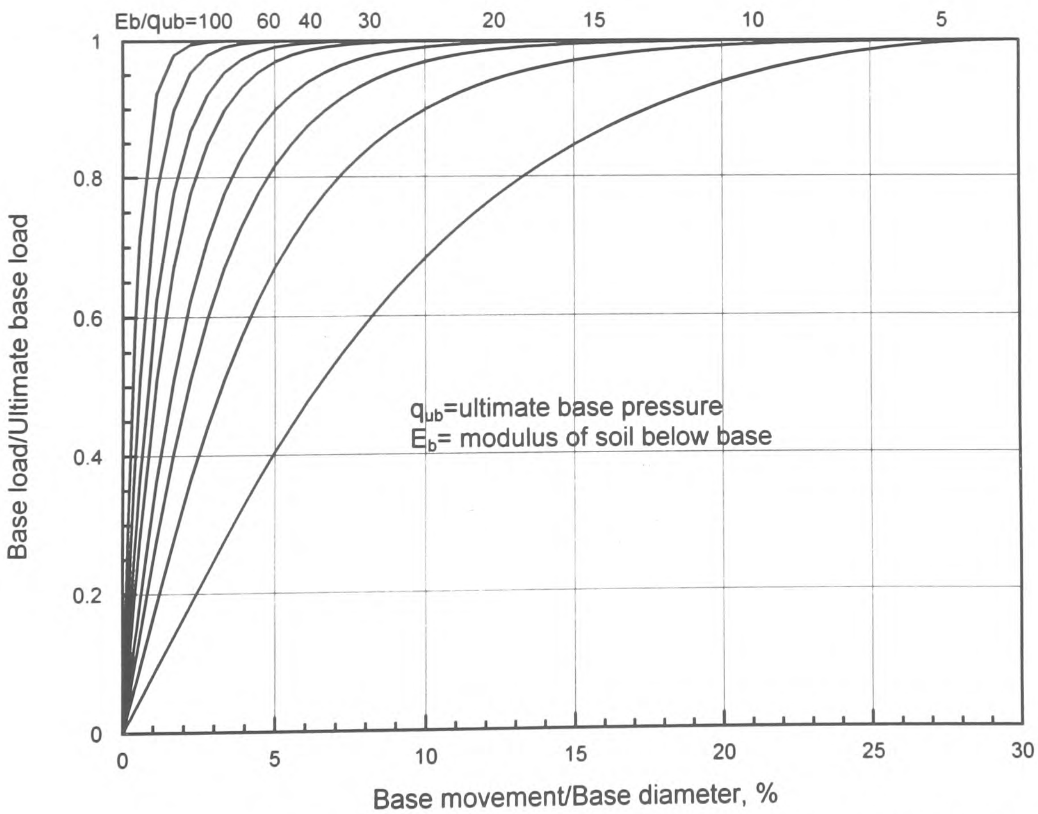

Fig. 6.6(b): Normalised plot of base resistance versus settlement relationships for a range of soils from soft to very stiff : E_b/q_{ub}=5-100

CHAPTER 7

APPLICATION OF THE NUMERICAL MODEL TO PILE ANALYSIS AND DESIGN

CHAPTER 7: APPLICATION OF THE NUMERICAL MODEL TO PILE ANALYSIS AND DESIGN

7.1 INTRODUCTION

A large and growing number of pile load test data have been analysed using the proposed numerical model. The objective of this exercise is to demonstrate the validity and accuracy of the method. The pile test data analysed using the model include bored piles in Keuper marl as well as test piles formed in other soil types. Where it is possible to find instrumented pile test results, the data further supports the validity of the assumptions made in the numerical model.

Some examples have been selected from the database of pile test results back-analysed using the proposed method. When a large database has been gained, it is a simple matter to apply the method to predict the load-settlement behaviour of a pile, since the main parameters involved are easily linked to the prevailing ground conditions. The database currently includes 50 test pile case histories and is expanding, as more information becomes available. Of the test piles already analysed, 25 are presented here. These data show that the proposed model gives accurate and reliable predictions of the load-settlement behaviour, up to failure. Where the observed load-settlement curve for a pile does not include the failure stage, the ultimate load capacity has been extrapolated using Chin's(1972) method.

7.2 TEST PILES FOR THE BUTETOWN ROAD LINK, P.D.R.-CARDIFF

7.2.1 Introduction

Most classical methods of pile load-settlement analysis have not been developed to sufficient depths to be used solely as design tools. For this reason, foundation designers often rely on established soil parameters, supported by site experience. Pile load testing for the Butetown road link has already been discussed in chapters 3 and 4. The results of the load tests and the site investigation are now utilised in testing the validity of the proposed numerical model.

7.2.2 Test pile TP1 (Voided toe pile)

The ultimate base resistance determined by both the M.L and C.R.P. tests was found to be approximately 12MN. The observed load-settlement curve for the voided toe test revealed that, at a settlement of 90mm (10% pile diameter) the ultimate shaft resistance was not yet mobilised. By extrapolation, the estimated ultimate shaft resistance was 15.9MN. This value has been adopted in the numerical model to predict the load-settlement behaviour of the pile.

A comparison between the observed and predicted load-settlement curves is shown in Figures 7.1(a). Figure 7.1(b) shows the predicted variation of pile shortening with applied load. It can be seen that the numerical model is capable of predicting the load-settlement response even for pile TP1 where base resistance was deliberately eliminated.

7.2.3 Test pile TP2

Figs. 7.2(a)-7.2(d) illustrate comparisons between the observed and the predicted behaviour of Pile TP2. No load cell was installed in this pile as a result of certain construction difficulties. Therefore an attempt has been made to utilise the strain gauge data to calculate the shaft load at each applied pile head load increment. However, the results obtained are considered unreliable since the differences in strain gauge readings from level 2 to level 3 were too high, resulting in unreasonable values of local unit shaft resistance. The data is discussed in chapter 4. It is thought that either the level 3 gauges appeared to over-read, or the actual cross-sectional area of the pile at this level was smaller that intended.

Failure was not fully developed in the load test, hence the peak shaft resistance and the ultimate base load has been obtained by extrapolation, for use in the analytical model. The variation of Young's modulus of concrete with strain has been evaluated from the first strain gauge readings within the sleeved portion of the pile.

The coefficients R_s and r have been taken as R_s=0.8 and r=0.035 respectively. The latter value has been deliberately made larger than the average range given in Table 6.1 in order to allow for additional settlement due to shortening. This is necessary since Eqn.(6.4a) is based on total settlement at a point along the shaft, in accordance with Reese et al.(1969). Even under these conditions where a number of assumptions have been made based on other test pile data the analytical model produces reasonably accurate results.

7.2.4 Test pile TP3

The observed and predicted curves for TP3 are shown in Figs. 7.3(a)- 7.3(d). As part of the input data in the analysis, the maximum shaft load has been taken as the approximate value determined by the load test. Failure in end bearing did not occur, and the ultimate base resistance has been obtained by extrapolation. The ultimate base load to be input into the program was estimated by subtracting the extrapolated value of peak shaft load from the observed ultimate pile head load.

Based on the Keuper marl weathering zone for the stratum beneath the base, an E_b value has been selected from the values given by Davis and Chandler(1973). Since the shaft flexibility factor, *r* varies inversely as the rigidity of the pile shaft, a longer pile is expected to have *r* value slightly greater than that for a shorter pile. Pile TP3 was slightly longer than pile TP2, hence *r* value for TP3 was taken to be 4.5% of shaft diameter and proved appropriate. This is marginally higher than that adopted for TP2 (3.5%), due to differences in lengths and ground conditions.

7.2.5 Test pile TP4

The results for the pile TP4 are given in Figs.7.4(a)-7.4(d). The measured value of peak shaft load has been adopted in the analytical model, whereas the ultimate end bearing has been estimated by extrapolation. There is some scepticism regarding the quality of the data in this test pile, since there was a sudden collapse of the inner steel casing during the formation of the test pile. Nevertheless, the predicted results seem to be in reasonable agreement with the experimental data.

7.2.6 Test pile TP5

The predicted behaviour of pile TP5 is presented in Figs. 7.5(a)-(d). In addition, the predicted and measured axial force variations with depth are shown in Fig. 7.5(e). Both the maximum shaft load and ultimate base load values input into the model are as obtained from the load test. Similarly, the observed variation of Young's modulus of concrete with strain has been adopted in the analysis. The test data also reveal that the residual shaft resistance was likely to be less than 60% of the peak shaft resistance. In the analytical model, the value of R_s has been taken as 0.7. There is a remarkable agreement between the predicted and actual behaviour of the pile, not only in the load-settlement response but also in the load transfer characteristics.

7.2.7 Test pile TP6

The last of the Butetown test piles (TP6) measured and predicted curves are shown in Figs. 7.6(a)- 7.6(d). Obviously, pile failure was not realised and the observed load-settlement graph is still steep at the last data point reached. In order to obtain the required input data for the application of the analytical model, both P_{us} and P_{ub} were determined by extrapolation since failure was not reached. It is again demonstrated that the proposed model gives accurate results even for relatively low displacements of the pile head.

7.3 PREVIOUS PILE TESTING IN KEUPER MARL (CARDIFF P.D.R.)

7.3.1 Test piles at Eastmoors Link

The Eastmoors link viaduct, which was opened in 1984, forms part of a new Peripheral Distributor Road network in Cardiff. Three bored, cast in-situ piles, each 1.05m in diameter, were installed and load tested. No instrumentation to measure axial load variation was placed in these piles, except pile head movement gauges. The piles were tested to loads approaching their ultimate capacities. However, use has been made of other voided-toe piles tested in similar ground conditions in Cardiff in order to project the load capacities in both shaft and end resistance.

7.3.2 Eastmoors link-pile No.2

Table 7.1 shows the mean standard penetration test (S.P.T.) "N" values obtained at the Eastmoors site of pile No.2. The ultimate head load was not reached and the method of Mazurkiewicz(1972) was used to extrapolate the ultimate head load. Using the method proposed by Kilbourn et.al.(1988), the maximum shaft resistance was estimated from the observed load-settlement data. This was supported by data from a voided-toe test. A comparison between the observed and predicted response of the pile is shown in Figs. 7.7(a). The shaft resistance, base resistance and shortening predictions are presented in Figs. 7.7(b)-(d). It is again demonstrated that the proposed model provides accurate load-settlement predictions.

Depth (m)	Zones	Mean "N" value
11.74-14.62	IVa	40
14.62-20.03	III/II and IVa	140
20.03-24.90	III/II and IVa	100

Table 7.1: S.P.T. "N" values at Eastmoors link site (Pile-2)

7.3.3 Eastmoors link-pile No.3

The S.P.T. mean "N" values at the site of pile No.3 are given in Table 7.2.

Depth (m)	Zones	Mean "N" value
10.93-12.00	IV and III	30
12.00-17.00	IV and III	50
17.00-20.93	III	80
20.93-23.78	III	130

Table 7.2: S.P.T. "N" values at Eastmoors link site (Pile-3)

The tabulated S.P.T. "N" values were used to calculate the peak shaft resistance, as before. For the purpose of application of the analytical method, the peak shaft and base loads calculated by the Kilbourn et al.(1988) procedure have been adopted. Figures 7.8(a)-(d) illustrate the comparison between the observed and the predicted pile performance. It is clear that the present method of analysis produces reliable and accurate predictions.

7.3.4 Eastmoors link-pile No.4

The S.P.T. "N" values obtained at the site of pile No.4 are shown in Table 7.3.

Depth (m)	Zones	Mean "N" value
9.45-10.11	Sand and Gravel	25
10.11-12.00	IV and III	75
12.00-16.18	III/II and IV	150
16.18-21.27	III/II and IV	100

Table 7.3: S.P.T. "N" values at Eastmoors link site (Pile-4)

The peak shaft and base loads were calculated using the same procedure as in the previous test piles. In this test pile, failure was approached very closely at a settlement of 100mm and the maximum applied pile head load of about 15.1MN is consistent with the extrapolated load capacity vale of 15.5MN. The predicted and measured curves are illustrated in Figs 7.9(a)-(c).

7.3.5 Test piles at Grangetown Link

Three piles were installed and load tested for the design of the Grangetown road link. Two of these piles were of the voided toe type and were 1.3m and 0.9m in diameter. The third pile was normally constructed. It was 0.9m in diameter and was loaded to 4182kN, close to its ultimate capacity. This result was used as a guideline in estimating the peak shaft load for the working piles.

Based on extrapolation of the data for the 1.3m diameter voided toe pile, the peak shaft load for the normal pile was estimated as 32.49MN. Assuming that at the ultimate load capacity of the pile, 88% of the load was carried in shaft resistance, the ultimate base load was estimated as 4430kN. The predicted and measured load-displacement curves are compared in Figures 7.10(a). Figure 7.10(b)-(c) present plots of the predicted shaft load and base load versus base movement, while Fig. 7(d) shows the variation of shortening with applied load.

7.3.6 Test piles at Ely Bridge

Load testing was carried on a 0.9m diameter bored, cast in-situ pile installed in Keuper marl. No S.P.T. testing was carried out at the site, but preliminary pile design was based on percentage total core recovery and rock quality designation, alongside other published information and data. The test pile was 21.5m long and was embedded 10.5m into the Keuper marl. At the maximum applied load of 10.5MN in the test, the load-settlement curve was observed to be steep and the pile was still below its ultimate capacity.

Extrapolation of the observed load-settlement curve gave an ultimate load of 18.074MN. Using the method suggested by Kilbourn et al.(1988) of separating shaft resistance and base resistance, the peak shaft load was estimated to be 10.38MN. The ultimate base load was therefore obtained by subtracting the peak shaft load from the ultimate total load. This gave P_{ub}=7.69MN. These values have been used as guidelines when analysing the test pile using the numerical model.

Figure 7.11(a) illustrates a plot of load versus settlement where the observed test data are compared with the predicted curve. The choice of the parameter r is dictated by the rigidity of the pile-soil system.

7.3.7 Test pile at Clarence Road Bridge

In 1973, trial pile testing was carried out using 790mm diameter piles for the Clarence road bridge project in Cardiff. One test pile was provided with a voided toe while the other was normally constructed. The skin resistance was interpreted based on the results of the voided toe test pile. Both piles were of the same overall length and both were embedded 4.5m into the Keuper marl.

The load-settlement curve for the voided toe test pile approached failure and the peak shaft load was estimated to be about 3100kN. For various increments of settlement, the base resistance of the normally constructed pile was estimated as the difference between the pile head load in the normally constructed pile and that in the voided toe test pile. It was found that the resulting graph of base load versus pile head settlement was linear. Extrapolation of the load-settlement curve gave an ultimate load of 13.12MN for the normal pile, and 3.89MN for the voided toe pile. The latter prediction is higher than that obtained from the actual test. These values were input in the analytical model and the predicted performance curves are shown in Figs. 7.12(a)-(d).

7.3.8 Test piles at Cogan spur

For the Cogan Spur contract a test pile 0.9m in diameter was constructed and load tested. The ground profile at the site of the Cogan Spur test pile was found to be comparable to the site of the Grangetown link pile tests. The voided toe test pile at

Grangetown (pile-3) gave a peak shaft load of 4458kN (equivalent to 225.24kN/m^2) by extrapolation. Using the same shaft resistance per unit area for the Cogan Spur test pile, a peak shaft load value of 7.0MN was estimated. The ultimate total load capacity for the Cogan Spur pile was projected to be 14.23MN. Hence the ultimate base load was estimated to be 7.23MN. Using the numerical model, it was found that the peak shaft and base loads of 6.5MN and 7.0MN respectively produced the correct load-displacement curve. The results are shown in the plots of Fig. 7.13(a)-(d).

7.4 PILES FORMED IN KEUPER MARL AT OTHER LOCATIONS

7.4.1 Test pile at Kilroot, County Antrim, Northern Ireland

Pile loading tests were carried out for the construction of the a power station for Northern Ireland Electricity Service at Kilroot, County Antrim, Northern Ireland. Three test piles A, B and C were constructed and load tested in order to measure the peak shaft resistance of bored piles in the marl. Piles A and B were formed with voided toe while pile C was normally constructed to allow both shaft resistance and end bearing resistance to be developed.

In the C.R.P. test in pile A, the failure load due to shaft resistance alone was 3110kN, which corresponded to a penetration of 0.9% of the pile diameter. In pile C, where both shaft and base resistance were developed, the failure load was assessed as 6030kN. This was the load corresponding to a settlement of 10% of the pile diameter. Sudden failure occurred in the M.L. test on pile B when the load, due to shaft resistance only, reached 2490kN.

Leach et.al(1976) showed that the ultimate load of pile C was most accurately calculated using Davis and Chandler's(1973) method with pressuremeter c_u values and adhesion factor α=0.45, for the shaft; and effective stress parameters for undisturbed zone III marl (for the base). The calculated ultimate shaft resistance and ultimate base resistance values have been used in the analytical model to predict the load-settlement curve for the test pile. Figures 7.14(a)-(d) illustrate the results obtained.

7.4.2 Test piles for the Birmingham International Arena

Two piles were installed and load tested for the design of the foundations of the Birmingham International Arena. The first pile was 750mm in diameter and 13.6m long. The upper 5m length of this pile was sleeved and the pile was tested in compression. The second pile was 600mm in diameter by 18.8m long and was load tested in upward loading. The upper 3.5m length of this pile was 750mm in diameter and was sleeved.

The ultimate capacities of the trial piles were not achieved in either test and the method of Mazurkiewicz(1972) was used to extrapolate the maximum loads. The estimated ultimate capacity of the compression pile was 5400kN whilst that of the tension pile was 3780kN. Hence, the ultimate base capacity of the compression pile was estimated to be 1920kN. From these projections, the peak shaft resistance values were therefore deduced as 3220kN and 3580kN, for the compression pile and the tension pile respectively. From back-analysis, the deformation modulus E_b of the material beneath the base of the compression pile was evaluated as E_b=40 MN/m^2. This was based on the assumption that the peak shaft resistance was fully developed at a pile head movement of 20mm (at which the applied load was 4400kN). Based on the data given by Dauncey and Woodland(1984), the settlement response of pile C has been predicted using the numerical model. The results are shown in Figs. 7.15(a)-(d).

7.4.3 Test piles at Kings Norton, Birmingham

Two bored piles, each 400mm in diameter by 6.7m long, were installed and load tested at Kings Norton, Birmingham. The piles were embedded 4.6m into a stratum of Keuper marl strata having c_u values in the range 103-208kN/m^2. This was overlain by harder marl with c_u values varying from 138-276kN/m^2. These values were determined from quick undrained triaxial tests.

One of the test piles was constructed normally to allow both shaft resistance and end resistance to be developed. However, the other pile was specially constructed to allow the mobilisation of end bearing resistance only. The piles were load-tested under C.R.P. conditions at a settlement rate of 0.75mm/min. The failure stage in end base resistance was not reached.

The plot of settlement divided by load versus settlement, for the end bearing pile, was found not to be a straight line hence the ultimate base load value could not be evaluated. A similar plot for the normal pile gave a projected ultimate total load of 3153kN. It was also observed that at 25mm settlement, on comparing the two piles, the base load and the shaft load mobilised in the normal pile were 192kN and 1676kN respectively. Hence, assuming that 88% of the ultimate capacity of the normal pile was carried in shaft resistance, the peak shaft resistance has been estimated to be 2775kN. Therefore the ultimate base load the remainder 12% which is 378kN. The predicted performance of the pile is shown in Figs. 7.16(a)-(d).

7.4.4 Test piles at Coventry (rock-socket piles)

A test pile 1.06m in diameter was installed with its lower 3.75m length socketed into mudstone and siltstone strata. The upper 4.6m passing through fill was sleeved. The pile was loaded in increments up to about 6.75MN which was still below the ultimate capacity. This test pile was left to become part of the foundation.

Cole and Stroud(1976) analysed the test pile by considering the distribution of load between the base and the shaft of the socket in terms of two rock "spring stiffnesses". These are (i) a compressive stiffness $s_q=q/\rho$ and (ii) a shear stiffness $s_\tau=\tau/\rho$, where

q= base stress

τ= shear stress developed on the shaft

ρ= settlement of the rock socket pile

The ratio s_τ/s_q of the spring constants was taken as constant at 0.06, while s_τ and s_q varied with the S.P.T "N" value of the materials. This conclusion is supported by Poulos and Davis(1968) and Butterfield and Banerjee(1971) who considered the distribution of load between the base and the shaft for a pile in a homogeneous isotropic linear elastic soil. The analysis showed that the ratio of the base load to the shaft load depended on the length to diameter ratio (L/D) and was only slightly influenced by Poisson's ratio. Assuming Poisson's ratio to be 0.3, for typical rock socket pile dimensions where L/D lies between 2 and 5, the shaft to base load ratio varies from 2 to 5. However, τ/q varies only from 0.22-0.25. Hence s_τ/s_q for a given material might be expected to be constant, for these pile dimensions.

The equivalent spring stiffness for each stratum on the shaft was computed from the ratio of its "N" values to the "N" value for the base material and based on s_τ/s_q=0.06. Hence the base stress was evaluated to be 3650 kN/m^2, for a design load of 4500kN. At this load, the settlement of the pile was 12mm. Reducing this value by 3mm, in order to allow for the elastic compression of the pile, the settlement of the socket ρ was estimated as 9mm. The modulus of elasticity of the sandstone beneath the base was therefore back computed to be 0.15kN/mm^2. This value has been used in the numerical model to predict the performance of the pile. The results are given in Figs.7.17(a)-(d) which further demonstrate the accuracy of the predictive model.

7.4.5 Test piles at Leicester

Two test piles, each 0.6m in nominal diameter by 18m long, were tested. One pile was constructed with a voided toe in order to allow only shaft resistance to be mobilised while the other pile was normally constructed. Both piles were constructed considerably larger than expected. The voided toe pile turned out to be 762mm whilst the normally constructed pile was 813mm in diameter. These dimensions were confirmed by excavating the top 0.5m and then drilling down against the voided toe pile to check if any belling had occurred.

The voided toe pile was loaded to 2940kN at which the settlement of the pile head was 3.35mm whilst in the normally constructed pile, the maximum test load was 4410kN which produced a settlement of 6.60mm. The available loads were considerably short of those required to produce failure conditions in either pile. Foley and Davis(1971) estimated the average peak shaft resistance using (a) a total stress analysis and (b) an effective stress analysis. The adhesion factor was taken as α=0.45 and c_u was obtained from correlation with the measured "N" values. In the effective stress method (Chandler,1968), the mean coefficient of earth pressure at rest K_o was taken as 1.5, which was supported by the results of capillary tension measurements. The effective cohesion was assumed to be zero while the effective angle of friction was determined from triaxial tests on remoulded and softened samples.

The calculated average shaft resistance from the two methods was averaged and found to be 1.75 t/ft^2. It was recognised that this value was close to the 1.5 t/ft^2 measured at Tees Dock as reported by the C.I.R.I.A. report No.13. Using this value, the peak shaft resistance values were found to be 590 tons and 710 tons, for the voided toe pile and the normal pile respectively.

The peak resistance values have been used in applying the numerical model to predict the behaviour of the normal pile. The results of the analysis are shown in Figs. 7.18(a)-(d). It is therefore seen that accurate predictions are possible if appropriate soil parameters are input into the analysis program.

7.4.6 Test piles at Redcar, Teeside (End bearing-only pile)

A total of four piles each 0.5m in diameter were installed and load tested. The load test was organised as follows follows:

1) Pile 3- base resistance only

2) Pile 4- shaft resistance only (embedded 3.3m into the marl)

3) Pile 1 and Pile 2- shaft and base resistance (these were embedded 1.1m and 2.0m respectively, into the Keuper marl)

Another complete pile (Pile 6) was tested later during the contract at another part of the site. Plate loading tests were carried out on 865 and 584mm diameter plates in 900mm diameter holes. A total of 8 plate tests were carried out in the marl, four at the top of the weathered zone near the marl surface and four at the top of the relatively unweathered zone at a depth of 2.5-4.0m into the marl. Jorden and Dobie(1976) reported values of equivalent elastic moduli ranging from around 50MN/m^2 in the highly weathered marl and increasing to 3000MN/m^2 in the unweathered marl were deduced.

Pile 3 yielded an equivalent secant modulus of 1230MN/m^2, which is significantly greater than the result obtained from the plate loading tests. The proposed numerical has been used to analyse pile 3, utilising the deformation modulus value back analysed from the load test. The analysis of this pile is unique, since it is the only occasion where good quality load test data are found to test the validity of the suggested function for end bearing response. The predicted curves are shown in Figs. 7.19(a)-(d). It is therefore shown that accurate predictions are possible even for pile conditions where shaft resistance is negligible.

7.5 PILES FORMED IN OTHER SOIL TYPES

7.5.1 Pile in clay overlying sand

O'Riordan(1982) reported data obtained from pile testing for the design of the foundations of the British Library which was to be built adjacent to St. Pancras Station, London. The site investigation revealed the following soil stratification profile:

Depth (m)	Strata description
0.0-2.0	Fill
2.0-20.5	London clay
20.5-35.0	Silty clays (Woolwich and Reading Clay)
35.0-40.0	silty clays, increased sand content (Woolwich and Reading Sand)
40.0-43.5	Thanet Sands
Below 43.5m	Chalk (more than 88 mm thick)

Two bored, cast in-situ piles were installed and load tested. One test pile was 1.05m in diameter while the other was 1.53m in diameter. The smaller pile was fully sleeved in order to the development of end resistance only. The larger test pile, which was 38.5m long, was designed to measure both shaft resistance and end bearing behaviour. The upper two-thirds of the pile length was sleeved so as to found the pile 2m into the Woolwich and Reading Sand. A 50mm polystyrene base was installed at the pile toe to enable the measurement of shaft resistance only initially. The pile was instrumented with vibrating wire strain gauges, rod extensometers and magnetic extensometers.

The pile was tested under maintained load conditions, in 7 load cycles, taking the equilibrium settlement rate as 0.1mm per hour. The full shaft resistance was mobilised when the polystyrene base crashed at an applied load of about 10.4MN. Subsequent to this, any additional loads were resisted in both shaft resistance and end bearing. The data from strain gauges were interpreted in order to determine the axial force variation along the pile shaft. The final load cycle was carried out using a C.R.P. test procedure. The ultimate bearing capacity of the pile was attained at an applied load of 27MN at which the pile head settlement was 190mm.

The analytical model has been used to predict the load settlement variation and the load transfer of this test pile using input data directly obtained from the load test results. After making adjustments for residual loads due to the self weight of the pile (O'Riordan,1982), the ultimate shaft and base loads have therefore been taken as 9.205MN and 19.795MN respectively. The deformation modulus of the soil beneath the base has been back-figured to be 0.1 kN/mm^2. Figure 7.20(a) illustrates the predicted and observed load-settlement variation. The measured and predicted axial force variation with depth, corresponding to the ultimate load capacity of 27MN, is shown in Fig. 7.20(b). There is a good agreement between the observed and predicted behaviour. This demonstrates that the analytical model is capable of producing accurate and reliable results even for piles formed in clay/sand strata.

7.5.2 Piles in layered soils

Hirayama(1990) has reported loading tests of large diameter bored piles (2-3m in diameter and 40-70m in length) carried out for the design of a Viaduct at Honshu-Shikoku Bridge, West Japan. The point of failure was not reached in any of the test piles. The numerical model has been used to analyse the data from 3 instrumented test piles (T1, T2 and T3). In order to estimate the input data, the ultimate shaft resistance P_{us} and ultimate base resistance bearing P_{ub} were deduced from empirical correlation (Hirayama,1990) with S.P.T. results as given in Table 7.4.

Ultimate shaft resistance, q_{us} (kN/m^2)	Sand: q_{us}= 5N (≤200 kN/m^2) Clay: q_{us}= c_u or 10N (≤ 150 kN/m^2)
Ultimate shaft resistance, q_{us} (kN/m^2)	Sand: 400N Clay: $9c_u$ or 100N

Table 7.4:Estimation of shaft and base resistances from S.P.T results (Hirayama,1990)

The dimensions of the test piles were:

Pile No.	Diameter (m)	Length (m)
T1	3 m	70 m
T2	2 m	40 m
T3	2 m	70 m

To obtain the input data, the ultimate shaft loads were evaluated by summing the contribution ΔQ_{us} to shaft resistance of each stratum. The calculations for test piles T1 and T2 are shown in Tables 7.5 and 7.6.

Depth (m)	Thickness (m)	Stratum	S.P.T. N	q_{us} (kN/m^2)	ΔQ_{us} (MN)
Up to 2.9m	2.9	Sand	5	30	0.819
2.9-10.9m	8	Sand	10	60	4.524
10.9-14.9m	4	Sand	20	100	3.770
14.9-17.9m	3	Sand	30	120	3.393
17.9-20.9m	3	Sand	40	160	4.524
20.9-28.9m	8	Clay	20	120	9.048
28.9-32.9m	4	Clay	8	80	3.016
32.9-38.9m	6	Sand	30	225	12.723
38.9-48.9m	10	Clay	20	375	35.343
48.9-53.9m	5	Clay	50	375	17.671
53.9-67.9m	14	Sand	50	500	65.973
67.9-70m	2.1	Sand	50	500	9.896
			q_{ub}=20000	Total =	170.7

Table 7.5: Evaluation of P_{us} and P_{ub} for pile T1 from data by Hirayama(1990)

Depth (m)	Thickness (m)	Stratum	S.P.T. N	q_{us} (kN/m^2)	ΔQ_{us} (MN)
Up to 2.9m	2.9	Sand	5	30	0.546
2.9-10.9m	8	Sand	10	60	3.016
10.9-14.9m	4	Sand	20	100	2.513
14.9-17.9m	3	Sand	30	120	2.262
17.9-20.9m	3	Sand	40	160	3.016
20.9-28.9m	8	Clay	20	120	6.032
28.9-32.9m	4	Clay	8	80	2.011
32.9-38.9m	6	Sand	30	225	8.482
38.9-40.0m	1.1	Clay	20	375	2.592
			q_{ub}=18000	Total =	30.47

Table 7.6: Evaluation of P_{us} and P_{ub} for pile T2 from data by Hirayama(1990)

A calculation Table for pile T3 is not necessary since this pile had the same length as pile T1 and was installed in the same types of soil strata. The only difference was in the diameters (2 m for pile T3 and 3 m for pile T1). Therefore the ultimate shaft load for pile T3 can be obtained by multiplying that for pile T1 by a factor of two-thirds. Fig. 7.21(a) shows the predicted and measured load-settlement curves for pile T1 while the Fig. 7.21(b) illustrates a comparison of the axial force variations at an applied load of 40 MN. There is a remarkable agreement between the predicted and observed results. This demonstrates the suitability and success of the proposed analytical method. Similar comparisons for test piles T2 and T3 are given in Fig.7.22 and Fig 7.23. It demonstrated strongly that provided the correct input data are determined, the proposed method is reliable and accurate for a wide range of soil conditions and pile sizes.

7.6 SUMMARY OF THE INVESTIGATION OF PILE BEHAVIOUR

The above examples favourably suggest that, using the proposed method, both the nature of the load-settlement representation and the imposed parameters produce a very reliable prediction of pile response. Additional test pile cases are currently being examined, in a wide range of soil types, to verify if the method is capable of predicting the performance of piles in soil strata of random geometry and under different conditions.

Attempts have been made to predict the complete load-settlement behaviour of different piles, covering not only clean pile bases but also the effects of a pile base formed on debris. These studies show that

1) Reliable predictions of shaft and base resistance mobilisation are uniquely and successfully achieved by utilising basic soil parameters easily available from the results of soil investigations. The major parameters are the ultimate shaft and base resistance, modulus of deformation of the soil beneath the pile base and modulus of rigidity of the soil around the pile shaft.
2) Considerable errors in the computed load-settlement curve can occur if the soil properties are not established accurately. In addition, the effect on pile settlement of any soil debris present at the bottom of the hole should be considered.
3) The calculation of pile shortening under applied load must take into account the true stress- strain response of concrete. The use of a constant static modulus value for the pile concrete results in an overestimate of the pile shortening. This is because concrete tends to exhibit much higher stiffness values at low strains than at strains in excess of about 0.0002.
4) The possible decrease in shaft resistance with increasing pile settlement, subsequent to the point of peak shaft resistance, should be taken into consideration in order to determine the load capacity of a pile accurately.

7.7 CONCLUSION

The analytical model described is simple and accurate, provided that the input data and the soil parameters are determined accurately. The manner in which the model is linked to soil properties is straightforward and easy to understand. Moreover, the required soil parameters are those that would be readily available from conventional site investigation. The success of the method relies on the correct determination of these soil parameters. For test piles analysed, the predicted aand observed load-settlement curves agree remarkably well. However, there is no complacency in proposing that the model is infallible in all cases. Hence, further investigation of the method using additional test pile data will obviously be helpful. More pile test data are being sought and as relevant information becomes available, updating of the existing database will take place progressively.

The model can be readily adopted for use in designing a single pile, based on known soil properties. The process requires input of the various pile material and soil properties. The program is driven by the input data and enables the determination of whether or not the pile satisfies the design requirements. The model may also be used to back-analyse a test pile, provided that sufficient settlement has been achieved, so that a reasonable part of the load-settlement characteristic is extracted.

The program is coded such that it can be identified with the parameters available from any routine site investigation activity. The remaining parameters are available from well-cited design codes of practice and the appropriate standards and publications such as C.I.R.I.A. reports. In other words, the program provides all the information relevant to the design of piles short of being a "design program". The versatility of the proposed numerical model demonstrates that there is potential in theoretical investigation of pile performance, since pile behaviour is not a random phonomenon.

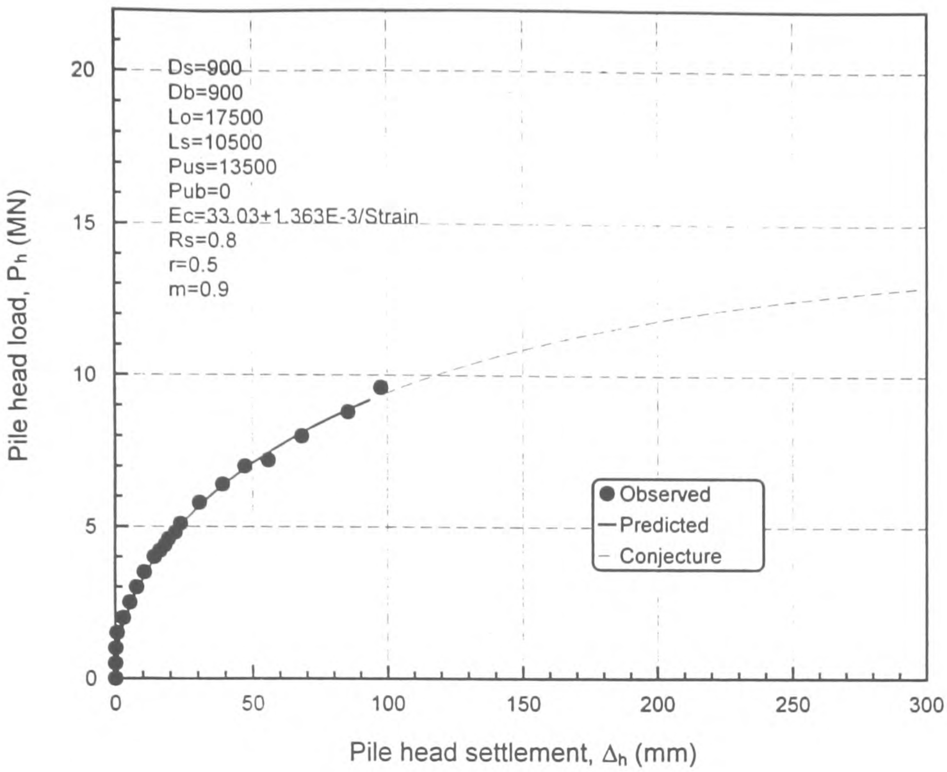

Fig. (7.1a):Test pile TP1 in Keuper marl at Butetown link road site, Peripheral Distributor Road, Cardiff -Load Vs settlement (voided toe pile)

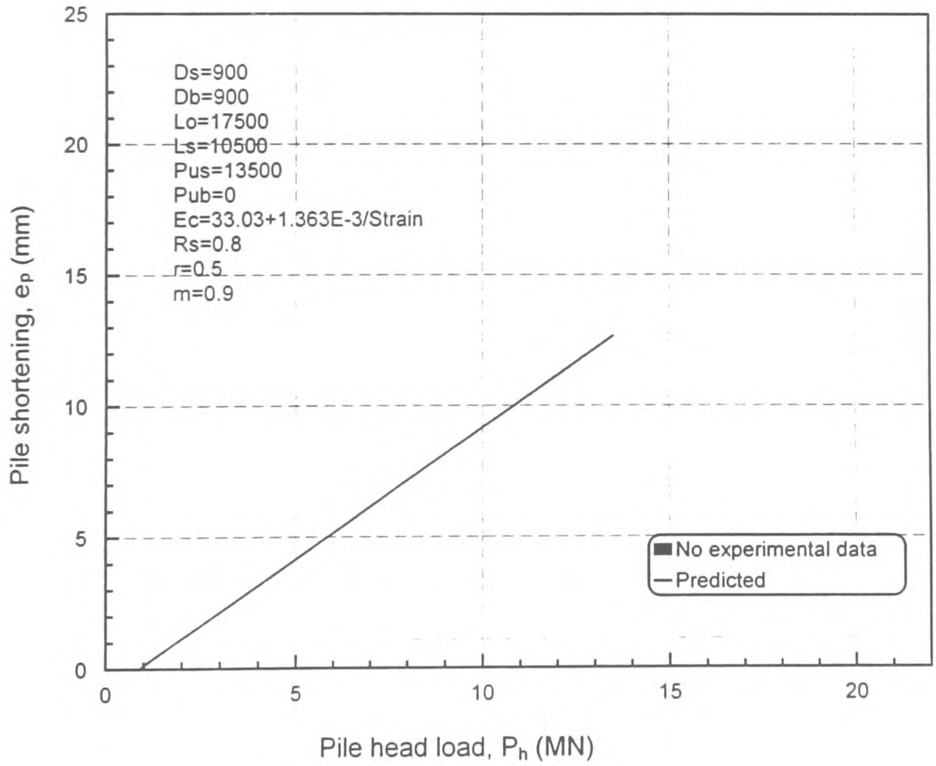

Fig. (7.1b):Test pile TP1 in Keuper marl at Butetown link road site, Peripheral Distributor Road, Cardiff -Shortening versus applied load (Voided toe test)

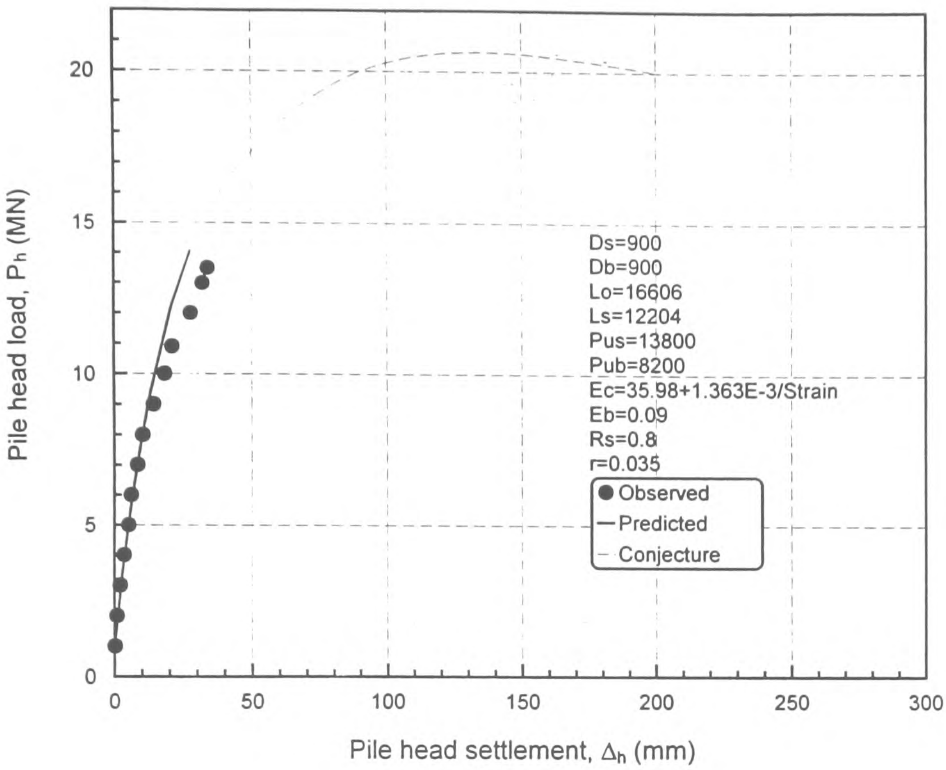

Fig. 7.2(a):Test pile TP2 in Keuper marl at Butetown link road site, Peripheral Distributor Road, Cardiff -Load settlement plot

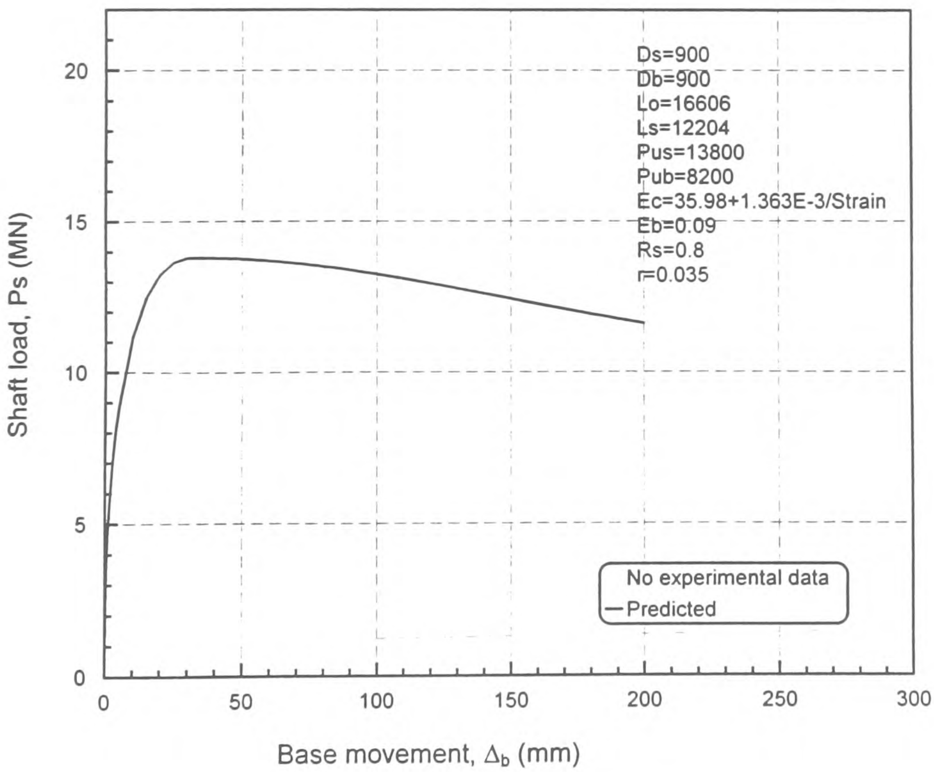

Fig. 7.2(b):Test pile TP2 in Keuper marl at Butetown link road site, Peripheral Distributor Road, Cardiff -Shaft load Vs base movement

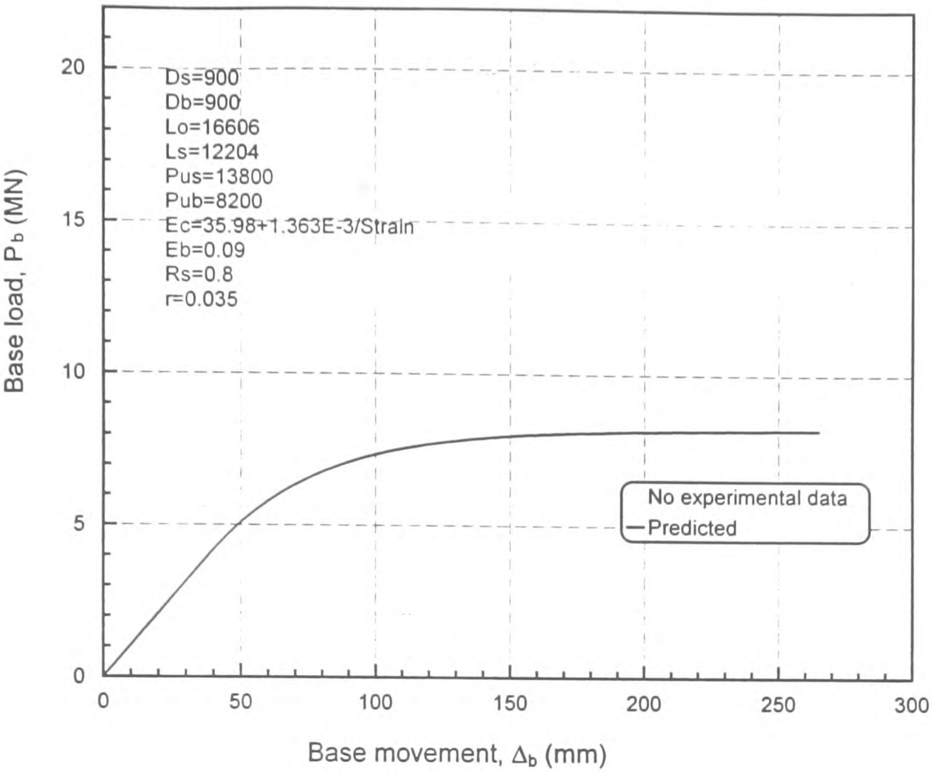

Fig. 7.2(c):Test pile TP2 in Keuper marl at Butetown link road site, Peripheral Distributor Road, Cardiff -Base load Vs base movement

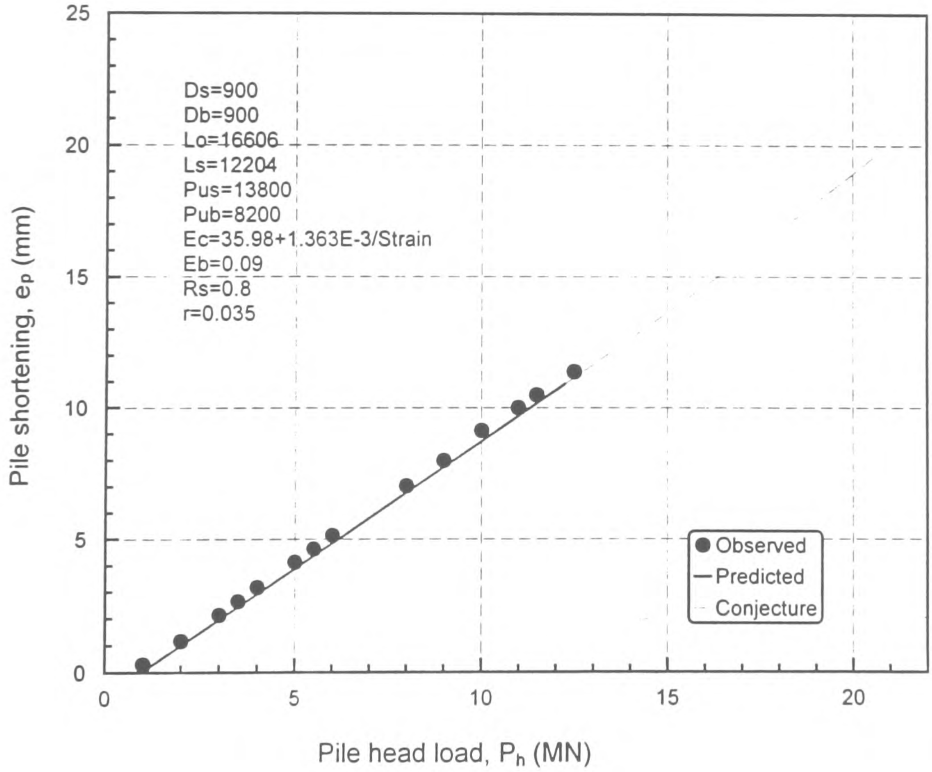

Fig. 7.2(d):Test pile TP2 in Keuper marl at Butetown link road site, Peripheral Distributor Road, Cardiff -Shortening Vs applied load

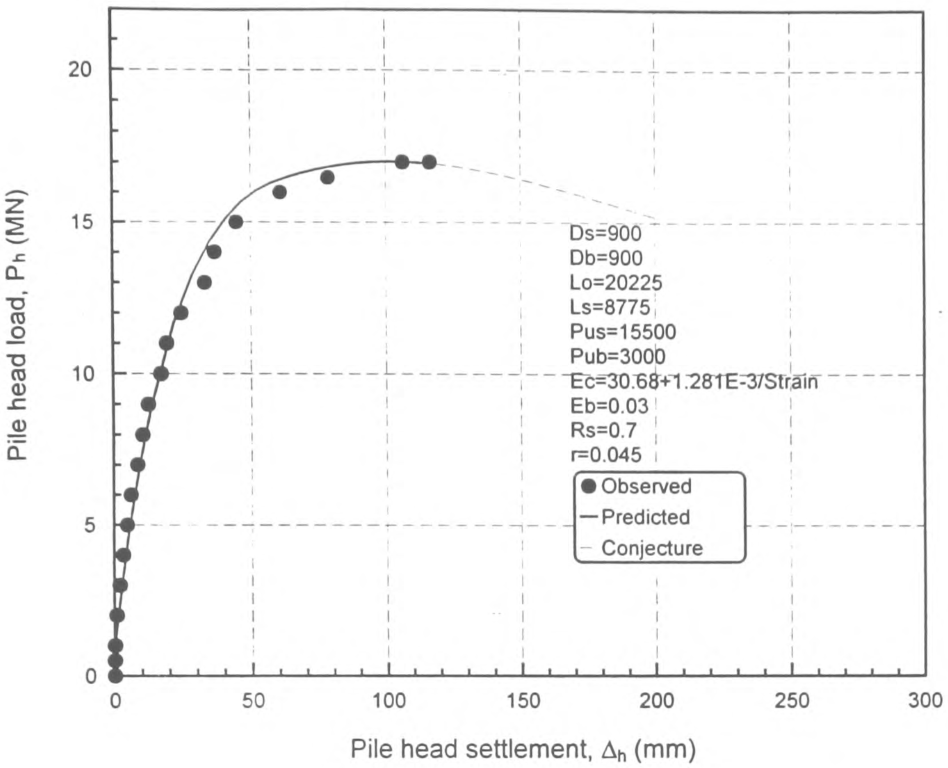

Fig. 7.3(a):Test pile TP3 in Keuper marl at Butetown link road site, Peripheral Distributor Road, Cardiff -Load settlement plot

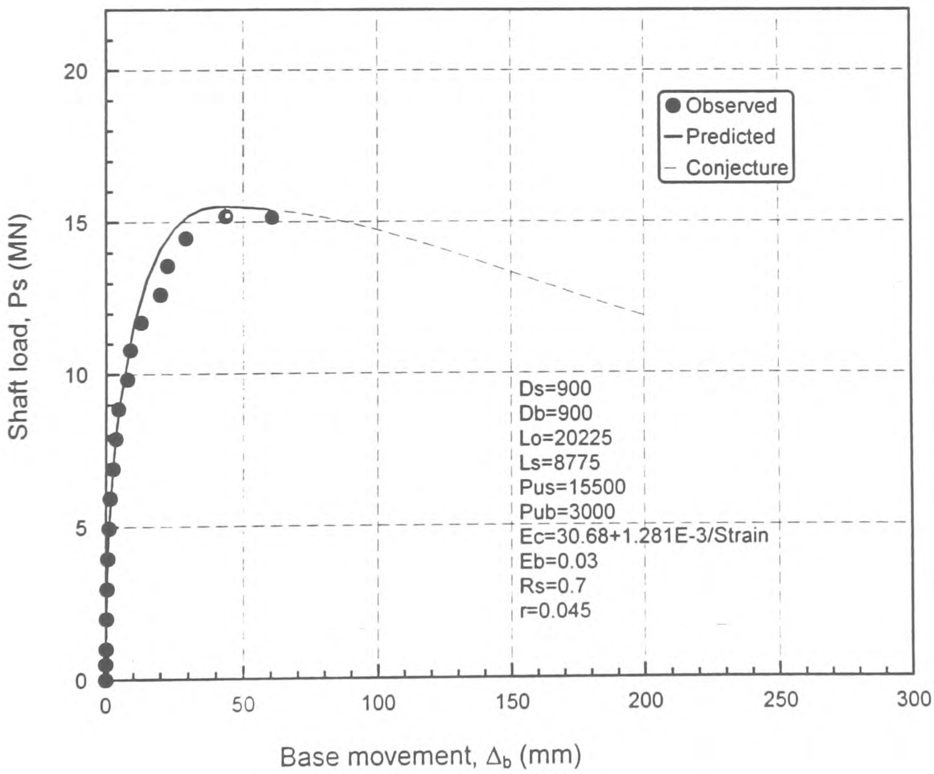

Fig. 7.3(b):Test pile TP3 in Keuper marl at Butetown link road site, Peripheral Distributor Road, Cardiff -Shaft load Vs base movement

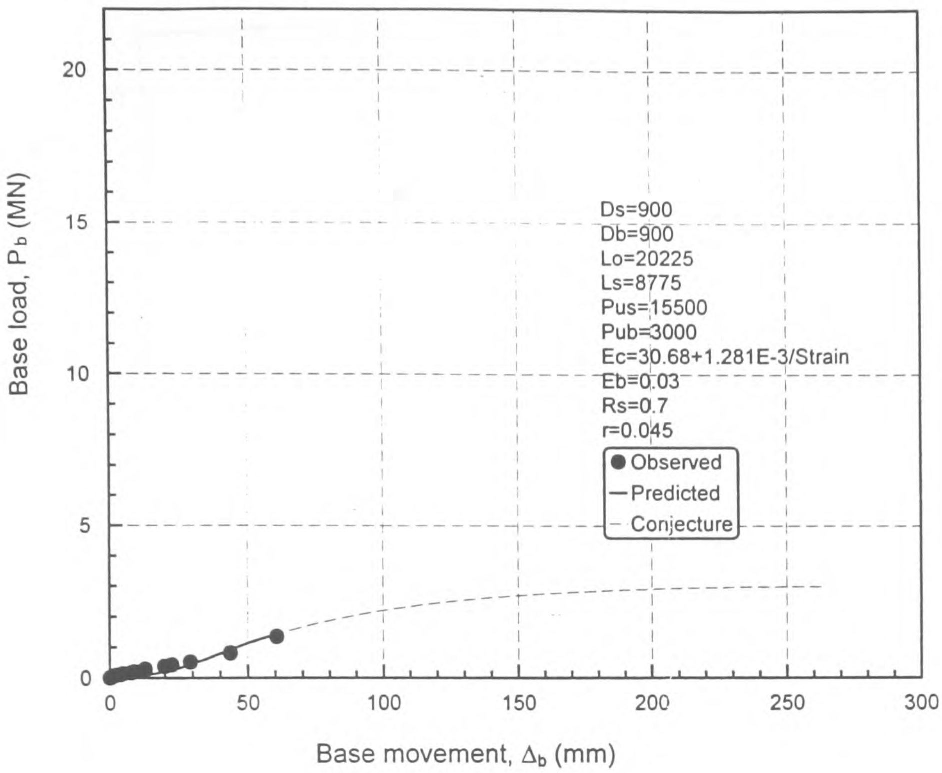

Fig. 7.3(c):Test pile TP3 in Keuper marl at Butetown link road site, Peripheral Distributor Road, Cardiff -Base load Vs base movement

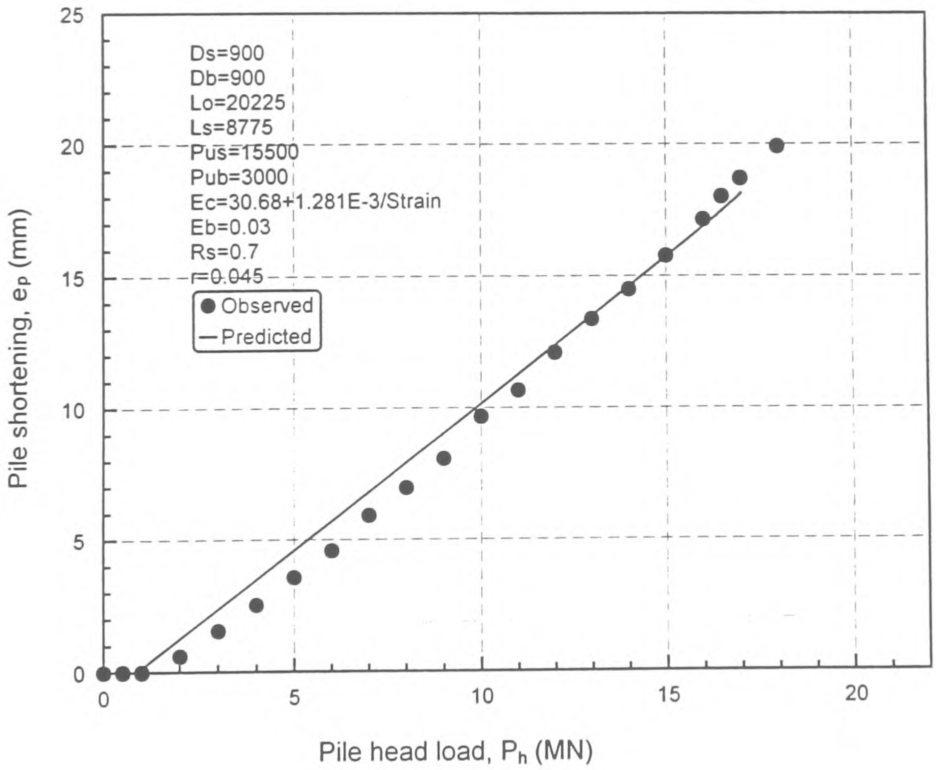

Fig. 7.3(d):Test pile TP3 in Keuper marl at Butetown link road site, Peripheral Distributor Road, Cardiff -Shortening Vs applied load

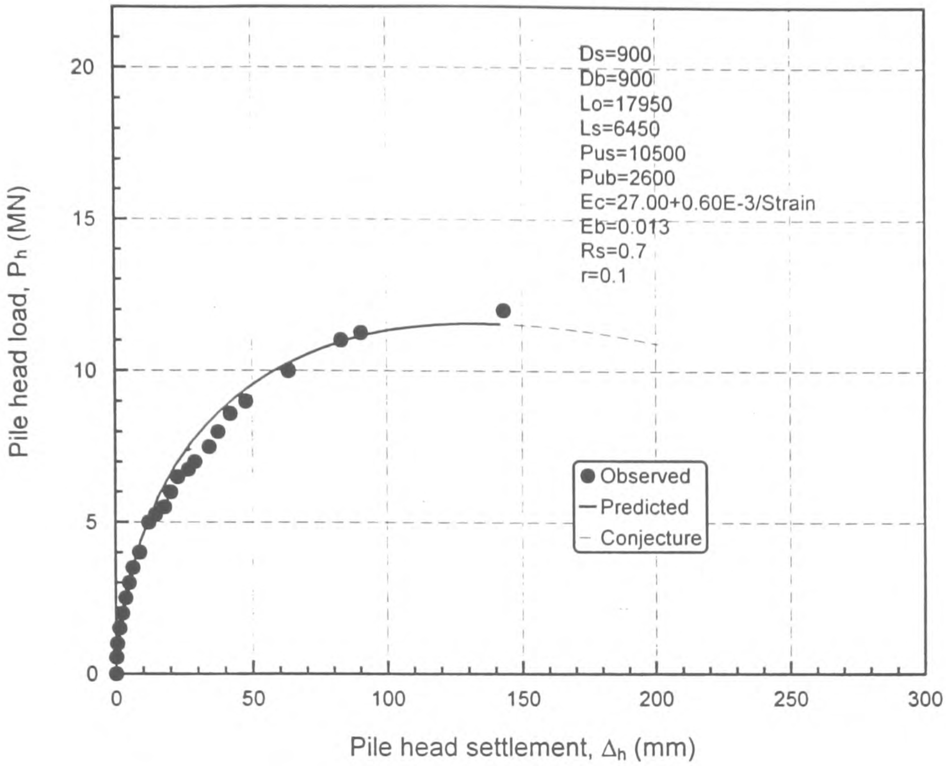

Fig. 7.4(a):Test pile TP4 in Keuper marl at Butetown link road site, Peripheral Distributor Road, Cardiff -Load settlement plot

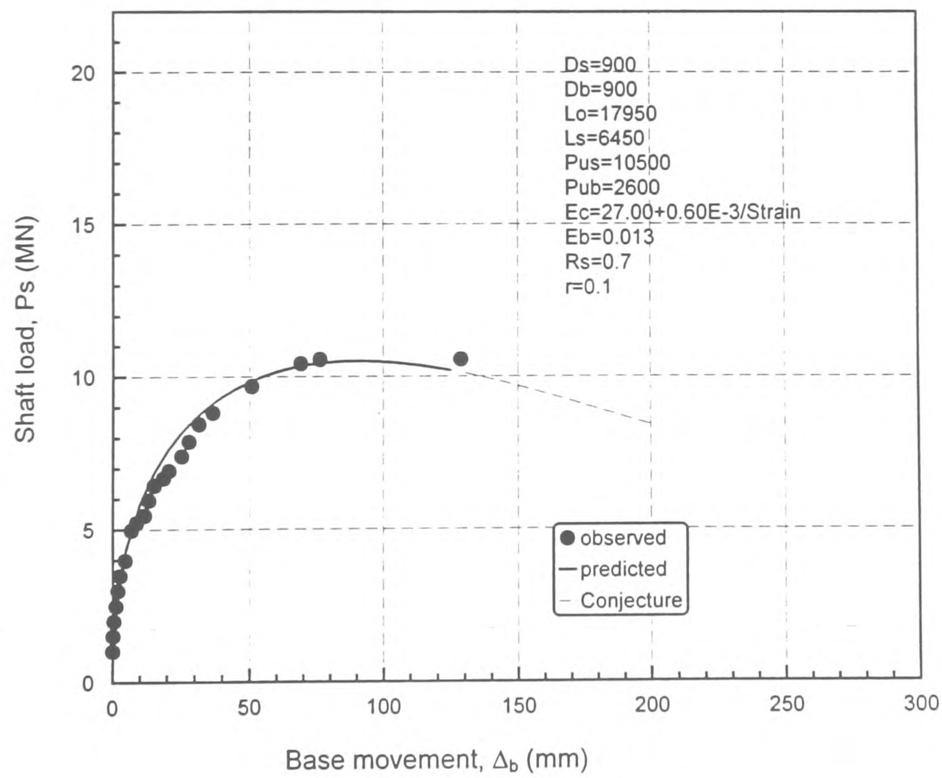

Fig.7.4(b):Test pile TP4 in Keuper marl at Butetown link road site, Peripheral Distributor Road, Cardiff -Shaft load Vs base movement

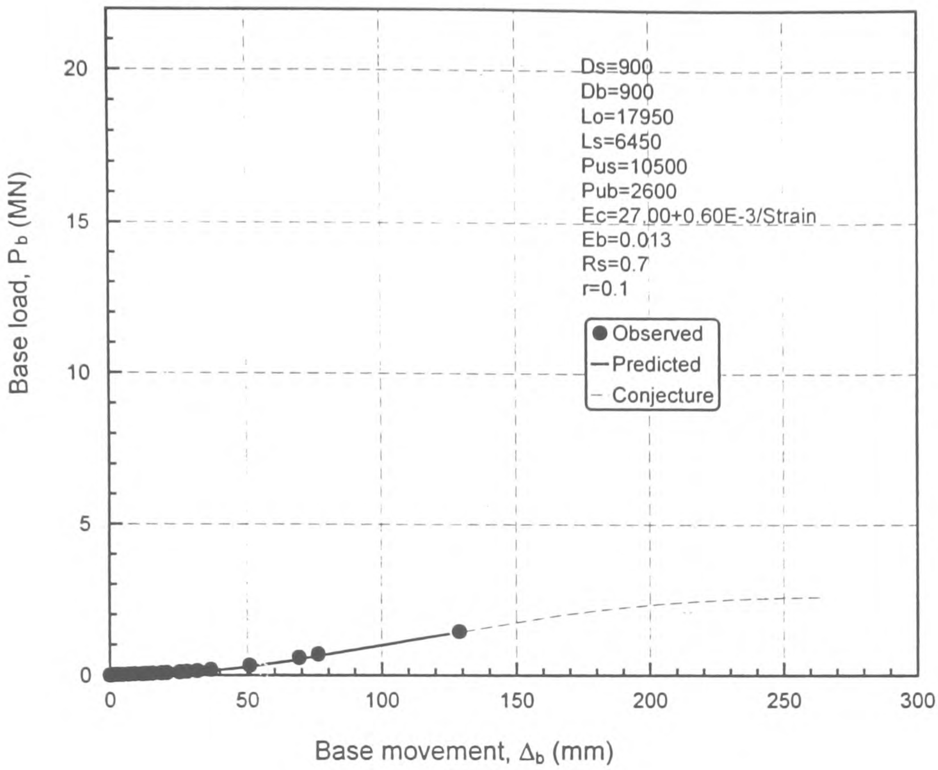

Fig.7.4(c):Test pile TP4 in Keuper marl at Butetown link road site, Peripheral Distributor Road, Cardiff -Base load Vs base movement

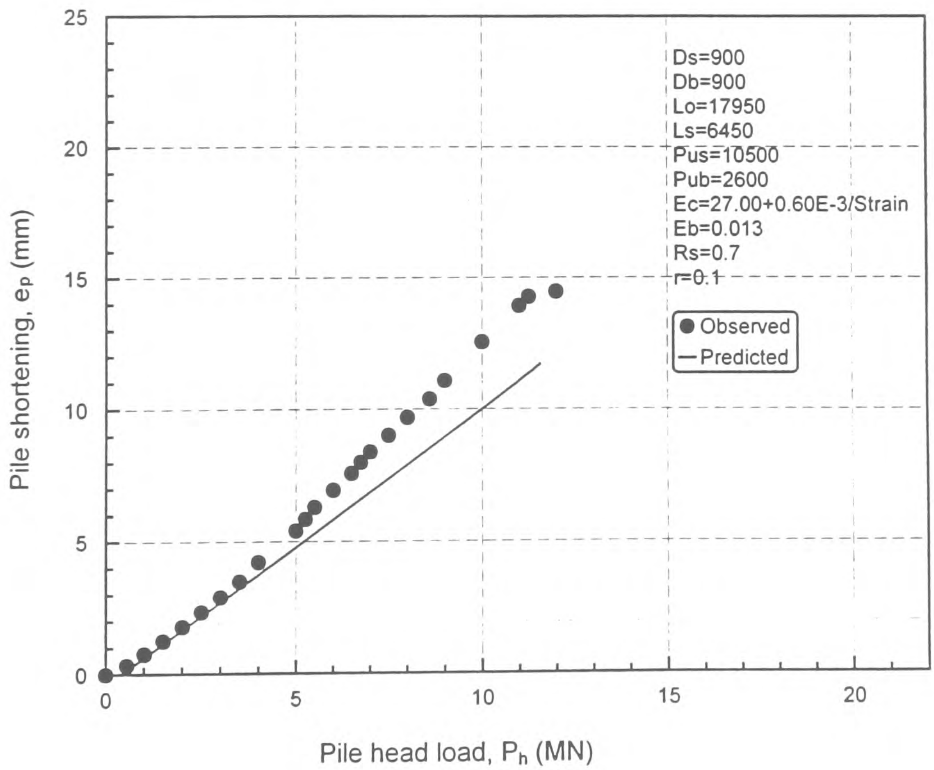

Fig. 7.4(d):Test pile TP4 in Keuper marl at Butetown link road site, Peripheral Distributor Road, Cardiff -Shortening Vs applied load

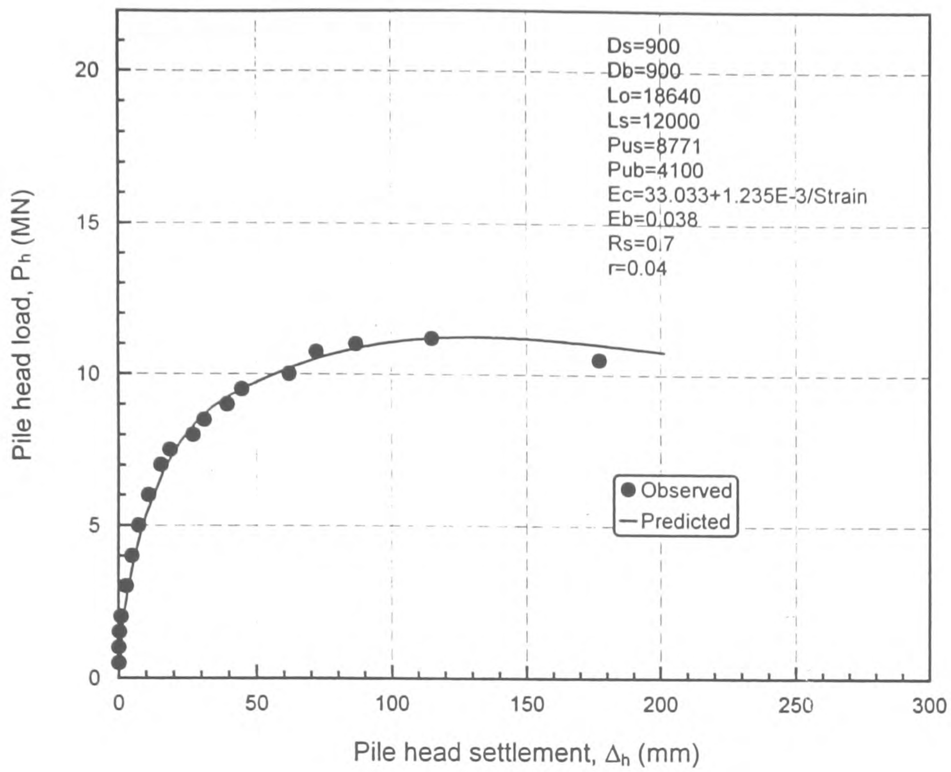

Fig. 7.5(a):Test pile TP5 in Keuper marl at Butetown link road site, Peripheral Distributor Road, Cardiff -Load settlement plot

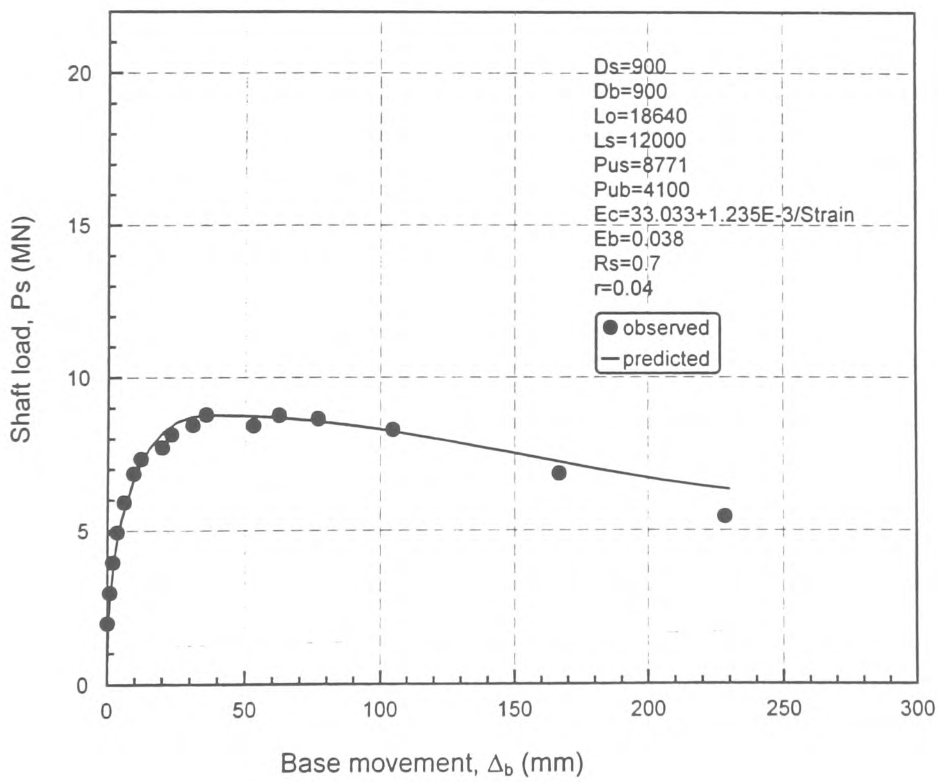

Fig. 7.5(b):Test pile TP5 in Keuper marl at Butetown link road site, Peripheral Distributor Road, Cardiff -Shaft load Vs base movement

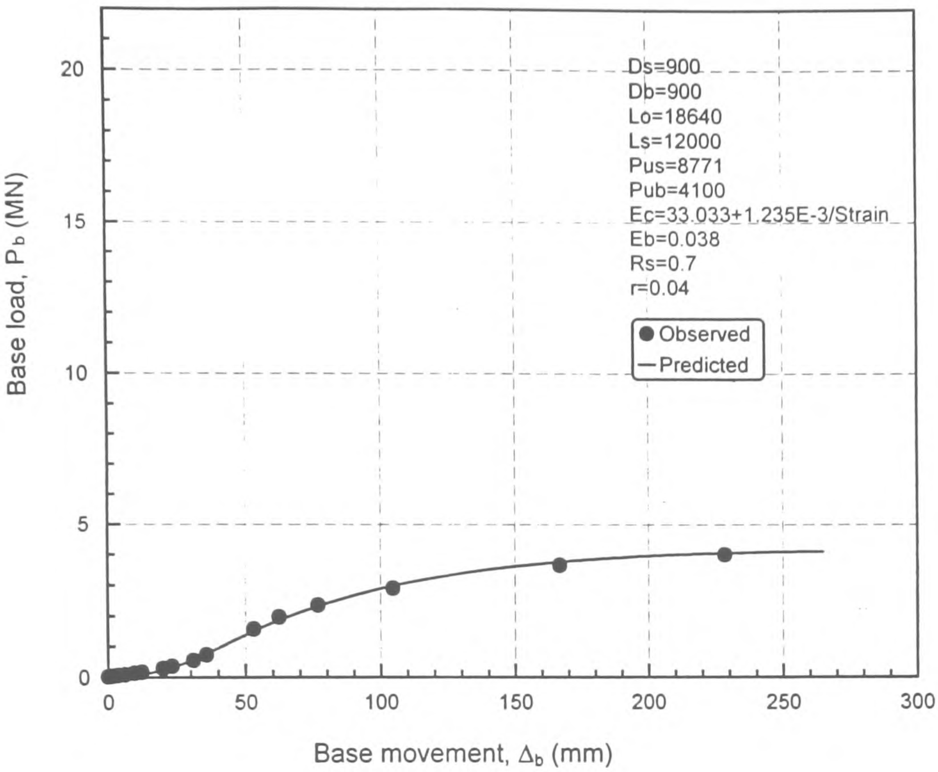

Fig. 7.5(c):Test pile TP5 in Keuper marl at Butetown link road site, Peripheral Distributor Road, Cardiff -Base load Vs base movement

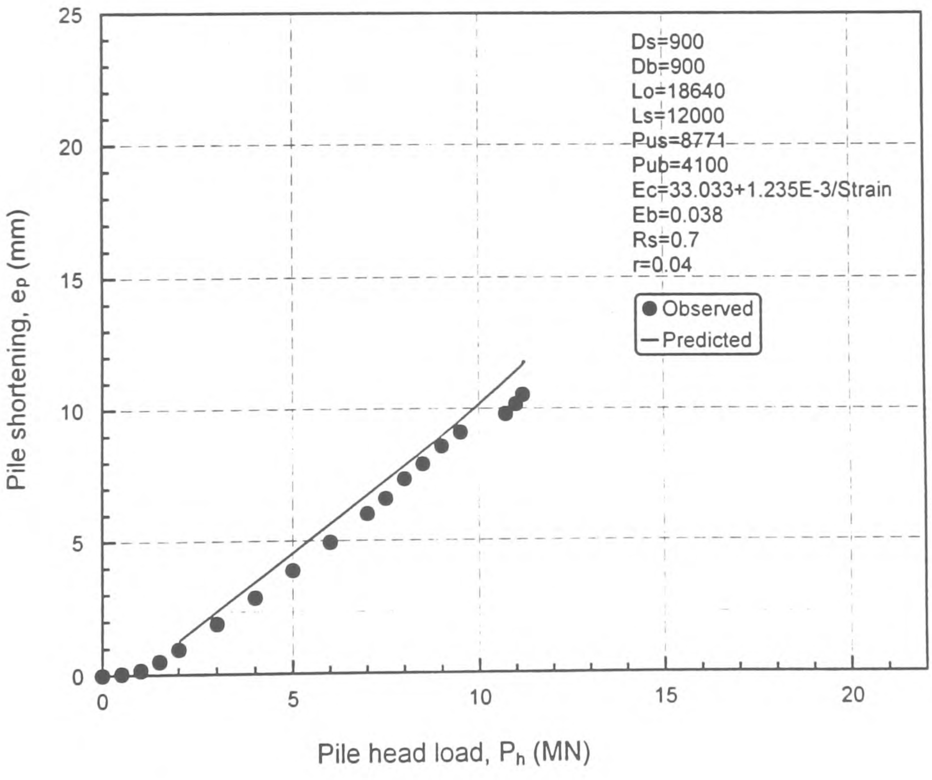

Fig. 7.5(d):Test pile TP5 in Keuper marl at Butetown link road site, Peripheral Distributor Road, Cardiff -Shortening Vs applied load

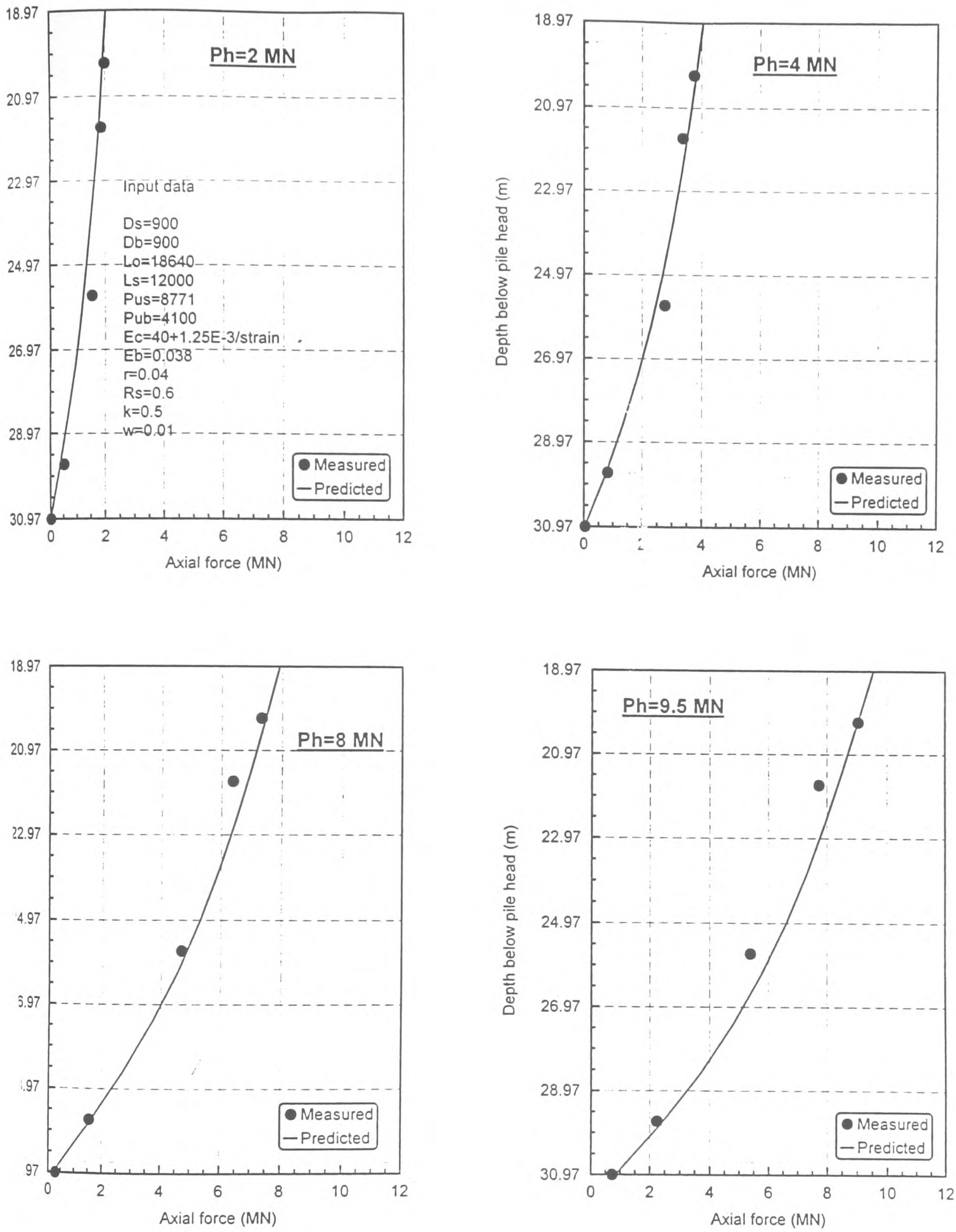

Fig 7.5(e): Comparison between predicted and measured axial force variation with depth-TP5
(for applied pile head loads of 2MN, 4MN, 8MN and 9.5MN:Locus of load increments)

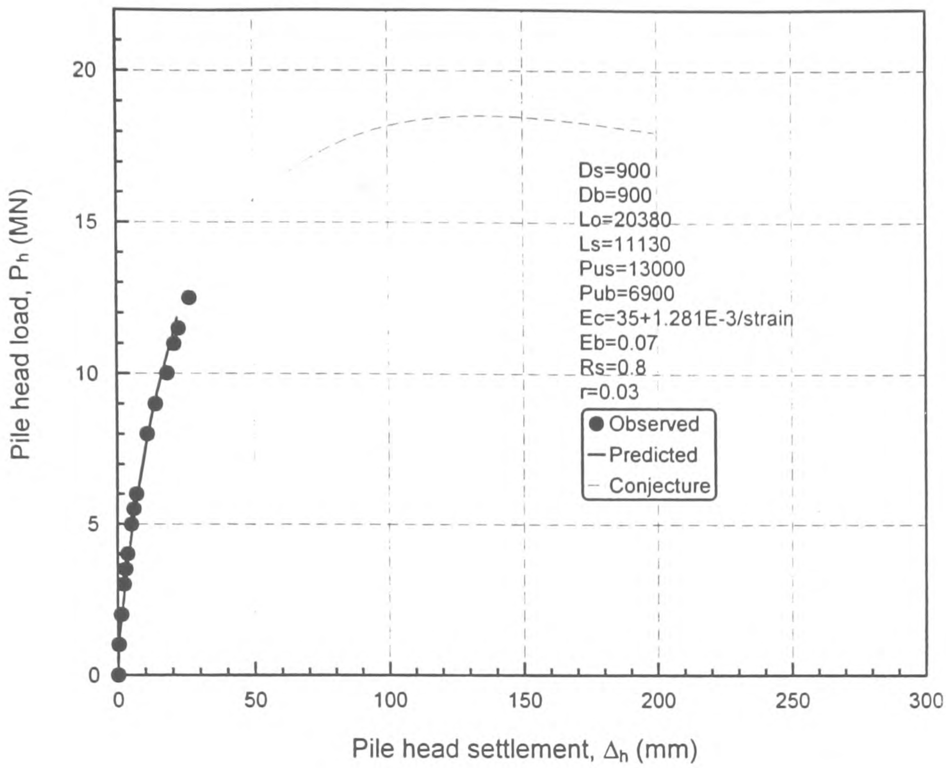

Fig. 7.6(a):Test pile TP6 in Keuper marl at Butetown link road site, Peripheral Distributor Road, Cardiff -Load settlement plot

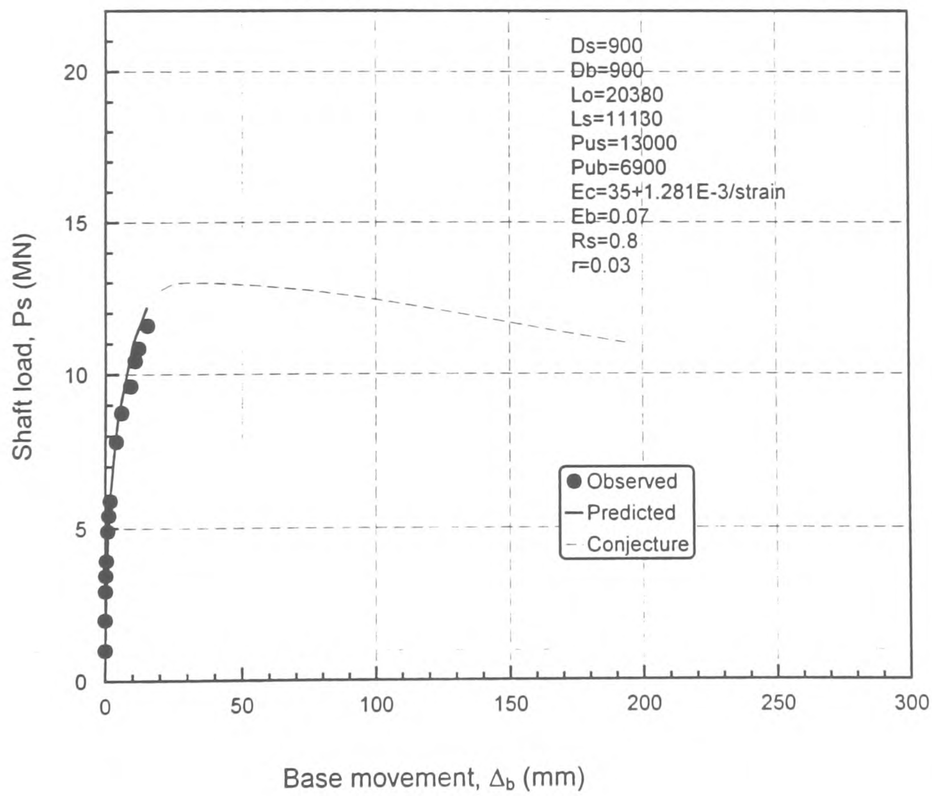

Fig. 7.6(b):Test pile TP6 in Keuper marl at Butetown link road site, Peripheral Distributor Road, Cardiff -Shaft load Vs base movement

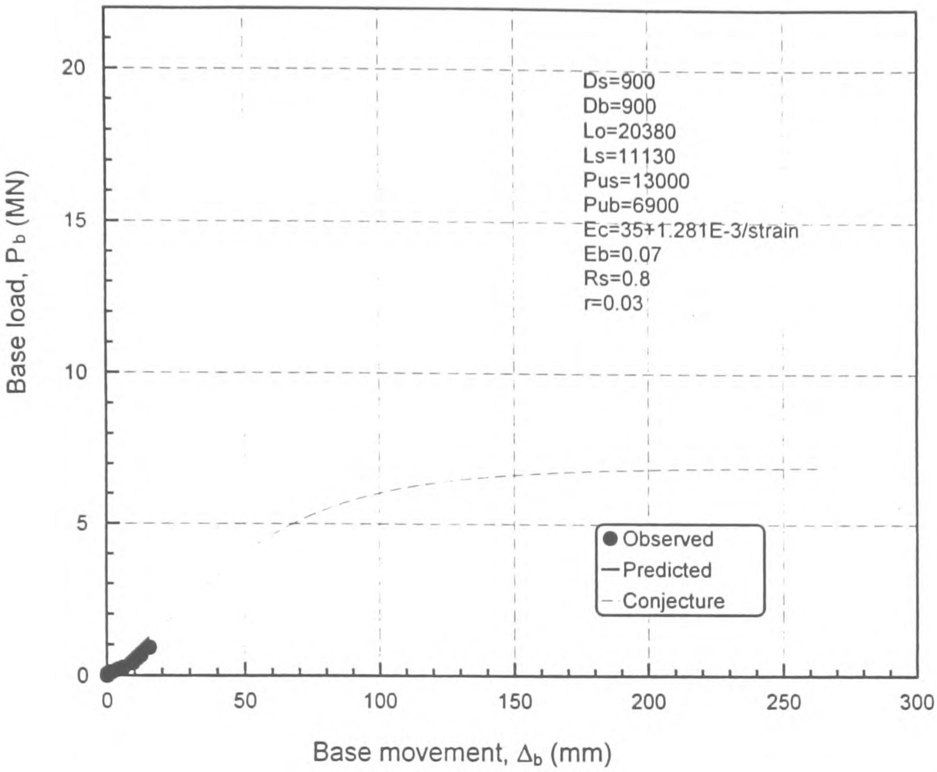

Fig. 7.6(c):Test pile TP6 in Keuper marl at Butetown link road site, Peripheral Distributor Road, Cardiff -Base load Vs base movement

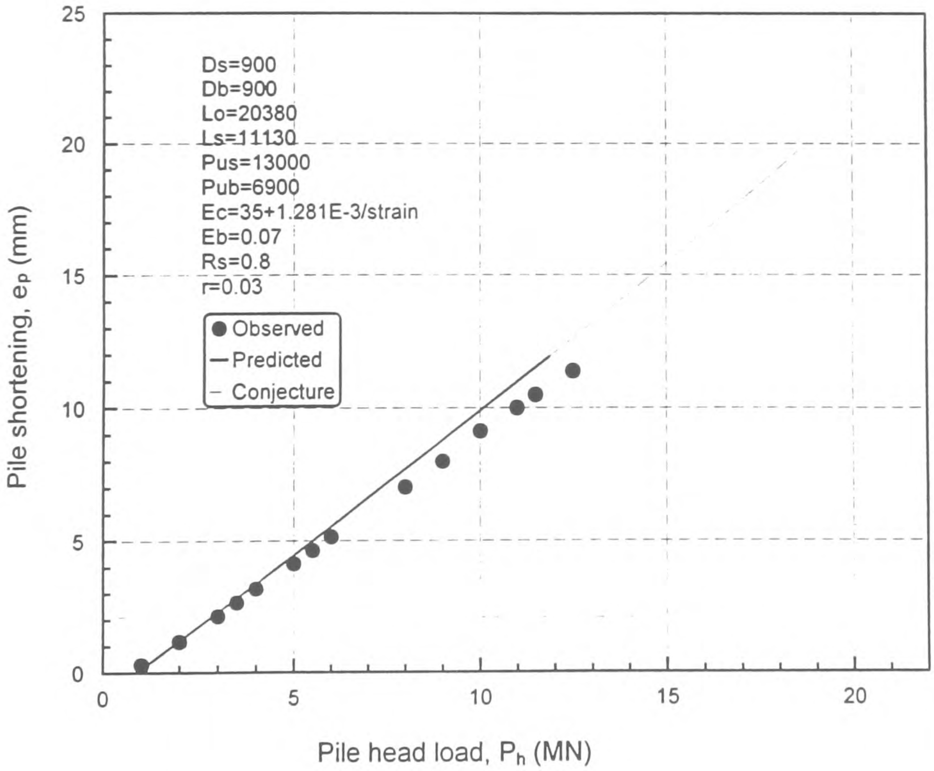

Fig. 7.6(d):Test pile TP6 in Keuper marl at Butetown link road site, Peripheral Distributor Road, Cardiff -Shortening Vs applied load

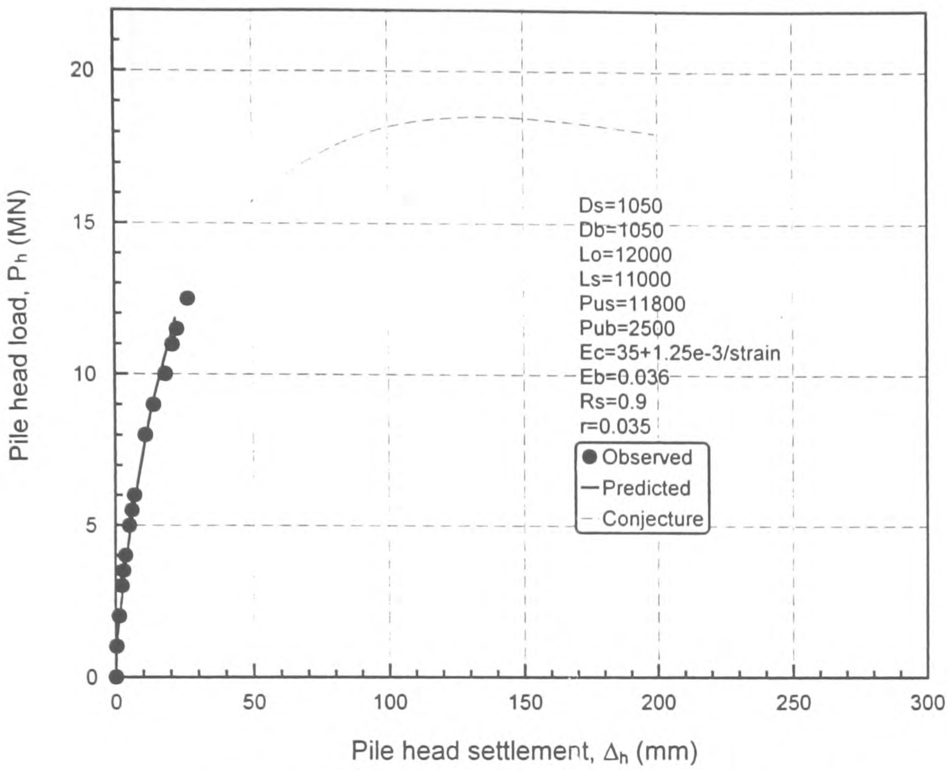

Fig. 7.7(a):Test pile in Keuper marl at Eastmoors link(Pile No.2), Peripheral Distributor Road, Cardiff (Kilbourn et al.1988)
-Load versus settlement plot

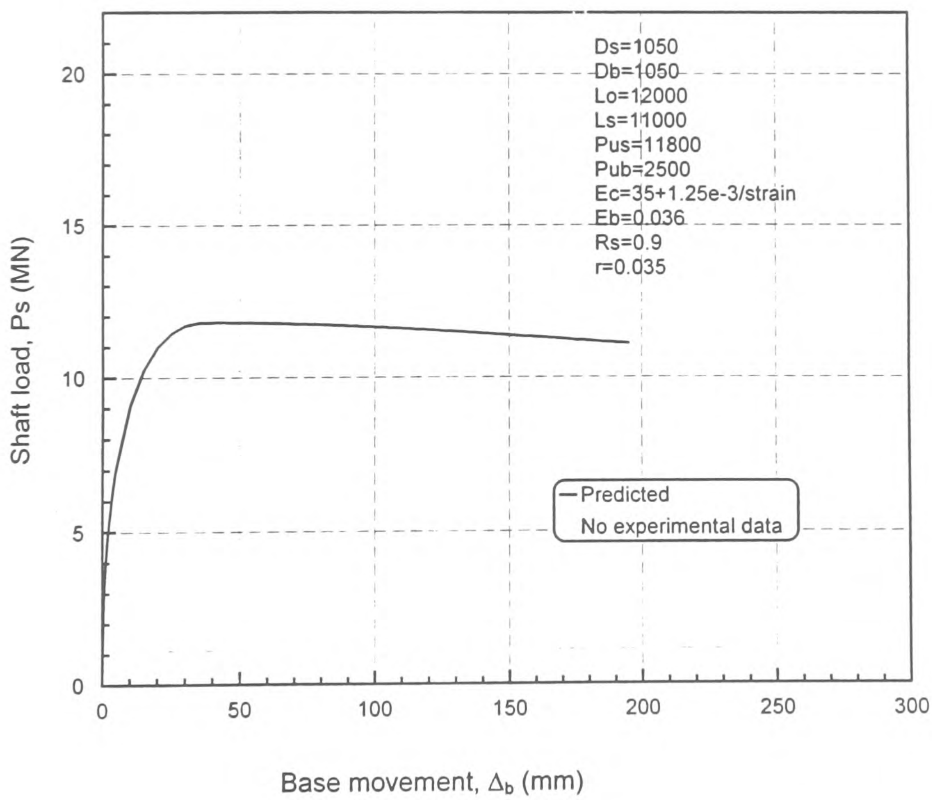

Fig. 7.7(b):Test pile in Keuper marl at Eastmoors link(Pile No.2), Peripheral Distributor Road, Cardiff (Kilbourn et al.1988)
-Shaft load versus base movement plot

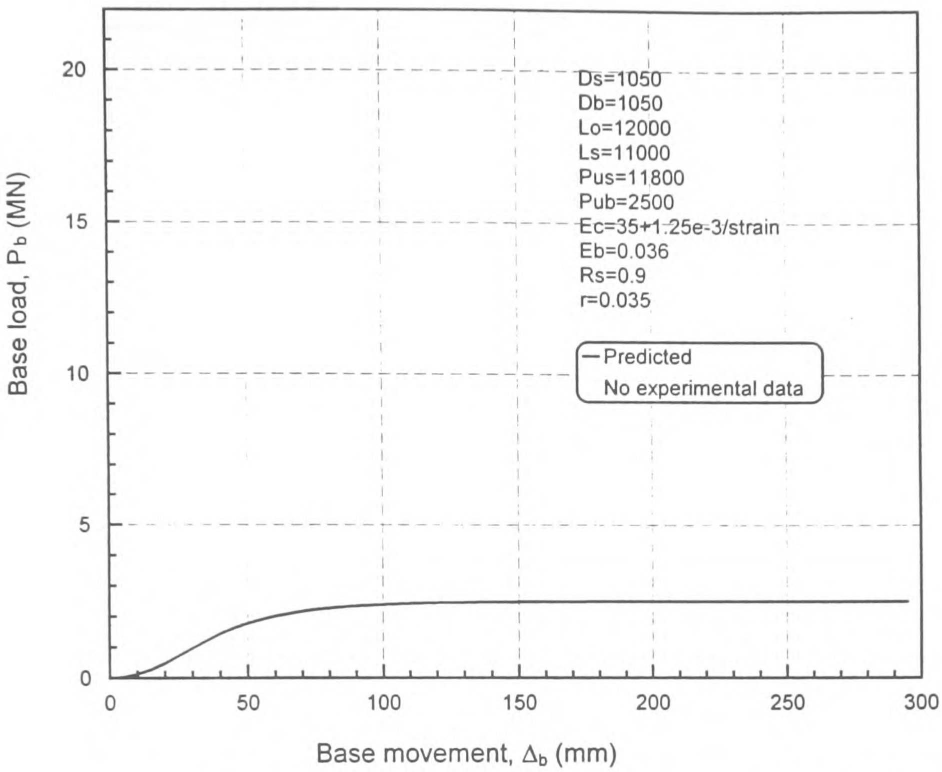

Fig. 7.7(c):Test pile in Keuper marl at Eastmoors link(Pile No.2), Peripheral Distributor Road, Cardiff (Kilbourn et al.1988)
-Base load versus base movement plot

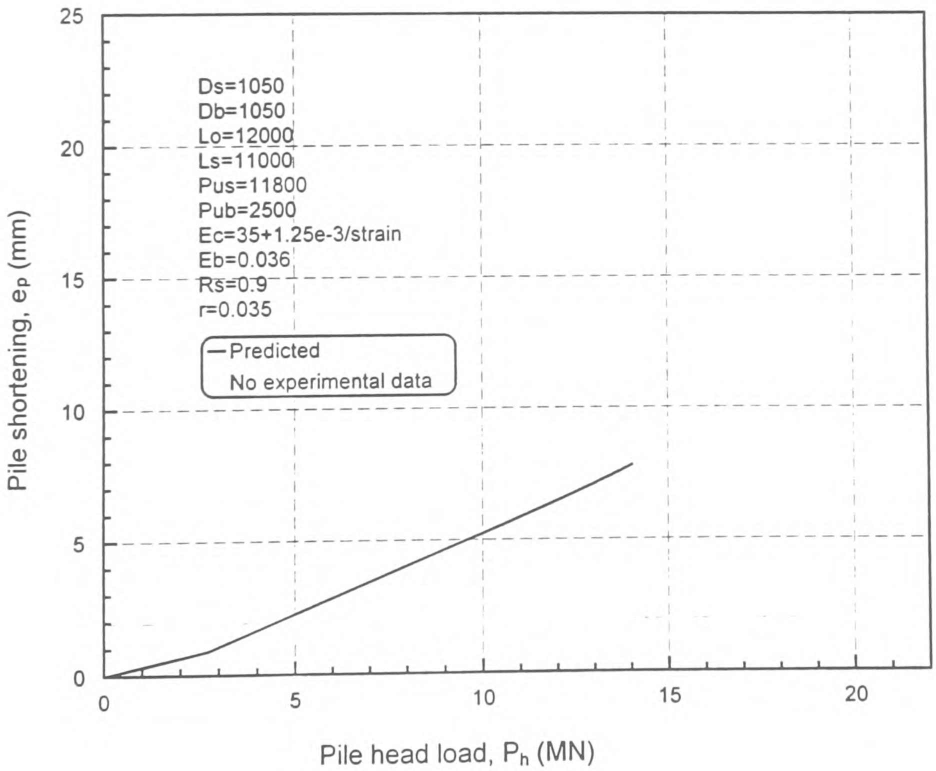

Fig. 7.7(d):Test pile in Keuper marl at Eastmoors link(Pile No.2), Peripheral Distributor Road, Cardiff (Kilbourn et al.1988)
-Shortening versus applied load

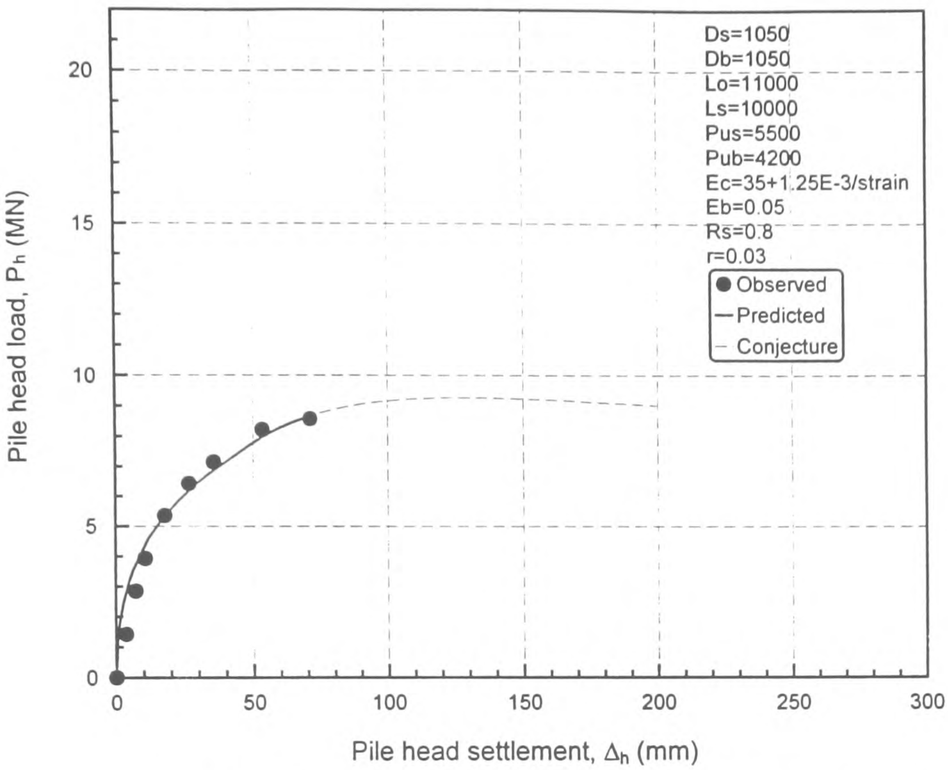

Fig. 7.8(a):Test pile in Keuper marl at Eastmoors link(Pile No.3), Peripheral Distributor Road, Cardiff (Kilbourn et al.1988)
-Load versus settlement plot

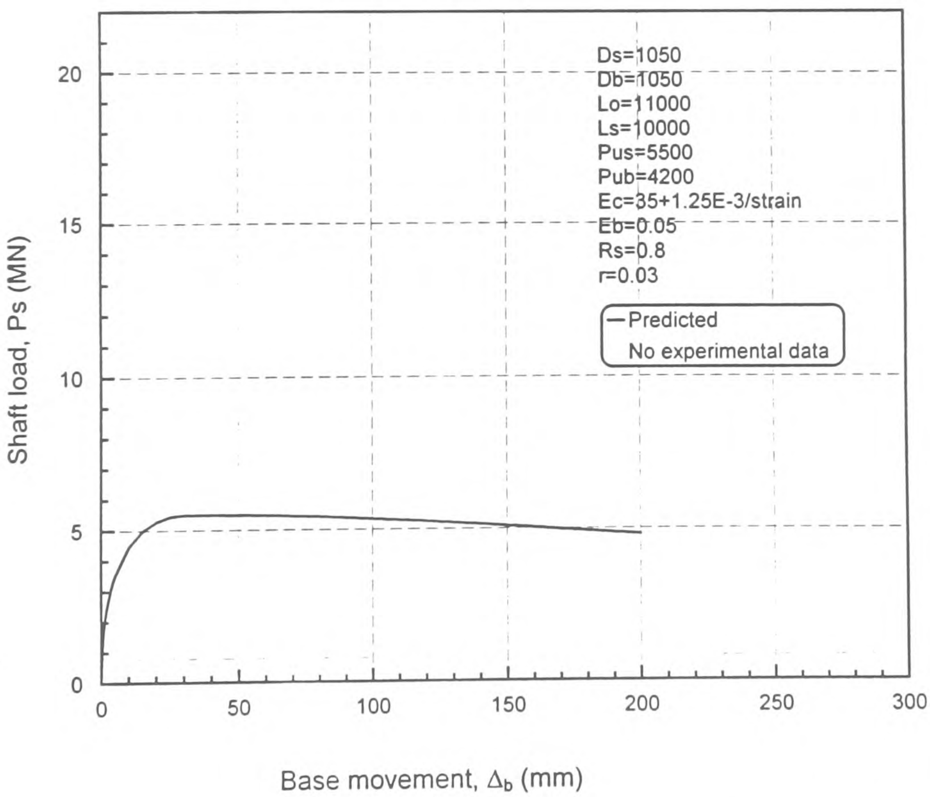

Fig. 7.8(b):Test pile in Keuper marl at Eastmoors link(Pile No.3), Peripheral Distributor Road, Cardiff (Kilbourn et al.1988)
-Shaft load versus base movement plot

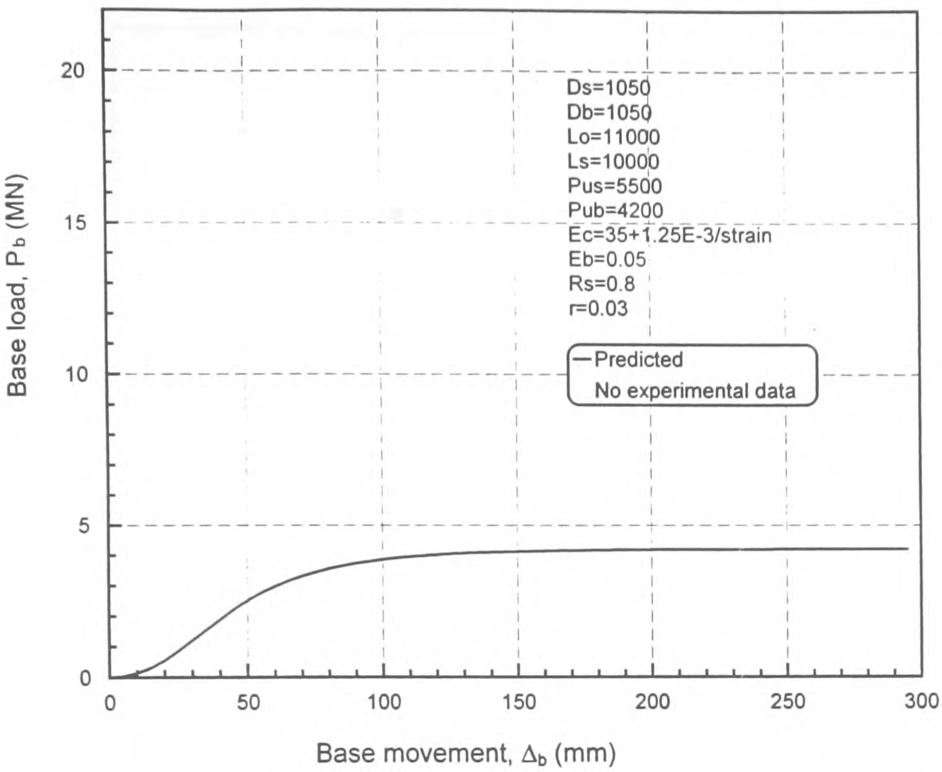

Fig. 7.8(c):Test pile in Keuper marl at Eastmoors link(Pile No.3), Peripheral Distributor Road, Cardiff (Kilbourn et al.1988)
-Base load versus base movement plot

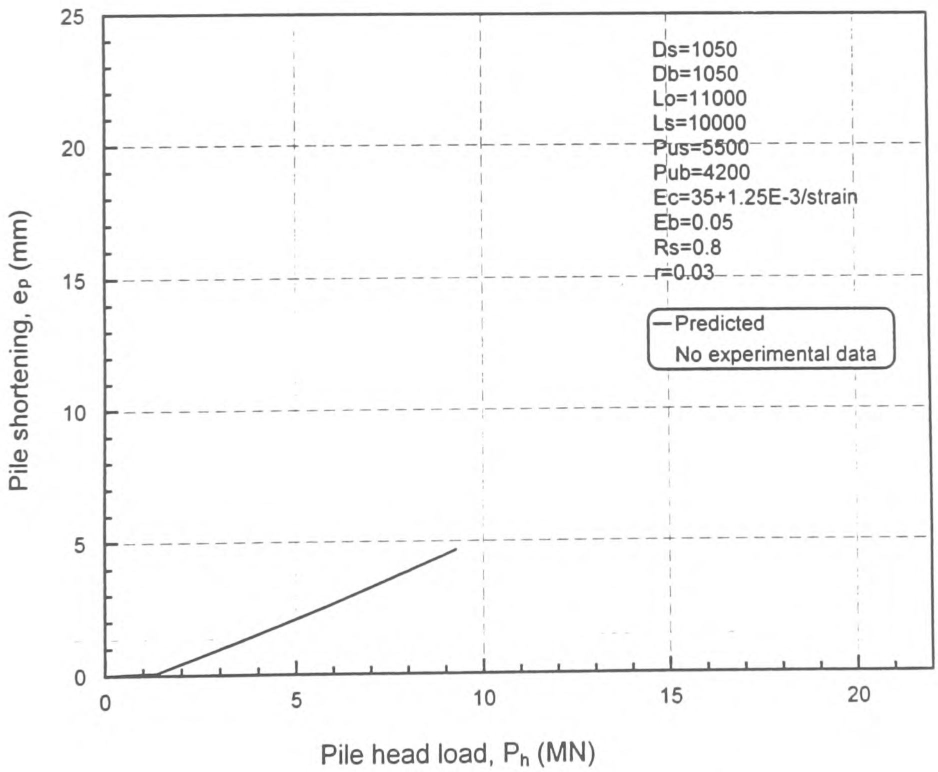

Fig. 7.8(d):Test pile in Keuper marl at Eastmoors link(Pile No.3), Peripheral Distributor Road, Cardiff (Kilbourn et al.1988)
-Shortening versus applied load

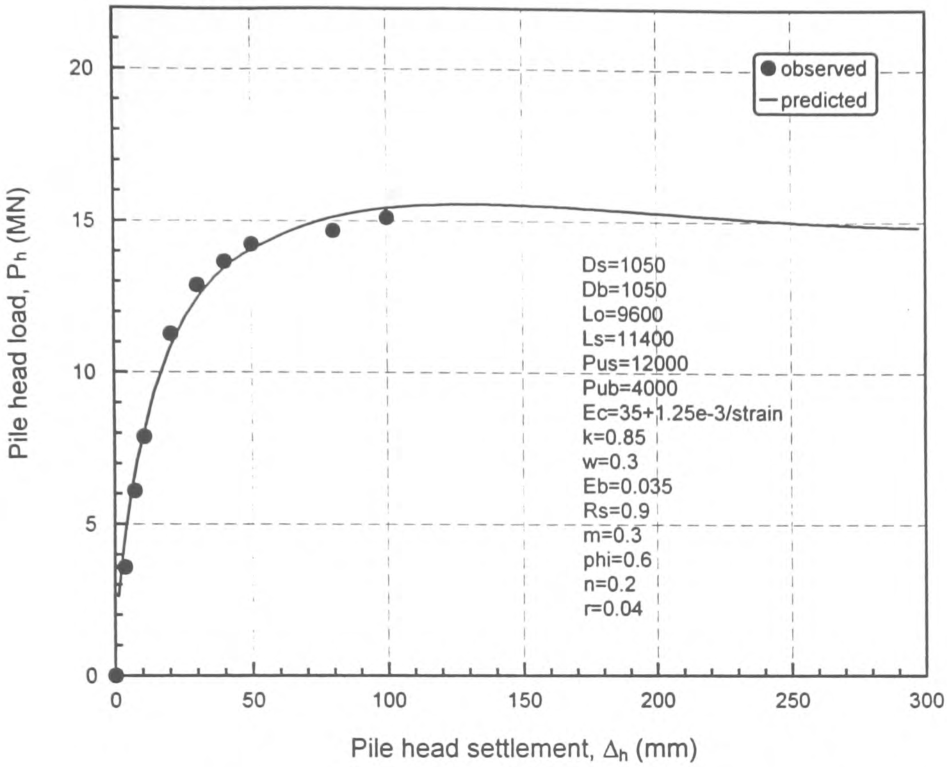

Fig. 7.9(a):Test pile in Keuper marl at Eastmoors link(Pile No.4), Peripheral Distributor Road, Cardiff (Kilbourn et al.1988) -Load versus settlement plot

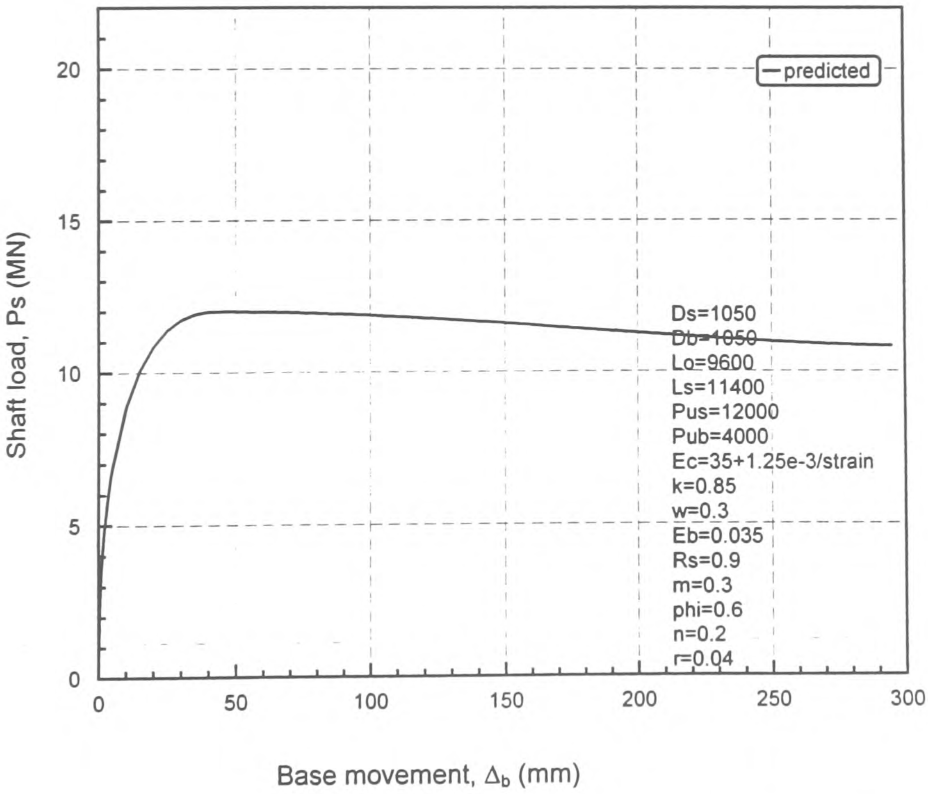

Fig. 7.9(b):Test pile in Keuper marl at Eastmoors link(Pile No.4), Peripheral Distributor Road, Cardiff (Kilbourn et al.1988) -Shaft load versus base movement plot

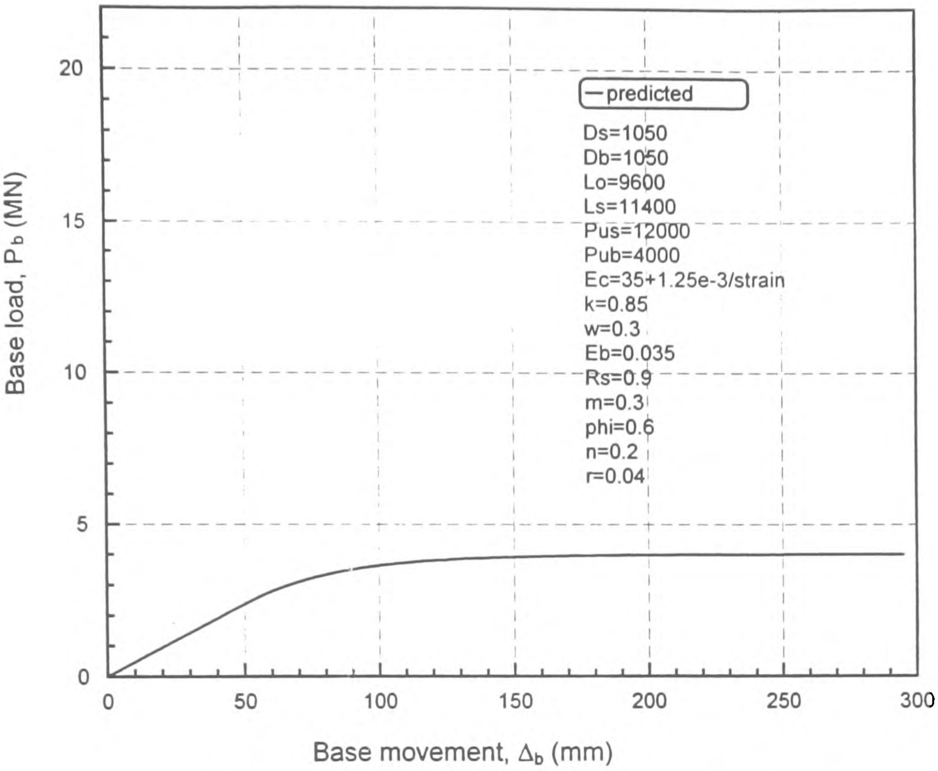

Fig. 7.9(c):Test pile in Keuper marl at Eastmoors link(Pile No.4), Peripheral Distributor Road, Cardiff (Kilbourn et al.1988) -Base load versus base movement plot

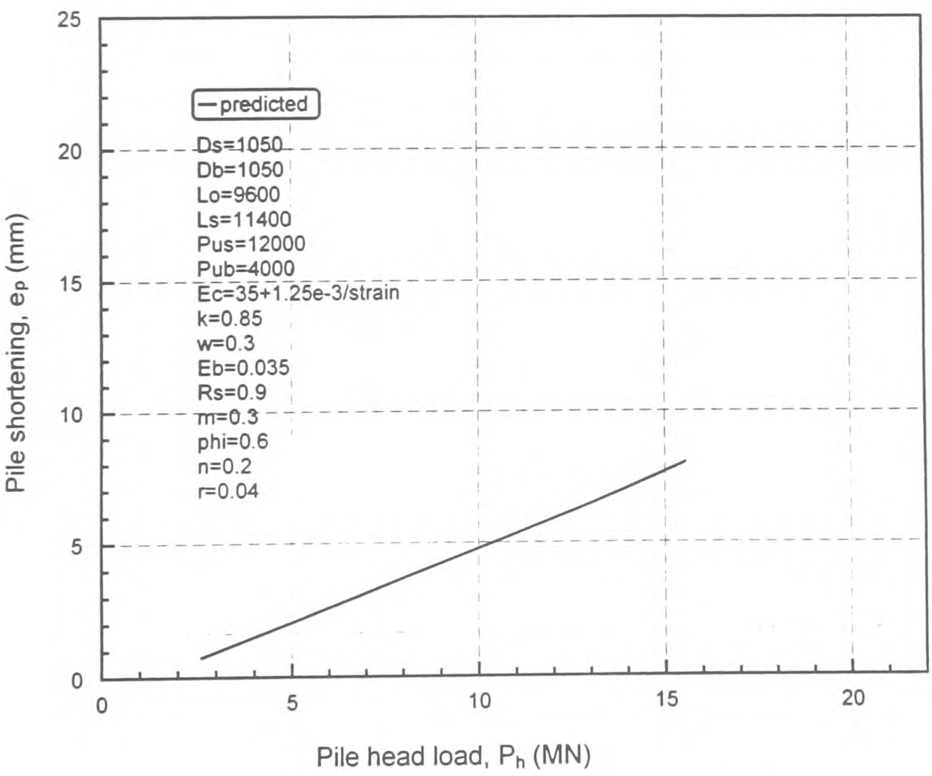

Fig. 7.9(d):Test pile in Keuper marl at Eastmoors link(Pile No.4), Peripheral Distributor Road, Cardiff (Kilbourn et al.1988) -Shortening versus applied load

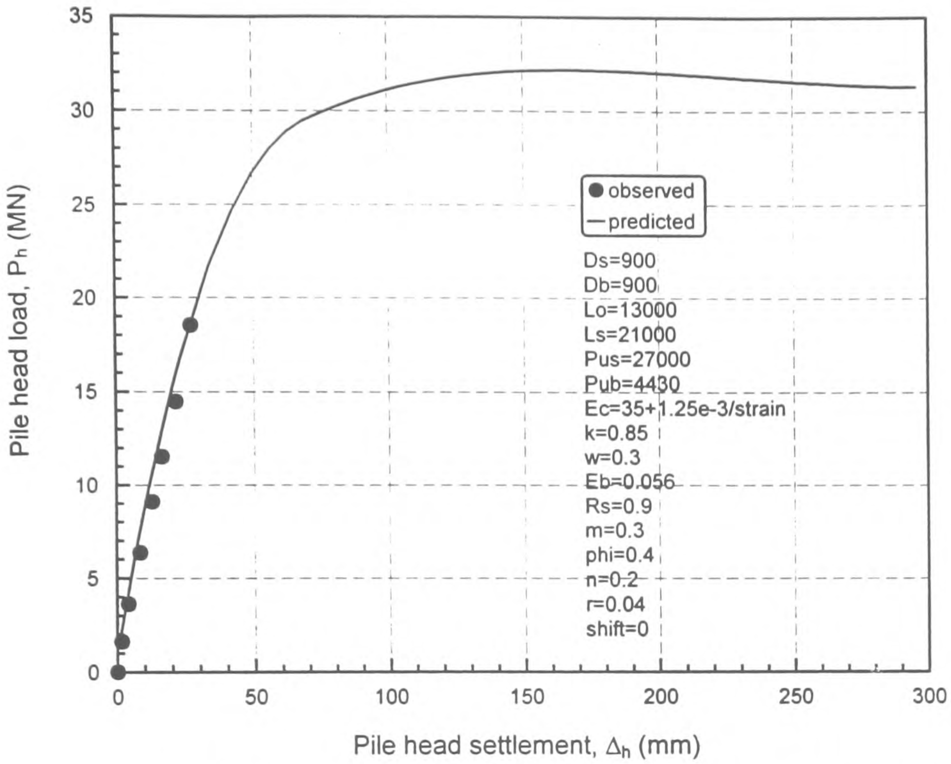

Fig. 7.10(a):Test pile in Keuper marl at Grangetown link(Test 1), Peripheral Distributor Road, Cardiff (Kilbourn et al.1988) -Load versus settlement plot

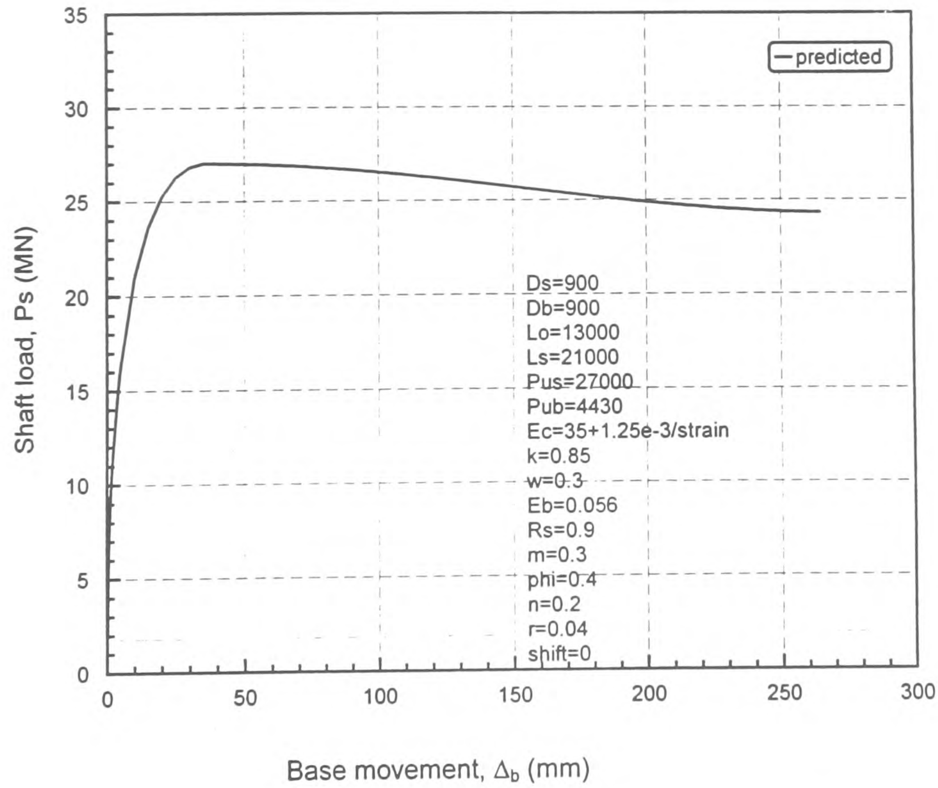

Fig. 7.10(b):Test pile in Keuper marl at Grangetown link(Test 1), Peripheral Distributor Road, Cardiff (Kilbourn et al.1988) -Shaft load versus base movement plot

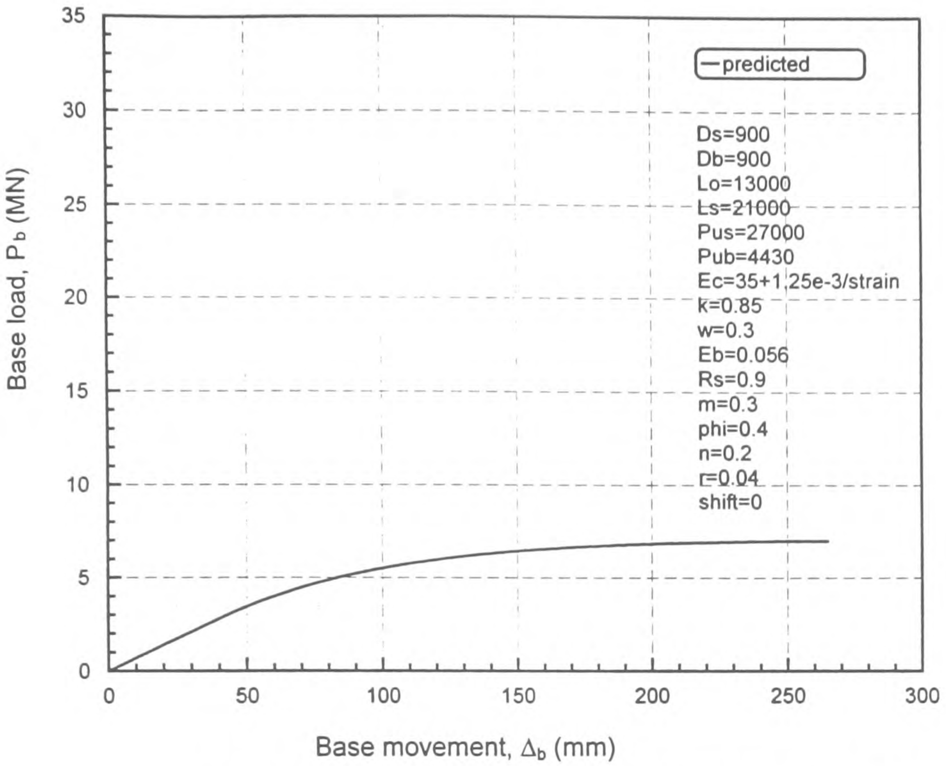

Fig. 7.10(c):Test pile in Keuper marl at Grangetown link(Test 1), Peripheral Distributor Road, Cardiff (Kilbourn et al.1988)
-Base load versus base movement plot

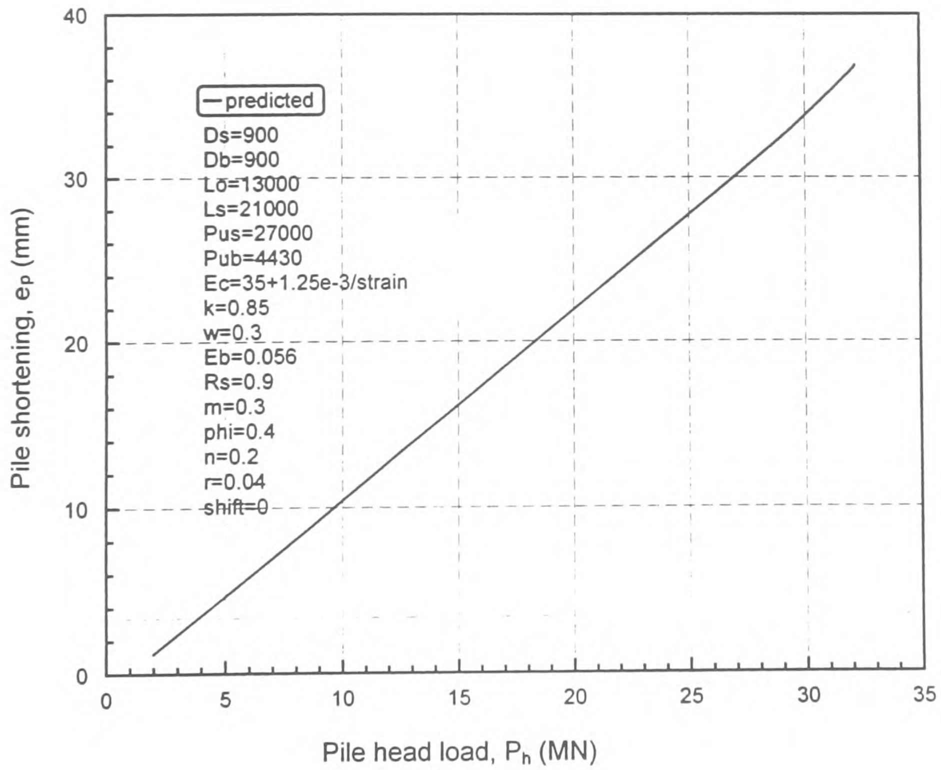

Fig. 7.10(d):Test pile in Keuper marl at Grangetown link(Test 1), Peripheral Distributor Road, Cardiff (Kilbourn et al.1988)
-Shortening versus applied load

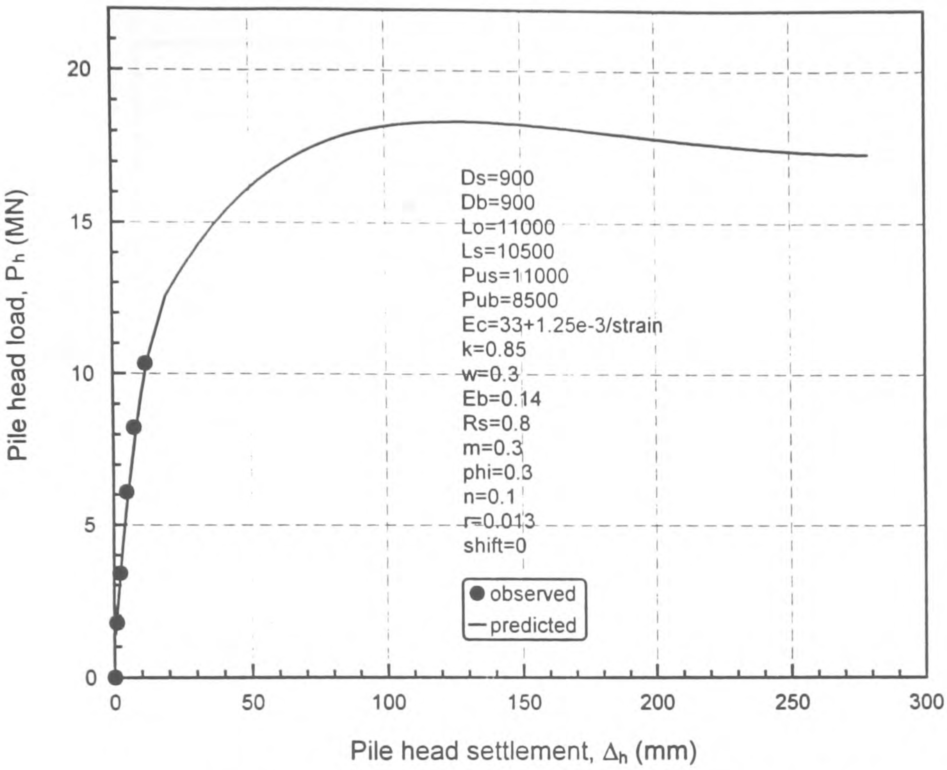

Fig. 7.11(a):Test pile in Keuper marl at Ely bridge, Peripheral Distributor Road, Cardiff (Kilbourn et al.1988) -Load versus settlement plot

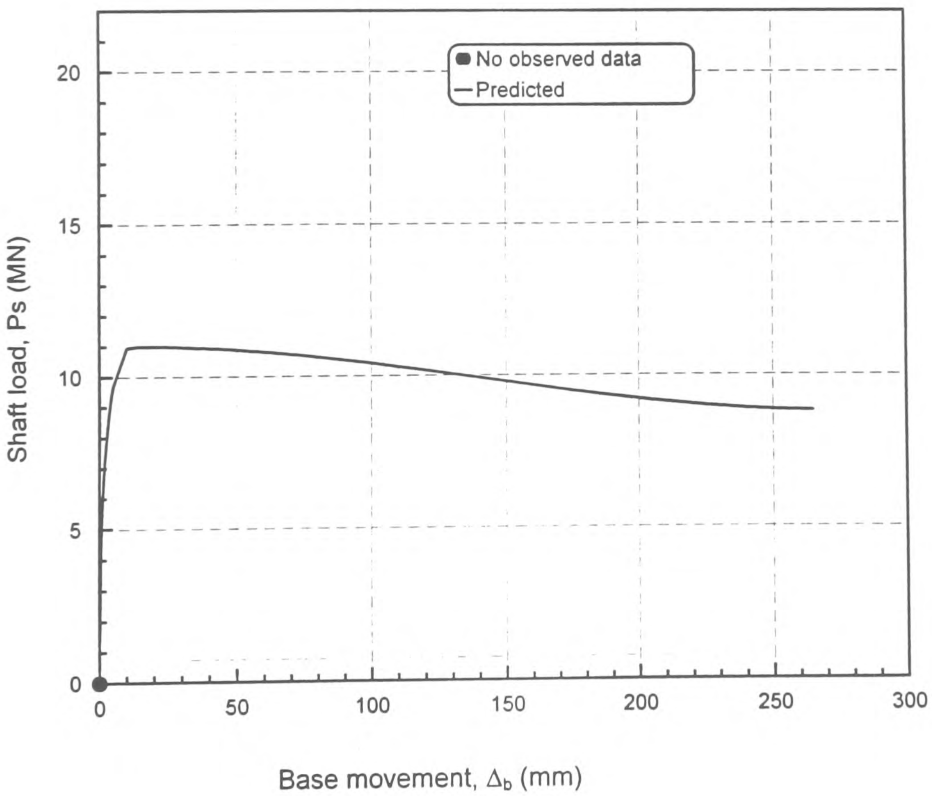

Fig. 7.11(b):Test pile in Keuper marl at Ely bridge, Peripheral Distributor Road, Cardiff (Kilbourn et al.1988) -Shaft load versus base movement plot

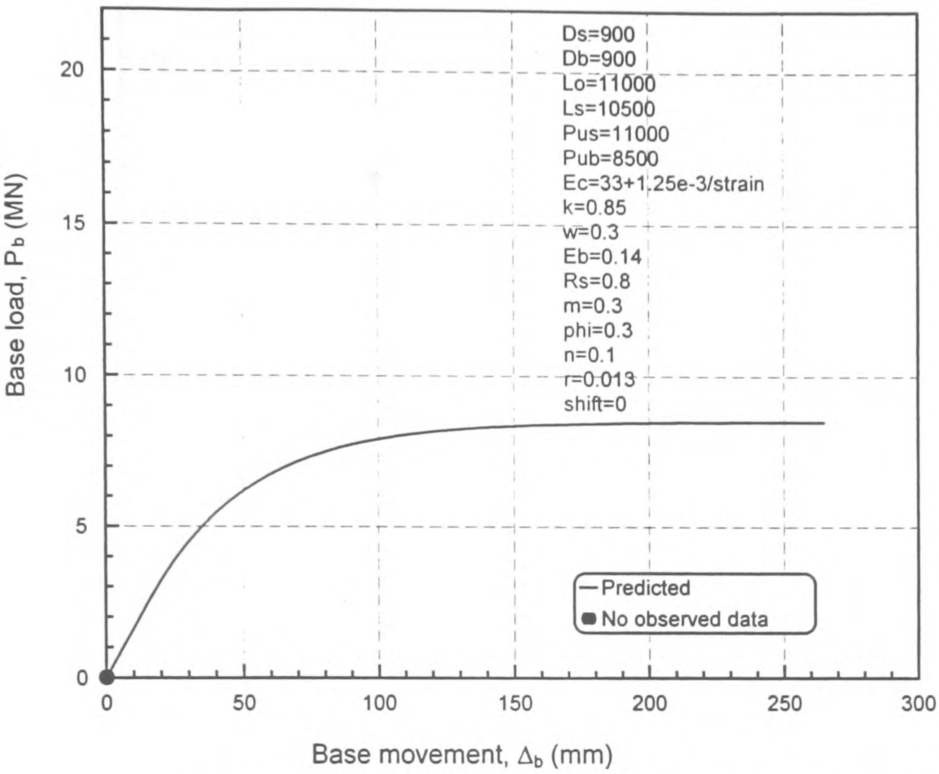

Fig. 7.11(c):Test pile in Keuper marl at Ely bridge, Peripheral Distributor Road, Cardiff (Kilbourn et al.1988) -Base load versus base movement plot

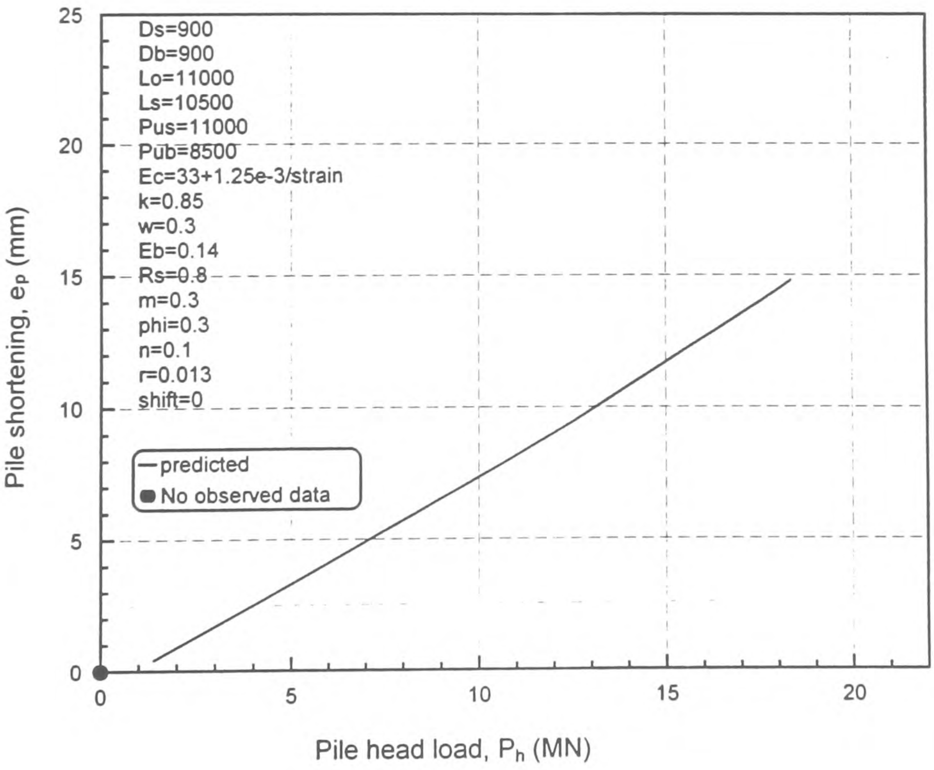

Fig. 7.11(d):Test pile in Keuper marl at Ely bridge, Peripheral Distributor Road, Cardiff (Kilbourn et al.1988) -Shortening versus applied load

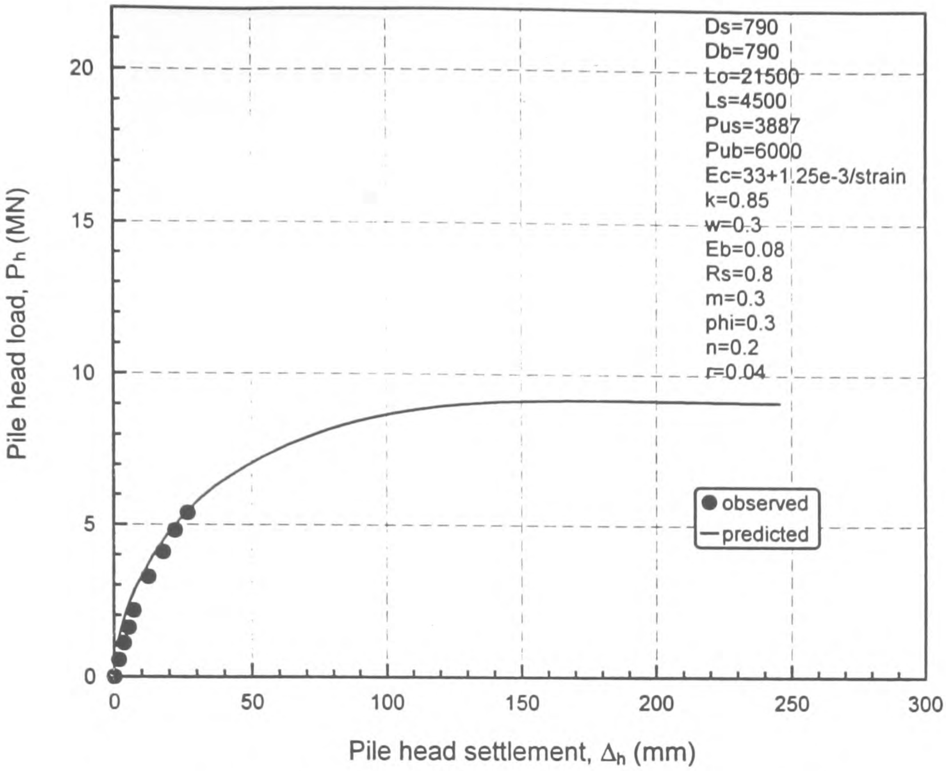

Fig. 7.12(a):Test pile in Keuper marl at Clarence road bridge, Peripheral Distributor road, Cardiff (Kilbourn et al.1988)
Load versus settlement plot

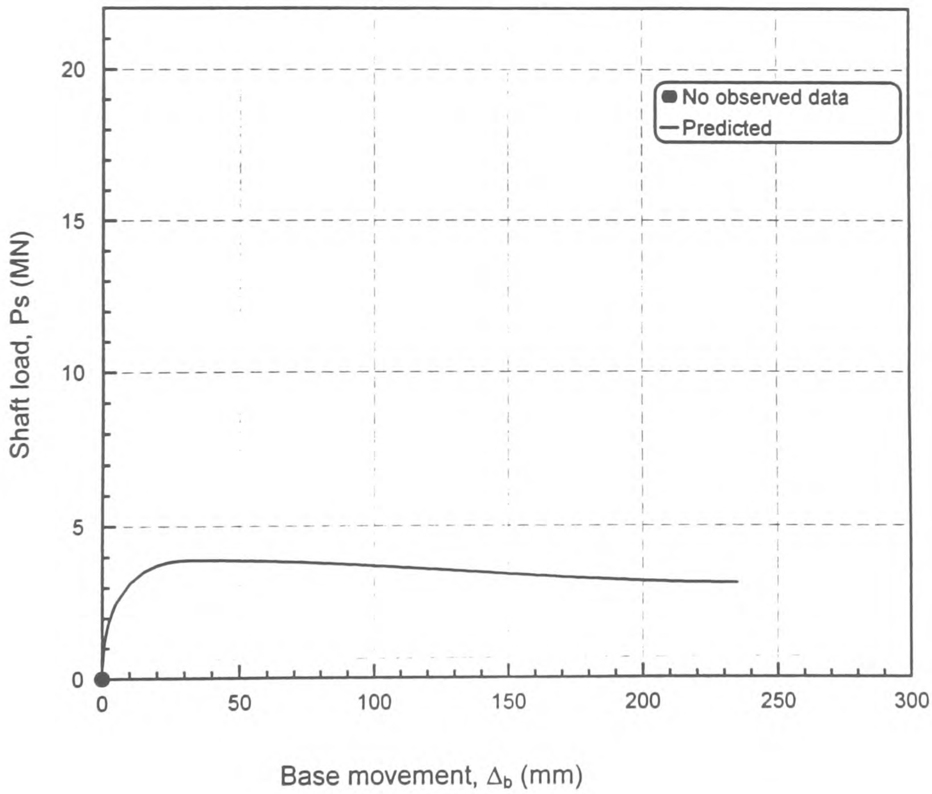

Fig. 7.12(b):Test pile in Keuper marl at Clarence road bridge, Peripheral Distributor road, Cardiff (Kilbourn et al.1988)
Shaft load versus base movement plot

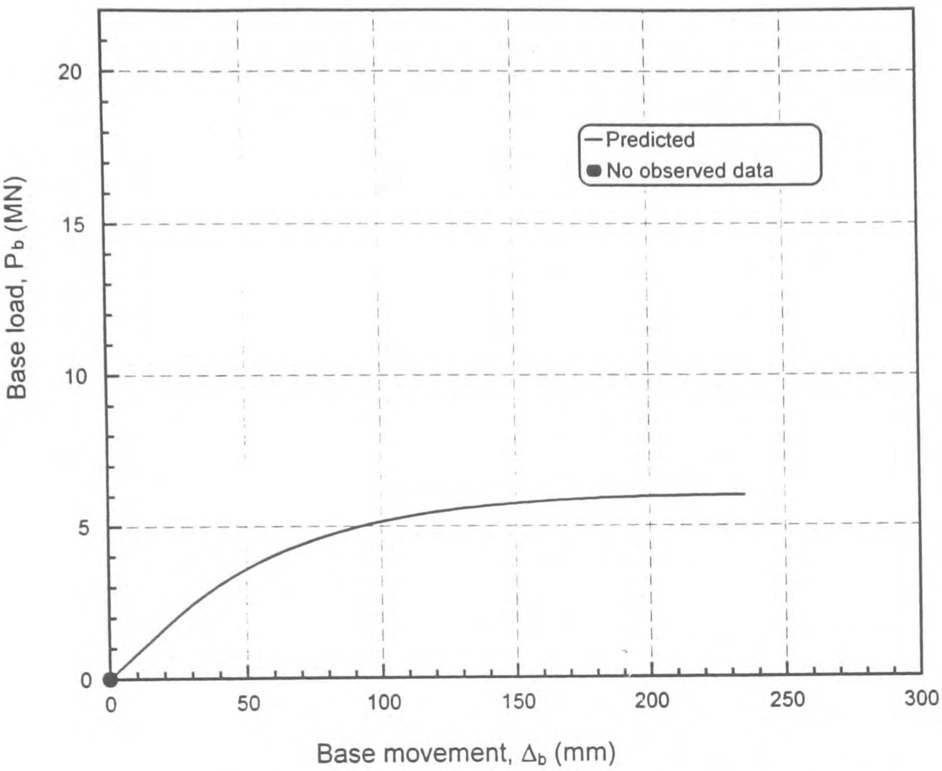

Fig. 7.12(c):Test pile in Keuper marl at Clarence road bridge, Peripheral Distributor road, Cardiff (Kilbourn et al.1988)
Base load versus base movement plot

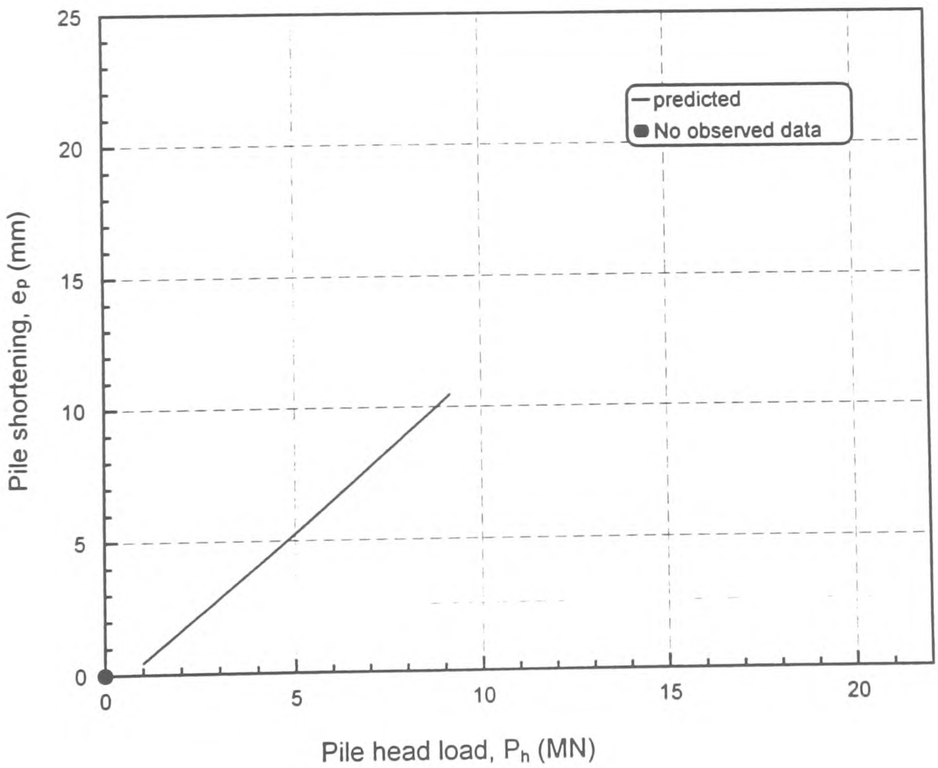

Fig. 7.12(d):Test pile in Keuper marl at Clarence road bridge, Peripheral Distributor road, Cardiff (Kilbourn et al.1988)
Shortening versus applied load

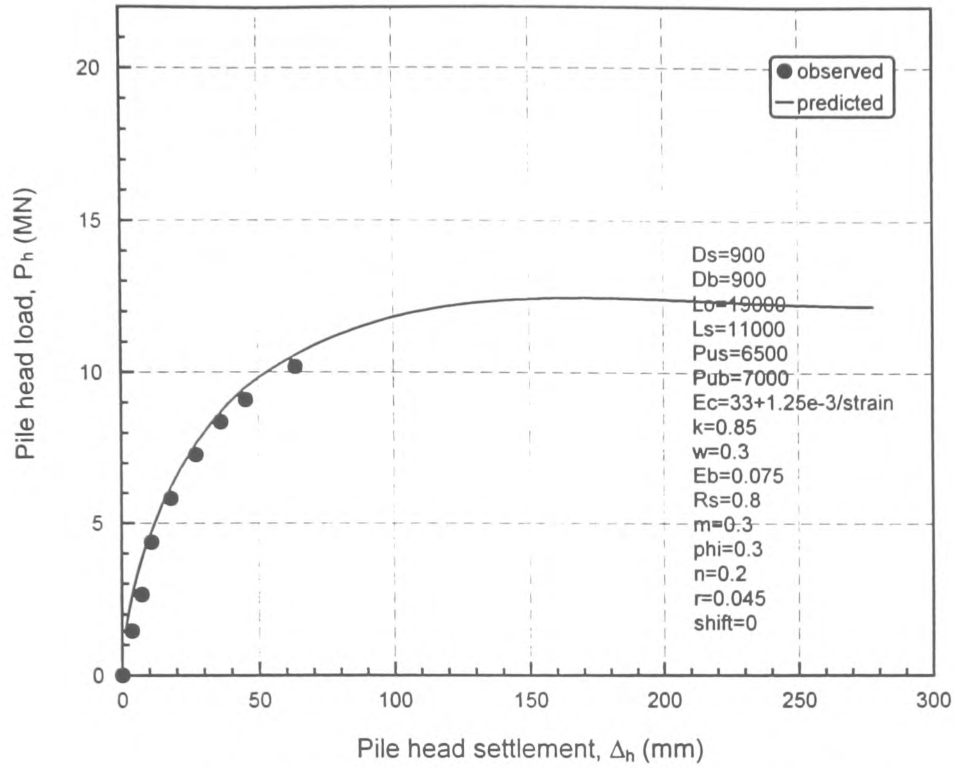

Fig. 7.13(a):Test pile in Keuper marl at Cogan spur, Peripheral Distributor road, Cardiff (Kilbourn et al.1988)
Load versus settlement plot

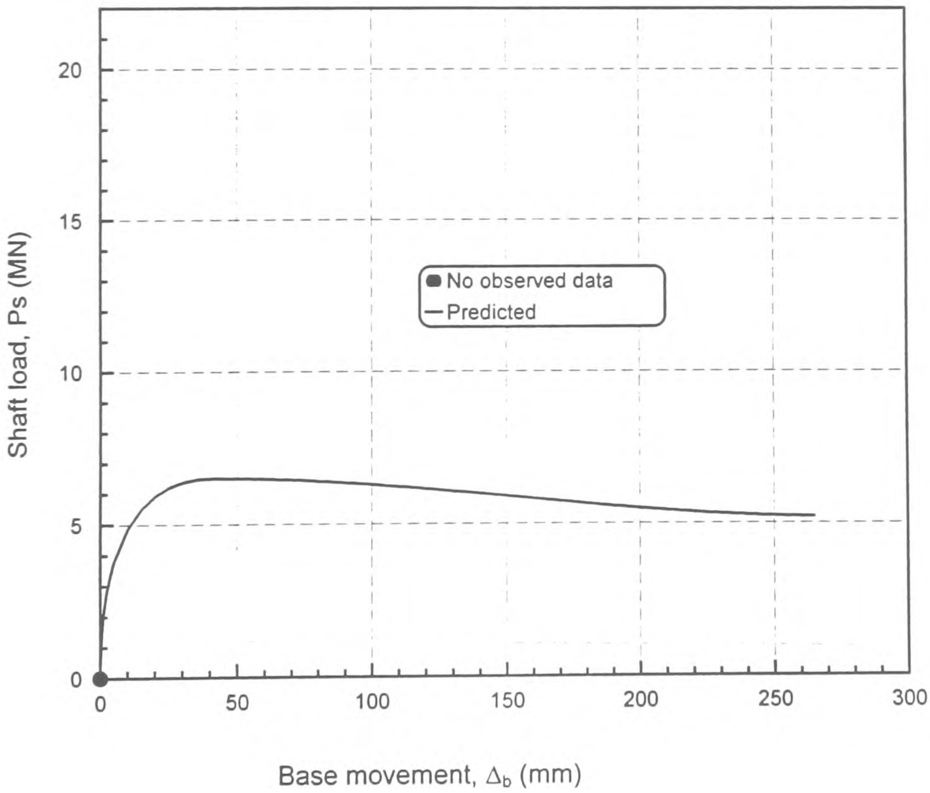

Fig. 7.13(b):Test pile in Keuper marl at Cogan spur,Peripheral Distributor road, Cardiff (Kilbourn et al.1988)
Shaft load versus base movement plot

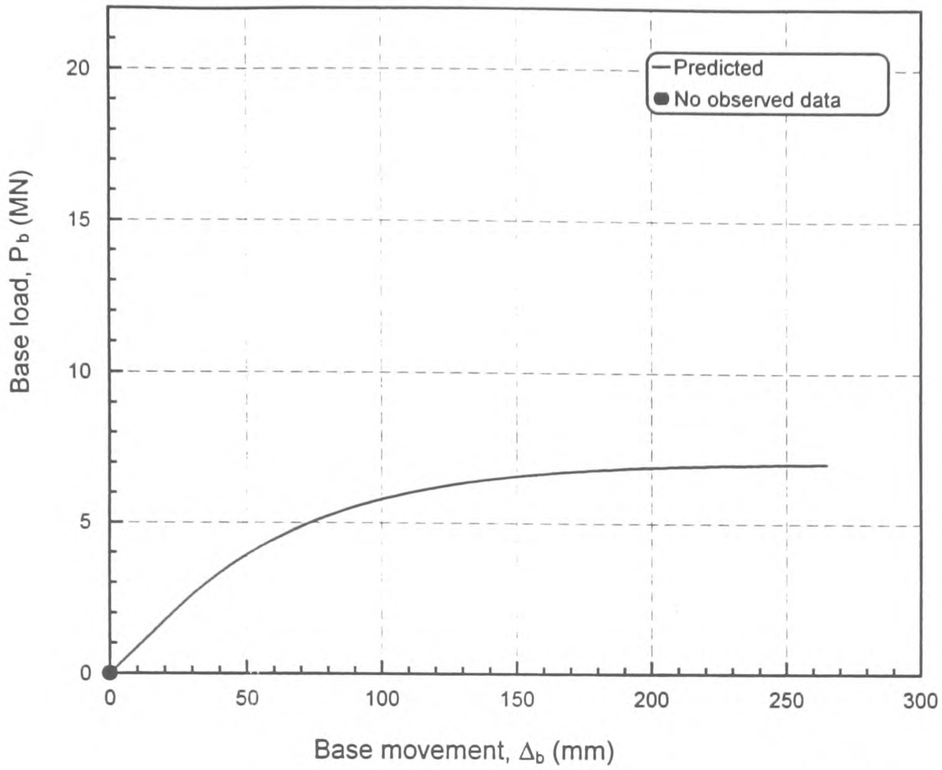

Fig. 7.13(c):Test pile in Keuper marl at Cogan spur, Peripheral Distributor road, Cardiff (Kilbourn et al.1988)
Base load versus base movement plot

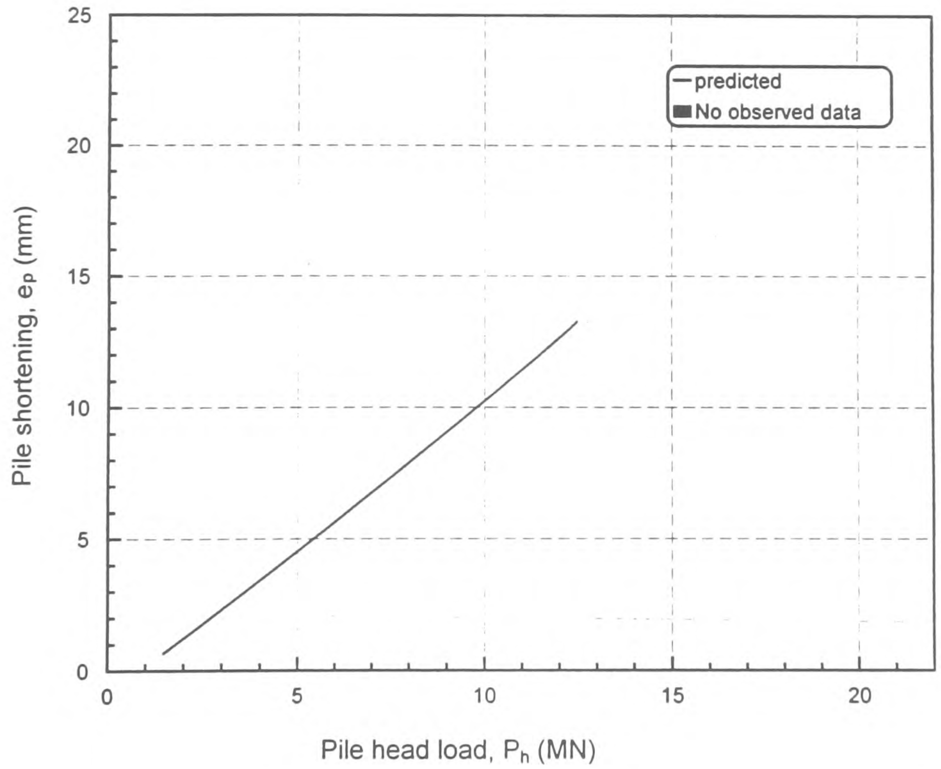

Fig. 7.13(d):Test pile in Keuper marl at Cogan spur,Peripheral Distributor road, Cardiff (Kilbourn et al.1988)
Shortening versus applied load

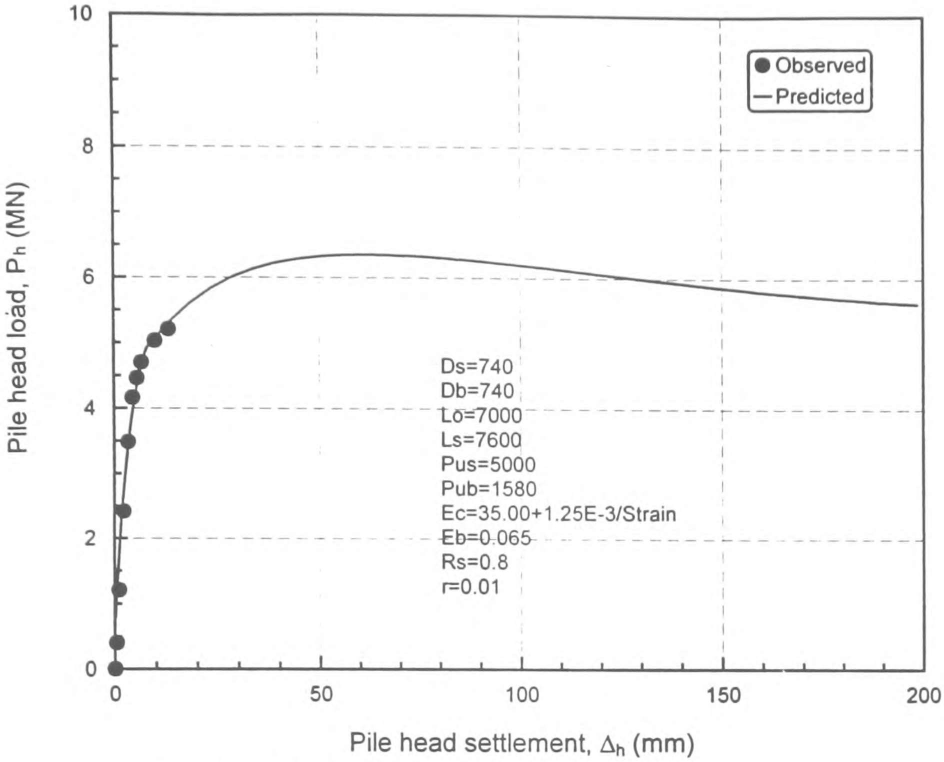

Fig.7.14(a)Test pile in Keuper marl at Kilroot, County Antrim, Northern Ireland (Leach et.al.1976)-Load Vs settlement plot

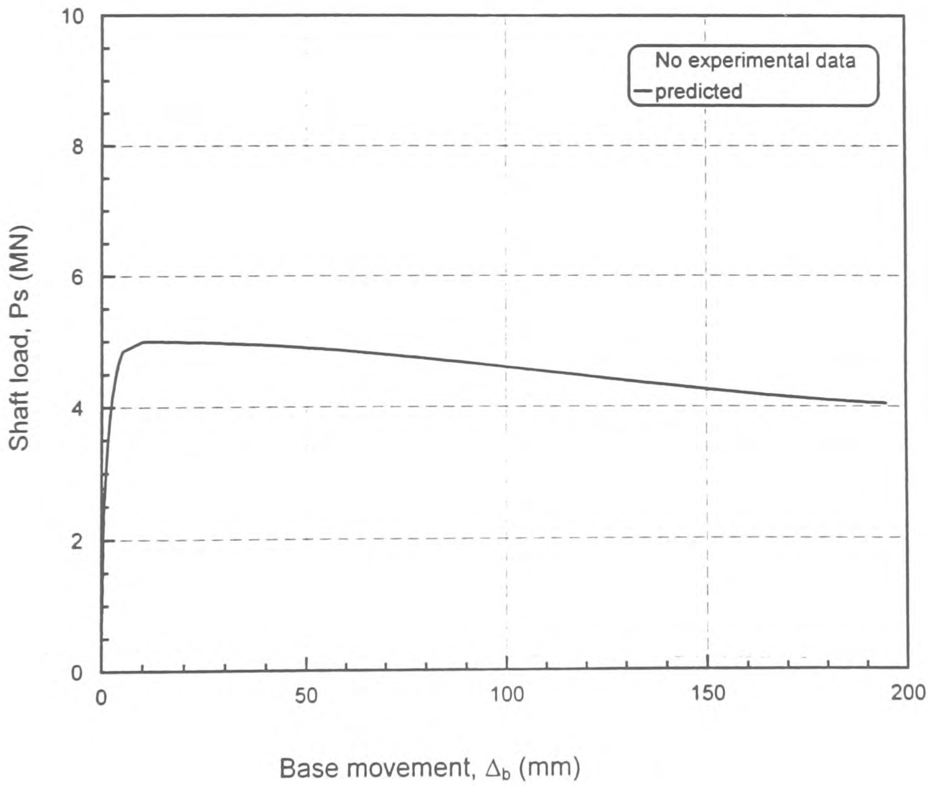

Fig.7.14(b)Test pile in Keuper marl at Kilroot, County Antrim, Northern Ireland (Leach et.al.1976)-Shaft load Vs base movement

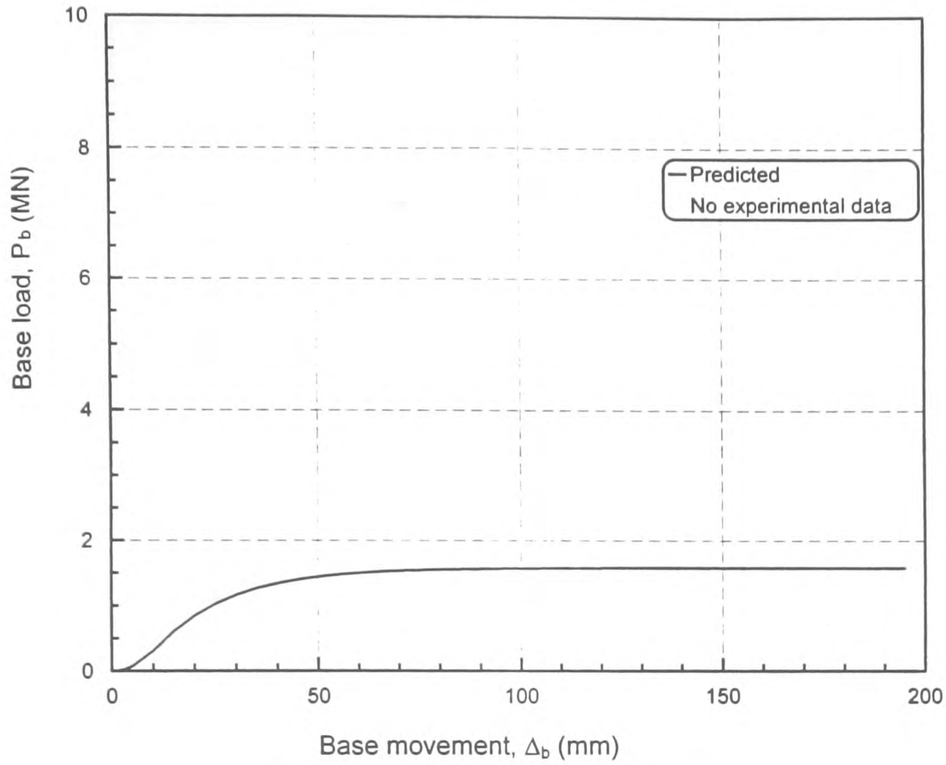

Fig.7.14(c)Test pile in Keuper marl at Kilroot, County Antrim, Northern Ireland (Leach et.al.1976)-Base load Vs base movement

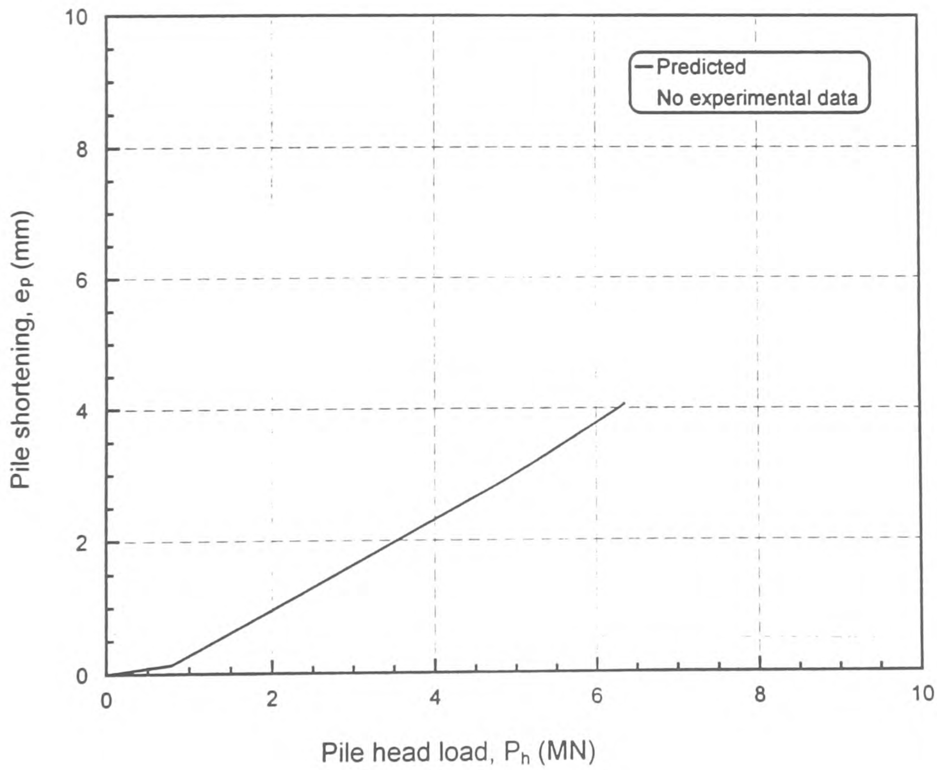

Fig.7.14(d)Test pile in Keuper marl at Kilroot, County Antrim, Northern Ireland (Leach et.al.1976)-Shortening Vs aplied load

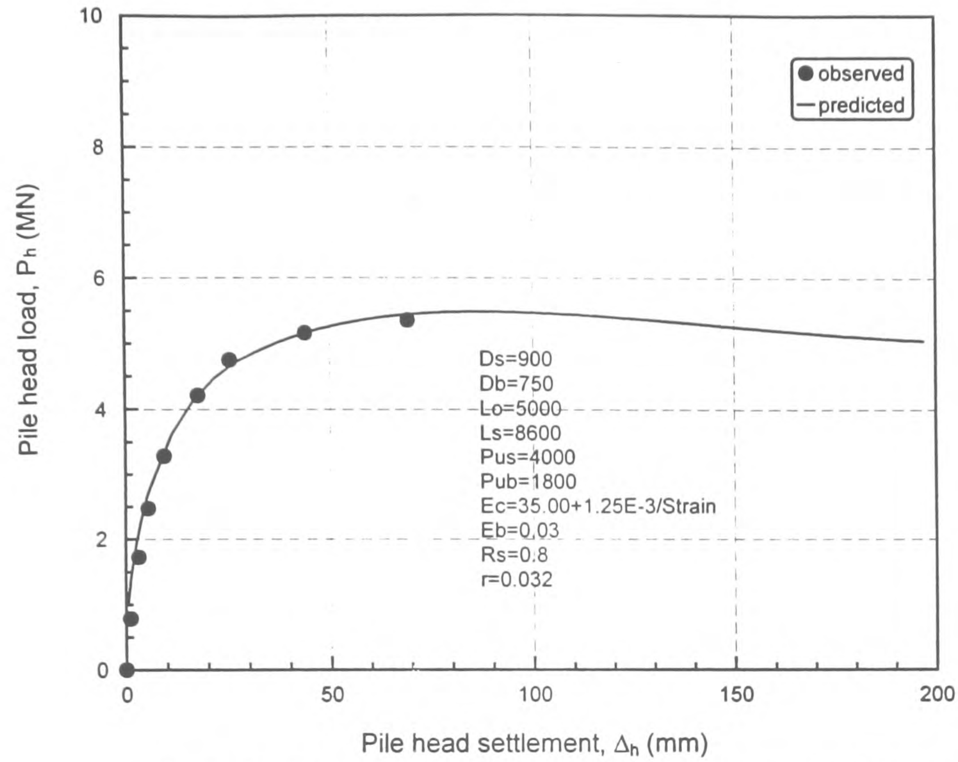

Fig.7.15(a)Test pile in Keuper marl-Birmingham International Arena, (Dauncy and Woodland,1983)-Load Vs settlement plot

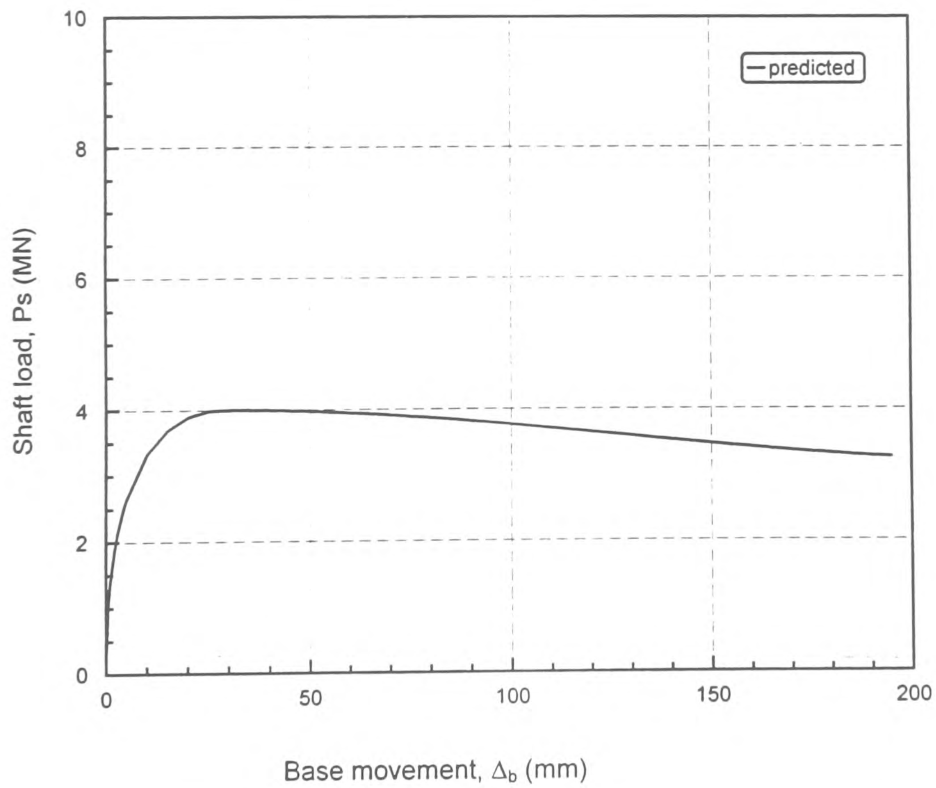

Fig.7.15(b)Test pile in Keuper marl-Birmingham International Arena, (Dauncy and Woodland,1983)-Shaft load Vs base movement

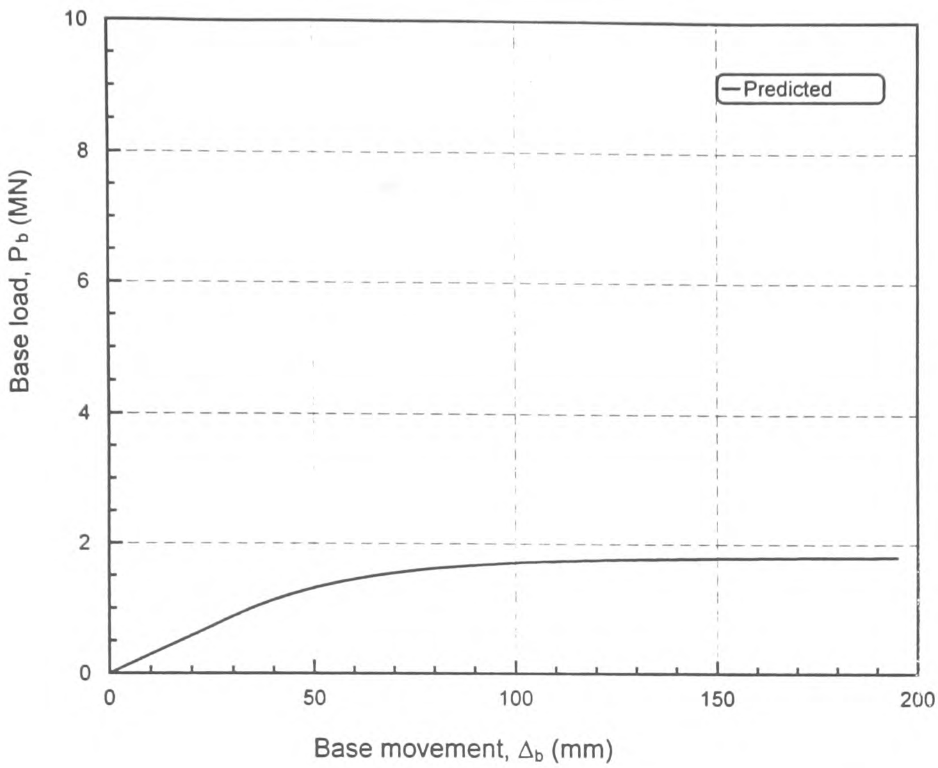

Fig.7.15(c)Test pile in Keuper marl-Birmingham International Arena, (Dauncy and Woodland,1983)-Base load Vs base movement

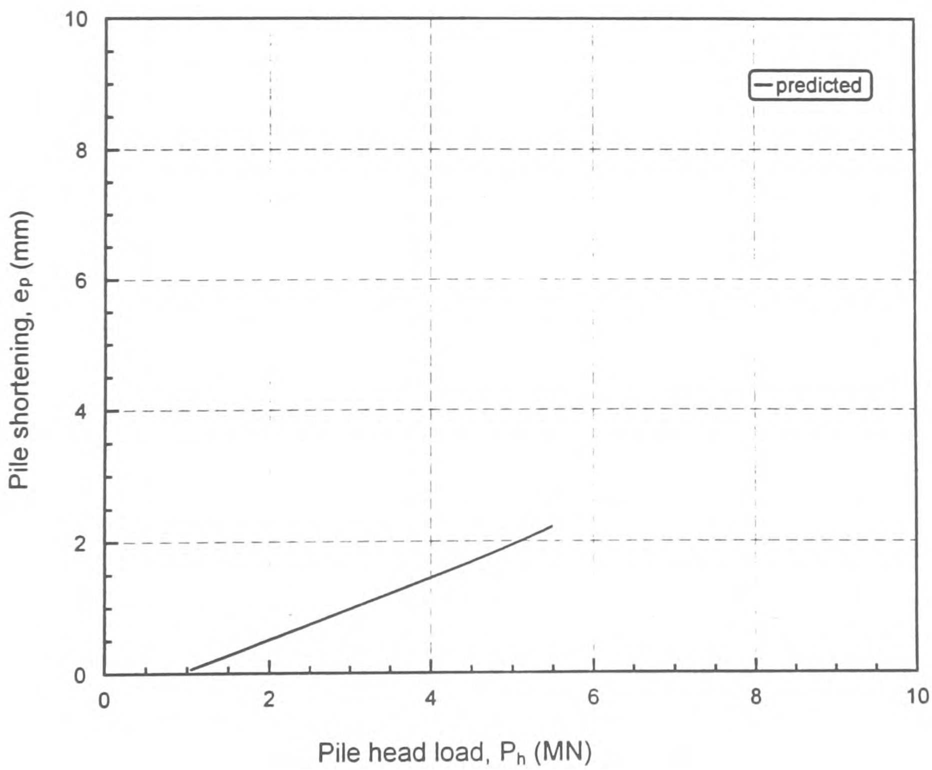

Fig.7.15(d)Test pile in Keuper marl-Birmingham International Arena, (Dauncy and Woodland,1983)-Shortening Vs aplied load

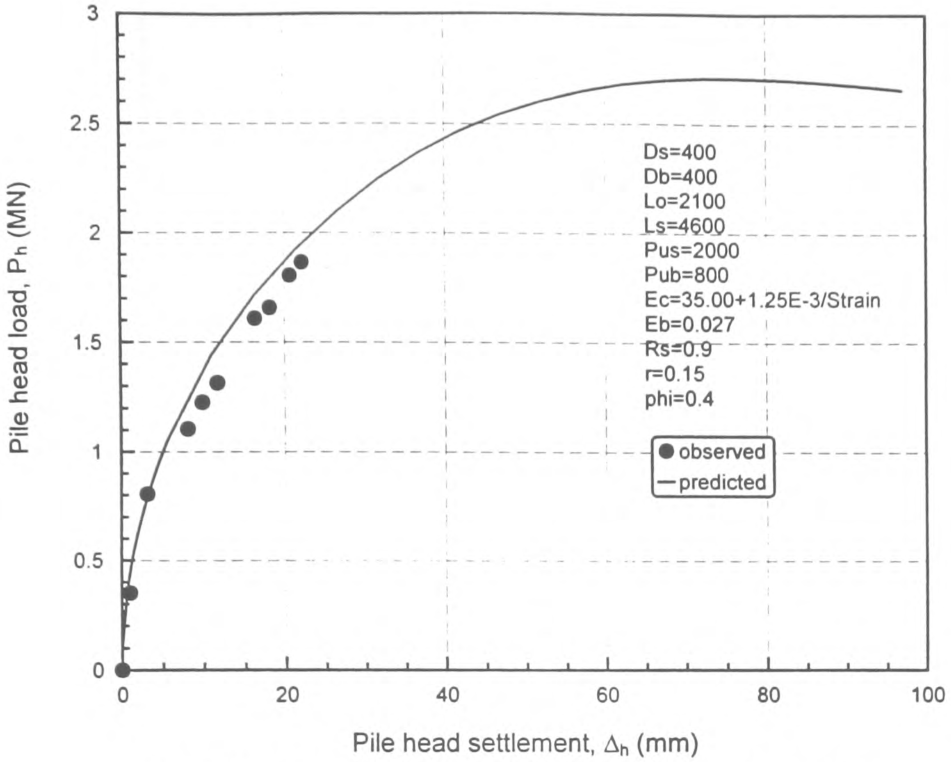

Fig.7.16(a)Test pile in Keuper marl-King's Norton, Birmingham (Chandler and Davis, 1973)-Load Vs settlement plot

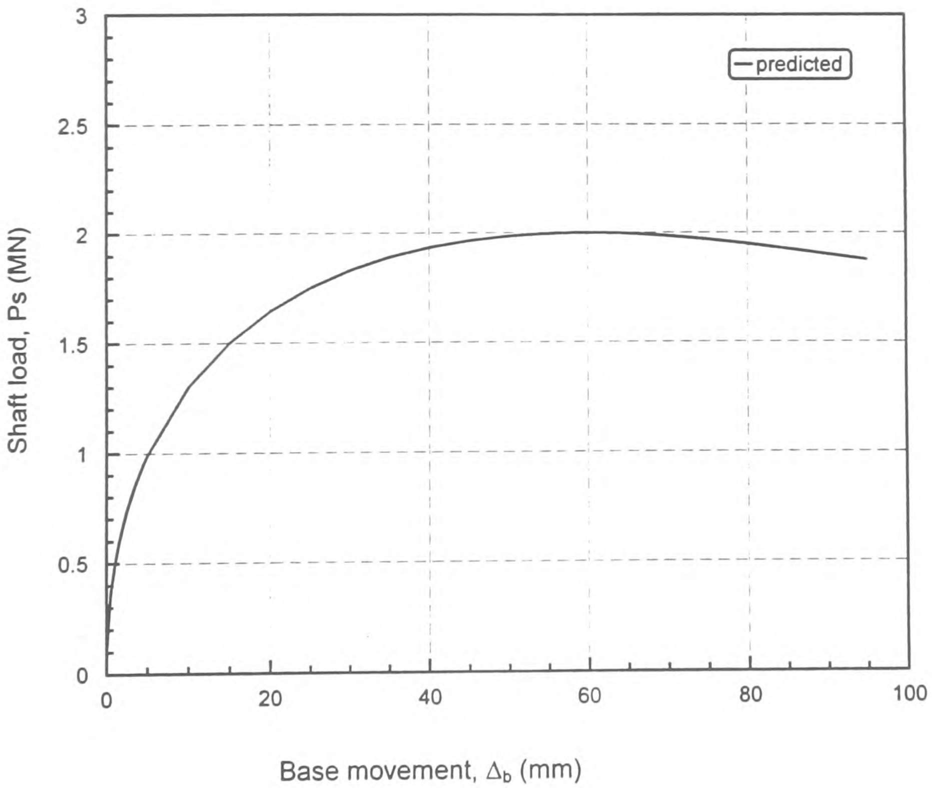

Fig.7.16(b)Test pile in Keuper marl-King's Norton, Birmingham (Chandler and Davis, 1973)-Shaft load Vs base movement

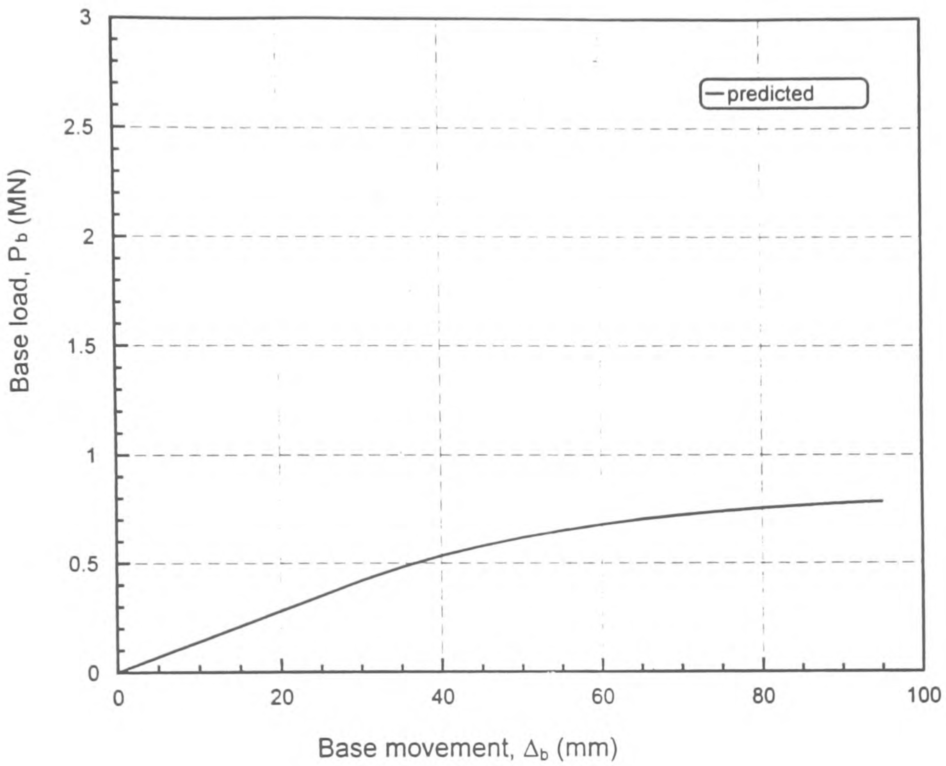

Fig.7.16(c)Test pile in Keuper marl-King's Norton, Birmingham (Chandler and Davis, 1973)-Base load Vs base movement

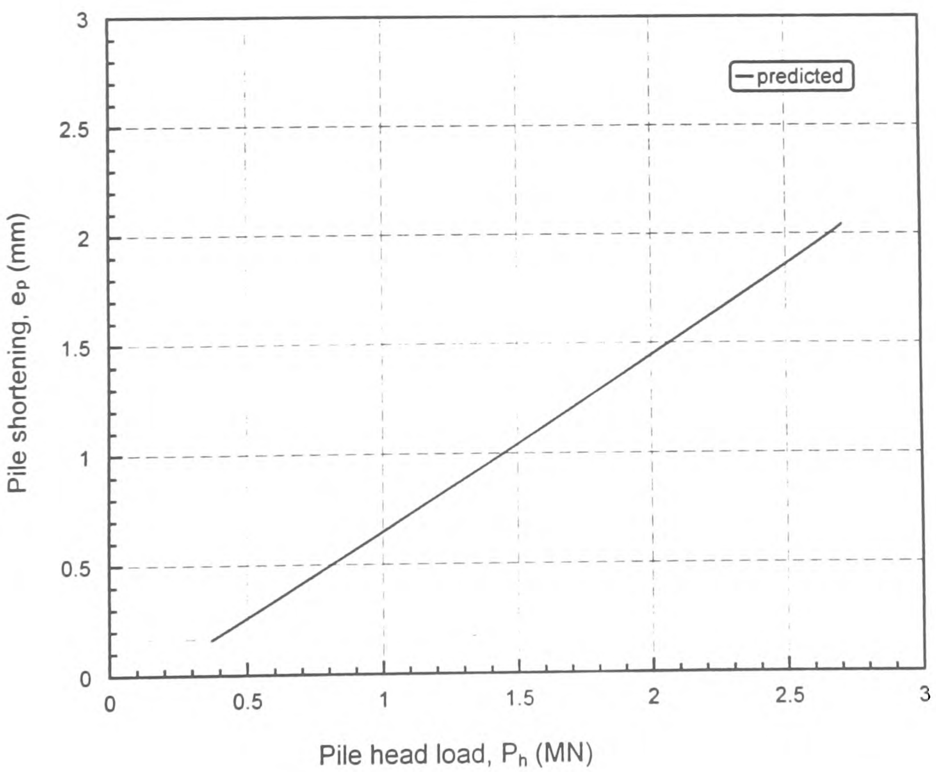

Fig.7.16(d)Test pile in Keuper marl-King's Norton, Birmingham (Chandler and Davis, 1973)-Shortening Vs aplied load

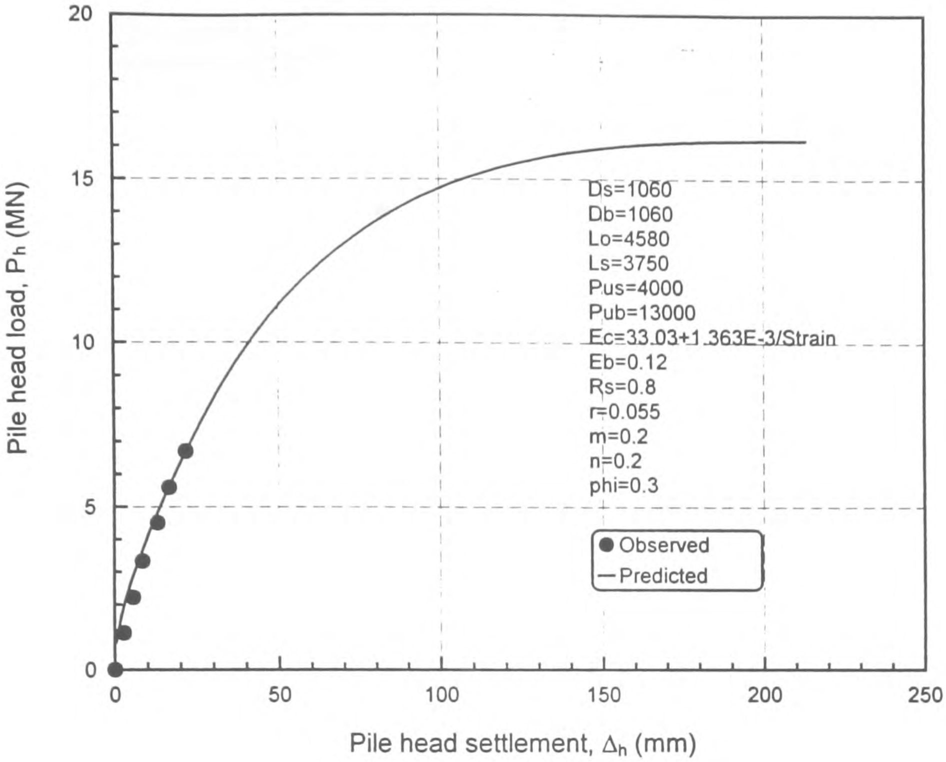

Fig. 7.17(a):Test pile at Coventry Point,Coventry (Rock socket pile)
-Load Vs settlement

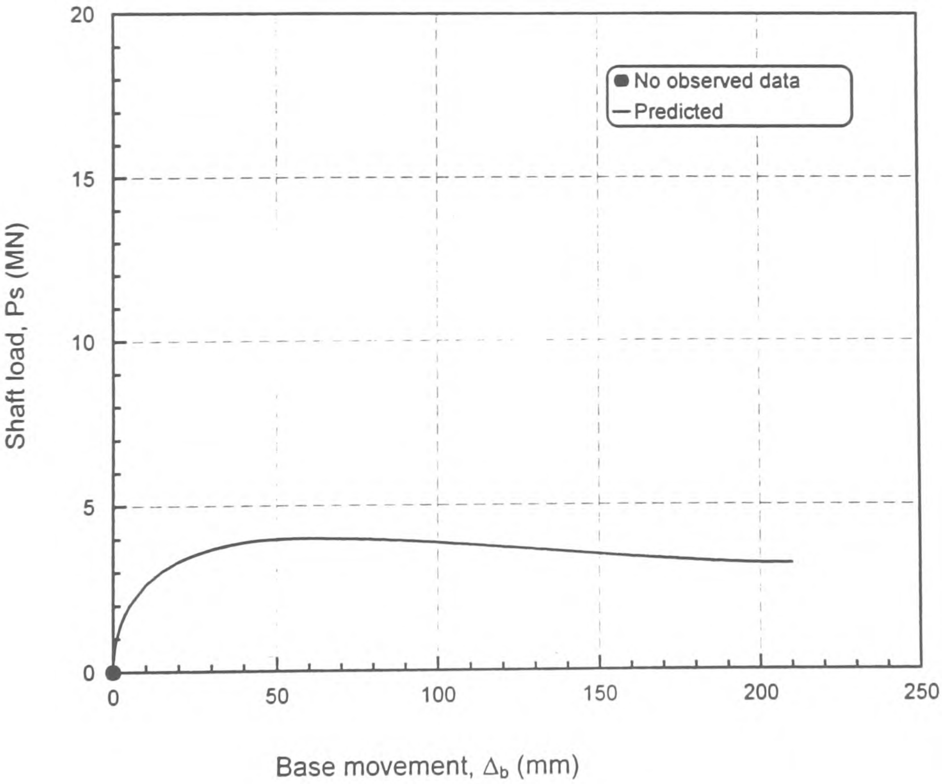

Fig. 7.17(b):Test pile at Coventry Point,Coventry (Rock socket pile)
-Shaft load Vs base movement

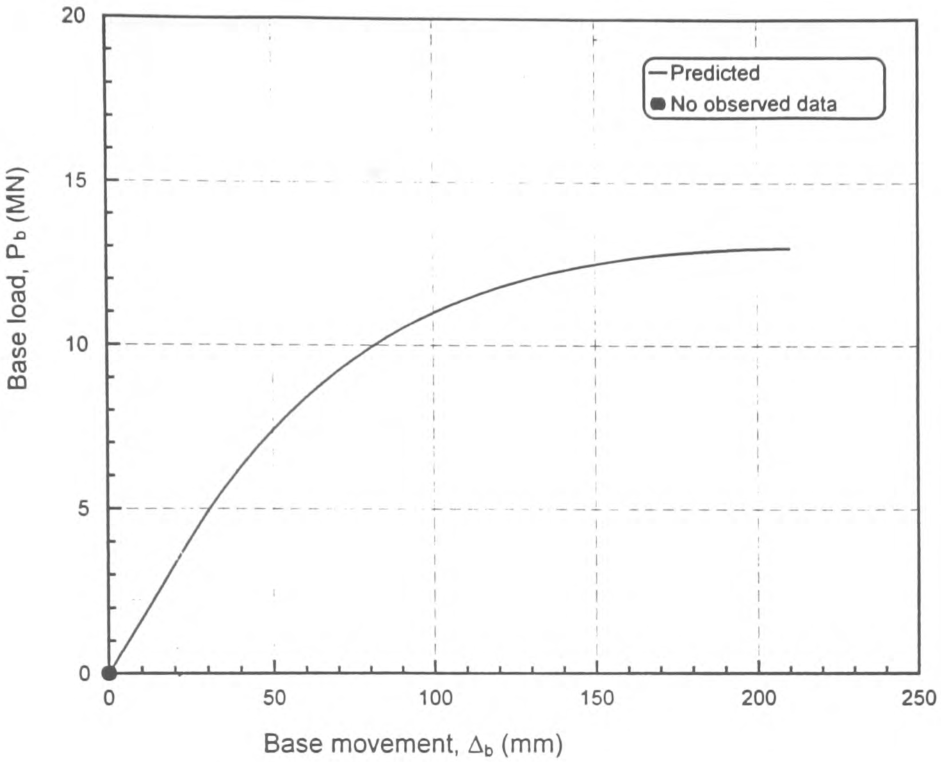

Fig. 7.17(c):Test pile at Coventry Point,Coventry (Rock socket pile)
-Base load Vs base movement

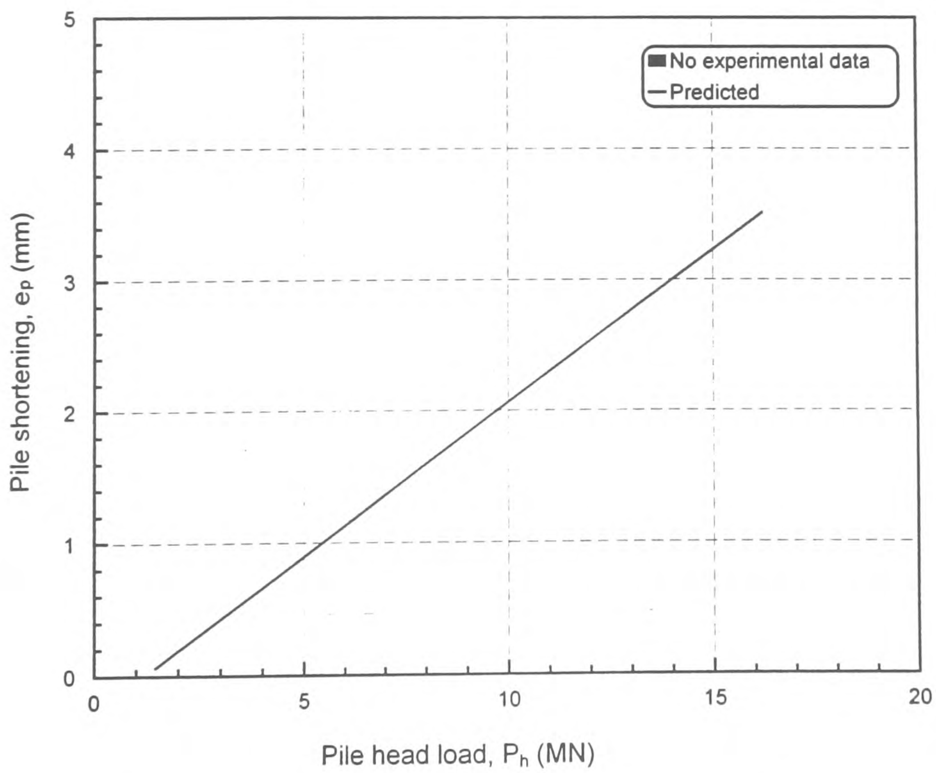

Fig. 7.17(d):Test pile at Coventry Point,Coventry (Rock socket pile)
-Shortening Vs applied load

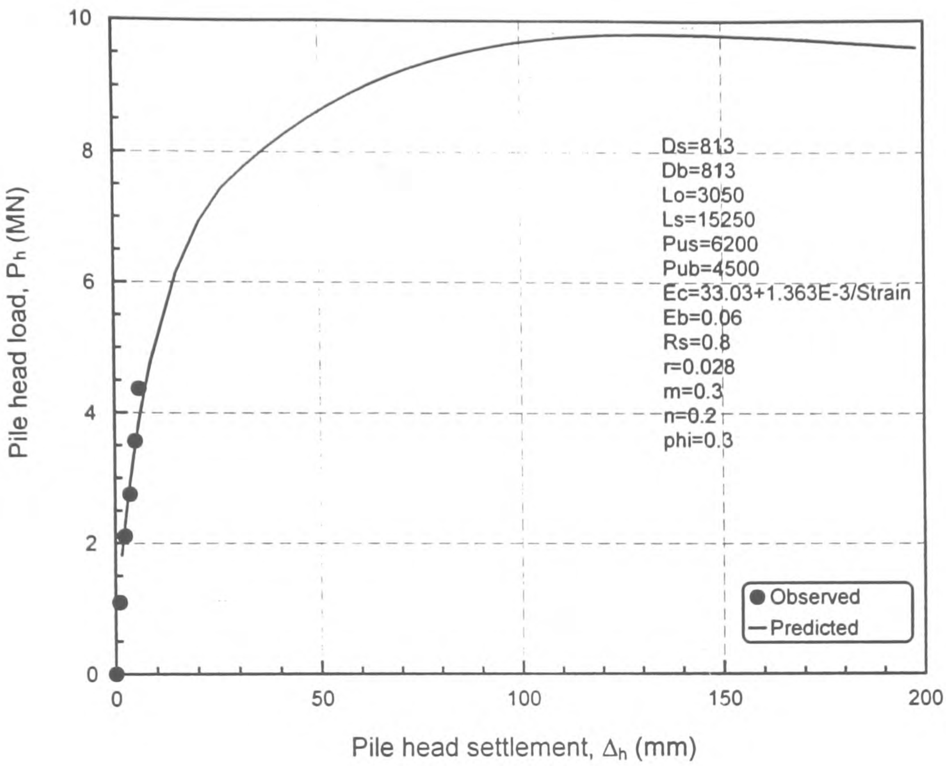

Fig. 7.18(a):Test pile at Leicester -Load Vs settlement

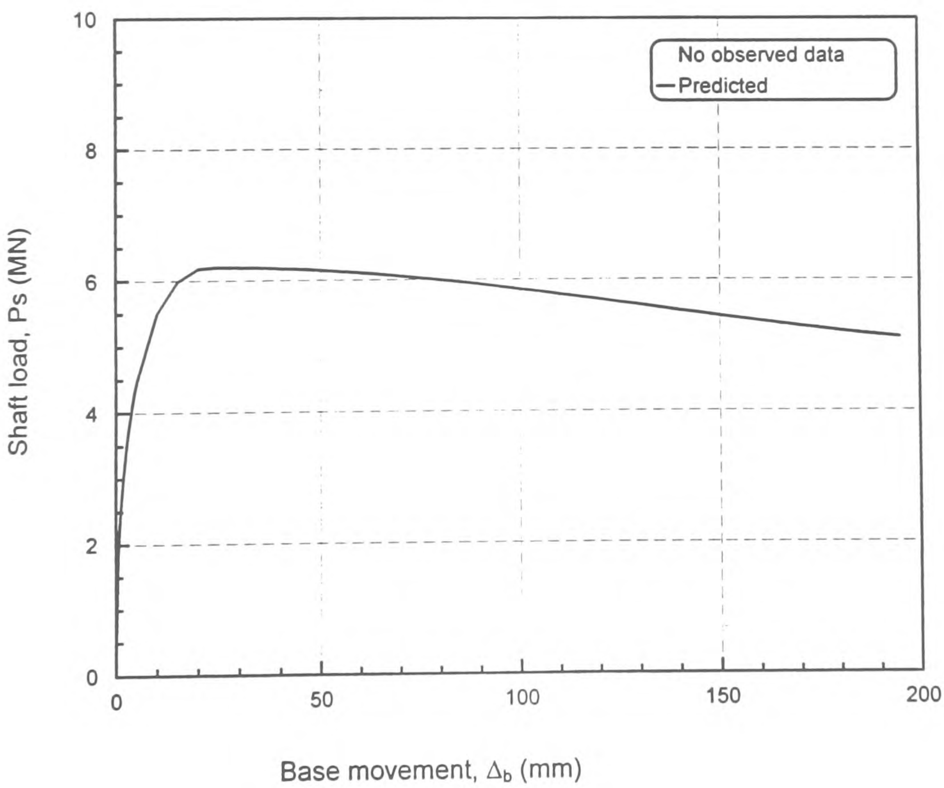

Fig. 7.18(b):Test pile at Leicester -Shaft load Vs base movement

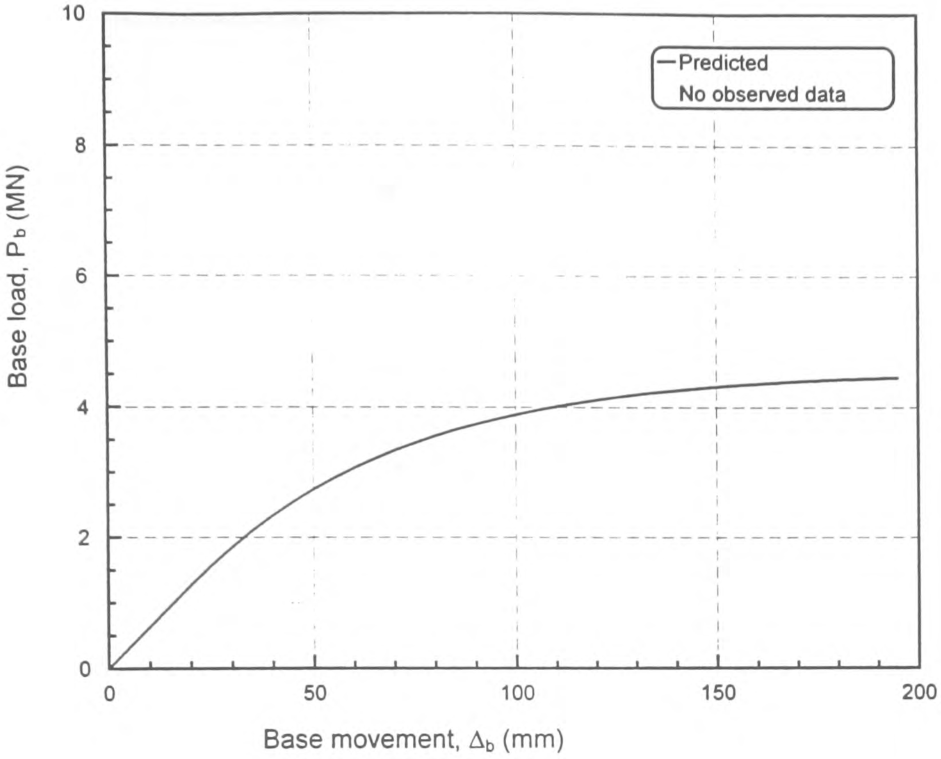

Fig. 7.18(c):Test pile at Leicester -Base load Vs base movement

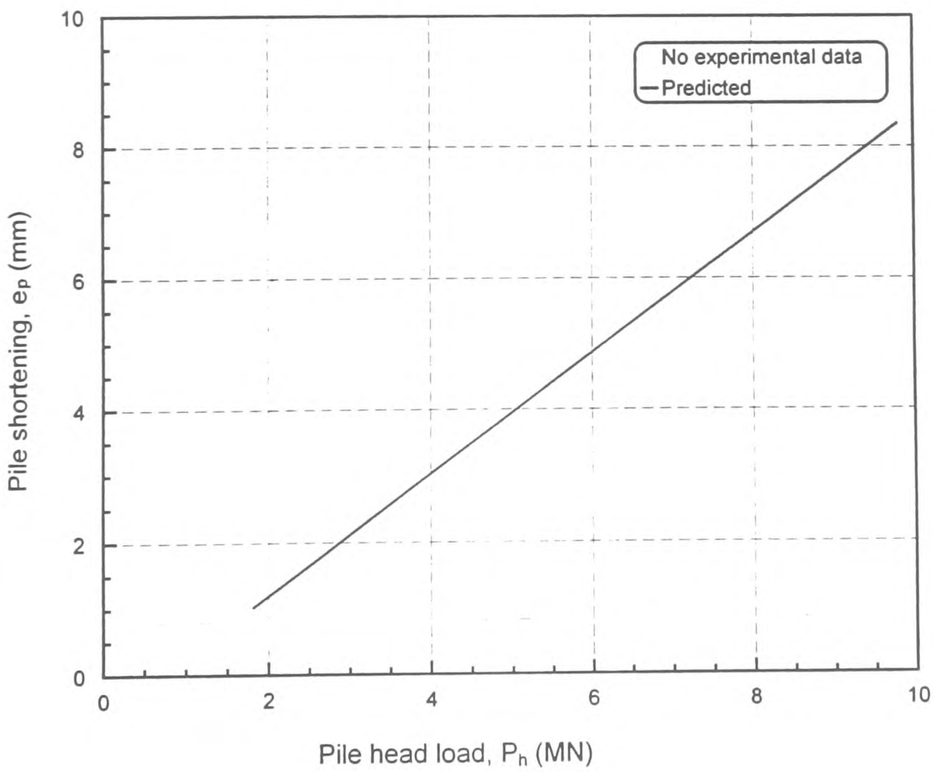

Fig. 7.18(d):Test pile at Leicester -Shortening Vs applied load

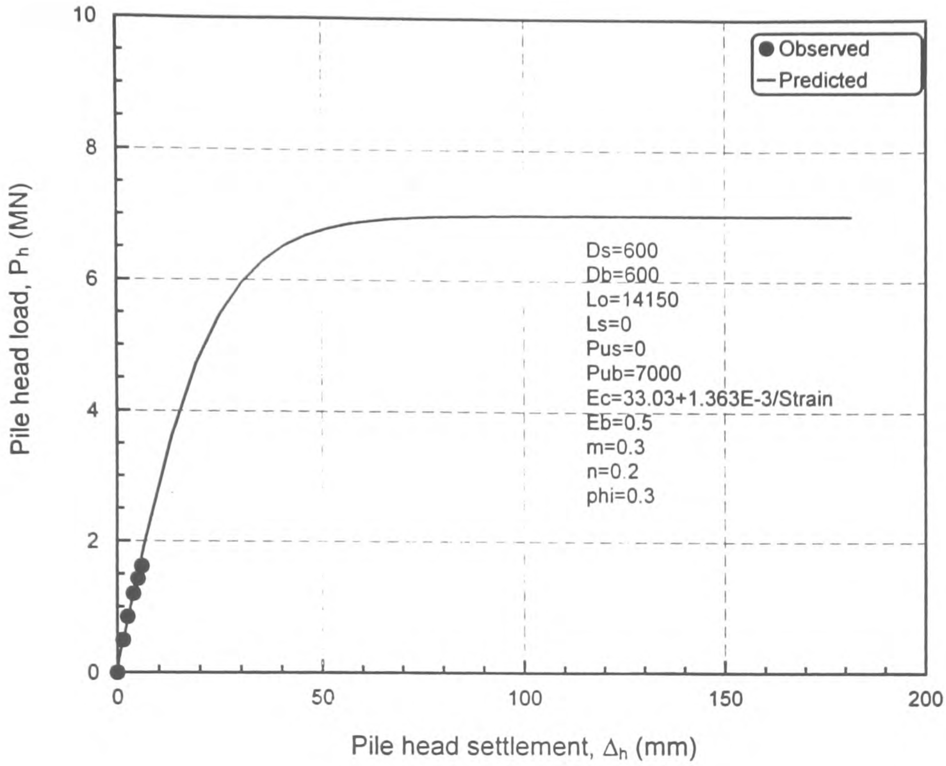

Fig. 7.19(a):Test pile at Redcar, Teesside (end bearing pile)
-Load Vs settlement

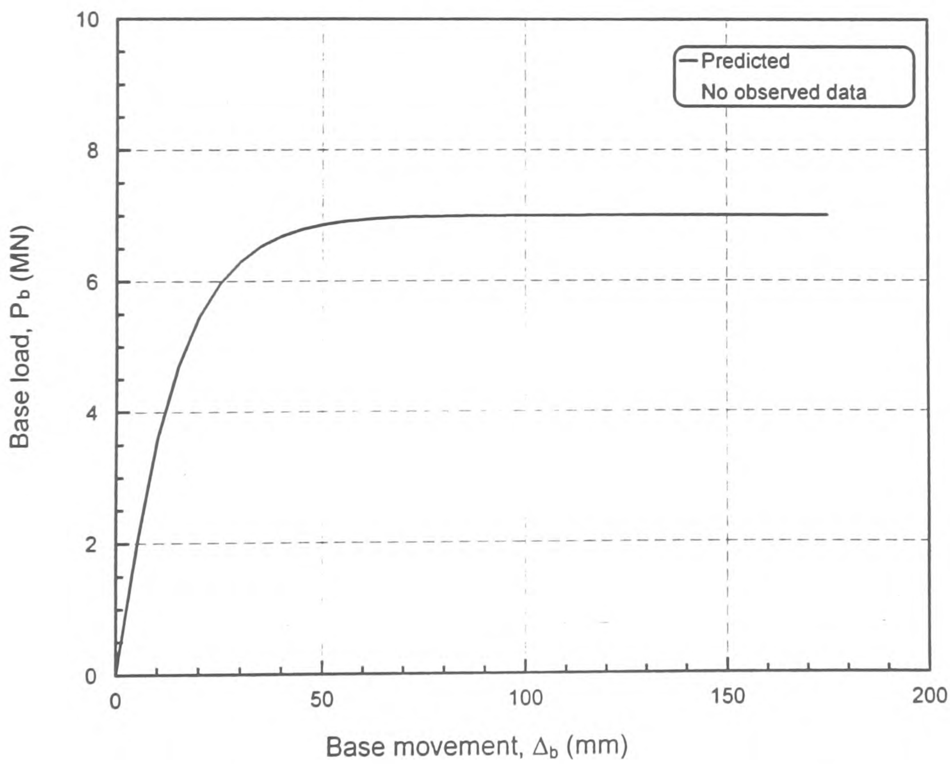

Fig. 7.19(b):Test pile at Redcar, Teesside (end bearing pile)
-Base load Vs base movement

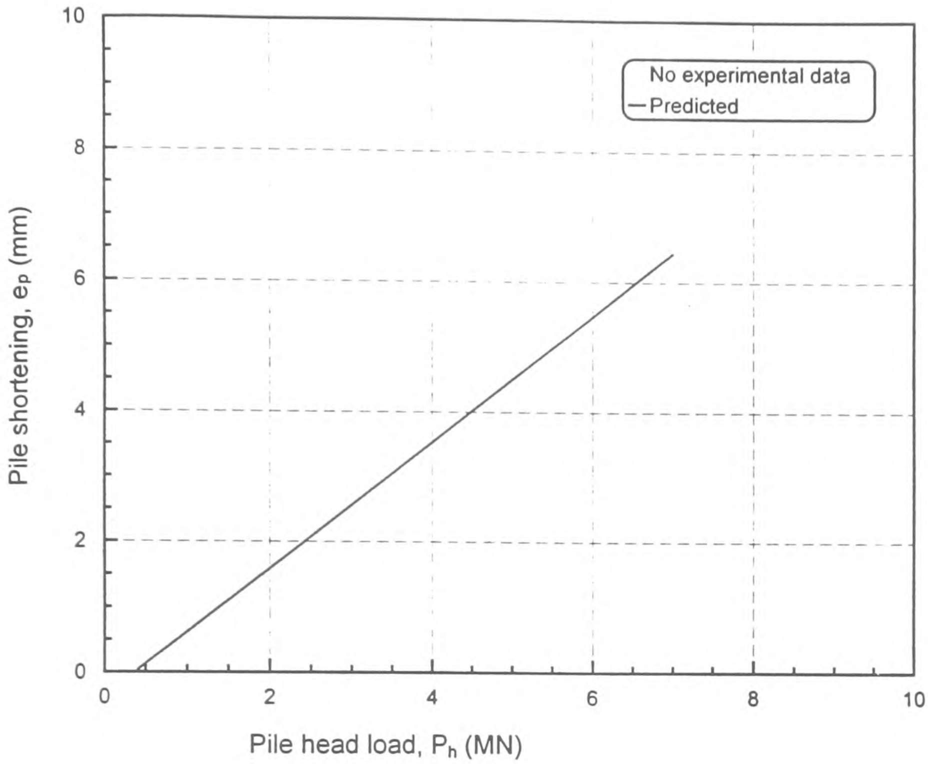

Fig. 7.19(c):Test pile at Redcar, Teesside (end bearing pile)
-Shortening Vs applied load

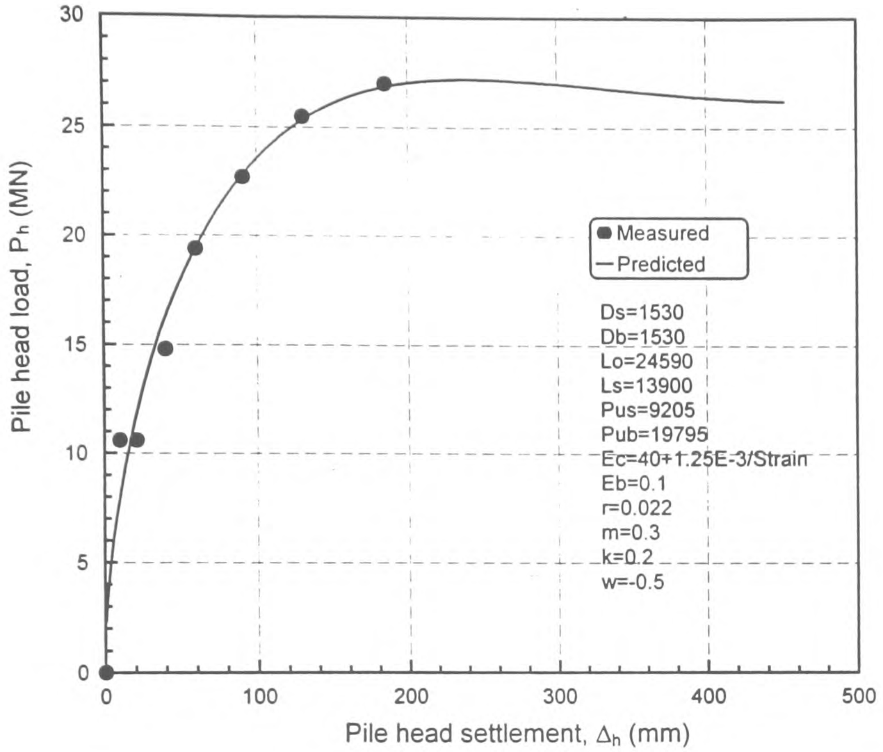

Fig. 7.20(a):Test pile in clay overlying sand at St. Pancras,London (O'Riordan,1982) -Applied load Vs settlement

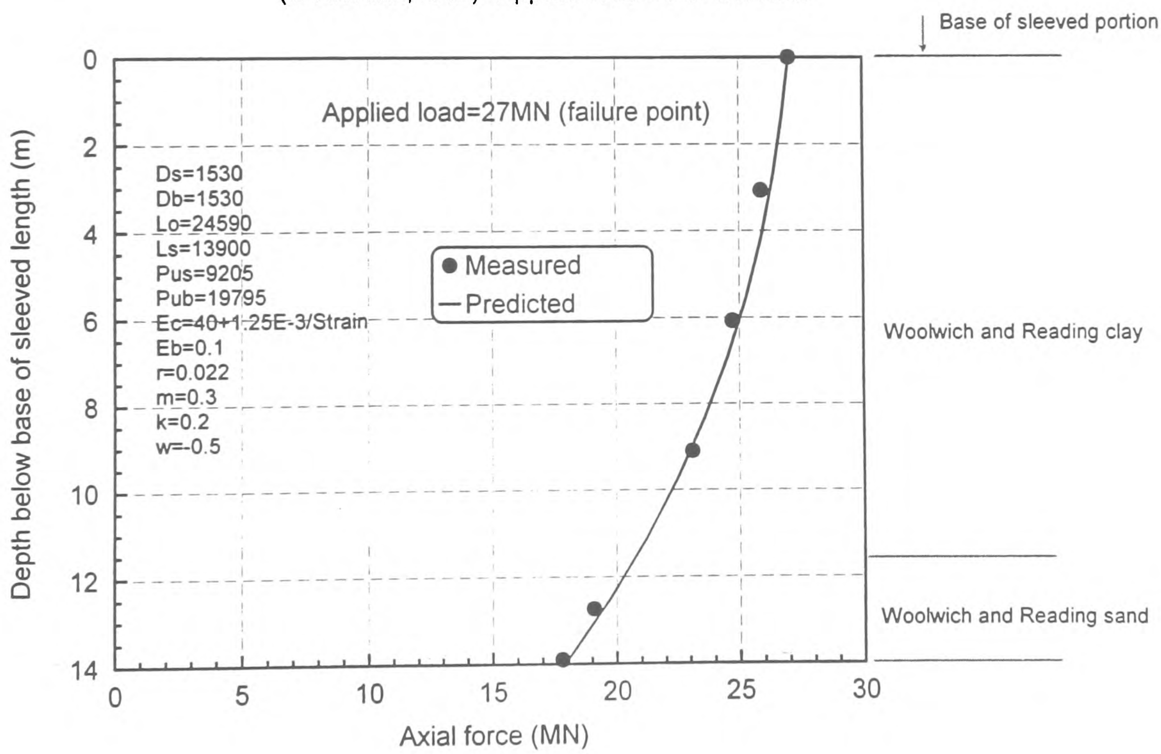

Fig. 7.20(b):Test pile in clay overlying sand at St. Pancras,London (O'Riordan,1982) -Axial force Vs depth for 27MN load

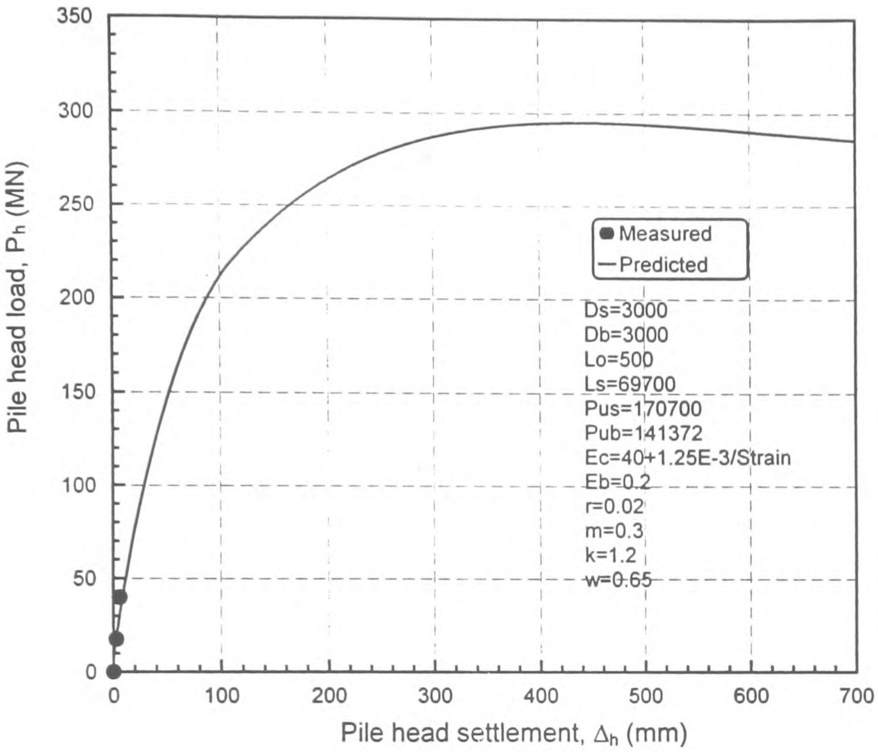

Fig. 7.21(a):Test pile T1 in layered so: Bannosu Viaduct, Honshu-Shikoku bridge,Japan (Hirayama,1990)- Applied load Vs settlement

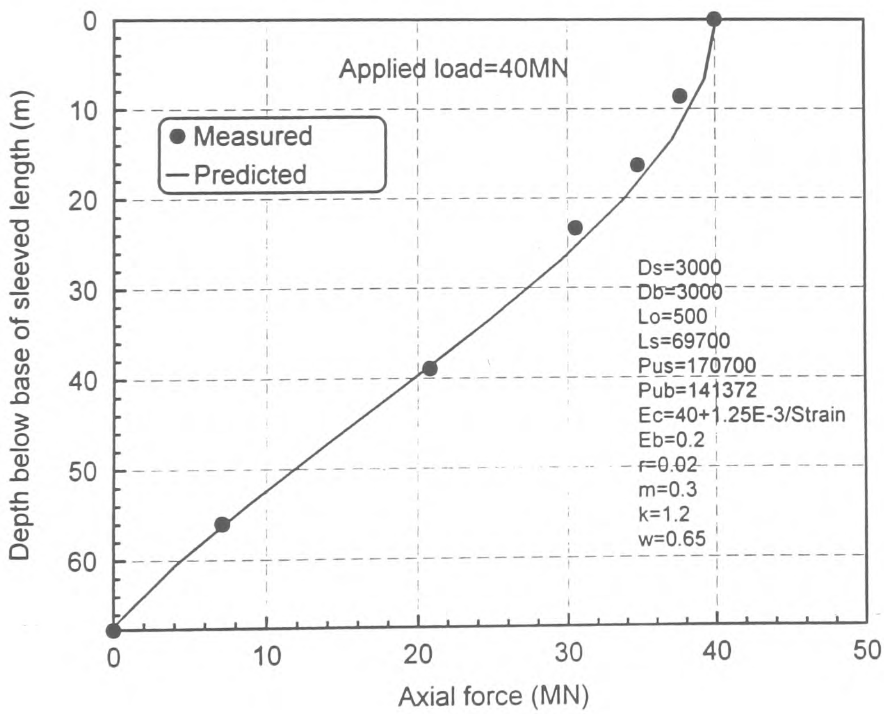

Fig. 7.21(b):Test pile T1 in layered soi: Bannosu Viaduct, Honshu-Shikoku bridge,Japan (Hirayama,1990)- Axial force Vs depth at 40 MN appliedpile head load

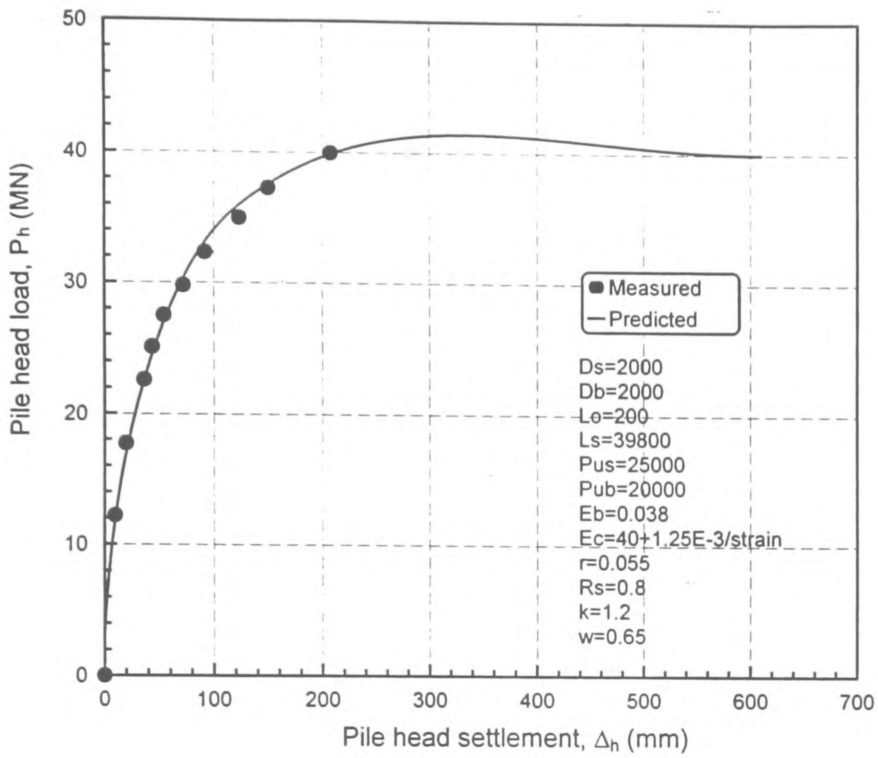

Fig. 7.22(a):Test pile T2 in layered so: Bannosu Viaduct, Honshu-Shikoku bridge,Japan (Hirayama,1990)- Applied load Vs settlement

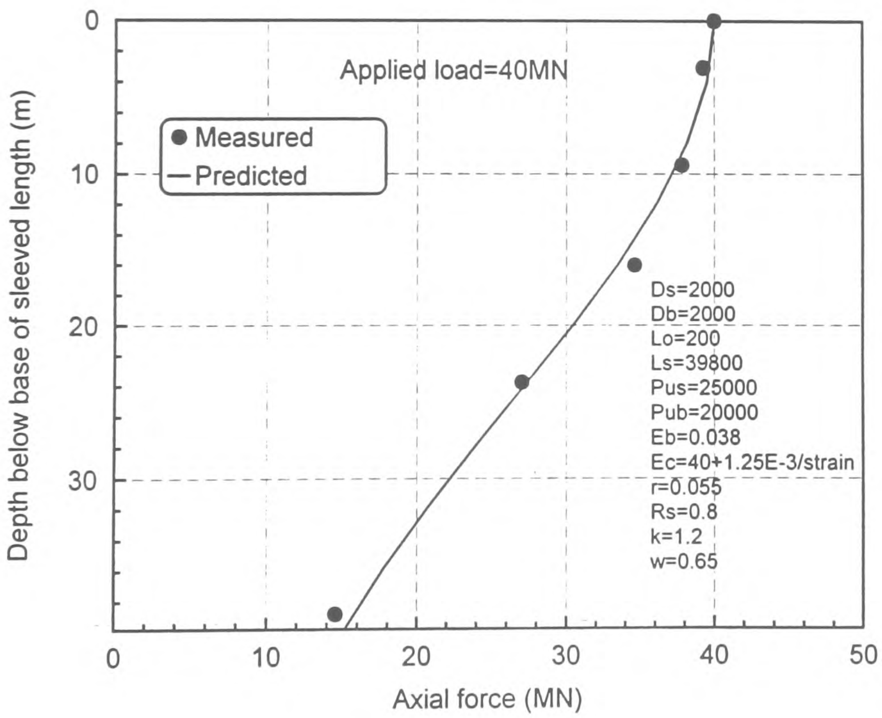

Fig. 7.22(b):Test pile T2 in layered soi: Bannosu Viaduct, Honshu-Shikoku bridge,Japan (Hirayama,1990)- Axial force Vs depth at 40 MN appliedpile head load

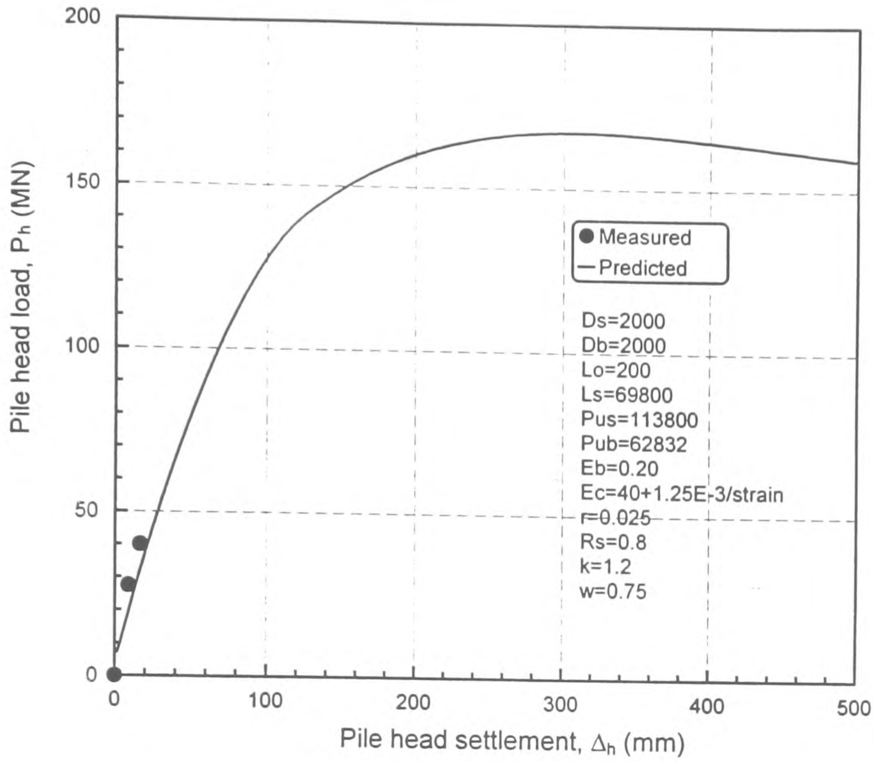

Fig. 7.23(a):Test pile T3 in layered so: Bannosu Viaduct, Honshu-Shikoku bridge,Japan (Hirayama,1990)- Applied load Vs settlement

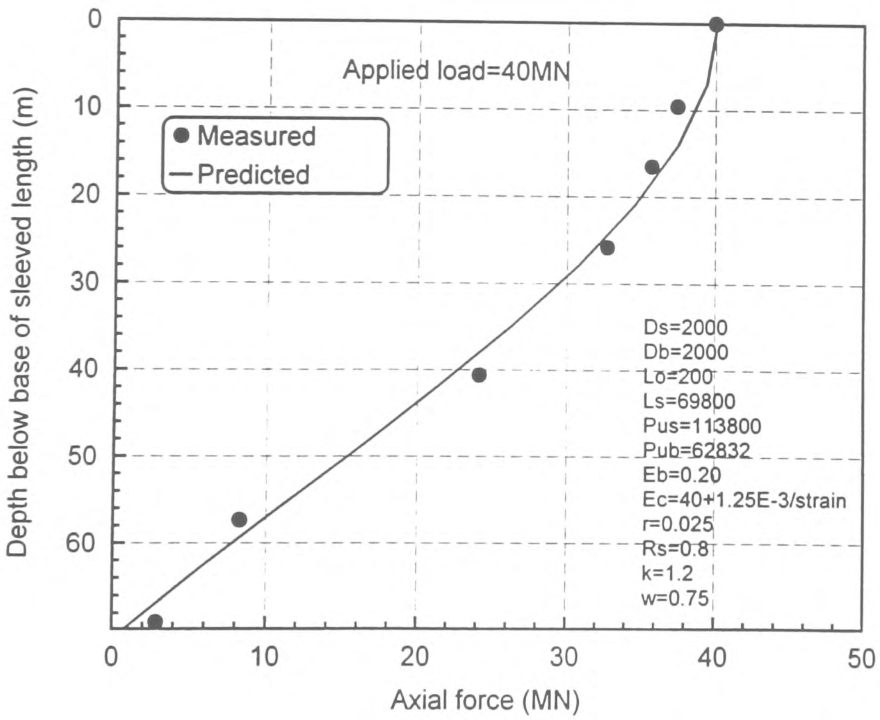

Fig. 7.23(b):Test pile T3 in layered soi: Bannosu Viaduct, Honshu-Shikoku bridge,Japan (Hirayama,1990)- Axial force Vs depth at 40 MN appliedpile head load

CHAPTER 8

CONCLUSIONS AND RECOMMENDATIONS

uncertainties. Hence a detailed soil investigation at the particular site of interest remains the most suitable method of assessing the appropriate correlation formula. In one case study of rock socket piles, cross-jacking tests and cube crushing tests were found to produce reasonable predictions of the in-situ shear strength parameters whereas the point load index test method significantly overestimated the shear strength of the rock.

d) The effective stress approach to the calculation of peak shaft resistance gave reasonable results, subject to the testing methods adopted. It was observed that drained triaxial tests on recompacted soil samples lead to a good estimate of the peak shaft resistance. Pressuremeter test methods provided reasonable values of the coefficient of earth pressure at rest K_o for use in predicting maximum shaft resistance based on the effective stress approach by Chandler(1968).

e) There is substantial evidence that the process of installation of bored piles has a significant effect on the load-settlement response. Changes in the properties of the soil caused by drilling affect the shaft resistance of the pile. The extent of influence is more pronounced in the development of shaft resistance than in end bearing performance. With respect to a bored cast-in-place pile, the suitability of a particular design formula depends on its capability to take into account the effects of pile installation.

8.1.2 Performance of pile instruments

A successful pile loading test programme was carried out and useful data obtained which showed that:

a) The observed readings from the embedded vibrating wire gauges were both accurate and consistent during all loading stages.

b) The extensometer readings at all levels were reasonably consistent and were found to confirm and support the strain gauge data. The pile shortening per unit applied load was calculated using both the strain gauge and extensometer readings. The results revealed that, for each test pile, a good correlation existed between the strains experienced by the strain gauges and extensometers.

c) At every loading stage, the force recorded by the base load cell was consistent with axial force calculations obtained from strain gauge readings. On consideration of all forces acting on a given pile, vertical equilibrium was satisfied at all loading stages.

8.1.3 Force-strain calibration of the test piles

The difficulties of establishing the correct load- deformation function for the test piles was overcome by applying two calibration methods which were all based on the "as built" condition of the test piles. These are (i) the gauge stiffness and (ii) the curve fitting method for Young's modulus versus strain variations. The calibration was necessary in order to take the following points into consideration:

1) Possible eccentric transmission of the applied load down the pile, which would alter the stress distribution from one cross-section to another.

2) Difficulty in reproducing the actual test pile material properties, as constructed, in laboratory testing of concrete specimens.

3) Non-homogeneity of the pile concrete surrounding the strain gauges.

By applying these calibration methods to predict the shortening of the test piles, a remarkable agreement between the two methods was achieved. The results of the shortening prediction were found to be consistent with the measured values deduced from the extensometers.

8.1.4 Elastic constants from a model short pile

The material characteristics of the composite reinforced concrete short column were assessed accurately and successfully using a simple mathematical model. The stiffening effect of steel on concrete has been accurately determined. This was by projecting the effective Young's modulus and Poisson's ratio of the reinforced zone of concrete at a given pile cross-section. The validity of the model was demonstrated by comparing predicted strains with measured values in three mutually perpendicular directions. An excellent agreement, to within 5% was observed between the measured and the predicted strain values at several locations. The results indicate the following:

a) The change in material properties due to reinforcing of concrete was found to affect the effective Poisson's ratio more than the Young's modulus.
b) For a specific amount of reinforcement, it was found that the Poisson's ratio of concrete increased by 25% whilst the Young's modulus increased by 10.5%.
c) There was evidence that the elastic constants for plain concrete were position sensitive, which support previous observations by other researchers. The evidence arose from the fact that lower strain values were recorded near the central axis of the column. This suggested that there was compression of concrete centrally.

8.1.5 Load transfer of large bored piles in Keuper marl

The development, distribution and magnitude of shaft resistance were calculated using the two independent calibration methods. It was found that:

a) The calculated results were consistent using both methods and the differences were considered nominal. The maximum difference in the calculated axial force at any point along a typical test pile was found to be less than 4%, in comparing the two methods.

b) Through continuous force equilibrium checks for each test pile, the maximum out of balance force was less than 5% of the applied pile head. The apparent loss of force within the sleeved portion could be attributed to frictional losses at the knuckles installed at various points to ensure constant clearance between the inner and outer casings.

c) The percentage of nominal force resisted by the pile base varied from approximately 0.1% to 15%, for applied loads varying from zero to the maximum pile capacity. The load transfer profile varies with the intensity of applied load and so do the proprtionate shaft and base resistance mobilised.

d) In every test pile case, the rate of development of shaft resistance with increasing pile penetration was much more rapid than that of base resistance. The peak shaft load was attained at net settlement values in the range 35-50mm (4%-5% diameter). In contrast, the base resistance had not been reached, even at penetrations in excess of 230mm (26% diameter). There was a decrease in the shaft resistance with increasing penetration beyond the point of peak shaft load. Due to this behaviour, the total load capacity of the pile consisted of a portion of the ultimate base resistance and a portion of the peak shaft load.

8.1.6 Verification of the design of the contract piles for Butetown road link

The design of the contract piles for the Butetown road link was based on the recommendations of the site investigation report. The report gave values of maximum shaft resistance for various weathering zones, empirically correlated with S.P.T. "N" values. The pile load capacity predictions were compared with the results of the following alternative design methods:

1) Effective stress method (Burland,1973) for shaft resistance prediction utilising the strength parameters given by Davis and Chandler(1973) and allowing for the variation of the in-situ earth pressure coefficient with depth.
2) Empirical method using the S.P.T. "N" values obtained from the site investigation and converted to equivalent undrained cohesion based on the coefficients given by Kilbourn et al(1988).
3) Total stress method based on the point load strength data obtained from the site investigation cohesion.
4) Observed load capacity values from the pile tests.

The design for end bearing was carried out using the use of effective stress parameters for different weathering zones, as given in the site investigation interpretative report. The design results showed that:

a) The design method suggested in the site investigation report resulted in shaft resistance being underestimated by 40-57%. However, this method produced reasonable predictions of base resistance. The calculated base resistance of pile TP1, where the full base capacity was realised, was found to be accurate to within 5%.
b) The effective stress design method produced shaft resistance values consistent with

the results of the S.P.T design method suggested in the site investigation report. The predicted shaft resistance values were 41%-59% of the observed values. By back-analysis, it was found that, on average, value of $\bar{\beta}$ (in Burland's,1973 notation) is 1.42.

c) The use of measured S.P.T. "N" values in the design formula suggested by Kilbourn etal(1988) produced shaft resistance predictions of 62%-79% of the measured values. By back-analysis, it has been shown that accurate shaft resistance predictions (with a maximum error of 5%) may be obtained using an adhesion factor of 0.53 when a factor of 6 is applied to convert S.P.T "N" values to equivalent undrained cohesion. Alternatively, back-analysis also showed that a factor of 3.2 is appropriate for converting the average "N" value (along the pile shaft) into average unit shaft resistance (in kN/m^2).

d) The design method utilising point load data with an adhesion factor of 0.5 resulted in calculated shaft resistance of 30%-40% of the observed values. In order to match the observed shaft resistance values, it was found that an average adhesion factor of 1.45 was required. It was therefore shown that the use of point load data seriously underestimated the strength of the Keuper marl.

8.1.7 Prediction model for large diameter piles

The proposed analytical model is simple and has been proven accurate, provided that the input data and the soil parameters are determined accurately. The manner in which the model is linked to soil properties is straightforward and easy to understand. Moreover, the required soil parameters are those that would be readily available from conventional site investigation. The success of the method relies on the correct determination of these soil parameters. The numerical model has been applied to 19 test pile case histories, some of which include full instrumentation. In all the test piles analysed, there is a very good agreement between the predicted and the measured data. However, there is no complacency in proposing that the model is infallible in all cases. The improved predictive capability of this model is likeky to lead to a more cost-effective pile design. This is by enabling the use of shorter pile lengths and smaller pile diameters to achieve the same design criteria, with respect to load capacity as well as settlement limits.

The model can be readily adopted for use in designing a single pile, based on known soil properties. The model may also be used to back-analyse a test pile, provided that sufficient settlement has been achieved, so that a reasonable part of the load-settlement characteristic is extracted. All the available pile test results have been utilised in checking the validity of the model. The results strongly reveal the influence of the condition of a pile base on the settlement of the pile head The proposed method demonstrates that there is potential in theoretical investigation of pile performance, since piles behave according to certain identified trends.

The following are the salient points regarding the capability of the program:

1) Input data utilises site investigation and/or existing British Standard, or C.I.R.I.A. information.
2) Estimates the pile elastic (and non-recoverable) shortening.
3) Predicts the load transfer mechanism along the embedded pile length.

4) Predicts the actual and weighted displacements corresponding to gradual and full mobilisation of the shaft resistance and end bearing resistance.
5) Projects the complete pile head load-settlement curve for the loaded pile to include an adjustment for the condition of the pile base, whether clean or resting on soil debris.
6) The prediction is extended to the stage of sequential failure in both shaft resistance and end bearing, together with the percentage make-up of these components.

8.1.8 Validation of the proposed mathematical model

All the available pile test results have been utilised in checking the validity of the model. The results strongly demonstrate that:

a) The numerical model is capable of predicting the load-settlement behaviour of large diameter, bored piles installed in soils having a wide range of properties. The load-settlement curve is determined by the soil properties at a particular site, the geometrical and material properties of the pile.
b) The proposed model may be used to analyse not only conventionally constructed piles but also piles with either negligible shaft resistance or end bearing.
c) The model is capable of separating shaft resistance and end bearing, at any stage of loading, for piles with different length to diameter ratios. It is also possible to predict the elastic shortening of the pile and the variation of axial force in the pile with depth.

8.2 RECOMMENDATIONS AND PROPOSALS FOR FURTHER WORK

A comprehensive analysis of the pile test data and further numerical modelling has been carried out to predict pile response under loading. Although the studies have been successful in describing the characteristics of large bored piles in Keuper marl, the analyses are not definitive. The hypotheses put forward are tested using the current and other pile test data. However, more work is needed to further validate and prove the reliability of these theories.

The following points are considered to be of further interest for future research into pile response in Keuper marl:

1) Work is needed to establish the appropriate design approach, especially for shaft resistance capacity of bored cast in-situ piles. It is also important to determine the most suitable and accurate method of evaluating the required soil strength parameters from laboratory or in-situ testing. Currently, there are numerous claims as to which design methods and laboratory test methods should be used. However, it seems as yet not possible to identify a single method, which can be said to produce consistent and reliable pile load capacity predictions.
2) Further investigations are necessary using instrumented test piles, with strains monitored at close intervals along the pile shaft, in order to study the exact load transfer mechanism of large diameter, bored piles.
3) Additional work is required to address the influence of multi-layered ground on the development of load resistance and the settlement response of the pile.
4) The available design methods for bored piles in Keuper marl such as the C.I.R.I.A. method are informative and useful. However, further research is necessary in order

to produce a more flexible and universal method that could be applicable to as many different sites as possible.

5) Although the proposed analytical model is reliable and accurate, additional research work should be carried out in order to help relate the input parameters of the model to the soil and pile properties at a given site.
6) Further work is necessary in order to include the effect of time dependent functions on the load-settlement behaviour of a pile system.

REFERENCES

REFERENCES

AISI(1975) "Steel Pile Load Test Data"., **American Iron and Steel Institute.**, Washington, DC, pp84.

ALPAN,I.(1967) "The Empirical Evaluation of K_O and K_{OR}"., **Soil and Foundations., Tokyo.**, Vol.7., No.1,pp31-40.

AL-SHAIKH-ALI, M.(1971) "Creep in Keuper marl". Proc. Symposium on Interaction of Structure and Foundations. **University of Birmingham**, pp50-71.

AL-SHAIKH-ALI, M. & DAVIS,A.G(1975) "The In-Situ Creep In Soft Rocks Using a Prolonged Model Test Pile". **Proc. Conf. Soil Mech. & Found. Engng**, Istanbul Technical University, Vol.1, pp213-229.

ALTAEE,A., EVGIN,E. & FELLENIUS, B.H.(1993) "Load Transfer for Piles in Sand and the Critical Depth". **Canadian Geotechnical Journal**. Vol.30, No.3, pp455-463.

AMERICAN PETROLEUM INSTITUTE(1984) "Recommended Practice for Planning, Designing, and Constructing Fixed Offshore Platforms"., **15/e, API.., RP2A.**, pp 115.

AZZOUZ,A.S & LUTZ,D.G(1986) "Shaft Behaviour of a Model Pile in Plastic Empire Clays". **Jnl.Getech. Engng.,ASCE.,** Vol.112, No.4, Paper No.2054., pp389-407.

BAGUELIN, F et al.(1975) "La Capacite Portante des Pieux"., **Annales de l'Institut Technique du Batiment et des Travaux Publics., Supplement 330., Serie SF/116.**, July-Aug., 1975.

BANERJEE, P.K.(1970) "A Contribution to the Study of Axially Loaded Pile Foundations"., **Ph.D Thesis., University of Southampton., England.**

BANERJEE, P.K & DAVIES, T.G.(1977) "Analysis of Pile Groups Embedded in a Gibson Soil"., **Proc. 9th Int. Conf. S.M.& F.E., Tokyo.**, Japan.

BARKER,W.R & REESE,L.C(1970) "Load Carrying Characteristics of Drilled Shafts Constructed With the Aid of Drilling Fluids"., **Res. Rep 89-9.,Center For High. Res., Univ. of Texas, Austin.**

BARNES, G.E.(1995) **Soil Mechanics Principles and Practice**. Macmillan., pp229. ISBN 0-333-59654-4.

BHUSHAN,K.(1982) "Discussion:, New Design Correlations For Piles In Sand"., **Jnl. Geotech. Eng. Div., ASCE., GT11.,** Nov., pp1508-1510.

BIENIAWSKI,Z.T.(1975) "The Point Load test in Geotechnical practice". **Engineering Geology**, Vol.9, No.1, pp1-11.

BISHOP,A.W.,WEBB,D.C & LEWIN,P.I(1965) "Undisturbed Samples of London Clay From Ashford Common Shaft:Strength/Effective Stress Relationships., **Geotechnique., Vol.15.**,pp1-31.

BOND,A.J&JARDINE,R.J(1991)"Effects of Installing Displacement Piles in a High OCR Clay"., Geotechnique., Vol.41., No.3, pp341-363.

BOOKER,J.R & POULOS,H.G(1976) "Analysis of Creep Settlements of Pile Foundations"., **Jnl. Goet. Eng. Div.,ASCE**.,Vol.102, No. GT1,pp1-14.

BOWLES,J.E.(1996) Foundation Analysis and Design. 5th Edition., McGraw-Hill., pp886-888., ISBN 0-07-114052-2

BJERRUM,L.(1973) "Problems of Soil Mechanics and Construction in Soft Clay",**Proc. 8th Int. Conf. ISSMFE**,Moscow,Vol.3,pp150-157.

BRIERLEY, G.S. et al.(1979) "Interpreting End-Bearing Pile Load Test Results." **ASTM** STP No.670, pp181-198.

BREWER,R(1964) "Fabric and mineral analysis of soils". **John Wiley and Son** (New York).

BROMHAN,S.B & STYLES,J.R(1971) "An analysis of Pile Loading Tests in Stiff Clay"., **Proc. 1st Aust.-N.Z. Conf. Geomechs., Melbourne**., Vol.1,pp246-253.

BRITISH STANDARDS INSTITUTION(1981) BS 5930 "Code of Practice for Site Investigations"

BRITISH STANDARDS INSTITUTION (1973) BS 1881:Part 121 "Determination of static modulus of elasticity of concrete"

BRITISH STANDARDS INSTITUTION(1986) BS 8004 "Code of practice for Foundations"

BRITISH STANDARDS INSTITUTION(1990) BS5950 "Structural Use of Steelwork in Buildings".,Part 1.

BRITISH STANDARDS INSTITUTION BS 8110 "Structural Use of concrete", Part 1., pp 2/3.

BURLAND,J.B.(1969) "Contribution To Discussion On "Comparison of Full Scale Performance with In-Situ and Laboratory Measurements"., **Proc. British Geotechnical Society Conference on In-Situ Investigations of Soils and Rocks**., British Geotechnical Society., London., England., pp61.

BURLAND,J.B.(1973) "Shaft Friction of Piles in Clay -A simple fundamental approach". **Ground Engineering**, Vol.60, No.3, pp30-42.

BURLAND,J.B. & BURBRIDGE,M.C.(1985) "Settlement of Foundations on Sand and Gravel., **Proc., I.C.E.,** Part 1., Vol.85., Dec., pp1325-1381.

BURLAND,J.B., BUTLER,F.G., & DANICAN,P.(1966) "The Behaviour and Design of Large Diameter Bored Piles in Stiff Clay". **Proc. Symp. on Large Bored Piles,** Inst.Civil Engnrs.,London,pp51-57.

BURLAND,J.B & COOKE,R.W(1974) "The Design of Bored Piles in Stiff Clays"., **Ground Engineering., Vol.7., No.4.**, July.

BURLAND,J.B. and TWINE,D.(1988) "The shaft friction of bored piles in terms of effective strength".**Proc. 1st Int.Geot.Sem. on Deep Foundations on Bored and Auger Piles**,Ghent,pp411-420.

BUTTERFIELD, R & BANERJEE, P.K.(1970) "A Note on The Problem of a Pile reinforced Half-Space., **Geotechnique**., London., Vol.20., pp100-103.

BUTTERFIELD, R & BANERJEE, P.K.(1971) "The Elastic Analysis of Compressible Piles and Pile Groups"., **Geotechnique.,** London., Vol.21., pp43-60..

CAMBERFORT,H & CHADEISSON,R.(1961) "Critere Pour l'Evaluation de la Force Portante d'un Pieu"., **Proc. 5th Int. Conf. S.M. & F.E. Vol. 2**, pp23-31.

CARRIER,W.D.(1993) "Discussion: Hyperbolic Method For Consolidation Analysis"., **Jnl. Geotech. Eng. Div., A.S.C.E., Vol.119., No.1**., Jan., pp186-190.

CARRUBBA,P.(1997) "Skin Friction of Large-Diameter Piles Socketed into Rock". **Canadian Geotechnical Journal**, Vol. 34, pp230-240.

CASTELLI, F., MAGUERI, M., & MOTTA, E.(1992) Anolisi non lineare del cedimento di un palo singolo. Rivista Italiana di Geotecnica , 26, pp115-135.

CHANDLER,R.J.(1966) Discussion to paper by Whitaker & Cooke. Proc. Symposium on Large Bored Piles. Pp95-97.

CHANDLER,R.J(1968) "The Shaft Friction of Piles in Cohesive Soils in Terms of Effective Stress".**Civil Engineering Public Works Review**, January,pp49-51

CHANDLER,R.J(1969) "The Effect of Weathering on the Shear Strength Properties of Keuper Marl" **Geotechnique**,Vol.21,pp321-334.

CHIN,T,K.(1970) "Estimation of the Ultimate Load of Piles From Tests Not Carried to Failure". **Proc. 2nd South East Asian Conference on Soil Mechanics & Foundation Engineering, Singapore**, pp81-92.

CHIN,T..K(1972) "The Inverse Slope as a Prediction of Ultimate Bearing Capacity of Piles". **Proc. 3rd SE Asian Conf.Soil Engng,Hong Kong**,pp83-91

CHIN,T..K & VAIL,A.J(1973) **Proc. 8th Int. Conf. Soil Mech., Moscow**, Vol.2, Part 1, pp47-52.

CHOW, Y.K.(1986) "Analysis of Vertically Loaded Pile Groups". **Int. Journal Numerical Analysis Methods Geomechanics,** Vol.10, No.1, pp59-72.

CHOW,F.C., JARDINE,R.J., NAUROY,J.F. & BRUCY,F.(1997) "Time-Related Increases in the Shaft Capacities of Driven Piles in Sand. **Geotechnique**. Vol.47, No.2, pp353-361.

CHRISTOULAS,S.G.(1988) "Dimensionnement De Pieux"., **Quelques Expe'riences et Recherches en Grece., Bull. Laison Labs., P.et**. Ch 154., pp 5-10.

CLAYTON, C.R. & MILITITSKY,J.(1983) "Installation Effects and the Performance of Bored Piles in Stiff Clay". **Ground Engineering**, Vol.116, No.2, pp17-32.

COLE,K.W & STROUD,M.A(1976) "Rock Socket Piles at Coventry Point, Market Way, Coventry". **Geotechnique**,Vol.26,No.9,pp47-62

COOKE,R.W & PRICE,G(1973) "Strains and Displacements Around Friction Piles". **Proc. 8th Int. Conf. Soil Mech. and Found. Engng., Moscow**

COOKE,R.W., PRICE,G. & TARR,K.(1979) "Jacked Piles in London Clay: A Study of Load Transfer and Settlement Under Working Conditions". **Geotechnique, Vol.29, No.2**, pp113-147.

COOKE,R.W. & WHITAKER,R.(1961) "Experiments with Model Piles with Enlarged Bases"., **Geotechnique**., Vol.11., pp1-13.

COOP,M.R. & WROTH,C.P.(1989) "Field Studies of an Instrumented Model Pile in Clay." **Geotechnique,** Vol.4, pp 679-696.

COYLE,H.M & REESE,L.C.(1966) "Load Transfer of Axially Loaded Piles in Clay"., **Jnl. Soil Mech. & Found. Division., A.S.C.E., Vol.92**., SM2., March., pp1-26.

DASGUPTA,G.(1985) "Stochastic Finite Element Analysis of Soil-Structure Systems". **Proc. 4th Int. Conf. on Structural Safety and Reliability., 2 Kobe, Japan,** pp528-532.

DAUNCEY,P.C & WOODLAND,A.R(1984) "Bored Cast In-Situ Piled Foundations in Keuper Marl for the Birmingham International Arena" **Piling and Ground Treatment for Foundations**, Thomas Telford, London.

DAVIS,A.G(1967) "The Mineralogy and Phase Equilibrium of Keuper Marl". **Journal of Engineering Geology**, pp39-45.

DAVIS,A.G(1974) "Contribution to Discussion in Session IV, Rocks, Cambridge". **Conf. Settlement of Structures., British Geotechnical Society**., London., pp757-759.

DAVIS,A.G & CHANDLER,R.J(1973) "Further Work on the Engineering Properties of Keuper Marl". **CIRIA Report 47,October.**

DE BEER,E., LOUSBERG,E., DE JONGHE,A., WALLAYS,M. & CARPENTIER,R. (1979) "Prediction of the Bearing Capacity of Displacement Piles, Penetrating Into a Very Dense Sand Layer. **Proc. 7th European Conference on Soil Mechanics., London**., Vol.3., pp51-59.

DECOURT,L.(1982) "Prediction of the Bearing Capacity of Piles Based Exclusively on the N Values of The S.P.T., **Proc. ESOPT2.,Amsterdam,**Vol.1,pp29-34.

DE MELLO,V.F.(1971) "The Standard Penetration Test"., **4th Pan American Conf. On S.M. & F.E. San Juan., Puerto Rico., Published by ASCE,** Vol.1., pp1-86.

GERMAN STANDARDS DIN 4014(1990) Bored Piles: Construction Procedure; Design and Bearing Behaviour. Beuth Verlag, Berlin.

DOWNS,D.I & CHIEURZZI,R(1966) "Transmission Tower Foundations" **Journal of Power Division., ASCE,**Vol.92., PO2, pp91-114.

DUMBLETON,M.J(1967) "Origin and Mineralogy of African Red Clays and Keuper Marl". **Journal of Engineering Geology**,p39-45.

ENGLAND,M.(1993) "A Method of Analysis of Stress Induced Displacement in Soils With Respect to Time". **Deep Foundations on Bored and Auger Piles. Van Impe (ed.) © Balkema, Rotterdam**, ISBN 90 54103132, pp241-245.

ESRIG,M.I and KIRBY,R.C.(1979) "Soil Capacity For Supporting Deep Foundations in Clay"., **ASTM., STP No. 670**, pp27-63.

EUROCODE(1992) "Design of Concrete Structures"., Eurocode 2., Part 1 (General Rules and Rules For Buildings)., ENV 1992-1-1., pp68.

FELLENIUS,B.H(1980) "The Analysis of Results From Routine Pile Tests"., **Ground Engineering.**, Vol. 6., September., pp19-31.

FELLENIUS,B.H(1991) "Summary of Pile Capacity Predictions and Comparison With Observed Behaviour"., **Journal of Geotechnical Division., A.S.C.E.**, Vol.117., No.1., pp192-195.

FELLENIUS,B.H & ALTAEE,A.A.(1995) "Critical Depth: How It Came Into Being And Why It Does Not Exist"., **Proceedings., I.C.E., London., Vol.113., April.**, pp107-111.

FELLENIUS,B.H. & SAMSON,I.(1976) "Testing of Drivability of Concrete Piles and Disturbance to Sensitive Clay"., **Canadian Geotechnical Journal., Vol.13., No.2.**, pp139-160.

FLAATE,K. & SELNES,P.(1977) "Side Friction of Piles in Clay"., Proc. **9th Int. Conf. S.M. & F.E.**, Vol.1., pp517-522.

FLEMING,W.G.K., WELTMAN,A.J., RANDOLPH,M.F, & ELSON,W.K.(1992) **Piling Engineering.**, 2nd Edition., Blackie (Glasgow and London), pp104.

FLEMING,W.G.K(1992) "A New Method for Single Pile Settlement Prediction and Analysis",**Geotechnique**,Vol.42,No.3

FLEMING, W.G.K. THORBURN,S.(1983) "Recent Piling Advances- State of The Art Report". In *Proc. Conf. on Advances in Piling and Ground Treatment for Foundations*, ICE, London.

FOLEY,G.P & DAVIS,A.G(1971) "Piling in Keuper marl at Leicester",**Civil Engineering Public works Review**, September

FORT,D.S & MARTIN,P.L(1989) "Installation, Instrumentation and Load Testing of a Large Diameter Bored Pile in Upper Chalk". **Int. Chalk Symposium**, Thomas Telford, London.

FOX,E.N.(1948) "The Mean Elastic Settlement of a Uniformly Loaded Area at Depth Below Ground Surface". **Proc. 2nd Int. Conf. S.M.&F.E., London., England.**

FRANK, R.(1974) "Etude Theorique du Comportement des Pieux sous Charge Verticale. Introduction de la Dilatance"., **Doctor-Engineer Thesis., University Paris (Pierre et Marie Curie University)., France., November.**

FRANK, R.(1975) "Etude Theorique du Comportement des Pieux sous Charge Verticale"., **Rapport de recherche no.46., Laboratorie Central des Ponts et Chaussees., Paris.**, France.

FRANKLIN,J.A.,BROCH,E.& WALTON,G.(1972) "Logging the Mechanical Character of Rock"., **Trans. Inst. Min & Metall., A81**, ppA43-A51. Also A80, ppA1-A9(1971).

GEOLOGICAL SOCIETY ENGINEERING GROUP(1970): **Working Party Report., Vol.3., No.1., 1970.**

GIBBS,H.J & HOLZ,W.T(1957) "Research on Determining the Density of Sand by Spoon Penetration Testing". **Proc. 4th Int. Conf. Soil Mech.and Found. Engng**,Vol.1,pp35.

GUO,D.J., THAM,L.G. & CHEUNG,Y.K.(1987) "Infinite Layer for Analysis of Single Piles". **Computers and Geotechnics**, Vol.3, No.4, pp229-249.

HANNA,T.H & TAN,R.H.S(1973) "The Behaviour of Long Piles Under Compressive Loads in Sand"., **Canadian Geotechnical Journal., Vol.10., No.2.**, pp311-340.

HIRAYAMA,H.(1990) "Load-Settlement Analysis For Bored Piles Using Hyperbolic Transfer Functions". **Soils and Foundations, Japanese Society of Soil Mechanics and Foundation Engineering**, Vol.30, No.1, pp55-64, March.

HOBBS,N.B & HEALY,P.R(1979) "Piling in Chalk".,**Construction Industry Research Information Association (C.I.R.I.A.) report PG6.**

HOLEYMAN,A.(1985) "Dynamic Non-Linear Skin Friction of Piles"., **Proc. Symp. On Penetrability, Drivability of Piles., 11th Int. Conf. S.M. & F.E.**, San Francisco.

HORVATH,R.G.(1978) "Field Load Test Data on Concrete-to-rock Bond Strength for Drilled Pier Foundations. **Publication 78-07, Dept. of Civil Engineering, University of Toronto**, Canada.

HORVATH, R.G & KENNEY, T.C.(1979) "Shaft Resistance of Rock-Socketed Drilled Piers". **Proc. ASCE, Symposium on Deep Foundations, Atlanta, Georgia**, October 25th, pp182-214.

HUNTER,A.H & DAVISSON,M.T(1969) "Measurement of Pile Load Transfer". **Performance of Deep Foundations, ASTM STP 444,ASTM**,pp 106-117.

INDRASURYA,B., MOCHTAR, & TURNER,B., EDIL(1988) "Shaft Resistance of Model Piles in Clay". **Journal Geotech. Eng. Div., ASCE, Vol.114, No.11**, November.

INSTITUTION OF CIVIL ENGINEERS(1988) **Specification for Piling**. ICE, London

INSTITUTION OF CIVIL ENGINEERS(1979) **Recent Developments in the Design and Construction of Piles.** ICE, London

IRELAND,H.O(1957) "Pulling Tests on Piles in Sand"., **Proc. 4th Int. Conf. S.M.& F.E.**,Vol.2,pp43-54.

JEFFERS, E.(1995) "Steel H-bearing Piles Driven into Mercia Mudstone". **Ground Engineering**, June, pp33-37.

JOHNSTON, I.W. & HABERFIELD, C.M.(1993) "Side Resistance of Piles in Weak Rock". **Proc. International Symposium - Geotechnical Engineering of Hard Soils and Soft Rocks**. Balkema, Rotterdam, Vol.2, pp969-975. ISBN 90 5410 3442.

JONES,A.J.(1991) "Analysis of Shallow and Deep Foundations Using Soil-Structure Interaction Techniques"., **Ph.D Thesis, Polytechnic of Wales.**

JORDEN,E.E & DOBIE,M.(1977) "Tests on Piles in Keuper Marl for the Foundations of a Blast Furnace at Redcar, Teesside". Proc. **Symp. Piles in Weak Rock., I.C.E., London.,** pp105-113.

KAY,W.F.(1980) "The Development of Shaft Friction in Semi-Full Scale Piles Passing Through Ganular Soils".,**Ph.D Thesis,Polytechnic of Wales.**

KERISEL,J.(1964) "Deep Foundations-Basic Experimental Facts". **Proc. North American Conference on Deep Foundations, Mexico City, 1964.**

KILBOURN,TREHARNE & ZARIFIAN(1988) "The use of Standard Penetration Test for the Design of Bored piles in Keuper Marl of Cardiff". **Geotechnology Conference on Penetration Testing in U.K**, University of Birmingham, July.

KLINK,S.A.(1985a) "Actual Elastic Modulus of Concrete" ., Technical Paper., **A.C.I. Journal.,** 82-54, pp630-633.

KLINK,S.A.(1985b) "Actual Poisson Ratio of Concrete"., Technical Paper., **A.C.I. Journal.**, 82-74, pp813-817.

KONDNER,R.L.(1963) "Hyperbolic Stress-Strain Response: Cohesive Soils". **Journal of the Soil Mechanics and Foundations Division, ASCE**, Vol.89, SM 1, pp115-143.

KRAFT,L.M. (1981) "Friction Capacity of Piles Driven into Clay"., **Jnl. Geotech. Eng. Div., ASCE., GT11.,** Nov., pp1521-1541.

KULHAWY,F.H.(1984) "Limiting Tip and Side Resistance: Fact or Fallacy?". Proc. **Symposium on Analysis and Design of Piled Foundations. R.J. Meyer, Editor, San Francisco, ASCE**, New York, pp80-89.

KULHAWY,F.H & GOODMAN,R.E.(1980) "Design Of Foundations On Discontinuous Rock"., **Proc. Int. Conf. On Structural Foundations On Rock., Sydney**., Vol.., pp209-220.

KULHAWY,F.H & GOODMAN,R.E.(1987) "Foundations In Rock"., **Chapter 15., Reference Book., Ground Engineering., F.G Bell., Butterworth**., London.

KULHAWY,F.H. & PHOON, K.K.(1993) "Drilled Shaft Side Resistance in Clay Soil to Rock." **Proc. On Conf. on Design and Performance of Deep Foundations: Piles and Piers in Soil and Soft Rock. Geotechnical Special Publication, No.38, ASCE**, pp172-183.

LAI,J.Y, & BOOKER, J.R.(1989) "Application of Discrete Fourier Series to the Finite Element Stress Analysis of Axi-symmetric Solids". **Research Report 605, University of Sydney**, Australia.

LAKE,G.C.(1986) "The Development of Shaft Friction and End Bearing Resistance for Dynamically Driven Model Piles"., **Ph.D Thesis, Polytechnic of Wales.**

LEACH,B.A, MEDLAND,J.W & SUTHERLAND,H.B(1976) "The Ultimate Bearing Capacity of Bored Piles in Weathered Keuper Marl". **Proc.6th European Conf. Soil Mech. & Founds**, Paper No.30,pp507-514,March

LEACH,B & MELLARD,D.J(1980) "The Design and Installation of Precast Concrete Piles in the Keuper Marl of The Severn Estuary.,**Proc. Conf. Recent Developments in the Design and Construction of Piles.,I.C.E.,London**.,pp33-43.

LEE,C.Y.(1993) "Settlement of Pile Groups- Practical Approach". **Journal of Geotechnical Engineering Division, ASCE, Vol.119, No.9**, September, pp1449-1461.

LEE,C.Y. & SMALL,J.C.(1991) "Finite Layer Analysis of Axially Loaded Piles". **Journal of Geotechnical Engineering Division, ASCE, Vol.117, No.11**, November, pp1706-1721.

LEONARDS,G.A. & LOVELL, D.(1979) "Interpretation of Load Tests on High Capacity Driven Piles". **ASTM** STP No.670, pp388-415.

LIAO,S.S.& WHITMAN,R.V.(1986) "Overburden Correction Factors For Sand"., **Jnl. Geotech. Eng. Div., ASCE.**, Vol.112, March., pp373-377.

LINGS,M.L.(1997) "Predicting The Shaft Resistance of Driven Pre-Formed Piles in Sand. **Proc. ICE, Geotechnical Engineering,** Vol.125, April, Paper 11001, pp71-84.

LORD,J.A.(1989) "Keynote Address: Design And Construction in Chalk".,**Proc. Int. Chalk Symposium., Brighton., England.**

MARSLAND,A.(1971) "Laboratory and In-Situ Measurements of the Deformation Moduli of London Clay"., **Symposium on Interaction of Structures and Foundation., Midland Soil Mechanics Society., Birmingham University**., Birmingham., England.

MAYNE,P.W.(1984) "K_0 - c_u /σ'_{vo} Trends for Overconsolidatad Clays"., **Jnl. Gotech. Eng. Div., ASCE.**, Vol.110., No.10., October., pp1511-1516.

MAZURKIEWICZ,B.K.(1972) "The Loading of Piles According to Polish Regulations., **Royal Swedish Academy of Engineering Sciences**., Committee on Pile Research., Report No.35., Stockholm.

McCLELLAND,B(1974) "Design of Deep Penetration Piles For Ocean Structures"., **Jnl.Geot.Eng.Div.,A.S.C.E.,**Vol.100.,No.GT7., pp705-747.

MEIGH,A.C.(1987) "Cone Penetration Testing- Methods and Interpretation"., **C.I.R.I.A., London., Butterworth**.

MENARD,L(1965) "Regles pour le calcul de la force portante et du tessament des fondations en fonction des resultats pressiometriques",**Proc. 6th Int.Conf Soil Mech & Found. Engng, Montreal**,Vol.2,pp295-299.

MEYERHOF, G.G.(1992) Various authors. Proc. **Conference on Recent Large-Scale Fully Instrumented Pile Tests in Clay. I.C.E.**, London

MEYERHOF,G.G(1976) "Bearing Capacity and Settlement of Pile Foundations". The 11th Terzaghi Lecture, 5 Nov 1975. **Proc. ASCE., GT3, March.**, pp197-228.

MEYERHOF,G.G. & MURDOCK,L.J.(1953) "An investigation of the Bearing capacity of some Bored and Driven Piles in London Clay", **Goetechnique**,Vol.3,No.7,pp267-282.

MINDLIN,R.D.(1936) "Force at a Point in the Interior of a Semi-Infinite Solid"., **Physics.,** May 1936.

MOHAN,D, JAIN,G.S. & JAIN,M.P.(1967) "A New Approach to Load Tests". **Geotechnique**, Vol.17, pp274-283.

MOORE, J.F.A. & JONES, C.W.(1974) "In-situ Deformation of Bunter Sandstone". **Cambridge Conference on Settlement of Structures**, pp311-319, London, British Geotechnical Society.

MURAYAMA,S & SHIBATA,T(1960) "The Bearing Capacity of a Pile Driven into Soil and Its New Measuring Methods". **Soils and Foundations., Japanese Society of Soil Mechanics and Foundation Engineering,** Vol.1., No.2,pp2-11.

NORWEST HOLST SOIL ENGINEERING(1990) "Butetown Link : Interpretative report, Detailed Considerations, Recommendations and Conclusions for South Glamorgan County Council".

OMER,J.R.(1994) "Elastic Constants Assessment in a Short Concrete Column for the Analysis of Large Bored Piles in Keuper Marl".,**Engineering-South Wales.**,Proc. South Wales Inst. of Engineers.,Vol.102., pp32-44., ISSN: 0969-6539.

OMER,J.R., DELPAK,R. & ROBINSON,R.B.(1995) "Elastic Analysis Of A Short Instrumented Composite Column For Use In The Design Of Large Bored Piles"., **Proc. 4th Int. Conf. Modern Building Materials, Structures & Techniques., Vilnius., Lithuania.,** May., pp 230-236.

O'RIORDAN,N.J(1982) "The Mobilisation of Shaft Adhesion Down a Bored, Cast In-Situ Pile in the Woolwich and Reading Beds". **Ground Engineering**, April 1982, pp17-26.

ORRJE,O & BROMS, B. (1967) "Effects of Pile Driving on Pile Properties"., **Jnl. Soil Mech. & Found. Div., A.S.C.E., Vol. 93., SM 5.**, Sept., Part 1., pp59-74.

OTTAVIANI, M.(1975) "Three Dimensional Finite Element Analysis of Vertically Loaded Pile Groups"., **Geotechnique., London., England.**, Vol.25., pp238-241.

PALMER,D.J & HOLLAND,G.R(1966) "The Construction of Large Diameter Bored Piles With Particular Reference to London Clay"., **Symp. On Large Bored Piles., I.C.E, London,** pp105-120.

PANDEY,V.J(1967) "Some Experiences With Bored Piling"., **J.S. M.F.D., A.S.C.E., Vol.93., SM5, pp75-87.**

PATEL,D.C.(1992) "Interpretation of Results of Pile Tests in London Clay". **Piling Europe. Thomas Telford, ICE, London.**

PECK,R.B(1958) "A Study of The Comparative Behaviour of Friction Piles"., **Highway Research Bulletin., Rep 36., U.S.A.**

PELLS,P.J.N.& TURNER,R.M.(1980) "End-Bearing On Rock With Particular Reference To Sandstone"., **Proc. Int. Conf. On Structural Foundations On Rock., Sydney**., Vol.1., pp 181-190.

PERREN,F.J.(1978) "A Case History of Piling in the Glacial Material of South Wales".,**M.Phil Thesis., Polytechnic of Wales.**

PHOON,K.K, QUEK,S.T., CHOW, Y.K. & LEE, S.L.(1990) " Reliability Analysis of Pile Settlement". **Journal of Geotechnical Engineering,. ASCE**, Vol.116, No.11, pp1717-1735.

POPOV,E.P(1976) **Mechanics of materials**, 2nd Edition, Prentice- Hall Inc., pp562.

POULOS,H.G.(1968) "Analysis of the Settlement of Pile Groups"., **Geotechnique**., London., Vol.18., pp449-471.

POULOS,H.G.(1987) "Analysis of Residual Stress Effects in Piles", **J.Geotech. Engng, Am.Soc.Civ.Engs**,Vol.113,No.3,pp216-229.

POULOS,H.G.(1989) "Pile Behaviour-Theory and Application", **Goetechnique, Vol.39, No.3**,pp365-415.

POULOS,H.G & DAVIS,E.H.(1980) "Pile Foundation Analysis and Design"., **John Wiley & Sons., ISBN 0-471-09956-2**.

POULOS,H.G & DAVIS,E.H.(1968) "The Settlement Behaviour of Single Axially Loaded Incompressible Piles and Piers"., **Geotechnique**., London., Vol.18., pp351-371.

PRICE,G. & WARDLE,I.F.(1982) "A Comparison Between Cone Penetration Test Results and the Performance of Small Diameter Instrumented Piles in Stiff Clay". **Proc. 2nd European Symposium on Penetration Testing**, Amsterdam, 24-27 May, pp775-780.

RANDOLPH,M.F. & MURPHY,B.S.(1985) "Shaft Capacity of Driven Piles in Clay". In **Proc. 17th Offshore Technology Conference, Houston,** Paper OTC 4883, pp371-378.

RANDOLPH,M.F & WROTH,C.P(1982) "Recent developments in understanding the axial capacity of piles in clay". **Ground Engineering**,Vol.15,No.7.

RANDOLPH,M.F & WROTH,C.P(1978) "Analysis of Deformation of Vertically Loaded Piles".,**Jnl. Geotech. Engng. Div., ASCE**., Dec 1978.,GT12.

RANDOLPH,M.F.(1993) "Pile Capacity in Sand- The Critical Depth Myth". **Australian Geomechanics Jounal**., Vol.24, pp30-34.

REESE,L.C, HUDSON,B.S. & VIJAYVERGIJA,B.S.(1969) "An Investigation of the Interaction Between Bored Piles and Soil"., **Proc. 7th Int. Conf. Soil Mech. & Found. Eng**. Vol.2., pp211-215.

REESE,L,C., TOUMA,F.T. & O'NEILL,M.W.(1976) "Behaviour of Drilled Piers Under Axial Loading". **Proc. Journal of the Geotechnical Engineering Division, ASCE**, Vol.102, GT5.

ROBINSON,R.B.(1989) "Piles in Sand and in Sand Overlying Clay"., **Ph.D Thesis, The Polytechnic of Wales.**

ROWE,R.K & ARMITAGE,H.H.(1987) "A Design Method for Drilled Piers in Soft Rock". **Canadian Geotechnical Journal, Vol. 24**, pp126-142

SAN-SHYAN LIN(1997) "Use of Filamented Beam Elements for Bored Pile Analysis". **Journal of Structural Engineering, ASCE**, Vol.123, No. 9, September, pp1236-1244.

SCHMERTMANN,J.H.(1975) "The Measurement of In-situ Shear Strength"., **7th. Proc. Of Soil Mech. & Foundation Division., ASCE.**, Vol.2, pp57-138.

SCHMIDT,H.H & RUMPELT, T.K.(1993) "Pile Load Capacity in Pre-consolidated Keuper Marls of South West Germany: Design and Performance". **Proceedings, International Symposium on Geotechnical Engineering of Hard Soils- Soft Rocks, Balkema, Rotterdam, Vol.2,** pp1021-1027, ISBN 90 54103442.

SEIDEL,J.P. & HABERFIELD,C.M.(1995) "The Axial Capacity of Pile Sockets in Rocks and Hard Soils." **Ground Engineering, March, 1995.**

SEMPLE,R.M & RIGDEN,W.J(1984) "Shaft Capacity of Driven Pipe Piles in Clay"., **Symposium on Analysis and Design of Pile Foundations., ASCE., San Fransisco.**,pp59-79.

SHARMAN,F.A.(1961) "The Anticipated and Observed Penetration Resistance of Some Friction Piles Entirely in Clay".,**Proc. 5th Int. Conf. S.M.& F.E.**, Vol.2.,pp135-141.

SHIOI,Y. and FUKUI,J.(1982) "Application of N-value to the Design of Foundations in Japan.,**Proc. ESOPT2,Amsterdam**, Vol.1, pp159-164.

SKEMPTON,A.W(1951) "The Bearing Capacity of Clays", **Building Research Congress**, ICE, London, pp180-189.

SKEMPTON,A.W(1959) "Cast In-situ Bored Piles in London Clay", **Goetechnique**, Vol.9,No.4,pp153-173.

SKEMPTON,A.W(1961) "Horizontal Stresses in Overconsolidated Eocene Clay".,**Proc. 5th Int. Conf. Soil Mech. & Found. Engng.,pp35-357.**

SKEMPTON,A.W(1966) "Summing up". **Symposium on Large Bored Piles**, London, pp 155.

SLADEN,J.A.(1992) "The Adhesion Factor: Applications and Limitations"., **Canadian Geotechnical Journal., Vol.29., No.2.**, April., pp322-326.

SMALL,J.C & BOOKER,J.R.(1984) "Finite Layer Analysis of Layered Elastic Materials Using a Flexibility Approach-Part 1: Strip Loadings". **International Journal of Numerical Methods in Engineering. Vol.20**, pp1025-1037.

SMALL,J.C & BOOKER,J.R.(1986) "Finite Layer Analysis of Layered Elastic Materials Using a Flexibility Approach-Part 2: Circular and Rectangular Loadings". **International Journal of Numerical Methods in Engineering.** Vol.23, Vol.5, pp959-978.

SMOLTCZYK,U.(1985) "Axial Pile Loading Test-Part 1: Static Loading". **Geotechnical Testing Journal, ISSMFE**, pp79-90.

SOWA,V.A(1970) "Pulling Capacity of Cast in-situ Bored Piles".,**Canadian Geotechnical Journal.**,Vol.7, pp482-493.

ST. JOHN, H.D., RANDOLPH,M.F., MCAVOY, R.P. & GALLAGHER,K.A. (1983) "The Design of Piles for Tethered Platforms". **Proceedings of the Conference on the Design and Construction of Offshore Structures.** Institution of Civil Engineers, London, pp53-64.

STROUD,M.A.(1989) "The Standard Penetration Test- Its Application And Interpretation"., **In ICE conference: Penetration Testing., Birmingham. Thomas Telford**., London., pp29-49.

TAN,T. et.al. (1991) "Hyperbolic Method For Consolidation Analysis"., **Jnl. Geotech. Eng. Div., A.S.C.E., Vol.117., No.11**., Nov., pp1723-1737.

TAVENAS,F.A. & AUDY, R.(1972) "Limitations of the Driving Formulae for Predicting the Bearing Capacity of Piles in Sand". **Canadian Geotechnical Journal**, Vol.9, No.1, February, pp47-62.

TAYLOR,P.T.(1966) "Age Effect on Shaft Resistance and Effect of Loading Rate on Load Distribution of Bored piles"., **Ph.D Thesis, University of Sheffield., England.**

TERZAGHI,K.(1942) "Discussion of The Progress Report of the Committee on Bearing Value of Pile Foundations". **Proc. ASCE., Vol.68**., pp311-323

TERZAGHI,K & PECK(1948) **Soil Mechanics in Engineering Practice**. John Wiley & Sons, New York and Toronto, pp125-169.

THORBURN,S. (1966) "Large Diameter Piles Founded in Bedrock". Proc. **Symp. Large Bored Piles., I.C.E.,** London., pp121-129.

THORBURN,S. & MaC VICAR,R.S.L.(1971) "Pile Load Tests to Failure in the Clyde Alluvium". In *Proc. Conf. on Behaviour of Piles*, ICE, London, pp1-7; pp53-54.

TIMOSHENKO,S.P & GERE,J.M(1972) **Mechanics of materials**, D.Van Nostrand Co., pp19-20.

TIMOSHENKO,S.P. & GOODIER,J.N. (1970) "Theory of Elasticity. 3rd Edition **McGraw-Hill Book Co**. Inc. New York..N.Y.

TOMLINSON,M.J.(1957) "The Adhesion of Piles Driven in Clay Soils",**Proc.4th Int. Conf. Soil Mech. & Found. Eng**.,Vol.2, pp66-71.

TOMLINSON,M.J.(1970) "The Adhesion of Piles in Stiff Clay". **CIRIA. Research Report** No. 26., London.

TOMLINSON,M.J.(1971) "Some Effects of Pile Driving on Skin Friction"., **Proc. Conf. Behaviour of Piles., I.C.E., London**., pp107-114.

TOMLINSON,M.J.(1994) **Pile Design and Construction Practice**.,4th edition,E&F.N. Spon,pp113-115.

TWINE,D.& GROSE, W.(1989) "Discussion on Foundation in Chalk., **pp 147., London., Thomas Telford.**

VAN WEELE, A.A.(1957) "A Method of Separating the Bearing Capacity of a Pile into Skin-Friction and Point Resistance". Proceedings, 4th **International Conference on Soil Mechanics and Foundation Engineering, London**, England, Vol.2, pp76-80.

VESIC,A.S(1963) "Bearing capacity of deep foundations in sand". **National Academy of Sciences, National Research Council,** Highway Research Record 39, pp112-153.

VESIC,A.S.(1964) "Investigations of Bearing Capacity of Piles in Sand". **Proc. North American Conference on Deep Foundations,** Mexico City, 1964.

VESIC,A.S(1967) "A Study of Bearing Capacity of Deep Foundations", **Final report, Project B-189, Engineering Experiment Station, Georgia Institute of Technology**, Atlanta.

VESIC,A.S(1969) "Load Transfer, Lateral Loads and Group Action of Deep Foundations". **Performance of deep foundations, ASTM STP 444, ASTM,** pp5-14.

VESIC,A.S.(1970) "Tests on Instrumented Piles. Ogeechee River Site. Journal of Soil Mechanics and Foundation Engineering Division. **American Society of Civil Engineers**. Vol.96, SM2, pp561-584.

VESIC,A.S.(1977) "Design Of Pile Foundations"., **National Cooperative Highway Research Programme., Synthesis Practice No.42., Transportation Research Board., Washington, D.C.,** pp68.

VIJAYVERGIYA,V.N and FOCHT,J.R(1972) "A New Way to Predict Capacity of Piles in Clay"., **OTC Paper 1178., 4th Offshore Technology Conf., Houston, Texas.**

WARDLE,I.F., PRICE,G. & FREEMAN,T,J.(1992) "Effect of Time and Maintained Load on the Ultimate Capacity of Piles in Stiff Clay". **Piling Europe., Thomas Telford, I.C.E.**, London, pp83-90.

WELTMAN,A.J and HEALY,P.R(1978) "Piling in Boulder Clay and other Glacial Tills".,**Construction Industry Research and Information Association (CIRIA)** Report PG5.

WERSCHING,S.N.(1987) "The Development of Shaft Friction and End Bearing of Piles in Homogeneous and layered Soils"., **Ph.D Thesis, Polytechnic of Wales.**

WHITAKER,T.(1957) "Experiments With Model Piles in Groups"., **Geotechnique**., Vol.7., pp147-167.

WHITAKER,T.(1963) "The Constant Rate of Penetration Test for the Determination of the Ultimate Bearing Capacity of a Pile". **Proc. ICE.**, Vol.26., pp119-123.

WHITAKER,T.(1970) "The Design of Piled Foundations"., **Oxford: Pergamon.**

WHITAKER,T & COOKE,R.W(1961) "A new approach to pile testing".**Proc.5th Int. conf. Soil Mech & Found. Engng.**,Vol.2, pp171-176.

WHITAKER,T & COOKE,R.W(1966) "An Investigation of the Shaft and Base Resistances of Large Bored Piles in London clay". **Proc., Symposium on large bored piles, ICE, London,** pp7-49.

WILLIAMS, A.F.(1980) "The Design and Performance of Piles Socketed into Weak Rock". **PhD Thesis, Monash University, Melbourne**, Australia.

WILSON,L.C(1977) "Tests on Bored and Driven Piles in Cretaceous Mudstone at Port Elizabeth, South Africa". Proc. **Symp. Piles in Weak Rock., I.C.E., London**, pp5-12.

WOODWARD,R & BOITANO,J.(1961) "Pile Loading Tests in Stiff Clays"., **Proc. 5th Int.Conf. S.M.& F.E., Vol.2**,pp177.

WYLLIE,D.C.(1991) "Foundations On Rock"., **E & FN Spon**, 1st Edition.

YAMAGATA,K(1963) "The Yield Capacity of Bearing Piles"., **Proc. Int. Conf. S.M. & F.E., Budapest**., pp325-342.

YAMASHITA,K.,TOMONO,M. and KAKURAI,M(1987) "A method for Estimating the Immediate Settlement of Piles and Pile Groups"., **Soils and Foundations**,Vol.27,No.1,pp61-76.

ZEITLEN,J.G & PAIKOWSKY,S.(1982) ""Discussion:, New Design Correlations For Piles In Sand"., **Jnl. Geotech. Eng. Div., ASCE., GT11.**, Nov., pp1515-1518.

VOLUME 11-APPENDICES

BH No	Description	Depth (m)	Moisture content % Natural	Moisture content % Saturated	Bulk density Mg/m^3	S.P.T Sampler	S.P.T "N"	Cu (from Point load tests) Field MN/m^2	Cu (from Point load tests) Laboratory Ax/Dia	Cu (from Point load tests) Laboratory MN/m^2	U.C.S MN/m^2	Triaxial (undrained) c_u MN/m^2	Triaxial (undrained) ϕ_u (deg)	Triaxial (drained) c' MN/m^2	Triaxial (drained) ϕ' (deg)
49	Red brown highly to completely weathered clayey	16.50				Split	58								
	fragmented to fine gravel sized silty MUDSTONE	18.00				Split	61								
	very weak with weak lithorelicts (Zone IVa K.marl)														
	Red brown and locally grey green intact to slightly	26.00							A	20.92					
	fractured,fresh to slightly weathered silty	26.05							A	21.21					
	MUDSTONE,moderately strong (Zone I-II)	26.10							D	11.68					
		26.10							A	17.39					
		26.25						31.68							
		26.30		5.0	2.68						6.60				
		26.55						34.26							
		26.59						44.07							
		26.62						43.44							
		26.64						44.56							
		26.68						25.16							
		26.70		4.1	2.68						11.70				
		26.95		3.8	2.72						13.20				
	Grey green slightly fractured,fresh to slightly	27.15							A	40.53					
	weathered SILTSTONE,strong (Zone I-II)	27.20							A	25.42					
		27.25							A	14.97					
	Grey green moderately fractured fresh to slightly	29.45													
	weathered silty MUDSTONE,strong. (Zone I-II).														
50	Red brown,slightly to highly weathered,clayey	16.50				Split	75/150								
	fragmented to fine to medium gravel sized silty	17.50				Split	50/75								
	MUDSTONE. Very weak with weak lithorelicts.														
	(Zone III-IVa)														
	Red brown fragmented to fine medium gravel,	21.35	3.8						A	20.39					
	moderately to highly weathered silty MUDSTONE,														
	weak to moderately weak:(Zone II-III)														
	Red brown and locally grey green slightly fractured	26.10						45.20							
	slightly weathered silty MUDSTONE moderately	26.25	2.5						A	28.80					

BH No.	Description	Depth (m)	Moisture content % Natural	Saturated	Bulk density Mg/m^3	S.P.T Sampler	"N"	Cu (from Point load tests) Field MN/m^2	Laboratory Ax/Dia	MN/m^2	U.C.S MN/m^2	Triaxial (undrained) c_u MN/m^2	ϕ_u (deg)	Triaxial (drained) c' MN/m^2	ϕ' (deg)
50	weak and moderately strong with occassional	26.50	2.9					46.85	A	5.41					
	strong bands (Zone II)	26.57						38.62							
	Red brown and locally grey green slightly fractured	26.65						25.83							
	slightly weathered silty MUDSTONE moderately	26.71						38.10							
	weak and moderately strong with occassional	26.75		3.7	2.73			21.64			22.20				
	strong bands (Zone II)	26.95		3.2	2.71						32.30				
		27.10		3.9	2.66						5.10				
	Red brown moderately fractured,moderately to	27.47						4.89							
	slightly weathered silty MUDSTONE,moderately	27.51						24.46							
	weak (Zone II-III)	27.55						23.68							
		27.60						19.95							
		27.70						23.46							
		27.90						5.48							
		27.92						21.31							
		27.94						8.39							
		27.98						5.84							
		28.12						9.36							
		28.17						8.87							
		28.22						10.76							
		28.25		3.9	2.61						7.40				
	Red brown and locally grey green intact to slightly	28.37	2.7						A	24.73					
	fractured,fresh to slightly weathered silty	28.40						17.63							
	MUDSTONE,moderately weak to moderately strong	28.43						23.03							
	(Zone II)	28.47						21.85							
		28.60						20.76							
		28.65						11.62							
		28.70						19.37							
		28.75						11.02							
		29.05	5												
		29.20		2.1	2.67						46.70				

BH No.	Description	Depth (m)	Moisture content % Natural	Saturated	Bulk density Mg/m^3	S.P.T Sampler	"N"	Cu (from Point load tests) Field MN/m^2	Laboratory Ax/Dia	MN/m^2	U.C.S MN/m^2	Triaxial (undrained) c_u MN/m^2	ϕ_u (deg)	Triaxial (drained) c' MN/m^2	ϕ' (deg)
50	Grey green intact to slightly fractured,fresh to slightly	29.30							D	36.07					
	weathered SILTSTONE,strong (Zone I)	29.30							A	55.33					
		29.30							A	42.65					
		29.55						80.93							
		29.60						26.62							
	Red brown slightly fractured,moderately weathered	30.60							D	5.30					
	silty MUDSTONE,moderately weak to moderately	30.60							A	13.95					
	strong (Zone I-II)	30.78							A	15.85					
		30.78	2.3						D	34.43					
		30.78	2.3						A	42.78					
		30.90						28.41							
	Red brown slightly fractured,fresh to slightly	38.10						20.78							
	weathered silty MUDSTONE,moderately strong	38.19						23.24							
	(Zone II-I)	38.24						24.62							
	Red brown moderately fractured,slightly	40.00						31.90							
	weathered,silty MUDSTONE,moderately strong														
	(Zone II-I)														
51	Red brown,highly to completely weathered silty	16.00				Split	39								
	MUDSTONE,very weak clayey with fine gravel size	17.00				Split	58								
	lithorelicts (Zone IVa)														
	Red brown with grey green bands,fresh,slightly	28.00		3.0	2.64						31.00				
	fractured silty MUDSTONE,strong (Zone I)	28.27		4.1	2.58				D	2.65	5.00				
		28.27							A	7.08					
		28.35							D	7.95					
		28.35							A	14.45					
		28.40	3.6						A	21.39					
		29.10	2.2						A	52.05					
		29.20							A	0.80					

BH No.	Description	Depth (m)	Moisture content % Natural	Saturated	Bulk density Mg/m^3	S.P.T Sampler	"N"	Cu (from Point load tests) Field MN/m^2	Laboratory Ax/Dia	MN/m^2	U.C.S MN/m^2	Triaxial (undrained) c_u MN/m^2	ϕ_u (deg)	Triaxial (drained) c' MN/m^2	ϕ' (deg)
51	Red brown slightly weathered,silty MUDSTONE,	30.20							D	17.22					
	moderately strong (Zone II)	30.20							A	23.11					
		30.25							A	20.11					
		30.25							A	5.78					
		30.30							D	5.75					
		30.30							A	28.41					
		30.35							A	55.86					
		30.40	7.8						A	4.58					
		30.40							D	1.60					
	Red brown slightly weathered,silty MUDSTONE,	30.45							A	2.46					
	moderately strong (Zone II)														
	Grey green,slightly weathered SILTSTONE,	30.90		3.1	2.64						10.50				
	moderately strong (Zone II)														
	Red brown,fragmented to fine gravel,moderately to	59.00							D	12.45					
	highly weathered silty MUDSTONE ,fragments	59.00							A	18.83					
	weak to moderately weak (Zone III-II)														
52	Red brown,completely weathered silty MUDSTONE	17.30				Split	37								
	(stiff clay;Marl zone IVa)														
	Red brown fragmented to fine gravel,moderately to	25.75						39.03							
	highly weathered,silty MUDSTONE ,strong (Zone I-II)														
	Red brown highly fractured to fragmented to fine-	29.40							A	21.31					
	medium gravel,moderately to highly weathered	29.45							A	11.03					
	silty MUDSTONE,fragments weak to moderately	29.50							A	8.57					
	weak. (Zone II-III)														
	Red brown and locally grey green intact to slightly	31.10	1.5						D	46.77					
	fractured,fresh to slightly weathered silty	31.10							A	61.29					
	MUDSTONE,moderately weak to moderately strong.	31.25						6.98							
	(Zone I-II)	31.30						21.53							

BH No.	Description	Depth (m)	Moisture content % Natural	Saturated	Bulk density Mg/m^3	S.P.T Sampler	"N"	Cu (from Point load tests) Field MN/m^2	Laboratory Ax/Dia	MN/m^2	U.C.S MN/m^2	Triaxial (undrained) c_u MN/m^2	ϕ_u (deg)	Triaxial (drained) c' MN/m^2	ϕ' (deg)
52	Red brown moderately fractured to fragmented, moderately weathered silty MUDSTONE,fragments moderately weak.(Zone II)	36.80						13.87							
	Red brown and locally grey green intact to slightly fractured,fresh to slightly weathered silty MUDSTONE,moderately weak. (Zone II-I)	41.50						10.92							
		41.55						10.64							
		41.60						7.14							
		41.65						11.21							
	Red brown fragmented to fine medium gravel, moderately weathered silty MUDSTONE,fragments moderately weak. (Zone II)	43.70						34.25							
	Dark rey green slightly fractured,slightly weathered MUDSTONE,strong. (Zone I-II)	49.82						29.88							
	Dark grey green moderately fractured,fresh to slightly weathered MUDSTONE,moderately strong to strong. (Zone I-II with many joints infilled gypsum)	50.90						11.82							
	Dark grey green slightly fractured,fresh to slightly weathered MUDSTONE,moderately strong. (Zone I-II with many joints infilled with gypsum)	53.20						20.89							
	Red brown slightly fractured,fresh to slightly weathered silty MUDSTONE,moderately strong (Zone I-II with many joints infilled with gypsum)	53.40						43.05							
	Red brown moderately fractured,fissured,fresh to slightly weathered silty MUDSTONE,moderately weak to moderately strong (Zone I-II with many joints infilled with gypsum)	54.10						24.77							
		54.30						14.29							

BH No.	Description	Depth (m)	Moisture content % Natural	Moisture content % Saturated	Bulk density Mg/m^3	S.P.T Sampler	S.P.T "N"	Cu (from Point load tests) Field MN/m^2	Cu (from Point load tests) Laboratory Ax/Dia	Cu (from Point load tests) Laboratory MN/m^2	U.C.S MN/m^2	Triaxial (undrained) c_u MN/m^2	Triaxial (undrained) ϕ_u (deg)	Triaxial (drained) c' MN/m^2	Triaxial (drained) ϕ' (deg)
52	Red brown moderately fractured,fresh to slightly weathered silty MUDSTONE,moderately weak to moderately strong (Zone III-I with occassional joints infilled with gypsum	54.90						11.22							
	Red brown intact to slightly fractured,fissured,fresh to slightly weathered silty MUDSTONE,moderately weak to moderately strong (Zone I-II with many joints infilled with gypsum)	56.40						23.89							
		57.30						17.84							
		58.10						8.95							
53	Red brown moderately weathered silty MUDSTONE moderately weak.(Zone II-III)	15.60				Cone	12								
	Red brown completely weathered sandy MUDSTONE,with occassional weak fine grave sized lithorelicts (Zone IVa)	17.00				Split	77/150								
	Grey fresh SILTSTONE,moderately strong (Zone II)	18.00				Split	50/75								
	Grey fresht SILTSTONE,moderately strong (Zone II with red brown MUDSTONE bands).	19.00				?	49								
	Red brown completely weathered,clayey fragmented to fine to medium gravel sized silty MUDSTONE (stiff clay) :Zone III-IVa	20.00				Split	32								
		21.00				Split	22								
	Red brown completely weathered,silty MUDSTONE stiff clay (Zone IV)	22.00				Split	21								
		23.00				Split	34								
	Red brown completely weathered,silty MUDSTONE stiff clay with occassional moderately weathered bands,moderately weak (IVa with bands of III)	24.00				Split	50/75								

BH No.	Description	Depth (m)	Moisture content % Natural	Moisture content % Saturated	Bulk density Mg/m^3	S.P.T Sampler	S.P.T "N"	Cu (from Point load tests) Field MN/m^2	Laboratory Ax/Dia	Laboratory MN/m^2	U.C.S MN/m^2	Triaxial (undrained) c_u MN/m^2	Triaxial (undrained) ϕ_u (deg)	Triaxial (drained) c' MN/m^2	Triaxial (drained) ϕ' (deg)
53	Red brown and locally grey green intact to	34.30	1.3						D	12.99					
	moderately fractured,fresh to slightly weathered	34.30	1.3						A	79.26					
	silty MUDSTONE,moderately weak to moderately														
	strong. (Zone I-II with occassional small cavities).														
	Red brown and locally grey green moderately to	35.10						10.17							
	slightly fractured,weathered silty MUDSTONE,	35.20						22.89							
	moderately weak to moderately strong (Zone II with	37.80						10.92							
	occassional thin bands of fragmented zone III and	37.90						8.95							
	with occassional small solution cavities).														
	Red brown and locally grey green moderately to	38.30						30.12							
	slightly fractured,moderately to slightly weathered	38.40						20.89							
	silty MUDSTONE,moderately strong to strong (Zone	38.45						26.15							
	(II with occassional thin shaley bands with														
	some gypsum.														
54	Red brown clayey highly to completely weathered	13.20				Cone	50/35								
	silty MUDSTONE,very weak to a stiff clay with														
	occassional fine angular mudstone gravel (IVa-III)														
	Red brown highly fractured to fragmented clayey,	14.50				Cone	120/225								
	highly to completely weathered silty MUDSTONE,	15.00				Cone	100								
	fragments very weak to weak.(Zone III-IV with	15.50				Cone	50/35								
	occassional thin bands of moderately weak zone II)														
	Red brown highly occassionally completely	17.00				Cone	85/50								
	weathered silty MUDSTONE,very weak to weak.	17.50				?	87/150								
	(Zone III with some IVa,clayey in parts with	20.00				?	13								
	occassional thin bands of moderately weak zone II-III	20.50				Cone	18								
	Red brown clayey completely weathered silty	21.00				?	66								
	MUDSTONE,firm to stiff clay.(Zone IVa)														

BH No.	Description	Depth (m)	Moisture content % Natural	Moisture content % Saturated	Bulk density Mg/m^3	S.P.T Sampler	S.P.T "N"	Cu (from Point load tests) Field MN/m^2	Cu (from Point load tests) Laboratory Ax/Dia	Cu (from Point load tests) Laboratory MN/m^2	U.C.S MN/m^2	Triaxial (undrained) c_u MN/m^2	Triaxial (undrained) ϕ_u (deg)	Triaxial (drained) c' MN/m^2	Triaxial (drained) ϕ' (deg)
55	Red brown highly weathered,clayey,fragmented to fine to medium gravel sized MUDSTONE,very weak with weak lithorelicts. (Zone III-IVa becoming zone III with depth).	14.80				Split	58								
		16.00				Split	78/150								
	Red brown moderately weathered,silty MUDSTONE, weak. (Zone III-II).	20.60				Cone	150/265								
	Red brown and locally grey green fragmented, weathered,silty MUDSTONE,fragments moderately weak. (Zone II).	23.00				Cone	131/200								
	Red brown fragmented highly to completely weathered,silty MUDSTONE,fragments weak, (Zone III with some IVa;clayey in parts).	32.50				Cone	131/200								
	Red brown and locally grey green highly fractured slightly to moderately weathered silty MUDSTONE, moderately weak to moderately strong fragments. (Zone II).	35.60				Cone	127/195								
	Red brown fragmented to fine to medium sized gravel,moderately to slightly weathered silty MUDSTONE,fragments weak to mederately weak. (Zone II).	42.60				Cone	121/180								
	Red brown and locally grey green intact to slightly fractured,fresh to slightly weathered silty MUDSTONE,moderately strong and strong.(Zone I-II)	48.75		4.6	2.57				A	9.13	3.20				
		49.05						39.04							
		49.60						53.88							
56	Red brown completely to highly weathered,clayey fine medium graval sized,silty MUDSTONE,weak. (Zone III-IVa).	16.50				Split	75								
		17.50				Split	50/75								

BH No.	Description	Depth (m)	Moisture content % Natural	Moisture content % Saturated	Bulk density Mg/m^3	S.P.T Sampler	S.P.T "N"	Cu (from Point load tests) Field MN/m^2	Laboratory Ax/Dia	Laboratory MN/m^2	U.C.S MN/m^2	Triaxial (undrained) c_u MN/m^2	Triaxial (undrained) ϕ_u (deg)	Triaxial (drained) c' MN/m^2	Triaxial (drained) ϕ' (deg)
56	Red brown and locally grey green fragmented to fine-medium gravel sized,highly to completely weathered silty MUDSTONE-Fragments very weak to weak. (Zone III-IVa;clayey in parts with thin bands of zone II).	22.60				Cone	67								
	Red brown highly to completely weathered silty MUDSTONE,very weak. (Zone IVa-III).	35.80				Cone	89/245								
	Red brown and locally grey green intact to slightly fractured,fresh to slightly weathered silty MUDSTONE,strong. (Zone I-II).	43.20		4.1											
		43.50		3.9	2.73						16.60				
		45.70						53.69							
	Grey green intact to slightly fractured fresh SILTSTONE,strong. (Zone I-II).	46.15						20.03							
	Red brown and locally grey green intact to slightly fractured,fresh to slightly weathered silty MUDSTONE,moderately strong. (Zone I-II)	46.90						21.41							
57	Red brown moderately weathered,slightly clayey, completely fractured MUDSTONE,very weak. (Zone III and IVa)	16.50				Split	50								
		17.50				Split	79/150								
	Band of very weak zone IVa-III in within a layer of red brown highly fractured to fragmented to fine-medium gravel,slightly weathered silty MUDSTONE	25.30				Cone	92/90								
	Red brown highly to completely weathered silty MUDSTONE,very weak. (Zone III with occassional bands of zone IVa).	32.50				Cone	92								
		36.50				Cone	90								
	Red brown fragmented to fine gravel,highly to completely weathered silty MUDSTONE,fragments very weak to weak (Zone III;clayey in parts).	39.50				Cone	100								

BH No.	Description	Depth (m)	Moisture content %		Bulk density Mg/m^3	S.P.T		Cu (from Point load tests)			U.C.S MN/m^2	Triaxial (undrained)		Triaxial (drained)	
			Natural	Saturated		Sampler	"N"	Field MN/m^2	Laboratory Ax/Dia	Laboratory MN/m^2		c_u MN/m^2	ϕ_u (deg)	c' MN/m^2	ϕ' (deg)
57	Red brown highly fractured,slightly weathered silty MUDSTONE,moderately weak. (Zone II).	43.70						34.35							
	Red brown and locally grey green intact to slightly fracture,fresh to slightly weathered silty MUDSTONE moderately strong and occassionally stong. (Zone I-II).	44.10						22.41							
		44.20						16.03							
		44.30						21.92							
		44.40		3.8	2.69						22.50				
		44.60		3.1	2.63						14.90				
		45.00	1.4						D	15.89					
		45.00							A	32.77					
		46.60		6.8	2.5						2.70				
58	Red brown moderately weathered,clayey, fragmented to fine to medium gravel,silty MUDSTONE Moderately strong fragments. (Zone III).	16.40				Split	27								
59	Red brown highly weathered,clayey,fragmented to fine gravel sized,silty MUDSTONE,weak with moderately strong lithorelicts. (Zone IVa-III).	17.10				Split	56								
63	Red brown and locally grey green,highly to completely weathered,silty MUDSTONE,very weak with bands of silty clay. (Zone III-IVa with thin bands of zone II).	25.30				Cone	19/460								
	Red brown,slightly to moderately fractured,slightly weathered,silty MUDSTONE,moderately strong to strong. (Zone I-II).	37.30						9.38							
	Red brown and locally grey green,slightly to moderately fractured,fissured,fresh to slightly weathered,silty MUDSTONE,moderately weak to moderately strong. Locally strong. (Zone I-II).	41.20						14.28							

BH No.	Description	Depth (m)	Moisture content % Natural	Saturated	Bulk density Mg/m^3	S.P.T Sampler	"N"	Cu (from Point load tests) Field MN/m^2	Laboratory Ax/Dia	MN/m^2	U.C.S MN/m^2	Triaxial (undrained) c_u MN/m^2	ϕ_u (deg)	Triaxial (drained) c' MN/m^2	ϕ' (deg)
63	Red brown and grey green slightly to moderately fractured,fissured,fresh to slightly weathered,silty MUDSTONE,moderately strong to strong. (Zone I-II).	43.20						10.92							
		43.40						31.45							
		43.50						21.06							
		43.55						22.97							
		43.70						16.90							
		44.30						20.66							
64	Red brown highly weathered,silty MUDSTONE,weak with moderately weak bands. (Zone IVa-III).	17.00				Cone	90								
	Red brown and locally grey green,moderately fractured,moderately weathered,silty MUDSTONE, modrately weak to moderately strong. (Zone II).	21.60							D	3.71					
		21.60							A	10.39					
	Red brown slightly fractured,slightly to moderately weathered,silty MUDSTONE,moderately strong. (Zone II-I).	31.40						12.37							
	Red brown moderately to slightly fractured, moderately to highly weathered, silty MUDSTONE, moderately strong. (Zone II).	34.00						37.69							
	Red brown and locally grey green,slightly fractured, fresh to slightly weathered,silty MUDSTONE, moderately strong to strong. (Zone I-II with occassional thin bands of grey green siltstone.)	39.40						59.51							
		39.50		3.7	2.67			55.94			6.50				
	Red brown slightly fractured,slightly weathered, silty MUDSTONE,moderately strong to strong. (Zone I-II).	42.80						55.72							
		42.95						9.34							
65	Red brown highly weathered,clayey,fragmented silty MUDSTONE,very weak to weak. (Zone III-IVa).	18.50				Split	50/30								

BH No.	Description	Depth (m)	Moisture content % Natural	Saturated	Bulk density Mg/m^3	S.P.T Sampler	"N"	Cu (from Point load tests) Field MN/m^2	Laboratory Ax/Dia	MN/m^2	U.C.S MN/m^2	Triaxial (undrained) c_u MN/m^2	ϕ_u (deg)	Triaxial (drained) c' MN/m^2	ϕ' (deg)
65	Red brown and locally grey green fractured, moderately to slightly weathered silty MUDSTONE, moderately weak to moderately strong. (Zone II).	21.60						13.66							
	Red brown highly to completely weathered MUDSTONE,very weak. (Zone IVa-III;clayey).	26.00				Split	30								
	Red brown fragmented,highly weathered silty MUDSTONE. Fragments weak. (Zone II-III with thin bands of zone IVa).	29.30				Split	31								
	Red brown,slightly to moderately fractured,slightly to moderately weathered silty MUDSTONE, moderately weak to moderately strong. (Zone I-II).	35.00						20.92							
66	Red brown completely weathered,silty MUDSTONE, stiff clay with some moderately weak fine gravel sized lithorelictes. (Zone IVa).	19.55										24	0		
	Red brown,moderately weathered,fragmented to fine to coarse gravel sized silty MUDSTONE, moderately strong fragments. (Zone II).	20.55				Cone	92/100								
	Strong band of Zone I Keuper marl within a main layer of red brown,moderately to highly fractured, moderately weathered,silty MUDSTONE,moderately weak to moderately strong.	23.35		3.8	2.67						22.50				
	Rred brown,moderately to highly fractured, moderately weathered,silty MUDSTONE,moderately weak to moderately strong with bands of weak friable mudstone.(Zone II with thin bands of zone III).	23.55						25.05							

BH No.	Description	Depth (m)	Moisture content % Natural	Saturated	Bulk density Mg/m^3	S.P.T Sampler	"N"	Cu (from Point load tests) Field MN/m^2	Laboratory Ax/Dia	MN/m^2	U.C.S MN/m^2	Triaxial (undrained) c_u MN/m^2	ϕ_u (deg)	Triaxial (drained) c' MN/m^2	ϕ' (deg)
66	Red brown moderately fractured,moderately weathered silty MUDSTONE,moderately strong. (Zone II).	24.00	2.0						D	7.74					
		24.00							A	43.62					
		24.20						25.79							
	Band of moderately strong Zone I Keuper marl within a layer of red brown,moderately to very highly fractured,moderately weathered,silty MUDSTONE (fragments moderately weak and occassionally moderately strong).	37.15		5.6	2.59						0.40				
	Red brown and grey,moderately fractured, moderately weathered,silty MUDSTONE,moderately strong. (Zone II-I).	40.30		5.0	2.50						1.40				
		40.50						26.33							
	Red brown,slightly fractured,slightly to moderately weathered,silty MUDSTONE,moderately strong to strong. (Zone I-II).	44.70						23.67							
		44.80						29.88							
		44.90						36.11							
		45.20		5.6	2.57			27.24			6.50				
		45.40						18.61							
67	Red brown completely weathered,fragmented to fine to coarse gravel sized silty MUDSTONE,very weak with some hard bands. (Zone III with bands of II and IVa).	19.55				Cone	116								
		20.55				Cone	88/225								
		21.30				Cone	132/400								
	Red brown and locally grey green,slightly fractured,fresh to slightly weathered,silty MUDSTONE, moderartely strong. (Zone II locally to zone I).	22.10				Cone	50/225								
		22.55				Cone	79/125								
		22.80				Cone	50/200								
		23.00	3.1					26.68	A	4.64					
	Grey green,slightly weathered,calcerous SILTSTONE,moderately strong.	23.15						23.23							

BH No	Description	Depth (m)	Moisture content % Natural	Saturated	Bulk density Mg/m^3	S.P.T Sampler	"N"	Cu (from Point load tests) Field MN/m^2	Laboratory Ax/Dia	MN/m^2	U.C.S MN/m^2	Triaxial (undrained) c_u MN/m^2	ϕ_u (deg)	Triaxial (drained) c' MN/m^2	ϕ' (deg)
67	Red brown and locally grey green,slightly	23.40	1.6						D	22.82					
	fractured,fresh to slightly weathered,silty	23.40							A	45.16					
	MUDSTONE, moderartely strong. (Zone II locally to	23.80	2.0						A	39.60					
	zone I). Highly fractured from 24.10-24.50m.	24.00						45.71							
		24.20						32.41							
		24.30						27.75							
	Red brown and locally grey green,highlty	26.90							D	8.13					
	weathered,silty MUDSTONE,weak. (Zone III).	26.90							A	22.21					
	Red brown and locally grey green,moderately	28.50						31.57							
	fractured,moderately weathered,silty MUDSTONE;	28.60						26.68							
	fragments moderately weak to weak. (Zone II).														
	Red brown,fragmented,highly weathered,silty	31.00						20.56							
	MUDSTONE (weak fragments). Zone III to locally														
	zone II.														
	Red brown and locally grey green,highly to	36.50		6.4	2.63						0.99				
	moderately fractured,moderately weathered,silty	38.30						40.36							
	MUDSTONE,weak to modderately weak. (Zone II	38.70						18.43							
	with some III bands throughout). Becoming slightly	38.78						22.28							
	fractured and moderately strong between	38.85						16.94							
	36.00-37.00m; 38.60-38.80m; 39.30-39.60m.	40.00		6.6					A	1.40					
	Red brown,locally grey green,slightly to moderately	42.00							A	1.11					
	fractured,slightly weathered,silty MUDSTONE,														
	moderately weak. (Zone II).														
	Red,green and grey,moderately fractured,slightly	43.65						14.05							
	weathered,silty MUDSTONE,moderately strong and	44.00						8.58							
	locally strong. (Zone II).	44.40		2.6					D	14.93					
		44.40							A	32.63					
		44.40							A	71.38					

BH No.	Description	Depth (m)	Moisture content % Natural	Saturated	Bulk density Mg/m^3	S.P.T Sampler	"N"	Cu (from Point load tests) Field MN/m^2	Laboratory Ax/Dia	MN/m^2	U.C.S MN/m^2	Triaxial (undrained) c_u MN/m^2	ϕ_u (deg)	Triaxial (drained) c' MN/m^2	ϕ' (deg)
68	Firm,reddish brown,sandy silty CLAY with	18.00				Cone	71								
	occassional subrounded,fine to coarse gravel	19.00				Split	74								
	(weathered marl).	20.00				Split	59								
		21.00				Cone	80/150								
	Red brown,slightly fractured,fresh to slightly	23.30		4.1	2.67						11.40				
	weathered,silty MUDSTONE,moderately strong to	24.00	2.8						A	0.60					
	strong. (Zone I-II).														
69	Red brown,completely weathered MUDSTONE,	18.50				Cone	78/150								
	(stiff clay-Keuper marl zone IVa with some weak	19.55				?	94								
	bands of zone III-IVa).	20.50				Cone	96/150								
		21.50				Cone	50/75								
	Red brown,fragmented,moderately silty MUDSTONE	23.70							D	47.67					
	Fragments moderately weak to moderately strong.														
	Zone II).														
	Red brown,completely fractured,slightly weathered	25.10						21.28							
	silty MUDSTONE,moderately strong to strong. (Zone	25.20						18.43							
	II with some bands of zone I).	25.40						12.86							
		27.40							D	4.15					
		27.40							A	23.32					
	Grey green,slightly fractured, fresh to slightly	27.50	2.3						D	18.15					
	weathered SILTSTONE,moderately strong. (Zone I-II)	27.50							A	31.12					
		27.55	2.3						A	53.91					
	Red brown,slightly fractured,fresh to slightly	28.00						9.87							
	weathered,silty MUDSTONE,moderately strong to	28.10						25.46							
	strong. (Zone I-II).														
	Red brown,highly to completely weathered,silty	29.15							A	19.07					
	MUDSTONE,very weak. (Zone III-IVa).														

BH No.	Description	Depth (m)	Moisture content % Natural	Saturated	Bulk density Mg/m^3	S.P.T Sampler	"N"	Cu (from Point load tests) Field MN/m^2	Laboratory Ax/Dia	MN/m^2	U.C.S MN/m^2	Triaxial (undrained) c_u MN/m^2	ϕ_u (deg)	Triaxial (drained) c' MN/m^2	ϕ' (deg)
69	Red brown,slightly to moderately fractured, moderately weathered,silty MUDSTONE,moderately weak to moderately strong. (Zone II with thin bands of very weak zone III).	36.20						24.93							
		36.30						25.46							
		36.40						26.15							
	Red brown,slightly fractured,slightly weathered, silty MUDSTONE,moderately strong. (Zone II with thin bands of very weak zone III and strong zone I).	37.15							D	14.00					
		37.15							A	35.65					
		39.60						15.31							
	Red brown,highly fractured,moderately weathered silty MUDSTONE,moderately weak to moderately strong. (Zone II with very thin bands of very weak zone III).	44.00						16.39							
70	Red brown,completely weathered,fragmented to fine to coarse gravel sized,silty MUDSTONE,very weak with weak to hard bands. (Zone III with bands of II and IVa	19.20				Cone	63								
		20.30				Cone	89/150								
	Red brown,highly to completely weathered,silty MUDSTONE,very weak to hard. (Zone IVa and III with bands of very weak zone III from 22.50m to 22.60m and 23.20m to 23.30m.	22.00				Cone	83/112								
		22.80						5.38							
	Red brown and grey green,moderately to slightly weathered,silty MUDSTONE,moderately weak to moderately strong. (Zone II). From 26.80m to 27.10m moderately strong band.	25.60							A	49.61					
		25.65							A	33.30					
		25.70						41.89							
		26.80						67.82							
		27.50						15.05							
		27.50						18.82							
	Red brown moderately weathered,moderately fractured,highly silty MUDSTONE. (Zone II moderately weak with moderately strong bands from 30.90-31.18m.	30.00						45.56							
		31.00						58.09							

BH No.	Description	Depth (m)	Moisture content % Natural	Moisture content % Saturated	Bulk density Mg/m^3	S.P.T Sampler	S.P.T "N"	Cu (from Field MN/m^2	Point load tests) Laboratory Ax/Dia	Laboratory MN/m^2	U.C.S MN/m^2	Triaxial (undrained) c_u MN/m^2	Triaxial (undrained) ϕ_u (deg)	Triaxial (drained) c' MN/m^2	Triaxial (drained) ϕ' (deg)
70	Red brown,highly weathered,fractured,silty MUDSTONE,completely weathered and clayey in parts. (Zone III,very weak to weak with fragmented bands of zone II	31.40						41.21							
		31.50		4.3	2.64						1.10				
	Red brown,silty MUDSTONE,moderately strong. (Zone II-I).	34.90						1.32							
		35.00						8.53							
	Red brown,slightly fractured,slightly weathered silty MUDSTONE,strong. (Zone I).	38.00						19.99							
		38.10						18.59	A	12.61					
		38.15							A	18.86					
	Red brown,highly fractured,moderately to highly weathered,silty MUDSTONE,moderately weak to weak. (Zone II-III with bands of zone II and bands of completely weathered clayey zone IVa and III; weak to very weak;notably between 40.50-40.90m.	41.00						19.62							
		41.35						12.28							
		41.35						18.32							
71	Red brown,highly weathered,fragmented silty MUDSTONE,weak to moderately weak. (Zone III-II).	20.00				Split	50/40								
		21.00				Split	50/20								
	Grey green,slightly fractured,fresh to slightly weathered,SILTSTONE,moderately strong to strong. (Zone I-II).	25.40						41.25							
	Red brown and locally grey green ,slightly fractured fresh to slightly weathered,silty MUDSTONE, moderately strong to strong. (Zone I-II).	25.90						17.60							
		25.95						19.02							
		26.00						21.85							
		26.10		4.5	2.56						6.10				
		26.35		7.3											
		26.55							A	36.66					
		28.40						19.30							
		26.45		3.8	2.70						24.70				
		26.55	2.0												
		26.60							A	22.46					

BH No.	Description	Depth (m)	Moisture content % Natural	Moisture content % Saturated	Bulk density Mg/m^3	S.P.T Sampler	S.P.T "N"	Cu (from Point load tests) Field MN/m^2	Cu Laboratory Ax/Dia	Cu Laboratory MN/m^2	U.C.S MN/m^2	Triaxial (undrained) c_u MN/m^2	Triaxial (undrained) ϕ_u (deg)	Triaxial (drained) c' MN/m^2	Triaxial (drained) ϕ' (deg)
71	Red brown and locally grey green ,slightly fractured	28.65						16.39							
	fresh to slightly weathered,silty MUDSTONE,	28.75						12.02							
	moderately strong to strong. (Zone I-II).														
	Red brown and locally grey,intact to slightly to	30.00							A	18.58					
	moderately fractured,slightly weathered,silty	30.05							A	14.73					
	MUDSTONE,moderately strong with moderately														
	weak bands. (Zone II with occassional thin bands														
	of zone III).														
	Red brown,intact to moderately fractured,fresh to	40.90		3.6	2.63						12.70				
	highly weathered,silty MUDSTONE,moderately weak														
	to moderately strong. (Zone II-I).														
72	Red brown,highly to completely weathered,silty	19.00				Split	80								
	MUDSTONE,stiff clay with some moderately weak	20.00										135	0		
	fine gravel sized lithorelicts. (Zone IVa with bands														
	of zone II-III).														
	Red brown,locally grey green,highly to completely	24.50				Cone	50/25								
	weathered,silty MUDSTONE,very weak,clayey in														
	parts. (Zone III to IVa).														
	Red brown and grey green,slightly fractured,slightly	26.20						24.05							
	weathered,silty MUDSTONE,moderately strong to	26.30						20.96							
	strong. (Zone II with bands of strong zone II-I).	26.55		4.3	2.60						9.40				
		28.20	2.4						A	17.66					
	Red brown,occassionally grey green,moderately	28.55							A	3.83					
	fractured,moderately weathered,silty MUDSTONE,	28.80						26.01							
	moderately strong. (Zone II). Grey green strong	29.95							D	6.22					
	band at 30.30m to 30.65m.	29.95	3.5						A	11.42					
		30.25						20.58							
						(									

BH No.	Description	Depth (m)	Moisture content % Natural	Saturated	Bulk density Mg/m^3	S.P.T Sampler	"N"	Cu (from Point load tests) Field MN/m^2	Laboratory Ax/Dia	MN/m^2	U.C.S MN/m^2	Triaxial (undrained) c_u MN/m^2	ϕ_u (deg)	Triaxial (drained) c' MN/m^2	ϕ' (deg)
72	Red brown,highly to moderately fractured,slightly to	36.10						18.49							
	moderately weathered,silty MUDSTONE,bands of	36.15						14.07							
	moderately weak to moderately strong,becoming														
	strong from 36.30m to 37.00m. (Zone II).														
	Vertical fracture from 35.40-35.90m.														
	Red brown and locally grey green,moderately	40.30						3.81							
	fractured,slightly to moderately weathered,silty	42.65						9.15							
	MUDSTONE,moderately weak and moderately														
	strong bands. (Zone II with bands of zone III from														
	40.60m -40.90m and 41.00m-41.40m.).														
	Red brown,slightly fractured,slightly weathered to	43.70						20.07							
	fresh,silty MUDSTONE,moderately strong to strong.														
	(Zone II-I).														
73	Red brown,completely weathered silty MUDSTONE,	19.00										51	0		
	(stiff clay)- Keuper marl Zone IVa).														
	Red brown with some grey green moderately	26.00				Cone	50/10								
	weathered,moderately fractured silty MUDSTONE,	28.25							D	26.42					
	moderately strong with some stong bands. (Zone II	28.25							A	25.85					
	with some zone I). At 28.00-28.15m:Fragmented to	29.15						54.79							
	fine to coarse gravel sized. At 29.15m:Grey band.	29.95		6.3											
		30.40							D	6.47					
		30.40							A	39.65					
	Red brown,highly weathered,completely fractured	32.00				(Cone	108/225								
	to medium to coarse gravel size,silty MUDSTONE,	33.00				Cone	93/125								
	moderately weak;clayey in parts. (Zone III).														
	Light red brown,slightly weathered,slightly	44.00				Cone	91/100								
	fractured,silty MUDSTONE,strong. (Zone II-I).														

BH No.	Description	Depth (m)	Moisture content % Natural	Moisture content % Saturated	Bulk density Mg/m^3	S.P.T Sampler	S.P.T "N"	Cu (from Point load tests) Field MN/m^2	Laboratory Ax/Dia	Laboratory MN/m^2	U.C.S MN/m^2	Triaxial (undrained) c_u MN/m^2	Triaxial (undrained) ϕ_u (deg)	Triaxial (drained) c' MN/m^2	Triaxial (drained) ϕ' (deg)
74	Red brown,highly to completely weathered,	18.00				Split	91								
	completely fractured,silty MUDSTONE,very weak	19.50				Split	104								
	with weak fragments,clayey. (Zone III-IVa).														
	Red brown and grey,highly weathered,silty	21.00				Split	50/300								
	MUDSTONE, Very weak. (Zone III with some IVa).														
	Red brown and grey,moderately weathered,weak,	22.50				?	50/75								
	silty MUDSTONE. (Zone III to II).														
	Red brown and locally grey green,intact to slightly	26.65	2.9						A	1.28					
	fractured,slightly weathered,silty MUDSTONE,	26.70	2.2						A	42.34					
	moderately strong,occassionally strong. (Zone II-I).	26.80		3.8	2.60				A	17.37	17.90				
	Moderately weak band at 27.40m-27.80m.	27.00		4.3	2.66						5.20				
	Becoming moderately to highly fractured below	27.25						19.08							
	27.40m depth.	27.35						13.98							
	Red brown,moderately fractured,slightly weathered	28.50							A	27.38					
	silty MUDSTONE,moderately weak to moderately	28.55							A	62.74					
	strong. (Zone II).	29.30	2.7						A	37.62					
	Grey green,slightly weathered SILTSTONE,strong.	29.50	2.3												
	(Zone I-II).														
	Red brown,moderately weathered,moderately	44.50						22.43							
	fractured,silty MUDSTONE,moderately strong.														
	(Zone II with some III).														
76	Red brown,highly weathered,clayey,gravel sized	20.20				Split	52								
	silty MUDSTONE,very weak (fragments moderately	21.70				Cone	52								
	weak)...Zone III.	23.20				Cone	99								
	Light grey SILTSTONE and red brown silty	24.00				Cone	50/75								
	MUDSTONE,moderately weathered,fragmented to														
	medium to coarse gravel sized. Mod weak. (III-II).														

BH No.	Description	Depth (m)	Moisture content % Natural	Saturated	Bulk density Mg/m^3	S.P.T Sampler	"N"	Cu (from Point load tests) Field MN/m^2	Laboratory Ax/Dia	MN/m^2	U.C.S MN/m^2	Triaxial (undrained) c_u MN/m^2	ϕ_u (deg)	Triaxial (drained) c' MN/m^2	ϕ' (deg)
76	Grey,slightly weathered SILTSTONE,moderately strong. (Zone II).	29.25		3.3	2.57						35.20				
	Red brown,slightly weathered,moderately fractured silty MUDSTONE,moderately strong with strong bands and vertical fissures. (Zone II). At 29.45-34.20m:Joint 90 degrees with calcite infill. At 30.30-32.25m:Thin,completely fractured bands. At 31.90-32.05m:Grey band.	29.50							A	29.24					
	Red brown,slightly weathered,fragmented to coarse gravel and cobble size silty MUDSTONE. Moderately strong fragments. (Zone II-III). At level 41.80-41.85m:Void infilled with calcite.	41.00						8.40							
	Red brown,moderately weathered,silty MUDSTONE moderately strong. (Zone II). At 44.60-44.70m:Moderately weathered, completely fractured to medium gravel size,weak with moderately strong fragments. (Zone III). At 43.50-45.50m:Moderately weathered, completely fractured to medium to coarse gravel size,weak with moderately weak fragments.	43.90						20.35							
		43.95						16.39							
		44.90						5.46							
		44.95						12.77							
	Red brown,moderately weathered,moderately fractured,silty MUDSTONE,moderately strong and strong.(Zone II). At 55.20-55.50m:Solution cavities present.	55.40						5.91							
		55.80						5.91							
		55.90						8.01							
		55.95						6.85							
	Red brown,moderately weathered,moderately fractured,silty MUDSTONE,moderately strong with bands of strong and moderately weak. (Zone II with thin band of zone II-III). At 57.00-57.95m:Highly fractured.	56.60						25.57							
		57.30						12.68							
		57.34						17.34							
		57.45						16.82							

BH No.	Description	Depth (m)	Moisture content % Natural	Saturated	Bulk density Mg/m^3	S.P.T Sampler	"N"	Cu (from Point load tests) Field MN/m^2	Laboratory Ax/Dia	MN/m^2	U.C.S MN/m^2	Triaxial (undrained) c_u MN/m^2	ϕ_u (deg)	Triaxial (drained) c' MN/m^2	ϕ' (deg)
77	Red brown completely weathered,silty MUDSTONE,	22.00				Cone	98								
	very weak. (Zone IVa with occassional bands of	23.00				Cone	88/150								
	moderately weak zone II.)	24.00				Cone	91								
	Red brown,highly to completely weathered silty	28.60							D	79.65					
	MUDSTONE,very weak. Zone III-IVa with	28.70							A	38.53					
	occassional thin bands of zone II and with bands of														
	very weak zone IVa-III from 27.90-28.00m;28.35-														
	28.45m.														
	Red brown and locally grey green,slightly fractured	29.10							A	42.44					
	slightly weathered,silty MUDSTONE,moderately	29.40		4.4	2.74						3.00				
	strong to strong. (Zone I-II). Core length up to 0.4m.	29.70		3.8	2.68						20.80				
		29.90		3.8	2.66						17.70				
	Red brown,moderately weathered,highly to	30.70							A	92.23					
	moderately fractured,silty MUDSTONE,moderately														
	strong. (Zone II).														
	Red brown and locally grey green,moderately	32.60						9.53							
	fractured,moderately weathered,silty MUDSTONE,	33.10		4.1	2.50						8.40				
	(fragments moderately weak to moderately strong)														
	(Zone II).														
	Red brown and grey,slightly weathered silty	33.40		4.0	2.65						20.00				
	MUDSTONE,strong. (Zone I-II).														
78	Red brown,completely weathered silty MUDSTONE	23.50				Cone	117/225								
	(stiff clay). Zone IVa with moderately weak bands	24.50				Cone	50/75								
	of zone III-II.														
	Red brown and locally grey green,slightly fractured	27.35							A	12.96					
	slightly weathered,silty MUDSTONE,moderately	27.50						18.34							
	strong,locally strong. (Zone II with some I)	27.60						22.44							
		27.70						19.08							

BH No	Description	Depth (m)	Moisture content % Natural	Moisture content % Saturated	Bulk density Mg/m^3	S.P.T Sampler	S.P.T "N"	Cu (from Point load tests) Field MN/m^2	Cu (from Point load tests) Laboratory Ax/Dia	Cu (from Point load tests) Laboratory MN/m^2	U.C.S MN/m^2	Triaxial (undrained) c_u MN/m^2	Triaxial (undrained) ϕ_u (deg)	Triaxial (drained) c' MN/m^2	Triaxial (drained) ϕ' (deg)
78	Red brown and locally grey green,slightly fractured slightly weathered,silty MUDSTONE,moderately strong,locally strong. (Zone II with some I)	28.00						24.66							
		28.10		4.0	2.75						22.30				
		28.60		5.5	2.68			9.05	A	31.31	2.00				
		28.65							A	9.63					
	Red brown,slightly fractured,slightly weathered, silty MUDSTONE,moderately weak to moderately strong. (Zone II).	30.30	5.8												
		30.80						15.55							
		31.00						19.10							
	Red brown and locally grey green,slightly fractured, slightly weathered,silty MUDSTONE,moderately strong to strong. (Zone I-II).	31.65							D	8.86					
	Red brown,fragmented,highly weathered,silty MUDSTONE,moderately weak with weak bands. (Zone II with bands of very weak III-IVa).	36.85							A	11.43					
	Red brown,fragmented,highly weathered,silty MUDSTONE,very weak to weak. (Zone II-III with a band of very weak zone III from 37.40-37.50m.	37.65							D	9.53					
	Red brown and locally grey green,moderately fractured,moderately weathered,silty MUDSTONE, moderately strong. (Zone II).	38.90						8.50							
	Red brown and locally grey green,moderately to highly fractured,moderately to slightly weathered silty MUDSTONE,moderately strong with some moderately weak bands. Zone II).	41.90						20.01							
	Red brown,slightly fractured,moderately to slightly weathered,silty MUDSTONE,moderately weak to moderately storng. (Zone II).	43.70							D	7.26					
		43.70							A	37.31					

BH No.	Description	Depth (m)	Moisture content % Natural	Saturated	Bulk density Mg/m^3	S.P.T Sampler	"N"	Cu (from Point load tests) Field MN/m^2	Laboratory Ax/Dia	MN/m^2	U.C.S MN/m^2	Triaxial (undrained) c_u MN/m^2	ϕ_u (deg)	Triaxial (drained) c' MN/m^2	ϕ' (deg)
79	Red brown and grey green ,completely weathered,	22.70				?	88/400								
	silty MUDSTONE,(stiff clay with moderately weak	23.20				?	50/400								
	lithorelicts) (Zone IVa-III).														
	Red brown,highly to completely weathered,silty	23.80				?	50/200								
	MUDSTONE,very weak to hard. (Zone III with	24.00				?	86/150								
	bands of IVa-II).														
	Red brown and locally grey green,moderately to	27.75						10.31							
	highly weathered,silty MUDSTONE,very weak to														
	weak. (Zone III to locally zone II).														
	Red brown,locally grey green,slightly to moderately	28.30						39.10							
	fractured,slightly weathered,silty MUDSTONE,with	28.80		4.3	2.66						4.70				
	vertical fractures,moderately strong,with	30.30		5.4											
	moderately weak and strong bands. (Zone II with														
	some zone I).														
		31.15							D	2.49					
		31.15							A	27.45					
		31.20						14.64							
	Grey green,slightly weathered,calcerous	31.45							A	59.67					
	SILTSTONE,strong. (Zone I-II).														
	Red brown locally grey gren,moderately fractured,	31.75							A	24.37					
	slightly to moderately weathered,silty MUDSTONE,	31.80							A	24.41					
	moderately strong. (Zone II).	32.00							D	49.78					
		32.00							A	73.05					
		32.51	3.0						A	3.41					
		32.60							A	35.70					
	Red brown and locally grey green,highly to	38.20							A	10.92					
	moderately fractured,moderately weathered,silty	40.50						8.57							
	MUDSTONE,moderately weak with some moderately														
	strong and weak bands. (Zone to locally III).														

BH No.	Description	Depth (m)	Moisture content % Natural	Moisture content % Saturated	Bulk density Mg/m^3	S.P.T Sampler	S.P.T "N"	Cu (from Point load tests) Field MN/m^2	Laboratory Ax/Dia	Laboratory MN/m^2	U.C.S MN/m^2	Triaxial (undrained) c_u MN/m^2	Triaxial (undrained) ϕ_u (deg)	Triaxial (drained) c' MN/m^2	Triaxial (drained) ϕ' (deg)
79	Red brown and grey,slightly to moderately weathered,moderately fractured,silty MUDSTONE, moderately weak to moderately strong. (Zone II).	43.60		3.2	2.54						12.00				
80	Red brown,highly weathered,clayey,fragmented,	21.00				Split	132								
	silty MUDSTONE,very weak to hard. (Zone IVa,	22.60				?	50/75								
	becoming IVa-III and weak).														
	Grey green,slightly fractured,fresh to slightly	28.90							D	24.37					
	weathered,SILTSTONE,moderately strong to strong	28.90							A	53.46					
	(Zone I-II).	29.00							A	44.74					
		29.10		4.7				21.41							
	Red brown,slightly fractured,slightly weathered,	29.15						12.45							
	silty MUDSTONE,moderately strong and strong.Core	29.30						13.69							
	length upto 0.4m. (Zone I-II).	29.40						14.28							
		29.75		3.8	2.66						19.70				
		30.00		3.9	2.64						13.20				
		30.20		4.1	2.59						9.90				
	Red brown,slightly fractured,slightly weathered,	31.90							A	0.91					
	silty MUDSTONE,moderately strong to strong.	31.95							A	3.94					
	(Zone I-II).	32.00							A	6.46					
	Red brown and grey green,slightly fractured to	33.15		4.5	2.58						5.80				
	slightly weathered,silty MUDSTONE,moderately	33.50							D	29.66					
	strong,with vertical fractures. (Zone I-II).	33.50							A	46.44					
		33.60	1.9						D	48.87					
		33.80									17.30				
	Red brown and locally grey green,fragmented moderately weathered,silty MUDSTONE,fragments moderately strong. (Zone II).	36.50				?	50/20								

BH No.	Description	Depth (m)	Moisture content % Natural	Saturated	Bulk density Mg/m^3	S.P.T Sampler	"N"	Cu (from Point load tests) Field MN/m^2	Laboratory Ax/Dia	MN/m^2	U.C.S MN/m^2	Triaxial (undrained) c_u MN/m^2	ϕ_u (deg)	Triaxial (drained) c' MN/m^2	ϕ' (deg)
81	Red brown and locally grey green,intact to slightly	28.10						24.45							
	fractured,fresh to slightly weathered,silty	28.15						28.40							
	MUDSTONE,moderately weak to moderately strong,	28.20						21.28							
	with occassional strong bands. (Zone I-II).	28.30							A	11.62					
		28.45						39.79							
		28.65						21.41							
		28.75						38.42							
		29.00						39.78							
		29.40						71.00							
		29.60						42.77							
		29.70		5.3	2.60						6.60				
		30.15		3.6	2.60						10.90				
	Red brown,fragmented to fine-medium gravel,	30.60							D	5.15					
	slightly weathered,silty MUDSTONE,(fragments														
	moderately weak). (Zone II with a band of very														
	weak zone IVa-III from 31.30-31.40m.)														
	Red brown,highly fractured,slightly weathered,	36.50						15.69							
	silty MUDSTONE,moderately weak. (Zone II with														
	bands of moderately weak to moderately strong														
	zone I-II from 36.60-36.70m.														
	At 36.80-36.90m:...with occassional solution														
	cavities.														
	Red brown,intact to moderately fractured,fresh to	40.40						21.41							
	slightly weathered,silty MUDSTONE,moderately	40.44						38.79							
	weak,with occassional moderately strong bands.	40.60						20.33							
	(Zone II-I).	40.70						33.65							
		40.73						27.65							
		40.76						36.40							
		40.84						25.43							
		40.87						10.41							

BH No.	Description	Depth (m)	Moisture content % Natural	Saturated	Bulk density Mg/m^3	S.P.T Sampler	"N"	Cu (from Point load tests) Field MN/m^2	Laboratory Ax/Dia	MN/m^2	U.C.S MN/m^2	Triaxial (undrained) Cu MN/m^2	ϕ_u (deg)	Triaxial (drained) Cu MN/m^2	ϕ' (deg)
81	Red brown,highly fractured,fresh to slightly weathered,silty MUDSTONE,moderately weak to moderately strong. (Zone II-I,with occassional solution cavities.)	43.00						24.42							
84	Red brown,with grey green bands,highly weathered,fragmented to fine and occassionally medium gravel sized,silty MUDSTONE,very weak. (Zone III to IVa).	21.00				Split	88								
		22.50				Split	88/150								
	Red brown,moderately weathered,clayey,silty MUDSTONE,very weak. (Zone III).	23.50				Split	79/150								
	Red brown and locally grey green to slightly fractured,slightly weathered,silty MUDSTONE, moderately strong,occassionally strong. (Zone II-I).	29.40						27.91							
		29.50						27.71							
		29.75						23.87							
		29.90						22.10							
		29.95						30.75							
	Red brown and locally grey green,moderately to slightly fractured,moderately to slightly weathered, silty MUDSTONE,moderately weak to moderately strong. (Zone II).	30.00		3.6	2.56				D	12.45	19.40				
		30.05						15.64							
	Grey green,intact to slightly fractured,fresh to slightly weathered,SILTSTONE,strong. (Zone I-II).	32.30							D	28.88					
		32.45							D	33.81					
		32.45							A	11.39					
		32.52						45.84							
	Red brown,moderately fractured,moderately to slightly weathered,silty MUDSTONE,moderately weak to moderately strong. (Zone II with occassional shaly areas.	33.90						20.10							
		34.00						21.44							

BH No.	Description	Depth (m)	Moisture content % Natural	Saturated	Bulk density Mg/m^3	S.P.T Sampler	"N"	Cu (from Point load tests) Field MN/m^2	Laboratory Ax/Dia	MN/m^2	U.C.S MN/m^2	Triaxial (undrained) Cu MN/m^2	ϕ_u (deg)	Triaxial (drained) Cu MN/m^2	ϕ' (deg)
85C	Red brown and locally grey green,slightly	31.75		4.2	2.55						6.80				
	fractured,slightly weathered,silty MUDSTONE,	31.90		5.7	2.55						1.80				
	moderately strong to strong. (Zone II-I).	32.10		4.4	2.62						5.70				
87	Red brown,highly weathered,clayey,fragmented to	21.30				Cone	70								
	fine gravel sized silty MUDSTONE,very weak.														
	(Zone IVa with some III and thin grey siltstone														
	bands,moderately strong.														
	Red brown,moderately to highly fractured,slightly	26.45		3.7	2.71						16.30				
	weathered,silty MUDSTONE,moderately strong.	28.35		5.1	2.53						3.70				
	(Zone II).														
	25.80-26.30m..Fragmented to coarse gravel and cobble size.														
	26.30-27.55m..Slightly fractured.														
	27.55-28.00m..Highly fractured.														
	28.00-28.20m..Fragmented to fine to coarse gravel size.														
	28.20-28.40m..Fragmented to coarse gravel and cobble size fragments.														
	Red brown,slightly weathered,slightly fractured,	28.60							A	8.70					
	silty MUDSTONE,moderately strong to strong. (Zone	28.70							A	11.49					
	II with some some I). Grey green band at 30.30 to	28.75							A	7.36					
	30.50m.	29.00		4.4					A	12.20					
		29.00							D	8.13					
		29.00							A	31.52					
		29.15							D	7.11					
		29.15							A	22.55					
		30.05		4.1	2.64						10.00				
88	Red brown,moderately to highly weathered,	23.00				Cone	81/150								
	fragmented to fine to medium gravel size,silty														
	MUDSTONE,moderately weak,clayey. (Zone II-III).														

BH No.	Description	Depth	Moisture content %		Bulk	S.P.T		Cu (from Point load tests)			U.C.S	Triaxial (undrained)		Triaxial (drained)	
		(m)	Natural	Saturated	density	Sampler	"N"	Field	Laboratory		MN/m^2	Cu	ϕ_u	Cu	ϕ'
					Mg/m^3			MN/m^2	Ax/Dia	MN/m^2		MN/m^2	(deg)	MN/m^2	(deg)
88	Red brown,moderately to highly weathered,	24.00				Cone	50/75								
	fragemented to fine to medium gravel size,silty	25.00				Cone	81/150								
	MUDSTONE,clayey,weak. (Zone III to II with thin	26.00				Cone	50/75								
	bands of zone II).														
	Red brown and locally grey green slightly fractured	30.80						30.97							
	slightly weathered,silty MUDSTONE,moderately	31.70				Split	50/25								
	strong,occassionally strong. (Zone II-I). Vertical														
	fracture at 30.70-31.20m.														
	Red brown and locally grey green slightly fractured,	33.60		4.2	2.65						7.90				
	fresh to slightly weathered,silty MUDSTONE,	33.75	1.7						D	30.41					
	moderately strong and strong. (Zone I-II).	33.75							A	63.59					
		33.80		3.5	2.75										
	Red brown,fragmented,moderately weathered,silty	37.20				Cone	127/260								
	MUDSTONE. Fragments moderately weak to														
	moderately strong.(Zone II).														
	Red brown,slightly fractured,fresh to slightly	40.90						15.27							
	weathered,silty MUDSTONE,moderately strong,	41.00						17.66							
	slightly vuggy in parts,occassionally strong. (Zone	41.10						17.48							
	II-I with a moderately weak band of zone III from														
	39.50-39.60m.														
89A	Red brown,highly weathered,fragmented to fine	19.00				Split	50/75								
	gravel sized,silty MUDSTONE,very weak;lithorelicts														
	weak to moderately weak. (Zone III).														
	Red brown,highly to completely weathered,	21.00				Split	50/75								
	fragmented to coarse sand to medium gravel sized,	22.00				Cone	88/150								
	silty MUDSTONE,weak to very weak. (Zone II with														
	some IVa).														

BH No.	Description	Depth (m)	Moisture content % Natural	Saturated	Bulk density Mg/m^3	S.P.T Sampler	"N"	Cu (from Point load tests) Field MN/m^2	Laboratory Ax/Dia	MN/m^2	U.C.S MN/m^2	Triaxial (undrained) Cu MN/m^2	ϕ_u (deg)	Triaxial (drained) Cu MN/m^2	ϕ' (deg)
89A	Red brown and locally grey green,slightly	26.55						38.75							
	fractured,slightly weathered,silty MUDSTONE,	26.60		3.8	2.68				A	37.14	9.90				
	moderately strong to strong. (Zone II with some	26.70	1.3						D	46.23					
	zone I).	26.70							A	62.52					
		26.75	4.4												
		26.80							D	19.71					
		26.80							A	30.16					
		27.90							A	27.46					
		28.00	2.3						D	6.22					
		28.80		6.3	2.66						4.10				
		29.40						36.70							
		29.60						34.22							
	Red brown,fragmented,highly to completely	33.50				Cone	81/225								
	weathered,silty MUDSTONE. Fragments very weak														
	to weak. (Zone III-IVa;clayey in parts.)														
90	Red brown,completely weathered silty	18.00				Split	54								
	MUDSTONE,hard,very weak. (Zone IVa-III).	19.50				Split	59								
		21.00				Split	50/75								
	Grey green,slightly fractured,highly weathered	26.10						61.06							
	SILTSTONE,strong. (Zone I-II).														
	Red brown and locally grey green,moderately to	27.80	2.3						A	73.79					
	slightly fractured,slightly weathered,silty	28.40						16.18							
	MUDSTONE,moderately strong,occassionally	29.00	4.8												
	strong. (Zone II-I).	29.80							D	46.53					
		29.80							A	34.98					
		29.95							A	75.55					
	Red brown and locally grey green,moderately to	30.20						9.62							
	slightly fractured,slightly weathered,silty	30.30							A	26.79					
	MUDSTONE,moderately strong;occassionally strong	30.75							A	13.94					
	(Zone II-I with bands of III).	30.80						25.83							

BH No.	Description	Depth (m)	Moisture content % Natural	Saturated	Bulk density Mg/m^3	S.P.T Sampler	"N"	Cu (from Point load tests) Field MN/m^2	Laboratory Ax/Dia	MN/m^2	U.C.S MN/m^2	Triaxial (undrained) Cu MN/m^2	ϕ_u (deg)	Triaxial (drained) Cu MN/m^2	ϕ' (deg)
90	Red brown,fragmented,moderately weathered,silty MUDSTONE,fragments moderately weak and moderately strong. (Zone II).	32.00		5.2											
	Red brown,fragmented,moderately weathered,silty MUDSTONE,fragments moderately strong. (Zone II with bands of very weak zone III from 34.20-34.30m 34.50-34.60m. A band of zone II-I at 36.00-36.10m	35.10				Cone	88/105								
91	Red brown,highly to completely weathered,clayey, fragmented silty MUDSTONE,weak. (Zone IVa-III).	18.00				Split	80								
		19.50				Split	106								
	Red brown and locally grey green,highly to moderately fractured,moderately weathered,silty MUDSTONE,weak with bands of moderately strong. Zone III with bands of II and IVa).	25.00				Split	164/275								
	Red brown and grey green,moderately fractured, moderately weathered,silty MUDSTONE,moderately strong. (Zone III).	27.75							D	2.05					
		27.85							A	8.24					
		28.00				?	81/101								
	Red brown,moderately fractured to fragmented silty MUDSTONE,fragments moderately weak to moderately strong. (Zone II). Moderately strong to strong bands of grey green SILTSTONE from 30.60-30.70m and 30.90-31.10m.	30.00							A	52.02					
		31.10							A	10.41					
	Red brown,highly fractured,highly weathered,silty MUDSTONE,weak to moderately weak. (Zone III with a band of strong SILTSTONE from 32.90-33.10m.	33.00				Split	98/95								
	Red brown,moderately weathered,highly fractured silty MUDSTONE,fragments moderately strong. (Zone II,fragmented from 36.80-37.20m and 38.20-38.60m.	35.70				Split	127								

BH No.	Description	Depth (m)	Moisture content % Natural	Moisture content % Saturated	Bulk density Mg/m^3	S.P.T Sampler	S.P.T "N"	Cu (from Point load tests) Field MN/m^2	Laboratory Ax/Dia	Laboratory MN/m^2	U.C.S MN/m^2	Triaxial (undrained) Cu MN/m^2	Triaxial (undrained) ϕ_u (deg)	Triaxial (drained) Cu MN/m^2	Triaxial (drained) ϕ' (deg)
92	Red brown,completely weathered,fragmented to	19.30				Split	53								
	fine gravel sized,silty MUDSTONE,very weak to	20.50				?	50/40								
	weak with somr moderately strong fragments	21.55				Cone	50/75								
	(Zone IVa with thin bands of zone II).	22.50				Cone	76/105								
		22.55				Cone	98								
	Red brown,highly weathered,fine to coarse gravel	23.55				?	50/75								
	sized,silty MUDSTONE,weak with moderately														
	strong lithorelicts. (Zone II-III).														
	Red brown,slightly weathered,moderately	30.35						28.53							
	fractured,silty MUDSTONE,moderately strong and	31.25							D	35.79					
	strong,with vertical fractures. (Zone II).	31.25	1.8						A	64.35					
	At 27.45-30.10m: Joint 90 degrees.														
	At 30.55-30.70: Grey band.														
	At 31.90-32.00: Weak clay band.														
	At 32.00-32.20m: Fragmented to medium to coarse														
	gravel and cobble sized														
	Red brown,moderately weathered,fragmented to	35.00				Cone	127/235								
	coarse gravel and cobble size,silty MUDSTONE,	36.00				Cone	92/90								
	moderately strong with some strong bands.	37.20						21.71							
	(Zone II).														
93	Red brown,moderately fractured,slightly weathered	29.05						8.19							
	silty MUDSTONE,moderately strong. (Zone II with	29.10						9.19							
	a band of moderately strong zone I from 29.20 to	29.15						9.78							
	29.30m and 29.50-29.60m.														
	Red brown and slightly grey green, slightly	30.85		5.2	2.60						4.70				
	fractured,slightly weathered,silty MUDSTONE,	31.60		3.6	2.58						9.10				
	moderately strong to strong,with strong bands.														
	(Zone I-II).														

BH No.	Description	Depth	Moisture content %		Bulk	S.P.T		Cu (from Point load tests)			U.C.S	Triaxial (undrained)		Triaxial (drained)	
		(m)	Natural	Saturated	density	Sampler	"N"	Field	Laboratory		MN/m^2	Cu	ϕ_u	Cu	ϕ'
					Mg/m^3			MN/m^2	Ax/Dia	MN/m^2		MN/m^2	(deg)	MN/m^2	(deg)
94	Red brown,highly weathered,clayey,completely	17.30				Split	67								
	fractured,silty MUDSTONE,weak. Structure intact.	18.50				Split	91								
	(Zone III).	20.10				Split	77/150								
	Red brown and locally grey green,highly to	23.00				Cone	121/185								
	completely weathered,silty,friable MUDSTONE,weak	24.00				Cone	134/155								
	to moderately weak. (Zone III with some IVa).	25.00				Cone	125/165								
		26.00				Cone	98/80								
	Red brown and locally grey green,slightly to	27.50						15.64							
	moderately fractured,slightly weathered,silty	27.55						13.82							
	MUDSTONE,moderately strong;occassionally	27.64						22.05							
	strong. (Zone II with thin bands of moderately weak	27.70						27.12							
	zone II and occassional strong bands of zone I with	27.90						58.12							
	a thin band of siltstone from 29.50-29.55m.	28.00						42.34							
		28.05						37.67							
		28.12						37.08							
		28.20							D	19.98					
		29.20						12.32							
		29.30						10.27							
		29.38						5.20							
		29.42						5.94							
		29.60							D	8.82					
		29.80						6.41							
		29.85						13.42							
		29.90						24.98							
		30.00							A	13.77					
		30.20							D	2.07					
		30.20							A	13.54					
		30.70							A	20.48					
	Red brown and locally grey green,slightly fractured	31.10						20.22							
	slightly weathered,silty MUDSTONE,moderately	31.20	6.2						A	4.85					
	strong. (Zone I-II).	31.30	2.8						D	1.47					
		31.30							A	26.25					

BH No.	Description	Depth (m)	Moisture content % Natural	Moisture content % Saturated	Bulk density Mg/m^3	S.P.T Sampler	S.P.T "N"	Cu (from Point load tests) Field MN/m^2	Laboratory Ax/Dia	Laboratory MN/m^2	U.C.S MN/m^2	Triaxial (undrained) Cu MN/m^2	Triaxial (undrained) ϕ_u (deg)	Triaxial (drained) Cu MN/m^2	Triaxial (drained) ϕ' (deg)
94	Red brown and locally grey green,slightly fractured slightly weathered,silty MUDSTONE,moderately strong. (Zone I-II).	31.40	5.0						D	2.80					
		31.40							A	11.29					
		31.45							A	13.26					
		31.50						26.56							
	Red brown and locally grey green,highly weathered silty MUDSTONE,very weak to weak and friable. (Zone III with bands of moderately weak to weak zone III-II from 34.00-34.10m and with occassional thin bands of moderately weak zone II).	33.00				Cone	131/55								
		34.00				Cone	90/95								
		35.00				Cone	50/50								
		36.00				Cone	97/85								
	Red brown,moderately fractured,moderately weathered,silty MUDSTONE,moderately weak. (Zone II with occassional small solution cavities).	37.00				Cone	76/40								
	Red brown and locally grey green,moderately fractured,slightly weathered,silty MUDSTONE, moderately weak to moderately strong. (Zone II with thin bands of fragmented zone II).	39.10							A	27.98					
95	Red brown,completely weathered,silty MUDSTONE, very weak;clayey. (Zone IVa).	18.00				Split	88								
	Red brown,highly weathered,silty MUDSTONE,weak (Zone IZa-III).	19.50				Split	50/75								
	Red brown,highly weathered,silty MUDSTONE, moderately weak. (Zone III with some II).	25.50						34.94	A	4.02					
		25.60						48.92	A	6.58					
		25.65						58.12							
	Red brown,slightly to moderately fractured,fresh to slightly weathered,silty MUDSTONE,moderately weak to moderately strong. (Zone I-II).	26.65							A	3.04					

BH No.	Description	Depth (m)	Moisture content % Natural	Moisture content % Saturated	Bulk density Mg/m^3	S.P.T Sampler	S.P.T "N"	Cu (from Point load tests) Field MN/m^2	Laboratory Ax/Dia	Laboratory MN/m^2	U.C.S MN/m^2	Triaxial (undrained) Cu MN/m^2	Triaxial (undrained) ϕ_u (deg)	Triaxial (drained) Cu MN/m^2	Triaxial (drained) ϕ' (deg)
95	Red brown,slightly to moderately fractured,slightly	28.50						9.62							
	weathered,silty MUDSTONE,moderately strong.	28.70						10.53							
	(Zone I-II).														
96	Red brown,completely weathered,silty MUDSTONE weak to very weak;clayey,(Zone III-IVa).	18.00				Split	64								
	Red brown,completely to highly weathered,silty MUDSTONE,weak with thin clay bands. (Zone III-IVa).	19.50				?	50/75								
	Red brown,slightly weathered,moderately fractured silty MUDSTONE,moderately strong. (Zone II).	26.10						12.89							
	Red brown,slightly to moderately weathered,silty	29.90						9.54							
	MUDSTONE,moderately strong with thin grey bands	30.15						7.73							
	and patches. (Zone II). Becoming highly fractured	30.20		4.3							5.00				
	and moderately weak from 30.80m.	30.42	6.0								8.00				
	Red brown,highly weathered,clayey,completely fractured,to fine to medium gravel sized,silty MUDSTONE,weak. (Zone II-III).	35.00				Cone	84/150								
97	Red brown,completely weathered,silty MUDSTONE, stiff caly with some fine gravel sized lithorelicts. (Zone IVa).	17.20				Split	76								
	Red brown,completely weathered,clayey, fragmented to fine gravel sized silty MUDSTONE, moderately weak fragments. (Zone III-IVa).	18.20				Split	66								
	Red brown,completeley weathered,fragmented to fine to medium gravel sized silty MUDSTONE, moderately weak fragments. (Zone III-II).	19.00				Split	76								

BH No.	Description	Depth (m)	Moisture content % Natural	Saturated	Bulk density Mg/m^3	S.P.T Sampler	"N"	Cu (from Point load tests) Field MN/m^2	Laboratory Ax/Dia	MN/m^2	U.C.S MN/m^2	Triaxial (undrained) Cu MN/m^2	ϕ_u (deg)	Triaxial (drained) Cu MN/m^2	ϕ' (deg)
97	Red brown,completely weathered,silty MUDSTONE, hard clay with weak fine gravel sized lithorelicts. (Zone IVa-III).	20.00				Split	88/150								
	Red brown,highly weathered,fragmented to fine to medium and occassionally coarse gravel sized silty MUDSTONE. Moderately weak fragments. Clayey in parts. (Zone II-III).	21.00				Split	98								
	Red brown,highly weathered,fragmented to fine to coarse gravel sized silty MUDSTONE, moderately weak fragments. (Zone II-III).	22.00				Cone	78/150								
	Red brown,highly weathered,clayey,fragmented to fine to medium gravel sized silty MUDSTONE,very weak with moderately weak bands. (Zone III with bands of II-III).	23.00				Split	98								
	Red brown and grey green,highly weathered,silty MUDSTONE,moderately weak. (Zone II).	24.00				Cone	115/150								
	Red brown,highly weathered,clayey,fragmented to fine to medium gravel sized silty MUDSTONE,very weak with moderately weak bands. (Zone III with bands of zone II-III).	25.00				Split	101								
	Red brown,completely weathered,silty MUDSTONE hard with some weak lithorelicts. (Zone IVa-III).	26.00				Cone	111								
	Red brown,highly weathered,clayey,fragmented to	27.00				Cone	91/150								
	fine to coarse gravel sized silty MUDSTONE,	27.10		4.1					A	9.38					
	moderately weak fragments. (Zone III-II).	28.00				Cone	110/150								
	... 27.80-28.00m:thin weak clay bands.														

BH No.	Description	Depth (m)	Moisture content % Natural	Moisture content % Saturated	Bulk density Mg/m^3	S.P.T Sampler	S.P.T "N"	Cu (from Point load tests) Field MN/m^2	Laboratory Ax/Dia	Laboratory MN/m^2	U.C.S MN/m^2	Triaxial (undrained) Cu MN/m^2	Triaxial (undrained) ϕ_u (deg)	Triaxial (drained) Cu MN/m^2	Triaxial (drained) ϕ' (deg)
97	Grey,moderately weathered SILTSTONE,moderately weak to moderately strong. (Zone II ,becoming red brown and locally grey green,moderately weathered,silty MUDSTONE,moderately weak. (Zone II).	29.00				Cone	50/75								
	Red brown and locally grey green,intact to slightly fractured,fresh to slightly weathered,silty MUDSTONE,moderately strong. (Zone I-II).	30.05	4.3		2.79						11.03				
		30.20		3.5	2.60						19.70				
		30.70							A	17.76					
		30.72							D	14.07					
		30.72							A	54.84					
	Red brown,locally grey green,intact to slightly fractured,fresh to slightly weathered ,silty MUDSTONE,moderately strong with occassional thin strong bands. (Zone I-II).	34.00		4.0	2.62						10.90				
98	Red brown,completely to highly weathered,silty MUDSTONE,very weak to weak. (Zone IVa -III).	19.00				Cone	97								
		20.00				Split	91/150								
		22.00				Cone	121								
	Red brown,highly weathered,silty MUDSTONE,weak becoming moderately weak. (Zone III with some IVa and then II bands from 23.70m ownwards).	23.00				?	87/150								
		24.00				Cone	50/75								
	Grey,slightly weathered,fine grained SILTSTONE, moderately strong. (Zone II).	28.75							A	73.38					
		28.78	2.2												
	Red brown,slightly weathered,silty MUDSTONE, moderately strong and strong with occassional thin grey bands. (Zone II-I).	29.65		3.7	2.61						20.55				
		30.10							A	22.19					
		30.20						31.70							
		30.24						15.17							

BH No.	Description	Depth	Moisture content %		Bulk	S.P.T		Cu (from Point load tests)			U.C.S	Triaxial (undrained)		Triaxial (drained)	
		(m)	Natural	Saturated	density	Sampler	"N"	Field	Laboratory		MN/m^2	Cu	ϕ_u	Cu	ϕ'
					Mg/m^3			MN/m^2	Ax/Dia	MN/m^2		MN/m^2	(deg)	MN/m^2	(deg)
100	Red brown,completely weathered,clayey,	17.00				Split	91/225								
	fragmented to fine gravel sized silty MUDSTONE,	18.00				Split	116/225								
	very weak with weak lithorelicts. (Zone III-IVa).	19.00				Split	116/225								
	Lithorelicts moderately strong below 17.80m.	20.00				Split	112/225								
		21.00				Cone	101								
	Red brown,highly weathered,fragmented to fine to	22.00				Split	94/150								
	medium gravel sized,silty MUDSTONE,fragments	23.00				Split	49/75								
	moderately weak. (Zone III).														
	Red brown and locally grey green,moderately	29.25						7.34							
	fractured,slightly weathered silty MUDSTONE,	29.30						7.14							
	moderately strong with vertical fractures. (Zone II	29.35						7.34							
	with some I).														
	Red brown,fragmented,moderately weathered,silty	31.85							D	51.91					
	MUDSTONE,moderately strong. (Zone II).	31.85							A	37.44					
		31.85	1.1						A	46.98					
	Red brown,intact to slighlty fractured,fresh to	31.90							A	50.96					
	slightly weathered,silty MUDSTONE,moderately	32.00							A	17.88					
	weak to moderately strong. (Zone I-II).	32.00						11.82							
	Red brown,slightly fractured,slightly weathered,	39.60						7.76							
	silty MUDSTONE,moderately strong. (Zone II-I).	39.70						9.62							
101	Red brown,completely weathered,silty MUDSTONE	16.50				Split	36								
	(stiff clay),with occassional weak,fine gravel sized	18.00				Cone	34								
	lithorelicts. (Zone IVa).														
	Red brown,highly weathered,clayey,fragmented to	19.50				Cone	54								
	fine to medium gravel sized,silty MUDSTONE,weak.														
	(Zone III-IVa).														

BH No.	Description	Depth (m)	Moisture content % Natural	Moisture content % Saturated	Bulk density Mg/m^3	S.P.T Sampler	S.P.T "N"	Cu (from Point load tests) Field MN/m^2	Cu (from Point load tests) Laboratory Ax/Dia	Cu (from Point load tests) Laboratory MN/m^2	U.C.S MN/m^2	Triaxial (undrained) Cu MN/m^2	Triaxial (undrained) ϕ_u (deg)	Triaxial (drained) Cu MN/m^2	Triaxial (drained) ϕ' (deg)
101	Red brown,highly fractured to fragmented,slightly to moderately weathered,silty MUDSTONE,(fragments moderately weak). Zone II.	21.00				?	50/75								
	Red brown,highly weathered,clayey,fragmented to fine gravel sized,silty MUDSTONE,weak with moderately weak lithorelicts. (Zone III with some IVa	23.00				?	95/100								
	Red brown with some grey green,slightly weathered,slightly fractured,silty MUDSTONE, moderately strong to strong with vertical joints at 26.80-27.30m. (Zone II). ...27.45-27.60m:Fragmented to medium to coarse gravel sized. ...27.85-27.95m:Fragmented to medium to coarse gravel sized.	26.65	1.8						D	11.93					
		26.65							A	41.06					
	Grey,slightly weathered SILTSTONE,moderately strong. (Zone II).	29.65						6.69							
	Red brown,some grey green,slightly weathered, moderately to slightly fractured,strong,silty MUDSTONE. (Zone II-I).	30.25		3.8	2.67						12.06				
	Red brown,highly fractured to fragmented, moderately weathered,silty MUDSTONE. Fragments moderately strong. (Zone II).	37.55							D	12.18					
		37.55							A	21.70					
	Red brown,completely weathered,silty MUDSTONE, hard clay. (Zone IVa).	42.50				Cone	75/150								
102	Red brown,completely weathered,silty MUDSTONE, (soft to hard clay). Keuper marl zone IVa	16.60				Cone	16								

BH No.	Description	Depth (m)	Moisture content % Natural	Saturated	Bulk density Mg/m^3	S.P.T Sampler	"N"	Cu (from Point load tests) Field MN/m^2	Laboratory Ax/Dia	MN/m^2	U.C.S MN/m^2	Triaxial (undrained) Cu MN/m^2	ϕ_u (deg)	Triaxial (drained) Cu MN/m^2	ϕ' (deg)
102	Red brown,higlhy weathered,clayey,fragmented,	18.00				Split	56								
	silty MUDSTONE,weak. (Zone III-IVa).	19.50				Split	73								
	Red brown,moderately weathered,silty MUDSTONE	22.50				Cone	50/75								
	moderately weak. (Zone II).														
	Red brown,moderately weathered,moderately	31.10	2.4						A	83.97					
	fractured,silty MUDSTONE,moderately strong.	31.65	1.4						D	24.38					
	(Zone II with thin highly fractured bands and	31.65							A	74.14					
	vertical fractures.	32.55							D	11.41					
	...27.45-27.50m:Clayey weak band (Zone II).	32.55							A	34.61					
	...28.80-28.90m:Clayey weak band (Zone III).														
	...28.90-29.85m:Completely fractured (Zone II-III).														
	...31.00-31.20m:Strong grey band														
	...31.20-31.40m:Weak,clayey band (Zone II-III).														
	...31.50-31.60m:Weak clayey band (Zone II-III),with														
	some grey green areas below 31.20m														
	Red brown,moderately to highly weathered,silty	37.00				Split	67/50								
	MUDSTONE,moderately weak. (Zone II-III).														
	Red brown,moderately weathered,highly fractured	40.00				Split	50/30								
	silty MUDSTONE,moderately weak to moderately														
	strong,clayey in parts. (Zone II).														
103	Red brown,completely weathered,clayey,	16.50				Cone	21								
	fragmented,silty MUDSTONE,very weak. (Zone	18.00				Cone	43								
	III-IVa).	19.50				Cone	71								
	Red brown,highly weathered,fragmented to fine to	21.00				?	88/150								
	medium gravel sized silty MUDSTONE,weak														
	fragments. (Zone III).														

BH No.	Description	Depth (m)	Moisture content % Natural	Saturated	Bulk density Mg/m^3	S.P.T Sampler	"N"	Cu (from Point load tests) Field MN/m^2	Laboratory Ax/Dia	MN/m^2	U.C.S MN/m^2	Triaxial (undrained) Cu MN/m^2	ϕ_u (deg)	Triaxial (drained) Cu MN/m^2	ϕ' (deg)
103	Red brown,slightly fractured,slightly weathered,	27.50						17.44							
	silty MUDSTONE,moderately strong and strong	27.60						16.44							
	with grey green bands throughout. (Zone I-II).	28.20						38.11							
		29.00						7.82							
		30.70							D	25.42					
		30.70							A	44.70					
		30.80						24.68							
104	Red brown,highly weathered,clayey,fragmented to	18.50				Cone	56								
	fine to medium gravel sized silty MUDSTONE,weak														
	fragments. (Zone III with IVa).														
	Red brown,highly weathered,silty MUDSTONE,with	20.00				?	123								
	grey green SILTSTONE bands,clayey,fragmented to														
	fine to coarse gravel sized,weak;some moderately														
	strong fragments. (Zone III with thin bands of IVa).														
	Red brown,completely weathered,silty MUDSTONE,	26.10							A	8.79					
	moderately strong (Zone II). At 25.70-25.95m:														
	fragmented to coarse gravel sized.														
	Red brown with grey green bands,slighty	27.95						17.95							
	weathered,silty MUDSTONE,moderately strong;	28.00						22.30							
	occassionally strong. (Zone II).	28.04						19.08							
	...28.15-28.25m:moderately weak,completely	28.08						15.05							
	fractured clayey band.	28.15						15.61							
	...29.30-29.50m:moderately weak,completely	28.28						28.04							
	fractured clayey band.	28.40	1.6						D	53.06					
		28.40							A	64.45					
		28.90						13.45							
		29.20						23.45							
		29.55						8.01							
		29.70						14.21							
		29.75						12.33							
		29.77		5.6	2.71						1.17				

BH No.	Description	Depth (m)	Moisture content % Natural	Moisture content % Saturated	Bulk density Mg/m^3	S.P.T Sampler	S.P.T "N"	Cu (from Point load tests) Field MN/m^2	Laboratory Ax/Dia	Laboratory MN/m^2	U.C.S MN/m^2	Triaxial (undrained) Cu MN/m^2	Triaxial (undrained) ϕ_u (deg)	Triaxial (drained) Cu MN/m^2	Triaxial (drained) ϕ' (deg)
104	Red brown,slightly weathered,silty MUDSTONE, strong. (Zone II-I).	31.40		4.0	2.61				D	39.12					
		31.40							A	50.02					
		32.40							D	10.16					
		32.40							A	2.68					
	Red brown and locally grey green,highly fractured, moderately weathered,silty MUDSTONE,moderately strong. (Zone II with thin bands of weak zone II-III).	36.00						19.12							
	Red brown,highly fractured,moderately weathered silty MUDSTONE,moderately weak to moderately strong. (Zone II,with a band of weak zone II-III from 42.30-42.40m.	40.40						26.82							
		41.70						14.38							
		42.00						17.34							
		42.40							D	50.85					
		42.40							A	11.06					
		42.50							A	18.78					
		43.00						30.68							
	Red brown,moderately to slightly fractured,slightly weathered,silty MUDSTONE,moderately weak to moderately strong,with occassional thin bands of fractured zone II . (Zone II with some I).	51.10						4.24							
		51.40						10.33							
		51.80		6.6											
	Red brown and locally grey green,moderately fractured,slightly weathered,silty MUDSTONE, moderately weak to moderately strong. (Zone II with some zone I).	59.20						18.61							
		59.40						18.31							
105	Red brown,highly weathered,clayey,fragmented, silty MUDSTONE,very weak to weak. (Zone III).	13.80										26	0		
	Red brown,completely weathered with occassional fine gravel size lithorelicts,silty MUDSTONE, stiff. (Zone IVa).	16.80				Cone	45								
		18.30				Cone	92								
		19.80				Cone	94								
		21.30				Cone	111								

BH No.	Description	Depth (m)	Moisture content % Natural	Saturated	Bulk density Mg/m^3	S.P.T Sampler	"N"	Cu (from Point load tests) Field MN/m^2	Laboratory Ax/Dia	MN/m^2	U.C.S MN/m^2	Triaxial (undrained) Cu MN/m^2	ϕ_u (deg)	Triaxial (drained) Cu MN/m^2	ϕ' (deg)
105	Red brown and grey,highly weathered,fragmented to fine to medium gravel sized,silty MUDSTONE, weak to moderately weak. (Zone II-III).	22.80				Cone	48/225								
	Red brown,slightly weathered,moderately to slightly fractured,silty MUDSTONE,moderately strong. (Zone II). ...31.20-32.10:Fragmented.	27.80							D	12.45					
		27.80							A	35.77					
		27.85							A	40.14					
		28.00							A	4.94					
		28.45	2.0						D	31.30					
		28.45							A	64.51					
		28.65							D	18.29					
		28.65							A	40.74					
		29.50							A	4.32					
		29.80							D	11.69					
		29.80							A	28.43					
		29.85							A	13.98					
		29.90							D	12.18					
		29.90							A	39.31					
		29.95							D	6.36					
		29.95							A	40.60					
		30.05						16.90							
		30.15						20.76							
		30.65						26.21							
		30.80						32.86							
		30.90	2.3						D	16.77					
		30.90							A	40.57					
106A	Red brown,highly weathered,clayey with fine to medium gravel sized lithorelicts,silty MUDSTONE, very weak with moderately weak lithorelicts.(III-IVa).	18.50				Split	99								
	Red brown,highly weathered,clayey with fine to medium gravel and occassionally coarse gravel and cobble size lithorelicts,silty MUDSTONE.Moderately weak lithorelicts. (Zone III).	19.55				Split	100								

BH No.	Description	Depth (m)	Moisture content % Natural	Saturated	Bulk density Mg/m^3	S.P.T Sampler	"N"	Cu (from Point load tests) Field MN/m^2	Laboratory Ax/Dia	MN/m^2	U.C.S MN/m^2	Triaxial (undrained) Cu MN/m^2	ϕ_u (deg)	Triaxial (drained) Cu MN/m^2	ϕ' (deg)
106A	Red brown,highly weathered,clayey with fine to medium gravel and occassionally coarse gravel to cobble sized silty MUDSTONE,moderately weak lithorelicts. (Zone III).	20.55				Split	42								
	Red brown,highly to moderately weathered,silty MUDSTONE and grey SILTSTONE,moderately weak to moderately strong with occassional bands of highly weathered,clayey silty weak MUDSTONE. (Zone II with bands of III-IVa).	21.55				Split	91/150								
		22.55				Split	106								
		23.55				Split	50/75								
		25.50				Split	50/75								
107	Red brown,completely to highly weathered,clayey, completely fractured to fine to medium gravel sized silty MUDSTONE,very weak with moderately weak lithorelicts. (Zone III).	17.70				Split	70								
		18.50				Split	68								
	Red brown,moderately weathered,slightly clayey, completely fractured to fine to coarse gravel sized silty MUDSTONE,moderately weak fragments. (Zone II-III).	19.50				Split	80/150								
	Red brown and locally grey green,highly to moderately fractured,fresh,moderately weathered, silty MUDSTONE,weak to moderately strong. (Bands of zone III and II).	22.45	2.4						A	16.90					
108	Red brown,highly weathered,clayey,completely fractured to fine to medium gravel sized,silty MUDSTONE,very weak with weak lithorelicts. (Zone III-IVa with clay bands).	18.00				?	99								
	Red brown,highly to completely weathered,clayey fragmented to fine gravel sized,silty MUDSTONE, very weak. (Zone IVa).	19.00				Split	50/75								

BH No.	Description	Depth (m)	Moisture content % Natural	Moisture content % Saturated	Bulk density Mg/m^3	S.P.T Sampler	S.P.T "N"	Cu (from Point load tests) Field MN/m^2	Laboratory Ax/Dia	Laboratory MN/m^2	U.C.S MN/m^2	Triaxial (undrained) Cu MN/m^2	Triaxial (undrained) ϕ_u (deg)	Triaxial (drained) Cu MN/m^2	Triaxial (drained) ϕ' (deg)
108	Red brown,highly to completely weathered,clayey fragmented to fine and occassionally medium gravel sized,silty MUDSTONE,very weak with weak lithorelicts. (Zone III-IVa).	20.00				Split	152/225								
	Red brown,completely weathered,silty MUDSTONE with some fine gravel sized lithorelicts,very weak (Zone IVa).	21.00				Split	106								
	Red brown,highly weathered,clayey,fragmented to fine gravel sized,silty MUDSTONE,weak. (Zone III).	22.00				Split	118								
	Red brown,highly weathered,clayey,fragmented to fine gravel sized,silty MUDSTONE,very weak. (Zone IVa).	23.00				Split	118/225								
	Red brown,completely weathered,clayey, fragmented to fine gravel sized,silty MUDSTONE, very weak. (Zone IVa).	24.00				Split	92								
	Red brown,highly weathered,clayey,fragmented to fine to medium gravel sized,silty MUDSTONE,weak with some moderately strong lithorelicts. (Zone III).	25.00				?	90								
	Red brown,highly weathered,clayey,fragmented to fine and occassionally medium gravel sized,silty MUDSTONE,weak. (Zone III).	26.00				Split	87/150								
		27.00				Split	128								
	Red brown,moderately weathered,fractured to fine to coarse gravel and cobble sized,silty MUDSTONE, moderately weak with some moderately strong lithorelicts. (Zone II).	28.00				Split	50/75								
		28.70				Split	50/75								

BH No.	Description	Depth (m)	Moisture content % Natural	Moisture content % Saturated	Bulk density Mg/m^3	S.P.T Sampler	S.P.T "N"	Cu (from Point load tests) Field MN/m^2	Cu (from Point load tests) Laboratory Ax/Dia	Cu (from Point load tests) Laboratory MN/m^2	U.C.S MN/m^2	Triaxial (undrained) Cu MN/m^2	Triaxial (undrained) ϕ_u (deg)	Triaxial (drained) Cu MN/m^2	Triaxial (drained) ϕ' (deg)
108	Grey green,moderately fractured,fresh to slightly	29.60						36.07							
	weathered,SILTSTONE,moderately strong. (Zone II).														
	Red brown and locally grey green,intact to slightly	29.76						46.49							
	fractured,fresh to slighlty weathered,silty	29.90		3.6	2.75						22.34				
	MUDSTONE,moderately strong with bands of	30.10							D	22.35					
	moderately weak and strong. (Zone I-II).	30.10							A	71.50					
	...30.40-31.10m:Highly fractured.	30.15							A	28.49					
		31.20						24.42							
		31.30						18.81							
		31.50						23.24							
		31.60		4.0					A	8.18					
		31.65							A	2.02					
		31.80						14.42							
		32.70						20.76							
		32.75						35.44							
		32.80							A	8.34					
		32.85							A	2.00					
		32.90		3.5	2.66						12.06				
		33.00						9.78							
		33.10						14.92							
		33.20						26.48							
		33.30						29.07							
		33.50						33.20							
		33.60						30.42							
	Red brown,highly to completely weathered,silty	33.90						29.50							
	MUDSTONE,very weak. (Zone III-IVa).	35.00				Cone	50/5								
109	Red brown,completely to highly weathered,clayey,	17.55				Split	39								
	fragmented to medium to coarse gravel and														
	occassionally cobble sized,silty MUDSTONE,very														
	weak. (Zone III-IVa).														

BH No.	Description	Depth (m)	Moisture content % Natural	Moisture content % Saturated	Bulk density Mg/m^3	S.P.T Sampler	S.P.T "N"	Cu (from Point load tests) Field MN/m^2	Cu (from Point load tests) Laboratory Ax/Dia	Cu (from Point load tests) Laboratory MN/m^2	U.C.S MN/m^2	Triaxial (undrained) Cu MN/m^2	Triaxial (undrained) ϕ_u (deg)	Triaxial (drained) Cu MN/m^2	Triaxial (drained) ϕ' (deg)
109	Red brown,completely weathered,clayey,silty MUDSTONE,stiff to very stiff with weak fragments. (Zone IVa).	18.55				Split	43								
	Red brown,highly to moderately weathered,clayey, fragmented to coarse gravel and cobble sized, silty MUDSTONE,weak,becoming very weak. (Zone III).	19.55				Split	132								
		20.55				Split	56								
	Stiff,red brown,silty CLAY,with some fine to medium gravel sized lithorelicts (Zone IVa) with occassional thin bands of moderately weathered silty MUDSTONE. (Zone III).	21.55				Split	52								
		22.55				Split	17								
	Stiff,red brown and grey green,very silty CLAY with some fine to medium gravel sized,silty mudstone lithorelicts. (Zone IVa with some III).	23.55				Split	89/150								
		24.55				Split	37								
		25.55				Split	173								
		26.55				Split	76								
		27.55				Split	48								
		28.55				Split	45								
		29.55				Split	67								
	Red brown,highly to completely weathered,silty MUDSTONE,weak with fine gravel sized,moderately weathered lithorelicts. (Zone III).	30.55				Split	91/150								
	Red brown,completely weathered,silty MUDSTONE, (hard clay) with occassional fine gravel sized lithorelicts. (Zone IVa).	31.55				Split	64								
	Red brown,highly weathered,fragmented to fine to coarse gravel and cobble sized,silty MUDSTONE, weak fragments with thin bands of moderately weathered,grey green mudstone. (Zone III with bands of II and IVa).	32.55				Split	74								

BH No.	Description	Depth (m)	Moisture content % Natural	Moisture content % Saturated	Bulk density Mg/m^3	S.P.T Sampler	S.P.T "N"	Cu (from Point load tests) Field MN/m^2	Cu (from Point load tests) Laboratory Ax/Dia	Cu (from Point load tests) Laboratory MN/m^2	U.C.S MN/m^2	Triaxial (undrained) Cu MN/m^2	Triaxial (undrained) ϕ_u (deg)	Triaxial (drained) Cu MN/m^2	Triaxial (drained) ϕ' (deg)
109	Red brown,highly weathered,clayey,fragmented to	33.55				Split	82								
	fine gravel sized silty MUDSTONE,very weak with	34.55				Split	104/225								
	moderately weak lithorelicts. (Zone III).														
	Red brown,moderately weathered,fragmented to	35.55				Split	99/75								
	fine to coarse gravel and cobble sized,silty	36.55				Split	50/75								
	MUDSTONE,moderately weak to moderately strong.														
	(Zone II with some III).														
110	Grey,highly weathered SILTSTONE,moderately	19.50				Split	68/150								
	weak to weak. (Zone II-III).														
	Red brown,completely weathered,clayey,silty	21.50				Split	19								
	MUDSTONE,weathered to a silty shaly clay with	22.50				Split	76/150								
	very weak and weak mudstone bands. (Zone IV	23.50				Split	22								
	with bands of III and then occassional 0.05-0.10m	24.75				Split	74/150								
	bands of zone II).														
117	Red brown and locally green,highly to completely	13.30				?	8/150								
	weathered silty MUDSTONE,moderately strong.	13.80				?	87/150								
	(Zone IVa with some III).														
	Red brown and locally green grey,slightly	15.00				?	50/75								
	weathered,silty MUDSTONE,moderately strong to	16.70							D	60.97					
	strong. (Zone II with occassional weak bands of	16.70							A	55.08					
	zone III).														
	...At 17.50m:Band of green grey sandy SILTSTONE.														
	Red brown,slightly fractured,fresh to slightly	17.70							D	7.26					
	weathered,silty MUDSTONE,moderately strong.	17.70							A	4.42					
	(Zone I-II).	17.80							D	5.19					
		17.80							A	4.25					

BH No.	Description	Depth (m)	Moisture content % Natural	Moisture content % Saturated	Bulk density Mg/m^3	S.P.T Sampler	S.P.T "N"	Cu (from Point load tests) Field MN/m^2	Cu (from Point load tests) Laboratory Ax/Dia	Cu (from Point load tests) Laboratory MN/m^2	U.C.S MN/m^2	Triaxial (undrained) Cu MN/m^2	Triaxial (undrained) ϕ_u (deg)	Triaxial (drained) Cu MN/m^2	Triaxial (drained) ϕ' (deg)
118	Red brown,moderately weathered,silty MUDSTONE,	13.20				Cone	81/150								
	moderately strong fragments. (Zone III).														
	Green grey,moderately weathered,silty	15.20				Cone	77/150								
	SANDSTONE,moderately strong with bands of														
	weak silty mudstone. (Zone II with some III).														
	Red brown,highly to moderately weathered,silty	16.20				Cone	91/150								
	MUDSTONE,weak to moderately weak. (Zone III).	17.20				Cone	93/150								
	Red brown,slightly to moderately weathered,silty	20.95							D	4.98					
	MUDSTONE,moderately strong. (Zone II).	20.95							A	28.02					
	Red brown,moderately to slightly weathered,	27.05							D	77.80					
	moderately fractured,silty MUDSTONE with 10-20mm	27.05							A	50.46					
	solution cavities in parts,moderately strong,(Zone II														
	with thin bands of zone III).														
	...24.75-25.05m:fragmented band.														
	...26.50-26.80m:fragmented band.														
	...26.95-27.15m:fragmemted band.														
	Red brown,slightly weathered,slightly fractured,	27.80							D	1.00					
	silty MUDSTONE,moderately strong to strong.	27.80							A	21.03					
	(Zone II-I).	27.85							D	8.46					
		27.85							A	12.56					
	Red brown,moderately weathered,fragmented,	33.10							A	20.39					
	silty MUDSTONE,moderately weak. (Zone II-III).														
	Red brown,silty MUDSTONE,with bands of grey	38.20							D	8.96					
	green SILTSTONE,slightly to moderately weathered,	38.20							A	17.02					
	moderately strong to strong. (Zone II).														
	...38.30-38.75m:Fragmented to fine to medium gravel sized														

127	Red brown calcerous SILTSTONE,with numerous	17.50							D	66.03					
	angular gravel sized lithorelics upto 50mm (IVa-III)	17.50							A	10.75					
	At 18.75-18.83m:Grey green band.														
	Red brown and grey green,mottled and streaked,	19.02				Split	39								
	slightly calcerous SILT,with some to numerous sand	19.55				Split	55								
	and gravel angular siltstone lithorelics,firm to stiff	20.05				Split	11								
	(Zone IVa).	20.50										41	0		
127A	Red brown,closely fractured,very thinly bedded	15.80							D	32.23					
	slightly calcerous,slightly sandy SILTSTONE,weak	16.95							A	10.78					
	to moderately weak,with sub-horizontal and sub-														
	vertical fractures,rough planar and curved,with														
	silt coating. (Zone II-III).														
	Grey green,moderately fractured,slightly calcerous,	17.40	3.9	4.3	2.36						17.50				
	slightly sandy SILTSTONE,strong with sub-horizontal														
	and sub-vertical fractures,rough,planar. (Zone I-II).														
	Red brown,closely fractured,slightly calcerous	26.38	4.9	3.7	2.59						7.80				
	SILTSTONE,moderately weak.,with sub-horizontal														
	fractures,rough,planar with black stain. (Zone II)														
	...Locally with some silty matrix.														
	...26.20-26.58:Medium fractured.														
	Red brown with occassional grey green spots,	28.05							A	7.13					
	slightly fractured,slightly calcerous slightly sandy	28.30		2.7	2.50						8.40				
	SILTSTONE,moderately weak,becoming moderately	28.60							A	25.14					
	strong. (Zone II).	29.90							A	6.30					
	...With sub-horizontal and 45 deg fractures,rough														
	planar and irregular with black stained calcite														
	coating.														
	...With occassional frequently calcite lined vugs up														
	to 5 mm.														
	Red brown with occassional grey green spots,	30.05							A	10.90					
	medium fractured,slightly calcerous slightly sandy														
	SILTSTONE,moderately weak to moderately strong														

BH No.	Description	Depth (m)	Moisture content % Natural	Saturated	Bulk density Mg/m^3	S.P.T Sampler	"N"	Cu (from Point load tests) Field MN/m^2	Laboratory Ax/Dia	MN/m^2	U.C.S MN/m^2	Triaxial (undrained) Cu MN/m^2	ϕ_u (deg)	Triaxial (drained) Cu MN/m^2	ϕ' (deg)
127A	(Zone II).														
	...With sub-horizontal and 45 deg fractures,rough planar and irregular with black stained calcite coating.														
	...With occassional frequently calcite lined vugs up to 5 mm.														
	Red brown with grey green spots,,moderately fractured,slightly calcerous,SILTSTONE,moderately weak to moderately strong. (Zone II).	43.45							A	15.09					
	...With sub-horizontal and sub-vertical fractures, rough,planar with black speckling and calcite coating														
	...Occassional frequently calcite lined vugs up to 3 mm.														
128	Red brown with grey green streaks and bands,	15.40							A	24.73					
	medium fractured,slightly calcerous,slightly sandy	15.50							D	27.05					
	SANDSTONE,moderately strong.	15.50							A	36.14					
	...With sub-horizontal fractures,rough,planar with	15.50							A	56.06					
	silt coating. (Zone II).														
	...15.90-16.00m:Prominent grey green band.														
	Red brown,closely fractured,thinly bedded,slightly	16.85							A	1.69					
	calcerous,slightly sandySILTSTONE,moderately	17.10							D	4.31					
	weak. (Zone II).	17.10							A	14.77					
	...With sub-horizontal and 70 deg fractures,rough,	18.30							D	26.03					
	planar,some black stain,occasional calcite coating.	18.30							A	57.76					
	...Closely fractured at 16.30-16.60m,16.95-17.05m and 17.24-17.30m.														
	Red brown with occassional grey green spots,	19.45							A	2.39					
	closely to very closely fractured,indistinctly	19.50							D	14.08					
	laminated calcerous,slightly sandy SILTSTONE,	19.50							A	13.88					
	...With 45 deg to 70 deg fractures,slightly rough, planar,some delamination on surfaces up to 1 mm														

BH No.	Description	Depth (m)	Moisture content % Natural	Saturated	Bulk density Mg/m^3	S.P.T Sampler	"N"	Cu (from Point load tests) Field MN/m^2	Laboratory Ax/Dia	MN/m^2	U.C.S MN/m^2	Triaxial (undrained) Cu MN/m^2	ϕ_u (deg)	Triaxial (drained) Cu MN/m^2	ϕ' (deg)
128	calcite and silt coating. (Zone II).														
	...18.76-18.97m:Hard silt (Zone IVb)														
	...19.44-19.58m:Moderately strong														
	...19.58-19.66m:stiff silt. (Zone IVb).														
128A	Red brown with grey green spots and bands,	16.52						29.59	D						
	medium fractured,slightly calcerous,sandy	16.52						70.09	A						
	SILTSTONE,moderately weak to moderately strong.														
	Zone II).														
	...Sub-horizontal to horizontal fractures,very rough,														
	planar,occassionally calcite coated and thin silt infill.														
	...Also medium to closely spaced 70 deg fractures,														
	rough,planar,and occassionally calcite coated.														
	Red brown with occassional grey green spots	33.00						2.47	A						
	moderately fractured,calcerous,muddy SILTSTONE														
	moderately weak to weak. (Zone II-III).														
	...Sub-horizontal 20 and 70 deg fractures,rough,														
	planar,occassionally black stained and calcite coated.														
	...with closely spaced calcite filled vug horizons.														
	...33.50-33.70m:Closely fractured zone recovered														
	as gravel.														
	Grey green closely fractured,slightly calcereous,	40.99						9.91	A						
	slightly silty MUDSTONE,moderately strong.														
	...Sub-horizontal fractures,rough,irregular,black														
	stained and calcite coated. (Zone II).														
	Red brown with some grey green,medium fractured	42.90						8.61	D						
	calcerous silty MUDSTONE,moderately strong to	42.90						24.85	A						
	strong.(Zone II).	42.90						31.77	A						
	...Sub-horizontal fractures,slightly rough,planar with														
	thin silt coating. Also randon fractures,slightly rough														
	irregular calcite coated and grey stained with														
	occassional calcite coated vugs before 41.90m.														

BH No.	Description	Depth	Moisture content %		Bulk	S.P.T		Cu (from Point load tests)			U.C.S	Triaxial (undrained)		Triaxial (drained)	
		(m)	Natural	Saturated	density	Sampler	"N"	Field	Laboratory		MN/m^2	Cu	ϕ_u	Cu	ϕ'
					Mg/m^3			MN/m^2	Ax/Dia	MN/m^2		MN/m^2	(deg)	MN/m^2	(deg)
128A	Red brown with occassional thin grey green spots	43.90						15.48	A						
	and bands,fractured,calcerous clayey SILTSTONE,	45.47						9.25	A						
	moderately strong.(Zone II).														
	...random fractured,rough,irregular with thin calcite														
	coating.														
	...also incipient sub-hirizontal fractures,rough,														
	stepped,planar and occassional calcite coated vugs														
	becoming gypsum infilled with depth														
	..44.95-45.15m:Extremely closely fractured calcerous														
	silty MUDSTONE,weak,recovered as gravel..random														
	fractures,rough,irregular,black stained and silt														
	infilled (Zone III).														
	Red brown with thick grey green bands and patches	47.40		3.2	2.36						5.80				
	medium fractured,calcerous silty MUDSTONE,strong.	49.81						18.09	A						
	...Sub-horizontal to 20 deg fractures,slightly rough	49.81						1.72	A						
	stepped planar with white fibrous gypsum infill up to	51.30						22.37	A						
	20mm. ...also incipient random random fractures,														
	rough,irregular and clean. (Zone II-I).														

Vioded toe test						End-bearing test (M.L. test)						End bearing test	
Load cycle 1		Load cycle 2		Load cycle 3		Load cycle 1		Load cycle 2		Load cycle 3		(C.R.P.) -Cycle 4	
P_h	Δ_h	P_h	Δ_h	P_h	Δ_h	P_h	Δ_h	P_h	Δ_h	P_h	Δ_h	P_h	Δ_h
(kN)	(mm)	(kN)	(mm)	(kN)	(mm)	(kN)	(mm)	(kN)	(mm)	(kN)	(mm)	(kN)	(mm)
0	0.00	500	10.20	800	39.57	800	0.15	16	0.78	22	3.76	16	20.25
500	0.15	1000	10.71	1600	40.45	1600	0.81	1600	1.71	4000	8.58	1600	21.89
1000	0.20	1500	11.24	2400	41.43	2400	1.64	3200	3.70	8000	14.75	3200	24.23
1500	0.73	2000	11.76	3200	42.65	3200	2.69	4800	5.61	12000	30.00	4800	26.71
2000	2.90	2500	12.31	4000	43.87	4000	3.70	5600	6.74			6400	29.36
2500	5.27	3000	12.94	4800	45.10	4800	4.86	6400	7.72			8000	32.15
3000	7.79	3500	13.99	5600	46.65	5600	5.98	7200	8.79			9600	37.57
3500	10.56	4000	15.44	6400	49.52	6400	7.05	8000	9.98			10600	42.62
4000	14.22	4200	16.27	7200	55.84	7200	8.17	8800	11.14			10850	45.62
		4400	18.13	8000	68.20	8000	9.69	9600	12.70			11010	48.62
		4600	19.41	8800	85.38			10400	14.47			11170	52.62
		4800	21.93	9600	97.60			11200	17.31			11350	56.62
		5100	23.74					12000	19.97			11630	60.62
		5800	30.59									11690	64.62
		6400	39.14										
		7000	47.28										
3000	13.59	6000	46.82	0	87.00	7000	9.19	8000	16.63	10600	34.84	10890	64.28
2000	12.26	5000	45.85			6000	8.22	4000	11.56	10000	34.81	5000	59.58
1000	11.26	4000	44.93			5000	7.19	0	4.87	8000	32.88	110	53.01
16	10.27	3000	43.84			4000	6.08			6000	30.72	28	52.59
		2000	42.65			3000	4.95			4000	28.17		
		1000	41.43			2000	3.78			2000	24.93		
		0	39.70			1000	2.37			80	20.84		
						0	1.27						

Table A.2: Pile head load and pile head displacement readings-TP1

P_h (kN)	Δ_h (mm)	VIBRATING WIRE STRAIN GAUGE READINGS AT LEVELS (MICRO UNITS)																P_b (kN)
		LEVEL 1.650 m				LEVEL 17.450 m				LEVEL 21.950 m				LEVEL 26.450 m				
		1	2	3	AVG	1	2	3	AVG	1	2	3	AVG	1	2	3	AVG	
0	0	-1	2	-1	0	0	0	0	0	0	0	0	0	-1	0	0	-0.2	
1000	0.22	10	17	1	13.5	6	8	9	7.6	4	4	4	4.0	3	3	3	3.0	
2000	0.93	33	58	10	45.5	24	34	33	30.1	17	21	20	19.2	18	13	12	14.4	
3000	2.05	62	87	38	74.5	51	73	63	62.2	35	43	42	40.1	40	28	26	31.3	
4000	3.48	91	118	66	104.5	79	113	95	95.8	54	67	64	61.5	62	42	39	47.4	
5000	5.09	119	148	96	133.5	108	154	128	129.9	73	92	87	84.0	83	56	52	63.6	
6000	6.07	146	176	122	161.0	134	190	160	161.1	89	113	107	103.1	101	67	63	77.0	
6000	6.81	149	181	124	165.0	140	199	166	168.1	94	121	113	109.5	108	71	66	81.6	
5000	6.45	120	154	91	137.0	113	167	138	139.3	80	105	97	94.4	97	61	57	71.8	
4000	5.87	94	124	66	109.0	87	135	109	110.3	66	88	81	78.2	86	52	48	61.7	
3000	5.04	70	96	42	83.0	59	101	77	79.2	49	69	62	59.8	72	41	37	49.8	
2000	4.20	45	69	21	57.0	31	66	46	47.5	32	48	42	40.8	57	29	26	37.2	
1032	3.22	20	44	0	32.0	5	32	16	17.6	16	28	23	22.6	42	18	15	25.3	
29	2.55	4	5	0	4.5	-4	9	-2	0.9	6	17	11	11.5	32	12	9	17.5	

Table A.3(i):Strain gauge readings-TP2 (load cycle 1)

P_h (kN)	Δ_h (mm)	VIBRATING WIRE STRAIN GAUGE READINGS AT LEVELS (MICRO UNITS)																P_b (kN)
		LEVEL 1.650 m				LEVEL 17.450 m				LEVEL 21.950 m				LEVEL 26.450 m				
		1	2	3	AVG	1	2	3	AVG	1	2	3	AVG	1	2	3	AVG	
28	2.56	4	5	-1	4.0	-5	9	-3	0.4	6	16	11	11.0	32	11	9	17.3	
2000	3.75	40	64	19	52.0	30	54	41	41.9	27	41	36	34.4	49	25	22	31.8	
4000	5.56	92	120	66	106.0	84	127	103	105.0	60	82	75	72.4	79	48	44	57.0	
6000	7.09	149	178	121	164.0	140	201	165	168.6	95	125	115	111.8	113	73	68	84.4	
7000	8.48	179	207	127	193.0	168	241	200	203.0	114	150	138	134.0	134	84	80	99.4	
8000	10.31	209	236	138	223.0	196	287	237	240.1	134	178	162	158.1	160	98	92	116.6	
9000	14.27	247	272	150	260.0	224	347	279	283.1	158	214	191	187.7	196	117	105	139.2	
8000	13.90	217	249	114	233.0	196	315	252	254.5	144	193	175	170.6	184	108	96	129.3	
7000	13.53	190	218	89	204.0	169	284	224	225.5	128	180	157	155.3	172	97	86	118.3	
6000	13.11	164	188	66	176.0	140	250	193	194.2	113	160	138	137.2	158	86	75	106.3	
4028	11.85	112	133	25	123.0	81	180	128	129.7	78	118	98	97.8	127	61	50	79.4	
2050	10.03	60	81	-11	71.0	23	107	63	64.4	41	73	55	56.2	92	35	26	50.7	
33	7.47	13	9	-8	11.0	-15	24	2	3.8	4	26	12	14.0	53	8	4	21.8	

Table A.3(ii):Strain gauge readings-TP2 (load cycle 2)

Note: Due to unacceptable amount of scatter,the readings of strain gauge No.3 have been excluded when computing average strains at level 1.650 m.

P_h (kN)	Δ_h (mm)	VIBRATING WIRE STRAIN GAUGE READINGS AT LEVELS (MICRO UNITS)																P_b (kN)
		LEVEL 1.650 m				LEVEL 17.450 m				LEVEL 21.950 m				LEVEL 26.450 m				
		1	2	3	AVG	1	2	3	AVG	1	2	3	AVG	1	2	3	AVG	
32	7.48	13	10	-9	12.0	-15	25	2	3.8	4	26	11	13.8	52	8	4	21.5	
2000	9.10	50	70	8	60.0	22	84	53	53.1	30	57	43	43.4	73	25	20	39.3	
4000	11.07	98	121	37	110.0	75	159	117	117.0	66	102	85	84.3	107	50	42	66.7	
6000	12.59	152	175	73	164.0	133	235	181	182.8	103	148	128	126.4	143	78	68	96.4	
8000	14.18	211	233	121	222.0	192	310	246	249.2	139	195	172	168.6	182	106	94	127.2	
9000	15.56	244	265	144	255.0	225	351	280	285.2	159	220	195	191.2	205	120	106	143.7	
10000	18.49	275	294	162	285.0	253	397	315	321.4	177	248	219	214.5	233	135	117	161.6	
10896	21.20	303	318	177	311.0	279	438	346	354.2	195	273	240	236.0	258	149	127	178.2	
9000	20.57	245	272	114	259.0	226	378	293	299.0	167	239	207	204.4	234	129	108	157.2	
7000	19.72	191	204	72	198.0	165	312	228	235.0	133	199	168	166.6	205	106	85	132.1	
5000	18.46	136	157	28	147.0	102	238	162	167.3	96	154	125	124.7	171	78	59	102.8	
3000	16.61	82	105	0	94.0	40	164	96	99.7	58	106	80	81.4	134	50	33	72.2	
17	11.94	17	27	-11	22.0	10	4	-5	3.3	-3	27	8	10.6	66	6	-5	22.4	

Table A.3(iii):Strain gauge readings-TP2 (load cycle 3)

P_h (kN)	Δ_h (mm)	VIBRATING WIRE STRAIN GAUGE READINGS AT LEVELS (MICRO UNITS)																P_b (kN)
		LEVEL 1.650 m				LEVEL 17.450 m				LEVEL 21.950 m				LEVEL 26.450 m				
		1	2	3	AVG	1	2	3	AVG	1	2	3	AVG	1	2	3	AVG	
2000	13.70	48	75	7	62.0	63	56	47	55.3	27	63	43	44.3	90	25	13	42.0	
4000	15.80	87	120	32	104.0	127	122	109	119.3	63	108	85	85.5	124	50	35	69.6	
6000	18.03	135	174	57	155.0	192	190	173	185.1	100	155	128	127.7	161	78	61	99.7	
8000	20.17	185	228	96	207.0	258	260	236	251.4	137	202	172	170.5	198	107	88	131.2	
9000	21.47	213	258	120	236.0	291	297	271	286.1	156	226	195	192.3	219	123	102	148.0	
10000	22.89	243	290	146	267.0	326	334	305	321.7	175	250	217	214.0	240	138	116	164.8	
11000	25.24	276	326	173	301.0	362	374	340	359.0	195	275	240	236.9	265	155	129	183.2	
12000	27.94	308	357	195	333.0	398	413	377	396.0	216	302	264	260.6	293	172	142	202.4	
13000	32.09	339	387	218	363.0	437	455	410	434.1	238	332	292	287.2	326	195	157	225.9	
13500	33.96	353	402	227	378.0	455	475	429	453.1	248	346	304	299.7	343	206	165	237.7	
10000	31.66	249	300	123	275.0	348	361	324	344.4	191	279	239	236.3	293	164	124	193.8	
7000	29.12	174	211	56	193.0	250	257	228	245.4	137	212	174	174.6	242	122	85	149.8	
4033	26.35	101	128	9	115.0	154	157	134	148.1	82	142	109	111.2	186	78	46	103.2	
45	21.42	34	25	-4	30.0	27	26	12	21.6	7	42	18	22.5	97	16	-5	36.1	

Table A.3(iv):Strain gauge readings-TP2 (load cycle 4)

Note: Due to unacceptable amount of scatter, the readings of strain gauge No.3 have been excluded when computing average strains at level 1.650 m.

P_h (kN)	Δh (mm)	EXTENSOMETER MOVEMENT (mm)		
		LEVEL 3 0-13 m	LEVEL 4 0-19 m	LEVEL 5 0-24 m
0	0	0.000	0.000	0.000
1000	0.22	0.085	0.003	0.226
2000	0.93	0.282	0.058	0.756
3000	2.05	0.697	0.667	1.381
4000	3.48	1.118	1.285	2.015
5000	5.09	1.556	1.910	2.664
6000	6.07	1.946	2.485	3.238
6000	6.81	2.042	2.603	3.371
5000	6.45	1.636	2.080	2.882
4000	5.87	1.248	1.547	2.346
3000	5.04	0.844	0.973	1.787
2000	4.20	0.429	0.376	1.206
1000	3.22	0.043	0.121	0.656
25	2.55	-0.050	0.130	0.130

Table A.3(v):Extensometer readings-TP2 (cycle 1)

P_h (kN)	Δh (mm)	EXTENSOMETER MOVEMENT (mm)		
		LEVEL 3 0-13 m	LEVEL 4 0-19 m	LEVEL 5 0-24 m
28	2.56	-0.054	0.129	0.126
2000	3.75	0.399	0.288	1.063
4000	5.56	1.214	1.441	2.235
6000	7.09	2.037	2.617	3.388
7000	8.48	2.483	3.239	4.021
8000	10.31	2.939	3.910	4.661
9000	14.27	3.398	4.616	5.438
8000	13.90	2.982	4.056	4.992
7000	13.53	2.601	3.519	4.468
6000	13.11	2.199	2.953	3.932
4028	11.85	1.395	1.773	2.812
2050	10.03	0.587	0.575	1.646
33	7.47	-0.114	0.106	0.169

Table A.3(vi):Extensometer readings-TP2 (cycle 2)

P_h (kN)	Δh (mm)	EXTENSOMETER MOVEMENT (mm)		
		LEVEL 3 0-13 m	LEVEL 4 0-19 m	LEVEL 5 0-24 m
32	7.48	-0.112	0.109	0.169
2000	9.10	0.470	0.369	1.303
4000	11.07	1.302	1.563	2.473
6000	12.59	2.144	2.776	3.663
8000	14.18	2.979	3.997	4.824
9000	15.56	3.406	4.650	5.435
10000	18.49	3.821	5.270	6.071
10896	21.20	4.199	5.859	6.639
9000	20.57	3.401	4.738	5.754
7000	19.72	2.630	3.587	4.633
5000	18.46	1.775	2.345	3.509
3000	16.61	0.944	1.108	2.326
17	11.94		0.295	0.934

Table A.3(vii):Extensometer readings-TP2 (cycle 3)

P_h (kN)	Δh (mm)	EXTENSOMETER MOVEMENT (mm)		
		LEVEL 3 0-13 m	LEVEL 4 0-19 m	LEVEL 5 0-24 m
2000	13.70	1.098	2.684	2.746
4000	15.80	1.768	2.835	3.101
6000	18.03	2.573	3.226	3.719
8000	20.17	3.457	4.500	4.863
9000	21.47	3.918	5.173	5.449
10000	22.89	4.380	5.483	6.033
11000	25.24	5.475	5.988	7.072
12000	27.94	5.375	7.264	7.303
13000	32.09	5.898	7.963	8.014
13500	33.96	6.146	8.308	8.364
10000	31.66	4.591	6.213	6.577
7000	29.12	3.309	4.368	4.893
4033	26.35	2.037	2.516	3.184
45	21.42	0.212	0.086	0.676

Table A.3(viii):Extensometer readings-TP2 (cycle 4)

P_h (kN)	LOAD START			LOAD END			CUMULATIVE TIME (HOURS)	
	DATE	TIME	Δ_h (mm)	DATE	TIME	Δ_h (mm)	START	END
0	27-6-91	12:41:01	0	27-6-91	12:42:39	0	0	0.03
1000		15:01:05	0.23		15:30:41	0.22	2.33	2.83
2000		15:34:52	0.87		16:35:57	0.93	2.90	3.92
3000		16:41:10	1.90		17:26:29	2.05	4.00	4.76
4000		17:30:31	3.09		18:16:33	3.48	4.83	5.59
5000		18:19:42	4.50		19:06:47	5.09	5.64	6.43
6000		19:10:17	6.00		22:41:31	6.81	6.49	10.01
5000		22:44:21	6.46		23:02:25	6.45	10.06	10.36
4000		23:04:48	5.88		23:16:41	5.87	10.40	10.60
3000		23:20:25	5.08		23:33:29	5.04	10.65	10.88
2000		23:36:32	4.23		23:47:32	4.20	10.92	11.11
1000		23:50:28	3.27	28-6-91	00:06:39	3.22	11.15	11.43
25	28-6-91	00:12:32	2.57		09:04:35	2.55	11.52	20.40

Table A.3(ix):Load-Displacement-Time record for TP2 (load cycle 1)

P_h (kN)	LOAD START			LOAD END			CUMULATIVE TIME (HOURS)	
	DATE	TIME	Δ_h (mm)	DATE	TIME	Δ_h (mm)	START	END
28	28-6-91	09:26:52	2.57	28-6-91	09:28:47	2.56	20.76	20.79
2000		09:36:05	3.74		10:37:54	3.75	20.92	21.94
4000		10:43:08	5.50		11:46:02	5.56	22.04	23.08
6000		11:52:25	6.93		12:54:13	7.09	23.19	24.21
7000		12:58:58	7.83		14:01:37	8.48	24.30	25.34
8000		14:07:10	9.34		15:08:06	10.31	25.44	26.45
9000		15:14:24	12.14		19:01:40	14.27	26.56	30.34
8000		19:08:26	13.90		19:24:35	13.90	30.46	30.72
7000		19:28:38	13.54		19:44:20	13.53	30.79	31.05
6000		19:48:01	13.13		20:03:12	13.11	31.12	31.36
4000		20:08:16	11.90		20:23:29	11.85	31.45	31.70
2000		20:28:26	10.10		20:44:12	10.03	31.79	32.05
60		20:53:45	7.67		20:54:53	7.68	32.21	32.23
33	29-6-91	08:38:27	7.47	29-6-91	08:40:58	7.47	43.96	43.99

Table A.3(x):Load-Displacement-Time record for TP2 (load cycle 2)

P_h (kN)	LOAD START			LOAD END			CUMULATIVE TIME (HOURS)	
	DATE	TIME	Δ_h (mm)	DATE	TIME	Δ_h (mm)	START	END
32	29-6-91	08:46:18	7.48	29-6-91	08:47:34	7.48	44.09	44.11
2000		09:46:21	9.04		10:17:16	9.10	45.09	45.61
4000		10:26:25	10.96		10:56:26	11.07	45.76	46.26
6000		11:04:30	12.49		11:36:37	12.59	46.39	46.93
8000		11:45:22	14.01		12:16:27	14.18	47.04	47.59
9000		12:22:44	14.96		13:09:21	15.56	47.70	48.47
10000		13:18:08	17.02		14:34:31	18.49	48.62	49.89
11000		14:51:14	20.70		15:03:13	21.20	50.17	50.37
9000		15:15:15	20.58		15:26:50	20.57	50.57	50.76
7000		15:30:45	19.74		15:41:19	19.72	50.83	51.00
5000		15:45:40	18.53		15:58:39	18.46	51.08	51.29
3000		16:08:34	16.63		16:17:40	16.61	51.46	51.61
50		16:33:10	12.76		16:34:35	12.75	51.87	51.89
16	30-6-91	09:36:13	11.94	30-6-91	09:37:24	11.94	68.92	68.94

Table A.3(xi):Load-Displacement-Time record for TP2 (load cycle 3)

P_h (kN)	LOAD START			LOAD END			CUMULATIVE TIME (HOURS)	
	DATE	TIME	Δ_h (mm)	DATE	TIME	Δ_h (mm)	START	END
2000	30-6-91	09:48:55	13.68	30-6-91	10:05:15	13.70	69.13	69.40
4000		10:14:43	15.61		10:59:50	15.80	69.56	70.31
6000		11:07:54	17.84		11:54:34	18.03	70.45	71.22
8000		12:03:38	19.99		12:34:54	20.17	71.38	71.89
9000		12:40:51	21.18		13:26:24	21.47	72.00	72.75
10000		13:32:57	22.48		14:18:13	22.89	72.86	73.62
10500		14:23:46	23.38		15:23:48	23.93	73.71	74.71
11000		15:31:31	24.48		16:30:55	25.24	74.84	75.83
11500		16:40:41	25.97		16:56:55	26.36	75.99	76.26
12000		17:18:07	27.59		17:27:24	27.94	76.62	76.77
12300		17:43:40	28.95		17:44:42	29.00	77.04	77.06
12500		17:58:37	30.01		17:59:42	30.07	77.29	77.31
12800		18:14:14	31.27		18:15:20	31.35	77.55	77.57
13000		18:21:39	32.00		18:22:37	32.09	77.68	77.69
13500		18:31:38	33.72		18:32:38	33.96	77.84	77.86
10000		18:39:03	31.66		18:40:06	31.66	77.97	77.98
7000		18:48:41	29.13		18:49:36	29.12	78.13	78.14
4000		18:57:06	26.36		18:58:03	26.35	78.27	78.28
46		19:08:16	21.45		19:09:17	21.42	78.45	78.47

Table A.3(xii):Load-Displacement-Time record for TP2 (load cycle 4)

P_h (kN)	Δ_h (mm)	VIBRATING WIRE STRAIN GAUGE READINGS AT LEVELS (MICRO UNITS)																				P_b (kN)
		LEVEL 1.550 m				LEVEL 21.225 m				LEVEL 23.735 m				LEVEL 26.235 m				LEVEL 28.735 m				
		1	2	3	AVG	1	2	3	AVG	1	2	3	AVG	1	2	3	AVG	1	2	3	AVG	
0	0.00																					
500	0.06	8	4	4	5.3	4	4	5	4.0	4	4	4	4.0	5	4	5	4.4	4	4	3	3.7	1.3
1000	0.16	15	7	7	9.6	6	8	9	7.5	7	8	8	7.5	7	7	7	7.0	6	6	5	5.6	2.7
2000	0.89	50	24	32	35.4	26	35	33	31.2	28	26	29	27.6	26	26	26	26.0	18	21	20	19.4	14.8
3000	2.11	86	60	71	72.3	56	71	69	65.3	60	54	60	57.9	55	56	57	55.9	36	42	41	39.6	30.2
4000	3.33	123	96	109	109.4	87	108	106	100.4	91	82	93	88.5	86	88	87	87.0	56	63	62	60.3	42.3
5000	4.72	163	134	150	148.9	121	147	145	137.8	125	111	127	121.1	120	121	119	119.6	77	82	83	81.0	52.5
6000	6.16	201	170	188	186.6	154	185	184	174.2	157	139	160	152.0	151	154	149	151.2	98	102	104	101.3	67.8
5000	6.53	174	154	173	167.1	140	174	170	161.2	149	131	154	144.7	148	151	145	147.9	99	98	103	99.8	55.1
4000	5.65	137	119	137	131.2	110	142	135	129.2	121	106	127	118.2	123	125	122	123.0	84	82	87	84.5	39.1
3000	4.72	103	84	102	96.4	81	111	101	97.4	92	80	99	90.4	95	97	96	96.2	67	66	70	67.8	21.1
2000	3.8	72	51	67	63.0	51	77	65	64.6	61	54	69	61.3	67	69	69	68.1	50	49	51	50.0	10.2
1000	2.6	36	15	25	25.4	16	39	23	26.2	25	23	33	27.2	34	35	36	35.1	30	25	27	27.4	0
500	2.01	17	6	9	10.8	4	21	26	10.3	11	11	18	13.3	21	21	22	21.1	22	15	18	18.4	0
25	1.90																					

Table A.4(i): Strain gauge readings-TP3 (load cycle 1)

P_h (kN)	Δ_h (mm)	VIBRATING WIRE STRAIN GAUGE READINGS AT LEVELS (MICRO UNITS)																				P_b (kN)
		LEVEL 1.550 m				LEVEL 21.225 m				LEVEL 23.735 m				LEVEL 26.235 m				LEVEL 28.735 m				
		1	2	3	AVG	1	2	3	AVG	1	2	3	AVG	1	2	3	AVG	1	2	3	AVG	
29	1.99																					
500	2.03	23	5	18	15.1	12	28	11	16.8	18	17	23	19.4	25	25	28	26.1	27	19	22	22.6	1.8
1000	2.07	31	9	21	20.0	16	33	18	22.3	22	22	27	23.6	29	30	32	30.4	30	21	24	25.1	0.6
2000	3.01	60	39	49	49.5	43	64	52	52.9	49	46	55	49.9	53	55	56	54.7	44	38	42	41.1	6.5
4000	5.21	128	109	122	119.7	103	131	123	119.2	109	98	109	105.7	108	112	109	109.6	78	73	79	76.5	30.8
6000	7.42	207	181	198	195.4	164	199	195	186.0	169	150	174	164.2	166	169	162	165.7	111	107	114	110.7	72.2
7000	8.63	245	218	236	233.1	196	235	232	220.7	195	177	205	192.4	195	199	190	194.6	130	123	133	128.9	91.8
8000	10.53	285	257	276	272.6	230	275	273	259.3	233	206	240	226.4	228	234	221	227.7	154	139	155	149.1	112.6
9000	12.68	329	298	317	314.2	265	315	315	298.4	268	236	277	260.2	263	271	254	262.9	180	154	180	171.2	142.0
8000	13.65	302	291	298	297.0	255	305	302	287.5	263	227	273	254.2	263	270	253	262.2	184	147	184	171.6	129.6
7000	12.70	263	256	263	260.4	225	274	267	255.2	236	203	247	228.4	238	245	229	237.4	169	133	168	156.6	103.3
6000	11.80	227	220	228	225.0	196	242	234	223.7	207	178	219	201.5	212	218	205	211.7	153	117	152	140.7	81.6
4000	9.68	160	148	157	155.0	135	177	162	158.0	147	125	160	144.0	154	160	151	154.7	116	83	114	104.3	36.4
2000	7.27	101	76	84	87.1	70	103	86	86.3	80	67	93	80.0	88	92	88	89.7	73	42	70	61.7	6.8
1000	5.85	66	40	46	50.7	34	61	42	45.6	42	35	55	43.8	53	55	53	53.5	51	18	43	37.3	-1.5
0	4.77																					

Table A.4(ii): Strain gauge readings-TP3 (load cycle 2)

P_h (kN)	Δ_h (mm)	VIBRATING WIRE STRAIN GAUGE READINGS AT LEVELS (MICRO UNITS)																				P_b (kN)
		LEVEL 1.550 m				LEVEL 21.225 m				LEVEL 23.735 m				LEVEL 26.235 m				LEVEL 28.735 m				
		1	2	3	AVG	1	2	3	AVG	1	2	3	AVG	1	2	3	AVG	1	2	3	AVG	
0	4.75																					
500	4.84	40	20	24	28.1	16	35	14	21.7	22	17	30	22.9	31	33	32	31.9	38	4	27	22.8	-2.7
1000	5.30	58	31	34	40.8	28	49	29	35.5	33	28	42	34.5	41	44	42	42.4	44	11	34	29.7	-1.6
2000	6.50	85	60	67	70.4	58	83	68	69.6	64	56	74	64.4	69	74	70	71.7	63	29	55	49.2	-0.8
4000	9.01	147	127	140	138.4	121	154	141	138.7	126	111	137	124.8	129	135	128	130.7	101	68	97	88.8	16.7
6000	11.5	221	200	217	212.9	185	226	216	208.8	189	167	200	185.6	191	199	186	191.7	141	105	137	127.9	53.1
8000	13.95	301	274	294	289.4	249	296	290	278.2	252	222	263	245.6	252	260	243	251.6	179	139	176	164.5	118.4
9000	15.14	345	312	334	330.2	282	334	329	314.9	285	250	295	276.9	284	292	273	282.9	199	156	198	157.1	157.1
10000	17.40	392	355	378	375.0	317	379	373	356.3	322	281	334	312.1	320	329	307	318.8	225	174	225	207.8	171.6
11000	19.48	429	394	416	413.0	350	417	413	393.2	355	307	367	342.9	352	362	337	350.0	247	190	248	228.3	200.2
12000	24.84	485	450	470	468.3	398	471	468	445.6	404	344	419	388.8	404	412	386	400.6	284	215	282	260.5	286.0
11000	25.69	445	432	443	440.1	380	452	448	426.6	390	326	406	374.1	392	398	375	388.3	277	207	276	252.9	263.4
10000	24.78	406	397	408	403.6	352	421	414	395.4	365	303	381	349.4	369	374	353	365.1	262	193	261	238.9	232.8
8000	22.68	331	326	335	331.0	291	356	345	330.8	308	252	325	294.9	314	319	302	311.9	229	162	228	206.2	176.8
6000	20.46	261	256	264	260.1	230	290	274	264.8	246	199	264	236.5	255	258	247	253.3	190	126	189	168.1	102.0
4000	17.93	199	184	191	191.4	166	216	200	194.2	180	141	197	172.6	189	191	184	187.9	144	83	144	123.7	44.9
2000	15.03	141	110	114	121.6	95	131	113	113.0	104	76	121	100.4	114	115	112	113.7	92	35	90	72.2	8.3
970	13.28	101	71	74	82.1	56	85	64	68.3	65	42	78	61.4	75	75	73	74.2	65	9	61	45.1	-0.2
25	11.56	58	46	38	47.3	23	44	22	29.8	31	13	41	28.6	44	40	41	41.4	44	-11	36	22.7	-5.4

Table A.4(iii): Strain gauge readings-TP3 (load cycle 3)

P_h (kN)	Δh (mm)	VIBRATING WIRE STRAIN GAUGE READINGS AT LEVELS (MICRO UNITS)																				P_b (kN)
		LEVEL 1.550 m				LEVEL 21.225 m				LEVEL 23.735 m				LEVEL 26.235 m				LEVEL 28.735 m				
		1	2	3	AVG	1	2	3	AVG	1	2	3	AVG	1	2	3	AVG	1	2	3	AVG	
0	11.44																					
1000	12.28	87	56	56	66.4	45	62	47	51.6	52	34	61	49.0	59	58	58	58.5	57	1	49	35.7	-3.2
2000	13.45	113	84	87	94.6	77	102	86	88.0	83	63	94	79.9	87	89	88	88.1	77	21	72	56.6	-0.6
4000	16.24	174	150	160	161.2	142	175	163	160.0	148	121	161	143.5	151	156	149	152.1	121	63	118	100.5	7.6
6000	18.90	243	223	239	235.1	209	253	242	234.5	215	180	229	208.2	218	224	212	217.9	167	104	163	144.8	51.5
8000	21.27	323	301	318	314.0	277	329	320	308.7	281	238	297	272.1	285	291	275	283.7	211	144	207	187.4	119.5
10000	24.91	407	378	397	394.2	344	405	399	382.6	348	296	364	336.1	352	358	337	349.0	254	180	250	227.9	247.6
12000	29.25	496	458	482	478.5	413	485	483	460.4	417	355	436	402.8	420	426	401	415.6	296	220	296	270.8	344.6
13000	33.25	538	499	523	520.0	448	525	524	499.4	453	381	472	435.4	455	459	433	448.8	317	243	318	292.6	367.6
14000	36.95	588	545	569	567.2	488	566	571	542.0	492	408	513	470.8	493	491	471	485.3	339	270	341	316.7	423.9
15000	44.89	649	599	623	623.9	532	612	623	589.0	538	434	559	510.1	539	526	516	527.0	360	304	367	343.7	521.5
16000	60.79	701	654	675	676.6	581	658	672	637.0	589	456	613	553.0	584	553	566	567.4	391	347	366	368.1	811.7
16500	78.56	739	691	707	712.2	612	683	709	668.1	631	473	656	586.7	623	576	604	601.0	428	374	355	385.7	1355.3
14000	82.51	635	604	625	621.2	540	608	630	592.7	569	414	598	526.8	568	513	552	544.7	399	340	311	350.2	****
12000	80.39	556	534	553	547.7	481	544	561	528.7	509	365	539	470.9	512	458	500	490.3	364	306	278	315.9	
10000	78.13	477	464	481	473.7	420	478	490	462.8	445	311	476	410.9	450	399	443	430.6	323	268	239	276.7	
8000	75.62	398	390	404	397.0	353	407	414	391.4	376	253	407	345.3	381	332	379	363.9	276	224	197	232.4	
6000	73.01	327	317	330	324.7	286	331	335	317.1	306	194	336	278.4	310	261	312	294.4	226	178	151	184.9	
4000	70.10	275	242	250	255.8	214	247	245	235.4	230	128	258	205.3	233	187	238	219.3	171	124	100	131.4	
2000	66.65	213	166	169	182.5	128	157	147	144.1	149	61	172	127.4	152	108	157	138.8	112	66	45	74.3	
80	62.89	126	93	98	105.5	56	71	55	60.6	76	-3	89	54.2	81	34	81	65.5	64	11	-2	24.3	
20	61.01																					

**** Load cell malfunction

Table A.4(iv): Strain gauge readings-TP3 (load cycle 4)

P_h (kN)	Δ_h (mm)	VIBRATING WIRE STRAIN GAUGE READINGS AT LEVELS (MICRO UNITS)																				P_h (kN)
		LEVEL 1.550 m				LEVEL 21.225 m				LEVEL 23.735 m				LEVEL 26.235 m				LEVEL 28.735 m				
		1	2	3	AVG	1	2	3	AVG	1	2	3	AVG	1	2	3	AVG	1	2	3	AVG	
0	61.48																					
2000	64.03	165	123	126	138.2	96	114	107	105.5	115	43	132	96.7	108	71	114	97.7	86	33	21	46.7	
4000	66.93	216	191	198	201.5	169	185	187	180.4	183	103	205	163.9	175	138	179	164.2	133	81	68	94.2	
6000	70.00	281	265	277	274.2	239	264	271	257.9	253	164	279	232.4	249	208	248	234.9	184	133	116	144.3	
8000	72.95	360	343	356	353.2	310	344	354	336.2	324	227	352	301.2	322	278	319	306.4	235	182	165	194.3	
10000	75.74	443	421	436	433.6	379	424	437	413.3	395	287	424	368.7	396	350	388	378.2	283	232	212	242.5	
12000	78.92	532	502	517	516.8	448	503	521	490.7	466	348	496	436.7	470	419	457	448.8	332	285	261	292.6	
14000	84.37	620	584	600	601.3	518	585	606	570.0	541	410	572	507.3	547	489	529	521.8	389	340	311	346.8	
15000	90.20	670	628	645	647.5	560	630	655	614.7	584	444	617	548.2	592	530	572	564.6	425	369	334	376.1	
16000	98.23	719	672	687	692.9	595	672	701	656.1	627	475	661	587.7	640	568	615	607.5	467	399	353	406.4	
17000	106.32	762	714	726	734.0	633	712	746	697.1	670	505	705	626.7	687	610	658	651.6	513	429	381	440.8	
18000	116.41	816	763	773	784.1	671	756	796	741.2	716	540	753	669.8	744	657	711	703.9	568	469	414	483.8	
14000	118.18	665	636	644	648.3	561	642	674	625.2	610	446	652	569.2	656	562	628	615.3	518	417	358	431.0	
10000	113.58	499	490	498	495.7	433	505	527	488.3	476	330	517	440.9	524	430	505	486.4	423	331	274	343.0	
8000	110.99	424	420	427	423.6	373	436	451	420.0	408	274	447	376.5	453	364	439	418.7	371	283	227	293.3	
6000	108.23	358	350	354	354.3	303	360	368	343.8	337	211	373	306.8	377	292	370	346.5	313	231	176	240.4	
4000	104.95	312	272	273	285.9	226	273	272	256.7	254	141	288	227.6	292	210	287	263.0	245	168	119	177.2	
2000	101.54	255	196	194	215.0	144	183	175	166.9	175	71	202	149.3	210	127	203	180.0	176	104	62	114.2	
0	99.49																					

Table A.4(v): Strain gauge readings-TP3 (load cycle 5)

P_h (kN)	Δ_h (mm)	EXTENSOMETER MOVEMENT (mm)		
		LEVEL 3 0-24 m	LEVEL 4 0-26 m	LEVEL 5 0-29 m
0	0.00			
500	0.06	0	0	0
1000	0.16	0.052	0.006	0
2000	0.89	0.579	0.596	0.599
3000	2.11	1.399	1.523	1.539
4000	3.33	2.252	2.499	2.515
5000	4.72	3.130	3.516	3.550
6000	6.16	3.989	4.494	4.567
5000	6.53	****	****	****
4000	5.65			
3000	4.72			
2000	3.80			
1000	2.60			
500	2.01			
25	1.90			

Table A.4(vi): Extensometer readings-TP3 (load cycle 1)

P_h (kN)	Δ_h (mm)	EXTENSOMETER MOVEMENT (mm)		
		LEVEL 3 0-24 m	LEVEL 4 0-26 m	LEVEL 5 0-29 m
29	1.99	****	****	****
500	2.03			
1000	2.07			
2000	3.01			
4000	5.21			
6000	7.42	4.303	4.913	4.970
7000	8.63	5.109	5.754	5.916
8000	10.53	6.015	6.748	6.967
9000	12.68	6.937	7.784	8.058
8000	13.65	****	****	7.834
7000	12.70			6.968
6000	11.80			6.104
4000	9.68			5.675
2000	7.27			****
1000	5.85			
0	4.77			

Table A.4(vii): Extensometer readings-TP3 (load cycle 2)

P_h (kN)	Δh (mm)	EXTENSOMETER MOVEMENT (mm)		
		LEVEL 3 0-24 m	LEVEL 4 0-26 m	LEVEL 5 0-29 m
0	4.75	****	****	****
500	4.84			
1000	5.30			
2000	6.50			
4000	9.01			
6000	11.50			5.644
8000	13.95	7.310		7.549
9000	15.14	7.313	8.246	8.532
10000	17.40	8.273	9.277	9.662
11000	19.48	9.112	10.206	10.646
12000	24.84	10.292	11.732	12.078
11000	25.69	9.940	****	11.586
10000	24.78	9.228		10.759
8000	22.68	7.926		9.019
6000	20.46	****		7.193
4000	17.93			5.233
2000	15.03			2.936
970	13.28			1.678
25	11.56			0.603

Table A.4(viii): Extensometer readings-TP3 (load cycle 3)

P_h (kN)	Δh (mm)	EXTENSOMETER MOVEMENT (mm)		
		LEVEL 3 0-24 m	LEVEL 4 0-26 m	LEVEL 5 0-29 m
0	11.44	****	****	
1000	12.28			1.215
2000	13.45			2.203
4000	16.24			4.262
6000	18.90			6.330
8000	21.27	7.947		8.340
10000	24.91	8.783		10.336
12000	29.25	10.487		12.361
13000	33.25	11.340		13.356
14000	36.95	12.320		14.481
15000	44.89	13.427		15.765
16000	60.79	14.654		17.142
16500	78.56	15.389		18.010
14000	82.51	13.695		16.042
12000	80.39	12.196		14.320
10000	78.13	10.682		12.571
8000	75.62	9.051		10.618
6000	73.01	8.221		8.615
4000	70.10	****		6.394
2000	66.65			3.897
80	62.89			1.468
20	61.01			

Table A.4(ix): Extensometer readings-TP3 (load cycle 4)

P_h (kN)	Δ_h (mm)	EXTENSOMETER MOVEMENT (mm)		
		LEVEL 3 0-24 m	LEVEL 4 0-26 m	LEVEL 5 0-29 m
0	61.48		****	
2000	64.03	****		2.709
4000	66.93			4.864
6000	70.00			7.026
8000	72.95			9.119
10000	75.74	9.493		11.185
12000	78.92	11.207		13.207
14000	84.37	12.991		15.276
15000	90.20	13.994		16.445
16000	98.23	14.983		17.592
17000	106.32	15.933		18.696
18000	116.41	16.929		19.901
14000	118.18	14.414		16.981
10000	113.58	11.196		13.253
8000	110.99	****		11.399
6000	108.23			9.373
4000	104.95			7.014
2000	101.54			4.556
0	99.49			

Table A.4(x): Extensometer readings-TP3 (load cycle 5)

P_h (kN)	LOAD START			LOAD END			CUMULATIVE TIME (HOURS)	
	DATE	TIME	Δ_h (mm)	DATE	TIME	Δ_h (mm)	START	END
0	13-8-91	12:39:07	0.00	13-8-91				
500		12:42:09	0.06		12:57:44	0.07	0.00	0.26
1000		13:01:23	0.16		13:13:04	0.19	0.32	0.52
1500		13:15:21	0.36		13:32:24	0.40	0.55	0.84
2000		13:35:19	0.89		14:03:11	0.97	0.88	1.35
3000		14:09:16	2.11		14:46:59	2.23	1.45	2.08
4000		14:50:54	3.33		14:50:35	3.50	2.14	3.14
5000		15:58:18	4.72		16:57:01	4.93	3.27	4.25
6000		17:01:45	6.16	14-8-91	08:41:37	7.33	4.33	19.99
5000	14-8-91	08:45:55	6.53		09:05:50	6.53	20.07	20.40
4000		09:09:26	5.65		09:27:16	5.65	20.46	20.75
3000		09:32:33	4.72		09:48:23	4.75	20.85	21.10
2000		09:52:42	3.80		10:11:58	3.76	21.18	21.50
1500		10:17:46	3.17		10:35:25	3.18	21.60	21.89
1000		10:39:50	2.60		10:55:38	2.56	21.97	22.23
500		10:59:49	2.01		11:16:05	1.99	22.30	22.57
25		11:30:06	1.90		12:35:36	1.75	22.81	23.89

Table A.4(xi): Load-Displacement-Time record for TP3 (load cycle 1)

P_h (kN)	LOAD START			LOAD END			CUMULATIVE TIME (HOURS)	
	DATE	TIME	Δ_h (mm)	DATE	TIME	Δ_h (mm)	START	END
29	14-8-91	13:37:00	1.99	14-8-91	14:32:36	1.94	24.93	25.86
500		14:35:29	2.03		14:52:54	1.97	25.90	26.20
1000		14:55:25	2.07		15:10:40	2.05	26.24	26.49
2000		15:16:33	3.01		15:33:14	3.02	26.59	26.87
4000		15:42:31	5.21		16:39:19	5.24	27.02	27.97
6000		16:49:33	7.42		17:50:18	7.55	28.14	29.16
7000		17:56:14	8.63		18:57:02	9.00	29.25	30.27
8000		19:03:43	10.53		20:05:57	11.03	30.38	31.42
9000		20:16:17	12.68	15-8-91	08:33:04	14.40	31.58	43.86
8000	15-8-91	08:42:40	13.65		09:00:06	13.65	44.02	44.31
7000		09:12:40	12.70		09:29:44	12.70	44.52	44.80
6000		09:34:27	11.79		09:51:11	11.79	44.89	45.16
4000		10:00:35	9.68		10:15:09	9.69	45.32	45.56
2000		10:22:11	7.27		10:35:22	7.24	45.68	45.90
1000		10:40:47	5.85		10:55:22	5.82	45.99	46.23
0		11:04:08	4.77		11:05:28	4.76	46.38	46.40

Table A.4(xii): Load-Displacement-Time record for TP3 (load cycle 2)

P_h (kN)	LOAD START			LOAD END			CUMULATIVE TIME (HOURS)	
	DATE	TIME	Δ_h (mm)	DATE	TIME	Δ_h (mm)	START	END
0	15-8-91	12:01:17	4.75	15-8-91	12:02:38	4.75	47.33	47.35
500		12:10:33	4.84		12:26:28	4.86	47.48	47.75
1000		12:30:40	5.30		12:47:08	5.33	47.82	48.09
2000		12:54:24	6.50		13:11:47	6.54	48.22	48.50
4000		13:21:40	9.01		13:39:26	9.07	48.67	48.96
6000		13:49:22	11.50		14:05:19	11.55	49.13	49.39
8000		14:13:44	13.95		14:51:44	14.05	49.54	50.17
9000		14:58:33	15.14		15:30:38	15.30	50.28	50.82
10000		15:43:30	16.93		16:45:27	17.40	51.03	52.06
11000		17:02:25	19.48		19:06:40	20.76	52.35	54.42
11500		19:16:17	21.46	16-8-91	00:43:44	24.32	54.58	60.04
12000	16-8-91	01:45:59	24.84		08:25:58	26.29	61.08	67.74
11500		08:39:30	26.08		08:40:55	26.09	67.96	67.99
11000		08:55:07	25.69		08:56:44	25.68	68.22	68.25
10000		09:07:03	24.78		09:21:22	24.71	68.42	68.66
8000		09:24:19	22.68		09:40:34	22.63	68.71	68.98
6000		09:46:44	20.46		10:02:04	20.26	69.08	69.34
4000		10:09:14	17.93		10:28:31	17.82	69.46	69.78
2000		10:34:29	15.03		10:50:19	14.98	69.88	70.14
1000		10:55:06	13.28		11:09:14	13.21	70.22	70.46
30		11:17:12	11.56		11:18:34	11.55	70.59	70.62

Table A.4(xiii): Load-Displacement-Time record for TP3 (load cycle 3)

P_h (kN)	LOAD START			LOAD END			CUMULATIVE TIME (HOURS)	
	DATE	TIME	Δ_h (mm)	DATE	TIME	Δ_h (mm)	START	END
0	16-8-91	12:51:19	11.44	16-8-91	14:02:49	11.43	72.16	73.35
1000		14:20:51	12.28		14:49:29	12.24	73.65	74.13
2000		14:56:12	13.45		15:29:22	13.56	74.24	74.79
4000		15:40:31	16.24		16:12:01	16.27	74.98	75.50
6000		16:22:02	18.90	17-8-91	08:50:47	18.95	75.67	92.12
8000	17-8-91	09:01:40	21.27		12:03:28	22.22	92.33	95.36
10000		12:13:04	24.91		12:45:23	25.36	95.52	96.06
11000		12:48:41	26.55		13:19:52	27.26	96.12	96.64
12000		14:02:31	29.25		14:34:07	29.86	97.35	97.87
13000		15:15:29	33.25		15:47:47	33.50	98.56	99.10
14000		16:26:53	36.95		16:58:07	39.18	99.75	100.27
15000		17:37:13	44.89		18:07:04	48.96	100.93	101.42
16000		18:46:36	60.79		20:26:04	76.34	102.08	103.74
16500		20:31:02	78.56		20:38:28	81.66	103.82	103.94
14000		20:53:52	82.51		20:55:41	82.49	104.20	104.23
12000		21:00:13	80.39		21:01:48	80.39	104.31	104.33
10000		21:05:01	78.13		21:06:29	78.12	104.39	104.41
8000		21:11:40	75.62		21:13:15	75.61	104.50	104.52
6000		21:19:44	73.01		21:30:07	72.90	104.63	104.81
4000		21:33:44	70.10		21:41:13	68.98	104.87	104.99
2000		21:45:54	66.65		21:56:04	66.44	105.07	105.24
80		22:03:08	62.89		22:04:42	62.79	105.36	105.38
20	19-8-91	10:42:21	61.01	19-8-91	10:44:31	61.48	142.01	142.05

Table A.4(xiv): Load-Displacement-Time record for TP3 (load cycle 4)

P_h (kN)	LOAD START			LOAD END			CUMULATIVE TIME (HOURS)	
	DATE	TIME	Δ_h (mm)	DATE	TIME	Δ_h (mm)	START	END
0	19-8-91	13:57:02	61.48	19-8-91	13:58:29	61.48	145.25	145.27
2000		14:05:28	64.03		14:19:53	64.04	145.39	145.63
4000		14:27:20	66.93		14:57:32	67.15	145.76	146.26
6000		15:06:06	70.00		15:32:20	70.11	146.40	146.84
8000		15:41:14	72.95		16:13:03	73.12	146.99	147.52
10000		16:24:47	75.74		16:56:50	75.98	147.71	148.25
12000		17:09:07	78.92		17:42:27	79.73	148.45	149.01
14000		17:56:46	84.37		18:29:42	86.38	149.25	149.79
14500		18:32:33	87.22		19:02:02	89.31	149.84	150.33
15000		19:05:22	90.20		19:37:13	92.85	150.39	150.92
15500		19:44:05	94.22		20:15:24	97.07	151.03	151.55
16000		20:19:42	98.23		20:54:41	101.62	151.63	152.21
16500		21:00:28	102.84		21:16:23	104.94	152.31	152.57
17000		21:20:46	106.32		21:36:41	109.37	152.64	152.91
17500		21:41:18	110.93		21:58:53	114.62	152.99	153.28
18000		22:04:10	116.41		22:37:05	122.08	153.37	153.91
14000		22:41:35	118.18		22:51:31	118.09	153.99	154.15
10000		22:54:51	113.58	20-8-91	09:44:15	113.31	154.21	165.03
8000	20-8-91	09:54:53	110.99		10:27:31	110.76	165.21	165.75
6000		10:33:40	108.23		11:07:04	108.04	165.86	166.41
4000		11:14:21	104.95		11:47:35	104.88	166.53	167.09
2000		11:55:12	101.54		12:25:52	101.37	167.22	167.73
0		12:35:58	99.49		13:37:19	97.03	167.89	168.92

Table A.4(xv): Load-Displacement-Time record for TP3 (load cycle 5)

Ph (kN)	Dh (mm)	VIBRATING WIRE STRAIN GAUGE READINGS AT LEVELS DOWN PILE SHAFT (MICRO STRAIN) LEVEL 1.250 m				LEVEL 17.950 m				LEVEL 18.750 m				LEVEL 21.500 m				LEVEL 24.250 m				EXTENSOMETER READINGS (mm) Pb (kN)	LEVEL 3 (0-19m)	LEVEL 4 (0-21m)	LEVEL 5 (0-24m)
		1	2	3	Mean	1	2	3	Mean	1	2	3	Mean	1	2	3	Mean	1	2	3	Mean				
540	0.17	20	4	-3	12	5	4	5	4.6	2	3	0	2.5	1	1	4	2.1	1	0	0	0.2	0.1	0.087	0.129	0.321
1000	0.56	34	20	0	27	14	13	16	14.2	8	9	0	8.5	3	4	6	4.3	2	1	1	1.1	0.0	0.382	0.574	0.749
1500	1.41	54	33	15	43.5	28	28	28	28.0	16	20	0	18.0	8	9	8	8.4	3	3	1	2.0	7.7	0.698	1.088	1.245
2000	2.38	73	48	27	60.5	43	40	42	41.6	28	31	0	29.5	12	14	11	12.5	3	4	1	2.3	13.3	1.026	1.649	1.776
2500	3.57	94	61	40	77.5	57	55	56	55.9	39	44	0	41.5	17	21	16	18.0	3	5	1	3.0	14.2	1.355	2.220	2.332
3000	4.82	113	76	50	94.5	72	69	71	70.7	51	58	0	54.5	23	27	23	24.3	5	7	1	4.2	17.1	1.686	2.798	2.895
3500	6.3	133	90	59	111.5	87	84	86	85.9	63	71	0	67.0	29	34	27	30.2	6	8	2	5.1	19.0	2.028	3.387	3.482
3000	7.3	125	81	49	103	87	82	84	84.4	60	71	0	65.5	28	35	29	30.5	5	9	2	5.3	14.2	2.152*	3.478	3.673
2500	6.91	108	67	36	87.5	73	73	76	73.8	50	61	0	55.5	24	30	23	25.8	5	8	1	4.6	11.3	2.152*	3.472*	3.676*
2000	6.5	90	54	25	72	65	60	64	63.0	41	51	0	46.0	19	26	19	21.2	4	7	1	3.7	7.6	2.152*	3.459*	3.673*
1500	5.99	69	39	14	54	50	46	51	48.9	31	39	0	35.0	14	20	14	16.2	3	6	0	3.0	2.9	2.152*	3.456*	3.681*
1000	5.43	50	23	-1	36.5	32	31	36	32.9	19	28	0	23.5	10	15	11	12.0	2	4	-1	1.8	-0.9	2.152*	3.452*	3.677*
480	4.84	33	8	-17	20.5	14	12	20	15.4	8	15	0	11.5	4	9	5	5.9	1	2	-1	0.7	-2.7	2.152*	3.450*	3.681*

Note Strain gauge No.3 at levels 1.250m and Level 18.750m excluded when computing average strains

Table A.5(i):Strain gauge,Extensometer and Base load cell readings-TP4 (load cycle 1)

Ph (kN)	Dh (mm)	VIBRATING WIRE STRAIN GAUGE READINGS AT LEVELS DOWN PILE SHAFT (MICRO STRAIN) LEVEL 1.250 m				LEVEL 17.950 m				LEVEL 18.750 m				LEVEL 21.500 m				LEVEL 24.250 m				EXTENSOMETER READINGS (mm) Pb (kN)	LEVEL 3 (0-19m)	LEVEL 4 (0-21m)	LEVEL 5 (0-24m)
		1	2	3	Mean	1	2	3	Mean	1	2	3	Mean	1	2	3	Mean	1	2	3	Mean				
500	4.64	31	6	-14	18.5	13	10	16	12.9	8	14	0	11	5	10	6	6.8	2	1	0	0.9	-2.8	2.151*	3.435*	3.692*
1000	5.03	45	20	-2	32.5	25	22	29	25.6	16	23	0	19.5	9	13	10	10.5	2	2	0	1.2	-0.1	2.152*	3.432*	3.699*
2000	5.98	46	21	-2	33.5	54	51	54	53	36	44	0	40	18	22	21	20.1	3	4	1	2.5	-1.9	2.149*	3.427*	3.690*
3000	7.08	114	78	46	96	81	77	79	79	56	65	0	60.5	27	32	27	28.8	5	7	1	4.2	13.2	2.151*	3.426	3.689
4000	8.75	157	108	68	132.5	107	103	103	104.3	78	90	0	84	37	44	36	39.1	8	12	2	7.1	23.6	2.447	3.945	4.211
5000	12.19	193	134	81	163.5	135	130	129	131.3	102	117	0	109.5	47	58	53	52.6	11	18	5	11.3	33	3.046	5.114	5.392
5250	14.64	207	143	87	175	144	140	138	140.6	110	127	0	118.5	50	65	62	59	13	22	7	14.1	36.8	3.299	5.506	5.834
5000	16.28	208	142	85	175	145	138	136	139.7	111	127	0	119	50	67	65	60.9	14	23	10	15.5	32.2	3.362*	5.571	5.926
4000	15.55	172	114	61	143	131	118	122	123.7	93	109	0	101	41	57	57	51.7	11	21	6	12.9	25.5	3.371*	5.563*	5.917*
3000	14.64	134	86	40	110	106	98	99	101.1	73	88	0	80.5	31	46	45	40.7	8	18	4	10.2	6.7	3.370*	5.557*	5.916*
2000	13.56	94	57	19	75.5	74	68	71	70.9	51	63	0	57	20	34	34	29.3	5	13	3	6.9	6.5	3.373*	5.556*	5.917*
1000	12.25	59	29	-3	44	40	36	41	38.7	26	37	0	31.5	9	22	23	18.2	3	8	1	4.1	-1.9	3.368*	5.554*	5.921*
500	11.52	42	15	-15	28.5	22	19	25	22	15	24	0	19.5	3	16	17	12.4	3	5	1	2.8	-1.9	3.371*	5.554*	5.920*

Note Strain gauge No.3 at levels 1.250m and Level 18.750m excluded when computing average strains

Table A.5(ii):Strain gauge,Extensometer and Base load cell readings-TP4 (load cycle 2)

Ph (kN)	Dh (mm)	VIBRATING WIRE STRAIN GAUGE READINGS AT LEVELS DOWN PILE SHAFT (MICRO STRAIN) LEVEL 1.250 m 1	2	3	Mean	LEVEL 17.950 m 1	2	3	Mean	LEVEL 18.750 m 1	2	3	Mean	LEVEL 21.500 m 1	2	3	Mean	LEVEL 24.250 m 1	2	3	Mean	Pb (kN)	EXTENSOMETER READINGS (mm) LEVEL 3 (0-19m)	LEVEL 4 (0-21m)	LEVEL 5 (0-24m)
500	10.95	37	12	-12	24.5	18	15	21	17.7	11	17	0	14	2	14	15	10.2	1	4	1	1.9	-4.7	3.366*	5.543*	5.925*
1000	11.44	52	25	1	38.5	32	27	34	31.2	21	28	0	24.5	7	18	21	15.2	2	4	1	2.1	-3.7	3.362*	5.536*	5.918*
2000	12.6	83	53	22	68	63	58	62	61.1	43	53	0	48	19	30	31	26.5	3	7	1	3.9	1.0	3.368*	5.534*	5.917*
3000	13.87	118	82	40	100	94	86	88	89.5	66	78	0	72	30	42	42	38.3	5	11	2	6.2	7.5	3.364*	5.532*	5.915*
4000	15.16	157	110	59	133.5	121	113	114	116	88	102	0	95	41	55	55	50.1	9	16	5	9.9	19.9	3.366*	5.531*	5.919*
5000	16.69	198	137	81	167.5	145	134	136	138.6	110	126	0	118	51	65	66	60.7	14	22	8	14.8	36.0	3.362	5.527	5.923
5500	18.02	220	152	92	186	159	151	149	152.9	123	140	0	131.5	57	72	71	66.7	17	28	11	18.5	43.4	3.552	5.874	6.286
6000	20.16	240	166	101	203	173	165	162	166.5	134	154	0	144	62	80	81	74.8	20	32	14	22.2	52.9	3.888	6.472	6.930
6500	22.81	258	180	107	219	187	179	174	180.2	147	168	0	157.5	68	89	92	82.8	24	39	21	27.9	62.3	4.224	7.093	7.567
6750	26.6	269	189	111	229	196	188	182	188.7	156	177	0	166.5	72	96	100	89.2	27	46	29	34	71.7	4.437	7.499	7.990
7000	28.99	279	197	116	238	204	196	189	196.2	163	185	0	174	77	102	106	95	30	51	34	38.5	80.2	4.623	7.836	8.378
6000	30.27	246	172	90	209	192	183	177	183.7	147	169	0	158	68	94	98	86.3	27	51	32	36.6	66.9	4.663	7.922	8.448*
5000	29.31	210	145	70	177.5	174	164	158	165.3	127	148	0	137.5	57	83	87	75.7	23	47	25	31.5	51.8	4.662*	7.920*	8.449*
4000	28.37	171	118	51	144.5	146	137	134	139.1	106	125	0	115.5	46	70	76	64.3	18	42	19	26.3	38.5	4.662*	7.919*	8.441*
3000	27.3	134	91	34	112.5	115	109	107	110.1	84	102	0	93	34	58	63	51.9	12	35	14	20.3	24.5	4.662*	7.921*	8.445*
2000	25.99	96	62	15	79	79	74	76	76.4	58	74	0	66	22	43	50	38.3	7	28	9	14.6	9.3	4.662*	7.917*	8.443*
1000	24.41	65	35	-1	50	45	40	45	43.5	31	43	0	37	8	28	35	23.9	3	19	4	8.9	0.8	4.662*	7.915*	8.448*
500	23.67	50	20	-10	35	29	24	30	27.6	20	30	0	25	3	22	29	18.1	2	16	3	6.7	-1	4.662*	7.911*	8.446*

Note Strain gauge No.3 at levels 1.250m and Level 18.750m excluded when computing average strains

Table A.5(iii):Strain gauge,Extensometer and Base load cell readings-TP4 (load cycle 3)

Ph (kN)	Dh (mm)	VIBRATING WIRE STRAIN GAUGE READINGS AT LEVELS DOWN PILE SHAFT (MICRO STRAIN)																				EXTENSOMETER READINGS (mm)			
		LEVEL 1.250 m				LEVEL 17.950 m				LEVEL 18.750 m				LEVEL 21.500 m				LEVEL 24.250 m				Pb	LEVEL 3	LEVEL 4	LEVEL 5
		1	2	3	Mean	1	2	3	Mean	1	2	3	Mean	1	2	3	Mean	1	2	3	Mean	(kN)	(0-19m)	(0-21m)	(0-24m)
1000	22.85	59	29	6	44.0	38	34	38	36.4	26	37	0	31.5	7	26	33	22.2	2	13	2	5.6	-1.9	4.662*	7.899*	8.455*
2000	23.96	88	54	23	71.0	68	62	65	65.0	47	60	0	53.5	19	38	44	33.8	5	16	4	8.1	1.9	4.662*	7.899*	8.453*
3000	25.31	118	81	37	99.5	98	93	93	94.6	72	86	0	79.0	32	51	56	46.5	7	21	6	11.3	9.4	4.660*	7.890*	8.449*
4000	26.68	155	108	53	131.5	129	122	120	123.9	95	112	0	103.5	45	65	70	59.7	12	27	9	16.0	20.8	4.661*	7.887*	8.453*
5000	28.08	194	135	71	164.5	157	149	146	150.6	118	138	0	128.0	57	78	81	72.0	17	33	14	21.4	37.7	4.658*	7.883*	8.454*
6000	29.66	234	163	90	198.5	183	175	170	175.9	141	163	0	152.0	68	90	94	84.3	24	42	22	29.3	59.4	4.656*	7.877*	8.457*
6500	30.68	255	177	102	216.0	195	187	182	188.0	153	176	0	164.5	74	97	101	90.9	29	48	29	35.4	76.4	4.655*	7.874*	8.463*
7000	32.02	276	191	112	233.5	207	200	193	199.8	166	188	0	177.0	80	104	108	97.3	34	56	37	42.4	94.2	4.652	7.872	8.469
7500	34.30	294	205	119	249.5	221	213	205	213.1	177	201	0	189.0	85	111	116	104.2	40	64	46	50.0	109.2	4.902	8.374	9.003
8000	37.53	313	216	127	264.5	234	225	217	225.7	189	214	0	201.5	92	119	125	111.8	45	72	58	58.4	127.0	5.231	9.005	9.664
8600	41.94	333	229	136	281.0	249	239	231	239.6	202	227	0	214.5	99	129	134	120.8	52	84	75	70.2	153.1	5.581	9.684	10.362
9000	47.62	352	242	143	297.0	263	253	244	253.8	214	240	0	227.0	107	139	144	130.1	61	99	100	86.5	191.2	5.943	10.395	11.062
10000	63.39	393	267	157	330.0	293	281	271	281.9	241	266	0	253.5	124	160	164	149.5	132	145	176	150.8	322.0	6.664	11.941	12.530
11000	82.95	435	290	173	362.5	321	309	299	309.7	264	290	0	277.0	141	171	186	166.2	270	234	297	267.1	582.9	7.352	13.581	13.914
11250	90.37	446	295	176	370.5	327	315	305	315.8	267	293	0	280.0	146	172	192	169.9	378	278	356	337.2	699.4	7.543	14.068	14.252
9500	93.56	392	253	137	322.5	298	289	280	289.1	230	260	0	245.0	130	151	178	152.8	346	311	369	342.0	662.0	7.618*	12.926	14.359
8000	96.74	334	215	104	274.5	273	264	257	264.4	200	229	0	214.5	112	132	161	134.8	328	301	344	324.5	577.8	7.615*	12.915	14.358*
6000	94.81	259	164	70	211.5	224	214	211	216.4	157	184	0	170.5	86	104	132	107.3	300	285	304	296.5	453.4	7.607*	12.909*	14.357*
4000	92.47	190	116	39	153.0	156	152	152	153.4	109	131	0	120.0	57	72	102	77.1	268	265	260	264.2	320.4	7.606*	12.903*	14.356*
2000	89.58	128	69	17	98.5	85	86	90	86.8	54	72	0	63.0	26	37	69	44.3	230	233	210	224.6	184.8	7.605*	12.899*	14.356*

Note Strain gauge No.3 at levels 1.250m and Level 18.750m excluded when computing average strains

Table A.5(iv):Strain gauge,Extensometer and Base load cell readings-TP4 (load cycle 4)

Ph (kN)	Dh (mm)	VIBRATING WIRE STRAIN GAUGE READINGS AT LEVELS DOWN PILE SHAFT (MICRO STRAIN)																				EXTENSOMETER READINGS (mm)			
		LEVEL 1.250 m				LEVEL 17.950 m				LEVEL 18.750 m				LEVEL 21.500 m				LEVEL 24.250 m				Pb	LEVEL 3	LEVEL 4	LEVEL 5
		1	2	3	Mean	1	2	3	Mean	1	2	3	Mean	1	2	3	Mean	1	2	3	Mean	(kN)	(0-19m)	(0-21m)	(0-24m)
3000	89.11	144	89	38	116.5	103	103	107	104.2	67	84	0	75.5	38	47	78	54.0	220	194	169	182.0	142.9	7.598*	12.874*	14.356*
6000	93.27	237	160	75	198.5	196	191	192	193.2	145	167	0	156.0	84	98	123	101.7	262	227	200	214.0	281.7	7.599*	12.871*	14.360*
9000	101.68	353	237	129	295.0	281	272	270	274.3	221	244	0	232.5	129	139	167	145.0	145	326	309	318.0	338.7	7.598*	12.858	14.358*
10000	110.72	395	268	152	331.5	305	297	295	299.1	243	267	0	255.0	144	153	182	159.4	373	359	425	392.0	769.1	7.598	13.383	14.357
11000	127.08	436	296	173	366.0	328	321	319	322.4	260	286	0	273.0	161	159	203	174.2	338	420	566	493.0	985.5	7.636	14.822	14.359
12000	155.60	476	321	188	398.5	348	343	345	345.4	273	297	0	285.0	181	163	240	194.9	173	529	1101	815.0	1452	8.301	16.553	14.458
11500	156.56	461	306	174	383.5	339	333	341	337.6	256	280	0	268.0	178	154	246	192.7	253	632	1731	1182.0	1552	8.372*	16.547	15.536
8000	155.45	334	210	103	272.0	272	270	279	273.7	186	207	0	196.5	133	108	200	146.8	173	606	1669	1138.0	1278	8.371*	13.106	15.541
5000	153.00	228	143	56	185.5	180	180	199	186.6	115	135	0	125.0	87	62	153	100.8	82	578	1567	1073.0	982.6	8.371*	11.326	15.537

Note Strain gauge No.3 at levels 1.250m and Level 18.750m excluded when computing average strains

Table A.5(v):Strain gauge,Extensometer and Base load cell readings-TP4 (load cycle 5)

P_h (kN)	LOAD START			LOAD END			CUMULATIVE TIME (HOURS)	
	DATE	TIME	Δ_h (mm)	DATE	TIME	Δ_h (mm)	START	END
0	2-9-91		0	2-9-91		0		
540		16:49:14	0.17		17:04:39	0.18	0	0.26
1000		17:10:23	0.56		17:40:14	0.71	0.35	0.85
1500		17:43:21	1.41		18:14:32	1.63	0.90	1.42
2000		18:17:04	2.38		18:49:59	2.68	1.46	2.01
2500		18:53:31	3.57		18:53:31	3.57	2.07	2.07
3000		19:45:12	4.82		20:31:42	5.31	2.93	3.71
3500		20:35:47	6.30	3-9-91	09:26:47	7.58	3.78	16.63
3000	3-9-91	09:33:26	7.30		09:50:10	7.29	16.74	17.02
2500		09:55:42	6.91		10:12:50	6.89	17.11	17.39
2000		10:15:18	6.50		10:32:04	6.47	17.43	17.71
1500		10:36:02	5.99		10:51:36	5.98	17.78	18.04
1000		10:54:51	5.43		11:08:35	5.42	18.09	18.32
500		11:12:34	4.84		11:28:20	4.83	18.39	18.65
0		11:39:09	4.37		12:28:16	4.39	18.83	19.65

Table A.5(vi): Load-Displacement-Time record for TP4 (load cycle 1)

P_h (kN)	LOAD START			LOAD END			CUMULATIVE TIME (HOURS)	
	DATE	TIME	Δ_h (mm)	DATE	TIME	Δ_h (mm)	START	END
500	3-9-91	12:33:11	4.64	3-9-91	12:52:35	4.65	19.73	20.06
1000		12:57:02	5.03		13:13:02	5.03	20.13	20.40
2000		13:20:16	5.98		13:35:48	6.02	20.52	20.78
3000		13:40:23	7.08		14:13:49	7.18	20.85	21.41
4000		14:22:06	8.75		15:23:11	9.33	21.55	22.57
5000		15:32:36	12.19		17:48:41	14.26	22.72	24.99
5250		17:54:59	14.64		21:56:30	15.96	25.10	29.12
5000	4-9-91	08:30:48	16.28	4-9-91	08:53:31	16.23	36.69	40.07
4000		08:57:14	15.55		09:13:27	15.53	40.13	40.40
3000		09:17:48	14.64		09:35:30	14.61	40.48	40.77
2000		09:38:39	13.56		09:55:29	13.53	40.82	41.10
1000		10:00:48	12.25		09:17:33	12.19	41.19	41.47
500		10:22:57	11.52		10:39:39	11.48	41.56	41.84
30		10:54:14	10.59		11:44:48	10.54	42.08	42.93

Table A.5(vii): Load-Displacement-Time record for TP4 (load cycle 2)

P_h (kN)	LOAD START			LOAD END			CUMULATIVE TIME (HOURS)	
	DATE	TIME	Δ_h (mm)	DATE	TIME	Δ_h (mm)	START	END
500	4-9-91	11:52:14	10.95	4-9-91	12:08:03	10.95	43.05	43.32
1000		12:14:36	11.44		12:31:53	11.46	43.42	43.71
2000		12:37:53	12.60		12:55:35	12.65	43.81	44.11
3000		13:04:14	13.87		13:23:05	13.92	44.25	44.57
4000		13:31:17	15.16		14:02:55	15.28	44.70	45.23
5000		14:10:02	16.69		15:10:54	17.12	45.35	46.37
5500		15:19:44	18.02		17:08:48	19.08	46.51	48.33
6000		17:17:11	20.16		19:49:05	21.89	48.47	51.00
6500		19:53:58	22.81	5-9-91	00:56:15	26.21	51.08	56.12
6750	5-9-91	01:05:24	26.60		05:36:16	28.54	56.27	60.79
7000		05:43:26	28.99		09:13:54	30.83	60.90	64.42
6000		09:22:55	30.27		09:38:48	30.25	64.56	64.83
5000		09:50:10	29.31		10:06:38	29.31	65.02	65.29
4000		10:11:21	28.37		10:28:44	28.32	65.37	65.66
3000		10:32:47	27.30		10:48:28	27.23	65.73	65.99
2000		10:54:35	25.99		11:09:45	25.95	66.09	66.35
1000		11:18:10	24.41		11:36:30	24.34	66.48	66.79
500		11:42:17	23.67		11:59:11	23.61	66.88	67.17
40		12:10:21	22.83		12:20:58	22.77	67.35	67.53

Table A.5(viii): Load-Displacement-Time record for TP4 (load cycle 3)

P_h (kN)	LOAD START			LOAD END			CUMULATIVE TIME (HOURS)	
	DATE	TIME	Δ_h (mm)	DATE	TIME	Δ_h (mm)	START	END
75	5-9-91	14:45:59	22.00	5-9-91	14:45:59	22.00	69.95	69.95
1000		14:51:06	22.85		15:22:01	22.89	70.03	70.55
2000		15:26:23	23.96		15:59:25	24.13	70.62	71.17
3000		16:04:15	25.31		16:37:43	25.42	71.25	71.81
4000		16:44:09	26.68		17:03:03	26.77	71.92	72.23
5000		17:09:58	28.08		17:43:09	28.22	72.35	72.90
6000		17:50:38	29.66		18:20:46	29.90	73.02	73.53
6500		18:26:16	30.68		18:57:40	31.18	73.62	74.14
7000		19:01:13	32.02		19:32:41	33.01	74.20	74.73
7500		19:37:16	34.30		20:07:55	35.90	74.80	75.32
8000		20:12:22	37.53		20:44:45	40.04	75.39	75.93
8500		20:49:10	41.94		21:21:41	45.78	76.00	76.54
9000		21:26:01	47.62		21:57:55	52.65	76.61	77.15
9500		22:02:41	54.55		22:34:38	60.69	77.22	77.76
10000		22:39:48	63.39		23:11:32	70.81	77.84	78.38
10250		23:14:13	71.71		23:14:51	71.98	78.42	78.43
10500		23:16:55	73.47		23:17:46	74.12	78.46	78.48
10750		23:20:15	77.61		23:20:57	77.61	78.52	78.53
11000		23:24:50	82.95		23:25:32	83.87	78.59	78.61
11250		23:30:05	90.37		23:30:49	91.38	78.68	78.70
11000		23:33:48	92.76		23:35:13	92.84	78.74	78.77
9500	6-9-91	09:07:34	93.56	6-9-91	09:09:02	93.55	88.30	88.33
8000		09:24:09	96.74		09:43:26	96.72	88.58	88.91
6000		09:48:13	94.81		10:03:14	94.71	88.98	89.24
4000		10:07:02	92.47		10:23:27	92.35	89.30	89.57
2000		10:26:38	89.58		10:44:01	89.43	89.62	89.92
60		10:53:22	85.87		10:54:49	85.81	90.07	90.10

Table A.5(ix): Load-Displacement-Time record for TP4 (load cycle 4)

P_h (kN)	LOAD START			LOAD END			CUMULATIVE TIME (HOURS)	
	DATE	TIME	Δ_h (mm)	DATE	TIME	Δ_h (mm)	START	END
0	6-9-91	12:26:26	86.00	6-9-91	12:27:42	86.00	91.62	91.64
3000		12:34:04	89.11		13:06:06	89.22	91.75	92.28
6000		13:14:31	93.27		13:47:26	93.48	92.42	92.97
9000		13:59:33	100.16		14:30:15	101.68	93.17	93.68
10000		14:37:09	106.85		14:58:48	110.72	93.80	94.16
11000		15:05:07	118.31		15:18:02	127.08	94.27	94.48
12000		15:25:40	143.20		15:38:14	155.60	94.61	94.82
11500		15:50:37	156.56		16:04:30	156.76	95.02	95.25
8000		16:08:13	155.45		16:14:08	155.43	95.32	95.42
5000		16:17:46	153.00		16:25:32	152.86	95.48	95.61
0		16:35:13	145.26		16:37:00	145.20	95.77	95.80

Table A.5(x): Load-Displacement-Time record for TP4 (load cycle 5)

P_h (kN)	Δ_h (mm)	VIBRATING WIRE STRAIN GAUGE READINGS AT LEVELS (MICRO UNITS)																				P_b (kN)
		LEVEL 3.340 m				LEVEL 20.200 m				LEVEL 21.700 m				LEVEL 25.700 m				LEVEL 29.700 m				
		1	2	3	AVG	1	2	3	AVG	1	2	3	AVG	1	2	3	AVG	1	2	3	AVG	
0	0																					
500	0.03	2	2	1	1.75	1	2	2	1.5	2	2	2	2.0	2	2	2	2.0	1	1	1	0.4	1.5
1000	0.09	6	4	7	5.7	4	5	5	4.7	5	5	5	5.0	4	4	4	4.0	1	0	1	0.4	6.1
1500	0.30	27	10	12	16.3	11	14	15	13.1	14	13	13	13.2	9	9	9	9.0	2	2	1	1.5	13.7
2000	0.94	45	25	25	31.7	24	27	30	26.8	28	27	27	27.2	19	19	18	18.7	2	2	2	2.0	24.7
3000	2.75	81	58	57	65.6	53	52	64	56.7	62	59	59	59.9	41	42	40	40.8	3	3	4	3.4	34.1
4000	4.78	118	93	89	99.8	82	79	99	86.7	96	91	92	92.8	63	64	61	62.7	4	5	5	5.1	46.2
5000	7.30	154	129	122	135.4	113	107	134	118.0	131	126	128	128.1	88	88	82	85.9	6	7	7	6.5	63.4
6000	10.86	193	168	157	172.7	143	137	175	151.5	167	163	166	165.2	113	113	103	109.7	9	9	8	8.7	85.1
5000	11.69	164	143	134	147.2	123	115	156	131.5	146	144	150	146.7	102	102	90	97.8	7	7	5	6.0	67.9
4000	10.69	129	110	104	114.1	94	85	124	101.0	115	114	120	116.3	81	82	70	77.7	3	4	1	2.9	43.6
3000	9.65	94	76	73	81.1	65	56	92	71.0	83	83	89	85.4	60	61	48	56.4	1	2	-3	-0.2	20.8
2000	8.50	60	43	42	48.0	36	30	59	41.6	50	51	58	53.1	36	39	26	33.7	-2	-1	-6	-2.9	2.0
1500	7.88	41	26	25	30.8	21	17	42	26.5	33	35	42	36.4	24	27	14	21.5	-2	-2	-7	-3.8	-7.2
1000	7.25	24	8	9	13.6	6	4	24	11.4	14	18	25	19.3	12	16	3	10.1	-3	-3	-8	-4.9	-16.4
500	6.48	3	-8	-7	-4.3	-10	-8	6	-4.1	-4	1	8	1.9	-1	3	-10	-2.8	-4	-4	-10	-6.0	-24.6
0	6.61	11	-3	-12	-1.1	-8	-7	7	-7.3	-3	1	9	2.2	-3	1	-13	-5.1	-4	-4	-10	-6.0	-25.7

Table A.6(i): Strain gauge readings-TP5 (load cycle 1)

P_h (kN)	Δ_h (mm)	VIBRATING WIRE STRAIN GAUGE READINGS AT LEVELS (MICRO UNITS)																				P_b (kN)
		LEVEL 3.340 m				LEVEL 20.200 m				LEVEL 21.700 m				LEVEL 25.700 m				LEVEL 29.700 m				
		1	2	3	AVG	1	2	3	AVG	1	2	3	AVG	1	2	3	AVG	1	2	3	AVG	
0	6.61																					
500	6.62	13	0	-5	2.6	-6	-3	10	0.5	1	5	12	5.9	1	4	-9	-1.5	-3	-4	-9	-5.2	-21.5
1000	6.65	19	5	2	8.4	-1	1	16	5.4	6	10	17	11.0	4	7	-6	1.9	-3	-4	-8	-4.9	-19.0
2000	7.35	55	33	32	40.0	27	25	46	32.5	37	40	46	40.9	23	26	13	21.0	-2	-2	-5	-3.1	-8.7
4000	9.64	127	100	94	106.9	85	79	112	92.2	103	103	108	104.6	69	69	57	65.1	2	2	1	1.5	32.0
6000	12.29	199	169	157	175.0	145	141	180	155.2	170	168	172	170.0	116	114	101	110.3	8	9	7	8.0	95.6
7000	15.37	235	206	190	210.1	176	171	219	188.7	204	202	207	204.2	139	136	123	132.6	12	13	9	11.3	136.7
7500	18.64	257	227	208	231.0	194	191	243	209.5	223	223	228	224.8	153	150	135	145.8	16	16	10	13.8	171.0
6000	22.14	218	193	178	196.5	165	161	215	180.2	194	197	205	198.8	136	132	115	127.5	14	14	4	11.0	162.5
4000	20.07	149	127	117	130.8	107	100	151	119.5	129	135	144	135.9	91	89	71	83.9	7	7	-4	3.4	88.1
2000	17.73	78	59	54	64.1	48	49	84	60.7	69	69	80	69.8	43	43	25	37.1	1	1	-11	-3.2	21.8
1000	16.25	41	24	20	28.3	17	22	47	28.6	23	33	45	33.7	17	19	1	12.0	-2	-3	-14	-6.3	-5.6
0	14.54	-2	-6	-7	-5.0	-11	-5	10	-2.0	-10	-5	12	-1.0	-8	-4	-21	-11.0	-3	-5	-16	-8.0	-25.63

Table A.6(ii): Strain gauge readings-TP5 (load cycle 2)

P_h (kN)	Δ_h (mm)	VIBRATING WIRE STRAIN GAUGE READINGS AT LEVELS (MICRO UNITS)																				P_b (kN)
		LEVEL 3.340 m				LEVEL 20.200 m				LEVEL 21.700 m				LEVEL 25.700 m				LEVEL 29.700 m				
		1	2	3	AVG	1	2	3	AVG	1	2	3	AVG	1	2	3	AVG	1	2	3	AVG	
0	14.70																					
2000	16.30	65	48	46	53.0	38	39	64	46.8	46	54	63	54.4	29	30	11	23.4	0	-1	-10	-3.6	0
4000	18.68	135	114	109	119.6	96	90	131	105.8	113	119	126	119.5	76	73	55	67.9	4	4	-4	1.5	52.3
6000	21.25	206	183	172	187.0	156	150	200	168.6	183	185	192	186.5	126	120	103	116.1	12	11	4	9.3	139.7
7000	22.85	243	220	203	221.9	186	183	235	201.3	217	218	225	219.8	149	143	126	139.3	16	16	8	13.5	204.6
7500	24.17	263	239	220	240.6	203	200	254	218.8	234	236	242	237.5	160	154	137	150.6	19	19	10	16.0	240.1
8000	27.11	284	259	238	260.3	218	218	274	236.7	252	255	261	255.9	173	166	149	162.4	23	22	12	19.3	283.1
8500	30.98	304	280	256	280.1	240	236	296	257.1	272	276	282	276.6	187	179	161	175.6	29	27	13	23.3	363.2
9000	39.41	328	306	277	303.9	264	259	323	282.2	297	300	309	301.7	205	195	177	192.4	44	38	16	32.8	554.7
9500	44.75	346	325	294	321.8	284	275	345	301.4	317	318	329	321.5	221	208	189	206.1	57	46	20	40.7	726.7
8000	50.99	295	280	254	276.3	246	234	309	263.1	279	282	297	285.9	202	187	164	184.2	65	50	13	42.7	821.1
6000	49.12	228	214	195	212.3	188	175	247	203.3	214	220	236	223.5	157	144	120	140.7	54	40	1	31.5	663.4
4000	46.96	160	145	133	145.9	129	119	181	142.8	145	153	172	156.6	107	97	72	92.3	43	29	-11	20.6	491.1
2000	44.49	91	77	69	79.1	69	69	112	83.3	73	85	105	87.9	55	49	24	42.4	32	18	-20	9.9	308.3
0	40.58	16	-1	-3	4.0	2	8	26	12.0	-7	9	30	10.6	-2	-4	-25	-10.3	17	5	-26	-1.4	108.9

Table A.6(iii): Strain gauge readings-TP5 (load cycle 3)

P_h (kN)	Δ_h (mm)	VIBRATING WIRE STRAIN GAUGE READINGS AT LEVELS (MICRO UNITS)																				P_b (kN)
		LEVEL 3.340 m				LEVEL 20.200 m				LEVEL 21.700 m				LEVEL 25.700 m				LEVEL 29.700 m				
		1	2	3	AVG	1	2	3	AVG	1	2	3	AVG	1	2	3	AVG	1	2	3	AVG	
0	41.42	8	-8	-11	-3.4	-6	-1	16	-3.4	-16	1	0	-5.0	-10	-12	-35	-3.4	14	3	-27	-13.4	120.0
3000	42.81	100	85	72	85.8	69	65	104	79.4	75	88	0	81.5	52	44	19	38.3	24	13	-16	7.0	290.3
6000	46.59	200	183	160	181.0	154	142	203	166.2	175	185	0	180.0	120	111	87	105.7	38	28	-1	21.6	593.8
8000	49.90	269	251	221	247.2	215	203	273	230.2	245	251	0	247.9	175	160	137	157.5	54	42	12	36.3	929.0
9000	52.95	305	286	251	280.7	245	235	307	262.3	279	285	0	282.0	199	183	160	180.8	68	53	19	46.8	1187.5
10000	62.02	340	322	283	314.8	276	267	343	295.3	314	322	0	317.8	232	209	183	208.1	96	72	23	63.3	1575.0
10726	71.98	366	348	304	339.3	297	289	371	319.0	336	351	0	343.3	262	230	201	230.6	122	88	28	79.3	1962.7
11000	86.76	377	360	313	349.8	304	299	385	329.3	342	367	0	354.5	287	244	208	246.1	148	104	36	96.1	2354.9
11189	115.07	383	369	320	357.0	311	304	392	335.6	346	374	0	360.3	326	265	219	270.1	182	127	53	120.6	2905.5
11116	118.06	377	363	315	351.5	306	299	387	330.8	341	370	0	355.3	326	264	216	268.9	183	128	54	121.2	2910.0
11000	118.38	374	360	313	348.9	304	297	384	328.5	338	367	0	352.6	324	263	215	267.2	12	127	54	120.7	2894.7
9000	117.12	308	299	262	289.4	255	244	332	277.0	285	313	0	298.9	284	225	177	228.7	166	112	39	105.9	2609.3
6000	114.63	210	202	176	196.3	172	159	240	190.3	191	219	0	204.7	211	158	109	159.4	144	92	17	84.4	2249.6
3000	112.04	114	105	88	102.6	86	88	144	106.3	90	120	0	105.1	131	87	38	85.2	120	72	-5	62.0	1777.3
136	107.96	23	0	8	10.4	3	16	37	18.9	-10	22	0	6.0	51	17	-27	13.5	93	48	-26	38.1	1156.0

Table A.6(iv): Strain gauge readings-TP5 (load cycle 4)

P_h (kN)	Δ_h (mm)	VIBRATING WIRE STRAIN GAUGE READINGS AT LEVELS (MICRO UNITS)																				P_b (kN)
		LEVEL 3.340 m				LEVEL 20.200 m				LEVEL 21.700 m				LEVEL 25.700 m				LEVEL 29.700 m				
		1	2	3	AVG	1	2	3	AVG	1	2	3	AVG	1	2	3	AVG	1	2	3	AVG	
0	105.56	15	-2	-6	2.3	-3	9	27	11.0	-17	14	0	-1.5	45	11	-33	7.7	90	45	-27	36.0	1109.4
5007	110.93	175	162	143	160.1	132	126	188	148.6	145	175	0	160.0	166	118	71	118.4	115	72	7	64.7	1711.7
10040	142.70	351	343	301	331.6	289	280	365	311.3	323	350	0	336.5	338	367	217	273.9	198	138	72	136.2	3277.1
10083	143.23	352	345	302	332.8	290	281	366	312.5	324	351	0	337.6	339	269	218	275.3	199	139	73	136.9	3287.9
10340	150.56	355	348	304	335.6	294	284	369	315.8	327	355	0	340.7	350	274	223	282.6	207	144	77	142.8	3380.3
10500	160.20	368	362	317	348.8	306	296	383	328.2	338	368	0	353.0	368	286	235	296.3	216	151	86	151.1	3572.5
10500	177.21	363	358	312	344.4	302	291	379	324.1	331	365	0	348.0	380	288	236	301.6	224	153	93	156.5	3653.3
10350	177.41	359	354	309	340.5	299	288	375	320.3	327	361	0	343.8	377	285	233	298.2	222	151	91	154.8	3619.5
5017	173.42	182	183	158	174.2	152	142	217	170.3	166	198	0	181.8	248	167	112	175.4	181	112	46	112.8	2928.8
0	165.11	9	-8	-9	-2.7	-12	4	19	3.7	-26	10	0	-5.3	74	15	-37	17.3	118	58	-12	54.7	1585.5

Table A.6(v): Strain gauge readings-TP5 (load cycle 5)

P_h (kN)	Δ_h (mm)	VIBRATING WIRE STRAIN GAUGE READINGS AT LEVELS (MICRO UNITS)																				P_b (kN)
		LEVEL 3.340 m				LEVEL 20.200 m				LEVEL 21.700 m				LEVEL 25.700 m				LEVEL 29.700 m				
		1	2	3	AVG	1	2	3	AVG	1	2	3	AVG	1	2	3	AVG	1	2	3	AVG	
3000	168.19	104	89	79	90.7	67	72	114	84.4	69	106	0	87.1	147	80	26	84.3	135	75	12	74.0	1954.0
6000	172.21	207	194	173	191.5	158	152	221	176.9	174	211	0	192.8	237	158	108	167.6	156	98	43	99.0	2505.1
8000	177.62	278	265	236	259.7	221	214	293	242.5	247	281	0	264.4	308	222	173	234.3	187	127	79	131.0	3181.6
8964	188.27	313	302	267	293.7	253	245	326	274.8	281	316	0	298.3	347	253	206	268.6	211	144	95	150.0	3544.8
10000	238.57	351	345	301	332.4	290	279	365	311.3	311	355	0	333.1	414	286	241	313.4	248	166	117	177.1	4005.6
7528	236.98	266	263	231	253.5	223	211	294	242.7	240	283	0	261.4	358	234	187	259.6	228	146	96	156.8	3691.1
5050	234.21	183	180	157	173.2	149	141	214	168.0	159	200	0	179.4	289	173	123	194.9	206	127	71	134.6	3344.1
2555	231.00	100	93	79	90.9	72	81	128	93.8	72	113	0	92.4	211	107	53	124.0	182	103	42	109.2	2840.2
87	227.05	20	3	1	7.9	-3	16	34	15.8	-15	24	0	4.2	129	38	-15	50.7	153	77	9	79.6	2144.0

Table A.6(vi): Strain gauge readings-TP5 (load cycle 6)

P_h (kN)	Δ_h (mm)	EXTENSOMETER MOVEMENT (mm)		
		LEVEL 3 0-21.7m	LEVEL 4 0-25.7m	LEVEL 5 0-29.7m
0	0			
500	0.03	0.027	0.052	0.043
1000	0.09	0.140	0.158	0.173
1500	0.30	0.399	0.396	0.485
2000	0.94	0.784	0.770	0.929
3000	2.75	1.606	1.602	1.876
4000	4.78	2.470	2.480	2.845
5000	7.30	3.389	3.426	3.872
6000	10.86	4.343	4.448	4.934
5000	11.69	3.856	3.959	4.442
4000	10.69	3.041	3.089	3.531
3000	9.65	2.223	2.254	2.615
2000	8.50	1.404	1.412	1.672
1500	7.88	0.988	0.998	1.201
1000	7.25	0.575	0.586	0.717
500	6.48	0.162	0.149	0.197
0	6.61	0.114	-0.004	-0.038

Table A.6(vii): Extensometer readings-TP5 (load cycle 1)

P_h (kN)	Δ_h (mm)	EXTENSOMETER MOVEMENT (mm)		
		LEVEL 3 0-21.7m	LEVEL 4 0-25.7m	LEVEL 5 0-29.7m
0	6.61			
500	6.62	0.135	0.025	0.102
1000	6.65	0.237	0.189	0.280
2000	7.35	1.036	0.991	1.199
4000	9.64	2.677	2.657	3.073
6000	12.29	4.393	4.456	4.997
7000	15.37	5.296	5.465	6.002
7500	18.64	5.810	6.059	6.578
6000	22.14	5.083	6.376	5.813
4000	20.07	3.438	6.373	3.975
2000	17.73	1.740	6.373	2.047
1000	16.25	0.827	6.367	1.002
0	14.54	0.137	6.370	-0.045

Table A.6(viii): Extensometer readings-TP5 (load cycle 2)

P_h (kN)	Δ_h (mm)	EXTENSOMETER MOVEMENT (mm)		
		LEVEL 3 0-21.7m	LEVEL 4 0-25.7m	LEVEL 5 0-29.7m
0	14.70			
2000	16.30	1.268	6.373	1.441
4000	18.68	2.946	6.359	3.355
6000	21.25	4.674	6.357	5.307
7000	22.85	5.550	6.375	6.281
7500	24.17	6.003	6.375	6.790
8000	27.11	6.464	6.850	7.323
8500	30.98	6.949	7.425	7.887
9000	39.41	7.504	8.079	8.563
9500	44.75	7.945	8.608	9.093
8000	50.99	7.050	8.704	8.117
6000	49.12	5.509	8.704	6.340
4000	46.96	3.802	8.692	4.426
2000	44.49	2.098	8.707	2.469
0	40.58	0.181	8.702	0.248

Table A.6(ix): Extensometer readings-TP5 (load cycle 3)

P_h (kN)	Δ_h (mm)	EXTENSOMETER MOVEMENT (mm)		
		LEVEL 3 0-21.7m	LEVEL 4 0-25.7m	LEVEL 5 0-29.7m
0	41.42	0.164	8.708	-0.045
3000	42.81	2.006	8.707	2.335
6000	46.59	4.482	8.708	5.129
8000	49.90	6.153	8.708	7.032
9000	52.95	6.962	8.709	7.978
10000	62.02	7.792	8.711	9.010
10726	71.98	8.403	9.131	9.780
11000	86.76	8.649	9.390	10.151
11189	115.07	8.861	9.589	10.503
11116	118.06	8.820	9.580	10.482
11000	118.38	8.783	9.575	10.449
9000	117.12	7.420	9.571	8.846
6000	114.63	5.174	9.570	6.237
3000	112.04	2.737	9.569	3.446
136	107.96	0.362	9.571	0.628

Table A.6(x): Extensometer readings-TP5 (load cycle 4)

P_h (kN)	Δ_h (mm)	EXTENSOMETER MOVEMENT (mm)		
		LEVEL 3 0-21.7m	LEVEL 4 0-25.7m	LEVEL 5 0-29.7m
0	105.56	0.137	9.570	0.385
5000	110.93	4.041	9.570	4.842
10040	142.70	8.301	9.572	9.941
10083	143.23	8.330	9.574	9.970
10340	150.56	8.503	9.572	10.234
10500	160.20	8.707	9.570	10.478
10500	177.21	8.716	9.570	10.556
10350	177.41	8.629	9.570	10.470
5017	173.42	4.629	9.568	5.784
0	165.11	0.304	9.568	0.715

Table A.6(xi): Extensometer readings-TP5 (load cycle 5)

P_h (kN)	Δ_h (mm)	EXTENSOMETER MOVEMENT (mm)		
		LEVEL 3 0-21.7m	LEVEL 4 0-25.7m	LEVEL 5 0-29.7m
3000	168.19	2.267	9.585	2.945
6000	172.21	4.899	9.585	5.970
8000	177.62	6.637	9.585	8.028
9000	188.27	7.476	9.584	9.083
10000	238.57	8.342	9.585	10.234
7528	236.98	6.656	9.585	8.260
5050	234.21	4.635	9.584	5.939
2555	231.00	2.471	9.585	3.448
87	227.05	0.310	9.584	0.850

Table A.6(xii): Extensometer readings-TP5 (load cycle 6)

P_h (kN)	LOAD START			LOAD END			CUMULATIVE TIME (HOURS)	
	DATE	TIME	Δ_h (mm)	DATE	TIME	Δ_h (mm)	START	END
0	19-11-91	12:06:15	0.00					
500		12:09:25	0.03	19-11-91	12:40:38	0.01	0.00	0.520
1000		12:44:28	0.09		13:15:39	0.07	0.584	1.104
1500		13:18:34	0.30		13:50:14	0.35	1.153	1.680
2000		13:52:52	0.94		14:25:42	1.08	1.724	2.271
3000		14:34:21	2.75		15:02:31	2.92	2.416	2.885
4000		15:10:16	4.78		16:11:10	5.26	3.014	4.029
5000		16:17:56	7.30		18:18:22	8.49	4.142	6.149
6000		18:27:01	10.86		22:26:50	12.53	6.293	10.290
5000		22:32:22	11.69		22:49:49	11.65	10.383	10.673
4000		22:53:07	10.69		23:09:07	10.63	10.728	10.995
3000		23:12:50	9.65		23:40:20	9.57	11.057	11.515
2000		23:45:01	8.50		23:59:12	8.44	11.593	11.830
1500	20-11-91	00:04:07	7.88	20-11-91	00:19:00	7.82	11.912	12.160
1000		00:23:05	7.25		00:54:24	7.10	12.228	12.750
500		01:00:27	6.48		01:16:28	6.41	12.851	13.118
0		01:24:29	6.29		09:27:10	6.61	13.251	21.296

Table A.6(xiii): Load-Displacement-Time record for TP5 (load cycle 1)

P_h (kN)	LOAD START			LOAD END			CUMULATIVE TIME (HOURS)	
	DATE	TIME	Δ_h (mm)	DATE	TIME	Δ_h (mm)	START	END
0	20-11-91	10:55:26	6.61				22.767	
500		10:59:03	6.62	20-11-91	11:13:30	6.62	22.827	23.068
1000		11:16:29	6.65		11:33:13	6.66	23.118	23.397
2000		11:41:36	7.35		12:12:06	7.45	23.536	24.045
4000		12:20:22	9.64		13:21:37	9.64	24.183	25.203
6000		13:28:04	12.29		14:29:30	12.82	25.311	26.335
7000		14:51:47	15.37		17:11:15	17.56	26.706	29.031
7500		17:18:04	18.64	21-11-91	10:36:21	23.41	29.144	46.449
6000	21-11-91	10:45:38	22.14		11:03:25	22.09	46.604	46.900
4000		11:09:31	20.07		11:27:39	20.00	47.002	47.304
2000		11:31:57	17.73		12:03:02	17.52	47.376	47.894
1000		12:08:28	16.25		12:40:50	16.10	47.984	48.524
0		12:51:59	14.87		13:56:00	14.49	48.709	49.776

Table A.6(xiv): Load-Displacement-Time record for TP5 (load cycle 2)

P_h (kN)	LOAD START			LOAD END			CUMULATIVE TIME (HOURS)	
	DATE	TIME	Δ_h (mm)	DATE	TIME	Δ_h (mm)	START	END
0	21-11-91	14:43:06	14.70				50.561	
2000		14:49:17	16.30	21-11-91	15:04:45	16.32	50.664	50.922
4000		15:10:23	18.68		15:28:55	18.72	51.016	51.325
6000		15:35:49	21.25		16:06:17	21.39	51.440	51.948
7000		16:11:52	22.85		17:13:28	23.41	52.041	53.068
7500		17:18:24	24.17		20:04:42	26.26	53.150	55.921
8000		20:17:28	27.11	22-11-91	00:51:06	30.19	56.134	60.695
8500	22-11-91	01:03:20	30.98		13:38:13	38.43	60.899	73.480
9000		13:46:42	39.41		17:04:30	43.31	73.621	76.918
9500		17:13:26	44.75		19:46:00	52.17	77.067	79.610
8000		19:50:29	50.99		20:06:11	50.98	79.684	79.946
6000		20:09:43	49.12		20:25:14	49.10	80.005	80.264
4000		20:27:55	46.96		20:45:33	46.89	80.308	80.602
2000		20:49:04	44.49		20:51:52	44.46	80.661	80.708
0		22:13:21	40.58		22:14:44	40.58	82.066	82.089

Table A.6(xv): Load-Displacement-Time record for TP5 (load cycle 3)

P_h (kN)	LOAD START			LOAD END			CUMULATIVE TIME (HOURS)	
	DATE	TIME	Δ_h (mm)	DATE	TIME	Δ_h (mm)	START	END
0	23-11-91	10:31:08	41.42	23-11-91	11:12:22	39.86	94.362	95.049
3000		11:23:17	42.76		11:41:56	42.81	95.231	95.542
6000		11:50:44	46.49		12:07:02	46.59	95.689	95.960
8000		12:18:06	49.47		12:51:16	49.90	96.145	96.697
9000		13:03:33	52.06		13:35:14	52.95	96.902	97.430
10000		13:43:58	56.86		14:29:26	62.02	97.576	98.333
10725		14:38:35	67.84		14:49:14	71.98	98.486	98.663
11000		14:55:36	76.05		15:15:17	86.76	98.770	99.097
11200		15:31:19	99.41		15:50:14	115.07	99.365	99.680
11055		15:54:22	118.06		15:55:08	118.38	99.749	99.761
9000		16:05:22	117.12		16:06:15	117.12	99.932	99.947
6000		16:16:44	114.63		16:17:41	114.63	100.122	100.137
3000		16:28:04	112.04		16:28:50	112.04	100.311	100.323
137		16:40:31	107.97		16:41:29	107.96	100.518	100.534
0		17:13:15	105.56				101.063	

Table A.6(xvi): Load-Displacement-Time record for TP5 (load cycle 4)

P_h (kN)	LOAD START			LOAD END			CUMULATIVE TIME (HOURS)	
	DATE	TIME	Δ_h (mm)	DATE	TIME	Δ_h (mm)	START	END
0	23-11-91	17:18:18	105.56	23-11-91	17:19:05	105.56	101.148	101.161
5007		17:30:22	110.81		17:40:57	110.93	101.349	101.525
10040		18:08:16	133.58		18:19:49	142.70	101.981	102.173
10083		18:20:40	143.23		18:20:40	143.23	102.187	102.187
10340		18:26:30	150.25		18:27:27	150.56	102.285	102.300
10500		18:39:31	158.76		18:40:19	160.20	102.502	102.515
10320		18:50:53	166.35		18:50:53	166.35	102.691	102.691
10263		18:51:46	166.83		18:51:46	166.83	102.706	102.706
10500		19:05:32	177.21		19:05:32	177.21	102.950	102.935
10350		19:06:30	177.41		19:06:30	177.41	102.966	102.952
5017		19:15:21	174.68		19:16:14	173.42	103.114	103.114
0		19:27:23	166.09	24-11-91	10:49:08	165.11	103.314	118.662

Table A.6(xvii): Load-Displacement-Time record for TP5 (load cycle 5)

P_h (kN)	LOAD START			LOAD END			CUMULATIVE TIME (HOURS)	
	DATE	TIME	Δ_h (mm)	DATE	TIME	Δ_h (mm)	START	END
0	24-11-91	10:52:18	165.10				118.715	
3000		10:56:06	168.10	24-11-91	11:10:53	168.19	118.778	119.025
6000		11:20:11	172.00		11:53:12	172.21	119.179	119.730
8000		12:03:29	176.33		12:35:30	177.62	119.901	120.435
9000		12:47:46	184.25		13:18:57	188.27	120.639	121.159
10000		13:39:47	207.61		14:47:00	238.57	121.506	122.626
7500		14:54:23	237.02		14:59:46	236.98	122.749	122.839
5000		15:02:49	234.31		15:09:43	234.21	122.890	123.005
2500		15:14:53	231.11		15:21:57	231.00	123.091	123.209
87		15:35:14	227.07		15:36:42	227.05	123.430	123.455
0		15:39:47	227.01				123.506	

Table A.6(xviii): Load-Displacement-Time record for TP5 (load cycle 6)

Ph (kN)	Dh (mm)	VIBRATING WIRE STRAIN GAUGE READINGS AT LEVELS DOWN PILE SHAFT (MICRO STRAIN)																					EXTENSOMETER READINGS (mm		
		LEVEL 1.690 m				LEVEL 10.980 m				LEVEL 20.380 m				LEVEL 25.880 m				LEVEL 30.260 m				Pb	LEVEL 3	LEVEL 4	LEVEL 5
		1	2	3	Mean	1	2	3	Mean	1	2	3	Mean	1	2	3	Mean	1	2	3	Mean	(kN)	(0-23m)	(0-26m)	(0-30m)
0	0.00	-1	-1	1	-0.3	0	1	0	0.3	-1	-1	-1	-1.0	-3	-2	-3	-2.7	-2	-1	-1	-1.3	-3.0	-0.046	-0.029	-0.004
514	0.06	8	2	4	4.7	4	5	4	4.3	2	3	3	2.7	-1	-1	-1	-1.0	-1	0	-1	-0.7	-1.2	0.036	0.072	0.048
1006	0.28	27	7	14	16.0	15	14	13	14.0	10	12	13	11.7	6	7	7	6.7	1	1	1	1.0	4.8	0.267	0.239	0.278
1500	0.69	42	24	29	31.7	26	29	27	27.3	22	24	26	24.0	15	16	18	16.3	5	2	5	4.0	13.8	0.590	0.622	0.712
2000	1.17	57	40	44	47.0	39	44	41	41.3	35	36	41	37.3	24	26	30	26.7	9	4	9	7.3	27.1	0.930	0.996	1.168
2507	1.71	72	58	61	63.7	51	60	56	55.7	48	49	57	51.3	35	37	42	38.0	12	6	11	9.7	42.2	1.299	1.389	1.663
3000	2.25	88	75	76	79.7	63	76	71	70.0	60	62	72	64.7	45	47	54	48.7	14	7	13	11.3	53.4	1.638	1.784	2.135
3500	2.89	106	95	92	97.7	76	92	87	85.0	74	75	88	79.0	55	56	66	59.0	14	9	12	11.7	52.8	2.000	2.211	2.648
2980	2.59	90	78	79	82.3	63	78	74	71.7	63	65	76	68.0	48	49	59	52.0	12	7	10	9.7	45.5	1.733	1.899	2.324
2000	1.93	62	47	53	54.0	39	50	49	46.0	40	43	51	44.7	36	37	46	39.7	8	6	7	7.0	33.5	1.195	1.237	1.549
1005	1.16	32	13	25	23.3	14	20	23	19.0	15	18	23	18.7	21	21	28	23.3	4	3	3	3.3	17.9	0.574	0.501	0.705
505	0.74	13	-5	10	6.0	0	4	8	4.0	2	5	8	5.0	12	11	17	13.3	2	2	1	1.7	9.6	0.223	0.128	0.245
17	0.56	0	-5	6	0.3	-6	-2	3	-1.7	-3	1	3	0.3	9	8	13	10.0	1	1	0	0.7	5.8	0.098	0.021	0.136

Table A.7(i): Strain gauge, Extensometer and Base load cell readings-TP6 (load cycle 1)

Ph (kN)	Dh (mm)	VIBRATING WIRE STRAIN GAUGE READINGS AT LEVELS DOWN PILE SHAFT (MICRO STRAIN)																					EXTENSOMETER READINGS (mm		
		LEVEL 1.690 m				LEVEL 10.980 m				LEVEL 20.380 m				LEVEL 25.880 m				LEVEL 30.260 m				Pb	LEVEL 3	LEVEL 4	LEVEL 5
		1	2	3	Mean	1	2	3	Mean	1	2	3	Mean	1	2	3	Mean	1	2	3	Mean	(kN)	(0-23m)	(0-26m)	(0-30m)
12	0.48	-1	-5	4	-0.7	-6	-2	2	-2.0	-3	-1	1	-1.0	7	6	12	8.3	1	2	0	1.0	6.5	0.083	-0.030	0.120
506	0.59	11	-4	9	5.3	-1	3	7	3.0	1	4	6	3.7	10	9	14	11.0	2	2	1	1.7	8.9	0.181	0.075	0.175
998	0.93	29	10	20	19.7	12	16	19	15.7	11	15	19	15.0	16	17	22	18.3	4	3	3	3.3	13.0	0.456	0.371	0.509
1998	1.76	59	44	49	50.7	37	47	46	43.3	37	40	47	41.3	32	32	40	34.7	8	5	7	6.7	29.3	1.089	1.114	1.381
3000	2.58	90	79	78	82.3	63	77	75	71.7	62	64	76	67.3	48	49	59	52.0	13	8	11	10.7	47.3	1.721	1.842	2.263
4000	3.60	122	114	109	115.0	90	109	103	100.7	88	90	105	94.3	67	68	82	72.3	17	12	14	14.3	70.8	2.381	2.572	3.168
5000	5.02	154	150	139	147.7	114	142	132	129.3	113	117	136	122.0	86	88	106	93.3	18	17	14	16.3	90.0	3.062	3.347	4.120
5506	5.90	172	170	156	166.0	128	160	149	145.7	128	132	155	138.3	97	98	121	105.3	19	19	14	17.3	97.0	3.435	3.770	4.629
5000	5.55	158	153	144	151.7	115	145	137	132.3	118	121	144	127.7	92	93	114	99.7	17	18	11	15.3	89.3	3.202	3.608	4.318
4005	4.81	128	120	115	121.0	89	116	110	105.0	94	98	117	103.0	79	79	100	86.0	13	15	8	12.0	73.0	2.635	3.596	3.549
2996	4.05	98	87	86	90.3	64	87	82	77.7	69	73	89	77.0	64	63	83	70.0	8	12	4	8.0	55.5	2.014	3.610	2.701
2009	3.26	69	53	57	59.7	40	57	55	50.7	43	48	61	50.7	48	47	64	53.0	4	10	-1	4.3	35.5	1.388	3.606	1.848
1002	2.37	36	17	29	27.3	13	24	27	21.3	16	22	31	23.0	29	27	42	32.7	-1	7	-5	0.3	17.0	0.711	3.600	0.922
502	1.92	18	-2	14	10.0	-1	7	12	6.0	3	8	15	8.7	19	17	30	22.0	-3	6	-7	-1.3	5.6	0.339	3.603	0.443
36	1.64	3	-7	7	1.0	-9	-1	4	-2.0	-4	0	7	1.0	13	10	24	15.7	-4	5	-8	-2.3	1.5	0.133	3.601	0.228

Table A.7(ii): Strain gauge, Extensometer and Base load cell readings-TP6 (load cycle 2)

Ph (kN)	Dh (mm)	VIBRATING WIRE STRAIN GAUGE READINGS AT LEVELS DOWN PILE SHAFT (MICRO STRAIN) LEVEL 1.690 m				LEVEL 10.980 m				LEVEL 20.380 m				LEVEL 25.880 m				LEVEL 30.260 m				Pb	EXTENSOMETER READINGS (mm LEVEL 3	LEVEL 4	LEVEL 5
		1	2	3	Mean	1	2	3	Mean	1	2	3	Mean	1	2	3	Mean	1	2	3	Mean	(kN)	(0-23m)	(0-26m)	(0-30m)
18	1.56	-1	-10	4	-2.3	-10	-3	2	-3.7	-6	-2	4	-1.3	12	10	22	14.7	-3	6	-7	-1.3	3.2	0.057	3.595	0.126
502	1.80	15	-5	9	6.3	-3	5	8	3.3	-1	5	11	5.0	16	13	26	18.3	-2	6	-6	-0.7	6.3	0.208	3.587	0.236
1004	2.24	32	12	23	22.3	10	20	22	17.3	12	17	25	18.0	23	21	36	26.7	0	7	-4	1.0	12.9	0.524	3.603	0.658
2009	3.06	62	47	50	53.0	37	51	50	46.0	38	43	54	45.0	39	39	54	44.0	5	9	0	4.7	26.6	1.173	3.603	1.544
3000	3.88	93	82	79	84.7	62	82	78	74.0	64	68	83	71.7	56	57	74	62.3	8	11	4	7.7	42.3	1.820	3.612	2.441
4003	4.70	124	117	109	116.7	88	114	107	103.0	90	94	112	98.7	73	74	93	80.0	13	13	8	11.3	64.0	2.481	3.609	3.347
5018	5.64	157	153	141	150.3	115	146	137	132.7	117	120	143	126.7	91	93	114	99.3	16	16	11	14.3	86.3	3.146	3.605	4.260
6004	6.92	190	187	171	182.7	142	177	166	161.7	143	148	175	155.3	109	111	135	118.3	19	21	14	18.0	118.1	3.812	4.204	5.132
7004	8.71	223	224	201	216.0	168	211	195	191.3	172	176	209	185.7	128	130	159	139.0	22	26	15	21.0	149.5	4.540	4.954	6.066
8003	10.92	257	262	233	250.7	193	246	225	221.3	204	218	242	221.3	148	148	181	159.0	26	31	15	24.0	195.5	5.302	5.620	7.016
9003	13.84	293	301	264	286.0	220	280	257	252.3	234	250	278	254.0	170	168	205	181.0	31	37	17	28.3	262.4	6.104	6.362	7.891
9009	14.47	302	310	272	294.7	226	287	263	258.7	240	256	285	260.3	176	174	210	186.7	33	37	17	29.0	255.4	6.309	6.487	8.211
8000	13.78	270	275	247	264.0	198	257	237	230.7	217	233	259	236.3	164	163	198	175.0	29	35	14	26.0	239.5	5.753	6.501	7.555
7000	12.91	237	241	218	232.0	171	227	209	202.3	193	209	232	211.3	152	150	185	162.3	27	33	11	23.7	227.0	5.143	6.495	6.782
6000	12.05	207	206	187	200.0	144	197	181	174.0	166	182	203	183.7	137	134	168	146.3	22	30	6	19.3	204.1	4.475	6.484	5.981
5009	11.19	176	173	158	169.0	118	167	153	146.0	139	156	174	156.3	120	117	150	129.0	16	27	2	15.0	176.7	3.821	6.507	5.169
4012	10.29	145	139	127	137.0	93	136	125	118.0	113	130	144	129.0	103	99	130	110.7	12	24	-3	11.0	149.7	3.171	6.509	4.329
3016	9.35	115	104	98	105.7	68	104	96	89.3	87	103	114	101.3	84	81	110	91.7	7	21	-8	6.7	119.7	2.522	6.529	3.449
2025	8.38	84	70	69	74.3	43	72	68	61.0	61	76	84	73.7	65	61	88	71.3	2	18	-13	2.3	89.8	1.834	6.499	2.519
1033	7.32	53	34	41	42.7	16	40	39	31.7	35	48	54	45.7	45	40	64	49.7	-3	15	-17	-1.7	58.8	1.112	6.532	1.563
19	6.09	18	-2	9	8.3	-12	4	7	-0.3	9	18	21	16.0	21	14	36	23.7	-8	13	-21	-5.3	27.9	0.310	6.559	0.491

Table A.7(iii): Strain gauge, Extensometer and Base load cell readings-TP6 (load cycle 3)

Ph (kN)	Dh (mm)	VIBRATING WIRE STRAIN GAUGE READINGS AT LEVELS DOWN PILE SHAFT (MICRO STRAIN)																					EXTENSOMETER READINGS (mm		
		LEVEL 1.690 m				LEVEL 10.980 m				LEVEL 20.380 m				LEVEL 25.880 m				LEVEL 30.260 m				Pb	LEVEL 3	LEVEL 4	LEVEL 5
		1	2	3	Mean	1	2	3	Mean	1	2	3	Mean	1	2	3	Mean	1	2	3	Mean	(kN)	(0-23m)	(0-26m)	(0-30m)
22	6.00	17	-3	9	7.7	-12	3	6	-1.0	8	18	21	15.7	20	14	36	23.3	-8	12	-21	-5.7	28.5	0.297	6.544	0.460
500	6.30	32	11	21	21.3	-1	16	19	11.3	19	29	32	26.7	27	21	42	30.0	-6	13	-19	-4.0	33.2	0.566	6.527	0.807
1002	6.71	48	30	33	37.0	14	33	33	26.7	32	41	47	40.0	35	30	52	39.0	-4	15	-17	-2.0	41.7	0.895	6.516	1.255
2002	7.58	77	64	60	67.0	40	64	60	54.7	58	68	76	67.3	52	48	72	57.3	1	17	-12	2.0	57.1	1.592	6.504	2.152
3004	8.49	108	98	89	98.3	65	95	89	83.0	82	94	105	93.7	70	66	92	76.0	6	18	-8	5.3	78.1	2.223	6.516	3.070
4002	9.42	138	133	118	129.7	91	127	117	111.7	107	120	134	120.3	88	86	113	95.7	11	21	-4	9.3	102.6	2.885	6.527	3.966
5010	10.39	169	168	147	161.3	116	159	146	140.3	133	147	165	148.3	106	104	133	114.3	15	23	1	13.0	132.1	3.556	6.525	4.858
5997	11.40	209	212	185	202.0	147	197	180	174.7	161	178	199	179.3	125	124	155	134.7	19	26	5	16.7	166.9	4.417	6.532	5.897
7002	12.45	234	239	208	227.0	168	222	203	197.7	185	201	225	203.7	142	141	173	152.0	23	29	9	20.3	188.4	4.943	6.523	6.576
8002	13.64	268	274	239	260.3	196	254	233	227.7	211	229	256	232.0	160	161	193	171.3	28	33	14	25.0	247.9	5.639	6.523	7.395
9004	15.27	302	310	270	294.0	225	285	263	257.7	239	259	288	262.0	178	178	213	189.7	36	39	18	31.0	319.8	6.311	6.538	8.234
10008	18.26	343	350	304	332.3	254	321	297	290.7	269	294	327	296.7	199	200	240	213.0	46	46	20	37.3	402.1	7.151	7.244	9.199
10495	19.41	362	366	320	349.3	268	336	312	305.3	283	310	343	312.0	209	210	252	223.7	53	50	23	42.0	476.9	7.534	7.543	9.605
10988	20.85	377	385	335	365.7	282	353	327	320.7	297	326	361	328.0	219	220	266	235.0	60	53	26	46.3	557.1	7.854	7.792	9.994
11490	22.58	392	404	350	382.0	293	371	342	335.3	311	342	379	344.0	231	231	282	248.0	71	58	31	53.3	658.2	8.281	8.098	10.473
11999	24.70	412	426	368	402.0	308	389	358	351.7	324	360	398	360.7	243	245	300	262.7	83	63	38	61.3	789.0	8.673	8.383	10.923
12495	26.62	429	448	384	420.3	322	407	374	367.7	339	377	417	377.7	256	257	316	276.3	94	68	45	69.0	909.4	9.064	8.672	11.365
9987	24.67	349	362	317	342.7	251	332	307	296.7	278	316	347	313.7	222	221	279	240.7	82	59	33	58.0	829.4	7.696	8.045	9.763
8008	22.99	285	295	256	278.7	197	272	250	239.7	226	263	289	259.3	189	185	242	205.3	69	51	22	47.3	746.5	6.398	8.042	8.258
6005	21.18	222	226	195	214.3	145	209	193	182.3	174	209	229	204.0	153	148	197	166.0	56	44	10	36.7	649.5	5.035	8.070	6.644
4009	19.37	161	158	138	152.3	95	147	137	126.3	123	155	169	149.0	115	109	159	127.7	43	37	-3	25.7	541.5	3.685	8.044	4.973
2009	17.29	99	88	80	89.0	44	81	79	68.0	72	99	108	93.0	73	66	111	83.3	28	31	-16	14.3	415.0	2.245	8.081	3.105
1010	16.21	68	52	53	57.7	16	48	51	38.3	47	70	78	65.0	52	44	87	61.0	21	28	-22	9.0	348.6	1.517	8.185	2.156
27	14.99	36	19	23	26.0	-9	15	22	9.3	22	42	46	36.7	30	20	60	36.7	14	24	-27	3.7	276.3	0.737	8.172	1.130

Table A.7(iv): Strain gauge, Extensometer and Base load cell readings-TP6 (load cycle 4)

P_h (kN)	LOAD START			LOAD END			CUMULATIVE TIME (HOURS)	
	DATE	TIME	Δ_h (mm)	DATE	TIME	Δ_h (mm)	START	END
0	18-2-92	10:55:50	0	18-2-92				
500		11:00:18	0.04		11:18:56	0.06	0	0.311
1000		11:24:37	0.27		11:43:53	0.28	0.405	0.726
1500		11:51:01	0.67		12:09:17	0.69	0.845	1.150
2000		12:17:07	1.14		12:36:38	1.17	1.280	1.606
2500		12:42:35	1.63		13:47:14	1.71	1.705	2.782
3000		13:52:11	2.16		14:55:33	2.25	2.865	3.921
3500		15:01:10	2.71		19:02:05	2.89	4.014	8.030
3000		19:08:11	2.59		19:28:18	2.59	8.131	8.467
2000		19:34:16	1.93		19:54:09	1.93	8.566	8.898
1000		20:00:42	1.16		20:19:13	1.15	9.007	9.315
500		20:25:11	0.75		20:44:04	0.74	9.415	9.729
20		20:55:47	0.57		20:57:41	0.56	9.925	9.956

Table A.7(v): Load-Displacement-Time record for TP6 (load cycle 1)

P_h (kN)	LOAD START			LOAD END			CUMULATIVE TIME (HOURS)	
	DATE	TIME	Δ_h (mm)	DATE	TIME	Δ_h (mm)	START	END
0	19-2-92	10:06:51	0.48	19-2-92				
500		10:12:01	0.59		10:31:11	0.59	23.195	23.515
1000		10:35:36	0.93		10:54:33	0.93	23.588	23.904
2000		11:01:19	1.75		11:18:17	1.76	24.017	24.300
3000		11:25:22	2.56		11:44:51	2.58	24.418	24.743
4000		11:51:44	3.49		12:54:18	3.60	24.857	25.900
5000		13:02:35	4.78		14:00:06	5.02	26.038	26.997
5500		14:06:09	5.57		18:11:06	5.91	27.098	31.180
5000		18:16:44	5.58		18:34:26	5.55	31.274	31.569
4000		18:40:55	4.82		18:58:51	4.81	31.677	31.976
3000		19:04:12	4.05		19:21:47	4.05	32.065	32.358
2000		19:26:42	3.27		19:43:34	3.26	32.440	32.721
1000		19:49:33	2.39		20:06:45	2.37	32.821	33.108
500		20:12:18	1.93		20:30:16	1.92	33.200	33.499
50		20:38:34	1.67		20:41:58	1.64	33.638	33.695

Table A.7(vi): Load-Displacement-Time record for TP6 (load cycle 2)

P_h (kN)	LOAD START			LOAD END			CUMULATIVE TIME (HOURS)	
	DATE	TIME	Δ_h (mm)	DATE	TIME	Δ_h (mm)	START	END
20	20-2-92	10:18:55	1.53	20-2-92	12:28:30	1.56	47.311	49.471
500		12:32:26	1.73		13:02:45	1.80	49.536	50.041
1000		13:07:24	2.19		13:41:34	2.24	50.119	50.688
2000		13:46:03	3.05		14:02:49	3.06	50.763	51.042
3000		14:07:00	3.87		14:26:56	3.88	51.112	51.444
4000		14:31:53	4.71		14:52:41	4.70	51.526	51.873
5000		14:58:10	5.55		16:00:25	5.64	51.965	53.002
6000		16:07:44	6.70		17:12:06	6.92	53.124	54.197
7000		17:19:31	8.24		18:23:01	8.71	54.320	55.379
8000		19:29:51	10.79		19:58:31	10.92	56.493	56.970
9000		20:09:36	12.60	21-2-92	10:57:42	14.47	57.155	71.957
8000	21-2-92	11:02:40	13.78		11:22:01	13.78	72.040	72.362
7000		11:26:42	12.98		13:05:09	12.91	72.441	74.081
6000		13:09:21	12.07		13:28:35	12.05	74.151	74.471
5000		13:33:48	11.22		13:51:49	11.19	74.559	74.859
4000		13:56:21	10.32		14:14:13	10.29	74.934	75.232
3000		14:19:33	9.41		14:41:35	9.35	75.321	75.688
2000		14:47:12	8.41		15:07:09	8.38	75.782	76.114
1000		15:12:18	7.37		15:32:18	7.32	76.200	76.533
20		16:16:30	6.11		17:01:28	6.09	77.270	78.019

Table A.7(vii): Load-Displacement-Time record for TP6 (load cycle 3)

P_h (kN)	LOAD START			LOAD END			CUMULATIVE TIME (HOURS)	
	DATE	TIME	Δ_h (mm)	DATE	TIME	Δ_h (mm)	START	END
20	21-2-92	18:05:47	6.00	21-2-92	18:10:50	6.00	79.091	79.175
500		18:17:18	6.30		18:36:16	6.30	79.283	79.599
1000		18:42:16	6.71		19:04:07	6.71	79.699	80.064
2000		19:08:47	7.57		19:29:01	7.58	80.141	80.479
3000		19:34:50	8.46		16:53:35	8.49	80.575	80.888
4000		19:58:58	9.40		20:17:19	9.42	80.977	81.284
5000		20:22:21	10.34		20:42:12	10.39	81.367	81.698
6000		20:48:48	11.32		21:23:25	11.40	81.808	82.385
7000		21:32:21	12.35		22:06:01	12.45	82.534	83.095
8000		22:15:52	13.47		23:10:22	13.64	83.259	84.168
9000		23:23:55	14.93	22-2-92	00:28:34	15.27	84.393	85.471
10000	22-2-92	00:42:53	16.83		10:30:55	18.26	85.709	95.510
10500		10:39:35	18.80		12:15:01	19.41	95.655	97.245
11000		12:25:38	20.06		14:14:11	20.85	97.422	99.231
11500		14:25:05	21.61		16:12:51	22.58	99.413	101.209
12000		16:19:41	23.22		19:22:44	24.70	101.323	104.374
12500		19:32:38	25.34		21:35:54	26.62	104.539	106.593
10000		21:40:43	24.71		22:00:27	24.68	106.673	107.003
8000		22:06:08	23.01		22:24:31	22.99	107.097	107.036
6000		22:29:31	21.25		22:47:36	21.18	107.487	107.788
4000		22:53:02	19.41		23:11:33	19.37	107.879	108.187
2000		23:15:57	17.45		23:48:55	17.29	108.261	108.810
1000		23:54:15	16.28	23-2-92	00:10:57	16.21	108.899	109.178
50	23-2-92	00:23:30	15.11		00:27:27	15.07	109.386	109.452
28		00:35:02	15.00		00:38:27	14.99	109.578	109.635

Table A.7(viii): Load-Displacement-Time record for TP6 (load cycle 4)

Ph (kN)	Dh (mm)	VIBRATING WIRE STRAIN GAUGE READINGS AT LEVELS DOWN PILE SHAFT (MICRO STRAIN) LEVEL 1.690 m				LEVEL 10.980 m				LEVEL 20.380 m				LEVEL 25.880 m				LEVEL 30.260 m				Pb	EXTENSOMETER READINGS (mm) LEVEL 3	LEVEL 4	LEVEL 5
		1	2	3	Mean	1	2	3	Mean	1	2	3	Mean	1	2	3	Mean	1	2	3	Mean	(kN)	(0-23m)	(0-26m)	(0-30m)
0	0.00	18	-3	6	7.0	-25	-1	3	-7.7	11	27	29	22.3	16	6	46	22.7	10	22	-30	0.7	326.0	0.000	0.000	0.000
250	0.18	12	-10	-1	0.3	-29	-9	-4	-14.0	6	22	23	17.0	12	2	41	18.3	8	22	-32	-0.7	321.0	-0.203	0.020	-0.305
502	0.57	1	-22	-11	-10.7	-36	-23	-16	-25.0	-2	11	11	6.7	3	-8	32	9.0	6	21	-34	-2.3	284.0	-0.554	0.037	-0.861
752	1.07	-10	-34	-21	-21.7	-43	-34	-28	-35.0	-10	-1	-1	-4.0	-5	-17	21	-0.3	4	20	-36	-4.0	243.0	-0.934	0.012	-1.403
1005	1.61	-21	-44	-30	-31.7	-51	-45	-39	-45.0	-19	-12	-13	-14.7	-13	-26	11	-9.3	2	18	-37	-5.7	202.0	-1.304	-2.489	-1.916
1499	2.83	-18	-49	-44	-37.0	-67	-67	-58	-64.0	-37	-35	-41	-37.7	-31	-46	-12	-29.7	-3	16	-40	-9.0	117.0	-2.138	-3.912	-3.047
2000	5.97	-368	-126	-31	-175.0	-84	-93	-71	-82.7	-59	-67	-67	-64.3	-51	-66	-36	-51.0	-8	13	-41	-12.0	39.0	-4.891	-8.717	-7.135
1946	5.99	-369	-126	-28	-174.3	-85	-93	-70	-82.7	-60	-68	-67	-65.0	-51	-67	-30	-49.3	-7	14	-40	-11.0	43.0	-4.893	-8.762	-7.149
1507	5.53	-335	-104	-15	-151.3	-72	-78	-56	-68.7	-48	-56	-56	-53.3	-45	-60	-22	-42.3	-6	14	-38	-10.0	47.0	-4.351	-7.797	-6.387
1004	4.72	-287	-83	-2	-124.0	-58	-59	-36	-51.0	-33	-41	-37	-37.0	-36	-49	-10	-31.7	-3	16	-35	-7.3	57.0	-3.539	-6.473	-5.227
503	3.75	-221	-63	9	-91.7	-43	-39	-18	-33.3	-18	-23	-16	-19.0	-24	-35	3	-18.7	0	17	-32	-5.0	71.0	-2.547	-4.854	-3.807
10	2.46	-149	-30	18	-53.7	-24	-11	3	-10.7	0	-2	8	2.0	-9	-19	22	-2.0	5	19	-27	-1.0	93.0	-1.219	-2.480	-1.869

Table A.8(i) Strain gauge, Extensometer and Base load cell readings-TP6:Pull-out test (load cycle 1)

Ph (kN)	Dh (mm)	VIBRATING WIRE STRAIN GAUGE READINGS AT LEVELS DOWN PILE SHAFT (MICRO STRAIN) LEVEL 1.690 m				LEVEL 10.980 m				LEVEL 20.380 m				LEVEL 25.880 m				LEVEL 30.260 m				Pb	EXTENSOMETER READINGS (mm) LEVEL 3	LEVEL 4	LEVEL 5
		1	2	3	Mean	1	2	3	Mean	1	2	3	Mean	1	2	3	Mean	1	2	3	Mean	(kN)	(0-23m)	(0-26m)	(0-30m)
11	2.64	-143	-29	18	-51.3	-24	-11	3	-10.7	1	-1	8	2.7	-9	-19	22	-2.0	5	18	-27	-1.3	89.0	-1.215	-2.475	-1.857
249	2.91	-155	-39	10	-61.3	-32	-21	-6	-19.7	-7	-10	-1	-6.0	-13	-24	17	-6.7	3	18	-28	-2.3	85.0	-1.505	-3.020	-2.267
499	3.33	-185	-47	4	-76.0	-40	-33	-17	-30.0	-15	-19	-11	-15.0	-19	-31	10	-13.3	2	16	-30	-4.0	76.0	-1.986	-3.895	-2.974
1002	4.27	-268	-68	-6	-114.0	-55	-54	-36	-48.3	-31	-37	-31	-33.0	-32	-43	-3	-26.0	-2	15	-34	-7.0	59.0	-3.073	-5.774	-4.574
1505	5.18	-327	-93	-18	-146.0	-70	-74	-54	-66.0	-45	-53	-51	-49.7	-43	-56	-16	-38.3	-6	14	-37	-9.7	46.0	-4.057	-7.358	-5.795
2000	6.07	-407	-121	-30	-186.0	-86	-94	-72	-84.0	-61	-69	-69	-66.3	-54	-70	-29	-51.0	-9	13	-41	-12.3	31.0	-4.997	-8.841	-7.299
3000	19.27	-802	-154	-66	-340.7	-1407	-1259	-67	-911.0	-62	-80	-77	-73.0	-102	-997	-40	-379.7	-16	4	-21	-11.0	-38.0	-11.324	-15.952	-13.850
3500	24.39	-860	-173	-87	-373.3	-1597	-1297	-84	-992.7	-68	-85	-79	-77.3	-107	-1128	0	-411.7	-19	3	-21	-12.3	-37.0	-13.041	-16.284	-16.624
2952	23.93	-809	-131	-61	-333.7	-1514	-1219	-80	-937.7	-59	-76	-69	-68.0	-100	-1101	0	-400.3	-18	4	-19	-11.0	-37.0	-13.089	-16.338	-15.989
2002	21.93	-712	-87	-32	-277.0	-1298	-1041	-59	-799.3	-42	-56	-47	-48.3	-80	-988	0	-356.0	-13	5	-16	-8.0	-35.0	-11.434	-16.078	-13.708
1003	18.92	-653	-58	-14	-241.7	-954	-757	-36	-582.3	-22	-34	-21	-25.7	-63	-811	0	-291.3	-8	5	-12	-5.0	-35.0	-8.259	-13.222	-10.077
517	17.04	-527	-51	-6	-194.7	-735	-570	-28	-444.3	-9	-23	-6	-12.7	-53	-685	0	-246.0	-5	5	-8	-2.7	-35.0	-6.192	-10.756	-7.628
16	14.62	-236	-33	13	-85.3	-511	-376	-9	-298.7	10	-6	14	6.0	-36	-484	0	-173.3	-1	5	-5	-0.3	-36.0	-3.777	-7.040	-4.709

Table A.8(ii) Strain gauge, Extensometer and Base load cell readings-TP6:Pull-out test (load cycle 2)

Ph (kN)	Dh (mm)	VIBRATING WIRE STRAIN GAUGE READINGS AT LEVELS DOWN PILE SHAFT (MICRO STRAIN) LEVEL 1.690 m				LEVEL 10.980 m				LEVEL 20.380 m				LEVEL 25.880 m				LEVEL 30.260 m				Pb	EXTENSOMETER READINGS (mm) LEVEL 3	LEVEL 4	LEVEL 5
		1	2	3	Mean	1	2	3	Mean	1	2	3	Mean	1	2	3	Mean	1	2	3	Mean	(kN)	(0-23m)	(0-26m)	(0-30m)
10	14.67	-232	-32	13	-83.7	-508	-373	-9	-296.7	10	-6	15	6.3	-36	-481	0	-172.3	-1	5	-5	-0.3	-34.5	-0.002	-0.008	-0.007
501	15.43	-273	-48	-5	-108.7	-547	-417	-35	-333.0	-8	-24	-3	-11.7	-48	-500	0	-182.7	-4	4	-7	-2.3	-34.5	-0.862	-1.679	-1.209
1001	16.85	-326	-51	-12	-129.7	-668	-541	-45	-418.0	-25	-41	-20	-28.7	-60	-569	0	-209.7	-6	4	-10	-4.0	-35.3	-2.427	-4.729	-3.323
1495	18.42	-375	-58	-19	-150.7	-868	-686	-53	-535.7	-37	-37	-34	-36.0	-69	-679	0	-249.3	-10	3	-12	-6.3	-35.3	-4.192	-8.175	-5.649
2000	20.01	-480	-76	-28	-194.7	-1060	-830	-64	-651.3	-47	-63	-48	-52.7	-77	-814	0	-297.0	-12	3	-15	-8.0	-34.5	-5.911	-11.556	-7.874
2499	21.61	-585	-98	-39	-240.7	-1235	-961	-75	-757.0	-57	-75	-62	-64.7	-89	-942	0	-343.7	-14	2	-17	-9.7	-34.5	-7.543	-14.588	-9.927
3004	23.34	-687	-124	-54	-288.3	-1395	-1080	-86	-853.7	-68	-88	-76	-77.3	-101	-1069	0	-390.0	-17	2	-19	-11.3	-36.0	-9.156	-17.355	-11.910
3497	25.29	-773	-153	-72	-332.7	-1541	-1179	-96	-938.7	-77	-104	-89	-90.0	-107	-1172	0	-426.3	-20	2	-20	-12.7	-36.9	-10.801	-20.026	-13.958
3997	28.69	-808	-168	-80	-352.0	-1681	-1263	-105		-82	-179	-103	-121.3	-113	-1270	0	-461.0	-23	2	-20	-13.7	-36.1	-12.968	-23.028	-16.594
4499	32.12	-800	-172	-72		-1806	-1331	-115		-86	-276	-130	-164.0	-117	-1377	0	-498.0	-27	2	-22	-15.7	-37.0	-15.264	-25.419	-19.123
4996	35.58	-770	-149	-58	-325.7	-1957	-1367	-127		-87	-375	-166		-121	-1508	0		-30	2	-23	-17.0	-34.5	-17.555	-26.826	-21.371
5442	40.14	-716	-95	-43	-284.7	-2148	-1402	-145		-82	-460	-202	-248.0	-123	-1660	0	-594.3	-34	2	-23	-18.3	-42.4	-19.711	-26.857	-23.417
4508	38.45	-659	-64	-22	-248.3	-1993	-1295	-126		-70	-427	-181	-226.0	-115	-1601	0	-572.0	-31	3	-21	-16.3	-35.4	-18.590	-26.811	-21.764
3501	35.84	-579	-52	-8	-213.0	-1728	-1148	-102	-992.7	-54	-377	-153	-194.7	-104	-1474	0	-526.0	-27	4	-18	-13.7	-34.5	-15.731	-25.707	-18.872
2502	32.62	-312	-41	6	-115.7	-1366	-934	-77	-792.3	-36	-330	-120	-162.0	-89	-1344	0	-477.7	-22	4	-15	-11.0	-35.3	-12.160	-21.945	-14.840
1506	28.93	-140	-15	28	-42.3	-962	-661	-61	-561.3	-19	-280	-88	-129.0	-71	-1171	0	-414.0	-16	5	-10	-7.0	-34.5	-8.201	-15.736	-10.113
503	24.57	-85	24	49	-4.0	-572	-385	-35	-330.7	9	-194	-50	-78.3	-47	-799	0	-282.0	-10	5	-6	-3.7	-35.3	-3.777	-7.407	-4.594
18	22.15	-70	45	57	10.7	-478	-308	-10	-265.3	32	-140	-21	-43.0	-9	-594	0	-201.0	-6	5	-4	-1.7	-36.0	-1.525	-2.911	-1.736

Table A.8(iii) Strain gauge, Extensometer and Base load cell readings-TP6:Pull-out test (load cycle 3)

Ph (kN)	Dh (mm)	VIBRATING WIRE STRAIN GAUGE READINGS AT LEVELS DOWN PILE SHAFT (MICRO STRAIN) LEVEL 1.690 m				LEVEL 10.980 m				LEVEL 20.380 m				LEVEL 25.880 m				LEVEL 30.260 m				Pb	EXTENSOMETER READINGS (mm) LEVEL 3	LEVEL 4	LEVEL 5
		1	2	3	Mean	1	2	3	Mean	1	2	3	Mean	1	2	3	Mean	1	2	3	Mean	(kN)	(0-23m)	(0-26m)	(0-30m)
19	21.98	-66	47	57	12.7	-473	-303	-10	-262	32	-135	-20	-41.0	-28	-582	0	-203.3	-5	5	-3	-1.0	-34.0	-1.435	-2.695	-1.622
505	22.82	-90	24	34	-10.7	-501	-335	-35	-290	13	-157	-40	-61.3	-41	-600	0	-213.7	-8	4	-5	-3.0	-35.0	-2.291	-4.462	-2.847
1002	24.36	-118	4	14	-33.3	-589	-413	-58	-353	-10	-186	-57	-84.3	-55	-654	0	-236.3	-11	3	-8	-5.3	-35.0	-3.810	-7.501	-5.036
2003	28.20	-208	-22	-7	-79.0	-988	-663	-72	-574	-38	-250	-92	-126.7	-74	-857	0	-310.3	-17	2	-12	-9.0	-34.0	-7.820	-15.075	-10.092
3000	31.95	-271	-31	-13	-105.0	-1350	-885	-88	-774	-57	-319	-126	-167.3	-89	-1136	0	-408.3	-22	1	-15	-12.0	-34.0	-11.887	-21.602	-14.911
4003	35.51	-349	-43	-16	-136.0	-1676	-1082	-109	-956	-74	-402	-161	-212.3	-105	-1402	0	-502.3	-27	1	-18	-14.7	-44.0	-15.701	-25.644	-19.018
4997	39.45	-450	-66	-28	-181.3	-1953	-1259	-130		-86	-507	-194	-262.3	-119	-1632	0	-583.7	-32	1	-21	-17.3	-37.0	-19.238	-26.758	-22.335
5989	45.47	-434	-58	-27		-2097	-1375	-137		-84	-599	-264	-315.7	-127	-1790	0	-639.0	-38	0	-23	-20.3	-37.0	-19.638	-26.821	-24.630
6471	48.78	-425	-52	-24	-167.0	-2171	-1420	-140		-82	-603	-275	-320.0	-131	-1856	0		-41	-1	-24	-22.0	-36.0	-19.667	-26.749	-24.520
6961	53.11	-416	-49	-22	-162.3	-2256	-1460	-141		-79	-584	-264	-309.0	-132	-1921	0	-684.3	-45	-2	-25	-24.0	-35.0	-19.667	-26.779	-24.537
7466	58.41	-411	-47	-21	-159.7	-2354	-1505	-143		-77	-562	-250	-296.3	-134	-1976	0	-703.3	-50	-3	-25	-26.0	-36.0	-19.660	-26.818	-24.433
7947	63.62	-406	-44	-19	-156.3	-2459	-1547	-143		-76	-541	-237	-284.7	-134	-2017	0	-717.0	-55	-3	-25	-27.7	-35.0	-19.640	-26.785	-24.552
8500	70.79	-404	-42	-18	-154.7	-2507	-1585	-146		-75	-527	-227	-276.3	-132	-2030	0	-720.7	-61	-5	-26	-30.7	-35.0	-19.603	-26.873	-24.572
6000	65.00																								
4000	58.40																								
2000	51.30																								

Table A.8(iv) Strain gauge, Extensometer and Base load cell readings-TP6:Pull-out test (load cycle 4)

Depth (m)	Applied pile head load											
	1MN	2MN	3MN	4MN	5MN	6MN	5MN	4MN	3MN	2MN	1MN	
1.65m	909	2001	2991	4015	5004	5943	5014	3963	2987	2011	1072	
17.45m	926	1569	2485	3445	4419	5310	4867	3901	2864	1808	811	
21.95m	487	918	1512	2120	2759	3302	2895	2379	1794	1189	610	Load cycle 1
26.45m	458	782	1262	1720	2180	2561	2176	1854	1476	1074	696	
28.806m	405	622	935	1206	1492	1693	1429	1320	1156	961	776	

Depth (m)	Applied pile head load											
	2MN	4MN	6MN	7MN	8MN	9MN	8MN	7MN	6MN	4MN	2MN	
1.65m	2117	3950	5919	6903	7921	9177	8061	6992	5960	4007	2090	
17.45m	1710	3787	5881	7013	8234	9650	7479	6576	5602	3594	1560	
21.95m	1264	2336	3448	4075	4775	5590	4867	4391	3287	2601	1305	Load cycle 2
26.45m	1190	1902	2675	3098	3584	4222	3581	3239	2865	2028	1134	
28.806m	1076	1422	1834	2077	2370	2807	2213	2091	1931	1508	1000	

Depth (m)	Applied pile head load										
	2MN	4MN	6MN	8MN	9MN	10.9MN	9MN	7MN	5MN	3MN	
1.65m	2184	3937	5829	7862	9019	10982	9095	6864	4999	3061	
17.45m	1626	3500	5430	7378	8433	10457	8907	6933	4844	2758	Load cycle 3
21.95m	1341	2541	3776	5013	5678	6990	5989	4822	3529	2193	
26.45m	1221	2025	2896	3799	4283	5295	4532	3758	2854	1910	
28.806m	1074	1524	2029	2558	2835	3480	3004	2650	2160	1616	

Depth (m)	Applied pile head load									
	4MN	6MN	6MN	10MN	12MN	13.5MN	10MN	7MN	4MN	
1.65m	3997	5809	7656	9787	12132	13730	10012	6957	4050	
17.45m	3810	5771	7742	9842	12057	13758	10665	7542	4473	Load cycle 4
21.95m	2802	4060	5336	6632	8021	9186	7255	5309	3309	
26.45m	2329	3226	4165	5166	6287	7339	5914	4526	3059	
28.806m	1802	2332	2904	3484	4172	4943				

Table A.9: Variation of pile axial forces with depth below pile head-TP2

Depth (m)	Applied pile head load									
	2MN	3MN	4MN	5MN	6MN	5MN	4MN	3MN	2MN	
1.550	2018	2991	3970	5012	6007	5017	3983	2981	2018	
21.225	1907	2807	3733	4719	5680	4847	3925	3009	2065	
23.735	1419	2045	2678	3351	3990	3504	2892	2250	1579	Load cycle 1
26.235	1386	2004	2647	3320	3973	3578	3003	2384	1736	
28.735	1250	1667	2095	2523	2942	2467	2114	1729	1318	
Load Cell	15	30	42	53	68	55	39	21	10	

Depth (m)	Applied pile head load											
	2MN	4MN	6MN	7MN	8MN	9MN	8MN	7MN	6MN	4MN	2MN	
1.550	2084	3943	5946	6944	7990	9091	8036	6989	5976	3973	2030	
21.225	2174	3929	5698	6616	7638	8673	7764	6840	5939	4059	2007	
23.735	1642	2800	4015	4600	5305	6007	5450	4860	4244	2927	1462	Load cycle 2
26.235	1742	2881	4046	4645	5332	6063	5634	5066	4477	3172	1684	
28.735	1460	2194	2904	3282	3701	4160	3559	3216	2852	2018	1043	
Load Cell	7	31	72	92	113	142	130	103	82	36	7	

Depth (m)	Applied pile head load														
	2MN	4MN	6MN	8MN	9MN	10MN	11MN	12MN	11MN	10MN	8MN	6MN	4MN	2MN	
1.550	2258	3981	5868	7805	8839	9973	10936	12336	11041	10009	7956	5951	4009	2035	
21.225	2238	3988	5764	7522	8451	9500	10434	11762	10659	9777	7950	6084	4088	1792	Load cycle 3
23.735	1631	2815	4008	5184	5798	6488	7093	7993	7319	6762	5533	4216	2774	1145	
26.235	1762	2931	4127	5302	5916	6620	7232	8224	7640	7116	5916	4594	3119	1445	
28.735	1333	2109	2876	3594	3976	4443	4845	5477	4585	4270	3532	2673	1671	509	
Load Cell	-1	17	55	118	157	172	200	286	263	233	177	102	45	8	

Depth (m)	Applied pile head load																
	2MN	4MN	6MN	8MN	10MN	12MN	14MN	16MN	16.5MN	14MN	12MN	10MN	8MN	6MN	4MN	2MN	
1.550	2478	4084	5866	7769	9703	11376	13874	16512	17371	14034	12026	10004	7908	5932	4049	2046	
21.225	2319	4055	5852	7641	9423	11299	13267	15558	16308	13256	11507	9706	7755	5724	3492	997	Load cycle 4
23.735	1620	2790	3980	5156	6333	7560	8811	10324	10943	9058	7850	6554	5136	3690	2111	427	
26.235	1771	2948	4159	5369	6751	7796	9078	10588	11207	9445	8269	6979	5538	4036	2413	674	
28.735	1192	1999	2814	3598	4343	5132	5796	6922	7246	5242	4501	3654	2696	1670	514	-720	
Load Cell	0	8	52	120	248	345	423	812	1355	350	316	277	232	185	131	74	

Depth (m)	Applied pile head load																
	2MN	4MN	6MN	8MN	10MN	12MN	14MN	15MN	16MN	17MN	18MN	14MN	10MN	8MN	6MN	4MN	
1.550	2502	4052	5833	7768	9738	11776	13845	14977	16089	17095	18322	14132	9889	7884	5957	4054	
21.225	1701	3536	5434	7352	9240	11136	13078	14173	15187	16192	17272	13490	9683	7784	5665	3243	Load cycle 5
23.735	1139	2401	3686	4979	6246	7523	8848	9616	10358	11090	11900	9479	6645	5222	3683	1933	
26.235	1158	2406	3734	5076	6424	7750	9121	9924	10730	11558	12540	10498	7650	6155	4560	2715	
28.735	200	1092	2032	2971	3876	4817	5835	6385	6954	7600	8407	6426	4482	3384	2216	820	
Load Cell	47	94	144	194	243	293	347	376	406	441	484	431	343	293	240	177	

Table A.10: Variation of pile axial forces (kN) with depth below pile head-TP3

Depth (m)	Applied pile head load							
	2MN	2.5MN	3MN	3.5MN	3MN	2.5MN	2MN	
1.250	2000	2500	3000	3500	3000	2500	2000	
17.950	1444	1865	2300	2747	2400	2058	1709	
18.750	877	1161	1469	1765	1473	1207	955	Load cycle 1
21.500	474	605	754	894	544	419	297	
24.250	233	249	278	299	-125	-144	-168	
Load Cell	13	14	17	19	14	11	8	

Depth (m)	Applied pile head load								
	3MN	4MN	5MN	5.25MN	5MN	4MN	3MN	2MN	
1.250	2985	4045	4944	5278	4982	4017	3022	1981	
17.950	2491	3226	4010	4280	3918	3435	2753	1843	
18.750	1569	2117	2712	2922	2669	2229	1728	1153	Load cycle 2
21.500	830	1071	1385	1534	1249	1024	755	476	
24.250	257	324	422	488	139	75	9	-71	
Load Cell	13	24	33	37	32	26	7	7	

Depth (m)	Applied pile head load														
	2MN	3MN	4MN	5MN	5.5MN	6MN	6.5MN	6.75MN	7MN	6MN	5MN	4MN	3MN	2MN	
1.250	2046	2985	4026	4965	5507	6006	6475	6768	7032	5985	5016	4000	3016	1985	
17.950	1844	2677	3454	4117	4536	4935	5337	5586	5806	5207	4641	3834	2942	1905	Load cycle 3
18.750	1175	1742	2285	2828	3147	3442	3761	3973	4150	3593	3082	2531	1967	1290	
21.500	668	946	1225	1475	1617	1808	1997	2148	2285	1799	1533	1248	937	596	
24.250	134	188	276	391	479	566	701	845	951	554	426	296	145	3	
Load Cell	1	8	20	36	43	53	62	72	80	67	52	39	25	9	

Depth (m)	Applied pile head load															
	2MN	3MN	4MN	5MN	6MN	7MN	8MN	9MN	10MN	11.25MN	9.5MN	8MN	6MN	4MN	2MN	
1.250	2088	2960	3939	4948	5988	7059	8007	9002	10011	11250	9588	7896	5884	3932	2113	
17.950	1904	2810	3706	4523	5297	6028	6820	7680	8540	9577	8474	7649	6048	3945	1723	Load cycle 4
18.750	1553	2333	3082	3832	4566	5331	6080	6860	7671	8482	5802	4959	3742	2346	769	
21.500	950	1338	1742	2119	2495	2893	3336	3896	4489	5113	3253	2755	1994	1159	252	
24.250	164	262	405	571	812	1213	1703	2562	*	*	*	*	*	*	*	
Load Cell	2	9	21	38	59	94	127	191	322	699	662	578	453	320	185	

Depth (m)	Applied pile head load									
	3MN	6MN	9MN	10MN	11MN	12MN	11.5MN	8MN	5MN	
1.250	3203	5791	8837	9990	11079	12105	11547	7894	5060	
17.950	2814	5624	8184	8967	9702	10428	10043	7950	5096	Load cycle 5
18.750	1563	3643	5621	6203	6668	6978	6408	4475	2541	
21.500	1007	2240	3359	3761	4114	4649	4372	3130	1886	
24.250	*	*	*	*	*	*	*	*	*	
Load Cell	143	282	339	769	986	1452	1552	1278	983	

Table A.11: Variation of pile axial forces (kN) with depth below pile head-TP4

Depth (m)	Applied pile head load													
	2MN	3MN	4MN	5MN	6MN	5MN	4MN	3MN	2MN	1.5MN	1MN			Load cycle 1
3.340	2030	2993	3964	4976	6035	5001	4000	3002	2000	1480	960			
20.200	1891	2740	3592	4481	5433	4526	3604	2696	1807	1350	893			
21.700	1519	2261	3008	3809	4651	4043	3298	2540	1747	1338	918			
25.700	1326	1828	2325	2851	3391	2844	2351	1828	1271	972	692			
29.700	947	979	1018	1049	1099	592	516	440	516	351	324			
Load Cell	25	34	46	63	85	68	44	21	2	0	0			
Depth(m)	2MN	4MN	6MN	7MN	7.5MN	6MN	4MN	2MN						Load cycle 2
3.340	2035	3975	5950	6968	7574	5995	4010	1995						
20.200	1818	3547	5376	6348	6951	5502	3669	1892						
21.700	1655	3138	4661	5457	5937	4917	3376	1757						
25.700	1192	2218	3271	3790	4097	3170	2102	956						
29.700	631	738	889	966	1024	317	131	-31						
Load Cell	0	32	96	137	171	163	88	22						
Depth(m)	2MN	4MN	6MN	7MN	7.5MN	8MN	8.5MN	9MN	9.5MN	8MN	6MN	4MN	2MN	Load cycle 3
3.340	2114	3995	5898	6884	7412	7968	8527	9200	9705	7975	6030	4012	1982	
20.200	1939	3605	5378	6302	6796	7302	7878	8587	9129	7574	5756	3918	2109	
21.700	1717	3184	4693	5443	5841	6256	6722	7287	7733	6712	5172	3521	1826	
25.700	1019	2021	3107	3630	3884	4150	4447	4826	5134	4202	3129	1935	703	
29.700	411	526	702	796	852	927	994	1230	1409	711	434	165	-98	
Load Cell	0	52	140	205	240	283	363	555	727	821	663	491	308	
Depth(m)	3MN	6MN	8MN	9MN	10MN	10.73MN	11MN	11.19MN	11.12MN	10.99MN	9MN	6MN	3.01MN	Load cycle 4
3.340	3068	5942	7940	8951	9980	10720	11036	11254	11074	10989	9055	6028	2981	
20.200	2876	5495	7427	8396	9392	10107	10418	10608	10401	10326	8652	5833	3108	
21.700	2382	4792	6453	7287	8163	8787	9061	9203	9228	9156	7717	5194	2524	
25.700	1325	2974	4241	4811	5479	6030	6409	6996	6913	6868	5836	3979	1991	
29.700	560	917	1276	1533	1937	2238	2739	3339	2955	2942	2545	1969	1369	
Load Cell	290	594	929	1188	1575	1963	2355	2906	2910	2895	2609	2250	1772	
Depth(m)	5MN	10.04MN	10.08MN	10.34MN	10.5MN	10.35MN	10.5MN	5.02MN						Load cycle 5
3.340	5010	10074	10110	10192	10582	10350	10476	5017						
20.200	4670	9475	9510	9608	9974	9703	9825	4892						
21.700	4037	8240	8266	8340	8633	8592	8703	4323						
25.700	3047	6750	6783	6957	7283	7391	7480	4154						
29.700	1768	3471	3487	3628	3823	3612	3656	2505						
Load Cell	1712	3277	3288	3380	3573	3620	3653	2929						
Depth(m)	3MN	6MN	8MN	8.96MN	10MN	7.53MN	5.05MN	2.56MN	0.087MN					Load cycle 6
3.340	3033	5966	7951	8946	10066	7520	5064	2548	10					
20.200	2850	5541	7450	8390	9452	7190	4905	2636	251					
21.700	2353	4824	6498	7291	8105	6310	4272	2109	-84					
25.700	2287	4235	5795	6597	7644	6265	4657	2894	1072					
29.700	2047	2631	3379	3823	4457	3710	3158	2526	1790					
Load Cell	1954	2505	3182	3545	4006	3691	3344	2840	2144					

Table A.12: Variation of axial force (kN) with depth below pile head-TP5

Depth (m)	Applied pile head load												
	1MN	2MN	3MN	3.5MN	3MN	2MN	1MN						Load cycle 1
1.690	1014	1985	3009	3561	2970	2018	996						
10.980	942	1794	2700	3171	2605	1752	847						
20.380	864	1676	2528	2984	2479	1716	860						
25.880	581	1099	1659	1922	1624	1283	832						
30.260	443	599	706	714	457	385	276						
Load Cell	4.8	7.1	53.4	52.8	45.5	33.5	17.9						
Depth (m)	Applied pile head load												
	1MN	2MN	3MN	4MN	5MN	5.5MN	4MN	3MN	2MN	1MN			Load cycle 2
1.690	1043	2010	2986	3993	5010	5580	3992	3007	2023	990			
10.980	929	1787	2658	3563	4449	4963	3489	2610	1740	797			
20.380	903	1719	2531	3358	4220	4728	3415	2584	1747	858			
25.880	823	1237	1672	2183	2721	3024	2363	1939	1496	961			
30.260	441	535	626	717	775	795	415	310	204	110			
Load Cell	13	29.3	47.3	70.8	90	97	73	55.5	35.5	17			
Depth (m)	Applied pile head load												
	2MN	4MN	6MN	8MN	9MN	8MN	6MN	4.01MN	2.03MN	1.03MN			Load cycle 3
1.690	2043	3978	5989	8036	9113	8012	5992	4006	2030	1028			
10.980	1828	3554	5346	7160	8100	6956	5172	3398	1605	681			
20.380	1804	3441	5149	7154	8152	7142	5475	3571	2011	1125			
25.880	1270	2059	2885	3766	4251	4260	3514	2606	1582	1017			
30.260	414	562	707	834	931	410	240	24	-198	-296			
Load Cell	26.6	64	118.1	195.5	262.2	239.5	204	149.7	89.8	58.8			
Depth (m)	Applied pile head load												
	4MN	6MN	8MN	10MN	11MN	11.49MN	12.5MN	10MN	6MN	4MN	2MN	1.01MN	Load cycle 4
1.690	3975	6132	7875	10023	11017	11509	12643	10048	5986	4021	2008	1019	
10.980	3432	5312	6902	8779	9665	10107	11070	8587	4971	3197	1343	414	
20.380	3703	5458	7024	8961	9898	10369	11372	9129	5646	3919	2132	1254	
25.880	2388	3336	4219	5220	5756	6064	6754	5578	3645	2649	1508	921	
30.260	309	490	693	989	1206	1365	1749	843	290	7	-289	-432	
Load Cell	102.6	166.9	247.9	402.1	557.1	658.2	909.4	829	649.5	541.7	415	348.6	

Table A.13: Variation of pile axial forces (kN) with depth below pile head-TP6